

**Tailor-Made Structures for Molecular Junctions:
From Linear Wires to Molecular Loops**

Inauguraldissertation

zur

Erlangung der Würde eines Doktors der Philosophie

vorgelegt der

**Philosophisch-Naturwissenschaftlichen Fakultät
der Universität Basel**

Von

Ksenia Reznikova

Basel 2024

Genehmigt von der Philosophisch-Naturwissenschaftlichen Fakultät

auf Antrag von

Erstbetreuer: Prof. Dr. Marcel Mayor

Zweitbetreuer: Prof. Dr. Christof Sparr

Externer Expert: Prof. Dr. Michal Juríček

Basel, den 21.02.2023

Prof. Dr. Marcel Mayor (Dekan)

Für Joel

und meine Familie

We all wish we had superpowers.

We all wish we could do more than we can do.

Stan Lee

Acknowledgment

First and foremost, I would like to acknowledge my supervisor *Prof. Dr. Marcel Mayor* for giving me the opportunity to work on so many exciting and challenging projects in his group. I am deeply grateful for your support, encouragement, and guidance throughout the last years.

I would sincerely like to thank *Prof. Dr. Christof Sparr* for agreeing to be my second supervisor and *Prof. Dr. Michal Juríček* for accepting to be the external expert for this thesis.

Collaborative work is only possible with the best partners. I would like to thank our collaborators at EMPA, *Prof. Dr. Michel Calame* and his students *Oliver Schmuck* and *Dr. Davide Beretta*, for fruitful discussions, showing and explaining the experimental setup, as well as the junction chip preparation procedure. Furthermore, I want to thank the experimental physics at TUDelft, *Prof. Dr. S. J. Herre van der Zant*, *Chunwei Chu*, and *Sebastiaan van der Poel* and theoretical physics *Prof. Dr. Fabian Pauly*, *Werner M. Schosser*, *Dr. Katawoura Beltako*, and *Matthias Blaschke* from the University of Augsburg for making and explaining the MCBJ measurements and the theory behind them during our monthly Zoom meetings. I would also like to thank my co-workers, *Dr. Almudena Gallego*, *Dr. Eric Sidler*, *Dr. Patrick Zwick*, and *Charlotte Kress*, for the great collaboration.

I want to thank *Prof. Dr. Daniel Häussinger*, his students, and his research group (mainly *Daniel*, *Raphael*, and *Pascal*) for helping with the NMR analysis.

Thanks to *Dr. Loïc Le Pleux*, *Dr. Laurent Jucker*, *Camiel C. E. Kroonen*, *Manuel U. Hugo*, *Adriano D'Addio*, *Björn Pfund*, *Jöel F. Keller*, and *Dr. Joel L. Rösslein* for proofreading my thesis and their helpful advice and corrections.

I am also grateful to be a part of the QUIET program. It was a pleasure to meet so many highly motivated scientists and be at so many conferences, meetings, and networking events, as well as to have a lot of discussions and inspiring time together.

I want to thank all current and former members of the Mayor Group for the great working atmosphere, all scientific and non-scientific discussions, time in and outside the lab, and all the fun we had together. A special thank goes to my "Lab 8 Family", *Kevin*, *Linda*, *Tomáš*, *Florian*, *Marius*, *Adriano*, *Manuel*, *Ramon*, and *Camiel*. I have always enjoyed working with you, and I will really miss all the bad jokes, the unique taste in music, and the unforgettable discussions. Furthermore, I would like to thank *Laurent* for always having/founding time for me and my stories/challenges. *Björn* and *Adriano*, thank you for your crash course, patience, and several explanations of spectroscopy.

I want to thank *Sylvie Mittelheisser, Dr. Michael Pfeffer, and Jonas Zurflüh* for their analytical support.

Good working conditions at the chemistry department were only possible because of the excellent technical and administrative staff. I want to thank *Markus Ast, Andres Koller, Hisni Meha, Andreas Sohler, Oliver Ilg, Markus Hauri, Nathalie Plattner-Longhi, Olaf Lips, and Brigitte Howald*.

I want to thank *Prof. Dr. Bernhard Jung and Loreno Calisse* for their IT support.

I want to thank my family, future in-laws, and my friends outside the lab for their support. Especially my *Mom*. Without you, I would not be who I am. Thank you for everything you did for me.

Finally, I would like to thank my love and dearest friend *Joel*, who has been there all along to celebrate with me on the good days and cheer me up during the bad ones, and who never stopped believing in me, even when I did not.

Preface & Overview of the Thesis

In 1974, Aviram and Ratner suggested implementing molecules as the smallest building block, still providing structural diversity and functionality, allowing them to act as functional devices into electronic circuits.¹ This visionary concept still fascinates scientists worldwide, leading to the blossom of interdisciplinary research to understand charge transport through molecules in the electrode-molecule-electrode junctions.²⁻⁴ Over the past decades, several possibilities and techniques for probing and manipulating the molecules in the junctions were developed, for instance, scanning tunneling microscope break junctions (STM-BJ),⁵ mechanically controlled break junctions (MCBJ),⁶ electromigration breakdown junctions (EBJ),⁷ and graphene-molecule-graphene junctions.⁸⁻¹⁰ Beyond the initial interest in understanding electronic transport, these techniques also allowed scientists to explore interference of electron waves,^{11,12} mechanics,¹³ optical effects,¹⁴ and thermoelectric phenomena¹⁵ of molecular junctions.

This thesis contains the preparation of several molecules for investigations in molecular junctions, which were done in the scope of a highly interdisciplinary project named Quantum Interference Enhanced Thermoelectricity (QUIET), involving scientists from different disciplines and countries (theoretical and experimental physics and chemistry).

- I. The first chapter describes the design and synthesis of presumably suitable and stable molecular rods for the investigation of charge-transport properties of graphene-molecule-graphene junctions. It is a follow-up project to the one started during my master's thesis in the group of *Prof. Dr. Marcel Mayor* in collaboration with the experimental physicists from the group of *Prof. Dr. Michel Calame* at EMPA (Swiss Federal Laboratories for Materials Science and Technology) in Zurich, Switzerland. Due to the challenges that arose during the chip preparation and molecules immobilization, the synthesis was frozen in the next-to-the-last step.
- II. The second part of this thesis deals with a deeper understanding of the relationship between conductivity, quantum interference, and mechanical response of molecules implemented in mechanically controllable break junctions in dependence on difference substitution pattern. For this purpose, six molecular wires bearing the [2.2]paracyclophane as a central moiety were synthesized as model compounds. The realization of this project was only possible due to the fruitful and inspiring collaboration with the experimental physicists from the group of *Prof. Dr. S. J. Herre van der Zant* from the University of Technology in Delft, Netherlands, and theoretics from the group of *Prof. Dr. Fabian Pauly* from the University of Physics in Augsburg, Germany. The results of the first four structures are presented in the form of a

publication. The last two structures were successfully synthesized and are now under investigation; therefore, only synthesis is included in the thesis.

- III. The third chapter deals with the design and synthesis of the envisioned structure implementing molecular wire and loop scaffold, which combines two conductivity pathways: through-space and through-bond. This project was synthetically most challenging and provided surprising results. Our efforts, progress, and all challenges are summarized and will be discussed in this chapter.
- IV. The last chapter provides the elucidation of cyclic dimers. The initial structure was obtained as a by-product in the macrocyclization reaction in *Chapter 3* and was then transformed into the thiophene analogue. This synthetic step, as well as topological evidence and preliminary optical investigations of both dimers, are summarized in this chapter.

All chapters are constructed similarly, providing the introduction on the first pages to ease the reader into the topic. Afterward comes the project description, molecular design, synthetic strategy, results, and discussion. Also, each chapter is supplied with a summary and outlook. All the experimental parts can be found in the supporting information of the corresponding chapter and the spectra in the appendix.

Contents

| | |
|-------------------------------------------------------------------------------------------------------------------------------------------------------|------------|
| Acknowledgment | I |
| Preface & Overview of the Thesis | III |
| 1 Synthesis Towards Tailor-Made Molecular Rods for Graphene Junctions | 3 |
| 1.1 Introduction: Graphene Junctions..... | 3 |
| 1.1.1 Formation of Graphene Junctions | 3 |
| 1.1.2 Immobilization: Covalent Bond vs. π - π Stacking | 4 |
| 1.2 Project Description | 7 |
| 1.3 Molecular Design | 8 |
| 1.4 Synthetic Strategy | 9 |
| 1.5 Results and Discussion | 11 |
| 1.5.1 Synthesis of the Anchoring Group and the OPE Linker | 11 |
| 1.5.2 Synthesis of the Central Moiety | 13 |
| 1.5.3 Assembly of OPE5 Precursor and OPE5 Reference | 14 |
| 1.6 Summary..... | 16 |
| 1.7 Outlook: Hydrosilylation..... | 16 |
| 2 Quantum Interference Effects in [2.2]Paracyclophane-Based Structures | 21 |
| 2.1 General Introduction..... | 21 |
| 2.1.1 Two-Fold Substituted [2.2]Paracyclophanes | 21 |
| 2.1.2 Molecular Orbital-Based Quantum Interference..... | 29 |
| 2.2 <i>Meta</i> vs. <i>Para</i> : “Substitution Pattern Controlled Quantum Interference in [2.2]Paracyclophane-Based Single-Molecule Junctions.”..... | 32 |
| 2.3 Pseudo- <i>Ortho</i> -[2.2]Paracyclophane-Based Molecular Wires | 41 |
| 2.3.1 Project Description and Molecular Design | 41 |
| 2.3.2 Results and Discussion | 42 |
| 2.4 Summary..... | 45 |
| 2.5 Outlook..... | 46 |
| 3 Synthesis Towards a [2.2]Paracyclophane-Based Molecular Loop | 51 |
| 3.1 Introduction | 51 |
| 3.1.1 General Macrocyclization Strategies | 51 |
| 3.1.2 Ring Closure of Angle-Strained Diyne-Containing Macrocycles | 52 |
| 3.2 Project Description | 58 |
| 3.3 Molecular Design | 59 |
| 3.4 Synthetic Strategy | 60 |
| 3.5 Results and Discussion | 63 |
| 3.5.1 Synthesis of the Central PCP-Moiety | 63 |
| 3.5.2 Synthesis of the Terthiophene Derivative | 64 |

| | | |
|----------|----------------------------------------------------------------------------|------------|
| 3.5.3 | Borylation of Terthiophene Derivate and Assemble of Loop Precursor | 65 |
| 3.5.4 | Macrocyclization..... | 73 |
| 3.6 | Summary..... | 83 |
| 3.7 | Outlook: Redesign..... | 84 |
| 4 | Dimer: An Infinity Loop..... | 89 |
| 4.1 | Introduction | 89 |
| 4.1.1 | Optical-Active Pseudo-Ortho-[2.2]Paracyclophane Containing Macrocycles ... | 89 |
| 4.1.2 | Optical-Active Pseudo-Meta-[2.2]Paracyclophane Containing Macrocycles | 91 |
| 4.2 | Project Description | 92 |
| 4.3 | Results and Discussion | 93 |
| 4.3.1 | Topology | 93 |
| 4.3.2 | Formation of Thiophene Dimer..... | 95 |
| 4.3.3 | Preliminary Optical Investigations..... | 97 |
| 4.4 | Summary..... | 103 |
| 4.5 | Outlook..... | 103 |
| 4.5.1 | Chirality | 103 |
| 4.5.2 | Proof-of-Concept..... | 105 |
| 5 | Supporting Information..... | 109 |
| 5.1 | Contributions..... | 109 |
| 5.2 | General Information..... | 109 |
| 5.3 | Supporting Information: Chapter 1..... | 111 |
| 5.4 | Supporting Information: Subchapter 2.2 | 119 |
| 5.4.1 | Synthesis and Characterization | 119 |
| 5.4.2 | Transport Measurements | 127 |
| 5.4.3 | Transport Calculations | 132 |
| 5.5 | Supporting Information: Subchapter 2.3 | 139 |
| 5.6 | Supporting Information: Chapters 3 & 4..... | 141 |
| 6 | Abbreviations | 153 |
| 7 | References..... | 155 |
| 8 | Appendix..... | 169 |

Chapter 1

1 Synthesis Towards Tailor-Made Molecular Rods for Graphene Junctions

This chapter presents the results towards the synthesis of tailor-made molecular rods for immobilization in graphene junctions. For this purpose, the desired molecules were designed bearing flat π -conjugated subunits as outer anchoring groups to interact with graphene electrodes via π - π stacking. Furthermore, additional anchoring groups were introduced to increase the mechanical stability of molecules between two graphene electrodes and prevent the molecule's sliding out of the junction. The first generation of possible candidates was synthesized, measured, and reported in the scope of previous research (Ksenia Reznikova, Master Thesis supervised by *Prof. Dr. Marcel Mayor*). Therefore, this chapter will outline an elongated second generation of molecular wires with an improved synthetic strategy. The preparations of graphene junctions by molecules immobilization and consequent measurements were carried out in the group of *Prof. Dr. Michel Calame* at EMPA (Swiss Federal Laboratories for Materials Science and Technology) in Zurich, Switzerland. The following pages will introduce the benefits of graphene electrodes compared to commonly used gold ones, as well as a brief overview of the formation of graphene gaps and several possibilities of molecule immobilization.

1.1 Introduction: Graphene Junctions

Because of its remarkable electrical properties, graphene has become an attractive alternative to gold as a material for electrodes in molecular junctions.^{16–18} In addition, graphene electrodes allow to overcome the synthetic challenges arising during the late-stage introduction of linkage groups since graphene electrodes do not only allow to bind covalently^{14,18,19} but also via π - π stacking interactions of the aromatic rings.^{9,20} A further advantage of this flat two-dimensional scaffold is stability at room temperature and the possibility of preparing extremely thin electrodes, which can better interact with the investigated molecules.^{8,21}

1.1.1 Formation of Graphene Junctions

Graphene junctions are commonly prepared from single-layer graphene with a size of 10 μm obtained from chemical vapor deposition (CVD) grown on a copper foil, which is then transferred to the substrate (Si/SiO_2).^{22,23} The graphene construction can have different conformations, for example, triangular, hourglass-shaped, or H-shaped.²⁴ And the nanogaps can also be formed using several techniques and setups for the fabrication of graphene electrodes, for instance, electron beam lithography,¹⁶ focused ion and electron beam milling,^{25,26} selective hydrogen plasma etching,²⁷ scanning probe methods,²⁸ and electrical

breakdown.^{8,10,21,24} In our case, graphene electrodes are prepared using the electrical breakdown (EB) protocol. For this purpose, the graphene is conformed in H-shaped constriction with 400 nm wide and 800 nm long contacted to metal electrodes, such as platinum or gold (see Figure 1a).^{22,24} The EB process is performed by applying high voltage pulses with increasing amplitude through the constriction until the desired gap is formed (see Figure 1b).²² The obtained nanogap width can be only approximately estimated, making the preparation of suitable molecular wires more challenging. However, the presence of molecules implemented between two electrodes (see Figure 1c) can be determined according to the changes in the transport characteristics before and after deposition.²⁴

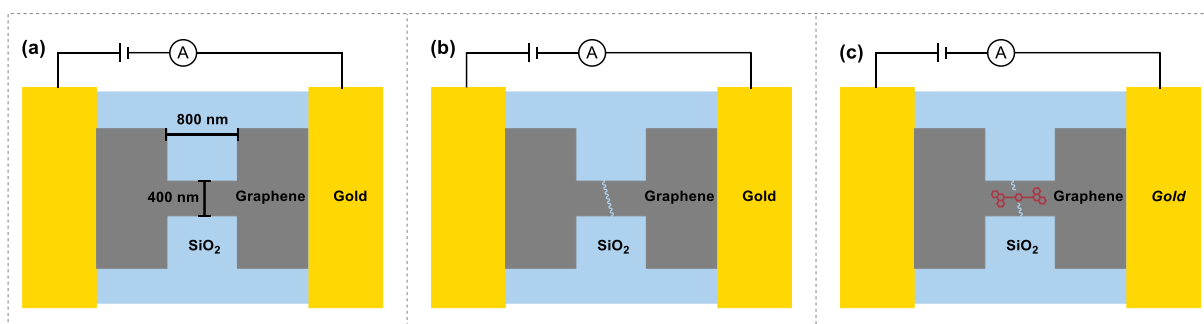


Figure 1: Schematic representation of H-shaped graphene junction before (a) and after (b) electrical breakdown, and (c) after molecule immobilization.

1.1.2 Immobilization: Covalent Bond vs. π - π Stacking

As mentioned above, there are several possibilities to attach molecules to graphene electrodes, and a short overview of selected examples will be presented in the following pages. The first option is a covalently binding of a molecule to the graphene electrode. For this approach, oxidized graphene edges are required (see Figure 2a), which can be obtained by reactive etching of graphene using an oxygen plasma. The carboxylic acid on the graphene edges can undergo a condensation reaction with amine anchoring groups providing the covalent bonds to the electrodes (see Figure 2). *Xu et al.* published this procedure on examples of 1,4-diaminobenzene (**1**) and 4,4'-diaminobiphenyl (**2**).¹⁹ However, the obtained yield of the electrode-molecule-electrode junction formation was pretty low, under 20%, which was presumed to be due to the lack of control during the etching process.

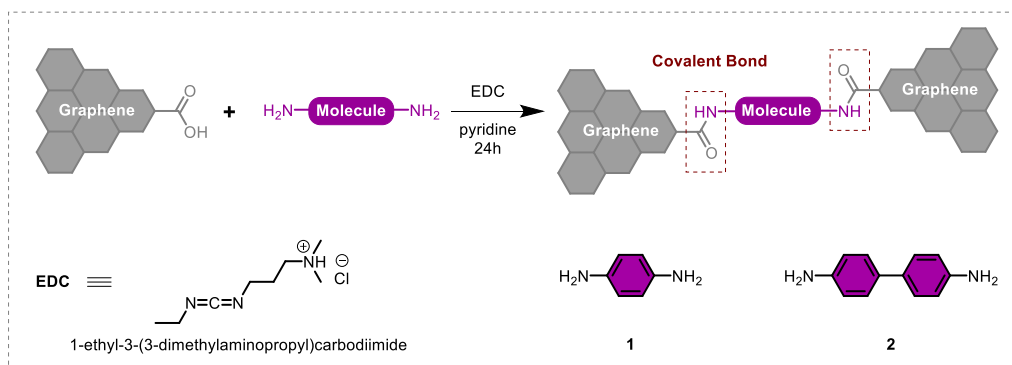


Figure 2: Schematic representation of oxidized graphene, which reacts with a diamine in pyridine with EDC as an activating agent providing a covalent bond between the molecule and graphene.

A second approach for the molecules to interact with graphene electrodes would be via π - π stacking, allowing to relinquish the introduction of anchoring groups either on graphene or molecular wire. This strategy requires the molecule to contain π -conjugated anchoring groups, which are flat and have suitable size, on both ends of the molecular wire to interact with electrodes. *Limburg et al.* investigated the non-covalent interfacing of different anchoring groups of porphyrin-based molecular wires with graphene electrodes (see Figure 3).²⁹

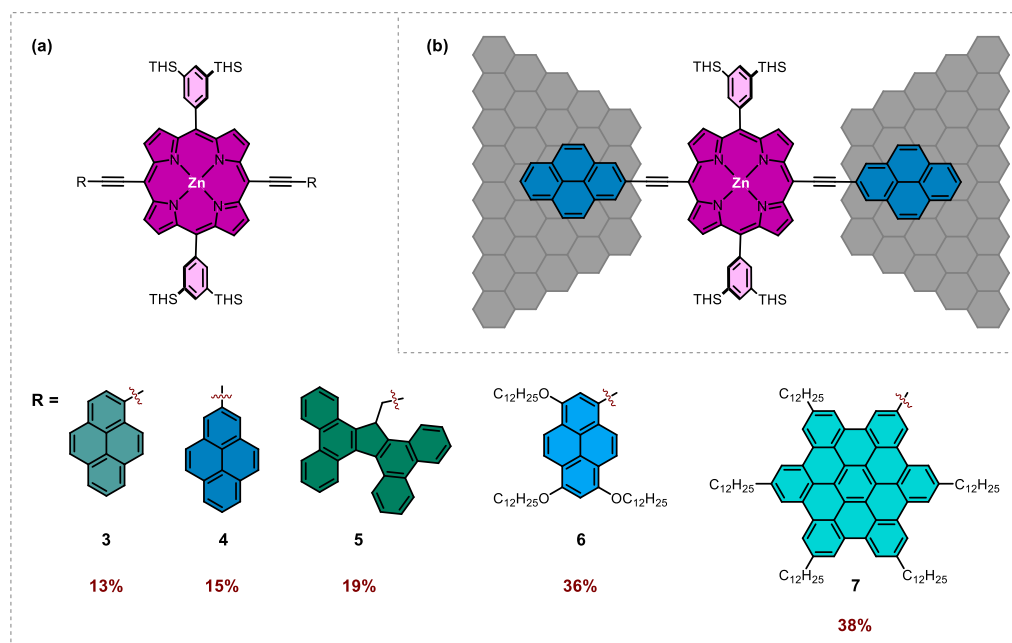


Figure 3: (a) Porphyrin wires with different anchoring groups. The numbers in red are junction formation probabilities that increase with the size of the anchoring group. (b) Schematic representation of graphene junction bridged by porphyrin-based molecular wire. THS is an abbreviation for trihexylsilyl.

They observed an increase in molecular junction formation probability with an increase in the size of the anchoring group from pyrene with different substitution pattern **3** and **4** (13% and 15%, respectively), over tetrabenofluorene (**5**) with 19%, up to values of 36% and 38% obtained with the best performing 1,3,8-tridodecyloxy pyrene (**6**) and 2,5,8,11,14-

pentadecylhexa-*peri*-hexabenzocoronene (**7**)³⁰ anchoring groups, respectively. These observations can be rationalized by the weak nature of π - π interactions, which leads to limited mechanical stability of molecules with small anchoring groups in the junction.

The aforementioned stability problem can be solved by introducing an additional anchoring option in the molecular design. *Calame* and co-workers demonstrated a possibility of stabilization of the molecules in the junction by implementing a silyl anchoring group in the design of investigated molecules.³¹ The silyl anchor formed a covalent bond with the silicone oxide substrate, increasing the electrode-molecule-electrode junction's mechanical robustness. On the other hand, stable electrical communication was achieved by a π - π overlap of several carbazoles arranged in a row between both graphene electrodes, as depicted in Figure 4.

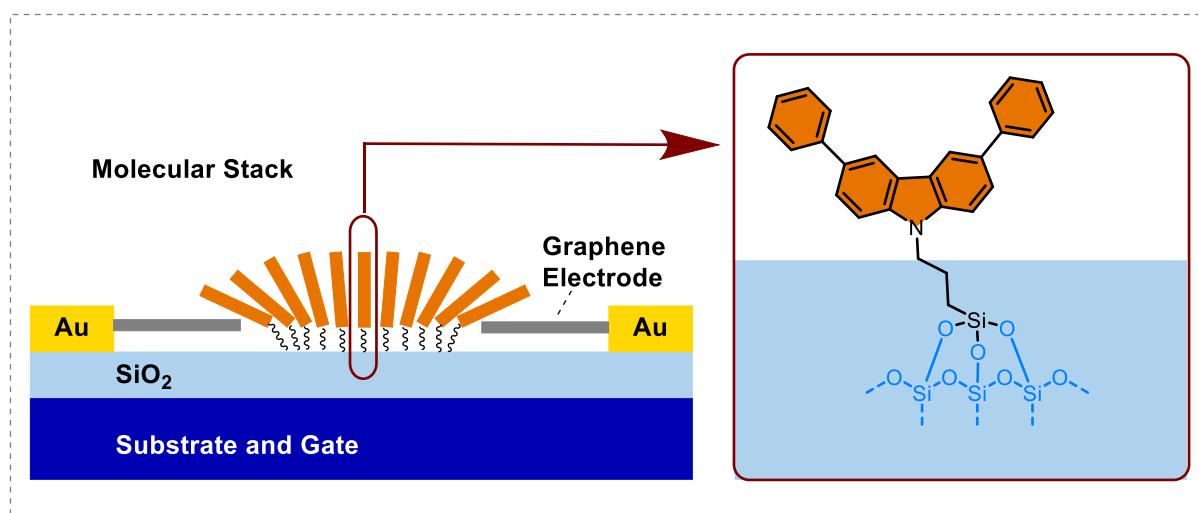


Figure 4: Schematic representation of graphene junction containing a row of π - π stacked molecules bridging between two graphene electrodes and a zoom-in of silyl anchor of carbazole-based molecule forming a covalent bond in the junction.

1.2 Project Description

The use of graphene as electrode material raises a question of a suitable and reliable design of molecular rods to achieve a mechanically stable molecular junction with controllable and reproducible current-voltage (I-V) characteristics. The potential candidate should fulfill several requirements. Firstly, the molecules should be well conjugated, flat, and rigid, with an appropriate size to bridge both electrodes. Secondly, the desired structure should be connected to the graphene electrodes covalently or via π - π stacking, implicating suitable outer anchoring groups for a molecular rod. By the covalent bonding of molecules to graphene electrodes, the edge etching strongly influences the electrodes' geometry and impacts the junction's current-voltage (I-V) characteristics.^{19,32} Therefore, connecting molecules to the graphene via π - π stacking seems to be a more suitable strategy,³² even with a lack of mechanical stability.¹⁸

The main goal of this project is to find a suitable molecular design allowing a balance between mechanical and electronic stability for molecular rods in graphene junctions. Therefore, we designed a molecular rod that allows the anchoring of molecules directly to the silicon insulator instead to the graphene electrodes. This additional anchoring possibility permits the task separation of outer and central anchoring groups, as depicted in Figure 5, where one is responsible for electrical communication and the other for mechanical stabilization, respectively.

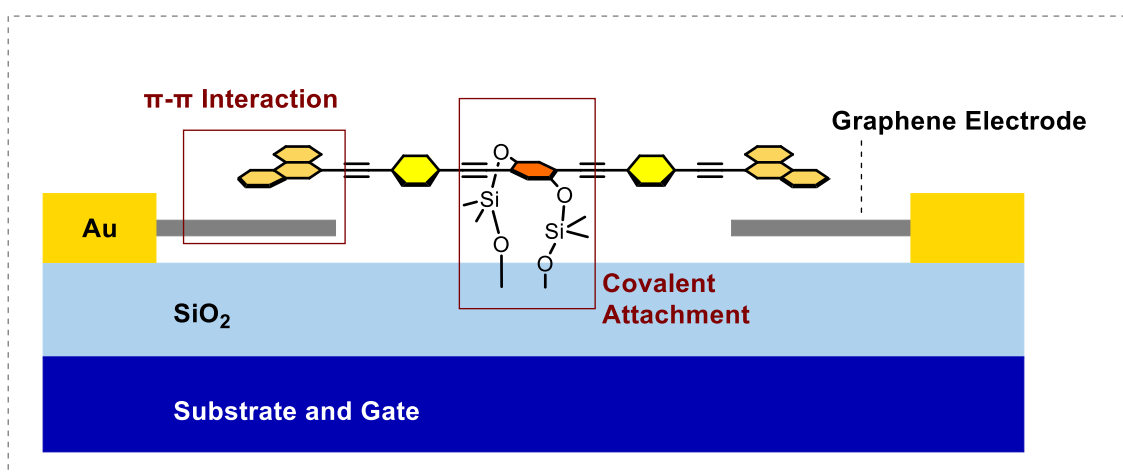


Figure 5: Schematical representation of a task separation between outer and central anchoring groups responsible for electronic transport and stability in the junction, respectively.

1.3 Molecular Design

The proposed molecular rod comprises two anchoring groups (see Figure 6): the silyl anchoring group attached to the central moiety that prevents the molecule's sliding out of the junction and the outer anchoring groups that interact with graphene. Both parts are connected via a linear π -conjugated system to establish electronic communication. For this purpose, good polarizable and rigid oligo(phenylene ethynylene) (OPE) linkers were chosen. The OPE linkers were functionalized with alkoxy chains to improve solubility of the molecular rod. The introduction of additional OPE linkers enables the prolongation of the structure and provides the possibility of preparing a library of molecules that are different in length. Further, we considered using phenanthrene as the outer anchoring groups to interact with graphene electrodes due to a flat conjugated system suitable for stable electrical communication but too small for mechanical stabilization. This feature of phenanthrene would allow us to prove our hypothesis of the possibility of additional mechanical stabilization of molecules due to the covalent attachment of the silyl anchoring group to the silicon dioxide substrate in the molecular junction.

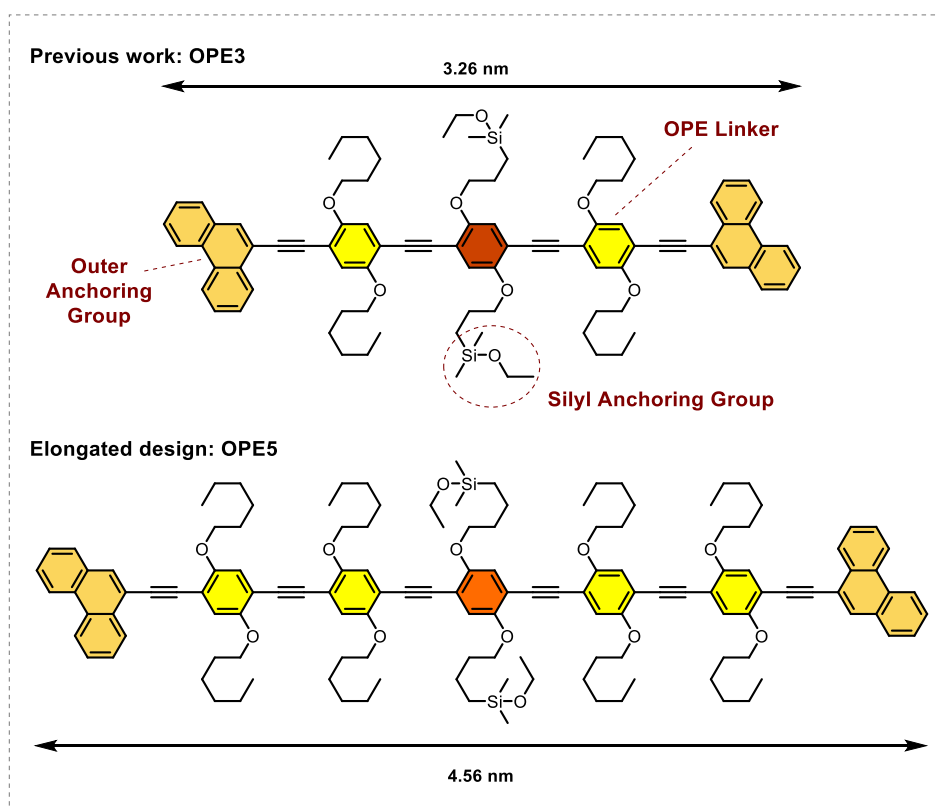


Figure 6: OPE3 structure (synthesized and fully characterized during the master thesis) and OPE5 structure with displayed lengths calculated by geometry optimization in Chem3D (MM2).

Firstly, we considered the length of **OPE3** to be suitable to bridge the graphene electrodes. Therefore, the desired structure was synthesized and fully characterized in the scope of my master thesis in the group of *Prof. Dr. Marcel Mayor*. Also, the preliminary measurements in the laboratories of *Prof. Dr. Michel Calame* at EMPA were performed during the master thesis, proving the yield of junction formation of about 20%, which was lower than expected. Therefore, we assume that the obtained width of the graphene junctions was bigger than estimated. As a result, improvement of junction formation was investigated from one side exploring possibilities to narrow the gap further and on the other via elongation of the molecular bridge. The latter will be achieved by implementing two additional OPE moieties that increase the length from approximately 3.26 nm of **OPE3** to 4.56 nm of **OPE5** (see Scheme 6), which can still be elongated by introducing additional OPE building blocks.

1.4 Synthetic Strategy

The synthetic strategy toward the desired **OPE5** structure is illustrated in Figure 7. The hydrosilylation step is performed as the last stage modification to facilitate the purification steps during the synthesis. In addition, the silyl anchoring group makes **OPE5** water labile; therefore, it cannot be stored for a long time and should be introduced briefly before immobilization. The assembly of the OPE backbone **8** is based on *Sonogashira-Hagihara* cross-coupling reactions³³, which are known to be suitable for synthesizing large OPE-based molecular architectures.^{34–36} Due to the fact that the desired structure is centrosymmetric, it can be stepwise assembled over the convergent synthesis strategy from the highly functionalized building blocks **9–11**. An ethynyl group or leaving group is required for coupling the desired subunits.³⁷ The ethynyl groups are masked with a protecting group (PG), which makes the synthesis vary between *Sonogashira-Hagihara* cross-coupling reactions and deprotections. On the other hand, iodine was chosen as a leaving group to enable cross-coupling reactions even at room temperature. The subunits for OPE linker **10** and central moiety **11** were decorated with alkyl and terminal alkene chains to improve the solubility and allow hydrosilylation, respectively. Due to stability reasons, the terminal alkene chain of the central moiety was exchanged for a more stable butene analogue for the **OPE5** molecular rod compared to the **OPE3**.

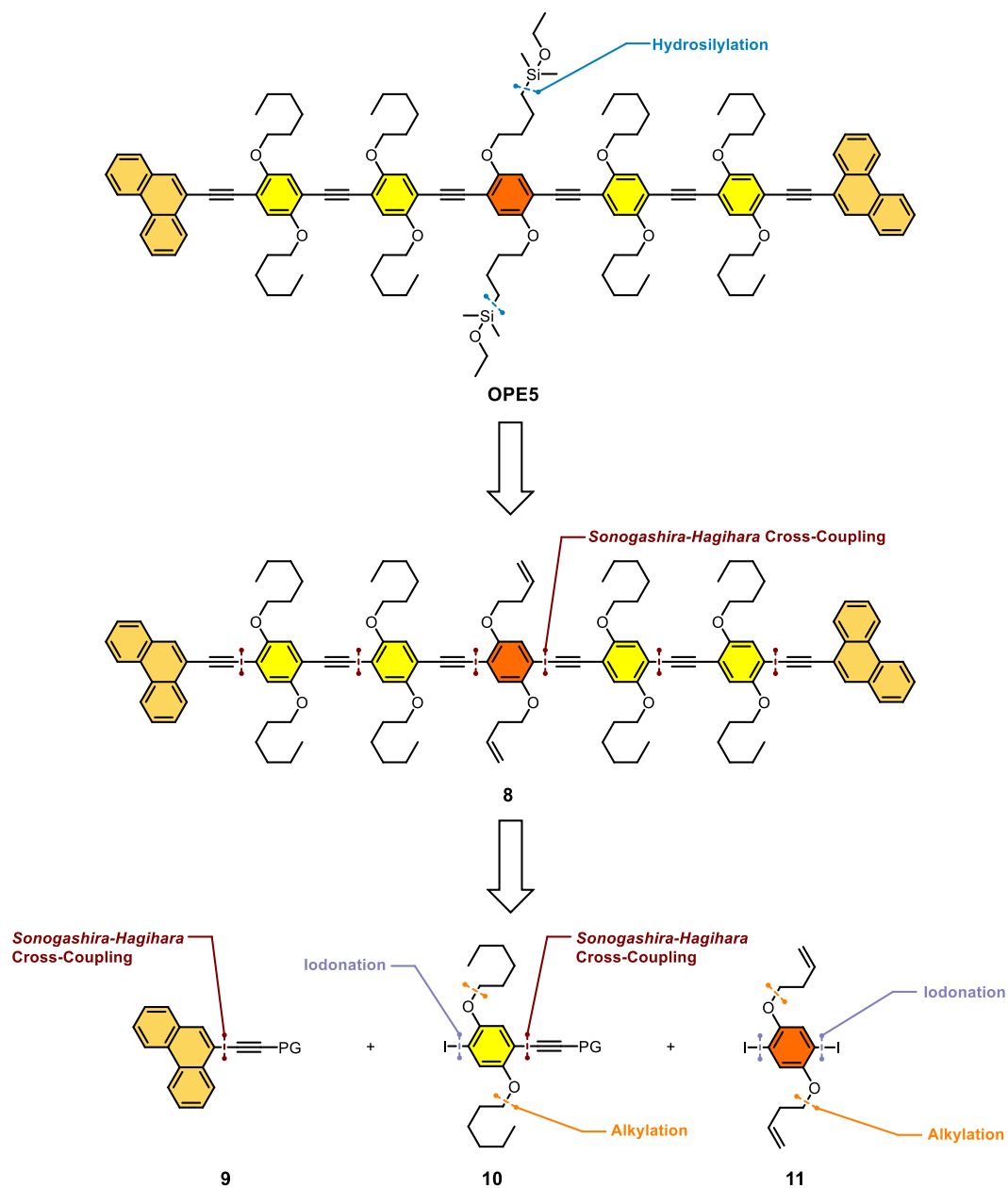
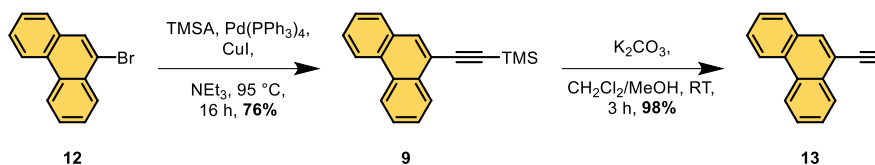


Figure 7: Synthetic strategy for the synthesis of OPE5. The abbreviation PG stands for protecting group. All disconnections in the retrosynthetic analysis are marked with colors dependent on the reaction type.

1.5 Results and Discussion

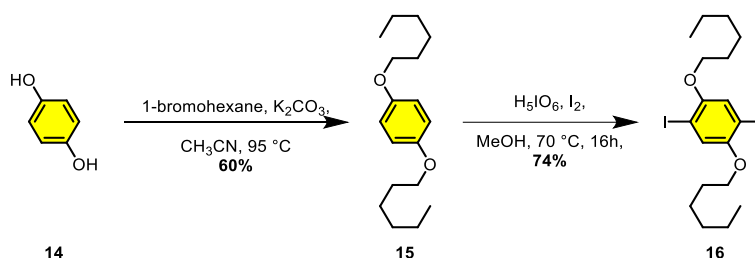
1.5.1 Synthesis of the Anchoring Group and the OPE Linker

The synthesis of the desired **OPE5** structure started with the preparation of 9-ethynylphenanthrene (**13**) (see Scheme 1), which was achieved on a gram scale in two steps following the modified procedure developed by Grunder and co-workers.³⁶ Commercially available 9-bromophenanthrene (**12**) was used in a *Sonogashira-Hagihara* cross-coupling reaction with trimethylsilylacetylene (TMSA), tetrakis(triphenylphosphine)palladium, and copper iodine in triethylamine as base and solvent. The TMS-protected acetylene **9** was obtained in 76% yield after the purification by column chromatography. Afterward, the TMS protecting group was cleaved using an excess of potassium carbonate in a mixture of dichloromethane and methanol, providing the free acetylene **13** in an excellent yield of 98%.



Scheme 1: Synthesis of the outer anchoring group **13** over the introduction of acetylene.

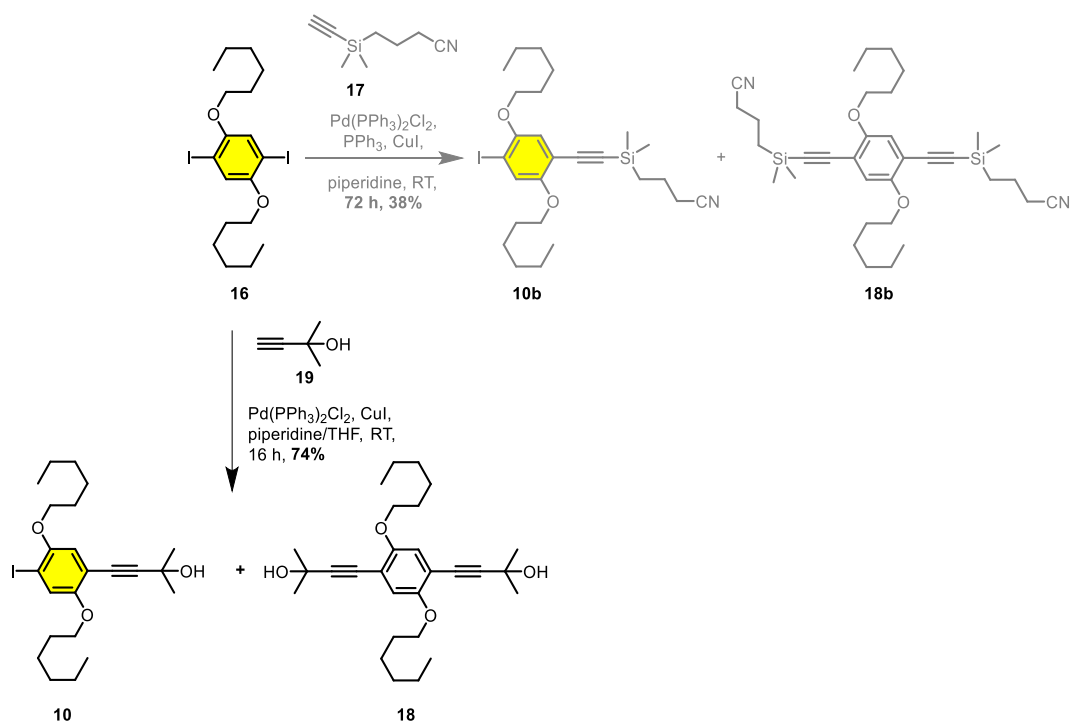
Next, building block **16** for the OPE linker was prepared (see Scheme 3). The commercially available hydroquinone **14** was alkylated using 1-bromohexane and potassium carbonate in acetonitrile, providing 1,4-bis(hexyloxy)benzene (**15**) in 60% yield. Iodination of **15** was performed by modification of literature known conditions³⁸ with periodic acid and iodine in methanol. After purification via recrystallization from ethanol, the desired diiodo compound **16** was isolated in 74% yield.



Scheme 2: Synthesis of diiodo compound **16**.

The bifunctional repeating unit **10** was prepared in a statistical *Sonogashira-Hagihara* cross-coupling reaction with masked acetylene (see Scheme 3). A statistically expected outcome for

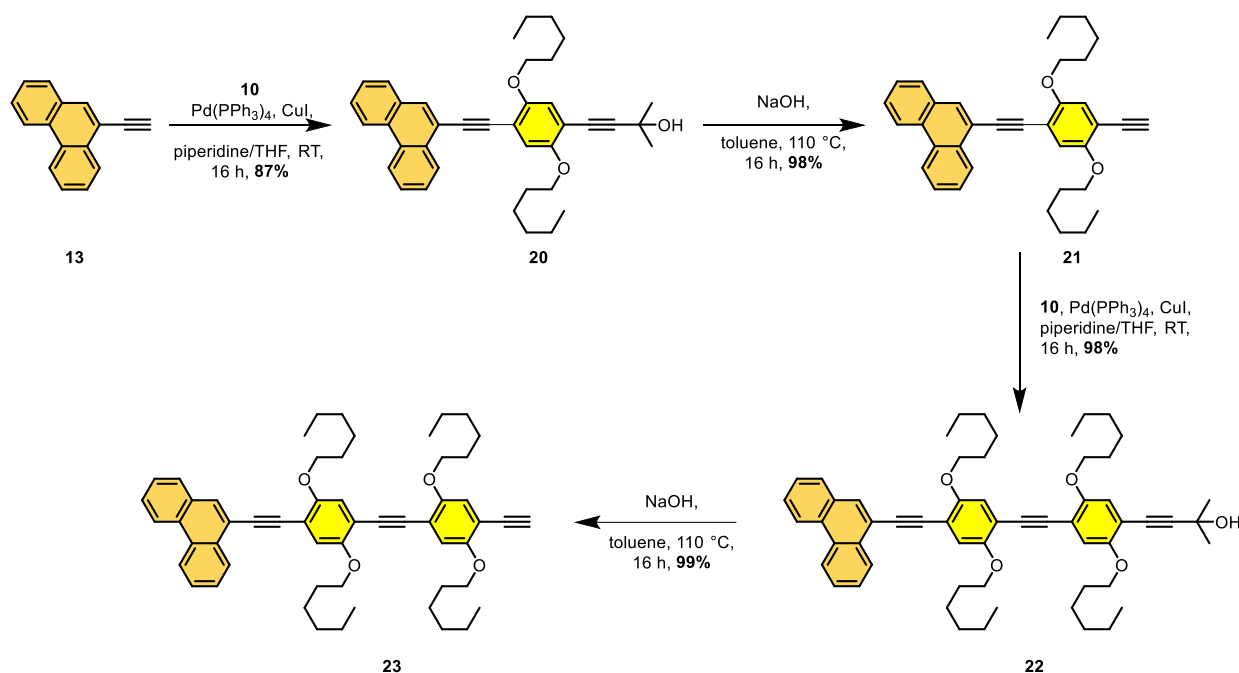
this reaction is starting material **16**, desired product **10**, and overreacted diacetylene **18** in a 1:2:1 ratio. Therefore, polar acetylene was required to ease the purification of this statistical mixture.³⁷ Thus, the acetylenes with a (3-cyanopropyl)dimethylsilyl (CPDMS) **17**^{36,39} and 2-hydroxyprop-2-yl (HOP) **19**⁴⁰ as protecting groups were used since they are known for being suitable for OPE-based systems. During the previous synthesis of **OPE3**, CPDMS was used as a masking group. This reaction step was limiting because of the low yield and loss of the material due to overreaction. However, by applying a HOP-acetylene **19** and an excess of diiodo **16** building block, the formation of undesired **18** was expected to be suppressed and increase yield for **10** as well as for starting material **16**. Therefore, 0.7 equivalents of HOP-acetylene **19** and 1.0 equivalent of diiodo compound **16** were used and reacted in a mixture of THF and piperidine (5:1) in the presence of bis(triphenylphosphine)palladium chloride and copper iodide. After the purification by column chromatography, the mono HOP-protected acetylene **10** was obtained in an excellent yield of 74%.



Scheme 3: Synthesis of bifunctional repeating unit **10** of the OPE backbone. The conditions and corresponding yields for the reactions performed during the master thesis are grayed out.

Previously prepared building blocks were assembled into OPE molecular wire subunit **23** over an alternating sequence of multiple *Sonogashira-Hagihara* cross-coupling reactions and deprotections (see Scheme 4). Such stepwise elongation of the wire started by coupling free acetylene **13** and monoiodine **10** using tetrakis(triphenylphosphine)palladium and copper iodide as a catalyst in a mixture of THF and piperidine (4:1). The desired HOP-protected acetylene **20** was obtained in 87% yield after column chromatography. Refluxing of **20** in

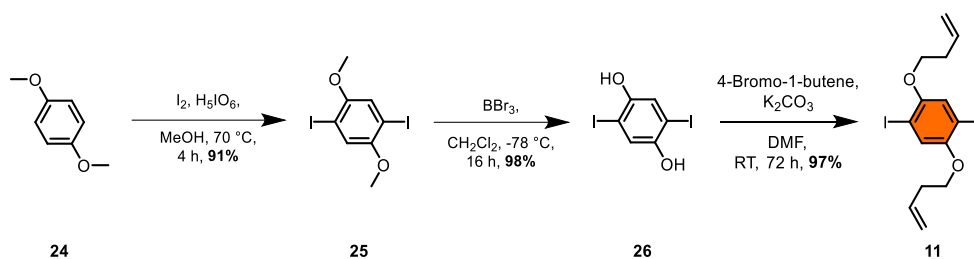
toluene in the presence of sodium hydroxide allowed the cleavage of protecting group,⁴¹ providing free acetylene **21** in an almost quantitative yield (98%). These *Sonogashira-Hagihara* cross-coupling and deprotection conditions were also used for the forthcoming reactions, providing HOP-protected acetylene **22** in 98% yield and free acetylene **23** in 99% yield.



Scheme 4: Synthesis of the OPE molecular wire building block **23** via stepwise elongation over *Sonogashira-Hagihara* cross-coupling reaction.

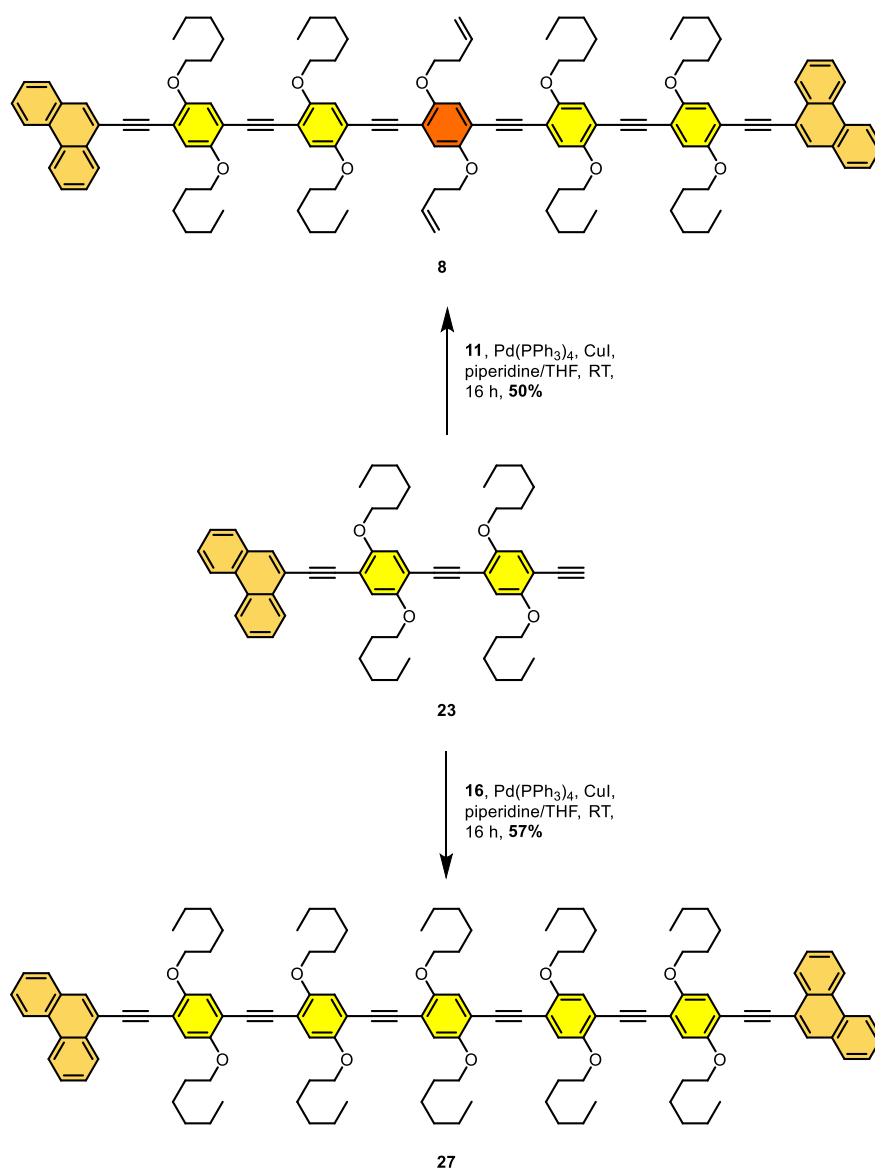
1.5.2 Synthesis of the Central Moiety

The synthesis of the central moiety **11** started with the iodination of hydroquinone dimethyl ether (**24**) (see Scheme 5). For this reaction, the same procedure³⁸ as for compound **16** was used to provide diiodo compound **24** in 91% yield. Next, demethylation of **25** was obtained by treatment with boron tribromide in dichloromethane at -78 °C to provide 2,5-diiodobenzene-1,4-diol (**26**)⁴² in 98% yield. Such a synthesis strategy⁴ allowed the modular etherification of **26**, which allows preparing a library of molecules with different side chain lengths. A first idea was to use allyl bromide in the design of the central moiety. However, the allyl group is known for being used as protecting group for alcohols which can be cleaved over the isomerization to more labile enol ether.⁴³ Therefore, the side chain with four carbons was more favored for stability reasons. Diol compound **26**, 4-bromo-1-butene, and potassium carbonate were dissolved in DMF and stirred at room temperature to provide central moiety **11** in 97% yield after column chromatography purification.

Scheme 5: Synthesis of the central moiety **11**.

1.5.3 Assembly of OPE5 Precursor and OPE5 Reference

With all building blocks in hand, the assembly of OPE5 precursor (**8**) and reference compound (**27**) were performed by applying the same conditions for the *Sonogashira-Hagihara* cross-coupling (see Scheme 6). The free acetylene **23** and diiodo compound **11** or **16** were coupled in a mixture of THF and piperidine (4:1) in the presence of tetrakis(triphenylphosphine)palladium and copper iodide as a catalytic system. The deprotected acetylene **23** was used in excess, leading to the formation of a homo-coupled by-product due to a *Glaser*-type reaction. However, column chromatography and manual gel-permeation chromatography (*BioBeads*, *SX-3* in toluene) easily removed the undesired by-product, providing OPE5 precursor (**8**) and OPE5 reference (**27**) in 50% and 57% yield, respectively. The obtained yields can be explained by poor solubility and loss of considerable amounts of the product during the purification. The identities of both OPE5 structures **8** and **27** were fully corroborated by ^1H and $^{13}\text{C}\{^1\text{H}\}$ NMR, as well as by 2D NMR spectroscopy measured in 1,1,2,2-tetrachloroethane- d_2 at 343 K due to low solubility at room temperature. The recorded spectra enabled the full assignment of proton and carbon atoms which are provided in the *Supporting Information for Chapter 1*. The elemental formulas of both molecular rods **8** and **27** were confirmed by the low-resolution matrix-assisted laser desorption ionization-time of flight (MALDI-ToF) mass spectrometry, where both found masses match the calculated values (OPE5 precursor **8**: m/z $[\text{M}]^+$ calcd. for $\text{C}_{126}\text{H}_{146}\text{O}_{10}$ 1819.092; found 1819.022 and OPE5 reference **27**: $[\text{M}]^+$ calcd. for $\text{C}_{130}\text{H}_{158}\text{O}_{10}$ 1879.186; found 1879.113) and isotopic distributions.



Scheme 6: Synthesis of OPE5 precursor **8** and OPE5 ref **27** via *Sonogashira-Hagihara* cross-coupling reaction.

The final hydrosilylation step to introduce the silyl anchoring group was not performed due to the graphene junction fabrication challenges. As mentioned above, silyl anchoring groups are water sensitive and cannot be stored for a long time; therefore, they should be freshly introduced before the immobilization into graphene electrodes. The conditions which favored hydrosilylation on the terminal alkene instead of internal alkyne were already elaborated during the previous work and will also be described in the *Outlook 1.7* of this *Chapter*.

1.6 Summary

In summary, the elongated design of a tailor-made molecular rod for graphene junctions was outlined. The envisioned design is based on assembling three different building blocks with various tasks. First, the outer anchoring groups are responsible for interaction with the graphene electrodes. The second one, OPE linker, allows the elongation of desired structure and makes the molecule suitable for larger nanogaps. The last one is the modified central moiety comprising the silyl anchoring groups, which is responsible for the mechanical stabilization of molecules in the junction. In this chapter, we presented a modified synthesis and assembly of building blocks. The exchange of the masking group for bifunctional OPE linker **10** from CPDMS to HOP increased the yield of the *Sonogashira-Hagihara* cross-coupling reaction and following deprotection compared to the previously published results.³⁶ In addition, replacement of the allyl chains of central moiety with the more stable butene analogue allowed to overcome isomerization and further stability issues. The precursor molecules **8** and corresponding reference compound **27** were successfully synthesized and fully characterized. However, the last step, introducing the silyl anchoring group, was not performed due to stability issues of **OPE5**, and challenges arose during the graphene junctions' preparation. Therefore, the following outlook subchapter will suggest a possible catalyst and conditions for hydrosilylation.

1.7 Outlook: Hydrosilylation

Hydrosilylation reaction allows the introduction of the previously discussed silyl anchoring group and will provide the desired **OPE5**. Typically for this type of reaction, platinum catalysts, such as Speier's (**28**)⁴⁴ and Karstedt's (**29**)⁴⁵ are used. However, platinum catalysts are also known for their advantage of forming several by-products, as well as low selectivity for terminal and internal alkenes and alkynes (see Figure 8).^{46,47}

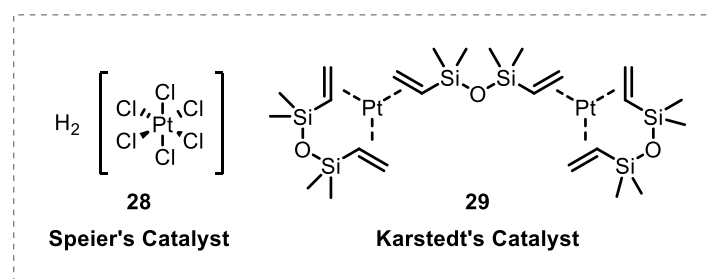
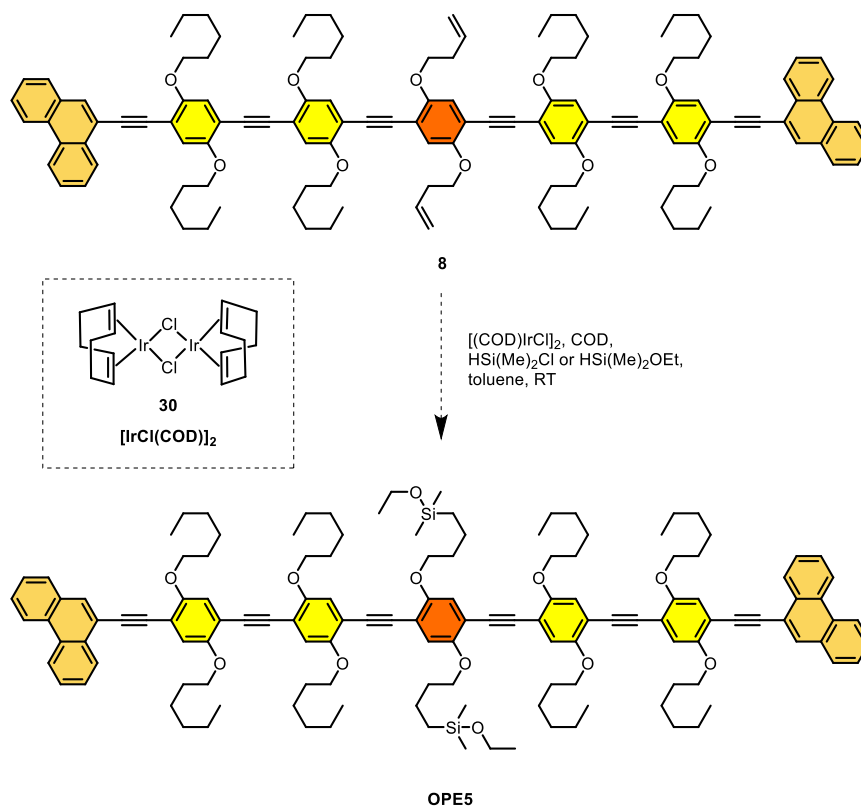


Figure 8: Examples of platinum catalysts for hydrosilylations.

The iridium catalyst, for instance [(COD)IrCl]₂ (**30**), would be a better candidate due to the higher selectivity.⁴⁸ However, the drawback of an iridium-based catalytic system is a short

lifetime which requires a large amount of catalyst for the full conversion due to the formation of elemental iridium during the reaction.^{46,49} A large amount of a co-catalyst, namely cyclooctadiene (COD), enables overcoming of such uneconomical challenges due to the suppression of deactivation of the catalyst.⁴⁸ The best results for the hydrosilylation of **OPE3** were obtained for 0.04 equivalents of iridium and 28.0 equivalents of COD, providing the desired **OPE3** in 36% yield after GPC purification. Therefore, we assume that the same conditions would also be suitable for the hydrosilylation of **OPE5** precursor (**8**).



Scheme 7: Proposed catalyst and conditions for hydrosilylation of terminal alkene to provide **OPE5**.

Chapter 2

2 Quantum Interference Effects in [2.2]Paracyclophane-Based Structures

This chapter presents the results of our investigations into the intriguing conductivity properties of different constitutional isomers of [2.2]paracyclophanes (PCPs). The combination of different substitution patterns on both the PCP core and the anchoring groups has allowed us to elucidate the conductance and mechanosensitivity in PCP-based molecular wires. Furthermore, all experimental findings were interpreted in terms of the quantum interference effect between the frontier molecular orbitals by theoretical calculations based on the density functional theory (DFT) and the Landauer formalism. All measurements were performed in the group of *Prof. Dr. Herre S. J. van der Zant* from the University of Technology in Delft, Netherlands, and the theoretical calculations were carried out in the group of *Prof. Dr. Fabian Pauly* from the University of Physics in Augsburg, Germany. To ease the reader into the topic, the results are preceded by an introduction covering two-fold substituted [2.2]paracyclophanes and molecular orbital-based quantum interference.

2.1 General Introduction

2.1.1 Two-Fold Substituted [2.2]Paracyclophanes

This subchapter provides insights into the history and applications of [2.2]paracyclophane. In addition, nomenclature, chirality, reactivity, and selectivity, of two-fold substituted [2.2]paracyclophane derivatives are introduced.

2.1.1.1 Synthesis and Applications of [2.2]Paracyclophane

The history of [2.2]paracyclophane (**33**) started in 1949 when Brown and Farthing⁵⁰ firstly prepared it by pyrolysis of *para*-xylene (**31**) over the formation of 1,4-quinodimethane intermediate (**32**) under low pressure and at 550 °C (see Figure 9a). Then, two years later, Cram and Steinberg⁵¹ developed a synthetic strategy to prepare the PCP **33** in a *Wurz*-type intramolecular cyclization of 1,2-bis(4-bromomethyl)phenylethane (**34**) with molten sodium (see Figure 9b). An alternative synthetic approach to obtaining the PCP structure would be the *1,6-Hofmann* elimination (*Winberg* cyclization).^{52,53} The reaction also takes place over the formation of 1,4-quinodimethane intermediate (**32**) prepared from (4-methylbenzyl)trimethylammonium bromide (**35**), where the optimized reaction conditions reported by *Chow et al.* in 2005 are illustrated in Figure 9c.⁵³ The several modifications and optimizations of the *Hofmann* elimination strategy allowed the preparation of PCP in a good yield and on a large scale,^{54,55} which allowed commercial production. Nowadays, the synthesis

of PCP-based molecules mostly starts with the functionalization of commercially available PCP, which will be described in detail in Subchapter 2.1.1.4.^{56–58}

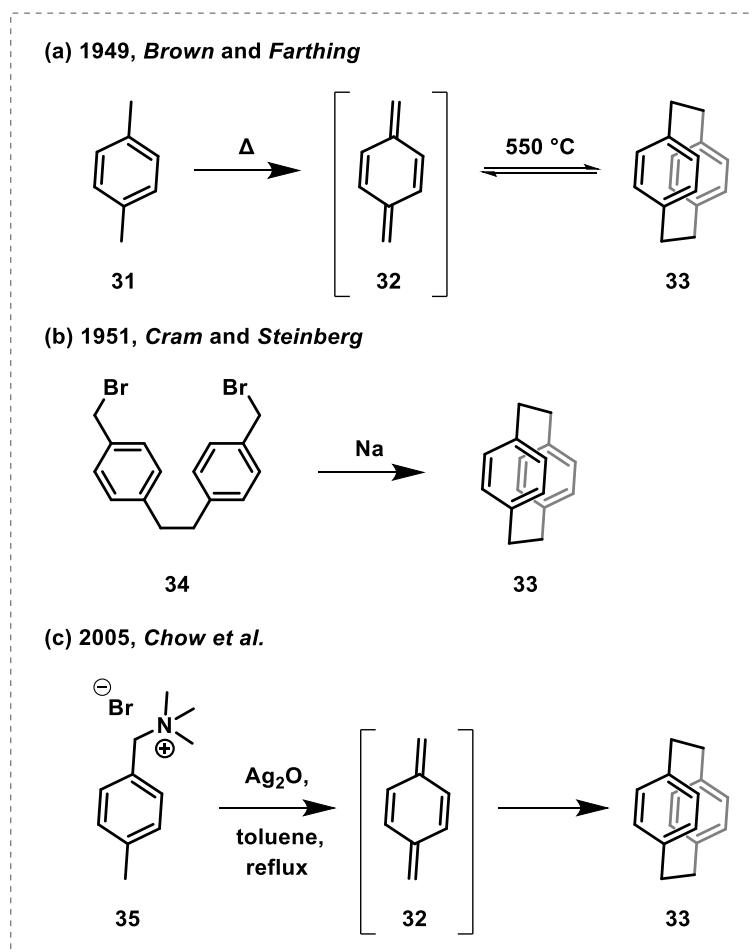


Figure 9: Synthesis of [2.2]paracyclophane (**33**): (a) via pyrolysis, (b) via *Wurcz*-type intramolecular reaction, and (c) via *Hofmann* elimination (*Winberg* cyclization).

[2.2]Paracyclophane is a remarkable three-dimensional aromatic compound with a "sandwich" orientation that has attracted the scientific community's interest due to its unique structural and electronic properties, which can be used in several applications. For instance, several PCP-based derivatives were reported in three-dimensional material chemistry^{59,60} and asymmetric catalysis.^{56,61–63} The PCP moiety is also used in molecular architectures, for example, as a building block for dendrimeric⁶⁴ and macrocyclic structures.^{65–70} Furthermore, PCP-based compounds are known for their chiroptical⁷⁰ and electronic⁷¹ properties, which makes them perfect candidates for organic electronic materials. Substituted PCPs were already incorporated into molecular wires,^{72,73} conjugated polymers,^{60,74} several emitters with circularly polarized luminescent (CPL),^{75,76} and thermally activated delayed fluorescence (TADF)^{58,77} properties.

2.1.1.2 Structure of [2.2]Paracyclophane

[2.2]Paracyclophane (**33**) belongs to the class of so-called cyclophane (**36**) compounds that consist of an arene motif bridged by an aliphatic chain, where the numbers in brackets indicate the length of the bridge, followed by prefix *para*, which describes the substitution pattern of the aromatic unit (see Figure 10a). Therefore, the compact skeleton of the PCP consists of two benzene rings (decks) in face-to-face orientation bridged with two ethylene chains. The decks are slightly bent with a decrease in ring-to-ring distance of 3.09 Å from the centrum of the deck to 2.83 Å from the outer carbon connected to the bridge, with a bridge carbon-carbon distance of 1.55 Å (see Figure 10b). The rings' distortion out of planarity decreases the inter-annular distance of PCP compared to other π - π stacked aromatic compounds. For instance, the distance between two graphene layers in graphite is 3.40 Å.^{58,57,78} Furthermore, one of the two co-facial benzene rings is slightly twisted by approximately 6° compared to the second ring to prevent an eclipsed conformation. This distortion of aromatic planarity allows better through-space charge transfers and leads to unusual reactivity, described in more detail in Subchapter 2.1.1.4.^{58,59}

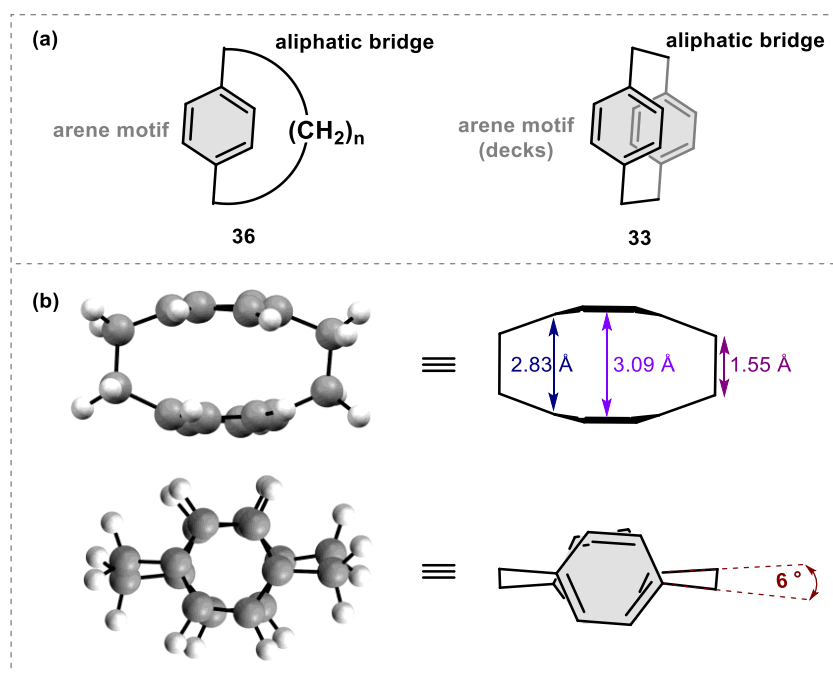


Figure 10: (a) General concept of cyclophane (**36**) and [2.2]paracyclophane (**33**). (b) Structural features of [2.2]paracyclophane with an aromatic-ring distance of 3.09 Å and 2.83 Å are depicted in violet and blue, respectively. The bond length between two carbons in the bridge is 1.55 Å, illustrated in purple. And the twist of co-facial benzene rings is represented in red.

2.1.1.3 Nomenclature and Stereochemistry of [2.2]Paracyclophane

The PCP-based molecules allow appealing structural diversity due to the spatial arrangement of substituents on its unique rigid scaffold. In the case of disubstituted PCP derivatives, the nomenclature indicates the connectivity pattern of the two substituents. The already known prefixes *ortho*-, *meta*-, and *para*- can be used for two-fold substitution on one phenyl ring, as shown in Figure 11. Reich and Cram⁷⁹ introduced an additional prefix pseudo (ps) to adequately describe the mutual arrangement of both substituents in the case of substitution on both benzene rings.

Therefore, the substitution pattern was defined by two prefixes instead of one, providing pseudo-*germinal*-, pseudo-*ortho*-, pseudo-*meta*-, and pseudo-*para*- as a naming convention for the PCP structures (see Figure 11). This nomenclature enables us to unequivocally distinguish between the regioisomers.

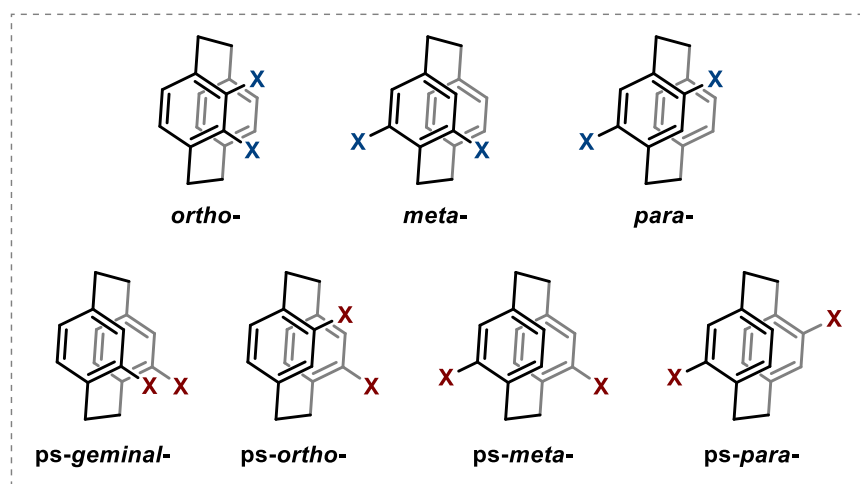


Figure 11: Overview of the two-fold homo-substituted PCP pattern on the same phenyl ring and different, where the spatial arrangement is depicted in blue and red, respectively. The nomenclature is based on the prefix system and describes the substitution pattern with ps as an abbreviation for pseudo.

However, the initial nomenclature differed.⁸⁰ The numbering started with the carbons on the ethylene bridge as one and two, continuing along the first aromatic ring (see Figure 12). Then, the second aromatic ring could be numbered in either an anti-clockwise or clockwise direction. This nomenclature provided two names for one structure, namely 4,16-disubstituted[2.2]paracyclophane and 4,12-disubstituted[2.2]paracyclophane. The alternative would be to start the numbering of the second phenyl ring in dependence on the substituent carrying carbon^{81,82} which leads to further confusion since two different molecules, pseudo-*para*-PCP and pseudo-*ortho*-PCP, would have the same name (4,12-disubstituted[2.2]paracyclophane, see Figure 12).⁸³ Therefore, due to the risk of confusion, only the pseudo-prefix-based nomenclature will be used in this thesis.

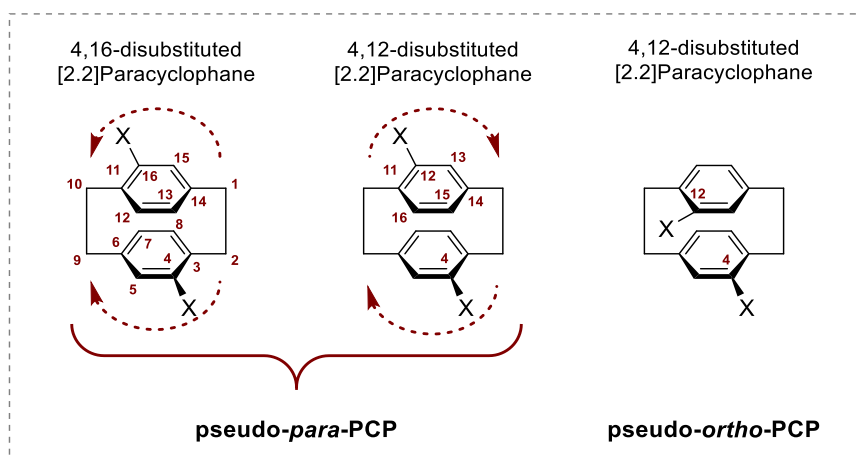


Figure 12: Example of different nomenclature systems used for disubstituted PCP derivatives. This figure was reproduced from Vorontsova *et al.*⁸³

The possibility of incorporating functional groups into ethylene bridges or benzene rings breaks the initial achiral D_{2h} symmetry^{83,84} of parent PCP. Introducing the substituents into ethylene bridges provides the stereogenic center chirality. On the other hand, implementing substituents in benzene rings may induce planar chirality depending on the substitution pattern. In the case of two-fold substitution with the same functional group, also called homo-substitution, on benzene rings, three substitution patterns lead to chiral molecules: *para*-, *ps-meta*-, and *ps-ortho*-PCP, which differ in the orientation of the C_2 -axis.

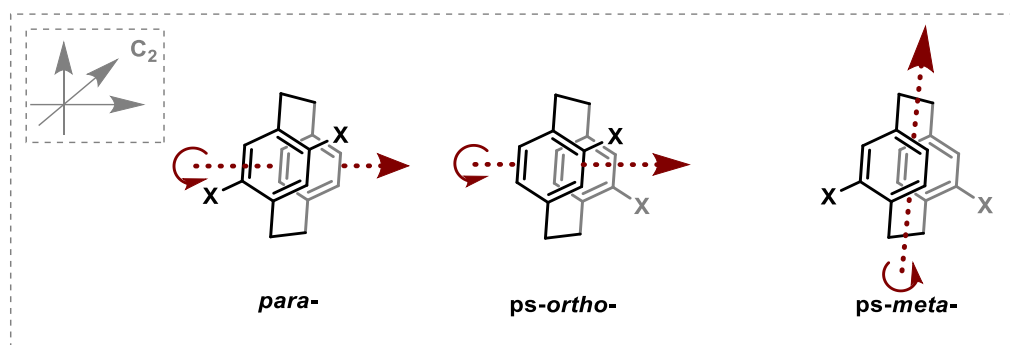


Figure 13: Chiral C_2 -symmetrical [2.2]Paracyclophanes. This figure was reproduced from Vorontsova *et al.*⁸³

In 1966, Cahn, Ingold, and Prelog proposed a rule for determining the absolute configuration of molecules with planar chirality.⁸⁵ The rule can be explained with the example of *ps-meta*-PCP depicted in Figure 14. Firstly, the most substituted ring is placed in the backplane. The next step is determining the first out-of-plane carbon, the pilot atom, which is then used as a point-of-view. Finally, the numbering to the highest priority substituent starts from the pilot atom. In our case, numbers from one to three were used. The configuration can be assigned depending on the direction of circulation 1-2-3 providing R_p for clockwise and S_p for

counterclockwise.^{57,86} In the case of several different substituents, the chirality is based on the substituent with the highest priority.

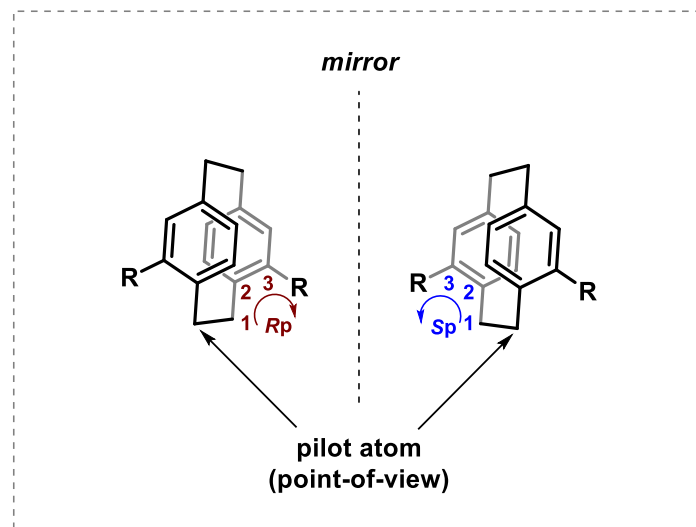


Figure 14: Absolute configuration of *ps-meta*-PCP derivatives; *ps-meta*-PCP (*R_p*) and *ps-meta*-PCP (*S_p*).

2.1.1.4 Derivatization of [2.2]Paracyclophane

As mentioned above, the PCP structures can be derivatized on the aromatic rings and the ethylene bridges. However, in the following part, we will only focus on the possible functionalizations of the aromatic system. Due to the unique structural features, such as abnormal distortion of aromatic planarity and a shorter distance between both rings, the substituent on the first ring can influence the reactivity and substitution pattern of the second one. The best example is the *ps-geminal*-PCP. This substitution pattern has the most sterically unfavored confirmation because of the repulsion of neighboring substituents. Indeed, the substitution in the *ps-geminal* position can be promoted due to the transannular directive effect.^{79,87} This effect is exemplified by the bromination of methyl ester monosubstituted PCP (**37**) depicted in Figure 15. The lewis base stimulates the substitution in the *ps-geminal* position in the electrophilic aromatic substitution. This specific stereoelectronic effect allows for synthesizing the *ps-geminal* core with several functional groups.^{57,58}

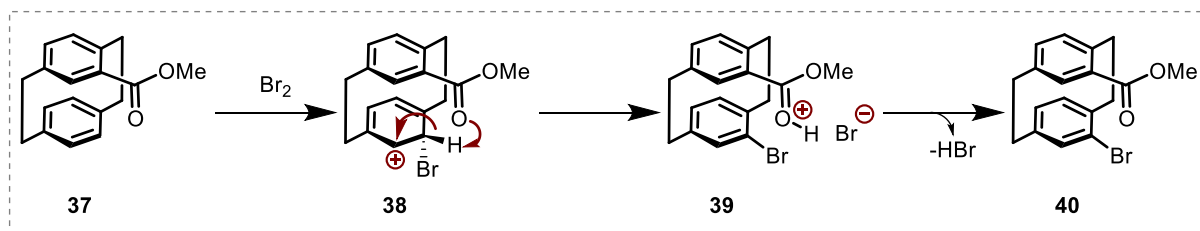


Figure 15: Transannular effect in methyl ester monosubstituted PCP-based molecule. The aromatic substitution of monosubstituted PCP bearing a Lewis base occurs via the *Wheland* intermediate.⁵⁷

The synthesis of the derivatives based on remaining regioisomers (*ps-para*-, *ps-ortho*-, and *ps-meta*-PCP) can be achieved via direct bromination. The initial iron-catalyzed bromination in tetrachloromethane developed by Cram⁸⁸ provided a mixture of several dibrominated compounds (see Figure 16), with *ps-para*-PCP (**41**, 26%) and *ps-ortho*-PCP (**42**, 16%) as the major products, followed by only a lower amount of *ps-meta*- (**43**, 6%) and *para*-PCP (**44**, 5%). In 2002, *Braddock et al.*⁸⁹ increased the yield of *ps-para*-PCP (**41**, 38%) by exchange of toxic tetrachloromethane with dichloromethane. Such improvement also enabled the crystallization of *ps-para*-PCP directly from the reaction mixture. However, later studies^{83,90} demonstrated that bromination without iron as a catalyst leads to the formation of almost exclusively *ps-para*- (**41**, 34%) and *ps-meta*-PCP (**43**, 43%), where the isomers can be separated using their different solubility.

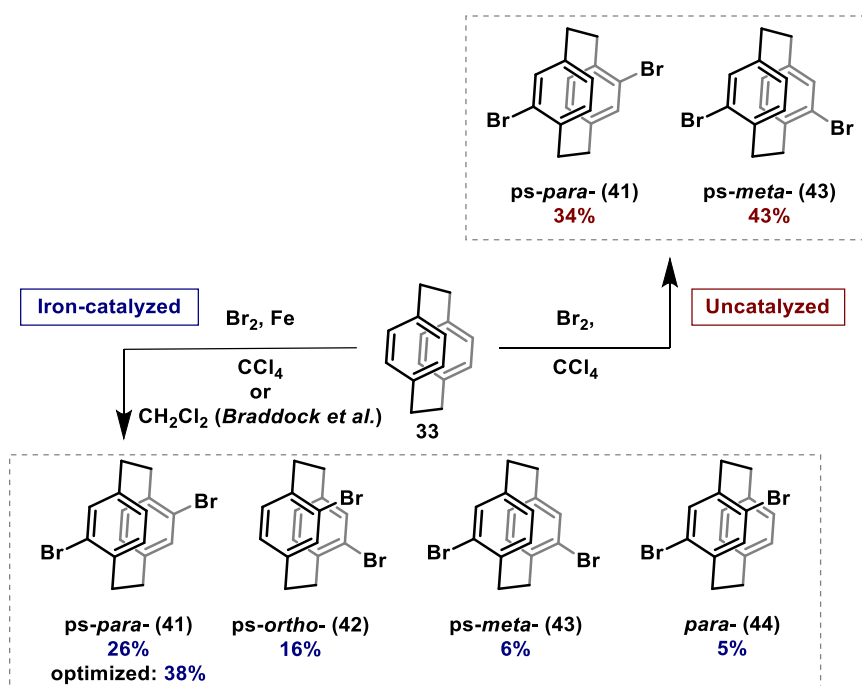


Figure 16: Synthesis of homo-substituted dibromo-PCP compounds with different connectivity pattern. The yield of catalyzed^{88,89} and uncatalyzed⁸³ reactions is given in blue and red, respectively.

Besides the direct bromination (see Figure 16), the main pathway to obtaining a *ps-ortho*-dibromo PCP (**42**) isomer is a thermal isomerization starting from the *ps-para*-substituted analogue (**41**). The latter can isomerize at a temperature above 200 °C. The process begins with the homolytic cleavage of a C-C bond on an ethylene chain, leading to the formation of a diradical. Next, one of the aromatic units rotates, and the diradical recombines to reform the ethylene bridge,⁹¹ which provides a *ps-ortho*-PCP (**42**) isomer (see Figure 17a). However, quantitative isomerization is impossible since the reaction is in equilibrium. There is a 1:1 mixture of both compounds with *ps-para* (**41**) and *ps-ortho* (**42**) connectivity, which can be separated by recrystallization. Therefore, to increase the obtained yield of *ps-ortho*-substituted PCP (**42**), previously separated *ps-para*-PCP (**41**) can be reused in the thermal isomerization cycle. The best-reported yield was 73% after four cycles.^{57,90} On the other hand, the equilibrium of *ps-geminal*- (**45**) and *ps-meta*-substituted PCP (**46**) favors the *ps-meta*-PCP derivative due to the steric repulsion of the *ps-geminal* substitution pattern (see Figure 17b).^{87,91}

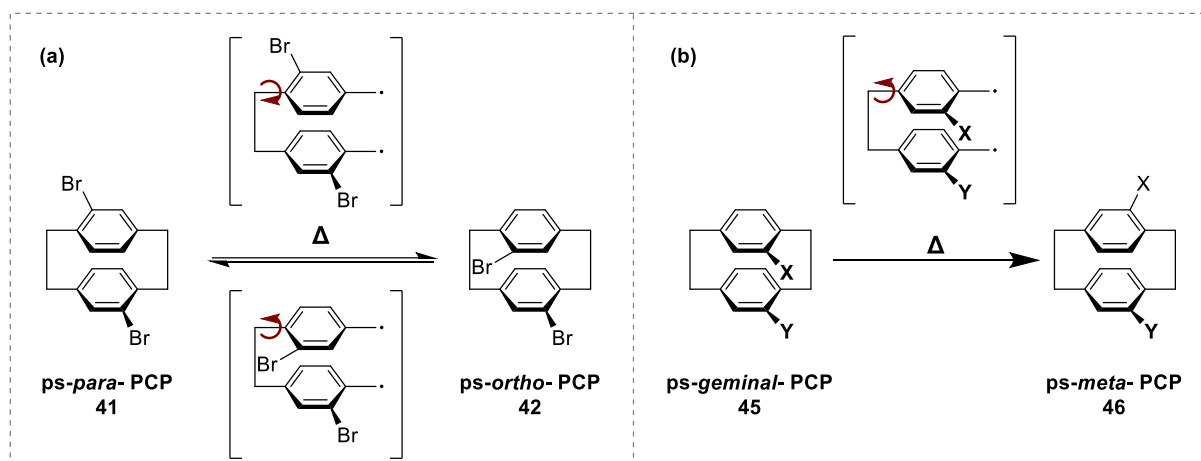


Figure 17: Thermal isomerization procedure. (a) Preparation of *ps-ortho*-PCP from *ps-para*-PCP via isomerization with balanced equilibrium (1:1 ratio) and (b) quantitative conversion of *ps-geminal*-derivative to *ps-meta*-analogue.

Dibromo PCP scaffolds with *ps-para*- (**41**), *ps-ortho*- (**42**), and *ps-meta*-substitution (**43**) can be employed to prepare homo- and hetero-substituted derivatives. The isomers can be converted to the desired structures in a mono- or double lithium-halogen exchange reaction followed by quenching with various electrophiles.^{35,46,49} Besides, dibromo-PCP can also react in palladium-catalyzed cross-coupling reactions to provide further PCP-based derivatives.⁵⁷ Unsurprisingly, the dibrominated PCP derivatives are essential building blocks and a common starting point for several synthetic strategies due to their incorporation possibilities.

2.1.2 **Molecular Orbital-Based Quantum Interference**

This subchapter provides insights into the relationship between conductivity and quantum interference. Furthermore, the possibility of predicting quantum interference using frontier molecular orbital theory is explained.

2.1.2.1 Quantum Interference

Nowadays, the phenomenon of quantum interference (QI) is one of the leading hot topics in the studies of molecular junctions.^{92–94} Firstly, the QI concept was introduced to describe the wave interference of electrons and photons in the double-slit experiments.^{95,96} Several years later, this term was adopted to describe the phase difference between the electron waves traversing different conduction pathways in a molecule in a single-molecule junction. These pathways can have either an atomic orbital or molecular orbital (MO) origin.⁹⁷ The latter is more general, was already well-established,^{98–101} and moved to the focus of interest for the investigations described in this chapter.

Constructive quantum interference (CQI) or destructive quantum interference (DQI) can enhance or suppress conductance and can be influenced by structural modifications such as variety in substituents^{102,103} or substitution pattern.^{104,105} The latter demonstrated significant conductance variations for the transmission through an aromatic ring, which were studied experimentally^{105,106} and theoretically.¹⁰⁷ The outcome of the investigation was that the phenyl ring with the anchoring groups in the *meta* position showed low conductance compared to the *para*- and *ortho*-substituted analogue. The reduction in electronic communication for *meta*-connectivity can be explained by the DQI. On the other hand, *para*- and *ortho*-connectivity showed an increase in conductance due to CQI.

2.1.2.2 Molecular Orbital Theory and Symmetry Rules

Yoshizawa, Tada, and their co-workers^{98–101} provided a method to predict the increase and decrease of electronic communication due to the presence or absence of DQI in aromatic π -systems. Such orbital rules are based on the Hückel molecular orbitals (MO) theory combined with the nonequilibrium Green's function (NEGF) methods.^{108,109} The underlying formulas are not reprinted within this chapter but are presented in the *Supporting Information* (see *Subchapter 5.4.3.3*). However, the following preconditions are necessary for the use of orbital symmetry rules: (a) the molecules have a weak electrode-molecule-electrode coupling, (b) there is electron-hole symmetry (pairing theorem) in orbital energies and MO expansion coefficients, and (c) the Fermi energy is located between the energy of the highest occupied MO (HOMO) and that of the lowest unoccupied MO (LUMO).^{98,99} Aromatic hydrocarbons and

their derivatives fulfill all these requirements and can be used for conductivity predictions. Therefore, the rules for symmetry and QI based on frontier MO theory can be summarized as follows.^{110,111} Firstly, the HOMO and LUMO need to have sizeable orbital coefficients to allow the contribution to transmission. Secondly, the products of the molecule's HOMO and LUMO need to be different in sign on the connection points to the electrodes to enhance transmission due to CQI. If this is not the case, the contributions of HOMO and LUMO will cancel each other out, resulting in DQI and low transmission.

The above-described rules can be used to predict the electron transport properties in benzene molecules with different connectivity pattern to electrodes. In the electrode-benzene-electrode junction, there are three configurations of how the molecule can be located: *para*-, *meta*-, and *ortho*- (see Figure 18a and c). Firstly, the frontier MOs should be determined to fulfill the first requirement. For *para*-substituted benzene, carbon 1 and 4 (C_1 and C_4) have a suitable size of the orbital amplitude in HOMO and LUMO, and therefore they are the relevant frontier orbitals for this case. Contrariwise, HOMO and LUMO do not achieve this requirement due to the smaller amplitude on one of the connection points in the case of *ortho*- and *meta*-connectivity. Thus HOMO' and LUMO' are used as frontier orbitals for such connectivity pattern.

Afterward, we can move to the second rule and determine the parities. In the case of *para*-connection, the sign of $C_{1\text{HOMO}}C_{4\text{HOMO}}^*$ is negative due to different orbital parities. On the other hand, the sign of $C_{1\text{LUMO}}C_{4\text{LUMO}}^*$ is positive (same parities); therefore, this connection would be symmetry-allowed and lead to CQI and high conductivity. Due to symmetry restrictions, the best contacts for the *meta*-substitution are C_2 and C_6 (or C_3 and C_5). In both cases, the sign is negative. Therefore, *meta*-connectivity is symmetry-forbidden and leads to DQI and low conductivity. There are also two possibilities for the last configuration, C_2 and C_3 (or C_5 and C_6). The sign in $C_{2\text{HOMO}}C_{3\text{HOMO}}^*$ is positive, and $C_{2\text{LUMO}}C_{3\text{LUMO}}^*$ is negative, providing the CQI and symmetry-allowed connection for *ortho*-substitution. The same result is also obtained for the prediction based on the other pair of carbons (C_5 and C_6).¹¹² Such predictions are in accordance with the previously described experimental results^{105,106} and can be performed for several other molecules to corroborate the experimental results.^{112,113}

To summarize, the rules of thumb for through-bond conductivity in benzene for *para*- and *ortho*-connectivity are CQI (high conductivity) and *meta*- DQI (low conductivity). In contrast, the trend of electronic communication in [2.2]paracyclophane-based molecules that allows the through-space conductivity is reversed (see Figure 18b and d).¹¹⁴ In the case of *ps-para*-PCP, both products of MO coefficients are the same, namely negative for $C_{1\text{HOMO}}C_{4'\text{HOMO}}^*$ and $C_{1\text{LUMO}}C_{4'\text{LUMO}}^*$. Thus, 1-4'-connection is symmetry-forbidden, and the conductance is

suppressed due to DQI. The same result can also be observed for the *ps-ortho*-connectivity. On the other hand, *ps-geminal* and *ps-meta* connections are now symmetry-allowed and enhance conductivity due to CQI due to the different parities in HOMO and LUMO.

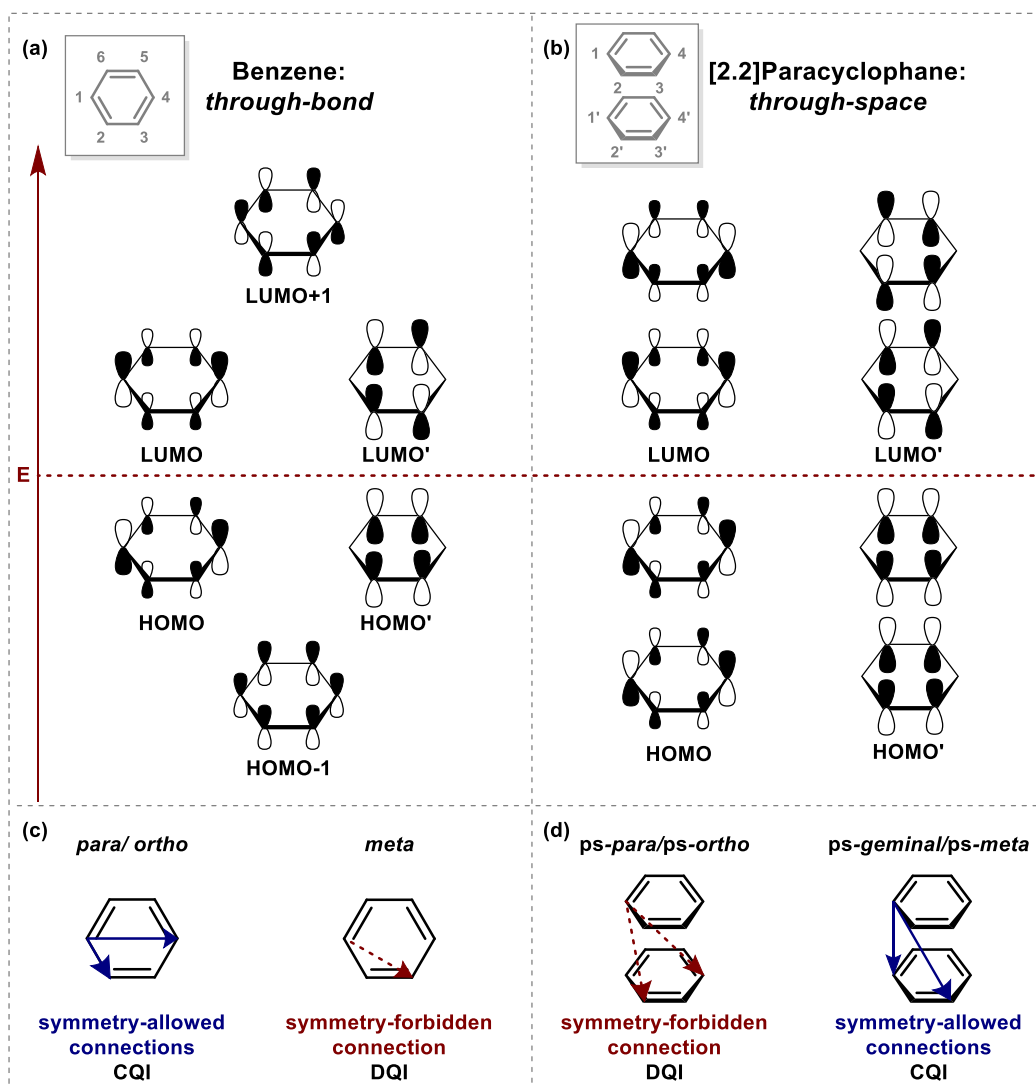


Figure 18: Comparison of electron transport properties in dependence of substitution pattern of benzene and [2.2]paracyclophane-based structures. (a) π -Based MOs of benzene¹¹² with the numbering of carbon atoms in grey; (b) frontier orbitals of two stacked benzene rings¹¹⁴ (similar to the structure of PCP) with the numbering of carbon atoms in grey. In this sketch, the Fermi energy which is placed between HOMO and LUMO, is indicated as a horizontal red dashed line. (c) and (d) symmetry-allowed and symmetry-forbidden connectivity pattern for electron transport (shown in blue and red, respectively) and consequential CQI and DQI.

Such an exciting trend of the QI for three-dimensional structures became the focus of our interest. Therefore, we decided to prove the theoretical predictions experimentally and prepared a series of molecules with different connectivity patterns on PCP-core and the anchoring groups. All investigations of *ps-para*-, *ps-meta*-, and *ps-ortho*-PCP derivatives are summarized and will be discussed in the remaining part of the chapter.

2.2 Meta vs. Para: “Substitution Pattern Controlled Quantum Interference in [2.2]Paracyclophane-Based Single-Molecule Junctions.”

This subchapter provides the results of our investigation of conductivity and mechanosensitivity properties of a combination of different substitution pattern in both PCP core and anchoring groups in molecular wires in the form of a publication entitled **“Substitution Pattern Controlled Quantum Interference in [2.2]Paracyclophane-Based Single-Molecule Junctions.”** published in *Journal of the American Chemical Society*.

Substitution Pattern Controlled Quantum Interference in [2.2]Paracyclophane-Based Single-Molecule Junctions

Ksenia Reznikova,[#] Chunwei Hsu,[#] Werner M. Schosser,[#] Almudena Gallego, Katawoura Beltako, Fabian Pauly,^{*} Herre S. J. van der Zant,^{*} and Marcel Mayor^{*}

Cite This: *J. Am. Chem. Soc.* 2021, 143, 13944–13951

Read Online

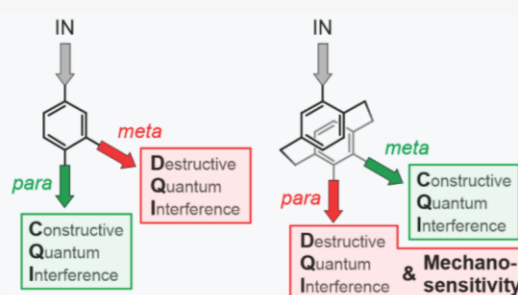
ACCESS |

Metrics & More

Article Recommendations

Supporting Information

ABSTRACT: Quantum interference (QI) of electron waves passing through a single-molecule junction provides a powerful means to influence its electrical properties. Here, we investigate the correlation between substitution pattern, conductance, and mechanosensitivity in [2.2]paracyclophane (PCP)-based molecular wires in a mechanically controlled break junction experiment. The effect of the *meta* versus *para* connectivity in both the central PCP core and the phenyl ring connecting the terminal anchoring group is studied. We find that the *meta*-phenyl-anchored PCP yields such low conductance levels that molecular features cannot be resolved; in the case of *para*-phenyl-coupled anchoring, however, large variations in conductance values for modulations of the electrode separation occur for the pseudo-*para*-coupled PCP core, while this mechanosensitivity is absent for the pseudo-*meta*-PCP core. The experimental findings are interpreted in terms of QI effects between molecular frontier orbitals by theoretical calculations based on density functional theory and the Landauer formalism.



INTRODUCTION

In recent years, great advancements have been made in the field of molecular electronics toward single-molecule junction studies.¹ The visionary idea of Aviram and Ratner² to profit from single molecules as functional units in electronic devices led to the development of several proof-of-concept molecular devices, such as molecular wires,^{3,4} switches,^{5,6} rectifiers/diodes,^{7,8} and thermo-electronic devices.^{9,10} The design of molecules incorporated in such electrode–molecule–electrode junctions is guided by our understanding of charge transport through the molecules. Indeed, even small structural modifications such as substituent effects,^{11,12} conformational flexibility,¹³ and changes in the anchoring groups and their positions^{14–18} can result in large conductance variations. Particularly strong variations are predicted for quantum interference (QI) effects originating from the interplay between different transport pathways. Destructive QI (DQI) or constructive QI (CQI) between the pathways can occur, reflected in a low or high conductance, respectively.¹⁹ QI effects thus become essential molecular design elements, on the one hand enriching the variety of functionalities emerging from the molecular structure but on the other hand making a full comprehension of the molecule's electronic transport behavior more challenging. A detailed understanding of these QI effects and of their origin in the molecule's structure is thus crucial to realize their full potential in future electronic components and devices.

Relationships between substitution pattern and single-molecule conductance were already theoretically predicted and experimentally confirmed in a variety of examples, ranging from simple phenyl rings²⁰ connected directly to the electrodes to more sophisticated oligo(phenylene vinylene) (OPV)²¹ and oligo(phenylene ethynylene) (OPE)-based molecular wires.¹⁵ Unanimously, these studies report a decrease in electronic transparency upon shifting the anchoring groups from the *para* to the *meta* position. This observation was rationalized by Yoshizawa and co-workers,^{22–24} who considered frontier orbital theory for simple organic molecules. Their set of rules predicts for benzene the *para* connection to be the symmetry-allowed one for charge transport, while charge transport involving the *meta* connection is symmetry-forbidden, resulting in high and low conductance, respectively.

Because the effects of substitution patterns in planar π -systems are well described and understood, our focus moved to three-dimensional structures like [2.2]paracyclophane (PCP), with two benzene systems facing each other interlinked by a pair of C_2H_4 bridges.²⁵ Initially, we considered the structure as

Received: July 5, 2021

Published: August 23, 2021



a model to investigate the through-space coupling of the stacked π -systems^{26,27} but realized quickly that their behavior is much richer. Already the first model compound²⁸ (ps-*para-para*-OPE PCP in Figure 1) displayed a sharp destructive QI

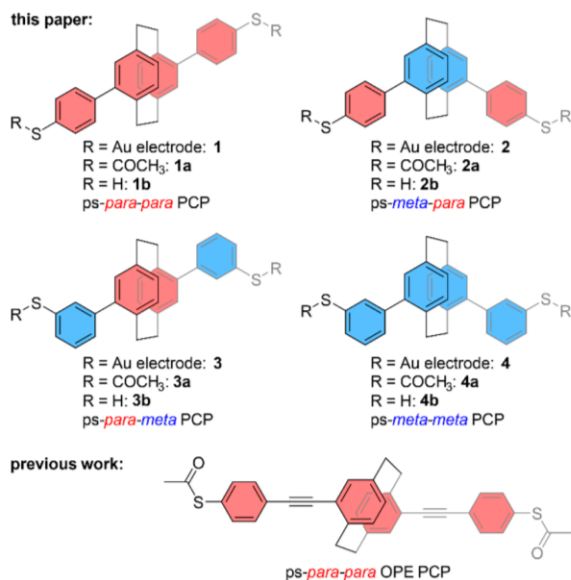


Figure 1. Schematic representation of target structures **1–4** together with the already reported model compound. The four molecules include either *para* or *meta* connection patterns in both the central PCP subunit and the peripheral phenyl subunits labeled in red and blue, respectively. For simplicity, the following text refers to the structures by their prefixes, with ps as an abbreviation for pseudo, followed by the prefix referring to the substitution pattern of the central PCP, and finally the prefix referring to the substitution pattern of the thiol anchor group in the phenyl subunits.

feature close to the Fermi level, but the phenomenon also depended substantially on the mechanical stress exposed to the molecule. It thus seemed that the rigid but squeezable PCP subunit provided mechanosensitivity to the molecular junction. Interestingly, Yoshizawa and co-workers²⁹ already provided their orbital view of PCP subunits and predicted that the charge transport through the pseudo-*para*-substituted PCP should be suppressed due to DQI, while CQI would prevail for pseudo-*meta*-substituted PCP. It thus seems that the rule-of-

thumb (*para* → good transport due to CQI; *meta* → bad transport due to DQI) is inverted for the PCP subunit.

Excited by this hypothesis, we explored the effects of the substitution pattern in more detail and designed the four PCP model compounds **1–4** (see Figure 1) consisting of comparable subunits but with various substitution patterns. The oligo(phenylene)-type PCP structures combine the compactness favoring electronic transparency on a detectable level with straightforward synthetic accessibility. Terminal acetyl masked thiol anchor groups enable their immobilization in a mechanically controlled break junction (MCBJ) by covalent S–Au bonds, guaranteeing both electronic coupling and mechanical stability. The latter is of particular importance to enable subtle mechanical manipulation of the integrated single molecule. The investigation of their transport properties and the influence of mechanical manipulations are studied with MCBJ experiments. The findings are rationalized by QI effects emerging from the interplay of frontier molecular orbitals, discussed with a theoretical model based on density functional theory (DFT). The electronic transport is described in terms of the Landauer formalism,³⁰ expressed through nonequilibrium Green's function (NEGF) methods.

RESULTS AND DISCUSSION

The PCP-based model compounds were assembled from the corresponding *para/meta* building blocks by Suzuki–Miyaura cross-coupling reactions. The literature known pseudo (ps)-*para-para*- or ps-*meta-para*-dibromo[2.2]paracyclophane³¹ and either 4- or 3-(*tert*-butylthio)phenyl boronic acid provided the PCP derivatives with four different combinations of substitution patterns. The adaption of a protocol from Jevric et al.³² enabled the subsequent transprotection and provided the target structures **1a–4a** in reasonable isolated yields ranging from 63 to 85%. The identity of the new PCP derivatives was corroborated by ¹H NMR, ¹³C{¹H} NMR spectroscopy, and high-resolution mass spectrometry (HR-MS). A detailed description of the synthetic protocols and the analytical data of all new compounds are provided in the Supporting Information (section 1).

The single-molecule electronic transport properties of PCPs **1–4** were investigated by integrating them into an electronic circuit using an MCBJ setup operated at ambient conditions. Two types of measurements were performed: fast-breaking and modulation experiments (see below). Details of the technique providing a pair of mechanically adjustable electrodes with a distance resolution of atomic dimensions have been reported

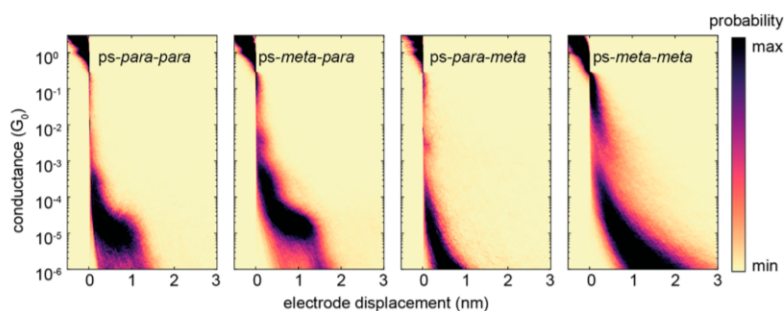


Figure 2. Two-dimensional conductance vs electrode displacement density histograms. The first (from the left) and second histograms are built up from 6 834 and 9 638 traces at 100 mV with ps-*para-para*- and ps-*meta-para*-PCP molecules, respectively. The third and fourth 2D histograms correspond to 3 780 and 10 000 traces at a bias voltage at 250 mV with ps-*para-meta*- and ps-*meta-meta*-PCP molecules, respectively.

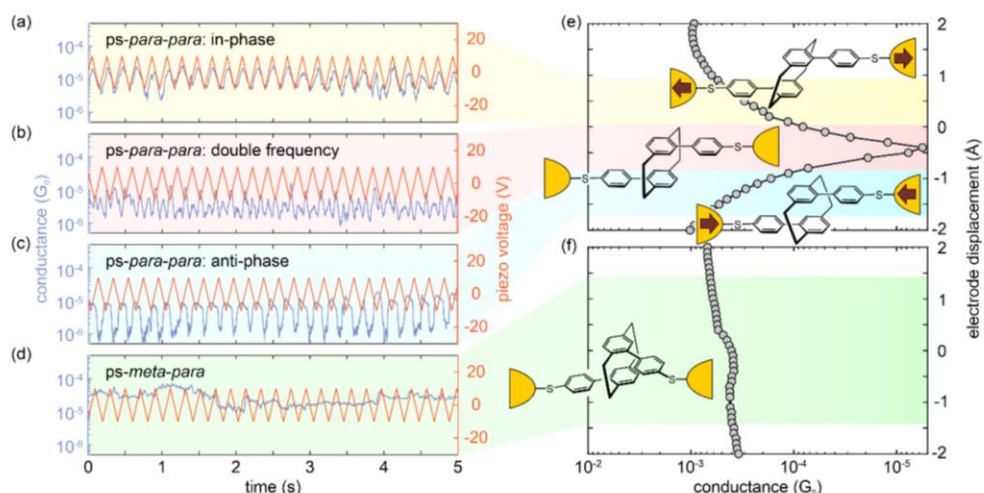


Figure 3. (a–c) Conductance traces of modulation experiments with *ps-para-para*-PCP (**1**), displaying (a) in-phase, (b) double frequency, and (c) anti-phase modulations. (d) Conductance traces of the modulation experiments with *ps-meta-para*-PCP (**2**). The red line in the distance–modulation traces represents the voltage applied to the piezoelectric stack, whereas blue represents the measured conductance. The total modulation time of the experiments is 15 s; for better visibility, only 5 s are displayed. (e) Calculated conductance of the *ps-para-para*-PCP molecular junction during the gap opening. The conductance displacement data is extracted from Figure 5b by evaluating the transmission function at the Fermi energy. The sketches rationalize the variety of conductance vs electrode displacement modulation behaviors observed for *ps-para-para*-PCP in dependence of the position of the DQI dip with respect to the trapping state of the molecule in the individual junction; see panels a–c and e. In particular, light background colors (yellow, red, and blue) relate the different situations of junctions, including molecules in prestretched, relaxed, or precompressed states, respectively, to the behavior in modulation experiments. (f) Same plot as in panel e but for *ps-meta-para*-PCP, where mechanosensitivity is basically absent. The green background color connects the conductance that is rather insensitive to electrode displacements to the observations made in the modulation measurements in panel d.

previously^{33,34} and are thus discussed in the Supporting Information (section 2.1).

In the fast-breaking experiments, several thousand conductance traces for each investigated molecule were collected and plotted as two-dimensional (2D) histograms displayed in Figure 2. For the case of *ps-para-para*- and *ps-meta-para*-PCPs with a constant bias voltage of 100 mV, clear conductance plateaus with a length of ~ 12.5 Å were observed. Through a reference-free clustering method³⁵ on the unfiltered data, the pure gold-to-gold tunneling traces and the molecular traces were separated. The molecular conductances of *ps-para-para*- and *ps-meta-para*-PCPs were obtained through a log-normal fit distribution yielding values of $1.3 \times 10^{-5} G_0$ and $2.2 \times 10^{-5} G_0$, respectively, where $G_0 = 2e^2/h$ is the quantum of conductance, as shown in the corresponding one-dimensional (1D) conductance histograms (see Supporting Information (section 2.2)).

For the molecules with the *meta*-phenyl anchoring (*ps-para-meta*-PCP and *ps-meta-meta*-PCP) the bias voltage in the transport experiment was increased to 250 mV in order to bring molecular levels closer to resonance, as the conductance of these PCPs was below the detection limit for a bias of 100 mV. However, even at this increased bias voltage, no clear conductance plateaus were detected, even when using the earlier-mentioned clustering method. Whether the lack of clear plateaus is due to molecular conductance below the detection threshold of the experimental setup of $10^{-6} G_0$ or the molecules' inability to form stable molecular junctions cannot be distinguished. The very short-breaking traces visible in Figure 2 at higher conductance values for both *ps-para-meta*- and *ps-meta-meta*-PCP are most likely due to direct electron

injection into the molecules' π -systems without controlled sulfur-to-sulfur immobilization.

Of particular interest are the distance-dependent single-molecule junction charge-transport studies of *ps-para-para*- and *ps-meta-para*-PCPs, as substantial differences in the transport behavior under mechanical stress are expected between the central *ps-para*- and *ps-meta*-PCP subunits. While the mechanosensitivity of the *ps-para*-PCP subunit was already evidenced in modulation experiments for the *ps-para-para*-OPE PCP (Figure 1)²⁸ and rationalized as being due to a distance-dependent conductance dip close to the Fermi level originating from DQI, similar behavior is not expected for the *ps-meta*-PCP subunit, as CQI has been predicted.²⁹

To study the presence of DQI in more detail, modulation experiments are useful. The modulation procedure consists of constricting the gold wire down to a conductance of $2 G_0$ with the piezo control.²⁸ The junction will then break by itself due to its surface tension.³⁶ The electrodes are then separated by 7.5 Å, and a pulse of a triangular waveform with an amplitude of 20 V_{peak-to-peak} is applied to the piezoelectric element, which corresponds to a modulation amplitude of 5 Å between the electrodes. The conductance is continuously monitored, and the modulation is applied at a frequency of 5 Hz for 15 s. Hereafter, the junction is fused again, and a new modulation trace is recorded. The results of electrode-modulation experiments on PCPs **1** and **2** are summarized in Figure 3.

Similar to *ps-para-para*-OPE PCP,²⁸ a rich variety of distance-modulated conductance responses has been observed for *ps-para-para*-PCP (**1**). The periodic electrode displacement caused a substantial conductance modulation, which was either in-phase (Figure 3a), anti-phase (Figure 3c), or even two times the frequency (Figure 3b) of the voltage applied to the piezo

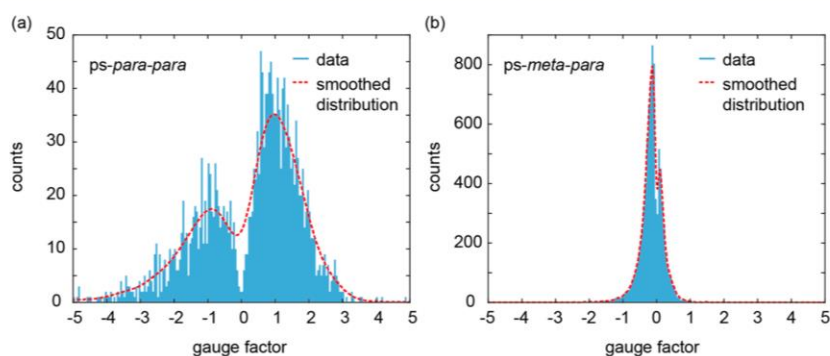


Figure 4. Gauge factors obtained from (a) 1 442 *ps-para-para*-PCP traces and (b) 2 236 *ps-meta-para*-PCP traces in modulation experiments. The counts are collected from fast Fourier transform (FFT) spectra over 1 s intervals of the traces, which means that there are 15 counts, with different GFs for each recording, lasting 15 s.

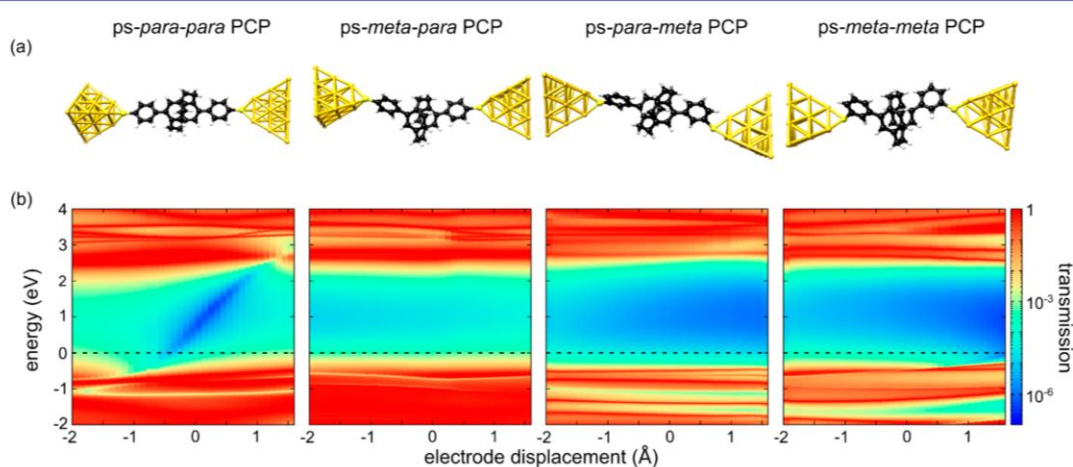


Figure 5. (a) Illustration of PCP derivatives 1–4 immobilized in junctions between two gold electrodes. (b) Transmission maps of the four types of PCP single-molecule junctions. The horizontal red resonances in the maps arise from molecular frontier orbitals. For the *ps-para-para*-PCP molecule, an antiresonance is observed inside the HOMO–LUMO gap that shifts in energy as the displacement is varied. Similar tunable DQI effects are absent for all other molecules, in particular for *ps-meta-para*-PCP junctions and *ps-meta-meta*-PCP junctions with central *ps-meta*-PCP systems. The position of the Fermi energy is indicated as a horizontal dashed line.

stack. As sketched in Figure 3e, this observed mechanosensitivity is caused by the DQI dip in the conductance versus molecular length relation (insets in Figure 3e), with the variety of observed behaviors reflecting the exact position of the conductance dip in the particular molecular junction. We take the in-phase case as an example to explain the observed behavior. This corresponds to a starting position in which the molecule is prestretched, as depicted in Figure 3e (top, light yellow background). In this case, whenever the molecule is stretched by increasing the voltage applied to the piezoelectric element, the conductance goes up, and the conductance goes down when the piezo voltage decreases, i.e., the conduction follows the applied piezo-voltage modulation in-phase.

The striking similarity of the mechanosensitivity of *ps-para-para*-PCP (1) and *ps-para-para*-OPE PCP, both comprising a central *para*-PCP subunit, not only points at this structural motif as the origin of the phenomenon but also further corroborates its rationalization based on the presence of a DQI dip in proximity of the Fermi level. Equally interesting are the modulation experiments performed with the *ps-meta-para*-PCP (2). As displayed in parts d and f of Figure 3, single-molecule

junctions with this structure do not feature significant conductance changes during the modulation experiments. Remarkably, the absence of mechanosensitivity of the *ps-meta-para*-PCP has not been reported experimentally before. Particularly, this behavior indicates the absence of a transmission dip as a function of electrode displacement (within the displacement window probed by the experiment), suggesting that DQI does not occur in the case of *ps-meta*-PCP cores. This is in agreement with previous predictions of π -stacked systems by the groups of Solomon^{26,27} and Yoshizawa.²⁹

To quantify the mechanosensitivity of the molecule under investigation, the gauge factor (GF) was determined as the ratio between logarithmic conductance variation and linear electrode displacement (see the Supporting Information (section 2.4) for more information). Figure 4 displays the GFs for (a) *ps-para-para*-PCP and (b) *ps-meta-para*-PCP. Indeed, the GFs of the measurements of both structures visualize their difference. While the absence of mechanosensitivity of *ps-meta-para*-PCP results in a sharp peak close to zero (Figure 4b), the GF values recorded for *ps-para-para*-PCP

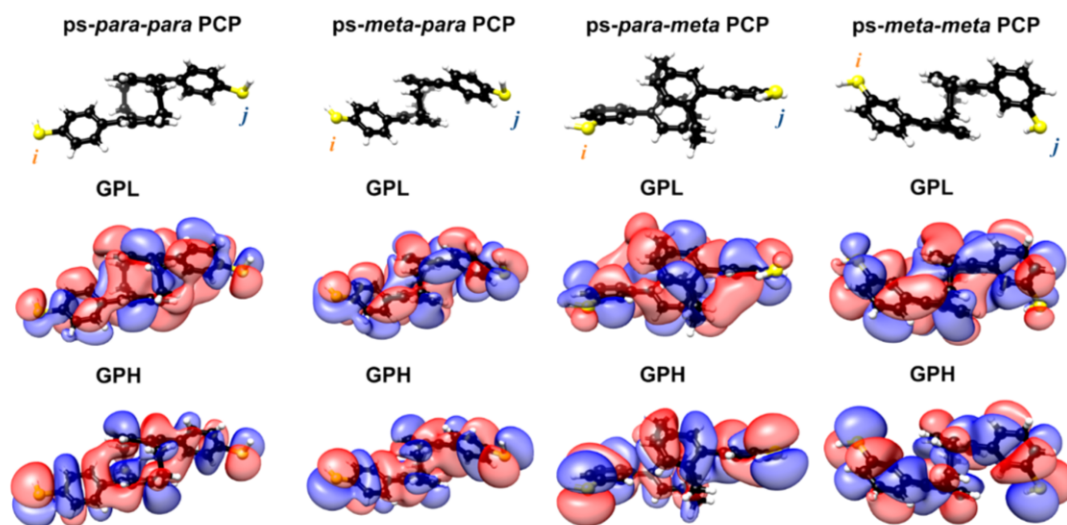


Figure 6. HOMO and LUMO molecular frontier orbitals of the *ps-para-para*-, *ps-meta-para*-, *ps-para-meta*-, and *ps-meta-meta*-PCPs. The anchoring sulfur atoms are marked *i* and *j*, respectively. Extended representations also including GPL+1 and GPH+1 for each molecule can be found in the [Supporting Information](#) (section 3.3).

(Figure 4a) display a broad distribution with a minimum at $GF = 0$, documenting its pronounced mechanosensitivity.

To rationalize the experimental observations described earlier, extensive DFT calculations were performed. First, the four model compounds *ps-para-para*-PCP (**1b**), *ps-meta-para*-PCP (**2b**), *ps-para-meta*-PCP (**3b**), and *ps-meta-meta*-PCP (**4b**) were optimized in the gas phase. The hydrogen atoms of the terminal thiol groups were removed, and the molecules were placed in model junctions, consisting of pairs of tetrahedral gold leads (Figure 5a). Optimizing the junction geometry, only the top three gold atoms in the first layer of each tip were allowed to relax, while the rest of the gold cluster remained fixed. Then, the systems were stretched in steps of 0.1 Å, and a geometry optimization was performed at every single step. A detailed description of the established approach³⁷ and explanations of the calculations are provided in the [Supporting Information](#) (section 3.1).

A closer look at the two-dimensional contour plots of transmission in dependence of energy and electrode displacement in Figure 5b reveals important information about the transmission behavior of the molecular junctions inside the electronic gap between the highest occupied molecular orbital (HOMO) and the lowest unoccupied molecular orbital (LUMO). In the case of the *ps-para-para*-PCP, a transmission valley (blue diagonal trace) with transmission values lower than 10^{-5} is observed between the molecular frontier orbitals (red horizontal traces). The transmission valley corresponds to the DQI conductance dip, as shown in Figure 3e. The energy position of the transmission minimum can be tuned by mechanical manipulation of the junction. It should be noted that the DQI crosses the complete HOMO–LUMO gap, making it a robust feature for experimental detection, because it does not depend on the precise position of the Fermi energy. A similar valley is not present for the *ps-meta-para*-PCP junction. Instead, the transmission stays rather constant in the range of $\sim 10^{-3}$ – 10^{-4} inside the molecule's HOMO–LUMO gap. Rather uniform transmission values are furthermore predicted in the molecules' electronic gap for both *ps-para*-

meta- and *ps-meta-meta*-PCP. Interestingly, for this pair of model compounds with terminal *meta*-benzene linkers, ~ 1 order of magnitude lower transmission values were calculated compared to the pair with terminal *para*-benzene linkers. This is also in line with the absence of measurable conductance plateaus for the *meta*-phenyl-connected PCPs in Figure 2.

The conductance that we compute within the DFT-NEGF formalism³⁷ at the Fermi energy is plotted in parts e and f of Figure 3 for *ps-para-para*- and *ps-meta-para*-PCP derivatives, respectively. Considering the example of the *ps-para-para*-PCP single-molecule junction, the conductance features a dip that is shifted toward negative displacements and is ~ 2 orders of magnitude lower than the base value. Molecular contacts constructed from *ps-meta-para*-PCP show instead a rather constant behavior in the studied displacement range without a DQI dip.

The behavior of another geometry that features a more complex stick–slip motion is discussed in the [Supporting Information](#) (section 3.2). In that case, remnants of transmission valleys are visible for the *ps-para-meta*-PCP molecular junction, further consolidating the hypothesis of the central *ps-para*-PCP subunit as the origin of the DQI phenomenon. Note, however, that we argue here on a qualitative level because we did not correct DFT quasiparticle energies and therefore expect uncertainties with respect to absolute conductance values,^{17,38–41} as a comparison of experimental and theoretical data in Figures 3 and 5 confirms.

While the calculated transmission plots perfectly support the hypothesis that mechanosensitivity can exclusively be observed for structures with a central *ps-para*-PCP subunit providing DQI, another qualitative argument is provided by considering orbital symmetry rules, as suggested by Yoshizawa and co-workers.^{29,42} The qualitative prediction of QI phenomena is based on the interplay of molecular frontier orbitals, especially the HOMO and LUMO, in transport models using Landauer–Büttiker scattering theory and Green's function methods (details are provided in the [Supporting Information](#) (section 3.3)). Thus, the gas-phase frontier orbitals of the model

compounds with terminal thiol groups were calculated and are displayed in Figure 6.

Assuming that the Fermi energy of the electrodes lies between the molecule's HOMO and LUMO energies due to charge neutrality, two orbital rules apply for the electronic transport properties.^{29,42} (1) The weights of the HOMO and LUMO wave functions on the anchoring atoms i and j (see Figure 6) need to be of decent size to yield a fair contribution to the transmission. (2) If the parities of the molecule's HOMO and LUMO on the anchoring atoms are different in sign, transport is symmetry-supported through CQI, which is typically reflected in a high transmission inside the HOMO–LUMO gap. If HOMO and LUMO parities are the same instead, the related molecular orbital resonances cancel each other out at a certain energy inside the HOMO–LUMO gap. As a consequence, transport is symmetry-inhibited, resulting in a DQI dip in the energy-dependent transmission function, typically leading to a reduced conductance of the single-molecule junction. This argument assumes that HOMO and LUMO orbital wave functions are of similar character on the termini i and j .

The analysis of the molecules started by defining the terminal sulfur atoms as anchoring sites i and j (see Figure 6). Comparing orbital wave functions on the terminal sulfur atoms shows that gas-phase HOMO (GPH) and gas-phase LUMO (GPL) of both model compounds comprising a central *para*-PCP (*ps-para-para*- and *ps-para-meta*-PCP) are of similarly oriented π -character at the sulfur atoms and have the same parities; thus, these structures should show DQI. In contrast, both molecules with a *ps-meta*-PCP subunit have different parities in their GPH and GPL on the terminal sulfur atoms and thus exhibit CQI. The orbital symmetry rules thus rationalize the experimental observations and numerical computations reported earlier, which identify the central *ps-para*-PCP subunit as the origin of DQI.

Let us point out that ferrocene recently emerged as a related 3D system to the PCP, where the angle between two cyclopentadienyl decks can be tuned rather continuously around the central Fe core atom.⁴³ The torsion can be compared to *meta* or *para* connection to the PCP. The mechanical distortion that explains the experimental results here is mainly the displacement of two benzene rings as compared to a rotation.

CONCLUSION

We have studied the electronic transport properties of single-molecule junctions based on π -stacked hydrocarbons. Our study confirms previous theoretical predictions for model compounds in terms of molecular orbital symmetry rules with regard to the suppression of electronic transport in PCP subunits when contacted in *ps-para* geometry as compared to *ps-meta* geometry. While the *ps-meta* subunit generally shows high conductance in comparison to the *ps-para* geometry (still relatively low compared to other conjugated molecular wires such as OPE3-dithiol⁴⁴) and little sensitivity to mechanical manipulation, the *ps-para* subunit offers an exceptional mechanoelectric sensitivity. Notably, our theoretical calculations predict that the DQI can be tuned through the complete electronic gap region, explaining the experimental robustness of the feature, as observations should be largely independent of the precise location of the Fermi energy. Similar to an optical Fabry–Pérot interferometer, the DQI feature can be used to detect minute displacement changes and hence serves as a

quantum sensor operating at ambient conditions, i.e., at room temperature.

ASSOCIATED CONTENT

Supporting Information

The Supporting Information is available free of charge at <https://pubs.acs.org/doi/10.1021/jacs.1c06966>.

Synthesis and characterization of all molecules, and details concerning transport measurements and calculations (PDF)

AUTHOR INFORMATION

Corresponding Authors

Fabian Pauly – Institute of Physics, University of Augsburg, 86159 Augsburg, Germany; orcid.org/0000-0001-8017-2379; Email: fabian.pauly@uni-a.de

Herre S. J. van der Zant – Kavli Institute of Nanoscience, Delft University of Technology, 2628 GJ Delft, The Netherlands; orcid.org/0000-0002-5385-0282; Email: h.s.j.vanderzant@tudelft.nl

Marcel Mayor – Department of Chemistry, University of Basel, 4056 Basel, Switzerland; Institute for Nanotechnology, Karlsruhe Institute of Technology (KIT), 76021 Karlsruhe, Germany; Lehn Institute of Functional Materials, School of Chemistry, Sun Yat-Sen University, Guangzhou 510274, P. R. China; orcid.org/0000-0002-8094-7813; Email: marcel.mayor@unibas.ch

Authors

Ksenia Reznikova – Department of Chemistry, University of Basel, 4056 Basel, Switzerland

Chunwei Hsu – Kavli Institute of Nanoscience, Delft University of Technology, 2628 GJ Delft, The Netherlands

Werner M. Schosser – Institute of Physics, University of Augsburg, 86159 Augsburg, Germany

Almudena Gallego – Department of Chemistry, University of Basel, 4056 Basel, Switzerland

Katawoura Beltako – Institute of Physics, University of Augsburg, 86159 Augsburg, Germany

Complete contact information is available at:

<https://pubs.acs.org/doi/10.1021/jacs.1c06966>

Author Contributions

[#]K.R., C.H., and W.M.S. contributed equally.

Notes

The authors declare no competing financial interest.

ACKNOWLEDGMENTS

This work was supported by a Horizon 2020 FET open project (QuIET; no. 767187). H.S.J.v.d.Z. and C.H. acknowledge support from The Netherlands Organisation for Scientific Research (NWO-Vrij program). M.M. acknowledges support from the Swiss National Science Foundation (SNF Grant no. 200020-178808) and the 111 project (90002-18011002).

ABBREVIATIONS

QI, quantum interference; DQI, destructive quantum interference; CQI, constructive quantum interference; OPE, oligo-(phenylene ethynylene); PCP, [2.2]paracyclophane; MCBJ, mechanically controlled break junction; DFT, density functional theory; NEGF, nonequilibrium Green's function; ps, pseudo; GF, gauge factor; FFT, fast Fourier transform;

HOMO, highest occupied molecular orbital; LUMO, lowest unoccupied molecular orbital; GPH, gas-phase HOMO; GPL, gas-phase LUMO.

REFERENCES

- (1) van der Molen, S. J.; Naaman, R.; Scheer, E.; Neaton, J. B.; Nitzan, A.; Natelson, D.; Tao, N. J.; van der Zant, H. S. J.; Mayor, M.; Ruben, M.; Reed, M.; Calame, M. Visions for a Molecular Future. *Nat. Nanotechnol.* **2013**, *8* (6), 385–389.
- (2) Aviram, A.; Ratner, M. A. Molecular Rectifiers. *Chem. Phys. Lett.* **1974**, *29* (2), 277–283.
- (3) Luo, L.; Choi, S. H.; Frisbie, C. D. Probing Hopping Conduction in Conjugated Molecular Wires Connected to Metal Electrodes. *Chem. Mater.* **2011**, *23* (3), 631–645.
- (4) Huber, R.; González, M. T.; Wu, S.; Langer, M.; Grunder, S.; Horhóiu, V.; Mayor, M.; Bryce, M. R.; Wang, C.; Jitchati, R.; Schönenberger, C.; Calame, M. Electrical Conductance of Conjugated Oligomers at the Single Molecule Level. *J. Am. Chem. Soc.* **2008**, *130* (3), 1080–1084.
- (5) Irie, M.; Fukaminato, T.; Sasaki, T.; Tamai, N.; Kawai, T. A Digital Fluorescent Molecular Photoswitch. *Nature* **2002**, *420* (6917), 759–760.
- (6) Liao, J.; Agustsson, J. S.; Wu, S.; Schönenberger, C.; Calame, M.; Leroux, Y.; Mayor, M.; Jeannin, O.; Ran, Y.-F.; Liu, S.-X.; Decurtins, S. Cyclic Conductance Switching in Networks of Redox-Active Molecular Junctions. *Nano Lett.* **2010**, *10* (3), 759–764.
- (7) Elbing, M.; Ochs, R.; Koentopp, M.; Fischer, M.; von Hanisch, C.; Weigend, F.; Evers, F.; Weber, H. B.; Mayor, M. A Single-Molecule Diode. *Proc. Natl. Acad. Sci. U. S. A.* **2005**, *102* (25), 8815–8820.
- (8) Lörtscher, E.; Gotsmann, B.; Lee, Y.; Yu, L.; Rettner, C.; Riel, H. Transport Properties of a Single-Molecule Diode. *ACS Nano* **2012**, *6* (6), 4931–4939.
- (9) Naher, M.; Milan, D. C.; Al-Owaedi, O. A.; Planje, I. J.; Bock, S.; Hurtado-Gallego, J.; Bastante, P.; Abd Dawood, Z. M.; Rincón-García, L.; Rubio-Bollinger, G.; Higgins, S. J.; Agraït, N.; Lambert, C. J.; Nichols, R. J.; Low, P. J. Molecular Structure–(Thermo)Electric Property Relationships in Single-Molecule Junctions and Comparisons with Single- and Multiple-Parameter Models. *J. Am. Chem. Soc.* **2021**, *143* (10), 3817–3829.
- (10) Stadler, R.; Markussen, T. Controlling the Transmission Line Shape of Molecular T-Stubs and Potential Thermoelectric Applications. *J. Chem. Phys.* **2011**, *135* (15), 154109.
- (11) Markussen, T.; Stadler, R.; Thygesen, K. S. The Relation between Structure and Quantum Interference in Single Molecule Junctions. *Nano Lett.* **2010**, *10* (10), 4260–4265.
- (12) Jiang, F.; Trupp, D. I.; Algethami, N.; Zheng, H.; He, W.; Alqorashi, A.; Zhu, C.; Tang, C.; Li, R.; Liu, J.; Sadeghi, H.; Shi, J.; Davidson, R.; Korb, M.; Sobolev, A. N.; Naher, M.; Sangtarash, S.; Low, P. J.; Hong, W.; Lambert, C. J. Turning the Tap: Conformational Control of Quantum Interference to Modulate Single-Molecule Conductance. *Angew. Chem., Int. Ed.* **2019**, *58* (52), 18987–18993.
- (13) Venkataraman, L.; Klare, J. E.; Nuckolls, C.; Hybertsen, M. S.; Steigerwald, M. L. Dependence of Single-Molecule Junction Conductance on Molecular Conformation. *Nature* **2006**, *442* (7105), 904–907.
- (14) Aradhya, S. V.; Meisner, J. S.; Krikorian, M.; Ahn, S.; Parameswaran, R.; Steigerwald, M. L.; Nuckolls, C.; Venkataraman, L. Dissecting Contact Mechanics from Quantum Interference in Single-Molecule Junctions of Stilbene Derivatives. *Nano Lett.* **2012**, *12* (3), 1643–1647.
- (15) Mayor, M.; Weber, H. B.; Reichert, J.; Elbing, M.; von Hänisch, C.; Beckmann, D.; Fischer, M. Electric Current through a Molecular Rod—Relevance of the Position of the Anchor Groups. *Angew. Chem., Int. Ed.* **2003**, *42* (47), 5834–5838.
- (16) Koga, J.; Tsuji, Y.; Yoshizawa, K. Orbital Control of Single-Molecule Conductance Perturbed by π -Accepting Anchor Groups: Cyanide and Isocyanide. *J. Phys. Chem. C* **2012**, *116* (38), 20607–20616.
- (17) Arroyo, C. R.; Tarkuc, S.; Frisenda, R.; Seldenthuis, J. S.; Woerde, C. H. M.; Elkema, R.; Grozema, F. C.; van der Zant, H. S. J. Signatures of Quantum Interference Effects on Charge Transport Through a Single Benzene Ring. *Angew. Chem., Int. Ed.* **2013**, *52* (11), 3152–3155.
- (18) Kiguchi, M.; Kaneko, S. Single Molecule Bridging between Metal Electrodes. *Phys. Chem. Chem. Phys.* **2013**, *15* (7), 2253–2267.
- (19) Lambert, C. J. Basic Concepts of Quantum Interference and Electron Transport in Single-Molecule Electronics. *Chem. Soc. Rev.* **2015**, *44* (4), 875–888.
- (20) Kiguchi, M.; Nakamura, H.; Takahashi, Y.; Takahashi, T.; Ohto, T. Effect of Anchoring Group Position on Formation and Conductance of a Single Disubstituted Benzene Molecule Bridging Au Electrodes: Change of Conductive Molecular Orbital and Electron Pathway. *J. Phys. Chem. C* **2010**, *114* (50), 22254–22261.
- (21) Arroyo, C. R.; Frisenda, R.; Moth-Poulsen, K.; Seldenthuis, J. S.; Bjørnholm, T.; van der Zant, H. S. Quantum Interference Effects at Room Temperature in OPV-Based Single-Molecule Junctions. *Nanoscale Res. Lett.* **2013**, *8*, 1.
- (22) Li, X.; Staykov, A.; Yoshizawa, K. Orbital Views of the Electron Transport through Polycyclic Aromatic Hydrocarbons with Different Molecular Sizes and Edge Type Structures. *J. Phys. Chem. C* **2010**, *114* (21), 9997–10003.
- (23) Yoshizawa, K.; Tada, T.; Staykov, A. Orbital Views of the Electron Transport in Molecular Devices. *J. Am. Chem. Soc.* **2008**, *130* (29), 9406–9413.
- (24) Yoshizawa, K. An Orbital Rule for Electron Transport in Molecules. *Acc. Chem. Res.* **2012**, *45* (9), 1612–1621.
- (25) Brown, C. J.; Farthing, A. C. Preparation and Structure of Di-*p*-Xylylene. *Nature* **1949**, *164* (4178), 915–916.
- (26) Solomon, G. C.; Vura-Weis, J.; Herrmann, C.; Wasielewski, M. R.; Ratner, M. A. Understanding Coherent Transport through π -Stacked Systems upon Spatial Dislocation. *J. Phys. Chem. B* **2010**, *114* (45), 14735–14744.
- (27) Solomon, G. C.; Herrmann, C.; Vura-Weis, J.; Wasielewski, M. R.; Ratner, M. A. The Chameleonic Nature of Electron Transport through π -Stacked Systems. *J. Am. Chem. Soc.* **2010**, *132* (23), 7887–7889.
- (28) Stefani, D.; Weiland, K. J.; Skripnik, M.; Hsu, C.; Perrin, M. L.; Mayor, M.; Pauly, F.; van der Zant, H. S. J. Large Conductance Variations in a Mechanosensitive Single-Molecule Junction. *Nano Lett.* **2018**, *18* (9), 5981–5988.
- (29) Li, X.; Staykov, A.; Yoshizawa, K. Orbital Views on Electron-Transport Properties of Cyclophanes: Insight into Intermolecular Transport. *Bull. Chem. Soc. Jpn.* **2012**, *85* (2), 181–188.
- (30) Perdew, J. P. Density-Functional Approximation for the Correlation Energy of the Inhomogeneous Electron Gas. *Phys. Rev. B: Condens. Matter Mater. Phys.* **1986**, *33* (12), 8822–8824.
- (31) Vorontsova, N. V.; Rozenberg, V. I.; Sergeeva, E. V.; Vorontsov, E. V.; Starikova, Z. A.; Lyssenko, K. A.; Hopf, H. Symmetrically Tetrasubstituted [2.2]Paracyclophanes: Their Systematization and Regioselective Synthesis of Several Types of Bis-Bifunctional Derivatives by Double Electrophilic Substitution. *Chem. - Eur. J.* **2008**, *14* (15), 4600–4617.
- (32) Jevric, M.; Petersen, A. U.; Mansø, M.; Madsen, A. Ø.; Nielsen, M. B. Bismuth(III)-Promoted Acetylation of Thioethers into Thioacetates. *Eur. J. Org. Chem.* **2015**, *2015*, 4675–4688.
- (33) Martin, C. A.; Ding, D.; van der Zant, H. S. J.; van Ruitenbeek, J. M. Lithographic Mechanical Break Junctions for Single-Molecule Measurements in Vacuum: Possibilities and Limitations. *New J. Phys.* **2008**, *10* (6), 065008.
- (34) Martin, C. A.; Smit, R. H. M.; van Egmond, R.; van der Zant, H. S. J.; van Ruitenbeek, J. M. A Versatile Low-Temperature Setup for the Electrical Characterization of Single-Molecule Junctions. *Rev. Sci. Instrum.* **2011**, *82* (5), 053907.
- (35) Cabosart, D.; El Abbassi, M.; Stefani, D.; Frisenda, R.; Calame, M.; van der Zant, H. S. J.; Perrin, M. L. A Reference-Free Clustering

Method for the Analysis of Molecular Break-Junction Measurements. *Appl. Phys. Lett.* **2019**, *114* (14), 143102.

(36) O'Neill, K.; Osorio, E. A.; van der Zant, H. S. J. Self-Breaking in Planar Few-Atom Au Constrictions for Nanometer-Spaced Electrodes. *Appl. Phys. Lett.* **2007**, *90* (13), 133109.

(37) Pauly, F.; Viljas, J. K.; Huniar, U.; Häfner, M.; Wohlthat, S.; Bürkle, M.; Cuevas, J. C.; Schön, G. Cluster-Based Density-Functional Approach to Quantum Transport through Molecular and Atomic Contacts. *New J. Phys.* **2008**, *10* (12), 125019.

(38) Quek, S. Y.; Venkataraman, L.; Choi, H. J.; Louie, S. G.; Hybertsen, M. S.; Neaton, J. B. Amine–Gold Linked Single-Molecule Circuits: Experiment and Theory. *Nano Lett.* **2007**, *7* (11), 3477–3482.

(39) Zotti, L. A.; Bürkle, M.; Pauly, F.; Lee, W.; Kim, K.; Jeong, W.; Asai, Y.; Reddy, P.; Cuevas, J. C. Heat Dissipation and Its Relation to Thermopower in Single-Molecule Junctions. *New J. Phys.* **2014**, *16* (1), 015004.

(40) Manrique, D. Z.; Huang, C.; Baghernejad, M.; Zhao, X.; Al-Owaedi, O. A.; Sadeghi, H.; Kaliginedi, V.; Hong, W.; Gulcur, M.; Wandlowski, T.; Bryce, M. R.; Lambert, C. J. A Quantum Circuit Rule for Interference Effects in Single-Molecule Electrical Junctions. *Nat. Commun.* **2015**, *6* (1), 6389.

(41) Garner, M. H.; Li, H.; Chen, Y.; Su, T. A.; Shanguan, Z.; Paley, D. W.; Liu, T.; Ng, F.; Li, H.; Xiao, S.; Nuckolls, C.; Venkataraman, L.; Solomon, G. C. Comprehensive Suppression of Single-Molecule Conductance Using Destructive σ -Interference. *Nature* **2018**, *558* (7710), 415–419.

(42) Tsuji, Y.; Yoshizawa, K. Frontier Orbital Perspective for Quantum Interference in Alternant and Nonalternant Hydrocarbons. *J. Phys. Chem. C* **2017**, *121* (17), 9621–9626.

(43) Camarasa-Gómez, M.; Hernangómez-Pérez, D.; Inkpen, M. S.; Lovat, G.; Fung, E.-D.; Roy, X.; Venkataraman, L.; Evers, F. Mechanically Tunable Quantum Interference in Ferrocene-Based Single-Molecule Junctions. *Nano Lett.* **2020**, *20* (9), 6381–6386.

(44) Frisenda, R.; Perrin, M. L.; Valkenier, H.; Hummelen, J. C.; van der Zant, H. S. J. Statistical Analysis of Single-Molecule Breaking Traces. *Phys. Status Solidi B* **2013**, *250* (11), 2431–2436.

2.3 Pseudo-*Ortho*-[2.2]Paracyclophane-Based Molecular Wires

This subchapter covers the synthesis of envisioned molecular wires with a substitution to the [2.2]paracyclophane in the pseudo-*ortho* position. Experimental and theoretical investigations of the pseudo-*ortho* PCP-based molecular wires are currently ongoing in collaboration with Prof. Dr. Herre S. J. van der Zant's group and Prof. Dr. Fabian Pauly's group using the same techniques as described in Subchapter 2.2.

2.3.1 Project Description and Molecular Design

DQI is an intriguing phenomena leading to conductance suppression and a sharp dip in the transmission function. The closer the DQI dip to the Fermi energy of electrodes, the distinctive the resulting suppression would be.^{13,96} This feature makes the cyclophane-based scaffold with DQI appealing for the investigation of mechanosensitivity, which was demonstrated recently in the example of mechanical stimuli of a porphyrin-cyclophane-based molecular wire.^{115,116}

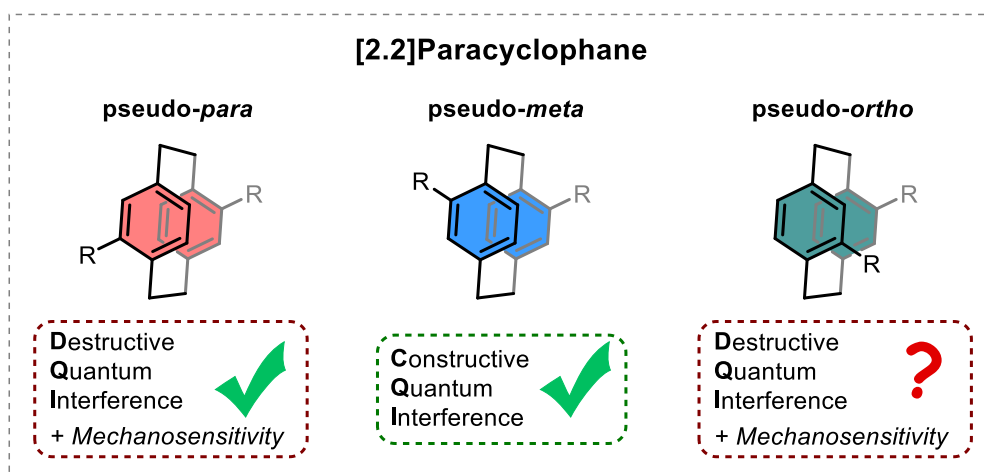


Figure 19: Overview of quantum interference effects and mechanosensitivity in PCP structures with different substitution pattern.

In addition, similar observations were also already confirmed for the PCP-based molecular wires (see Subchapter 2.2 and Figure 19), where only the molecular wire with a pseudo-*para*-PCP core and DQI demonstrated conductance changes upon the application of mechanical stress in the MCBJ.^{72,117} The observed strong conductance oscillation during the modulation experiments can be attributed to the shift in the overlap of the frontier orbital between the phenyl rings in the PCP scaffold. The orbital symmetry in a relaxed state with DQI is different from the one during stretching and compression, where DQI is lifted, providing a more efficient charge transport. According to the predictions of *Yoshizawa* and co-workers based on the frontier orbital analysis, pseudo-*ortho* substituted PCP would also demonstrate weak charge

transport due to the DQI (see 2.1.2.2).¹¹⁴ Therefore, these predictions make molecular wires comprising the pseudo-*ortho* PCP core promising candidates for a more pronounced understanding of the relationship between the DQI and mechanosensitivity.

Excited by this hypothesis, we embedded the pseudo-*ortho* PCP core into an OPE and an oligo(phenylene)-type backbone, providing two molecular wires that differ in length (see Figure 20). Both molecules comprise a thiol anchoring group which is masked by terminal acetyl to enable their immobilization in MCBJ. In junction, molecular wires will form a sulfur-gold covalent bond providing electronic communication and mechanical stability to allow mechanical manipulations.

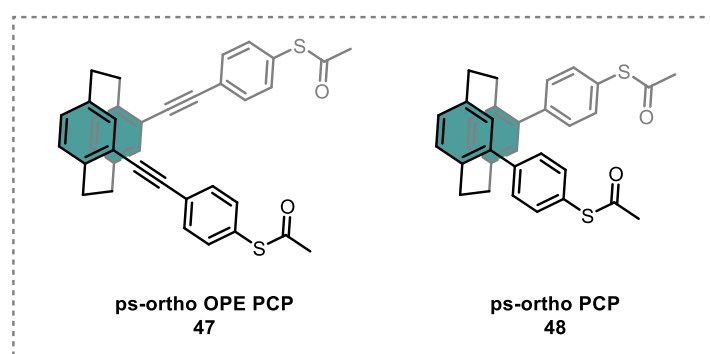
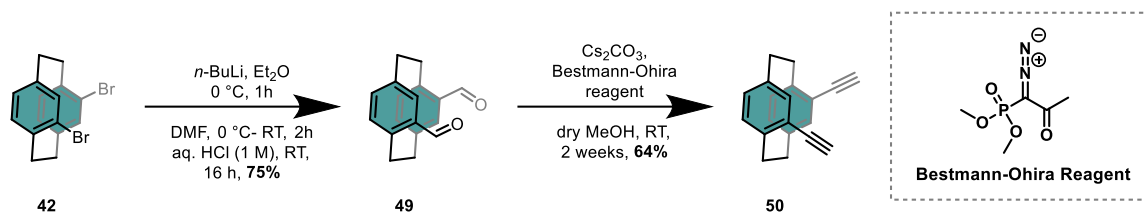


Figure 20: Molecular design of pseudo-*ortho* OPE PCP (**47**) and pseudo-*ortho* PCP (**48**) molecular wires. The central pseudo-*ortho* PCP core is coupled to either masked ethylphenylthiol (pseudo-*ortho* OPE PCP (**47**)) or directly to masked phenylthiol (pseudo-*ortho* PCP (**48**)).

2.3.2 Results and Discussion

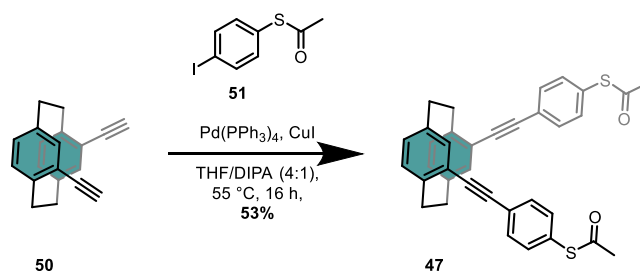
2.3.2.1 Synthesis of Pseudo-Ortho OPE PCP

To obtain the desired molecular wire **47**, diethynyl ps-*ortho* PCP (**50**) was prepared according to the literature-known procedure (see Scheme 8).^{90,118} First, the aldehydes were introduced via a formylation reaction. Two-fold lithiation of dibromo ps-*ortho* PCP (**42**)^{88–90} was carried out with *n*-BuLi in diethyl ether. Then *N,N*-dimethylformamide (DMF) was added, followed by quenching with aqueous hydrochloric acid (1 M) to provide ps-*ortho* dialdehyde (**49**) in 75% yield. Dialdehyde **49** was transformed to diethynyl by treating with *Bestmann-Ohira* reagent^{119,120} providing diethynyl ps-*ortho* PCP (**50**) in 64% yield.



Scheme 8: Synthesis of diethynyl *ps-ortho* PCP (**50**).

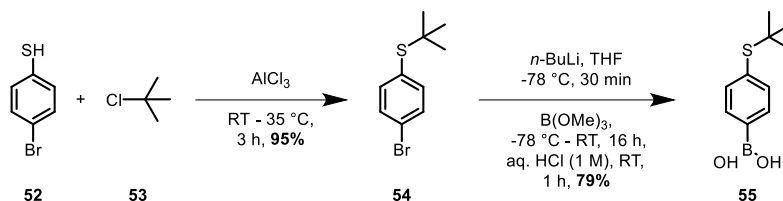
The envisaged coupling partner for a *Sonogashira-Hagihara* reaction was acetylthioiodobenzene (**51**),^{121,122} which comprised a masked sulfur moiety at the *para* position to the iodine and was prepared by *L. Jucker*. The cross-coupling reaction between free diacetylene PCP **50** and iodo compound **51** was achieved using tetrakis(triphenylphosphine)palladium and copper iodide as a catalyst in a mixture of THF and diisopropylamine (4:1). The target *ps-ortho* OPE PCP (**47**) was obtained in 53% yield after the purification by column chromatography and GPC (see Scheme 9). The *ps-ortho* OPE PCP (**47**) identity was corroborated by ^1H NMR, $^{13}\text{C}\{^1\text{H}\}$ NMR spectroscopy and high-resolution mass spectrometry, where the corresponding data is provided in the *Supporting Information for Subchapter 2.3*.



Scheme 9: Synthesis of *ps-ortho* OPE PCP (**47**).

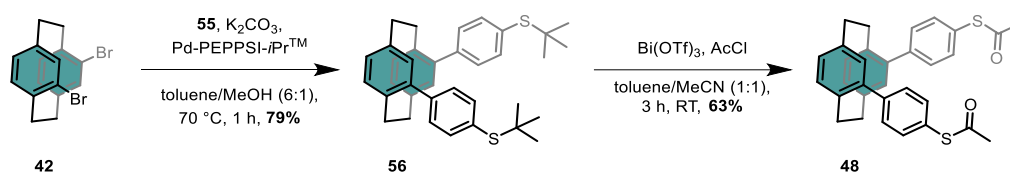
2.3.2.2 Synthesis of Pseudo-Ortho PCP

The synthesis of ps-*ortho* PCP **48** started with a preparation of literature known boronic acid derivative **55**. The free thiol **52** was protected by *tert*-butyl using 2-chloro-2-methylpropane (**53**) in a reaction catalyzed by aluminum trichloride to give 1-bromo-4-(*tert*-butylsulfanyl)benzene (**54**) in 95% yield.¹²³ The desired borylation of **54** was achieved via lithium-halogen exchange with *n*-BuLi, followed by the addition of trimethyl borate and aqueous hydrochloric acid (1 M), providing boronic acid **55** in 79% yield.^{124,125}



Scheme 10: Synthesis of boronic acid derivative **55**.

Then, a molecular wire was assembled from dibromo ps-*ortho* PCP (**42**) and previously described boronic acid **55** by *Suzuki-Miyaura* cross-coupling reaction. Building blocks were coupled using Pd-PEPPSI-*i*PrTM as a palladium source and potassium carbonate as a base in toluene/methanol to provide *tert*-butyl protected ps-*ortho* PCP **56** in 79% yield. The adaption of a strategy of *Jevric et al.*¹²⁶ enabled transprotection of **56** with bismuth triflate and acetyl chloride in toluene/methanol mixture, providing the desired ps-*ortho* PCP **48** in 63% yield after the purification by column chromatography and cyclic GPC. The identity of new compounds **56** and **48** were proven by ¹H NMR, ¹³C{¹H} NMR spectroscopy and high-resolution mass spectrometry (see Supporting Information for 2.3).



Scheme 11: Synthesis of ps-*ortho* PCP (**48**).

2.4 Summary

In this chapter, we demonstrated the potential of the π -stacked hydrocarbons scaffold as an appealing building block that enables us to gain more insights into the field of molecular electronics. All of the described results were only possible due to the extensive collaboration with groups of experimental and theoretical physicists.

First, four PCP-based molecular wires with a combination of different substitution patterns on both the PCP-core and the anchoring group were successfully synthesized and fully characterized. Unfortunately, the molecules with the *meta* substitution in the anchoring group (*ps-para-meta* and *ps-meta-meta* PCP) demonstrated a lack of clear plateaus, presumably due to the conductance values below the detection threshold or the formation of unstable molecular junctions. On the contrary, the molecules with *para*-phenyl, such as *ps-para-para* and *ps-meta-para* PCP, were successfully integrated and measured into an electronic circuit using the MCBJ setup at ambient conditions. The *ps-para-para* PCP shows lower conductance ($1.3 \times 10^{-5} G_0$) in comparison to the *ps-meta-para* PCP analogue ($2.2 \times 10^{-5} G_0$) and a pronounced response to mechanical manipulations. These observations were rationalized by theoretical calculations indicating the destructive and constructive quantum interference effects for *ps-para* and *ps-meta* PCP core, respectively. Furthermore, this trend is also in accordance with the predictions of *Yoshizawa* and co-workers.¹¹⁴

In the second part of this chapter, we discussed the implementation of the *ps-ortho* PCP subunit in the molecular wires to investigate our hypothesis of the relationship between the DQI and mechanosensitivity. Therefore, *ps-ortho* OPE PCP (**47**) and *ps-ortho* PCP (**48**) were successfully synthesized, fully characterized, and are currently under investigation.

2.5 Outlook

The knowledge gained through the investigation of QI effects and mechanosensitivity can be expanded, for instance, with the following model compounds (see Figure 21).

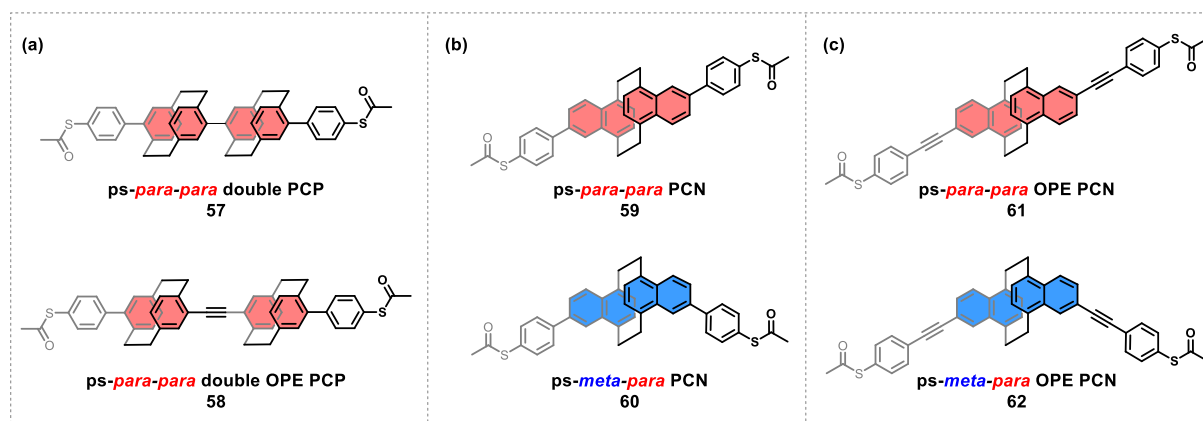


Figure 21: Model compounds for further investigations of QI effects and mechanosensitivity with the MCBJ setup. (a) Connecting two PCP-core linear to each other to increase the DQI. (b) and (c) PCN-based molecular wires, as an analogue to the PCP, would also demonstrate DQI features for the *ps-para* substitution (**59** & **61**).

The first idea for the model compound arises from the question of whether the mechanosensitivity would be enhanced or suppressed in the presence of two PCP-core exhibiting DQI features. The easiest way to prove this assumption is a connection of two parallel arranged *ps-para* PCP cores directly (**57**) or via acetylene (**58**) (see Figure 21a). The enlargement of the π -stacked hydrocarbons scaffold would allow the improvement of electron transport. The switch from benzene to naphthalenes would provide a highly delocalized *anti*-[2.2]paracyclonaphthanes (PCN) structure which can be substituted in *ps-para* (**59** & **61**) or pseudo-*meta* (**60** & **62**) positions exhibiting DQI and CQI features, respectively (see Figure 21b and c).

To complete the investigation of the disubstitution pattern on the PCP core, the last possible option, namely *ps-geminal* PCP, can be implemented in a molecular wire. According to our predictions, the target molecular wire **63** should demonstrate similar features as the *ps-meta* PCP analogue. The desired structure **63** can be prepared using a specific stereoelectronic effect of the *ps-geminal* PCP structure, which was already discussed in detail in *General Introduction 2.1.1.4*.

One of the possible synthetic strategies is depicted in Figure 22, where the *Sonogashira-Hagihara* cross-coupling to the anchoring groups is a last-stage modification. Free acetylene **64** for the cross-coupling reaction can be converted from dialdehyde **65**, by treating the latter with *Bestmann-Ohira* reagent similar to the synthesis of *ps-ortho* analogue **50**.⁹⁰ The required

dialdehyde **65** should be accessible by profiting from the trans-annular directive effect of **37** enabling the formulation in the *ps-geminal* position to provide **67**.⁵⁷ Afterward, the obtained ester aldehyde **67** can be reduced to diol **66** and oxidized to the desired dialdehyde **65**.¹²⁷

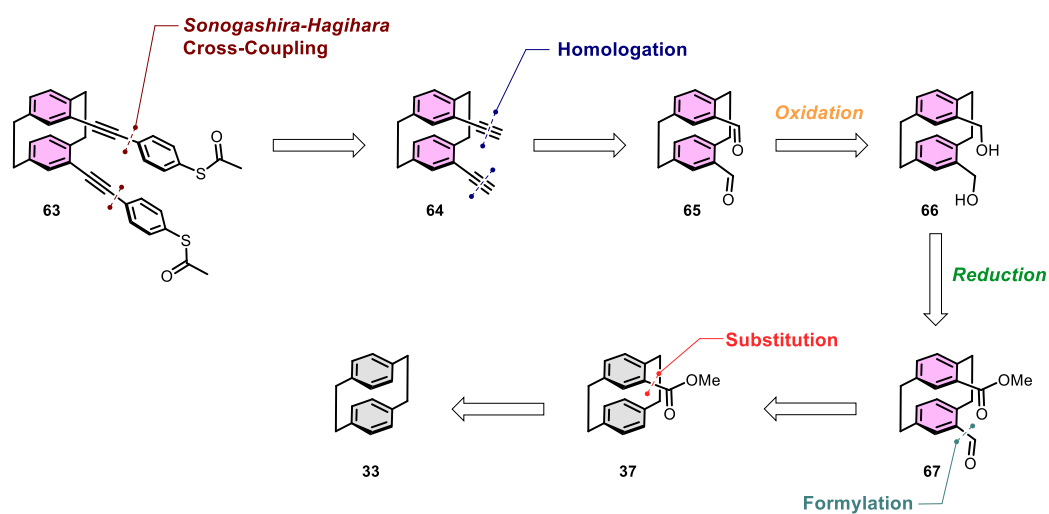


Figure 22: Retrosynthetic analysis for the *ps-geminal* OPE PCP (**63**) molecular wire.

Chapter 3

3 Synthesis Towards a [2.2]Paracyclophane-Based Molecular Loop

This chapter provides the results of the synthetic approaches towards a macrocyclic structure combining two conductivity pathways: through-space and through-bond. The molecular design was inspired by the work of *Dr. K. J. Weiland*^{65,66,128} and our results obtained from the investigations of the influence of the connectivity pattern on the conductance properties (see Chapter 2).^{72,117} The envisioned molecule comprises a PCP-based backbone linked in the pseudo-*meta* position to a septithiophene moiety, providing a macrocyclic structure. The key step in the synthetic strategy is macrocyclization by acetylene coupling to obtain the macrocycle comprising diacetylene, which enables the transformation to the corresponding thiophene providing the septithiophene moiety for the loop. Therefore, the following pages will introduce the general concept and several possibilities for the macrocyclization procedure of acetylene-containing precursors.

3.1 Introduction

3.1.1 General Macrocyclization Strategies

In recent years, chemists made a lot of advancements in the synthesis of acetylene-based macrocycles.^{34,129–134} These macrocycles became the focus of interest due to the possibility of extended conjugation and preparation of carbon-rich materials.³⁴ Furthermore, acetylene building blocks are easily accessible and allow a wide range of metal-catalyzed cross-coupling reactions to construct and close cyclic structures.^{37,129} The assembly of macrocycles can be generally divided into four major strategies,¹³⁵ illustrated in Figure 23.

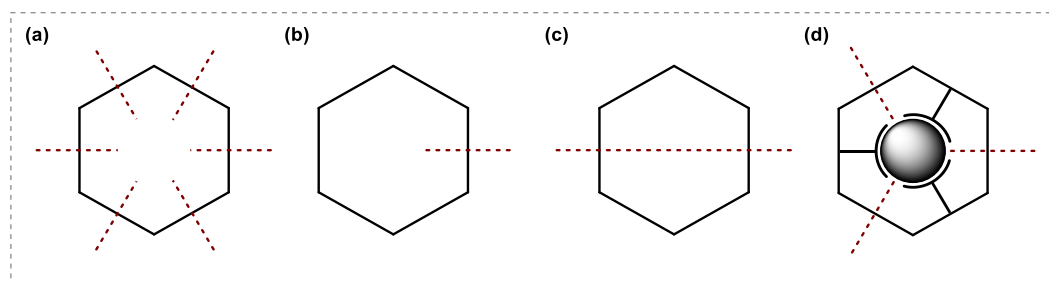


Figure 23: Schematic representation of four major kinetically controlled macrocyclization strategies: (a) cyclooligomerization; (b) intramolecular; (c) intermolecular and (d) templated cyclisation. The red dashed lines represent the retrosynthetic disconnection.

The first strategy is a so-called cyclooligomerization (see Figure 23a), which allows the formation of cyclic structures from several small building blocks. The cyclization occurs via homo- or cross-coupling reactions of monomers, which first build up linear oligomers that can

undergo ring-closure, providing macrocycles. Due to the random distribution of ring closure, this approach enables the preparation of various macrocycles, which differ in size, in one step.^{69,136} However, the competitive formation of linear oligomers and polymers leads to lower yields and requires more extensive purification. The intramolecular macrocyclization strategy can be applied as an alternative to random cyclization (see Figure 23b). The predefined precursor with a particular chain length allows a more controlled formation of macrocycles and minimizes the appearance of by-products, facilitating further purification.^{137,138} There are also several drawbacks, such as usually lengthier synthesis to the macrocyclization precursor and the requirement of optimized reaction conditions such as high-dilution or pseudo-high-dilution to suppress competing intermolecular reactions. The number of synthetic steps can be reduced for symmetrical macrocycles, which are synthesized via intermolecular dimerization (see Figure 23c).^{139,140} In this synthetic strategy, linear and cyclic polymers may form, which results in a decreased reaction yield of the desired macrocyclic dimer. The last strategy is templated cyclization (see Figure 23d). This strategy benefits from the preorganized arrangement of the monomer building blocks around a suitable template to overcome the disadvantages of random cyclization and long synthetic pathways, thereby potentially providing a high cyclization yield.^{141–143} Furthermore, the template can be chemically eliminated, releasing the desired structure. The disadvantage of the template strategy is a requirement to introduce and eliminate the template. Additionally, chosen template dictates the size and geometry of the structure. Therefore, the template strategy could not be easily implemented in each design, limiting the options for possible macrocycles.¹³⁵

3.1.2 Ring Closure of Angle-Strained Diyne-Containing Macrocycles

According to the work of *Krebs* and *Wilke*,¹⁴⁴ any bond angle of an alkyne smaller than 170 ° is defined as a strained angle.¹²⁹ Strained acetylenes are more reactive than a linear analogue, and this property is often exploited in strain-promoted click chemistry.^{145–147} Furthermore, the molecules containing strained diynes with an angle below 150° were only detectable until now but not isolable.¹²⁹ There are several strategies to assemble an angle-strained diyne-containing π -conjugated macrocycle. One of the options for macrocyclization would be a one-step coupling reaction, such as copper-mediated procedures or palladium-catalyzed couplings (see Figure 24).^{148,149} On the other hand, the desired macrocycle can also be prepared in two steps via the formation of platinum(II) diacetylide complexes, followed by oxidant-induced elimination of platinum complexes to release the strained butadiyne.¹⁵⁰

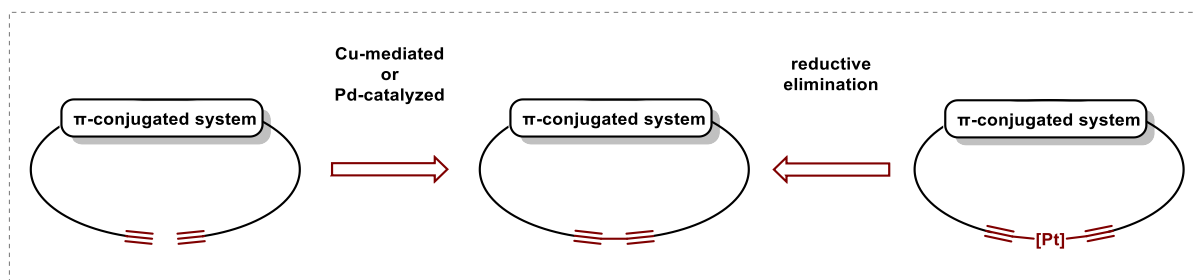


Figure 24: Synthetic options for ring closure of strained diyne-containing macrocycles.

3.1.2.1 Copper-Mediated vs. Palladium-Catalyzed Homocoupling for Intramolecular Cyclization

Glaser coupling¹⁵¹ and several variations of it, such as *Glaser-Eglinton*,¹⁵² *Glaser-Hay*,¹⁵³ and *Cadiot-Chodkiewicz* coupling^{154,155} (see Figure 25a), are the main source for providing symmetrical and unsymmetrical diacetylenes within small molecules, macrocycles, and polymers. Despite the long history of the *Glaser* coupling of over 150 years, there are still ongoing theoretical^{129,156–159} and experimental^{129,160} mechanistic studies to determine the possible intermediate for the reactions. The most widely accepted intermediate is the intermediate I depicted in Figure 25b, illustrating the formation of the dicopper(II) diacetylide complex, which collapses, providing the desired butadiyne. However, the proposed intermediate might not be ideally suitable for all copper-mediated reactions. The main difference between *Glaser-Hay* conditions to the initial copper-mediated homocoupling is the introduction of tetramethylethylenediamine (TMEDA) as a ligand for copper halides (see Figure 25a), which enables the solubility in almost any organic solvent. In addition, it leads to the possible formation of an alternative copper(III) intermediate (see Figure 25b, intermediate II), according to the density-functional theory (DFT) calculations of *Fomine* and co-workers.¹⁵⁶ The existence of a copper(III) intermediate was supported by extensive reaction mechanism studies using ¹³C NMR and UV/Vis spectroscopy methods, which suggested a different copper(III) intermediate that coordinated two acetylides (see Figure 25, intermediate III).¹⁵⁷ In 2016, *Lan* and co-workers proposed another possible intermediate for the *Glaser-Hay* reaction based on DFT calculations. This time, the proposed intermediate comprises two copper(II) ions, and the complex is illustrated in Figure 25b as intermediate IV.¹⁵⁸ Despite the inconclusive structural investigations of the intermediate, copper-mediated conditions are still prevalent in acetylene homocoupling reactions due to the high yield. Furthermore, a wide range of modification possibilities to optimize the conditions allow the preparation of several different macrocycles with intriguing shapes and properties.^{129,148,149,155,161}

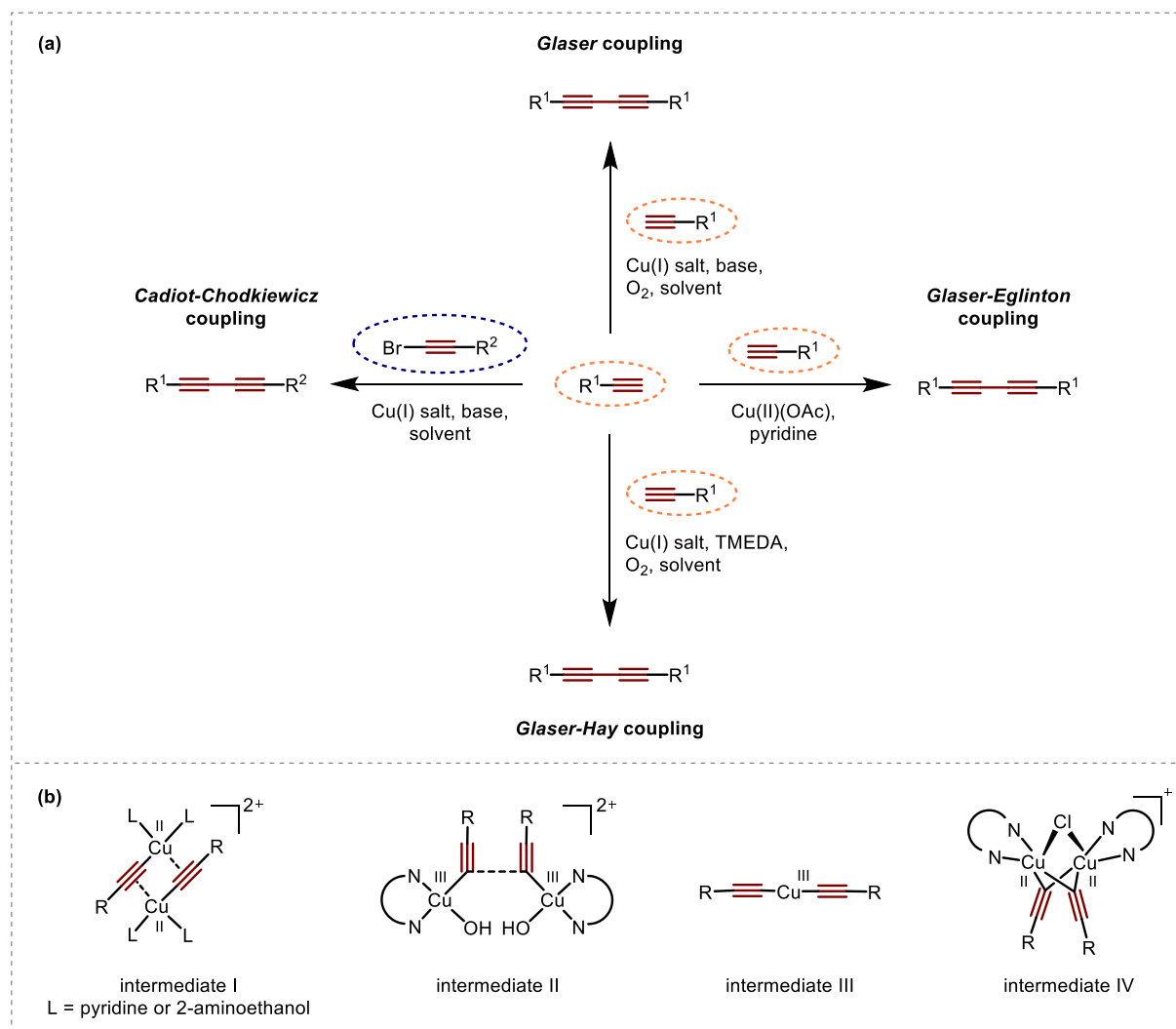


Figure 25: Proposed intermediates for Cu-mediated *Glaser*-coupling variations. The intermediates (a-d) depend on the copper catalyst which was used. This figure was reproduced from *Miki et al.*¹²⁹

An alternative to copper-mediated homocouplings are palladium-catalyzed reactions which favor strained angled molecules over linear ones. In 2004, *Haley and co-workers*¹⁶² investigated and described the selectivity differences between copper-mediated oxidative homocoupling of terminal alkynes compared to palladium-catalyzed procedures. The polyyne **68** was used as a precursor for possible homocoupling reaction, which can provide either bis[15]annulene (**69**) (cyclization across the *meta*-fused diynes) or more strained bis[14]annulene (**70**) (cyclization across the *ortho*-fused diyne) as a cyclization product (see Figure 26a). The cyclization using standard *Glaser-Eglinton* methods led to the formation of only *meta*-fused annulene (**69**) in 70% yield. Contrariwise, using a palladium catalyst with a *cis*-bidentate ligand provided the *ortho*-fused annulene (**70**) in 84% yield. However, if the monodentate ligand such as $Pd(PPh_3)_2Cl_2$ is used, the palladium-catalyzed reaction yields both *meta*- **69** and *ortho*-fused **70** products in 43% and 19%, respectively. The selectivity is rationalized by the geometry of the proposed intermediates (see Figure 26b). The copper-

containing intermediate prefers a pseudo-*trans* configuration and the formation of a not-strained angle ($> 170^\circ$). Conversely, various ligands can influence the geometry of the attached metal center in the case of a palladium-catalyzed reaction. The strained angle is more favorable for the reactions with *cis*-bidentate palladium-catalyst, which prefers *cis* geometry over *trans* and explains the formation of exclusively *ortho*-fused annulene (**70**).

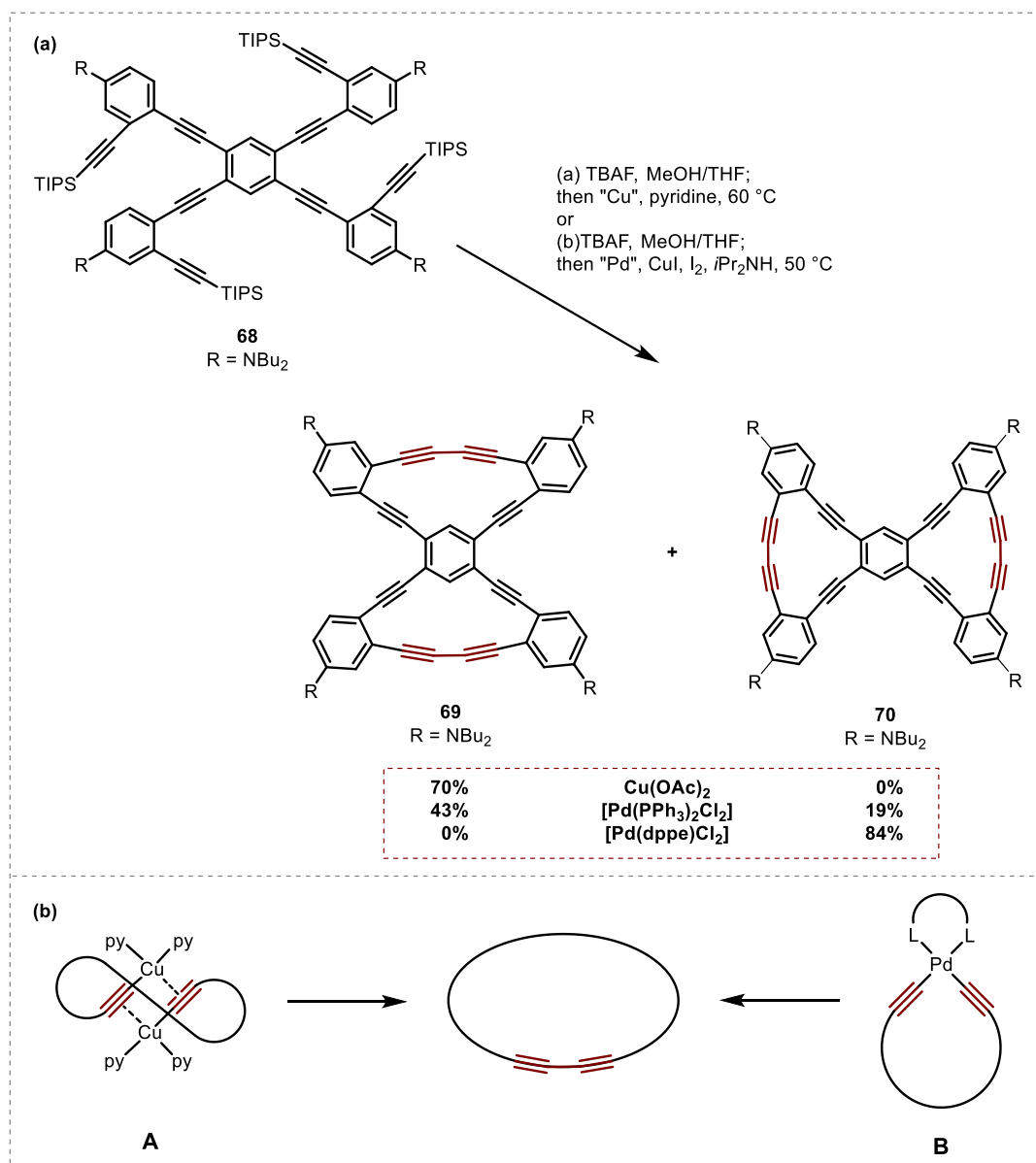


Figure 26: (a) An overview of reaction conditions for preparation of bis[15]annulene (**69**) and bis[14]annulene (**70**). (b) Proposed metal intermediates formed in copper-mediated **A** (left) and palladium-catalysed **B** (right) homocoupling reaction. This figure was reproduced from *Haley et al.*¹⁶²

3.1.2.2 Platinum Corner-Assisted Macrocyclization

The last strategy for closure of an angle-strained diyne-containing π -conjugated macrocycle is performed via the formation of platinum(II) diyne complexes similar to the palladium-catalyzed procedure. The desired macrocycle is assembled via the introduction of the transition metal center as a corner point in the cyclic backbone, followed by reductive elimination. However, compared to the unstable palladium-intermediate, which directly undergoes reductive elimination, the platinum-intermediate is stable even during purification and can be isolated in a good yield.¹⁵⁰ Afterward, the platinum-corner can be expelled under the simultaneous formation of a new C-C bond and provide the conjugated macrocycles via reductive elimination. A *cis*-platinum(II) complex is a perfect candidate for such a corner-assisted cyclization due to the unique pseudo-square planar geometry with an angle of about 90° .^{163,164} This particular angle allows the direct introduction of the platinum corner into the cyclic backbone and benefits the formation of a defined macrocycle. Due to this attractive geometry, the appearance of further macrocycles and linear polymers is suppressed. In addition, treating the platinum(II)-intermediate with iodine leads to the formation of octahedral platinum(IV)-complexes with two iodides attached to the metal center, providing the desired macrocycles under the liberation of $\text{Pt}^{\text{II}}\text{L}_2\text{I}_2$ -complexes (see Figure 27).^{164–167}

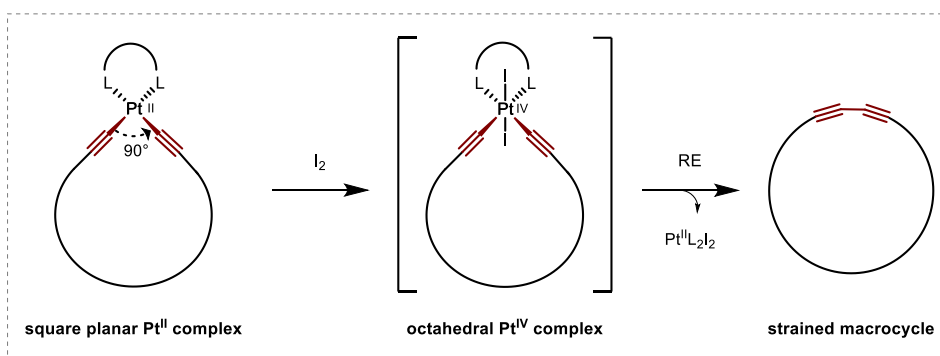
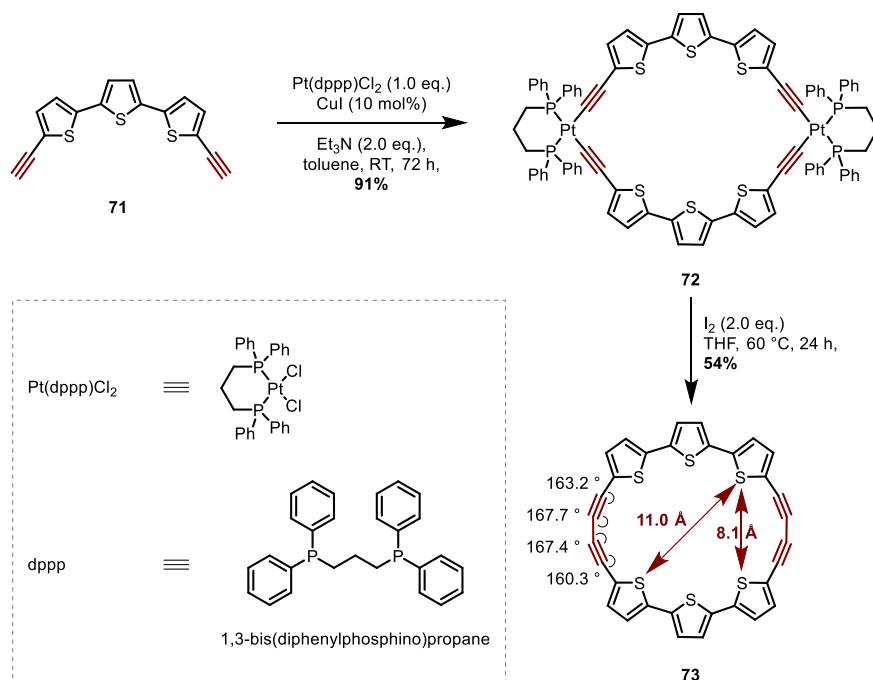


Figure 27: Schematic representation of the introduction of a Pt-corner followed by reductive elimination (RE) with iodine. L-L is an abbreviation for a ligand, and RE is an abbreviation for reductive elimination.

In 2003, *Bäuerle and co-workers*¹⁵⁰ reported the above-described ring closing strategy on the example of the preparation of the fully conjugated octithiophene macrocycle comprising exclusively thiophenes. This strategy provided corresponding strained-angle butadiyne precursor **73** (see Scheme 12), which was not accessible yet with the copper-mediated reactions.¹⁶⁸ The precursor molecule **73** was obtained using $\text{Pt}(\text{II})(\text{dppp})_2\text{Cl}_2$ as a metal corner, providing the platinum-intermediate **72** with an excellent yield of 91%. However, it turned out that the most significant disadvantage of this strategy was reductive elimination since the platinum(IV) complex can undergo *cis-trans* isomerization providing the most stable isomer. In dependence on the isomer configuration, the reductive elimination can provide the new C-C

bond or competitive halide alkyne formation.^{167,169} Nevertheless, the desired butadiyne compound **73** was isolated in 54% yield.¹⁵⁰



Scheme 12: *Cis*-Pt-corner assisted macrocyclization of diene-containing macrocycles **73**.¹⁵⁰ The angles, as well as the longest and shortest S-S distance for angle-stained cyclo[8]thiophene precursor, were adopted from *Miki et al.*¹²⁹

3.2 Project Description

The charge transport in single-molecule measurements can occur via two different pathways: through-bond (see Figure 28a) or through-space (see Figure 28b). The goal of this work is the preparation and examination of a molecule with competing conductivity pathways, where the envisioned design should combine the through-space and through-bond charge transport, as depicted in Figure 28c. The through-space pathway, which occurs via π - π interaction between vis-à-vis located molecular wires, can be achieved by the introduction of a PCP building block in the molecular wire, which is connected to the electrodes. The second requirement, the through-bond conductance pathway, can be accomplished by tethering the PCP moiety with a π -conjugated macrocycle. The introduction of the three-dimensional PCP building block induces a step in the macrocyclic structure, providing a loop shape for the through-bond pathway. This loop scaffold enables helical charge transport, making the pathway coil-like and susceptible to the applied magnetic field. Since the applied current can simultaneously proceed through both pathways, providing the observed conductivity as a mixture of both. This unique feature of coil-related scaffold enables the exploitation of a magnetic field, hopefully allowing unambiguous distinction between both pathways. In addition, the PCP scaffold induces the helical chirality in the macrocyclic ring, making the molecular loop not only intriguing for its potential physical properties in single-molecule junctions but also for the feasible chiroptical features.

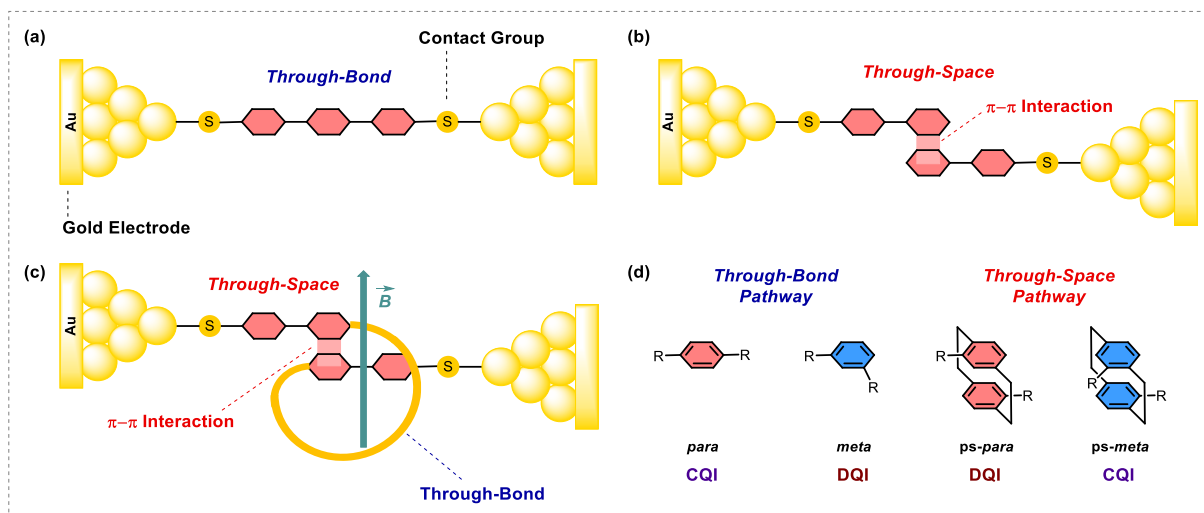


Figure 28: Schematic representation of (a) through-bond and (b) through-space electrical pathways implemented in an electrical circuit. (c) Combination of both pathways in one model compound, where the step in the macrocycles induces the helicity and makes it sensitive to an applied magnetic field. (d) QI depends on substitution pattern in benzene (through-bond pathway) and [2.2]paracyclophane (through-space pathway).

As we already know, through-bond coupled and through-space interacting benzene-based systems with the same substitution pattern possess different QI effects influencing the

conductivity properties (see Figure 28d and Chapter 2). Therefore, for our purpose, pseudo-*meta* substituted PCP core with CQI features and higher conductivity values seems to be a more appealing candidate as a pseudo-*para* analogue. Further advantages of pseudo-*meta* substitution are discussed in the following pages.

3.3 Molecular Design

Previous investigations of suitable model compounds within the group were performed by *Dr. K. J. Weiland*, where the first generation of possible candidates **75** and **76** were synthesized (see Figure 29). The first design comprises PCP-based molecular wire tethered in a pseudo-*para* position to oligothiophenes, which are known for their electronic properties.^{170,171} Molecular loops **75** and **76** were assembled using an iterative approach introducing thiophenes pair-wise in a sequential procedure to investigate the appropriate macrocycle size.⁶⁶ This strategy led to a long, linear, and complex synthesis providing an unstable target macrocycle **76a**, which unfortunately decomposed during purification attempts. Therefore, **76a** was not isolated and only confirmed by high-resolution mass spectrometry.¹²⁸ Accordingly, the design of the molecule was modified, and the linear ethynyl methyl benzoate **76b** was introduced instead of gold anchoring groups. Such replacement improved the molecule's stability.⁶⁵ However, due to the absence of the anchoring groups, the molecule was not integrated into the MCBJ setup to examine the electronic properties.

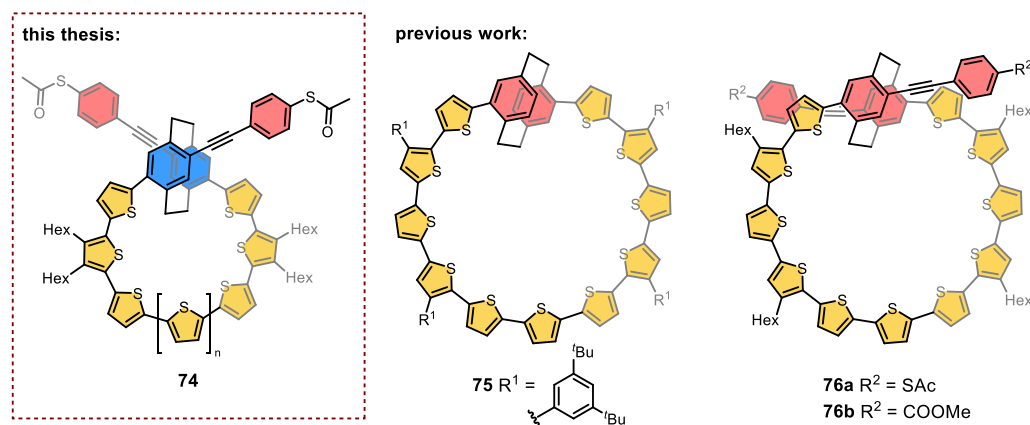


Figure 29: This thesis' ultimate target structure **74** and the *ps-para* PCP-based molecular loops **75**⁶⁶ and **76**⁶⁵ investigated by *Dr. Kevin J. Weiland*.¹²⁸

A novel design of molecular loop **74** was based on an exchange of the substitution pattern in the central PCP moiety (see Figure 29). A new PCP synthon with *ps-meta* connectivity demonstrates the CQI feature for both pathways, increasing the conductivity values compared to the first generation of model compounds. In addition, the through-bond conductivity is enhanced due to the decrease in the loop size. A lower number of thiophene repeating units

also enables the introduction of thiophene chains in a highly convergent synthesis, reducing the number of synthetic steps.

Cyclo[*n*]thiophenes (C_{*n*}T) were chosen as a motif for the helical subunit that imitates a coil and provides a through-bond conductivity in our conjugated macrocycles. The macrocyclic oligothiophenes were already prepared in different sizes (**77** and **78a – c**) and extensively studied by *Bäuerle et al.*, starting from the terminally ethynylated terthiophenes (see Figure 30).^{150,168} The library of macrocyclic terthiophene-diacetylenes **79a – c** was prepared in one pot in a statistical copper-mediated macrocyclization reaction.¹⁶⁸ However, the smallest possible so far reported macrocycle **73** was obtained via a platinum intermediate, where the synthetic pathway was discussed in the introduction 3.1.2.2.¹⁵⁰ Due to the fact that electronic properties of the molecules depend on the length of the conjugated chain, with the rule of thumb that the shorter one would lead to higher conductivity, the smallest possible cyclo[8]thiophene structure **77** was taken as a basis for the design of the desired structure. Therefore, one of the thiophenes units was replaced by PCP moiety, providing the desired loop structure **74a**.

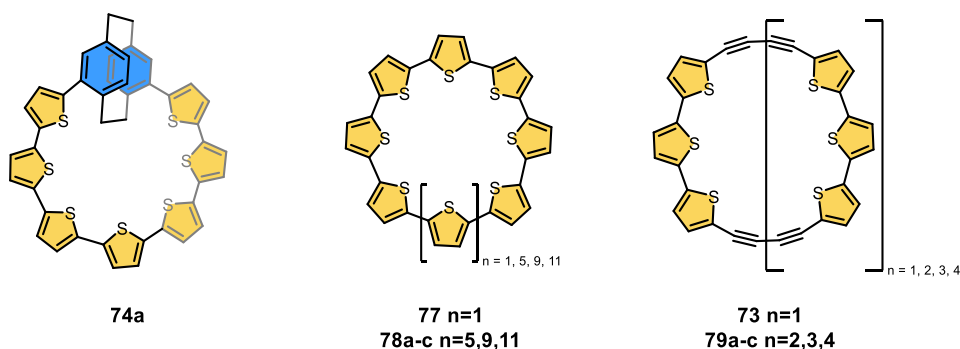


Figure 30: Ring size of envisaged oligothiophene macrocycle **74a** based on the size of smallest representative **77** of cyclo[*n*]thiophene family **78a – c** and macrocyclic terthiophene-diacetylene **73** and **79a – c** developed by *Bäuerle et al.*^{150,168} For simplicity, the solubilizing and anchoring groups were hidden.

3.4 Synthetic Strategy

The elaborate retrosynthetic plan toward the desired molecular loop **74** is illustrated in Figure 31. The last stage modification would be introducing phenyl rings bearing the thioacetate functional groups via *Sonogashira-Hagihara*³³ cross-coupling reaction. The free acetylene **80** can be formed via homologation. For instance, **80** can be obtained by treating the corresponding aldehyde **81** with the *Bestmann-Ohira*^{119,120} reagent or *Corey-Fuchs* reaction sequence.¹⁷² The envisioned molecular loop comprises an odd number of thiophene units. Therefore, the formation of a septithiophene macrocycle is expected to be achieved from the corresponding butadiyne macrocycles **81**, which can be prepared via acetylenes

intramolecular homocoupling reaction. Adequately functionalized terthiophene with hexyl chains on both β -position of central thiophene subunit for enhanced solubility and protected acetylene on a terminal α -position **83** can be introduced in a *Suzuki-Miyaura* cross-coupling. This disconnection enables the assembly of six thiophenes and the required terminal alkynes **83** in one synthetic step to the central tetrasubstituted PCP core **82**, compared to a previously used linear and iterative approach.

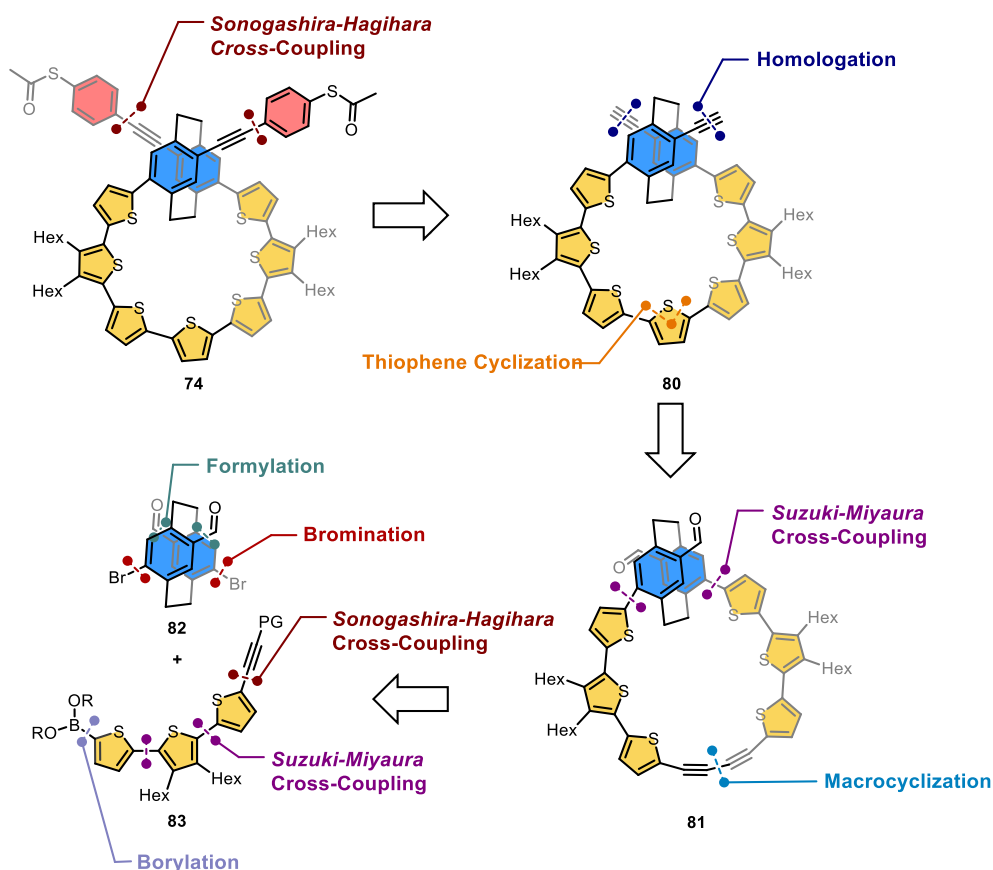


Figure 31: Synthetic strategy for the synthesis of molecular loop **74**. The abbreviation PG stands for protecting group. All disconnections in the retrosynthetic analysis are marked with colors dependent on the reaction type.

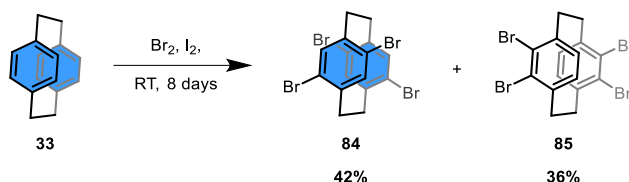
The terthiophene **83** should be accessible by *Sonogashira-Hagihara* cross-coupling reaction introducing the protected acetylene followed by borylation to previously prepared terthiophene scaffold, which can be constructed via a *Suzuki-Miyaura* cross-coupling reaction. The highly functionalized PCP-core **82** bearing two aldehydes and two bromines could be prepared in two different synthetic pathways. The first option would be to perform statistical four-fold bromination to get tetrabromo bis-(*ps-meta*)-*para* PCP followed by statistical lithiation¹⁷³ to obtain the desired bis-(*para*)-*ps-meta* PCP **82** on a gram scale. On the other hand, the desired structure can also be prepared from dibromo *ps-meta* PCP (**43**)⁸³ followed by regioselective double *Rieche* formylation, which has been reported so far only on mg scale.¹⁷⁴ Due to the

modification of the desired building block via several synthetic steps, the robust chemistry well established on a gram scale seems to be more appealing.

3.5 Results and Discussion

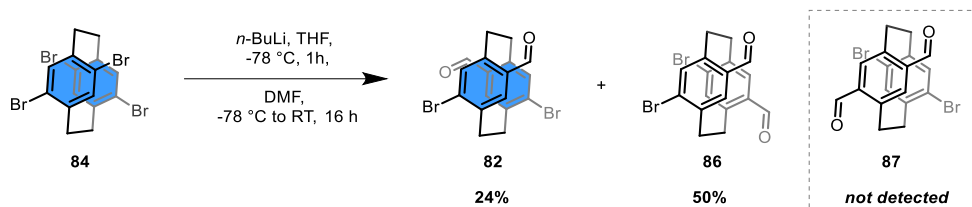
3.5.1 Synthesis of the Central PCP-Moiety

The first step of the synthesis consists of the four-fold bromination of commercially available PCP (**33**) to provide a mixture of constitutional isomers in a 1:1 ratio. There are several conditions for this bromination, for example, with *N*-bromosuccinimide (NBS)¹⁷⁵ or elementary bromine. The latter is used as bromine vapors,¹⁷⁶ neat¹⁷⁶, or iron-catalyzed in dichloromethane.¹⁷⁷ The best results on the gram scale were reported for an iodine-catalyzed reaction in neat bromine.^{176,178} Therefore, these conditions were used for the four-fold bromination, and the reaction provided a mixture of two isomers **84** and **85**, which could be separated by recrystallization. This purification strategy worked very well due to the lower solubility of undesired bis-(*ps-meta*)-*ortho*-PCP (**85**) in dichloromethane, providing tetrasubstituted PCP **84** in 42% and **85** in 36% yield, respectively.



Scheme 13: Synthesis of tetrabrominated bis-(*ps-meta*)-*para*- (**84**) and bis-(*ps-meta*)-*ortho*-PCP (**85**). The nomenclature used is based on the suggestion of Hopf and co-workers.⁸³ Abbreviation *ps* stands for pseudo and describes the spatial relation between the substituents of different PCP rings.

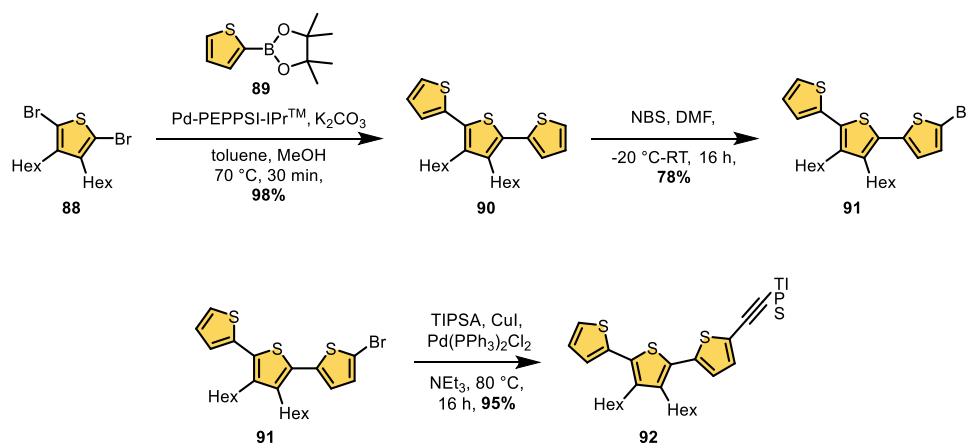
Next, the aldehydes were introduced via formylation reaction. The desired formylation was achieved using a selective lithiation approach.¹⁷³ For the two-fold lithiation, previously prepared tetrabrominated bis-(*ps-meta*)-*para*-PCP (**84**) was treated with a slight excess of 2.1 equivalents of *n*-BuLi followed by the addition of DMF to provide two isomers in a disadvantage 1:2 ratio of the desired structure **82** and by-product **86** determined by the crude NMR. However, the double lithiation on the same ring is not favored; therefore, **87** was not detected.



Scheme 14: Synthesis of bis-(*para*)-pseudo-*meta* (**82**), bis-(*para*)-pseudo-*ortho* (**86**) substituted PCP. Bis-(*ps-ortho*)-*para*-PCP (**87**) was not formed.

3.5.2 Synthesis of the Terthiophene Derivative

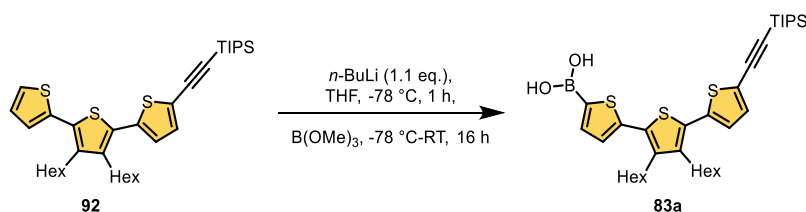
The synthesis of building block **92** started with assembling terthiophene from commercially available 2,5-dibromo-3,4-dihexylthiophene (**88**) and thiophene-2-boronic acid pinacol ester (**89**) (see Scheme 15). Both compounds were coupled via *Suzuki-Miyaura* cross-coupling reaction, providing the desired terthiophene scaffold (**90**) in 98% yield on a multigram scale. The next step is the asymmetrical bromination with NBS. The selectivity of the bromination can be controlled with a low temperature favoring the α -position over the β -positions. Even a tiny excess of NBS provides an overreaction and leads to bromination on the second α -position of terthiophene **91**. Therefore, the reaction was performed in the dark at $-20\text{ }^{\circ}\text{C}$ with only 1.1 eq. of NBS, providing the desired α -monobrominated compound (**91**) in 78% yield. Nevertheless, traces of α -dibrominated by-product were observed but could be easily separated by column chromatography. Subsequently, the α -monobrominated terthiophene **91** has reacted with triisopropylsilyl (TIPS) masked acetylene in the *Sonogashira-Hagihara* cross-coupling reaction to provide terthiophene **92** in 95% yield.



Scheme 15: Synthesis of terthiophene derivative **92**.

3.5.3 Borylation of Terthiophene Derivative and Assemble of Loop Precursor

With terthiophene building block **92** in hand, the next step is the introduction of a boronic acid or ester in the free α -position as a chemical handle for the planned *Suzuki-Miyaura* reaction. First, the preparation of boronic acid was usually more appealing since it is more reactive than a boronic ester analogue for the following *Suzuki-Miyaura* reaction. Therefore, terthiophene boronic acid **83a** was prepared by lithiation of terthiophene **92** with *n*-BuLi, followed by the addition of trimethyl borate and an acidic aqueous workup (see Scheme 16). While a color change to green was observed upon lithiation, only the mass of the starting material was detected by MALDI-ToF-MS. The reaction mixture was investigated by ^1H NMR; however, the obtained spectrum was not conclusive and showed a presence of starting material and several different borylated species. Since the purification of boric acids is difficult due to the reactivity and lability of the compounds, it was decided to use it in the next step without further purification and isolate the product after the following step.

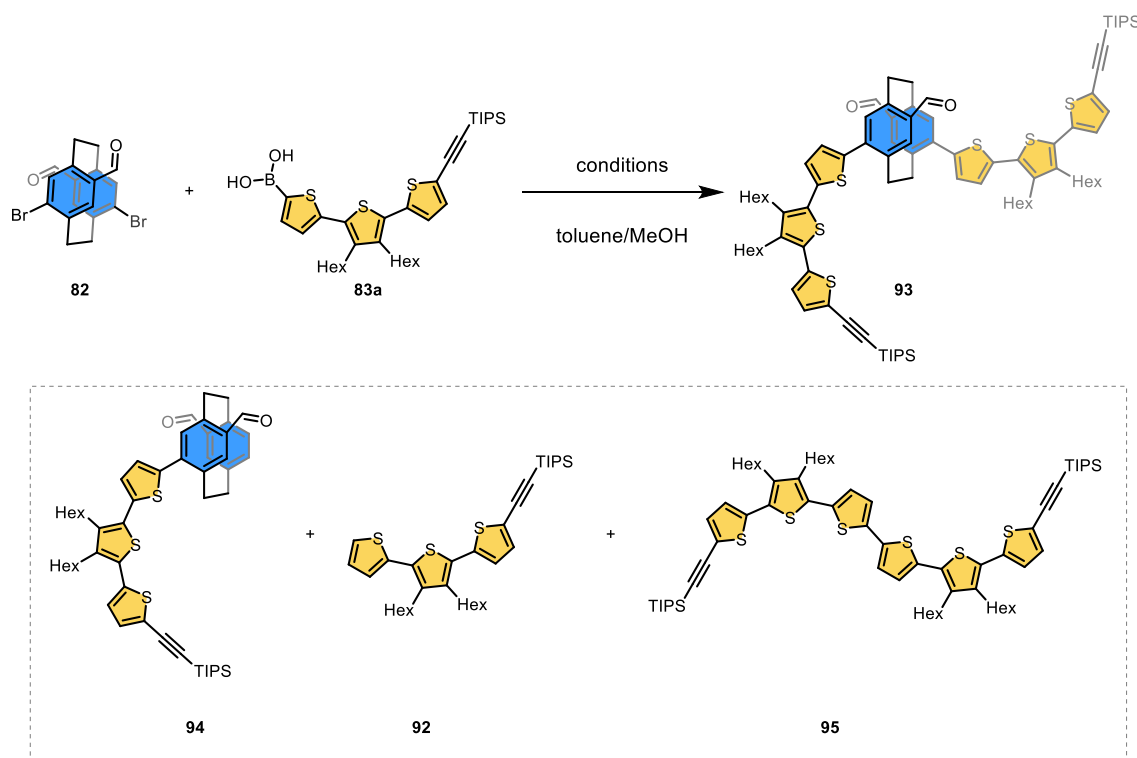


Scheme 16: Borylation of terthiophene building block **83a**.

The next step is the assembly of the previously prepared building blocks, namely PCP derivative **82** and boronic acid **83a** under *Suzuki-Miyaura* conditions (see Table 1). Firstly, the *Suzuki-Miyaura* conditions with Pd-PEPPSITM-*t*Pr and potassium carbonate as a catalytic system in toluene and methanol were tested following the procedure of *Weiland et al.* from a comparable system⁶⁵ (see entry 1). The reaction was carried out at 70 °C, and after 30 minutes, full conversion of the starting material **82** was observed according to TLC. However, these reaction conditions led to a complex product mixture, which contained the desired structure **93** and debrominated intermediate **94**, deborylated starting material **92**, and sexithiophene derivative **95** according to the MALDI-ToF-MS analysis. These observations also explain the low yield of 29% for the desired product **93**, which was obtained after purification by column chromatography. Increasing the temperature to 80 °C favored the formation of by-products (entry 2), which resulted in a lower yield of 12% for the target **93**. Thus, the catalytic system was changed for (Pd(dppf)Cl₂) and tripotassium phosphate, already established for the *ps-para*-PCP loop by *Weiland et al.*⁶⁵ The reaction mixture was heated to 80 °C and stirred for two hours providing the desired loop precursor **93** in 26% yield (entry 3). Since the previous reaction was not selective enough and unsuitable for purification techniques to provide only

the desired boric acid **83a**, the following *Suzuki-Miyaura* cross-coupling can not be optimized with impure starting material. Furthermore, the impurities probably led to the formation of several by-products.

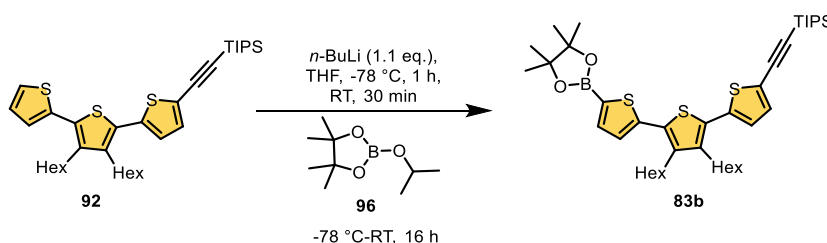
Table 1: Conditions for *Suzuki-Miyaura* cross-coupling reaction to obtain loop precursor **93**.



| Entry | Catalyst | Base | Temperature | Time ^[a] | MALDI-ToF-MS | Yield ^[b] |
|-------|------------------------------|--------------------------------|-------------|---------------------|-----------------------|----------------------|
| 1 | Pd-PEPPSI TM -iPr | K ₂ CO ₃ | 70 °C | 30 min | 93, 94, 92, 95 | 29% |
| 2 | Pd-PEPPSI TM -iPr | K ₂ CO ₃ | 80°C | 30 min | 93, 94, 92, 95 | 12% |
| 3 | Pd(dppf)Cl ₂ | K ₃ PO ₄ | 80°C | 120 min | 93, 92 | 26% |

^[a] Time until full consumption of the starting material (**82**); ^[b] isolated yield after column chromatography.

Therefore, we decided to change the strategy and move away from the boronic acid terthiophene derivative **83a** to the more stable boronic pinacol ester **83b** analogue. First, conditions for the borylation of thiophene-based compounds described in the literature,^{65,179–181} were tested. The terthiophene pinacol boronic ester **83b** was prepared by lithiation of terthiophene **92** with *n*-BuLi at -78 °C, where the reaction mixture was stirred for one hour at -78 °C, followed by allowing warming up to room temperature for 30 minutes. Afterward, the reaction mixture was cooled to -78 °C before 2-isopropoxy-4,4,5,5-tetramethyl-1,3,2-dioxaborolane (**96**) was added and stirred for additional 16 hours.



Scheme 17: Borylation of terthiophene building block **92**.

The obtained green-colored reaction mixture was analyzed by low-resolution MALDI-ToF-MS spectrometry using DCTB as a matrix in a reflective polarized (RP) mode. Thereby, a mixture of several compounds was identified (see Figure 32). The desired borylated compound **83b** (m/z $[M]^+$ calcd. for $C_{41}H_{63}BO_2S_3Si$ 722.385, found 722.573; see Figure 32c) was corroborated, with a isotop pattern perfectly matching the calculated pattern. However, there were several peaks that could be identified as either starting material **92** (m/z $[M]^+$ calcd. for $C_{35}H_{52}S_3Si$ 596.300; found 596.653; see Figure 32a), terthiophene bearing boronic acid **83a** (m/z $[M]^+$ calcd. for $C_{35}H_{53}BO_2S_3Si$ 640.307; found 640.609; see Figure 32b), and numerous overreacted compounds which were also lithiated in β position **97** – **99** (m/z $[M]^+$ calcd. for $C_{41}H_{64}B_2O_4S_3Si$ 766.392; found 767.142; m/z $[M]^+$ calcd. for $C_{51}H_{82}B_2O_4S_3Si$ 904.533; found 903.490; m/z $[M]^+$ calcd. for $C_{57}H_{93}B_3O_6S_3Si$ 1030.618; found 1029.324, respectively; see Figure 32d-f). Figure 32 illustrates only one of the possible constitutional isomers. Of course, there are more by-products due to the different connectivity opportunities. We also assume that the boronic acid derivatives were formed from the boronic pinacol ester analogue during the ionization in the MALDI-ToF-MS.

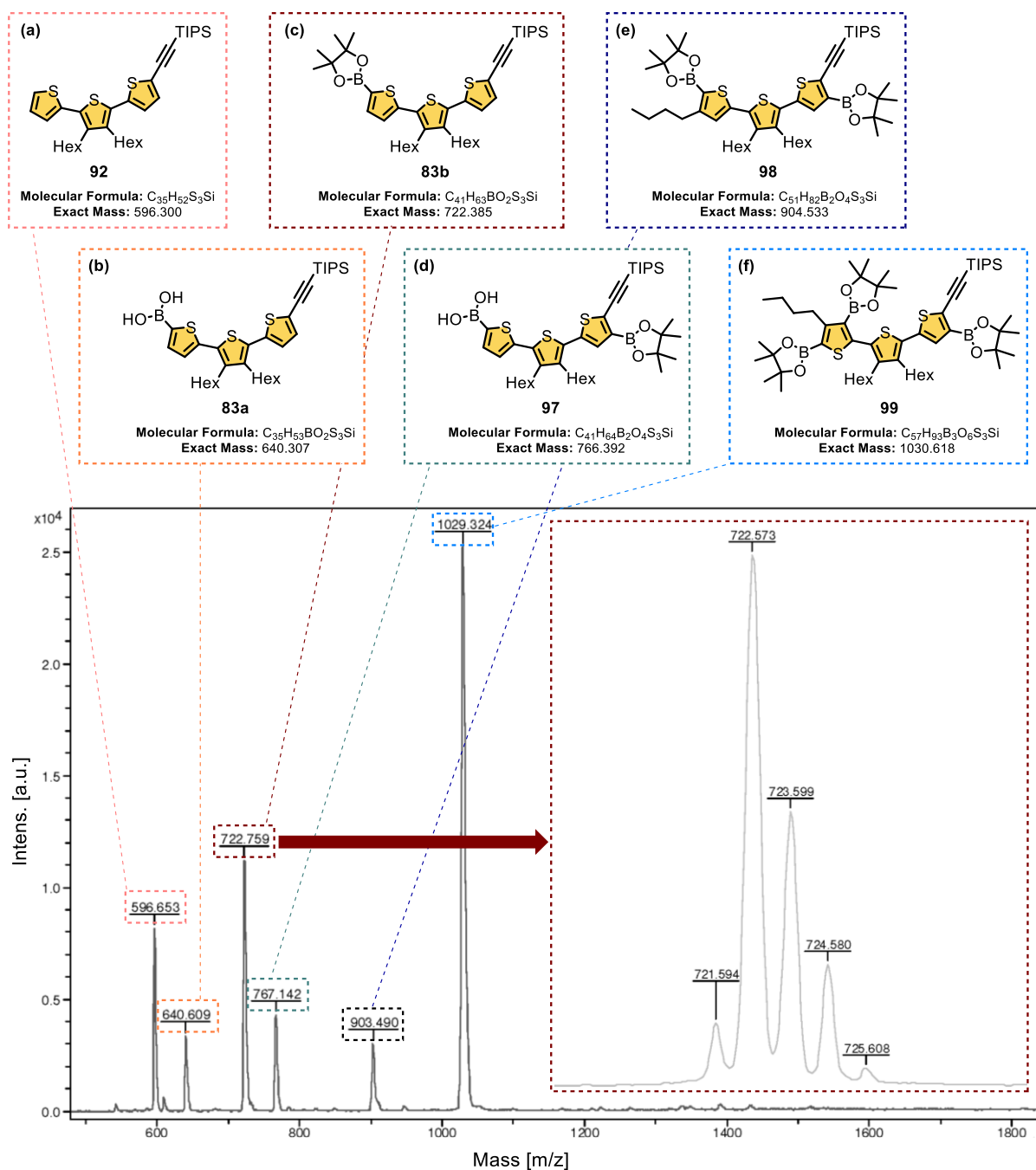


Figure 32: Proposed structures (a-f) and MALDI-ToF MS spectra of the reaction mixture obtained from the reaction shown in **Scheme 17** using DCTB as a matrix in reflective polarized mode. The mass assigned to according proposed structure are colored in the same color and connected with a dashed line. On the right side, the measured m/z pattern of the peak of desired structure **83b** is depicted.

The purification of the obtained complex mixture with oily texture seemed challenging since purification by column chromatography could lead to deborylation and the formation of additional by-products.¹⁸² Due to the significant difference in the size of by-products compared to the desired structure **83b**, automated cyclic gel GPC was considered as a purification technique of choice. Indeed, the separation of several compounds was achieved by GPC (see Figure 33a). Besides the expected overreacted compounds **97** – **99** (pink peak) and starting

material **92** (dark cyan peak), two peaks eluted a molecule with the mass (blue and violet) of the desired structure **83b**. The identity of both peaks was elucidated by NMR spectra (see Figure 33b). The blue peak (see NMR II) was identified as the desired structure **83b**, which was confirmed by ^1H NMR spectra due to the characteristic shift and symmetry of β -thiophene protons. Contrariwise, the violet peak (see NMR III) demonstrated a proton at the α -position, which interacts with both protons in the neighboring β -positions similar to the ^1H NMR of the starting material **92** (see NMR I). A further piece of evidence for the structural assignment came from the singlet at 7.27 ppm, which allowed us to assume the borylation on the β -position of the thiophene bearing the protected acetylene in terthiophene scaffold.

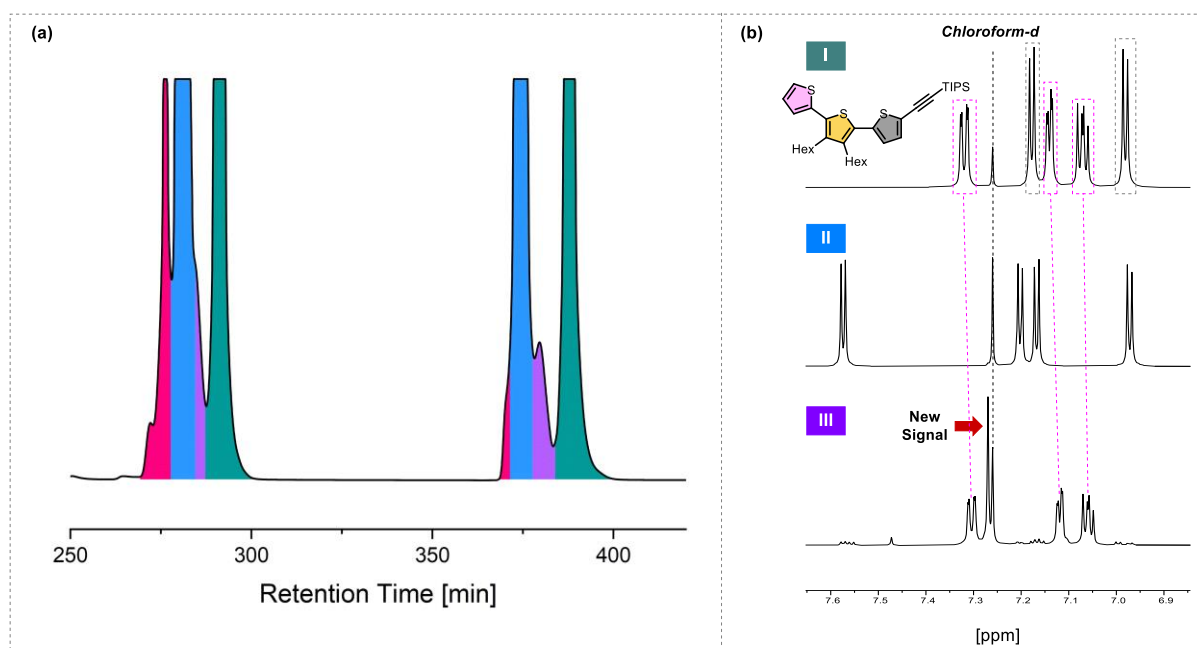
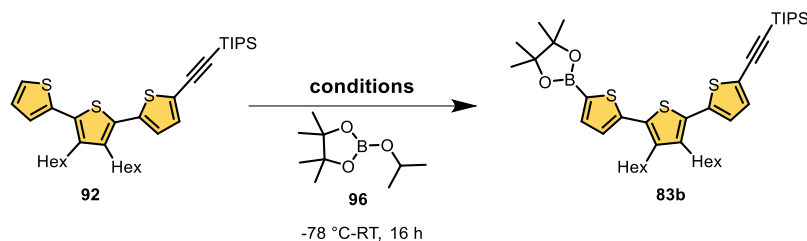


Figure 33: (a) GPC chromatogram traces of separation of borylated terthiophene, where the pink peak is overreacted terthiophene, blue is the desired structure **83b**, violet is a borylation in a β -position, and dark cyan is the starting material **92**. (b) Comparison of the aromatic region of ^1H NMR spectra of starting material (dark cyan) with both peaks (blue and violet) demonstrating the same peaks in the MALDI-ToF-MS. Second spectrum was assigned to the desired structure, and the third to the borylation in the β -position.

To prevent the formation of by-products, further lithiation attempts were performed, keeping the temperature permanent at $-78\text{ }^\circ\text{C}$ (see Table 2). The lithiation at a low temperature leads to a selective reaction at the α -position of terthiophene derivative **92**. However, it also provides a low conversion to the desired product **83b** (entry 1). Therefore, the time for the lithiation was increased, and the amount of $n\text{-BuLi}$ decreased (entry 2 - 4), which improved the conversion and provided the best result of the desired **83b** in 72% yield (entry 4) according to ^1H NMR spectra. The desired terthiophene derivative **83b** was used directly in the subsequent *Suzuki-Miyaura* reaction without further purifications. However, in order to obtain a full conversion, further reaction modifications are necessary, such as increasing the lithiation time to 120 min

or using a milder base such as lithium diisopropylamine (LDA)^{183,184} at higher temperature instead of *n*-BuLi.

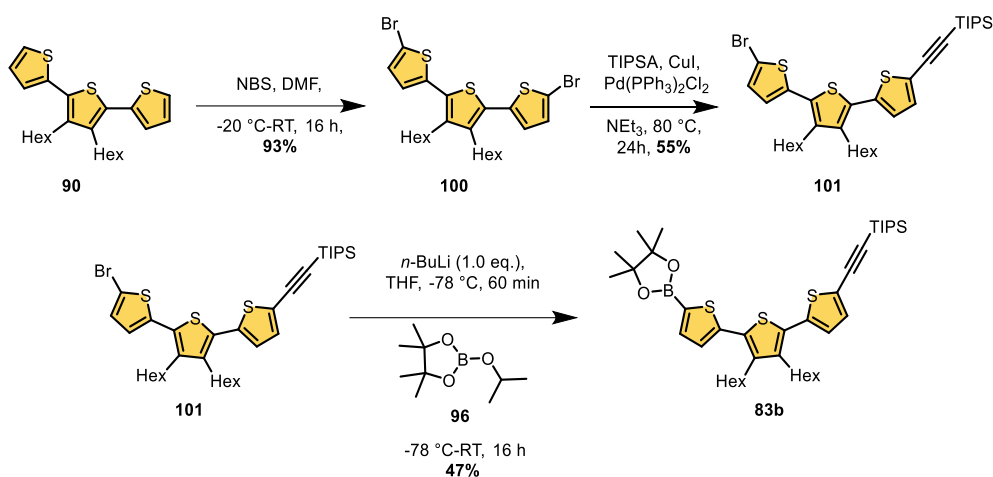
Table 2: Optimization of the terthiophene derivative **92** borylation reaction.



| Entry | <i>n</i> -BuLi [eq.] | Temperature [°C] | Time [min] | 92 : 83b ^[a] |
|-------|----------------------|------------------|------------|---------------------------------------|
| 1 | 1.1 | -78 | 30 | 3:2 |
| 2 | 0.95 | -78 | 30 | 1:1 |
| 3 | 1.0 | -78 | 60 | 2:3 |
| 4 | 1.0 | -78 | 90 | 1:2.8 |

^[a] determined by ¹H NMR spectra

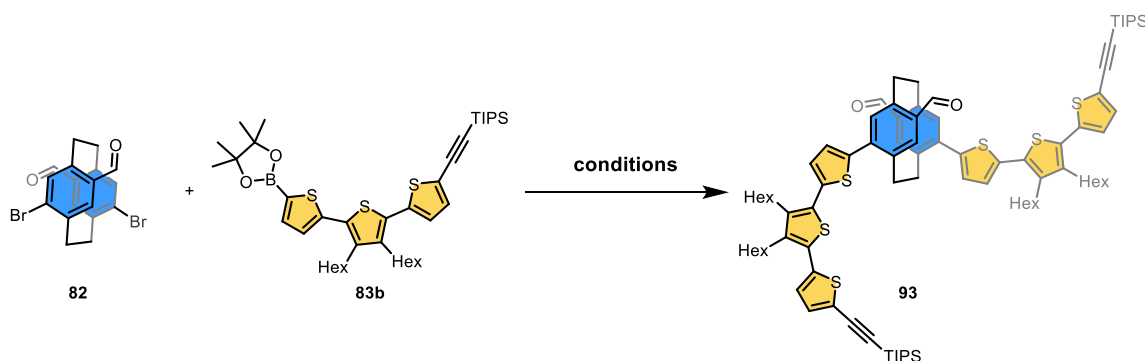
Parallel to the borylation investigations, we also examined another pathway to obtain terthiophene **83b** via a lithium-halogen exchange, where the reaction in α -position should be more preferred. However, another pathway requires an adaption of the synthetic approach (see Scheme 18). The first step was to increase the amount of NBS to 2.1 equivalents to obtain the desired two-fold brominated terthiophene **100** in 93% yield. The subsequent statistical *Sonogashira-Hagihara* cross-coupling was performed using an excess of **100**, and (triisopropylsilyl)acetylene to provide the desired bifunctional terthiophene **101** in a 55% yield. With the compound **101** in hand, the borylation of terthiophene was achieved analogously to the previous attempts (see Table 2). However, full conversion of starting material was still not obtained, and the yield was lower than entry 3 in the previous strategy. Furthermore, the overall yield over three reactions from the synthetic pathway with statistical bromination (see Scheme 15) to the pathway with statistical *Sonogashira-Hagihara* cross-coupling (see Scheme 18) dropped from 52% to 24%, respectively. Another advantage of the first synthetic pathway is the possibility of using the mixture containing **92** and **83b** directly in subsequent *Suzuki-Miyaura* coupling without the formation of further by-products and possible reisolation of **92** after this reaction step. Therefore, we decided to go on with the borylation results summarized in Table 2.



Scheme 18: Synthesis of terthiophene building block **101** followed by borylation reaction to provide **83b**.

The desired loop precursor **93** was obtained in a two-fold palladium-catalyzed *Suzuki-Miyaura* cross-coupling reaction from previously prepared building blocks **82** and **83b** (see Table 3). Initial conditions, with Pd-PEPPSITM-*i*Pr and potassium carbonate as a catalytic system in toluene and methanol, which demonstrated the best yield with the boronic acid analogue **83a**, showed no product formation and decomposition of starting material (entry 1). The conditions were modified by using water as an additive and increasing reaction time (entry 2); however, the product formation was still not observed. Therefore, the palladium source and base were changed (entries 3 and 4), and we found that using Pd(PPh₃)₄ as a catalyst with potassium carbonate as a base led to the formation of desired structure **93** in an excellent yield of 96% (entry 4).

Table 3: Condition screening for *Suzuki-Miyaura* cross-coupling reaction to obtain loop precursor (**93**).

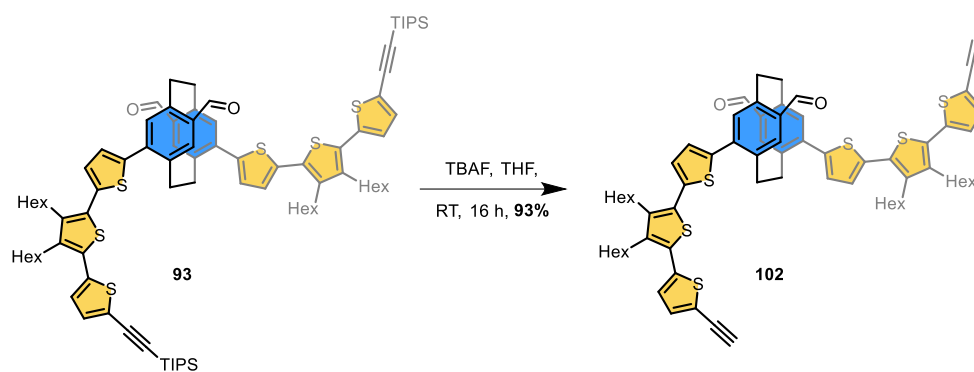


| Entry | Catalyst | Base | Solvent | Temperature [°C] | Time [h] | Yield ^[a] |
|-------|------------------------------------|--------------------------------|-------------------------------|---------------------|-------------|----------------------|
| 1 | Pd-PEPPSI TM -iPr | K ₂ CO ₃ | Toluene/MeOH | 70 | 0.5 | 0% |
| 2 | Pd-PEPPSI TM -iPr | K ₂ CO ₃ | Toluene/MeOH/H ₂ O | 70 | 16 | 0% |
| 3 | Pd(dppf)Cl ₂ | K ₃ PO ₄ | Toluene/H ₂ O | 70 | 16 | 80% |
| 4 | Pd(PPh ₃) ₄ | K ₂ CO ₃ | Toluene/H ₂ O | 70 | 16 | 96% |

^[a] isolated yield

3.5.4 Macrocyclization

The first step in the direction of the intermediate **81** was the deprotection of the TIPS masking group of **93** with tetrabutylammonium fluoride (TBAF) in wetted THF, which afforded the loop intermediate (PCP-based terthiophene-diyne) **102** in 93% yield (see Scheme 19) after purification by column chromatography.

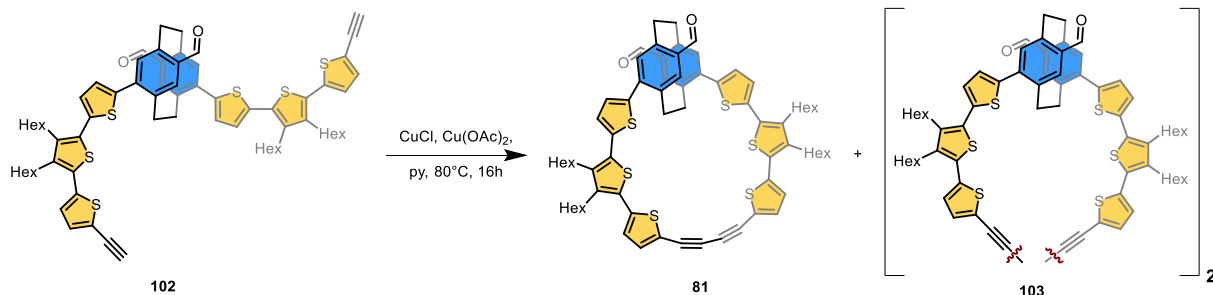


Scheme 19: Deprotection of loop precursor **93**.

3.5.4.1 Copper-mediated Macrocyclization Method

Since macrocyclization was the bottleneck reaction step towards the desired structure, several approaches described in the introduction were examined. The first attempt to achieve the desired molecular loop **81** was done by exploration of the *Eglinton-Breslow* conditions.^{185,186} These conditions were previously shown to result in the ring-closing of strained butadiynes^{187,188} and the molecular loop with *ps-para* connectivity.^{65,66} The oxidative acetylene homocoupling was performed using copper (I) chloride and copper (II) acetate as a copper source in dry and degassed pyridine under an argon atmosphere. The reaction was carried out under pseudo-high-dilution conditions, where the diacetylene **102** was dissolved in pyridine and slowly added (over 14 hours) with a syringe pump to the reaction mixture containing a copper mixture in pyridine at 80 °C (see Scheme 20 and Table 4, Entry 1). Afterward, the reaction was stirred for additional two hours to guarantee full consumption of starting material, which was monitored by TLC. The reaction mixture was analyzed by low-resolution MALDI-ToF-MS and indicated a mass that could be attributed to the desired structure **81** (m/z $[M]^+$ calcd. for $C_{70}H_{74}O_2S_6$ 1138.401, found 1138.943) and the twofold mass (m/z $[M]^+$ calcd. for $C_{140}H_{148}O_4S_{12}$ 2276.803, found 2276.286). Indeed, TLC indicated a formation of new species, which was then purified by column chromatography, isolated, and analyzed by NMR spectroscopy. A simple 1H NMR spectrum was very symmetrical, identifying a macrocyclic structure. However, it was impossible to distinguish between monomeric and dimeric macrocycles at this point. Therefore, diffusion-ordered spectroscopy (DOSY) was measured.

The DOSY spectrum of starting material **102** and the isolated compound were compared and showed that the isolated compound had approximately double the starting material size, unambiguously identifying the new structure as a cyclic dimer **103** (see Supporting Information for Chapter 3).



Scheme 20: Synthesis of the loop precursor **81** using *Eglinton-Breslow* conditions.

Attempting the suppression of dimer formation, the reaction was carried out at a lower concentration (see Table 4, Entry 2). However, instead of increasing the amount of desired macrocyclic structure **81**, such dilution led to the formation of a complex mixture containing exclusively poorly soluble linear polymers.

Table 4: Conditions to *Eglinton-Breslow* homocoupling reaction.

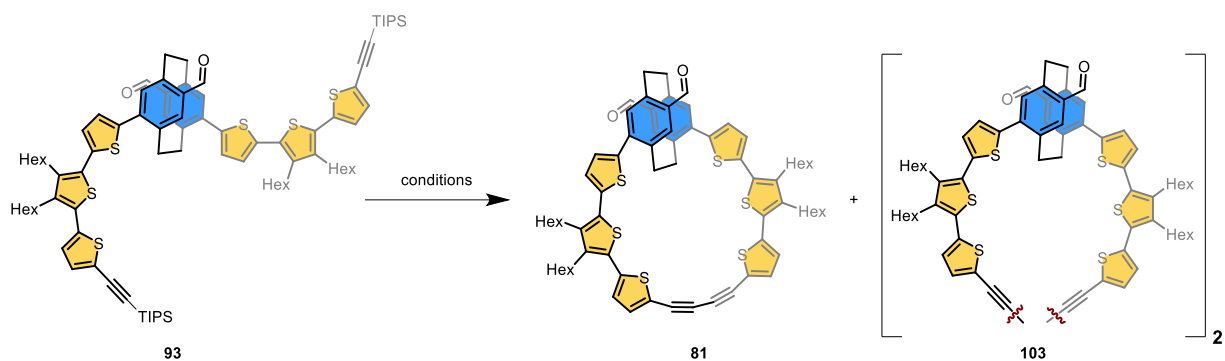
| Entry | 102 conc. [mM] | Time [h] | MALDI-ToF-MS |
|-------|--------------------|------------------------|-----------------------------------------------|
| 1 | 1.5 ^[a] | 16 (14) ^[c] | 81 and 103 (35%) ^[d] |
| 2 | 0.2 ^[b] | 84 (48) ^[c] | Complex mixture |

^[a] same concentration was used for the preparation of *ps-para* PCP-based molecular loop **75**;⁶⁶ ^[b] same concentration was used for the preparation of **76** (see Figure 29);⁶⁵ ^[c] addition time with syringe pump; ^[d] isolated yield.

In the next attempt, copper(II) fluoride dihydrate was used as a copper source. The advantage of such a strategy is deprotection from the masked acetylene and macrocyclization in one pot. These conditions were recently developed in our laboratories and were successful in the formation of strained butadiynes.¹⁸⁹ The initial conditions using DMSO as a solvent at 80 °C due to the low solubility at low temperatures lead only to deprotection (see Table 5, entry 1). Thus, tetramethylethylenediamine (TMEDA) was added to the reaction (entry 2). However, after stirring for 16 hours, no product or dimeric structure formation was identified in the complex mixture. Therefore, the solvent was exchanged for pyridine, in which the starting material was also well-soluble at room temperature. After one hour of stirring at room temperature, full deprotection was observed (entry 3). Again, however, there were no indications of the formation of the desired structure **81** or other cyclic oligomers. When the

reaction mixture was heated to 40 and 50 °C (entries 4 and 5), the dimer was obtained as a major product. Further increase in the temperature and reaction mixture concentration enhances the formation of linear polymers (entry 6).

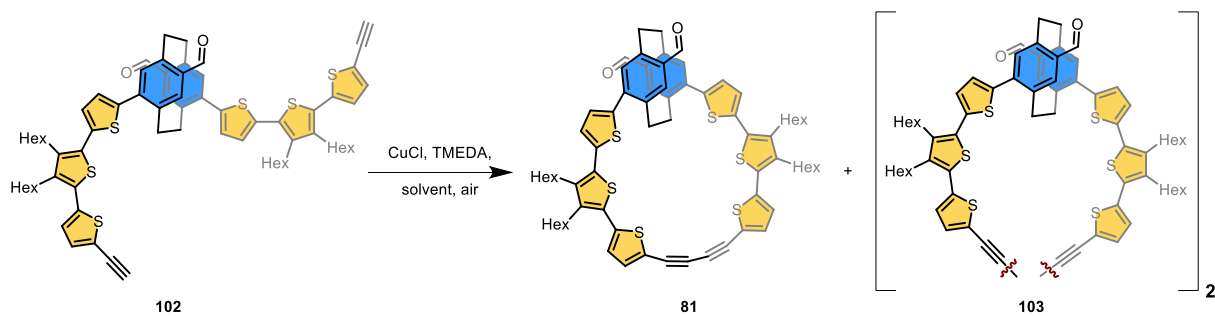
Table 5: Screening conditions for copper-mediated homocoupling with copper(II) fluoride as a copper source.



| Entry | 93 conc. [mM] | CuF ₂ x2H ₂ O [eq] | Solvent | Temp [°C] | Time [h] | MALDI-ToF-MS (Yield) ^[a] |
|-------|------------------|---------------------------------------------|------------|--------------|-------------|----------------------------------------|
| 1 | 0.3 | 6.0 | DMSO | 80 | 2 | Only deprotection (102) |
| 2 | 0.3 | 6.0 | DMSO/TMEDA | 80 | 16 | Complex mixture |
| 3 | 1.0 | 6.0 | pyridine | RT | 1 | Only deprotection (102) |
| 4 | 1.0 | 6.0 | pyridine | 40 | 1 | 103 (36%) |
| 5 | 1.0 | 6.0 | pyridine | 50 | 1 | 103 (38%) |
| 6 | 1.5 | 6.0 | pyridine | 80 | 16 | 103 (8%) |

^[a] isolated yield

In 2014, Hopf and co-workers^{129,190} published the synthesis of several PCP-based angle-strained alkyne-containing macrocycles. All the structures were obtained in a good yield and prepared using the *Glaser-Hay* conditions (see Scheme 21). The main difference between the *Glaser-Hay* conditions and the previously used is the introduction of bidentate ligand (TMEDA) for copper(I) halide, which improves the solubility of copper-source and provides presumably an alternative intermediate to the previously examined *Eglinton* modifications (see Introduction 3.1.2.1).¹²⁹ Therefore, we also decided to investigate these conditions.



Scheme 21: Synthesis of the loop precursor **81** using *Glaser-Hay* conditions.

First, the loop precursor **102** was dissolved in dichloromethane and methanol before adding copper(I) chloride and TMEDA. The copper-mediated homocoupling reaction provided a complete conversion of starting material after two hours of stirring at room temperature. Next, the reaction mixture was analyzed and indicated the formation of the desired loop **81** (m/z $[M]^+$ calcd. for $C_{70}H_{74}O_2S_6$ 1138.401, found 1138.434) and the dimeric macrocycles **103** (m/z $[M]^+$ calcd. for $C_{140}H_{148}O_4S_{12}$ 2276.803 m/z , found. 2277.812) by low-resolution MALDI-ToF-MS. Notably, the isotopic pattern recorded for loop structure **81** perfectly matched the corresponding elemental composition (see Figure 34).

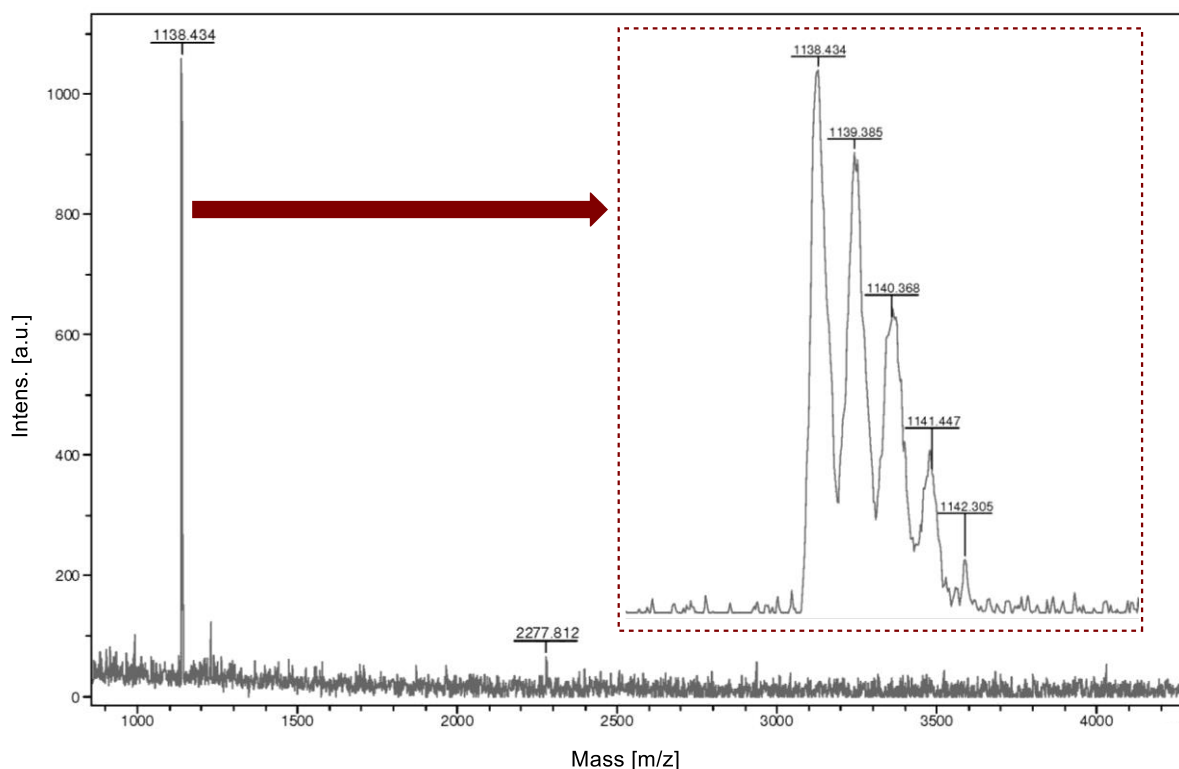


Figure 34: MALDI-ToF-MS spectrum of the reaction mixture with *Glaser-Hay* conditions.

However, isolation and characterization of the desired structure **81** was impossible due to the low amount. Since these conditions seemed to be the most promising ones, they were further investigated. The reactions were monitored by MALDI-ToF-MS and TLC, where the first analytic method indicated the formation of the desired structure, and the second allowed a distinction between the appearance of cyclic and linear oligomers and polymers, respectively. The screening began by looking for the perfect solvent and a ratio of copper chloride to TMEDA (see Table 6). Dichloromethane and toluene were selected due to the good solubility of free diacetylene **102** and the addition of methanol improved the solubility of copper chloride. However, the addition of methanol (entries 1 and 2) increased the formation of insoluble linear oligomers and polymers. On the other hand, the conditions with neat toluene led to no reaction (entry 3). If the reaction was performed in a mixture of toluene and methanol (entry 4) and stirred for 16 h, linear oligomers and polymers precipitated, and only cyclic dimer **103** could be identified from the remaining solution by MALDI-ToF-MS.

Table 6: Screening for *Glaser-Hay* conditions.

| Entry | 102 conc. [mM] | CuCl [eq.] | TMEDA [eq.] | Solvent | Time [h] | MALDI-TOF-MS | TLC^[e] (main spot) |
|-----------------------|-----------------------------|----------------------|-----------------------|---------------------------------------|--------------------|-------------------------------------------|-----------------------------------------|
| 1 | 0.4 | 42.0 | 14.0 | CH ₂ Cl ₂ /MeOH | 2 | 81 and 103 | polymers |
| 2 | 0.4 | 42.0 | 51.0 | CH ₂ Cl ₂ /MeOH | 1 | 81 and 103 | polymers |
| 3 | 0.4 | 42.0 | 84.0 | toluene | 2 | 102 (SM) | 102 (SM) |
| 4 | 0.4 | 42.0 | 84.0 | toluene/MeOH | 16 | 103 | polymers |
| 5 | 1.5 | 42.0 | 84.0 | CH ₂ Cl ₂ | 2 | 81^a and 103 | polymers |
| 6 | 1.0 | 42.0 | 84.0 | CH ₂ Cl ₂ | 2 | 81 and 103 | 103 and polymers |
| 7 | 0.2 | 42.0 | 84.0 | CH ₂ Cl ₂ | 16 | 81^a and 103 | polymers |
| 8 | 0.3 | 10.0 | 20.0 | CH ₂ Cl ₂ | 5 | 102 , 103 and polymers | polymers |
| 9 | 0.3 | 100.0 | 100.0 | CH ₂ Cl ₂ | 3(2) ^b | 102 , 103 , and polymers | polymers |
| 10 | 0.5 | 42.0 | 84.0 | CH ₂ Cl ₂ | 2 | 81 and 103 | 103 |
| 11 | 0.5 | 42.0 | 84.0 | CH ₂ Cl ₂ | 3(2) ^b | 81^a and 103 | 103 |
| 12^c | 0.5 | 42.0 | 84.0 | CH ₂ Cl ₂ | 2 | 81 and 103^d | 103 |

^[a] The mass of loop **81** was only detected after work up; ^[b] slow addition of SM; ^[c] CuCl and TMEDA were dissolved in dichloromethane and stirred for 10 min before SM was added; ^[d] most promising entry according to MALDI-ToF-MS and TLC, was purified by GPC. ^[e] Linear polymers stayed at baseline in pure dichloromethane.

Therefore, pure dichloromethane was chosen as the solvent for further entries. Instead of methanol, the amount of TMEDA was increased to improve the solubility of copper chloride. In the following entries 5 – 9, the influence of the concentration of the starting material was investigated. According to TLC, concentrations over 1.0 mM and under 0.4 mM lead to the exclusive formation of insoluble linear polymers. Furthermore, the increase and decrease in amount of copper chloride and TMEDA (entries 8 – 9) did not enhance formation of cyclic oligomers and of the desired structure **81**. Assuming that the slow addition of the starting material **102** would shift the equilibrium on the side of intramolecular ring closure, this hypothesis was tested (entry 11). However, both the rapid and slow addition of the starting material **102** to pre-dissolved copper chloride and TMEDA solution led to the formation of dimer as the major product according to a TLC. MALDI-ToF-MS also clearly indicated for all three attempts a product (**81**) formation. Therefore, according to the TLC, the most promising reaction mixture (entry 12) was purified by automated recycling GPC.

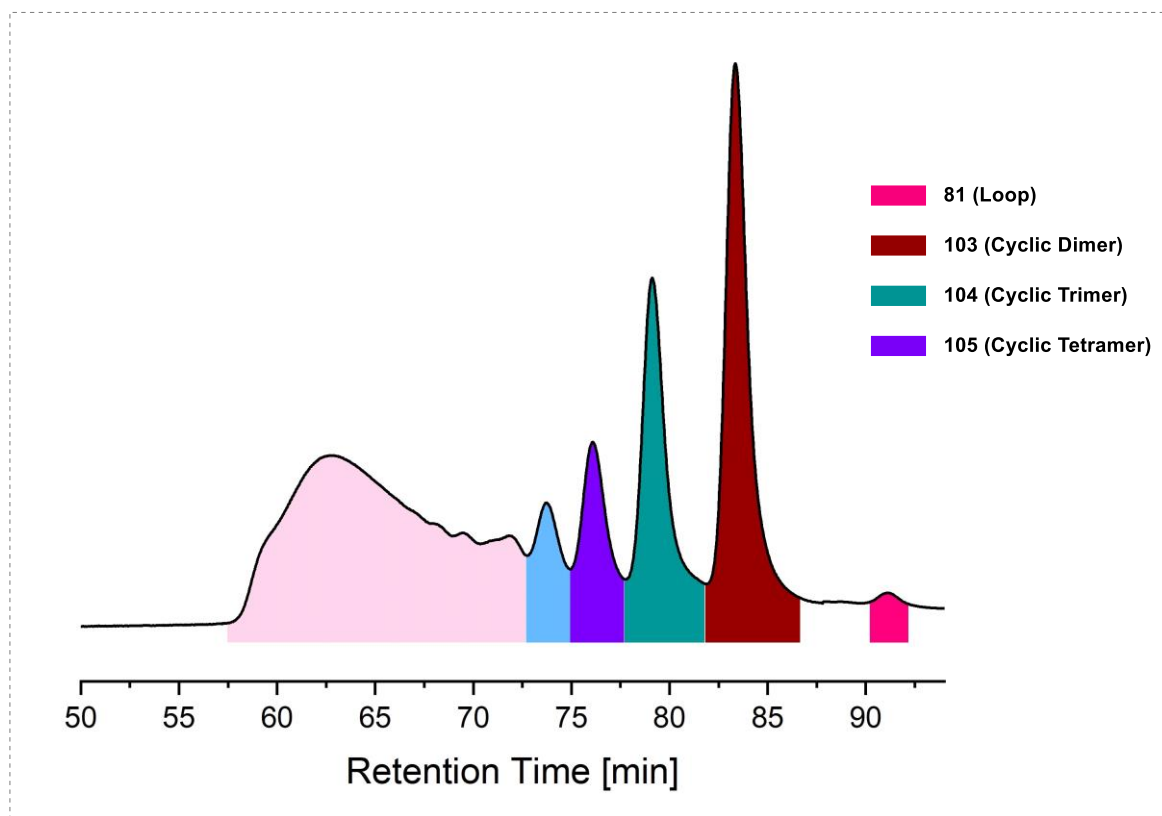


Figure 35: GPC traces of *Glaser-Hay* reaction, entry 12.

Already after the first cycle, the GPC purification provided surprising results (see Figure 35). Besides the linear polymers (light rosa), several cyclic macrocycles (blue to pink, from biggest to smallest) presumably differed in size according to the corresponding hydrodynamic radii of macrocycles derived from their retention time were synthesized. MALDI-ToF-MS also supported these observations, identifying violet peak as a cyclic tetramer **105**, dark cyan as a

cyclic trimer **104**, dark red as a cyclic dimer **103**, and pink as the desired loop structure **81**. Furthermore, the identity of the dimer **103** and trimer **104** was also confirmed by NMR spectroscopy. Unfortunately, the amounts of product **81** and cyclic tetramer **105** were too low for proper characterization.

3.5.4.2 Palladium-Catalyzed Macrocyclization Methode

In the next attempt, we considered using the conditions described by *Haley and co-workers*¹⁶² for palladium-catalyzed ring closure reactions. The advantage of using palladium is the preference for *cis* geometry over *trans* during intermediate formation and, therefore, the formation of a smaller ring with a strained angle, as already discussed in the introduction (see 3.1.2.1). The reported palladium-catalyzed homocoupling of the terminal alkyne is similar to the *Sonogashira-Hagihara* cross-coupling reaction (Pd-source, CuI, amine base) with additional oxidant (iodine) instead of organic electrophile.^{162,191}

Firstly, the palladium(II)-catalyst with the best-reported yield¹⁶² was tested (see Table 7, entry 1). Diacetylene **102** was dissolved in THF and slowly added to the reaction mixture containing a catalytic system in THF/DIPEA at 70 °C over 14 hours. The reaction with a palladium-catalyst bearing the *cis*-bidentate ligand was unsuccessful, demonstrating no conversion after 16 hours, monitored by MALDI-ToF-MS and TLC. These results were explained by the possibly not suitable angle of the bidentate ligand; therefore, palladium-catalyst with a monodentate ligand (Pd(PPh₃)₂Cl₂) was added to the reaction mixture and stirred for additional 16 hours (entry 2). Afterward, MALDI-ToF-MS only indicated the formation of cyclic dimer (**103**) and other cyclic (**104** – **105**) and linear oligomeric structures. In entry 3, the starting material was added slowly to the reaction mixture over two hours at 50 °C. Such temperature decrease and slow addition were expected to slow down the reaction and allow the formation of desired intramolecular homocoupling. However, after stirring for 16 hours, only the formation of cyclic dimer (**103**) and other cyclic (**104** – **105**) and linear oligomeric structures was detected, similar to the previous attempts.

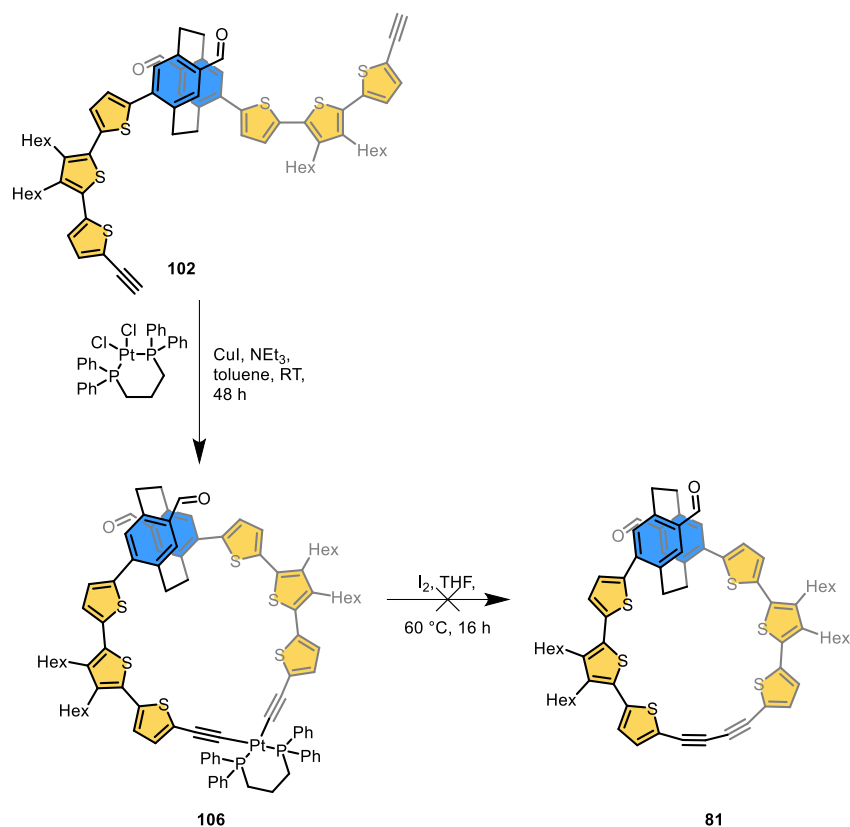
Table 7: Conditions screening for Pd-catalysed intramolecular homocoupling reaction.

| Entry | 102 conc. [mM] | Pd-source | Solvent | Temp [°C] | Time [h] | MALDI-ToF-MS |
|-------|--------------------------|----------------------------------------------------|-----------|--------------|-------------------------|--------------------|
| 1 | 0.5 | Pd(dppe)Cl ₂ ^[a] | THF/DIPEA | 70 | 16 (14) ^[b] | 102 (SM) |
| 2 | 0.5 | Pd(PPh ₃) ₂ Cl ₂ | THF/DIPEA | 70 | 16 | 103 (Dimer) |
| 3 | 0.5 | Pd(PPh ₃) ₂ Cl ₂ | THF/DIPA | 50 | 16 (2) ^[b,c] | 103 (Dimer) |

^[a] Pd(dppe)Cl₂ (dppe = 1,2-bis(diphenylphosphanyl)ethane); ^[b] additional time with syringe pump; ^[c] open flask.

3.5.4.3 Platinum Corner-Assisted Cyclisation Methode

The next option is the introduction of platinum centers as corner points in the cyclic backbone of the molecule, followed by reductive elimination. This strategy already demonstrated the efficiency of synthesizing a cyclo[8]thiophene precursor **73**,¹⁵⁰ which was used as a basis for desired molecular loop **74**. A. D'Addio prepared the employed *cis*-Pt(dppp)Cl₂ complex, which was inserted to form the platinum σ -acetylide complex. *Cis*-Pt(dppp)Cl₂ was chosen due to the chelating ligand, suppressing *cis-trans* isomerization and privileging the *cis* geometry around a platinum-metal center. Such geometry should prevent polymerization as well as the formation of bigger macrocycles. Therefore, the precursor molecule **102** and platinum-corner were stirred in the presence of copper(I) iodide and trimethylamine in toluene. After stirring the reaction mixture for 48 hours, the full consumption of starting material was observed. However, the desired structure **106** was not indicated by MALDI-ToF-MS or NMR spectroscopy. Furthermore, ¹H and ³¹P NMR were inconclusive, providing a spectrum of several compounds. The mixture's separation appeared impossible by normal or reverse phase column chromatography. Therefore, the reaction mixture was used in the next step without further purification. The reductive elimination was carried out in the presence of 2.0 equivalents of iodine at 60 °C.^{150,169} After stirring the reaction mixture for 16 hours, there was no evidence of the formation of the desired structure **81** in MALDI-ToF-MS.



Scheme 22: Synthesis of the loop precursor **81** via the introduction of a Pt-corner followed by reductive elimination.

However, a new species was detected by MALDI-ToF-MS and TLC. High-resolution electron spray ionization-time of flight (HR-ESI-ToF) MS indicated the formation of a diiodinated PCP-based terthiophene-diyne **107** (see Figure 36). The obtained mass of 1415.1966 m/z perfectly fits the calculated mass of **107** adduct (1392.2102 m/z) comprising sodium cation (1415.1995 m/z). Yet, the isolated amount was below 5% yield over two steps and did not allow to perform the complete characterization of the isolated compound due to insufficient amount. However, the iodination of the compound can occur either during the expel of the platinum-corner or after the loop closure on highly reactive strained butadiyne. Both proposed options are depicted in Figure 36b. However, inconclusive data made the determination of the exact structure and formation thereof challenging. Indeed, several challenges which arise during the reductive elimination with iodine, such as various side products and decompositions, were already described by the preparation of cyclo[*n*]thiophenes.¹⁶⁹ Furthermore, the mechanistic studies of reductive elimination with iodine also described the possibility of iodination of closing points as a potential reaction outcome.^{165,167,169}

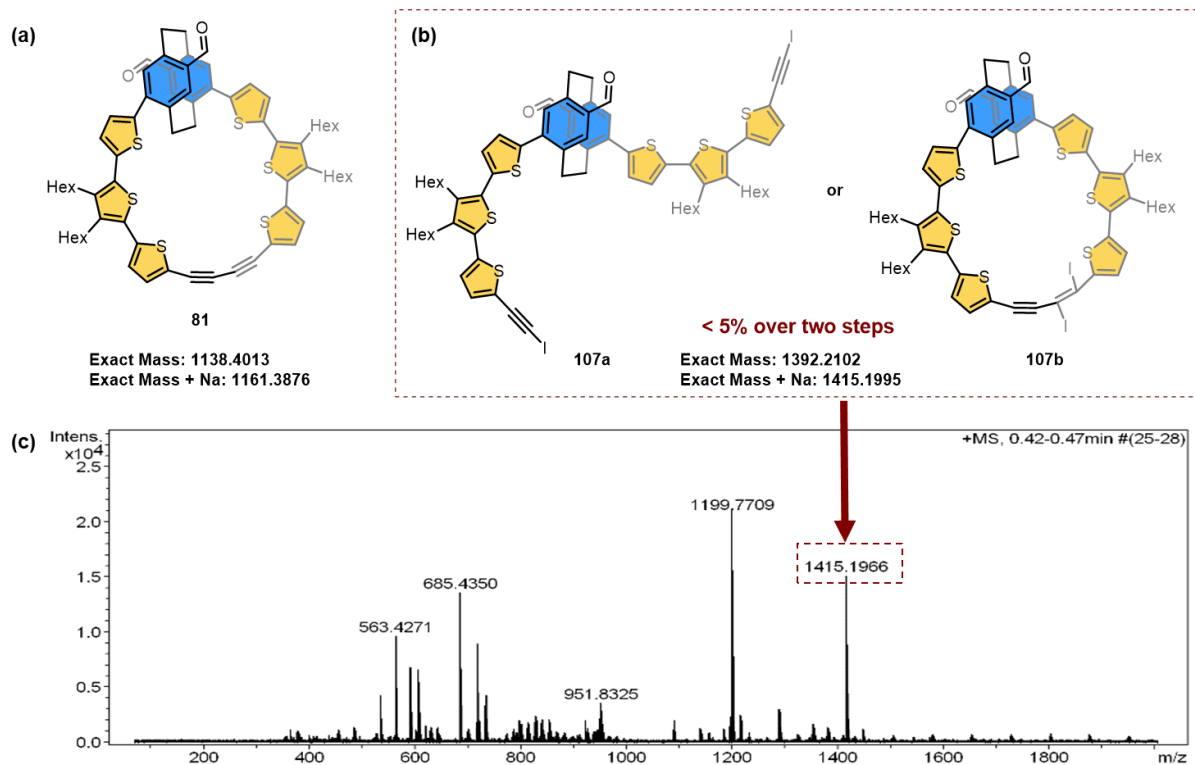


Figure 36: (a) structure and mass of the desired molecular loop (**81**); (b) proposed structures which are fitting the mass **107a** and **107b**; (c) HR-ESI-ToF MS spectrum of the isolated compound **107**.

With this result, we conclude that despite the evidence of the formation of desired loop **81**, investigated copper-mediated and palladium-catalyzed reactions demonstrated the preferred formation of intermolecular cyclization over intramolecular one. In the case of platinum-corner, the inconclusive data did not allow to prove the loop formation. Therefore, further investigations of the loop closure were stopped at this point due to the redesign of the initial structure. Thus, redesign ideas and new synthetic strategies are proposed and discussed in the following summary and outlook subchapter. In addition, further investigations of the isolated cyclic dimer (**103**) are outlined in Chapter 4.

3.6 Summary

In summary, a new design of the macrocyclic structure comprising two different charge pathways, namely through-space and through-bond, was outlined. The target structure consists of PCP-based molecular wire with *ps-meta* connectivity allowing the connection to a smaller loop size than for the *ps-para*-based analogue. This exchange of the connectivity pattern in the PCP core should enhance the through-space conductivity due to the CQI. In addition, the smaller loop size would make the structure more rigid, allowing better electronic communication as well as an increase in conductivity due to the lower number of thiophene moieties. Furthermore, the new design also allowed the convergent synthetic strategy and reduced the number of synthetic steps. All building blocks were synthesized and fully characterized. With the necessary building blocks in hand, the precursor molecule was assembled, followed by successful deprotection. The key step, the macrocyclization reaction, was performed using different synthetic strategies. Unfortunately, the intramolecular ring closure seems to be less favored as an intermolecular analogue, providing the formation of cyclic and linear oligomeric structures. Even the most promising reactions did not lead to the isolation of desired structure. The strategies using platinum and palladium for homocoupling were unsuccessful, providing several by-products and linear and cyclic oligomeric structures as the outcome of the reactions. The first evidence for the formation of desired loop (**81**) came from MALDI-ToF-MS analysis for the copper-mediated reactions. However, the amount of formed structure was too low for isolation as well as for further reaction steps. Several attempts to shift the equilibrium toward the formation of desired macrocycles were unsuccessful. A decrease in starting material concentration and concentration of catalyst, as well as a pseudo-high-dilution, lead to enhancement of the formation of poor soluble linear oligomers and polymers. The major product, mostly isolated from all investigated attempts, was a cyclic dimer formed via intermolecular ring closure, which was identified and confirmed by DOSY, two-dimensional NMR techniques, and MALDI-ToF-MS (see Chapter 4).

3.7 Outlook: Redesign

Therefore, redesigning the structure will be the most promising option. One of the possibilities is the elongation of the loop structure by the implementation of additional thiophene units providing molecular loop precursor **108**. This approach would improve the strained angle of butadiene-based macrocycles ($164.8 - 165.0^\circ$ for macrocycles **81** to $168.8 - 169^\circ$ for macrocycles **108**, see Figure 37). It is expected that the less strained angle and large distance of thiophenes units would enable the intramolecular ring closure.

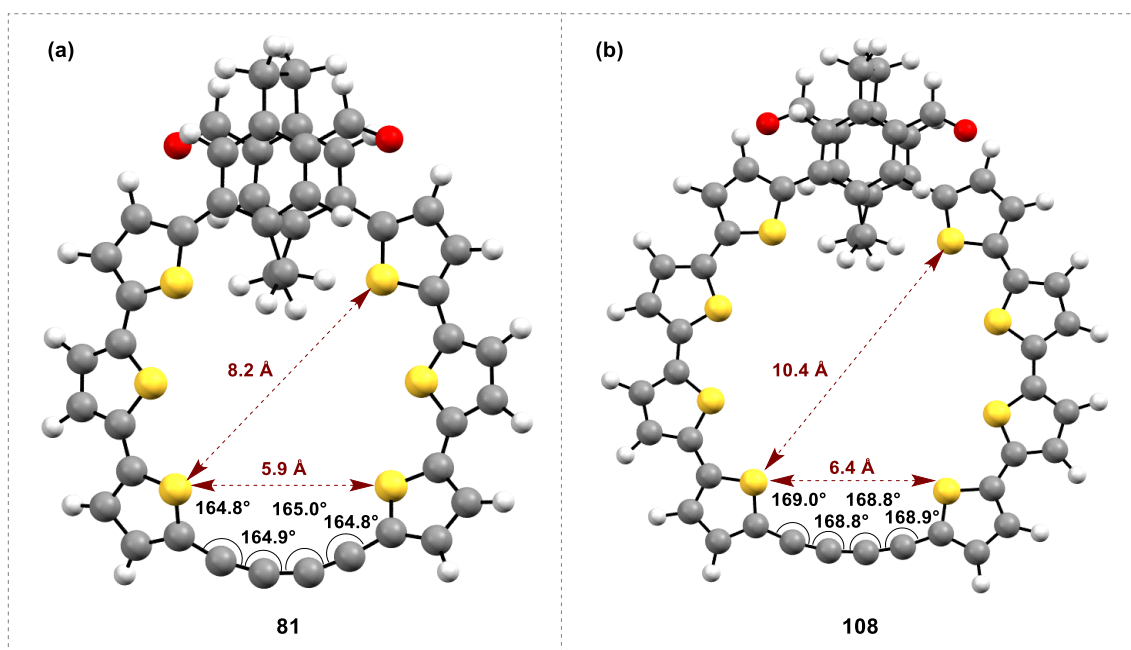


Figure 37: Calculated structures in Chem3D (MM2) for comparison of the loop size and strained angle in precursor molecules for (a) seven thiophene-based and (b) nine thiophene-based molecular loops. The hexyl solubility chains were omitted to facilitate the calculations.

The modified structure **108** can be synthesized as depicted in Figure 38, following pathway A (black arrow) or pathway B (grey arrows), where the precursor molecule for macrocyclization can be assembled in one step or stepwise, respectively. For example, in pathway A, quarterthiophene building block **109** can be constructed from previously established terthiophene building block (**83** or **101**) in a *Suzuki-Miyaura* cross-coupling reaction followed by borylation. Alternatively (pathway B), the quarterthiophene chain can be built-on via *Suzuki-Miyaura* cross-coupling of tetrasubstituted PCP **82** with a monothiophene building block, followed by bromination (see building block **110**) and a subsequent second *Suzuki-Miyaura* cross-coupling reaction to provide the desired precursor for the macrocyclization.

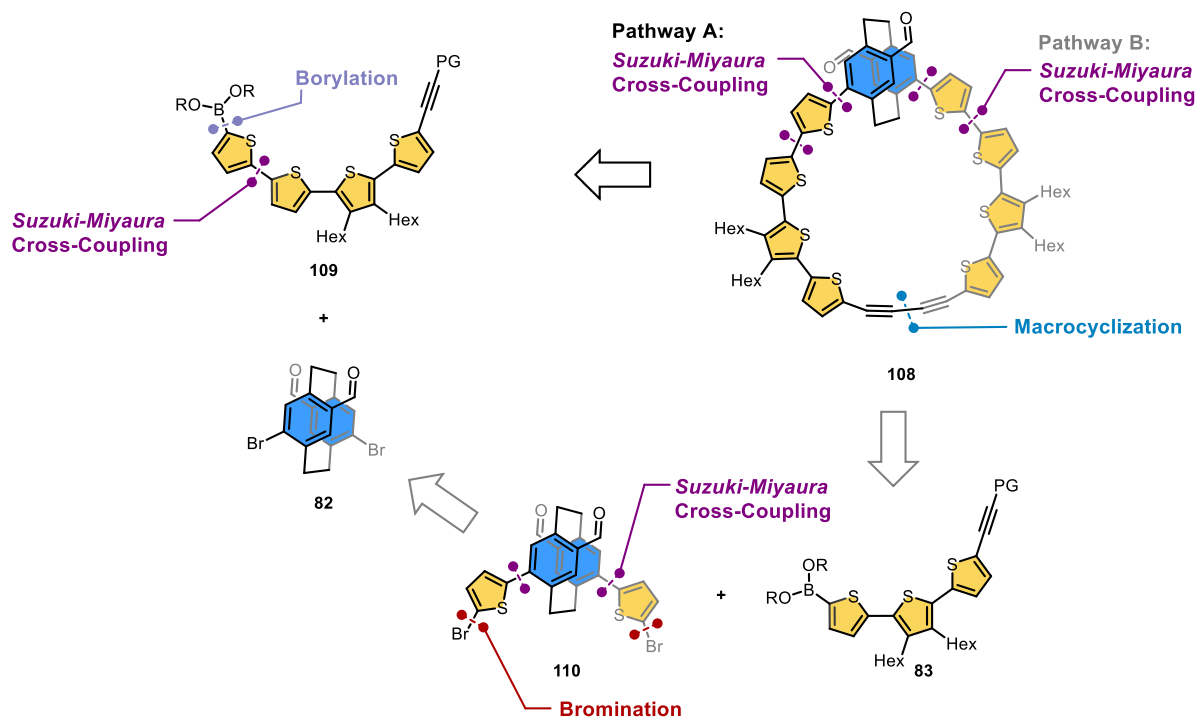


Figure 38: Possible synthetic strategies A and B for preparation of modified loop precursor **108** for nine thiophene-based molecular loop. PG is an abbreviation for protecting group.

On the other hand, the design of a loop scaffold can be revised by substituting thiophene moieties with cycloparaphenylenes (CPPs). Recently, *He et al.*⁶⁷ published a synthesis of a library of molecular loops where *ps-meta* PCP was implemented in the CPPs backbone. They prepared four molecular loops that differed in size bearing six to nine CPP moieties. The smallest of the reported structures **112** is illustrated in Figure 39 and can be used as a basis for the novel model compound **111**. Notably, all key intermediates and the final step of the reported macrocycles PCP-[6]CPP (**112**) were prepared in decent yield between 66 and 71%.⁶⁷

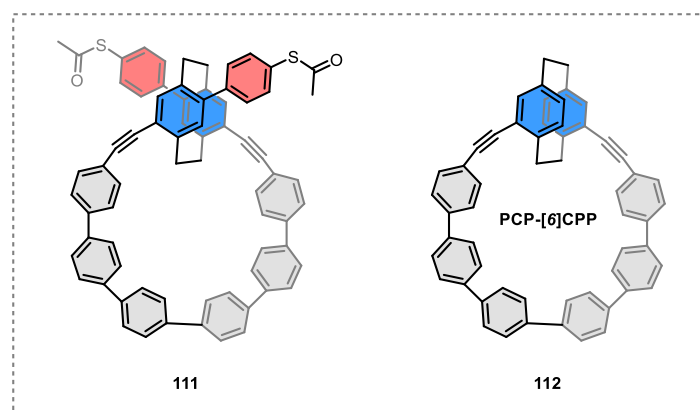


Figure 39: Development of new design **111** based on the previously published scaffold **112**.

Besides a small loop size, a new design enables the direct introduction of the masked thiol-bearing anchoring groups without an acetylene spacer. This direct connection would provide a higher conductivity, already demonstrated in previous work on the example of *ps-para* PCP-based model compounds where the molecules with acetylene spacer and without reveal conductance values of about $3.7 \times 10^{-6} G_0$ and $1.3 \times 10^{-5} G_0$, respectively.^{72,117} Therefore, a novel compact design seems to be encouraging for the investigations in the MCBJ junctions. The retrosynthetic analysis of the desired molecular loop (**111**) is drafted in Figure 40. For the immobilization of the molecule in the junction, thioacetate-functionalized anchoring groups are required. They can be introduced as a last-step modification via a transprotection of more stable sulfur thioether. The designed molecular loop architecture can be constructed via reductive elimination from the corresponding macrocycles **113**. The bottleneck of this strategy is also the macrocyclization reaction, which should be accessible by a nickel-mediated *Yamamoto* coupling¹⁹² similar to the macrocycles **112**.⁶⁷ The scaffold of the precursor molecule can be assembled via two-fold *Sonogashira-Hagihara* cross-coupling from monoiodo **115** and free acetylene **114** building blocks. The latter should be accomplishable from a two-fold *Suzuki-Miyaura* cross-coupling reaction and by profiting from the homologation of already available dialdehyde dibromo PCP **82**.

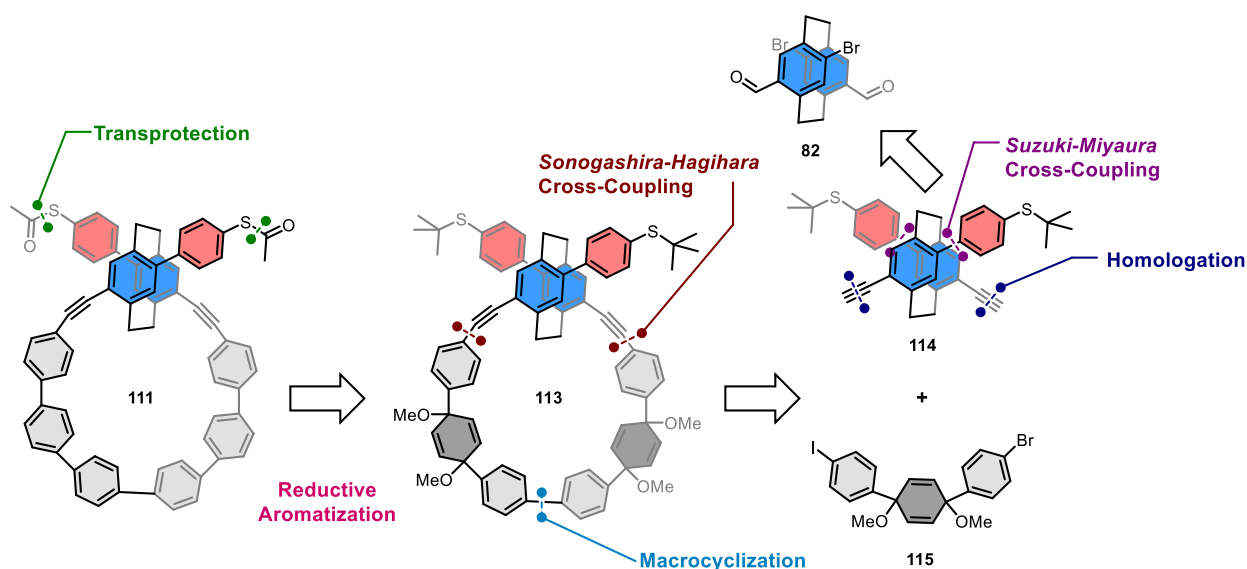


Figure 40: Proposed retrosynthetic analysis for the alternative molecular loop (**111**).

Chapter 4

4 Dimer: An Infinity Loop.

This chapter covers the question that arose in *Chapter 3*, namely the topology of the cyclic dimeric structure isolated during several loop closure attempts. Here we summarized all pieces of evidence for the conformation of the intriguing structure obtained from two-dimensional NMR spectroscopy and molecular mechanics geometry optimization (MM2 using Chem 3D), which allowed us to propose the possible structure. In addition, the butadiyne comprising dimer was transformed into the thiophene analogue. With both dimeric structures in hand, which were prepared from the racemic starting materials, preliminary investigations of the optical properties of PCP-containing cyclic dimers were performed to get insight into the topology and conjugation of macrocycles. The following introduction will provide an overview of already synthesized PCP-based macrocycles and elucidate their optical properties.

4.1 Introduction

4.1.1 Optical-Active Pseudo-Ortho-[2.2]Paracyclophane Containing Macrocycles

Macrocyclic structures have always fascinated scientists due to their beautiful topology and remarkable photophysical properties.^{135,193,194} The “simple” through-bond conjugated macrocycles comprising benzene, thiophene, and pyridine building blocks have already been extensively studied.^{150,195–199} But there is still a lack of studies for through-space conjugated examples, which can be constructed by implementing PCP building block in macrocyclic architecture.^{65–69}

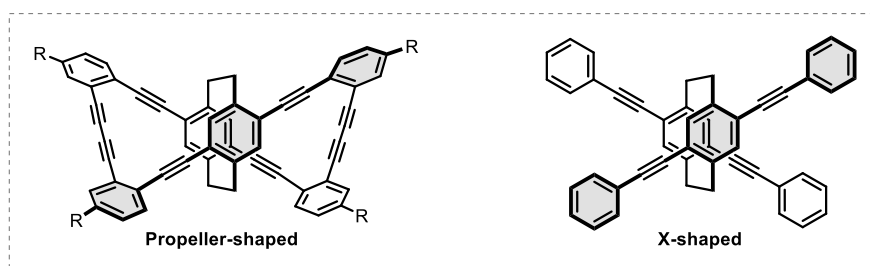


Figure 41: Propeller- and X-shaped PCP comprising structures.

However, chiral PCP-based building blocks have already demonstrated their efficiency in constructing optically active linear oligomers/polymers,^{200,201} propeller-^{202,203} and X-shaped structures (see Figure 41).²⁰⁴ All compounds showed good photoluminescence quantum yields (Φ_{PL}), intense circularly polarized luminescence (CPL) emission^{205,206} with excellent CPL dissymmetry factors (g_{lum}).²⁰⁷ Due to their potential application as CPL-active materials, PCP-based macrocycles with a right- and left-handed helicity induced by the three-dimensional scaffold are intriguing candidates for chiroptical investigations (*vide infra*).^{76,208}

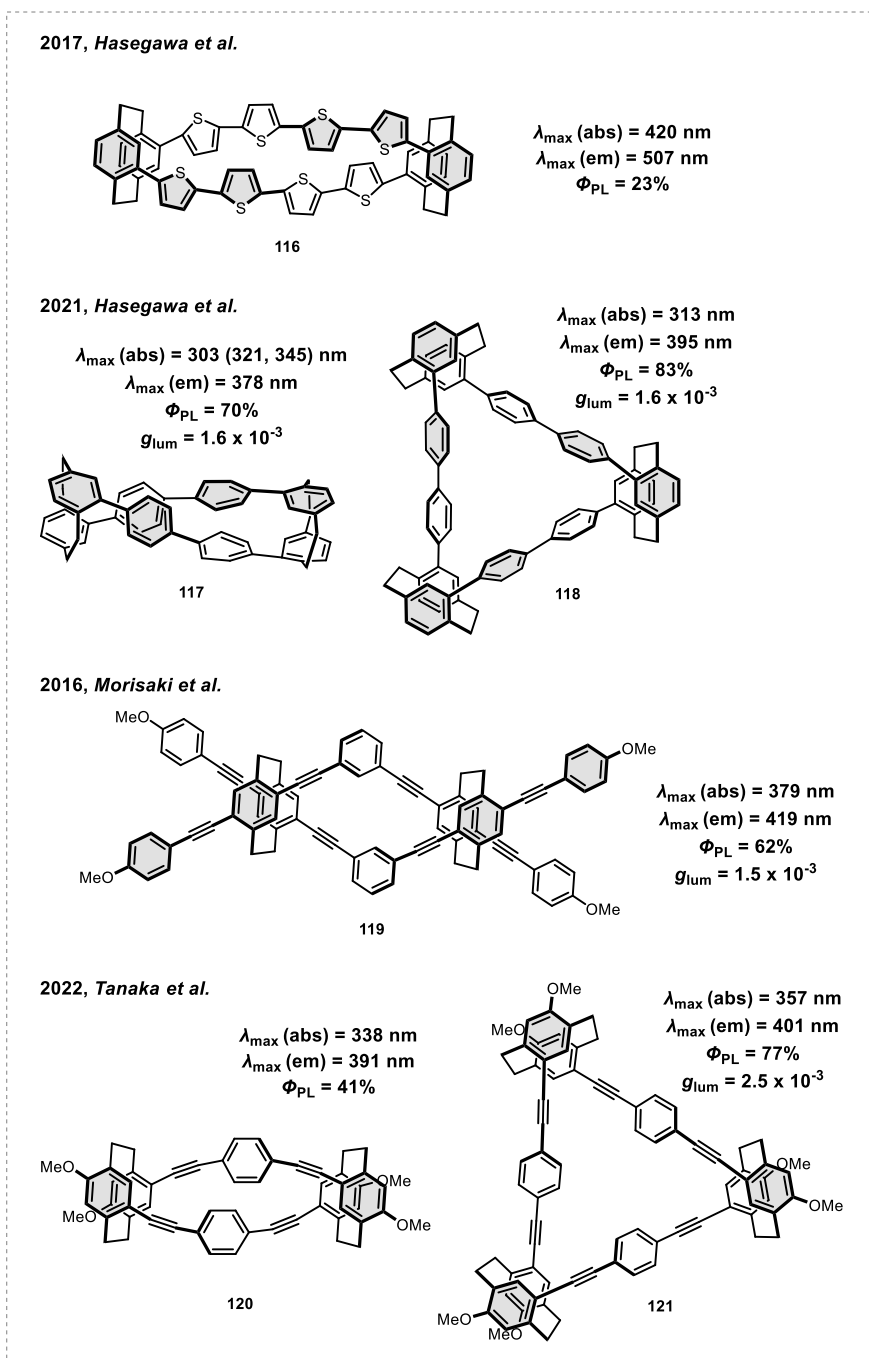


Figure 42: Overview of *ps-ortho*-PCP-based dimeric and trimeric macrocycles with selected optical characteristics. In parentheses are the λ_{\max} values of pronounced shoulders. Abs is an abbreviation for absorption and em for emission. Φ_{PL} is photoluminescence quantum yield, and g_{lum} is the CPL dissymmetry factor.

In 2017, Hasegawa *et al.* reported a pronounced enhancement in circular dichroism spectra of cyclic oligothiophene enantiomers bridged by two pseudo-*ortho* PCP corners (see Figure 42, **116**).⁷⁰ Furthermore, the oligothiophene double-decker exhibit an intriguing twisted topology according to single-crystal X-ray diffraction analysis and DFT calculations. Four years later, the same research group reported a similar conformation twist for the cyclic dimer **117**, where both *ps-ortho* PCP moieties were bridged by biphenyl.²⁰⁹ Besides the dimeric structure **117**; also cyclic trimer **118** was synthesized and analyzed. Both structures possess at least three-

fold higher photoluminescence quantum yields as thiophene bridged dimer **116**. In addition, both **117** and **118** demonstrated a similar high dissymmetry factor of 1.6×10^{-3} in CPL measurements. Not only the disubstituted (**116** – **118**) but also the tetrasubstituted PCP-based building blocks were implemented in a cyclic dimeric scaffold (see Figure 42, **119**), demonstrating excellent CPL emitters' behavior with significant CPL dissymmetry factors of 1.5×10^{-3} and good photoluminescence quantum yields of 62%.²⁰⁷ However, recently reported cyclic dimer analogue **120** by *Tanaka et al.* did not emit CPL. On the other hand, trimeric **121** analogue exhibited intense CPL emissions and showed high dissymmetry factors (2.5×10^{-3}) with a high quantum yield of 77% compared to the corresponding dimer **120** with only 41%.²¹⁰ A comparison of absorption and emission spectra of all four dimers revealed that thiophene bridged dimer **116** showed a bathochromic shift in absorption and emission (see Figure 42).

4.1.2 Optical-Active Pseudo-Meta-[2.2]Paracyclophane Containing Macrocycles

Notably, all the above-discussed molecules refer to the macrocycles with pseudo-*ortho* connectivity to the PCP building blocks. Implementing PCP with a pseudo-*meta*-connectivity in the macrocycles is not as popular as for pseudo-*ortho* analogue and still remains pretty underexplored. *He et al.* recently reported a library of cycloparaphenylenes (CPP)-based macrocycles with a ps-*meta*-diethynyl-PCP core, which differed in size from six (**112**) to nine (**124**) CPP units (see Figure 43).⁶⁷

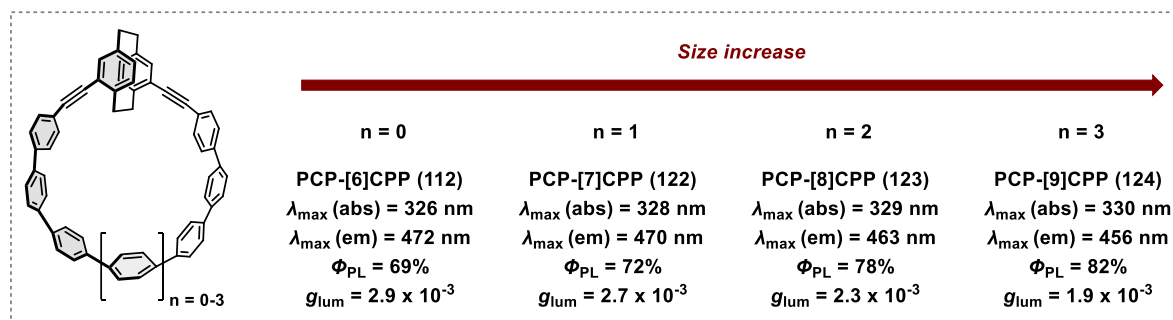


Figure 43: Schematic overview of prepared macrocycles and selected spectroscopic data. Abs is an abbreviation for absorption and em for emission. Φ_{PL} is quantum yield, and g_{lum} is the CPL dissymmetry factor.

The macrocycles exhibit a size-dependent increase in quantum yield from 69% to 82% and moderately large CPL dissymmetry factor from 2.9×10^{-3} to 1.9×10^{-3} . In addition, the absorption maxima showed a slight bathochromic shift from 326 nm to 330 nm according to the loop increase from the smallest macrocycles with six CPPs (**112**) to the biggest one with nine (**124**). Interestingly, the absorption maxima of CPP macrocycles are size-independent. In addition, emission spectra demonstrated a size-dependent hypochromic shift from 472 nm to 456 nm.⁶⁷

4.2 Project Description

The aim of this chapter is the corroboration of the topology of the dimeric structure isolated in Chapter 3. The intriguing cyclic dimer **103** was established via an intermolecular homocoupling reaction as a major by-product of the desired molecular loop **81**. Thus, the dimeric framework comprises two PCP moieties connected over butadiynes on thiophene chains (see Figure 44a). Initially, we considered the dimer as a proof-of-concept structure to investigate the conductivity from the first PCP moiety to the second via septithiophene chains (see 4.5.2). However, the dimeric topology's behavior is comprehensive and may provide unexpected photophysical properties.

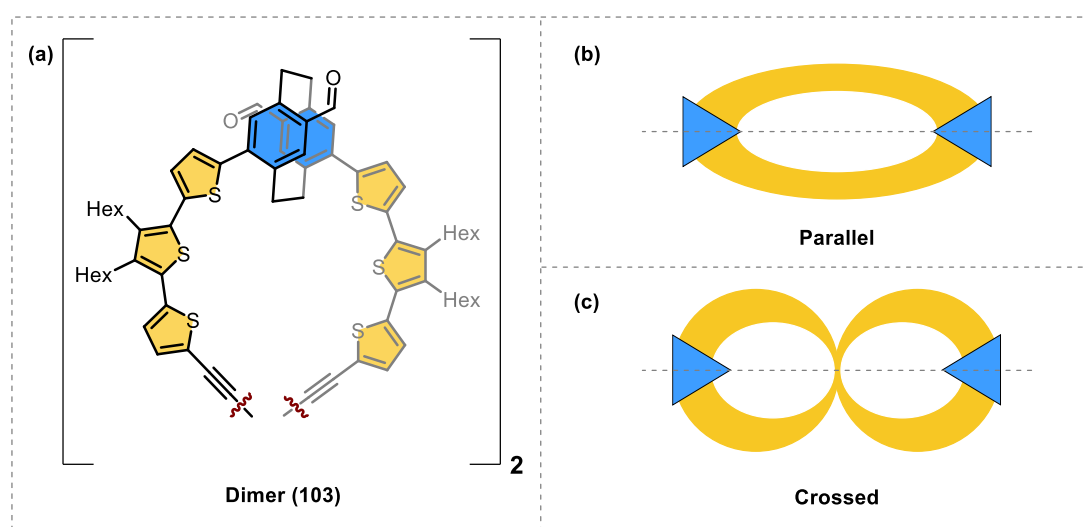


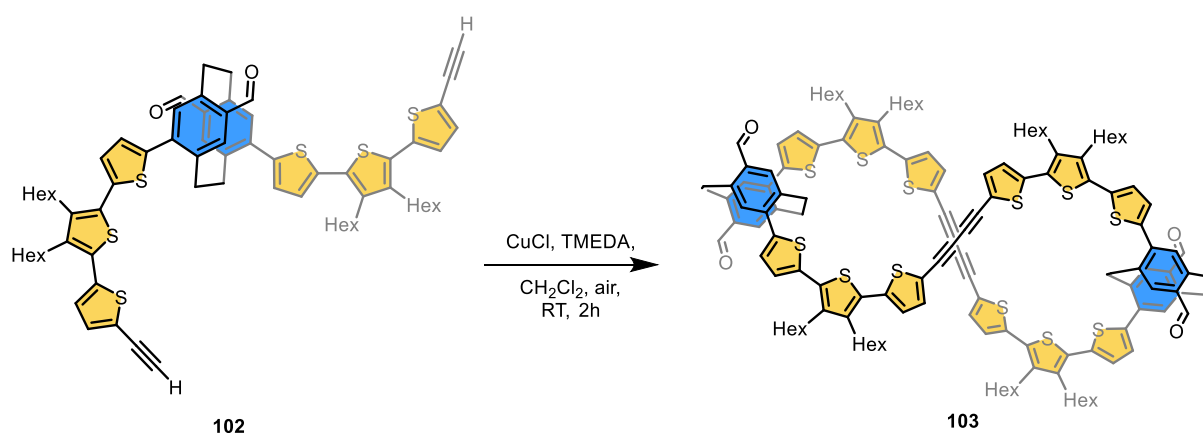
Figure 44: (a) Dimeric structure obtained via intermolecular homocoupling described in Chapter 3. (b - c) Sketch of proposed parallel (b) and crossed (c) topology for the investigated dimer.

Therefore, our focus of interest moved to the elucidation of the dimeric structure (**103**). In principle, there are two possible options for intermolecular ring closure: parallel or crossed (see Figure 44b-c). The first option implies that the thiophene chains are arranged parallel, and the second demonstrates the cyclic ribbon twisted around the central axis. The latter provides the figure-of-eight type (lemniscate) structure, indicating a higher degree of stability and symmetry than a parallel constitution. Furthermore, the lemniscate-type ribbon induces a helical chirality through a three-dimensional thiophene moiety, which is not intrinsically chiral. Besides the initial planar chirality of the PCP, such a helical chirality provides several possible enantio- and diastereoisomers of the dimer **103**.

4.3 Results and Discussion

4.3.1 Topology

The dimer was formed as a major product in the copper-mediated and palladium-catalyzed attempts to synthesize the macrocyclic loop structure (**81**) described in Chapter 3. The best yield was obtained for copper-mediated reactions (8 – 38%), depending on the used conditions (see Tables 4 and 6). An example of used conditions is illustrated in Scheme 23. Furthermore, the following scheme demonstrates a dimer topology on the instance of an enantiopure dimer **103** prepared from enantiopure starting material **102**. The further options for the configuration will be discussed in subchapter 4.5.1.



Scheme 23: Synthesis of the dimer **103** using *Glaser-Hay* conditions. The dimer is depicted as an enantiopure lemniscate structure as one of the possible configurations.

First insights concerning the macrocyclic dimeric structure **103** were observed in MALDI-ToF-MS and were supported by the retention times obtained in the GPC chromatogram (see Figure 35). The GPC separation allowed the isolation of macrocyclic dimer **103**, trimer **104**, and tetramer **105**. Unfortunately, the amount of the isolated tetrameric structure (**105**) was too low for a proper ^1H NMR characterization. Therefore, solely the dimer **103** and trimer **104** were examined. Comparing ^1H NMR spectra of starting material **102** to the obtained dimer **103** and trimer **104** validates the absence of free acetylene. Hence, this observation and assignment of all other protons verified the macrocyclic structure for dimer **102** and trimer **103**. Interestingly, the most pronounced chemical shift was indicated for the protons of thiophene moiety in both dimer **103** and trimer **104** (see Figure 45, yellow dashed frame) compared to starting material **102**. Furthermore, a slight chemical shift allows distinguishing between the dimeric and trimeric constitutions.

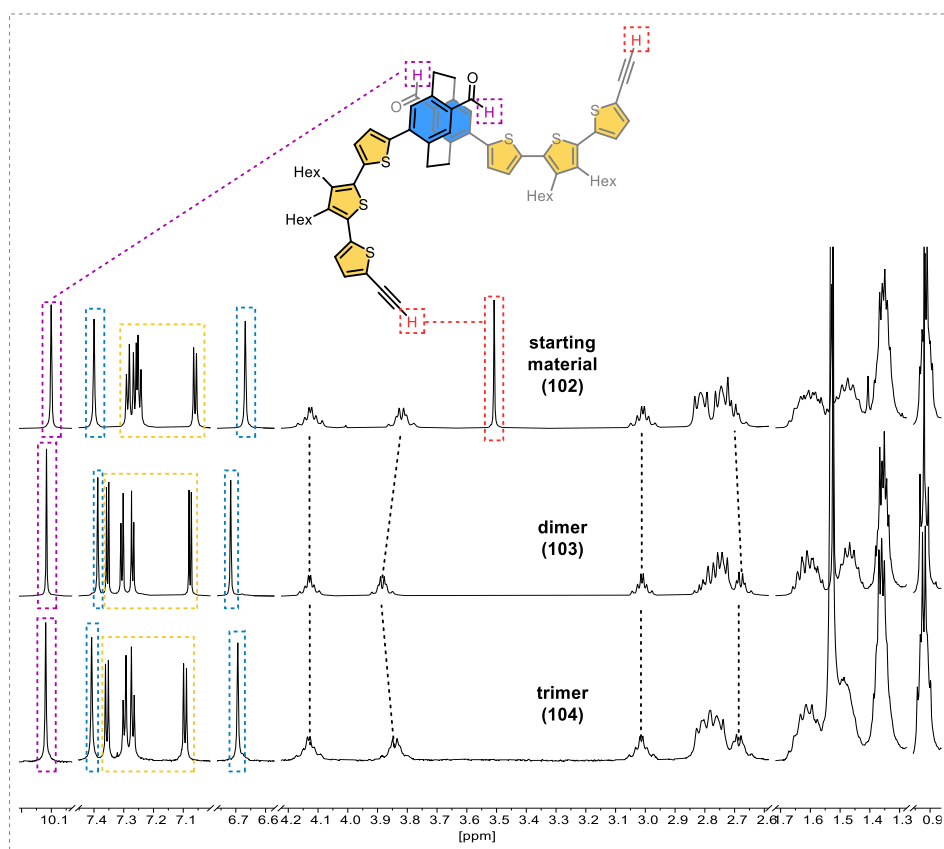


Figure 45: Comparison of ^1H NMR spectra (400/500 MHz, CH_2Cl_2 , 298 K) of starting material **102**, dimer **103**, and trimer **104**. For better visibility, the solvent peak was removed, and the main protons were assigned with dashed colored frames corresponding to the colors in depicted structure: violet for aldehyde, blue for aromatic protons for PCP-core, and yellow for thiophene. The protons of ethynyl bridges are indicated with a black dashed line. For simplicity, the protons corresponding to hexyl chains were not marked.

The ^1H NMR spectra of both the dimer (**103**) and trimer (**104**) demonstrated a high degree of symmetry. In the case of the dimer (**103**), such symmetry leads to the conclusion of a definite twist in the thiophene ribbon similar to the twist in the previously discussed structures **116** and **117**. To prove this hypothesis, the identity of the dimer **103** was corroborated by nuclear overhauser effect (NOE) spectroscopy to distinguish between crossed and parallel constitutions (spectrum is presented in the *Supporting Information*). However, the NOESY results were inconclusive, demonstrating that the structure is either crossed or opened. Therefore, combining all results and MM2 energy-minimization calculations, we proposed a possible configuration for the enantiopure dimer depicted in Figure 46. The front view demonstrated the figure-of-eight configuration and crossed topology. Nevertheless, the detailed view from the side indicates a considerable distance between the protons from *vis-à-vis* located thiophenes connected to the butadiynes (see Figure 46, red arrow in side view). This observation is in accordance with the aforementioned results of NOE spectroscopy.

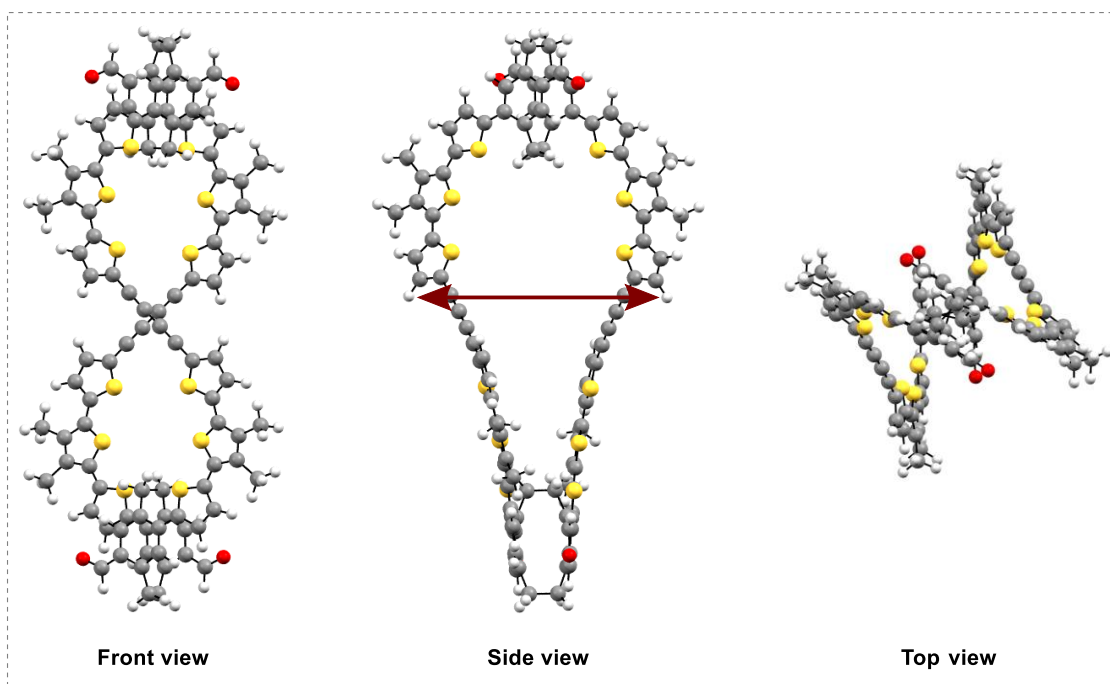


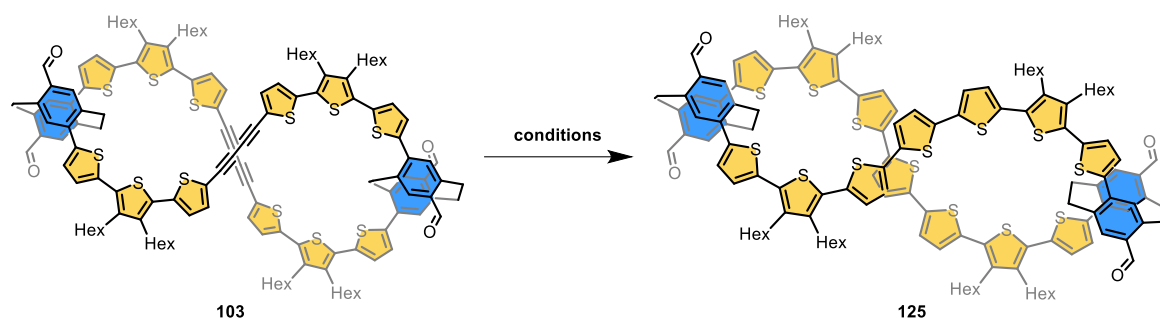
Figure 46: Proposed enantiopure dimeric structure. Geometry optimization performed MM2 level of theory using Chem3D. Methyl groups replaced the hexyl chains to facilitate the calculations. The distance *vis-à-vis* located thiophene protons is represented with a red arrow in the side view.

4.3.2 Formation of Thiophene Dimer

The next synthetic step was the transformation of the butadiyne motif of dimer **103** into a more stable bridging thiophene leading to the septithiophene-linked dimer **125**. Surprisingly, this transformation demonstrated several challenges leading to several side reactions and conclusively providing a complex mixture. The transformation investigation started with the mild method recently used in our laboratories and showed an almost quantitative yield of 96% after 10 minutes at room temperature.¹⁸⁹ Firstly, these conditions were appealing due to the short reaction time and complete conversion without the usage of elevated temperatures. The transformation occurred over the formation of trisulfur radical anions from elemental sulfur and base in DMF.^{211,212} Therefore, the sulfur was stirred with sodium hydrogen sulfide in DMF (see Table 8, entry 1), providing the desired product **125** and several by-products which were hardly separable. To facilitate the purification, screening for the most suitable conditions was performed. Next, we investigated the standard conditions for transformation using the disodium sulfide as a sulfur source for the thiophene cyclization. The reaction mixture was dissolved in wet DMF and stirred at 90 °C for 120 minutes providing the complex mixture with inconclusive products (entry 2). To exclude the insufficient amount of water as a proton source, 2-methoxy ethanol was added to the next attempt. The combination of 2-methoxy ethanol and DMF allowed increasing the temperature to 120 °C to accelerate the product formation (entry 3). Unfortunately, this modification also led to a complex mixture. To circumvent the solubility

issues of the starting material in DMF, THF was added to the reaction to improve the solubility (entry 4). After stirring at 80 °C for 90 minutes, by MALDI-ToF-MS the formation of the desired thiophene dimer and several by-products was detected. Thereby, we recognized that the exchange of the solvent is crucial for the reaction to provide the full conversion and minimize formation of by-products.

Table 8: Screening conditions for the transformation of butadiyne motif of dimer **103** into bridging thiophene **125**. For clarity, the schematical representation of the reaction is depicted in the example of enantiopure dimeric structure.



| Entry | Reagent | Additive | Solvent | Temp [°C] | Time [min] | MALDI-TOF-MS |
|-------|---------------------------------------------|----------------|-----------------------------|--------------|---------------|-----------------------------------------------|
| 1 | S ₈ , NaSH x H ₂ O | - | DMF | RT | 10 | Traces of 125 , several by-products |
| 2 | Na ₂ S x 9H ₂ O | - | DMF | 90 | 120 | Complex mixture |
| 3 | Na ₂ S x 9H ₂ O | - | DMF/2-methoxy ethanol | 120 | 120 | Complex mixture |
| 4 | Na ₂ S x 9H ₂ O | - | DMF/THF | 80 | 90 | 125 and several by- products |
| 5 | Na ₂ S x 9H ₂ O | - | xylene/2- methoxyethanol | 140 | 90 | 125 and several by- products |
| 6 | Na ₂ S x 9H ₂ O | CuI | xylene | 140 | 90 | No product, complex mixture |
| 7 | Na ₂ S x 9H ₂ O | 15- Crown-5 | xylene | 140 | 90 | 125 (49%) ^[a] |

^[a] isolated yield after upscaling of the reaction conditions.

Therefore, a high boiling solvent such as *para*-xylene was chosen. To our delight, the new solvent combined with 2-methoxy ethanol at 140 °C provided the formation of desired structure (entry 5).^{150,213} However, several by-products were still detected. For the next attempt, a catalytic amount of CuI, which is known to be an accelerator during the thiophene-cyclization step, was used.^{214,215} This strategy led to the formation of the complex mixture (entry 6), where the desired **125** structure was not detected. Therefore, 15-crown-5 ether was used as an additive, leading to the formation of desired structure almost exclusively according to the MALDI-ToF-MS (entry 7). Using the last discussed conditions, the desired thiophene dimer **125**

was isolated in 49% yield after purification by GPC. The isolated structure was identified and fully characterized by ^1H and $^{13}\text{C}\{^1\text{H}\}$ NMR spectroscopy. The latter was extracted from the two-dimensional NMR spectra due to the insufficient amount (see Supporting Information for Chapter 4).

4.3.3 Preliminary Optical Investigations

This subchapter summarizes and discusses the preliminary results of optical investigations of the molecules prepared in Chapters 3 and 4. All measurements were performed in chloroform at room temperature when nothing else was explicitly mentioned.

4.3.3.1 Steady-State Optical Spectroscopy

First, the absorption and emission spectra of linear building blocks, namely terthiophene derivative **92** and protected loop precursor **93**, were compared to the macrocyclic dimer **103** and thiophene dimer **125** structures, as depicted in Figure 47. Terthiophene derivative bearing TIPS-acetylene **92** shows its absorption maximum at 363 nm. After introducing a PCP moiety as the central subunit, the absorption maximum of the dimer precursor **93** demonstrates a bathochromic shift concerning the thiophene derivative **92** and is located at 424 nm. This redshift of 61 nm can be rationalized by an increase in π -conjugation length, which indicates the conjugation through the PCP core. In addition, the evidence of conjugation can be confirmed with the comparative literature known linear septithiophene, where the maximal absorption wavelength was found at 440 nm in chloroform.²¹⁶ Furthermore, **93** demonstrates a more or less pronounced shoulder around 375 nm, which disappears after the macrocyclization. The absorption maximum of dimer (**103**) and thiophene dimer (**125**) are also redshifted compared to the linear building blocks (**92** and **93**) and were found at 427 nm and 435 nm, respectively. These observations can also be associated with the further increase of conjugation for the macrocycles, implying higher conjugation due to better delocalization of the thiophene dimer **125** (sp^2 carbon) compared to the dimer **103** (sp center of acetylene), which is in accordance with previously published results.⁶⁶

The emission spectra of all four compounds (**92**, **93**, dimer (**103**), and thiophene dimer (**125**)) follow the same trend as the absorption spectra and demonstrate a bathochromic shift corresponding to the increased conjugation. Aside from that, the terthiophene derivative **92** has a distinctive shoulder at 445 nm nearby the intense emissions peak maxima at 466 nm, resulting in a comparable Stokes shift of 103 (82) nm. Unsurprisingly, the remaining **93**, dimer **103**, and thiophene dimer **104** demonstrated a further increase in Stokes shift of 148, 154, and 191 nm according to the corresponding emission maxima at 572, 581, and 626 nm,

respectively. These observations were assigned to increased molecules' size and probably an enhanced degree of freedom.

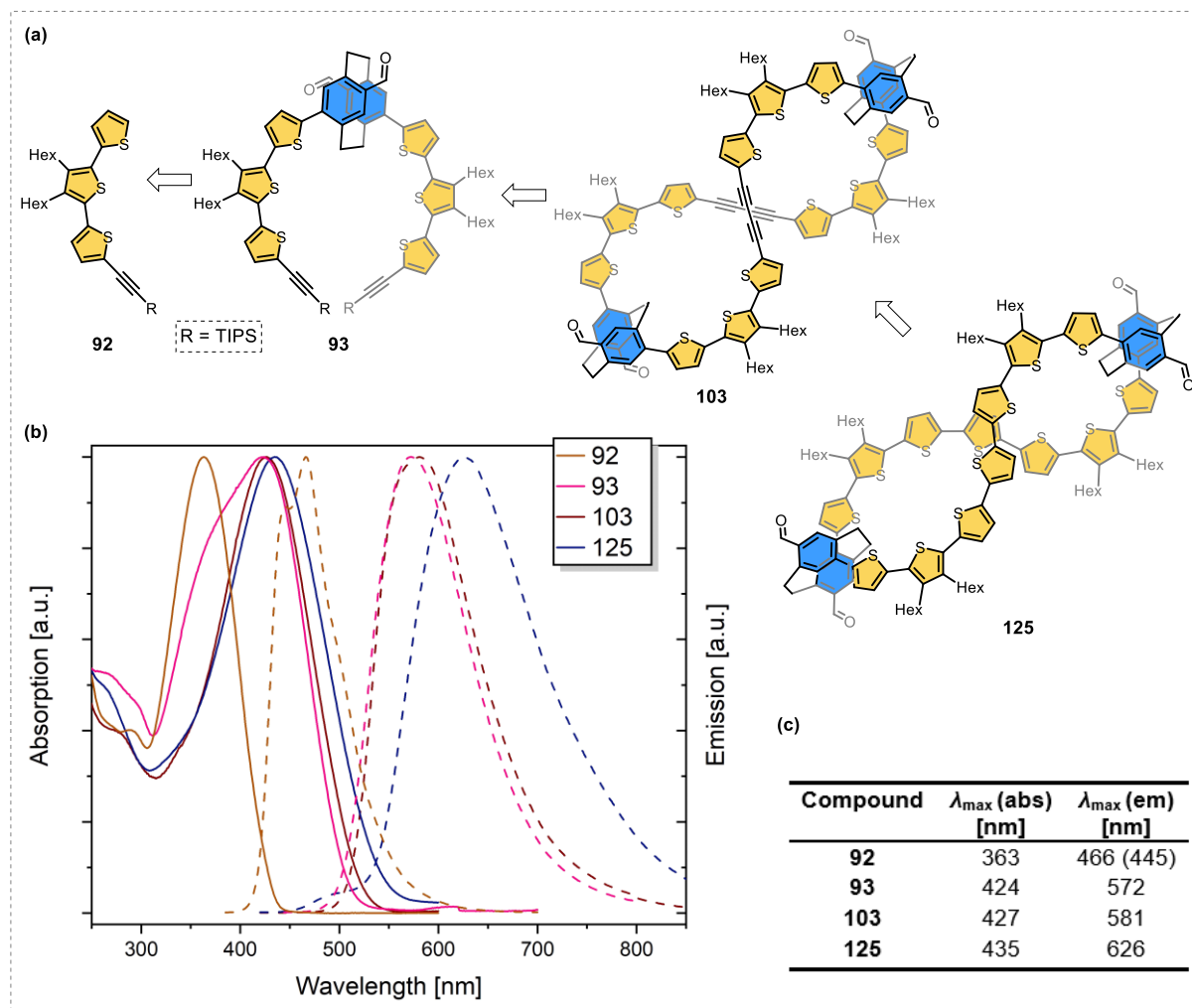


Figure 47: (a) Schematic representation of measured structures. For clarity, the dimer (**103**) and thiophene dimer (**125**) are depicted on the enantio pure example. (b) Absorption (solid lines) and emission (dashed lines) spectra of terthiophene derivative **92** (mustard yellow), protected loop precursor **93** (pink), dimer **103** (dark red), and thiophene dimer **125** (blue) in chloroform. Terthiophene derivative **92**, protected loop precursor **93**, dimer **103**, and thiophene dimer **125** were excited at 365, 424, 400, and 440 nm, respectively. Due to the limited substrate quantities, both absorption and emission spectra for all compounds were normalized. (c) **Table 9:** Comparison of the main absorption and emission values of terthiophene derivative **92**, loop precursor **93**, dimer **103**, and thiophene dimer **125**. In parentheses are the λ_{max} values of pronounced shoulders.

Previously isolated trimer (**104**) and tetramer (**105**) structures allowed us to elucidate the photophysical properties of macrocycles depending on their size (see Figure 48(b)). The absorption maxima of dimer (**103**), trimer (**104**), and tetramer (**105**) appeared at 427, 438, and 443 nm providing a redshift upon increasing the size, as depicted in Figure 48(a) and summarized in Figure 48(c). This observation also suggests an increase of a cyclic π -conjugation with the increasing ring size. Notably, this observation differed from the recently published results of the library of 1,3-butadiyne-linked pseudo-*meta*-PCP macrocycles providing the same absorbance and emission maxima independently of the size.⁶⁹

Furthermore, the emission spectra demonstrated a slight hypsochromic effect for trimer and tetramer relative to a dimer. Conclusively providing the decrease in *Stokes* shift from dimer to tetramer (154, 137, and 135 nm). The comparable size-dependent redshift in absorption and blueshift in emission trends were also found for cyclo[*n*]thiophene²¹⁷ and the pseudo-*meta*-PCP core implemented in cycloparaphenylene (CPP)⁶⁷ macrocycles (see Figure 43).

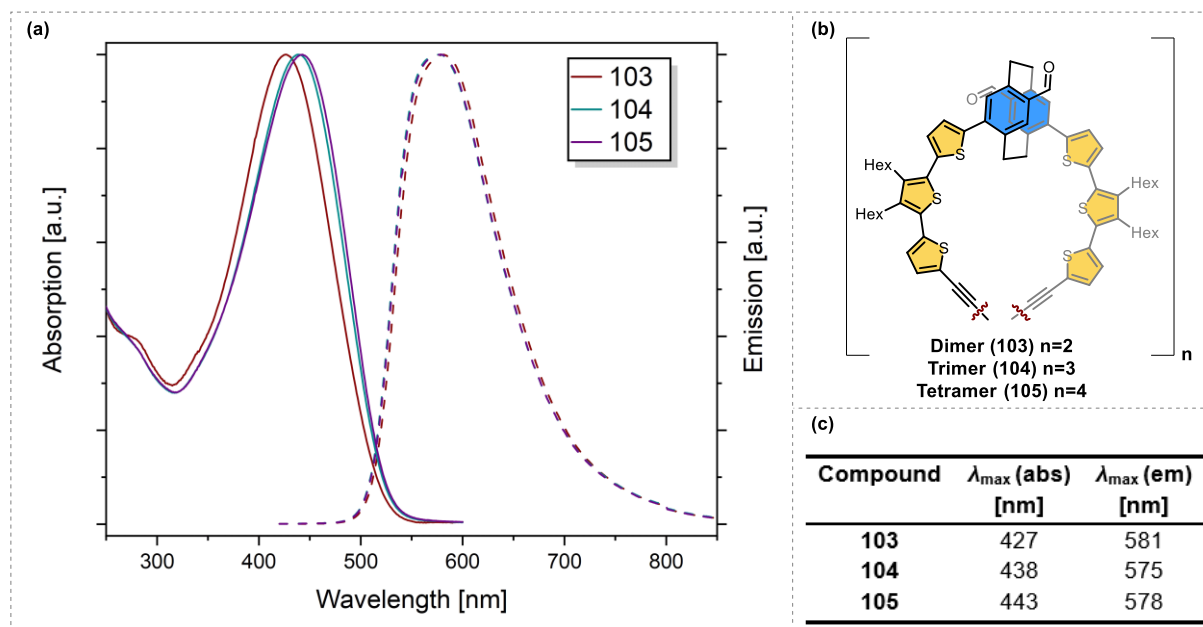


Figure 48: (a) Absorption (solid lines) and emission (dashed line) spectra of a dimer (**103**, dark red), trimer (**104**, dark cyan), and tetramer (**105**, purple) in chloroform. All three compounds were excited at 400 nm. Both absorption and emission spectra for all compounds were normalized due to the low quantity. (b) Schematic representation of measured structures. (c) **Table 10:** Comparison of the main absorption and emission values of dimer (**103**), trimer (**104**), and tetramer (**105**).

4.3.3.2 Solvatochromism

Next, the influence of solvent effects on the optical properties of terthiophene **92**, loop precursor **93**, dimer (**103**), and thiophene dimer (**125**) was explored (see Figure 49). Firstly, commonly used solvents in spectroscopy, such as acetonitrile and methanol, were investigated. Unfortunately, the desired loop precursor and macrocycles were not sufficiently soluble in these solvents. Therefore, the behavior of **92**, **93**, dimer (**103**), and thiophene dimer (**125**) was examined only in solvents allowing sufficient solubility, such as cyclohexane, toluene, ethyl acetate, and chloroform. Typically, the absorption spectra are less influenced by the solvent effects due to the short time in which absorption occurs.

In contrast, the first excited state of the investigated substrates can be stabilized with the surrounding (mostly polar) solvent molecules leading to a decrease in energy and hence a red shift in emission, the so-called solvatochromic effect. Such a solvatochromic effect is usually observed for excited state transitions where a charge transfer state is populated, and hence a dipole moment is generated. Such a charge transfer state can generally be stabilized with a more polar solvent, providing a red-shift emission with an increase in polarity (*vide infra*).²¹⁸

As mentioned above, the emission spectra provide apparent solvatochromic shifts, and therefore in the following discussion, we will focus on the comparison of fluorescence spectra of selected molecules in different solvents (see Figure 49). The emission peak maxima of terthiophene derivative (**92**) stay identical for the cyclohexane, toluene, and ethyl acetate measurements at 461 nm, demonstrating only a light redshift in chloroform to 466 nm. On the other hand, the shoulder gets more pronounced in the cyclohexane measurement compared to the other solvents. The solvatochromic shift is more distinct in the emission data of loop precursor (**93**), providing the solvent-dependent wavelength maxima at 510, 529, 540, and 572 nm in cyclohexane, toluene, ethyl acetate, and chloroform, respectively. Macrocycles also follow the same trend (the data is summarized in Figure 49f), demonstrating a bathochromic shift from cyclohexane to chloroform which is visualized in Figure 49e under 366 nm light. Notably, chloroform obscures the vibronic structures of **93**, dimer (**103**), and thiophene dimer (**125**). In contrast, they get more pronounced with decreased polarity from ethyl acetate to cyclohexane, demonstrating a defined shoulder in cyclohexane.

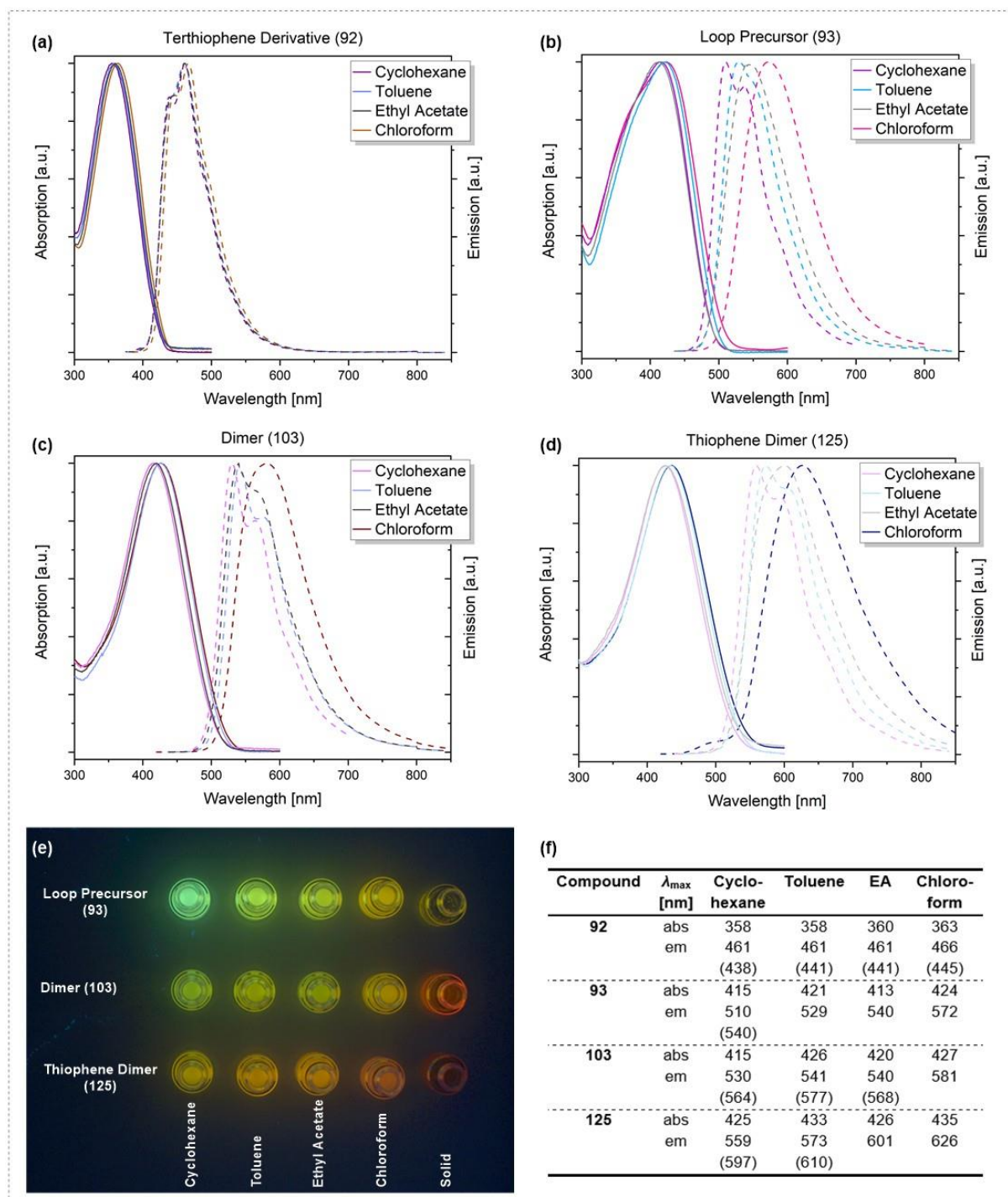


Figure 49: Absorption (solid lines) and emission (dashed lines) spectra of thiophene derivative (92), loop precursor (93), dimer (103), and thiophene dimer (125) in different solvents (a-d). Both absorption and emission spectra for all compounds were normalized. (e) Photograph showing the fluorescence for loop precursor (93), dimer (103), and thiophene dimer (125) in different solvents and solid state was taken under 366 nm wavelength light with a TLC visualizer. (f) **Table 11:** Comparison of the main absorption and emission values of 92, 93, dimer (103), and thiophene dimer (125) in different solvents. In parentheses are the λ_{\max} values of pronounced shoulders.

4.3.3.3 *Quantum Yield*

Intrigued by the solvatochromic results, we determined the absolute quantum yields (QY) for loop precursor (**93**) and macrocycles **103** and **125** in cyclohexane, toluene, ethyl acetate, and chloroform. The average of three cycles for each measurement was taken to decrease the noise level, and the obtained data are summarized in Table 12. Interestingly, the lowest efficiency was observed for dimer (**103**) with values of 9.3 (± 0.15) and 10.6 (± 0.19)% in apolar solvents compared to loop precursor (**93**) and thiophene dimer (**125**). On the other hand, this trend was turned in ethyl acetate and chloroform, providing the highest values for the dimer with efficiency of 8.9 (± 0.14) and 10.9 (± 0.52)%, respectively.

Table 12: Comparison of quantum yields of **93**, dimer (**103**), and thiophene dimer (**125**), which were taken in different solvents.

| Compound | Φ_f (%) ^[a] | | | |
|------------|-----------------------------|---------------------|--------------------|---------------------|
| | Cyclohexane | Toluene | Ethyl Acetate | Chloroform |
| 93 | 10.1 (± 0.23) | 11.6 (± 0.24) | 8.2 (± 0.05) | 7.7 (± 0.06) |
| 103 | 9.3 (± 0.15) | 10.6 (± 0.19) | 8.9 (± 0.14) | 10.9 (± 0.52) |
| 125 | 11.4 (± 0.35) | 11.4 (± 0.20) | 8.5 (± 0.07) | 9.6 (± 0.30) |

^[a]The data summarized in the table above are the average values calculated from three measurements to decrease the noise level. Standard deviation is given in paratheses. The measurements were done together with A. D'Addio.

4.4 Summary

In summary, the topology of dimeric structure (**103**) obtained by several macrocyclization attempts in *Chapter 3* was elucidated using several NMR techniques and molecular modeling on MM2 level of theory. Elaborated configuration consists of two PCP moieties connected via two parallel arranged chains of thiophenes joined in the middle via butadiyne. Due to the PCP and thiophene distortion, both chains exhibit a twisted geometry, leading to the topology of the dimer as a figure-of-eight structure from the front view. To further verify our findings, more insightful DFT calculations or single crystal X-ray diffraction are necessary, where the crystal breeding was ongoing during the writing of this thesis.

Initially, we considered the dimer (**103**) as a proof-of-concept structure (see 4.5.2) to investigate the conductivity from the first PCP moiety to the second via septithiophene chains. Therefore, the next step was successfully transforming butadiyne dimer into the thiophene analogue (**125**). The thiophene dimer (**125**) identity was proven by MALDI-ToF-MS and two-dimensional NMR techniques allowing the assignment of ^1H and $^{13}\text{C}\{^1\text{H}\}$ NMR spectra, where the latter was extracted from two-dimensional NMR.

Furthermore, the prepared dimers (**103** and **125**) demonstrated more comprehensive behavior and provided intriguing optical results. Firstly, the electronic communication through the PCP core and size-dependent conjugation in isolated macrocycles was confirmed by absorption data. In addition, PCP moiety bearing thiophene chains (**93**) and both dimers (**103** and **125**) demonstrated solvatochromism which can be assigned to the charge transfer from the pulling aldehydes. Unfortunately, the quantum yield was up to seven times lower than in PCP-containing cyclic structures discussed in the introduction. However, despite the already performed investigations, both dimeric structures have more exciting properties discussed in the following outlook.

4.5 Outlook

4.5.1 Chirality

Planar chirality of PCP-based derivatives was already discussed in detail in chapter 2.1.1.3, on the example of two-fold substituted PCP structures. Tetrasubstituted bis-(para)-pseudo-meta derivate (**93**) also demonstrates planar chirality (see Figure 50a). Therefore, the molecular loops bearing chiral PCP building block as central moiety would also lead to a planar chirality and have either *R_p* or *S_p* configuration. On the other hand, both thiophene moiety and cyclo[8]thiophene macrocycle (**77**) are achiral. However, replacing one thiophene building

block with PCP-moiety introduces a step in the planar macrocycle (**74**), which induces helical chirality (see Figure 50b).

The dimeric structures which were discussed (**103** and **125**) in this chapter consist of two chiral PCP-building blocks and, on account of this, can have the following configuration, namely (*R_p*,*R_p*), (*S_p*,*R_p*), and (*S_p*,*S_p*). Furthermore, the configuration of one PCP is twisted concerning the other one (see Figure 50). This twist in the double helix gets more pronounced after the transformation of butadiene to thiophene dimer. The distortion may also induce the helical chirality (*M* or *P*) in dimer (**103**) and thiophene dimer (**125**), providing another exciting point for further structural investigations.

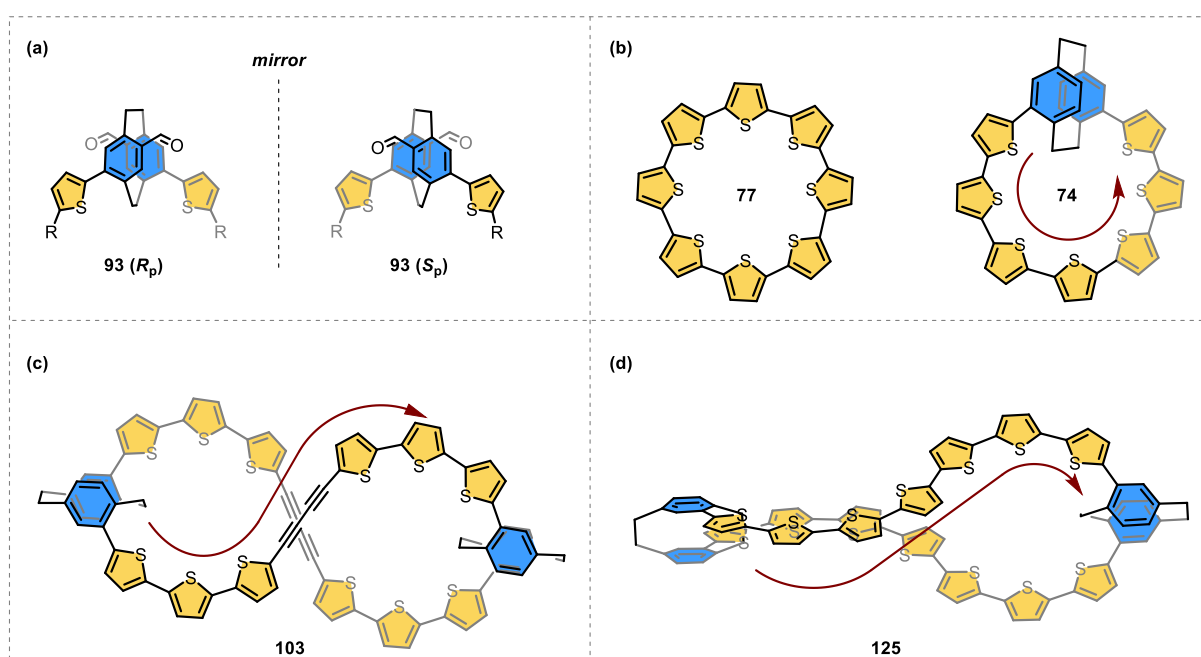


Figure 50: Development of possible chiralities in prepared dimers (**103** and **125**) compared to chiralities in initial molecular loop design **74**. (a) Schematic representation of planar chirality in building block **93** induced by tetrasubstituted PCP moiety used in the preparation of dimers. (b) Achiral cyclo[8]thiophene (**77**) and helical chirality in loop **74**, which is influenced by replacing thiophene with PCP-moiety. Dimer **103** (c) and thiophene dimer **125** (d) illustrate a double helix twist, which may also induce helical chirality. Red arrows demonstrate the twist direction. Aldehydes, solubility, and anchoring groups were hidden for clarity.

Tetrasubstituted *rac*-bis-(*para*)-pseudo-*meta* derivate **82** can be separated by chiral HPLC providing enantio pure isomers. However, in the scope of this thesis, only one of the enantiomers was converted to the corresponding dimer **103**. Therefore, all the previously discussed preliminary investigations were performed with dimeric structures **103** and **125** prepared from racemic starting material **82**.

4.5.2 Proof-of-Concept

Furthermore, the dimer skeleton can still be investigated in electrode-molecule-electrode junction as a proof-of-concept structure to approve whether the length of the thiophene chain is suitable or not, consequently facilitating further molecular design modifications. For this purpose, an appropriate compound **127** can be prepared in two or three steps from the already available thiophene dimer (**125**), as depicted in Figure 51. As previously described in the retrosynthetic analysis for the molecular loop **74**, the electrode anchoring groups can be introduced in the last step. However, the new architecture of the main skeleton requires a four-fold *Sonogashira-Hagihara* cross-coupling instead of a two-fold one to provide desired **127**. The free acetylene intermediate (**126**) for cross-coupling reaction should be accessible from the corresponding aldehyde **125** by treating with the *Bestmann-Ohira* reagent or *Corey-Fuchs* reaction sequence.

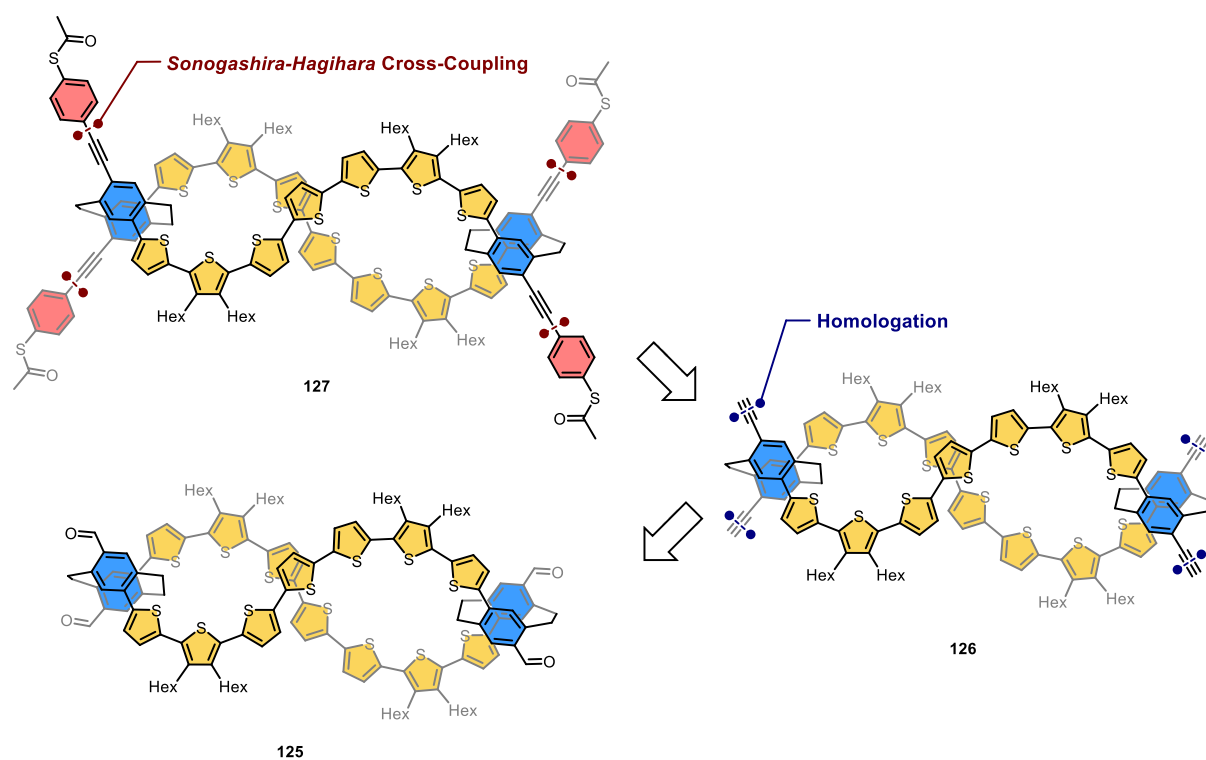


Figure 51: Synthetic strategy for the synthesis of proof-of-concept dimer **127**. All disconnections in the retrosynthetic analysis are marked with colors dependent on the reaction type.

Supporting Information

5 Supporting Information

5.1 Contributions

All compounds were synthesized and characterized by Ksenia Reznikova, except compound **51**, prepared by *Dr. Laurent Jucker*, and *cis*-Pt(dppp)Cl₂-complex, prepared by *Adriano D'Addio*. The measurement of two-dimensional NMR spectra and the full assignments for **OPE5** precursor (**8**), **OPE5** reference (**27**), and thiophene dimer (**125**) were done by *Prof. Dr. Daniel Häussinger* and his students. *Prof. Dr. Daniel Häussinger* also performed the NOESY and DOSY experiments for the dimer (**103**) and the following interpretation.

All MCBJ experiments were performed by *Chunwei Hsu* from *Prof. Dr. Herre S. J. van der Zant's group*. *Werner M. Schosser* and *Dr. Katawoura Beltako* from *Prof. Dr. Fabian Pauly's* group did theoretical calculations.

5.2 General Information

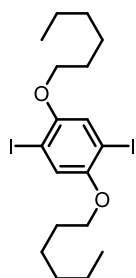
All commercially available chemicals and solvents were purchased from *Sigma-Aldrich*, *Acros*, *Apollo Scientific*, *Alfa Aesar*, and *Fluorochem* and used without further purification. Anhydrous solvents were purchased from Sigma-Aldrich and stored over molecular sieves (4 Å). All reactions with easily oxidized or hydrolyzed reagents were performed under Argon 4.8 or 5.0 from *PanGas* using *Schlenk* techniques and oven-dried glassware. Normal Phase column chromatography was performed on silica gel P60 (40-63 µm) from *SilicycleTM* using technical grade solvents. TLC was performed with silica gel 60 F254 aluminum sheets with a thickness of 0.25 mm purchased from *Merck*. Recycling gel permeation chromatography (GPC) was performed on a Shimadzu Prominence System equipped with SDV preparative columns from Polymer Standards Service (two Showdex columns in series, 20 x 600 mm each, exclusion limit: 30000 g/mol) with chloroform as solvent. NMR measurements were recorded using a Bruker DPX-400 (400 MHz for ¹H and 101 MHz for ¹³C), a Bruker DRX-500 (500 MHz for ¹H and 126 MHz for ¹³C), or a Bruker Ascend Avance III HD (600 MHz for ¹H and 151 MHz for ¹³C) spectrometer at 298 K if nothing else is explicitly noticed. The instruments were equipped with a direct observe 5 mm BBFO smart probe (400 and 600 MHz), an indirect detection 5 mm BBI probe (500 MHz), or a five-channel cryogenic 5 mm QCI probe (600 MHz). The chemical shifts are reported in parts per million (ppm) referenced to the residual solvent peak. The coupling constants (J) are given in hertz (Hz), and multiplicity is reported as follows: s (singlet), d (doublet), t (triplet), q (quartet), m (multiplet), and br (broad). All NMR solvents were purchased from *Cambridge Isotope Laboratories*, *Sigma-Aldrich* or *Fluorochem*. MALDI-ToF mass spectra were recorded on a Bruker MicroFlex LRF spectrometer using *trans*-2-[3-(4-

tert-Butylphenyl)-2-methyl-propenylidene]malononitrile (DCTB) as a matrix. High-resolution mass spectra (HR-MS) were measured as HR ESI-ToF-MS with a Bruker Maxis 4G instrument, where some of the investigated compounds were less prone to form adducts with common ions like H⁺, K⁺ or Na⁺. Therefore, silver ions were used to increase the signal intensity.^{219,220} UV-Vis absorption spectra were recorded on a Jasco V-770 spectrophotometer equipped with a Peltier-thermostatted cell holder (ETCR-762) set to 25°C. Emission spectra in solution were recorded on a Jasco FP-8600 spectrofluorometer equipped with a Peltier-thermostatted cell holder (ETC-815) set to 25°C. Quantum yields were determined on the same spectrofluorometer equipped with a nitrogen-flushed integrating sphere (ILFC-847S). Each measurement was repeated three times, and the average of the three calculated quantum yields was then reported. The UV-Vis and fluorescence spectra were measured in a 1 cm quartz glass cuvettes and quantum yield in 0.5 cm quartz glass cuvettes.

5.3 Supporting Information: Chapter 1

Previously reported compounds: 9-ethynyl-phenanthrene (**13**), 1,4-bis(hexyloxy)benzene (**15**) and 2,5-diiodobenzene-1,4-diol (**26**) were prepared following reported procedures.^{36,42,221}

Synthesis of 1,4-bis(hexyloxy)-2,5-diiodobenzene (**16**):



Periodic acid (10.9 g, 47.4 mmol, 0.7 eq.) was dissolved in methanol (180 ml) and stirred for 10 minutes before iodine (23.7 g, 93.3 mmol, 1.3 eq.) and hexyloxybenzene **15** (20.0 g, 71.8 mmol, 1.0 eq.) were added. The reaction mixture was stirred at 70 °C for 16 h. Afterwards, NaOH (aq. 1 M) was slowly added to the hot reaction mixture until the brown-red color disappeared. The precipitate was filtered off and recrystallized from ethanol to give the product **16**

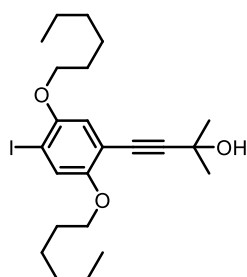
(28.2 g, 53.1 mmol, **74%**) as a colorless solid.

¹H NMR (400 MHz, CDCl₃): δ 7.17 (s, 2H), 3.93 (t, *J* = 6.5 Hz, 4H), 1.84 – 1.75 (m, 4H), 1.53 – 1.46 (m, 4H), 1.38 – 1.31 (m, 8H), 0.94 – 0.89 (m, 6H) ppm.

¹³C{¹H} NMR (101 MHz, CDCl₃): δ 153.03, 122.97, 86.47, 70.53, 31.62, 29.27, 25.86, 22.74, 14.18 ppm.

The analytical data are in agreement with the ones reported in ref.^{36,222}

Synthesis of 4-(2,5-bis(hexyloxy)-4-iodophenyl)-2-methylbut-3-yn-2-ol (**10**):



1,4-bis(hexyloxy)-2,5-diiodobenzene (**16**) (5.60 g, 10.6 mmol, 1.4 eq.) and 2-methyl-3-butyn-2-ol (**19**) (0.7 ml, 7.42 mmol, 1.0 eq.) were dissolved in THF (50 mL) and piperidine (10 mL). The reaction mixture was degassed with Argon for 20 min. Pd(PPh₃)₂Cl₂ (223 mg, 318 μmol, 3 mol%) and CuI (62 mg, 318 μmol, 3mol%) were added and the reaction mixture was stirred for 16 h at RT. Afterwards, the reaction mixture was

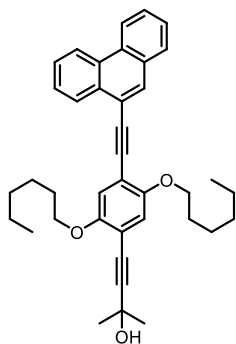
plugged over Celite® and the solvent was evaporated under reduced pressure. The crude product was purified by column chromatography (CH₂Cl₂) to give compound **10** (2.68 g, 5.50 mmol, **74%**) as a yellow oil which solidified at room temperature.

¹H NMR (400 MHz, CDCl₃): δ 7.25 (s, 1H), 6.79 (s, 1H), 3.92 (t, *J* = 6.4 Hz, 4H), 2.10 (s, 1H), 1.83 – 1.73 (m, 4H), 1.62 (s, 6H), 1.53 – 1.44 (m, 4H), 1.37 – 1.29 (m, 8H), 0.94. – 0.87 (m, 6H) ppm.

$^{13}\text{C}\{^1\text{H}\}$ NMR (101 MHz, CDCl_3): δ 154.50, 151.88, 123.84, 116.30, 113.12, 98.70, 87.59, 78.33, 70.24, 69.84, 65.90, 31.70, 31.62, 31.55, 29.41, 29.27, 25.87, 25.81, 22.77, 22.73, 14.19, 14.18 ppm.

HR-MS (ESI, +): m/z calcd. for $\text{C}_{23}\text{H}_{35}\text{IO}_3\text{Na}$ $[\text{M}+\text{Na}]^+$ 509.1523, found 509.1523.

Synthesis of Compound 20:



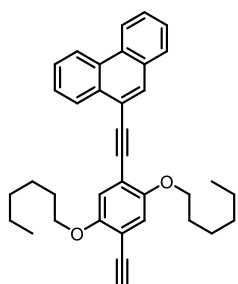
Previously prepared free acetylene **13** (594 mg, 2.94 mmol, 1.1 eq.) and iodo-compound **10** (1.30 g, 2.67 mmol, 1.0 eq.) were dissolved in THF (40 mL) and piperidine (10 mL). The reaction mixture was degassed with Argon for 20 min. $\text{Pd}(\text{PPh}_3)_4$ (309 mg, 267 μmol , 10 mol%) and CuI (52 mg, 267 μmol , 10 mol%) were added and the reaction mixture was stirred for 16 h at RT. Afterwards, the reaction mixture was plugged over celite and the solvent was evaporated under reduced pressure. The crude was

purified by column chromatography (silica gel, cyclohexane/ CH_2Cl_2 (1:2) to (pure CH_2Cl_2)) to give HOP-protected acetylene **20** (1.30 g, 2.32 mmol, **87%**) as a yellow solid.

^1H NMR (400 MHz, CDCl_3): δ 8.75 – 8.64 (m, 3H), 8.08 (s, 1H), 7.86 (dd, $J = 7.9, 1.5$ Hz, 1H), 7.74 – 7.63 (m, 3H), 7.62 – 7.57 (m, 1H), 7.11 (s, 1H), 6.97 (s, 1H), 4.10 – 4.00 (m, 4H), 2.26 (s, 1H), 2.03 – 1.92 (m, 2H), 1.89 – 1.79 (m, 2H), 1.67 (s, 6H), 1.61 – 1.49 (m, 4H), 1.43 – 1.28 (m, 8H), 0.97 – 0.90 (m, 3H), 0.90 – 0.83 (m, 3H) ppm.

$^{13}\text{C}\{^1\text{H}\}$ NMR (101 MHz, CDCl_3): δ 153.95, 153.72, 131.62, 131.42, 131.31, 130.45, 130.20, 128.69, 127.55, 127.49, 127.18, 127.06, 127.05, 122.80, 122.77, 120.08, 116.86, 116.56, 113.90, 113.56, 99.44, 93.41, 90.76, 78.76, 69.66, 69.52, 65.92, 31.79, 31.76, 31.59, 29.64, 29.47, 25.89, 25.87, 22.80, 22.76, 14.22, 14.15 ppm.

HR-MS (ESI, +): m/z calcd. for $\text{C}_{39}\text{H}_{44}\text{O}_3\text{Na}$ $[\text{M}+\text{Na}]^+$ 583.3183, found 583.3173.

Synthesis of Compound 21:

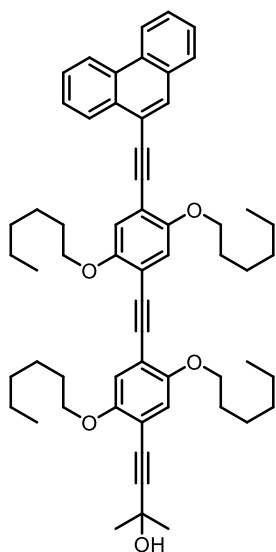
HOP protected compound **20** (1.0 g, 1.78 mmol, 1.0 eq.) and NaOH (712 mg, 17.8 mmol, 10 eq.) were dissolved in toluene (40 mL) and the reaction mixture was put in previously preheated oil bath and stirred for 16 h at 110 °C. Afterwards, the reaction mixture was diluted with toluene, washed with water (3x), brine, dried over Na₂SO₄, filtered, and the solvent was evaporated under reduced pressure. The crude was purified by column

chromatography (dry load, silica gel, cyclohexane/CH₂Cl₂) to give free acetylene **21** (880 mg, 1.75 mmol, **98 %**) as a yellow solid.

¹H NMR (400 MHz, CDCl₃): δ 8.75 – 8.65 (m, 3H), 8.08 (s, 1H), 7.87 (dd, *J* = 7.9, 1.5 Hz, 1H), 7.75 – 7.65 (m, 3H), 7.64 – 7.58 (m, 1H), 7.12 (s, 1H), 7.04 (s, 1H), 4.11 – 4.04 (m, 4H), 3.38 (s, 1H), 2.02 – 1.94 (m, 2H), 1.90 – 1.81 (m, 2H), 1.63 – 1.47 (m, 4H), 1.42 – 1.28 (m, 8H), 0.96 – 0.90 (m, 3H), 0.86 (t, *J* = 7.1 Hz, 3H) ppm.

¹³C{¹H} NMR (101 MHz, CDCl₃): δ 154.28, 153.86, 131.74, 131.42, 131.32, 130.50, 130.22, 128.73, 127.61, 127.49, 127.22, 127.10, 122.83, 122.80, 120.02, 117.25, 116.93, 114.60, 112.79, 93.62, 90.60, 82.54, 80.24, 69.86, 69.57, 31.80, 31.70, 29.63, 29.30, 25.90, 25.77, 22.78, 22.76, 14.19, 14.16 ppm.

The analytical data are in agreement with the ones reported in ref.³⁶

Synthesis of Compound 22:

Previously prepared free acetylene **21** (880 mg, 1.75 mmol, 1.3 eq.) and monoiodine **10** (640 mg, 1.32 mmol, 1.0 eq.) were dissolved in THF (50 mL) and DIPA (10 mL). The reaction mixture was degassed with Argon for 20 min. Pd(PPh₃)₄ (92 mg, 79.6 μmol, 6 mol%) and CuI (25 mg, 132 μmol, 10 mol%) were added and the reaction mixture was stirred for 16 h at room temperature. Afterwards, the reaction mixture was plugged over celite and the solvent was evaporated under reduced pressure. The crude was purified by column chromatography (silica gel, cyclohexane/ CH₂Cl₂ (1:1) to (pure CH₂Cl₂)) to give HOP-protected acetylene **22** (1.11 g, 1.29 mmol, **98%**) as a yellow amorphous solid.

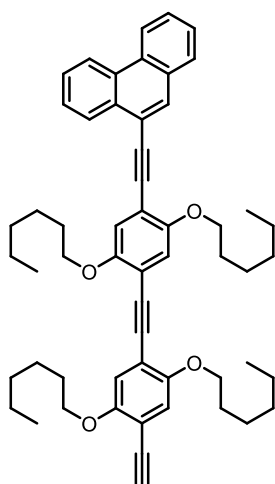
¹H NMR (400 MHz, CDCl₃): δ 8.76 – 8.65 (m, 3H), 8.09 (s, 1H), 7.87 (dd, *J* = 7.9, 1.5 Hz, 1H), 7.76 – 7.64 (m, 3H), 7.63 – 7.58 (m, 1H), 7.15 (s, 1H), 7.07 (s, 1H), 7.00 (s, 1H), 6.92 (s, 1H), 4.10 (t, *J* = 6.6 Hz, 4H), 4.00 (dt, *J* = 18.0, 6.5 Hz, 4H), 2.03 – 1.95

(m, 2H), 1.92 – 1.77 (m, 6H), 1.65 (s, 6H), 1.62 – 1.48 (m, 8H), 1.42 – 1.28 (m, 16H), 0.95 – 0.84 (m, 12H) ppm.

$^{13}\text{C}\{^1\text{H}\}$ NMR (101 MHz, CDCl_3): δ 154.06, 153.79, 153.63, 153.57, 131.65, 131.47, 131.36, 130.48, 130.24, 128.72, 127.57, 127.53, 127.21, 127.09, 122.83, 122.80, 120.14, 117.40, 117.18, 117.11, 116.62, 114.54, 114.43, 113.98, 113.46, 99.33, 93.60, 91.63, 91.58, 90.94, 78.74, 69.95, 69.85, 69.54, 65.95, 31.82, 31.79, 31.77, 31.76, 31.60, 29.69, 29.49, 29.47, 29.43, 25.94, 25.88, 25.84, 25.81, 22.80, 22.78, 14.21, 14.16 ppm.

MALDI-ToF-MS (RP, DCTB): m/z calcd. for $\text{C}_{59}\text{H}_{72}\text{O}_5$: 860.538, found 860.503.

Synthesis of Compound 23:

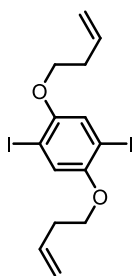


HOP-protected acetylene **22** (325 mg, 377 μmol , 1.0 eq.) and NaOH (151 mg, 3.77 mmol, 10 eq.) were dissolved in toluene (30 mL) and the reaction mixture was put in previously preheated oil bath and stirred for 16 h at 110 °C. Afterwards, the reaction mixture was diluted with toluene, washed with water (3x), brine, dried over Na_2SO_4 , filtered and the solvent was evaporated under reduced pressure to give free acetylene **23** (300 mg, 374 μmol , 99%) as a yellow solid which was used in the next step without further purification.

^1H NMR (400 MHz, CDCl_3): δ 8.77 – 8.66 (m, 3H), 8.09 (s, 1H), 7.88 (dd, $J = 7.9, 1.5$ Hz, 1H), 7.76 – 7.65 (m, 3H), 7.64 – 7.58 (m, 1H), 7.15 (s, 1H), 7.07 (s, 2H), 7.03 (s, 1H), 7.00 (s, 1H), 4.10 (t, $J = 6.6$ Hz, 4H), 4.02 (q, $J = 6.5$ Hz, 4H), 3.36 (s, 1H), 2.06 – 1.95 (m, 2H), 1.93 – 1.78 (m, 6H), 1.64 – 1.45 (m, 8H), 1.42 – 1.29 (m, 16H), 0.95 – 0.84 (m, 12H) ppm.

$^{13}\text{C}\{^1\text{H}\}$ NMR (101 MHz, CDCl_3): δ 154.31, 154.06, 153.67, 153.48, 131.66, 131.46, 131.35, 130.48, 130.24, 128.72, 127.58, 127.53, 127.21, 127.09, 122.83, 122.80, 120.13, 118.08, 117.18, 116.62, 115.10, 114.44, 114.06, 112.72, 93.63, 91.79, 91.47, 90.93, 82.46, 80.21, 69.94, 69.87, 69.76, 69.54, 31.82, 31.78, 31.76, 31.69, 29.69, 29.46, 29.40, 29.30, 25.94, 25.84, 25.81, 25.76, 22.80, 22.74, 14.20, 14.16 ppm.

The analytical data are in agreement with the ones reported in ref.³⁶

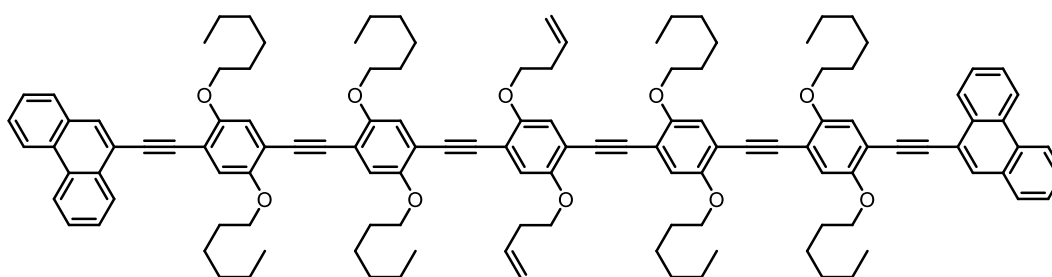
Synthesis of 1,4-bis(but-3-en-1-yloxy)-2,5-diiodobenzene (11):

2,5-Diiodobenzene-1,4-diol (**26**) (1.20 g, 3.32 mmol, 1.0 eq.), 4-bromo-1-butene (2.6 mL, 3.45 g, 25.6 mmol, 7.7 eq.) and K_2CO_3 (3.50 g, 25.2 mmol, 7.6 eq.) were dissolved in dry DMF (40 mL) and stirred at room temperature for 16 h. The reaction mixture was quenched with water, extracted with Et_2O (3x), washed with aq. HCl (aq., 1 M) and brine, dried over Na_2SO_4 , filtered, and the solvent was removed under reduced pressure. The crude was purified by column chromatography (pure cyclohexane to cyclohexane: EA 9/1) to provide the central moiety **11** (1.52 g, 3.23 mmol, 97%) as a beige oil that solidified at room temperature.

1H NMR (400 MHz, $CDCl_3$): δ 7.18 (s, 2H), 6.01 – 5.88 (m, 2H), 5.23 – 5.16 (m, 2H), 5.15– 5.10 (m, 2H), 3.98 (t, $J = 6.6$ Hz, 4H), 2.60 – 2.53 (m, 4H) ppm.

$^{13}C\{^1H\}$ NMR (101 MHz, $CDCl_3$): δ 152.96, 134.33, 123.14, 117.52, 86.49, 69.88, 33.79 ppm.

HR-MS (ESI, +): m/z calcd. for $C_{14}H_{16}I_2O_2Na$ $[M+Na]^+$ 492.9132, found 492.9122.

Synthesis of OPE Precursor (8):

Chemical Formula: $C_{126}H_{146}O_{10}$
Exact Mass: 1819.0916

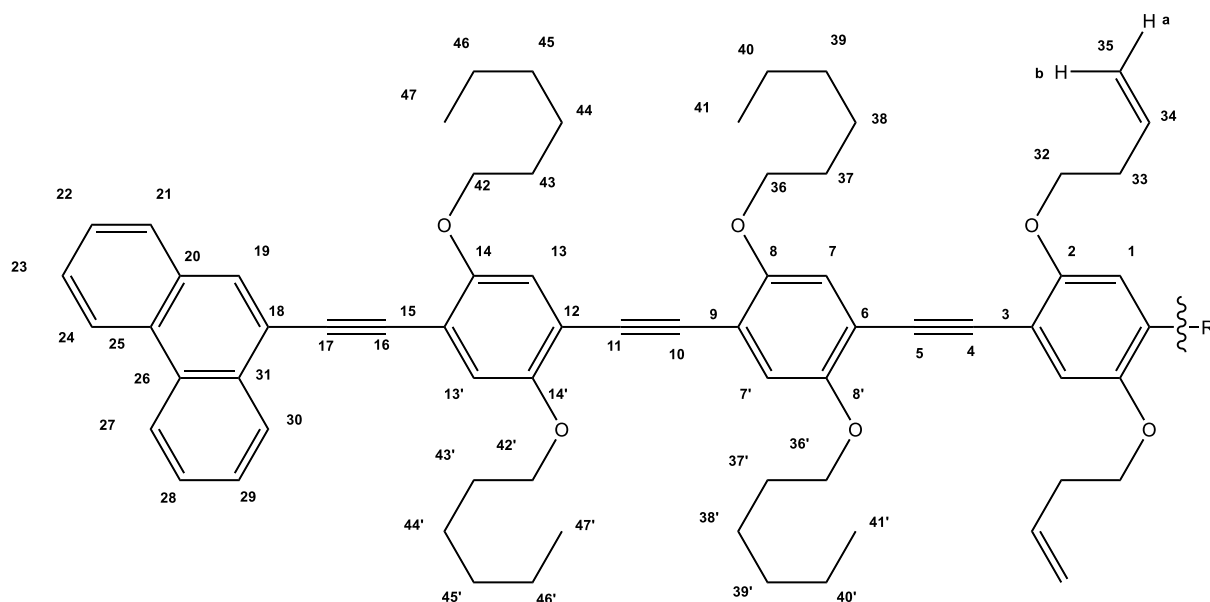
Previously prepared free acetylene **23** (200 mg, 249 μ mol, 2.4 eq.) and diiodo compound **11** (49 mg, 104 μ mol, 1.0 eq.) were dissolved in toluene (10 mL) and piperidine (4 mL). The reaction mixture was degassed with Argon for 20 min. $Pd(PPh_3)_4$ (6 mg, 5.2 μ mol, 5 mol%) and CuI (2 mg, 10.4 μ mol, 10 mol%) were added. The reaction mixture was stirred for 16 h at room temperature. Afterwards, the reaction mixture was plugged over celite and the solvent was evaporated under reduced pressure. The crude was purified by column chromatography (silica gel, toluene) and manual gel-permeation chromatography (Biobeads SX-3 in toluene) to give product (94 mg, 51.6 μ mol, **50%**) as a yellow amorphous solid.

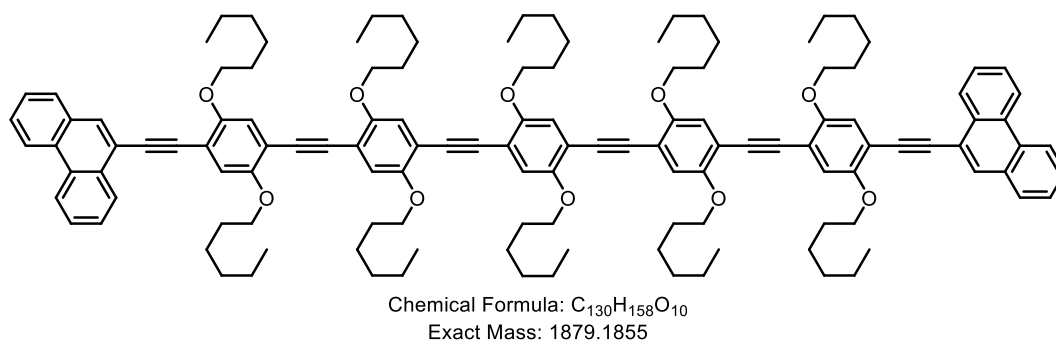
1H NMR (600 MHz, TCE- d_2 , 343 K): δ 8.78 – 8.74 (m, 4H, H27/30), 8.72 (d, $J = 8.3$ Hz, 2H, H24), 8.14 (s, 2H, H19), 7.93 (d, $J = 7.8$ Hz, 2H, H21), 7.80 – 7.69 (m, 8H, H23/28/29), 7.68 – 7.65 (m, 2H, H22), 7.22 (s, 2H, H13'), 7.13 (s, 2H, H13), 7.10 (s, 6H, H7/7'/1), 6.10 – 6.02 (m,

4H, H34), 5.30 – 5.25 (m, 2H, H35a), 5.20 -5.17 (m, 2H, H35b), 4.21 – 4.16 (m, 12H, H42/42'/32), 4.15 – 4.10 (m, 8H, H36/36'), 2.68 (q, $J = 6.7$ Hz, 4H, H33), 2.02 (p, $J = 6.9$ Hz, 4H, H43'), 1.97 – 1.88 (m, 12H, H43/37/37'), 1.69 – 1.57 (m, 16H, H44/44'/38/38'), 1.49 – 1.36 (m, 32H, H46/46'/45/45'/40/40'/39/39), 1.01 – 0.91 (m, 24H, H47/47'/41/41') ppm.

$^{13}\text{C}\{^1\text{H}\}$ NMR (151 MHz, TCE- d_2 , 343 K): δ 154.10 (C14'), 153.74(C8/8'/2), 153.71 (C14), 153.67 (C8/8'/2), 134.34 (C34), 131.40 (C19), 131.22 (C20), 131.09 (C31), 130.21 (C25), 130.01 (C26), 128.39 (C21), 127.25 (C23), 127.00 (C29), 126.89 (C22), 126.88 (C28), 122.58 (C24/27), 122.54 (C24/27), 119.99 (C18), 118.43 (C7/7'/1), 118.13 (C7/7'/1), 118.02 (C13'/7/7'/1), 117.21 (C13), 116.82 (C35), 115.04 (C9/6/3), 114.98 (C12), 114.92 (C9/6/3), 114.69 (C9/6/3), 114.31 (C15), 93.34 (C17), 91.92 (C10/5/4), 91.76 (C11), 91.71 (C10/5/4), 91.41 (C10/5/4), 90.94 (C16), 70.32 (C42'), 70.20 (C36/36'), 70.15 (C36/36'), 69.88 (C42), 69.59 (C32), 33.69 (C33), 31.44 (C45/45'/39/39'), 31.42 (C45/45'/39/39'), 31.41 (C45/45'/39/39'), 29.47 (C43/43'/37/37'), 29.44 (C43/43'/37/37'), 29.33 (C43/43'/37/37'), 29.29 (C43/43'/37/37'), 25.59 (C44/44'/38/38'), 25.54 (C44/44'/38/38'), 25.52 (C44/44'/38/38'), 22.41 (C46/46'/40/40'), 22.40 (C46/46'/40/40'), 22.38 (C46/46'/40/40'), 22.38 (C46/46'/40/40'), 13.79 (C47/47'/41/41'), 13.78 (C47/47'/41/41'), 13.74 (C47/47'/41/41') ppm.

MS (MALDI-ToF, RP, DCTB): m/z calcd. for $\text{C}_{126}\text{H}_{146}\text{O}_{10}$ $[\text{M}]^+$ 1819.0916, found 1819.022.



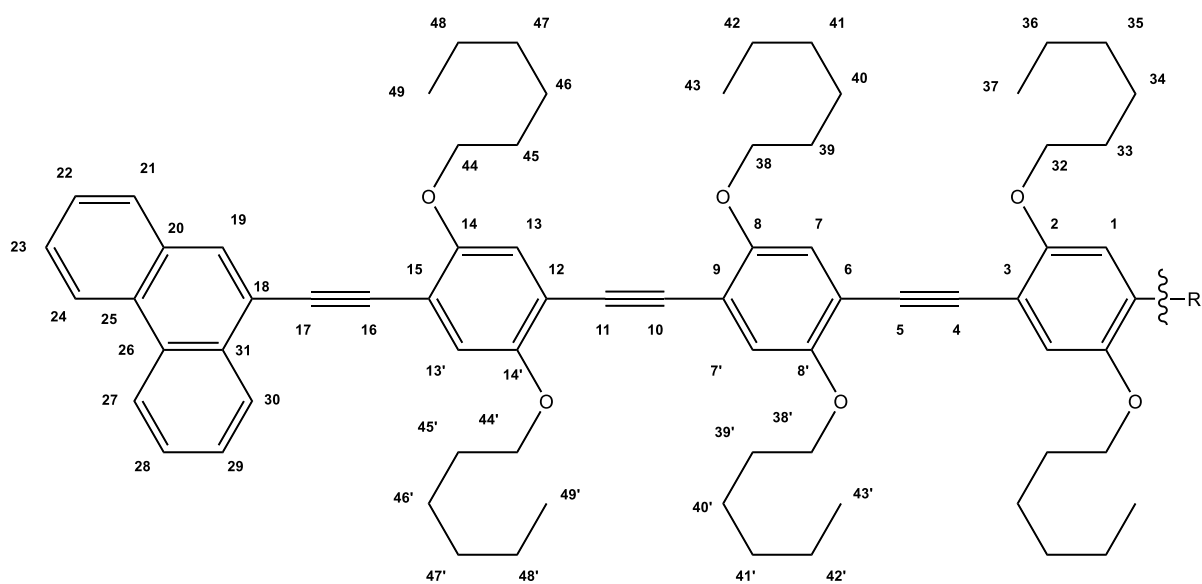
Synthesis of Referenz OPE5 (27):

Previously prepared free acetylene **27** (118 mg, 147 μmol , 2.6 eq.) and diiodo compound **16** (30 mg, 56.5 μmol , 1.0 eq.) were dissolved in toluene (4 mL) and piperidine (1 mL). The reaction mixture was degassed with Argon for 20 min. Pd(PPh₃)₄ (3 mg, 2.8 μmol , 5 mol%) and CuI (1 mg, 5.6 μmol , 10 mol%) were added and the reaction mixture was stirred for 16 h at room temperature. Afterwards, the reaction mixture was plugged over Celite® and the solvent was evaporated under reduced pressure. The crude was purified by column chromatography (silica gel, cyclohexane/ CH₂Cl₂ (1:2) to pure CH₂Cl₂) and manual gel-permeation chromatography (*BioBeads*, SX-3 in toluene) to give product **27** (60 mg, 32.2 μmol , **57%**) as a yellow amorphous solid.

¹H NMR (600 MHz, TCE-d₂, 343 K): δ 8.77 – 8.73 (m, 4H, H27/30), 8.71 (d, J = 8.3 Hz, 2H, H24), 8.14 (s, 2H, H19), 7.92 (d, J = 7.8 Hz, 2H, H21), 7.79 – 7.70 (m, 6H, H23/28/29), 7.68 – 7.64 (m, 2H, H22), 7.21 (s, 2H, H13'), 7.12 (s, 2H, H13), 7.10 – 7.07 (m, 6H, H7/7'/1), 4.20 – 4.15 (m, 4H, H44/44'), 4.14 – 4.09 (m, 14H, H38/38'/32), 2.02 (p, J = 6.9 Hz, 4H, H45'), 1.92 (m, 16 H, H45/39/39'/33), 1.96 – 1.87 (m, 20H, H46/46'/40/40'/34), 1.48 – 1.35 (m, 40H, H47/47'/48/48'/41/41'/42/42'/35/36), 0.99 – 0.90 (m, 30 H, H49/49'/43/43'/37) ppm.

¹³C{¹H} NMR (151 MHz, TCE-d₂, 343 K): δ 154.09 (C14'), 153.75 (C8/8'/2), 153.70 (C14), 131.40 (C19), 131.22 (C20), 131.08 (C31), 130.20 (C25), 130.00 (C26), 128.39 (C21), 127.36 (C23), 127.26 (C30), 127.01 (29), 126.90 (C22), 126.89 (C28), 122.58 (C27), 122.54 (C24), 119.99 (C18), 118.08 (C13'/7/7'/1), 117.19 (C13), 114.98 (C12), 114.82 (C9/6/3), 114.28 (C15), 93.33 (C17), 91.67 (C11/10/5/4), 90.94 (C16), 70.31 (C44'), 70.18 (C38/38'/32), 69.87 (C44), 31.44 (C47/47'/41/41'/35), 31.43 (C47/47'/41/41'/35), 29.47 (C45/45'/39/39'/33), 29.44 (C45/45'/39/39'/33), 29.32 (C45/45'/39/39'/33), 29.30 (C45/45'/39/39'/33), 25.60 (C46/46'/40/40'/34), 25.55 (C46/46'/40/40'/34), 25.53 (C46/46'/40/40'/34), 22.41 (C48/48'/42/42'/36), 22.40 (C48/48'/42/42'/36), 22.39 (C48/48'/42/42'/36), 22.38 (C48/48'/42/42'/36), 13.86 (C49/49'/43/43'/37), 13.79 (C49/49'/43/43'/37), 13.78 (C49/49'/43/43'/37), 13.75 (C49/49'/43/43'/37) ppm.

MS (MALDI-ToF, RP, DCTB): m/z calcd. for $C_{130}H_{158}O_{10}$ $[M]^+$ 1879.1855, found 1879.113.



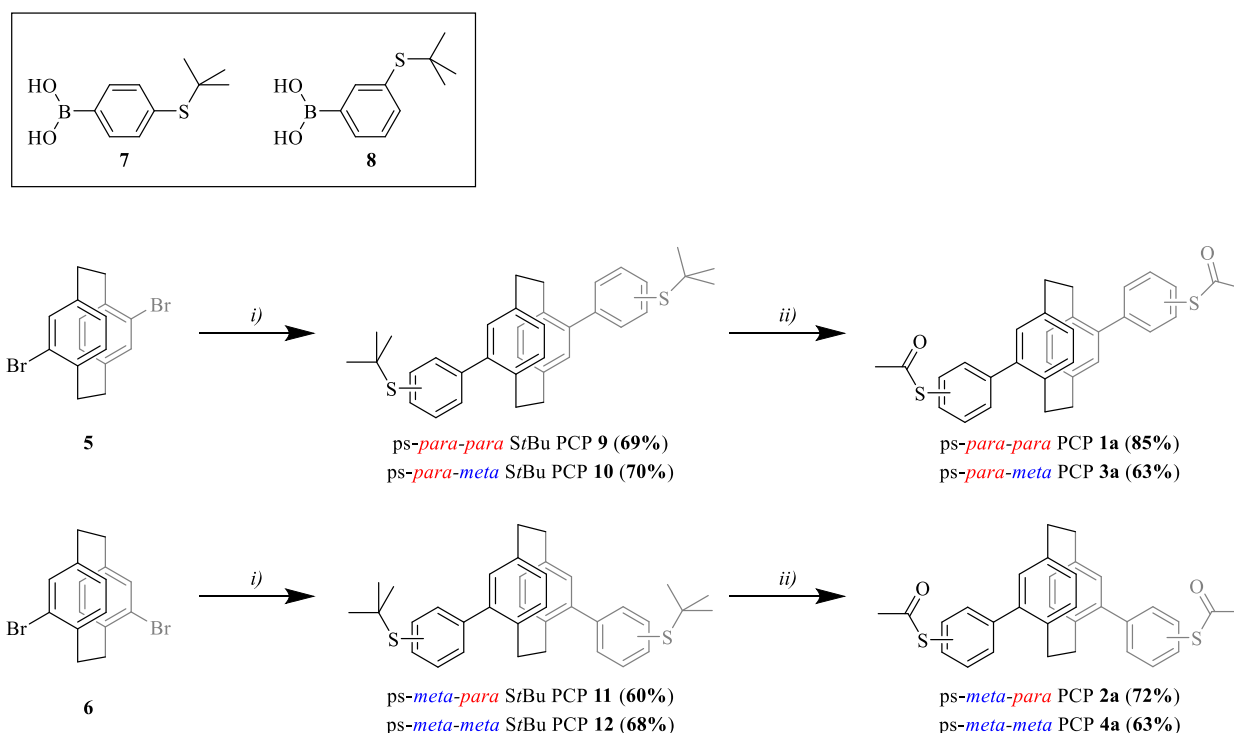
5.4 Supporting Information: Subchapter 2.2

The following Supporting Information was integrated as published with NMR and HR-MS spectra provided in the appendix.

Reznikova, K.; Hsu, C.; Schosser, W. M.; Gallego, A.; Beltako, K.; Pauly, F.; van der Zant, H. S. J.; Mayor, M. Substitution Pattern Controlled Quantum Interference in [2.2]Paracyclophane-Based Single-Molecule Junctions. *J. Am. Chem. Soc.* **2021**, *143* (34), 13944–13951.

5.4.1 Synthesis and Characterization

General Remarks: All commercially available compounds were purchased from Sigma-Aldrich, Acros, Apollo Scientific, Alfa Aesar, and Fluorochem and used without further purification. Anhydrous solvents were purchased from Sigma-Aldrich and stored over molecular sieves (4 Å). All reactions with reagents that are easily oxidized or hydrolyzed were performed under argon using *Schlenk* techniques with anhydrous solvents in oven-dried glassware. Column chromatography was performed on silica gel P60 (40-63 µm) from Silicycle™ using technical grade solvents. TLC was performed with silica gel 60 F254 aluminum sheets with a thickness of 0.25 mm purchased from Merck. Melting points were measured on a Büchi M-565 melting point apparatus and are uncorrected. ¹H NMR and ¹³C{¹H} NMR experiments were performed on Bruker Avance III NMR spectrometers operating at 500 MHz and 126 MHz proton frequencies, respectively. The instruments were equipped with an indirect-detection 5 mm BBI probe and with actively shielded z-gradients. The chemical shifts are reported in parts per million (ppm) referenced to the residual solvent peak, and the coupling constants (*J*) are given in hertz (Hz). All spectra were recorded at 298.15 K. For high-resolution mass spectra (HR-MS), a HR-ESI-ToF-MS measurement on a *maXis*™ 4G instrument from Bruker was used. Since the synthesized compounds **1a-4a** as well as **9-12** shown in this publication were less prone to form adducts with common ions like H⁺, NH₄⁺, K⁺ or Na⁺, the characteristic binding of silver ions to aromatic hydrocarbons^{219,220} was used to increase the signal intensity in the HR-ESI-ToF-MS analysis.

5.4.1.1 Experimental Procedures

Scheme S 1: Synthesis Overview: i) boronic acid **7** or **8**, K₂CO₃, Pd(PPh₃)₄, toluene/H₂O (6:1), 110 °C, 16 h; b) Bi(OTf)₃, AcCl, dry toluene/MeCN (1:1), RT, 2-3 h. The substitution patterns of the molecules in both the central PCP subunit and in the peripheral subunits are labeled in red and blue for *para*- and *meta*-substitution, respectively. For simplicity, the naming of structures was done according to the prefixes with ps as an abbreviation for pseudo, followed by the prefix referring to the substitution pattern of the central PCP subunit and the second one to the substitution pattern of the thiol anchoring group in the phenyl subunits.

Pseudo-*para*-dibromo[2.2]paracyclophane **5** and pseudo-*meta*-dibromo[2.2]paracyclophane **6** were synthesized over the bromination of [2.2]paracyclophane according to literature known procedure.⁸³ (3-(*Tert*-butylthio)phenyl)boronic acid **8** was commercially available. (4-(*Tert*-butylthio)phenyl)boronic acid **7** was prepared according to literature known procedures, starting from the respective 4-bromothiophenol and *tert*-butyl chloride in the presence of AlCl₃ to give the desired thioether¹²³, followed by lithium-halogen exchange, reacting with B(OMe)₃ and hydrolysis to the desired boronic acid **7**.¹²⁴

General Procedure 1: Suzuki-Miyaura Cross-Coupling Reaction

Dibromo[2.2]paracyclophane **5** or **6** (1.0 eq.), boronic acid **7** or **8** (2.4 eq.), and potassium carbonate (2.0 eq.) were dissolved in toluene/water (6:1). The reaction mixture was sparged with argon for 20 min. Pd(PPh₃)₄ (10 mol%) was added, and the reaction mixture was heated to 110 °C for 16 h. Afterward, the reaction mixture was cooled to room temperature, diluted with toluene and washed with water (3x), brine (1x), dried over Na₂SO₄, and filtered. The

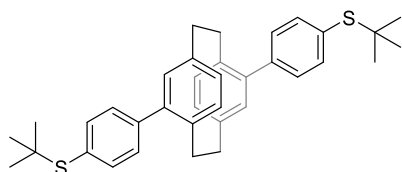
solvent was removed under reduced pressure, and the crude product was purified by flash column chromatography.

General Procedure 2: Transprotection Reaction

This reaction procedure was adopted from literature.²²³

Previously prepared compounds **9** – **12** (1.0 eq.) and acetyl chloride (50 eq.) were dissolved in dry toluene/MeCN (1:1) under argon atmosphere. Bismuth(III)trifluoromethanesulfonate (3.0 eq.) was added and the reaction mixture was stirred at room temperature till full conversion was observed by TLC (2-3 h). Then, water was added, and the aqueous layer was extracted with CH₂Cl₂ (3x). The combined organic layers were dried over Na₂SO₄ and filtered. The solvent was removed under reduced pressure and the crude product was purified by flash column chromatography.

Pseudo-*para*-bis((4'-*tert*-butylthio)phenyl)[2.2]paracyclophane (*ps-para-para* S*t*Bu PCP **9**):



Compound **9** was synthesized according to general procedure 1 using pseudo-*para*-dibromo[2.2]paracyclophane **5** (200 mg, 546 μmol, 1.0 eq.), (4-(*tert*-butylthio)phenyl)boronic acid **7** (275 mg, 1.31 mmol, 2.4 eq.), K₂CO₃ (151 mg, 1.09 mmol, 2.0 eq.), Pd(PPh₃)₄ (63 mg, 54.6 μmol, 10 mol%), toluene (12 mL) and water (2 mL). The crude was purified by flash column chromatography (cyclohexane/CH₂Cl₂ 2:1) to give *ps-para-para* S*t*Bu PCP **9** (201 mg, 386 μmol, 69%) as a white solid.

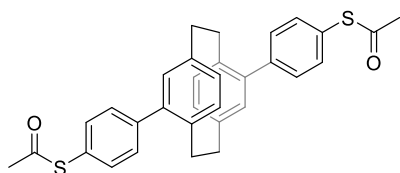
TLC (SiO₂, cyclohexane/CH₂Cl₂ 2:1): R_f = 0.15

m.p. > 270 °C (decomposition)

¹H NMR (500 MHz, CDCl₃): δ 7.68 – 7.62 (m, 4H, Ar-H), 7.51 – 7.47 (m, 4H, Ar-H), 6.69 – 6.64 (m, 4H, PCPAr-H), 6.60 (dd, *J* = 7.7, 1.9 Hz, 2H, PCPAr-H), 3.45 (ddd, *J* = 13.9, 9.9, 4.3 Hz, 2H, CH₂), 3.04 (ddd, *J* = 13.9, 10.0, 4.7 Hz, 2H, CH₂), 2.87 (ddd, *J* = 14.1, 10.0, 4.2 Hz, 2H, CH₂), 2.78 (ddd, *J* = 13.7, 9.9, 4.7 Hz, 2H, CH₂), 1.36 (s, 18H, *t*Bu-H) ppm.

¹³C{¹H} NMR (126 MHz, CDCl₃): δ 141.8, 141.5, 140.1, 137.7, 137.0, 135.0, 132.5, 131.4, 129.9, 129.6, 46.2, 34.9, 34.0, 31.2 ppm.

HR-MS (ESI, +): *m/z* calcd. for C₃₆H₄₀S₂Ag [M+Ag]⁺ 643.1617; found: 643.1604.

Pseudo-*para*-bis((4'-acetylthio)phenyl)[2.2]paracyclophane (ps-*para-para* PCP 1a):

Compound **1a** was synthesized according to general procedure 2 using compound **9** (51 mg, 95 μ mol, 1.0 eq.), acetyl chloride (0.34 mL, 4.75 mmol, 50 eq.), bismuth(III)trifluoromethane-sulfonate (189 mg, 282 μ mol, 3.0 eq.), toluene (10 mL) and acetonitrile (10 mL). The crude was purified by flash column chromatography (cyclohexane/ CH_2Cl_2 1:4) to give ps-*para-para* PCP **1a** (41 mg, 81 μ mol, 85%) as a white solid.

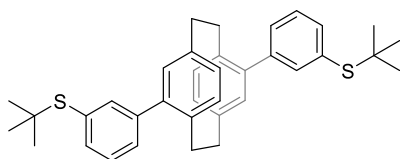
TLC (SiO_2 , cyclohexane/ CH_2Cl_2 1:4): R_f = 0.19

m.p. > 290 $^\circ\text{C}$ (decomposition)

^1H NMR (500 MHz, CDCl_3): 7.59 – 7.52 (m, 8H, Ar-H), 6.68 – 6.64 (m, 4H, PCPar-H), 6.59 (dd, J = 7.8, 1.9 Hz, 2H, PCPar-H), 3.44 (ddd, J = 14.0, 9.9, 4.4 Hz, 2H, CH_2), 3.05 (ddd, J = 14.0, 9.9, 4.8 Hz, 2H, CH_2), 2.90 – 2.78 (m, 4H, CH_2), 2.48 (s, 6H, SAc-H) ppm.

$^{13}\text{C}\{^1\text{H}\}$ NMR (126 MHz, CDCl_3): δ 194.2, 142.5, 141.2, 140.2, 137.1, 135.1, 134.6, 132.5, 130.6, 129.8, 126.6, 34.9, 33.9, 30.4 ppm.

HR-MS (ESI, +): m/z calcd. for $\text{C}_{32}\text{H}_{28}\text{O}_2\text{S}_2\text{Ag}$ [$\text{M}+\text{Ag}$] $^+$ 615.0576; found: 615.0572.

Pseudo-*para*-bis((3'-*tert*-butylthio)phenyl)[2.2]paracyclophane (ps-*para-meta* StBu PCP 10):

Compound **10** was synthesized according to general procedure 1 using pseudo-*para*-dibromo[2.2]paracyclophane **5** (150 mg, 410 μ mol, 1.0 eq.), (3-(*tert*-butylthio)phenyl)boronic acid **8** (207 mg, 984 μ mol, 2.4 eq.), K_2CO_3 (113 mg, 820 μ mol, 2.0 eq.), $\text{Pd}(\text{PPh}_3)_4$ (47 mg, 41 μ mol, 10 mol%), toluene (12 mL) and water (2 mL). The crude was purified by flash column chromatography (cyclohexane/ CH_2Cl_2 3:1) to give ps-*para-meta* StBu PCP **10** (154 mg, 287 μ mol, 70%) as a white solid.

TLC (SiO_2 , cyclohexane/ CH_2Cl_2 3:1): R_f = 0.15

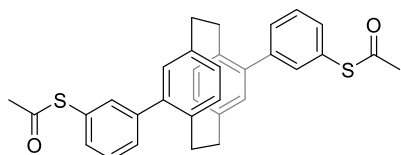
m.p.: 168 – 170 $^\circ\text{C}$

^1H NMR (500 MHz, CDCl_3): δ 7.72 (t, J = 1.7 Hz, 2H, Ar-H), 7.55 (m, 4H, Ar-H), 7.46 (t, J = 7.6 Hz, 2H, Ar-H), 6.69 – 6.66 (m, 4H, PCPAr-H), 6.60 (dd, J = 7.9, 1.9 Hz, 2H, PCPAr-H), 3.45 (ddd, J = 13.9, 10.0, 4.3 Hz, 2H, CH_2), 3.05 (ddd, J = 14.0, 10.0, 4.7 Hz, 2H, CH_2), 2.87 (ddd, J = 14.1, 10.0, 4.3 Hz, 2H, CH_2), 2.79 (ddd, J = 13.7, 9.9, 4.7 Hz, 2H, CH_2), 1.38 (s, 18H, $t\text{Bu-H}$) ppm.

$^{13}\text{C}\{^1\text{H}\}$ NMR (126 MHz, CDCl_3): δ 141.7, 141.5, 140.1, 138.9, 137.0, 136.0, 135.0, 133.0, 132.4, 130.4, 129.5, 128.8, 46.3, 34.9, 33.9, 31.2 ppm.

HR-MS (ESI, +): m/z calcd. for $\text{C}_{36}\text{H}_{40}\text{S}_2\text{Ag}$ $[\text{M}+\text{Ag}]^+$ 643.1617; found: 643.1610.

Pseudo-*para*-bis((3'-acetylthio)phenyl)[2.2]paracyclophane (ps-*para*-*meta* PCP 3a):



Compound **3a** was synthesized according to general procedure 2 using compound **10** (50 mg, 93.1 μmol , 1.0 eq.), acetyl chloride (0.33 mL, 4.66 mmol, 50 eq.), bismuth(III)trifluoromethane-sulfonate (187 mg, 279 μmol ,

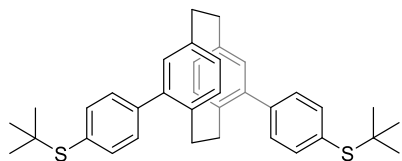
3.0 eq.), toluene (4 mL) and acetonitrile (4 mL). The crude was purified by flash column chromatography (cyclohexane/ CH_2Cl_2 1:2) to give ps-*para*-*meta* PCP **3a** (30 mg, 59 μmol , 63%) as a white amorphous solid.

TLC (SiO_2 , cyclohexane/ CH_2Cl_2 1:2): R_f = 0.15

^1H NMR (500 MHz, CDCl_3): δ 7.59 – 7.56 (m, 4H, Ar-H), 7.54 (t, J = 7.8 Hz, 2H, Ar-H), 7.43 (dt, J = 7.4, 1.6 Hz, 2H, Ar-H), 6.67 – 6.62 (m, 6H, PCPAr-H), 3.48 (ddd, J = 13.8, 9.9, 4.2 Hz, 2H, CH_2), 3.04 (ddd, J = 14.0, 10.0, 4.9 Hz, 2H, CH_2), 2.92 – 2.78 (m, 4H, CH_2), 2.49 (s, 6H, SAc-H) ppm.

$^{13}\text{C}\{^1\text{H}\}$ NMR (126 MHz, CDCl_3): δ 194.0, 142.4, 141.1, 140.2, 137.1, 136.0, 135.0, 132.5, 132.4, 130.9, 129.7, 129.5, 128.3, 34.8, 33.8, 30.5 ppm.

HR-MS (ESI, +): m/z calcd. for $\text{C}_{32}\text{H}_{28}\text{O}_2\text{S}_2\text{Ag}$ $[\text{M}+\text{Ag}]^+$ 615.0576; found: 615.0576.

Pseudo-*meta*-bis((4'-*tert*-butylthio)phenyl)[2.2]paracyclophane (ps-*meta*-*para* StBu PCP 11):

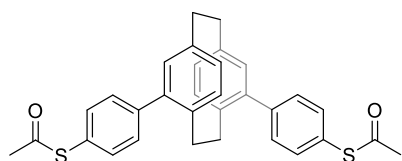
Compound **11** was synthesized according to general procedure 2 using pseudo-*meta*-dibromo[2.2]paracyclophane **6** (200 mg, 546 μmol , 1.0 eq.), (4-(*tert*-butylthio)phenyl)boronic acid **7** (275 mg, 1.31 mmol, 2.4 eq.), K_2CO_3 (151 mg, 1.09 mmol, 2.0 eq.), $\text{Pd}(\text{PPh}_3)_4$ (63 mg, 54 μmol , 2.0 eq.), toluene (12 mL) and water (2 mL). The crude was purified by flash column chromatography (cyclohexane/ CH_2Cl_2 3:1). The remaining impurities were precipitating in CH_2Cl_2 by adding MeOH, followed by filtration and evaporation of mother liquor to give ps-*meta*-*para* PCP **11** (175 mg, 344 μmol , 60%) as a colorless oil.

TLC (SiO_2 , cyclohexane/ CH_2Cl_2 2:1): $R_f = 0.23$

^1H NMR (500 MHz, CDCl_3): δ 7.65 – 7.61 (m, 4H, Ar-H), 7.48 – 7.44 (m, 4H, Ar-H), 6.72 (d, $J = 1.9$ Hz, 2H, PCPAr-H), 6.69 (d, $J = 7.8$ Hz, 2H, PCPAr-H), 6.58 (dd, $J = 7.7, 1.9$ Hz, 2H, PCPAr-H), 3.28 – 3.06 (m, 6H, CH_2), 2.56 – 2.48 (m, 2H, CH_2), 1.35 (s, 18H, *t*Bu-H) ppm.

$^{13}\text{C}\{^1\text{H}\}$ NMR (126 MHz, CDCl_3): δ 141.9, 141.6, 139.8, 137.7, 137.5, 132.5, 132.0, 131.6, 131.4, 129.8, 46.2, 35.3, 33.6, 31.2 ppm.

HR-MS (ESI, +): m/z calcd. for $\text{C}_{36}\text{H}_{40}\text{AgS}_2$ $[\text{M}+\text{Ag}]^+$ 643.1617; found: 643.1615.

Pseudo-*meta*-bis((4'-*tert*-acetylthio)phenyl)[2.2]paracyclophane (ps-*meta*-*para* PCP 2a):

Compound **2a** was synthesized according to general procedure 2 using compound **11** (20 mg, 37.3 μmol , 1.0 eq.), acetyl chloride (0.13 mL, 1.86 mmol, 50 eq.), bismuth(III)trifluoromethane-sulfonate (74.9 mg, 112 μmol , 3.0 eq.), toluene (2 mL) and acetonitrile (2 mL). The crude was purified by flash column chromatography (cyclohexane/ CH_2Cl_2 1:2) to give ps-*meta*-*para* PCP **2a** (13.6 mg, 33 μmol , 72%) as a white amorphous solid.

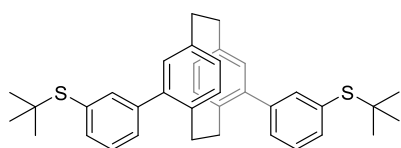
TLC (SiO_2 , cyclohexane/ CH_2Cl_2 1:2): $R_f = 0.32$

^1H NMR (500 MHz, CDCl_3): δ 7.54 – 7.50 (m, 8H, Ar-H), 6.72 (d, $J = 1.9$ Hz, 2H, PCPAr-H), 6.67 (d, $J = 7.9$ Hz, 2H, PCPAr-H), 6.57 (dd, $J = 7.8, 1.9$ Hz, 2H, PCPAr-H), 3.27 – 3.07 (m, 4H, CH_2), 2.62 – 2.54 (m, 2H, CH_2), 2.47 (s, 6H, SAc-H) ppm.

$^{13}\text{C}\{^1\text{H}\}$ NMR (126 MHz, CDCl_3): δ 194.2, 142.4, 141.7, 139.9, 137.6, 134.6, 132.6, 132.1, 131.8, 130.5, 126.6, 35.3, 33.5, 30.4 ppm.

HR-MS (ESI, +): m/z calcd. for $\text{C}_{32}\text{H}_{28}\text{O}_2\text{S}_2\text{Ag}$ $[\text{M}+\text{Ag}]^+$ 615.0576; found: 615.0583.

Pseudo-*meta*-bis((3'-*tert*-butylthio)phenyl)[2.2]paracyclophane (ps-*meta*-*meta* StBu PCP 12):



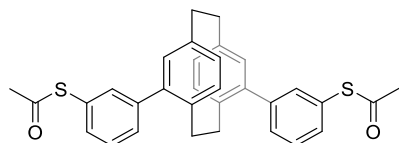
Compound **12** was synthesized according to general procedure **2** using pseudo-*meta*-dibromo[2.2]paracyclophane **6** (150 mg, 410 μmol , 1.0 eq.), (3-(*tert*-butylthio)phenyl)boronic acid **8** (200 mg, 952 μmol , 2.4 eq.), K_2CO_3 (113 mg, 820 μmol , 2.0 eq.), $\text{Pd}(\text{PPh}_3)_4$ (47.4 mg, 41 μmol , 10 mol%), toluene (12 mL) and water (2 mL). The crude was purified by flash column chromatography (cyclohexane/ CH_2Cl_2 4:1). The remaining impurities were precipitating in CH_2Cl_2 by adding MeOH, followed by filtration and evaporation of mother liquor to give ps-*meta*-*meta* StBu PCP **12** (149 mg, 278 μmol , 68 %) as a colorless oil.

TLC (SiO_2 , cyclohexane/ CH_2Cl_2 4:1): R_f = 0.13

^1H NMR (500 MHz, CDCl_3): δ 7.68 (t, J = 1.7 Hz, 2H, Ar-H), 7.54 (dt, J = 7.5, 1.5 Hz, 2H, Ar-H), 7.49 (dt, J = 7.7, 1.5 Hz, 2H, Ar-H), 7.44 (t, J = 7.6 Hz, 2H, Ar-H), 6.72 (d, J = 1.9 Hz, 2H, PCPAr-H), 6.68 (d, J = 7.8 Hz, 2H, PCPAr-H), 6.59 (dd, J = 7.8, 1.9 Hz, 2H, PCPAr-H), 3.27 – 3.06 (m, 6H, CH_2), 2.58 – 2.49 (m, 2H, CH_2), 1.36 (s, 18H, *t*Bu-H) ppm.

$^{13}\text{C}\{^1\text{H}\}$ NMR (126 MHz, CDCl_3): δ 141.9, 141.6, 139.9, 138.7, 137.5, 136.0, 133.0, 132.4, 132.0, 131.6, 130.2, 128.8, 46.3, 35.3, 33.6, 31.2 ppm.

HR-MS (ESI, +): m/z calcd. for $\text{C}_{36}\text{H}_{40}\text{AgS}_2$ $[\text{M}+\text{Ag}]^+$ 643.1617; found: 643.1604.

Pseudo-*meta*-bis((3'-*tert*-acetylthio)phenyl)[2.2]paracyclophane (ps-*meta*-*meta* PCP 4a):

Compound **4a** was synthesized according to general procedure 2 using compound **12** (50 mg, 93.1 μmol , 1.0 eq.), acetyl chloride (0.33 mL, 4.66 mmol, 50 eq.), bismuth(III)trifluoromethane-sulfonate (187 mg, 279 μmol , 3.0 eq.), toluene (4 mL) and acetonitrile (4 mL). The crude was purified by flash column chromatography (cyclohexane/ CH_2Cl_2 1:2) to give ps-*meta*-*meta* PCP **4a** (31 mg, 61 μmol , 66%) as a white amorphous solid.

TLC (SiO_2 , cyclohexane/ CH_2Cl_2 1:2): R_f = 0.26

^1H NMR (500 MHz, CDCl_3): δ 7.56 – 7.49 (m, 6H, Ar-H), 7.41 (dt, J = 6.7, 1.9 Hz, 2H, Ar-H), 6.73 (d, J = 7.8 Hz, 2H, PCPAr-H), 6.69 (d, J = 1.9 Hz, 2H, PCPAr-H), 6.58 (dd, J = 7.8, 1.9 Hz, 2H, PCPAr-H), 3.27 – 3.16 (m, 4H, CH_2), 3.14 – 3.06 (m, 2H, CH_2), 2.60 – 2.51 (m, 2H, CH_2), 2.47 (s, 6H, SAc-H) ppm.

$^{13}\text{C}\{^1\text{H}\}$ NMR (126 MHz, CDCl_3): δ 194.0, 142.2, 141.5, 139.8, 137.7, 135.7, 132.6, 132.5, 132.0, 131.7, 130.8, 129.5, 128.3, 35.2, 33.5, 30.5 ppm.

HR-MS (ESI, +): m/z calcd. for $\text{C}_{32}\text{H}_{28}\text{O}_2\text{S}_2\text{Ag}$ [$\text{M}+\text{Ag}$] $^+$ 615.0576; found: 615.0577.

5.4.2 Transport Measurements

5.4.2.1 Mechanically Controlled Break Junction

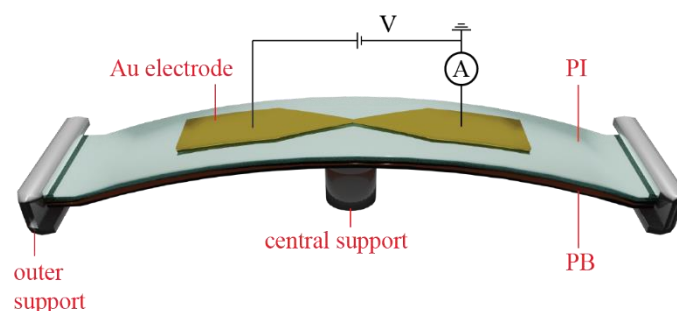


Figure S 1: Schematic illustration of the MCBJ setup.

The single-molecule measurements, described in the main text, were carried out with a mechanically controlled break junction. The MCBJ sample consists of a lithographically fabricated gold wire suspended on a flexible substrate made out of phosphor bronze (PB) with an insulating coating of polyimide (PI). The gold wire was defined with electron-beam lithography and evaporated with an electron-beam evaporator with a thickness of 80 nm together with a 3 nm titanium adhesive layer. In a typical room temperature MCBJ measurement, the gold wire is stretched through a three-point bending mechanism with a piezoelectric element and eventually ruptures, forming a nanogap between atomically sharp electrode surfaces for single-molecule characterization. During the breaking of the gold wire, the electrical conductance is recorded with or without the presence of molecules, and the closing of the junction is performed when the contact is broken, as signaled by a conductance below $10^{-6}G_0$. During the successive breaking and making of the gold contacts through the bending/unbending of the substrate, the electrical conductance is monitored, and a large number of “breaking traces” is collected. With a molecule of interest inside the junction, we can determine the single-molecule electrical conductance statistically.

5.4.2.2 Fast-Breaking Measurements

In the measurements performed for the PCP molecules, the MCBJ junctions were first characterized without the molecules for reference purposes. After the reference gold measurement, we deposited molecular solutions with concentrations ranging from 1 to 100 μM in CH_2Cl_2 onto the MCBJ samples. The fast-breaking measurements were performed at a constant DC bias voltage with the electrical current recorded by a homemade logarithmic current amplifier. During the fast-breaking measurements, the molecular junctions were continuously opened and closed by the piezoelectric element, creating thousands of

conductance breaking traces. The thousands of breaking traces were then plotted together to form a two-dimensional conductance histogram.

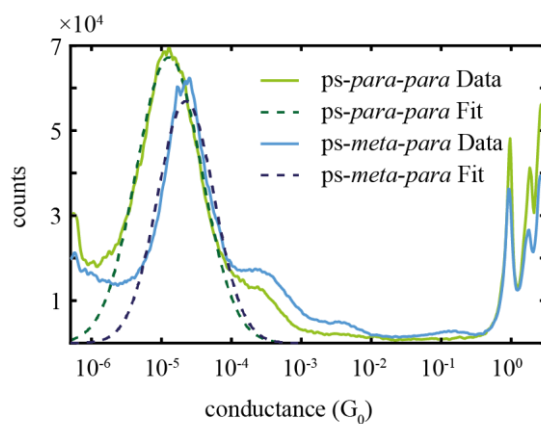


Figure S2: One-dimensional histogram of a fast-breaking measurement of *ps-para-para* and *ps-meta-para* PCP.

The one-dimensional conductance histogram, which is illustrated in Figure S2, was obtained by summing the counts at a fixed conductance level across all displacement values from a two-dimensional conductance vs. displacement histogram (see Figure 2). With a log-normal fit, the most probable conductance values for the *ps-para-para* and *ps-meta-para* PCP molecules are $1.3 \times 10^{-5} G_0$ and $2.2 \times 10^{-5} G_0$, respectively.

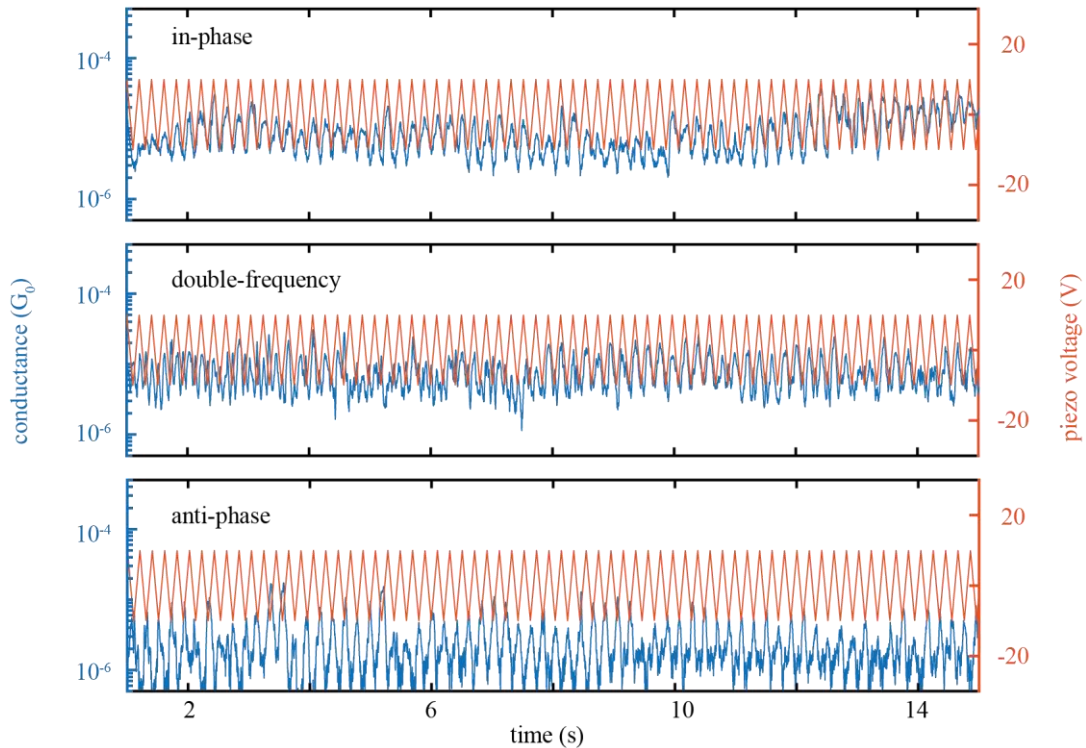
5.4.2.3 *Distance-Modulation Measurements*

Figure S3: Distance-modulation traces of *ps-para-para* PCP. The blue lines display three different types of conductance measurements, namely in-phase, double frequency, and anti-phase, and the red line displays the voltage applied to the piezoelectric stack. Note that an increase in piezo voltage corresponds to an increase in electrode displacement. The total modulation time of the experiment is 15 seconds.

An additional set of measurements of *ps-para-para* PCP is presented in Figure S3. The modulation traces clearly show in-phase and anti-phase behavior for the whole duration of 15 s. Note that the ascribed double frequency signal changes to the in-phase configuration after around 8 s during the modulation experiment. There are 112 traces in total showing a clear modulation signal in this modulation experiment, and the ratio of each behavior is provided in Figure S4.

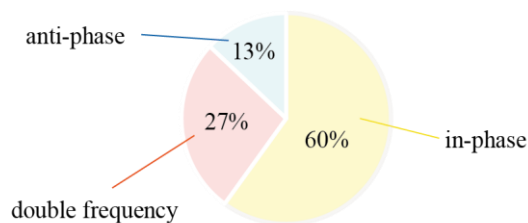


Figure S4: Ratio of phase response behaviors of *ps-para-para* PCP during the distance-modulation experiments.

The ratio between the in-phase, anti-phase, and double-frequency is 60:13:27. The in-phase case is clearly dominating the modulation behavior compared to the anti-phase case. This

difference also results in much fewer counts in the negative gauge factor shown in Figure 4a. The scarceness of the anti-phase behavior can be understood by looking at the starting electrode position in the modulation experiment. There, we first opened the junction up to 7.5 Å and then started modulating the junction with an amplitude of 5 Å. The total length of the molecular plateau is about 12.5 Å according to the fast-breaking measurement shown in Figure 2. Although the modulation size in the junction may not directly transform into the deformation of the molecule, we thus expect that the modulation occurs mostly in the strained molecular state. Considering the transmission vs. displacement chart for *ps-para-para* PCP shown in Figure 5b and the conductance dip depicted in Figure 3e, the in-phase behavior should be prevalent for a strained molecule.

5.4.2.4 Estimation of the Gauge Factor

In the main text, we introduced the gauge factor to quantify the mechano-sensitivity of the molecules. We define it as:

$$GF(f) \equiv \text{FFT} \left[\log \frac{G}{G_0} \right] (f) / \text{FFT} [d/d_0](f) \quad (1)$$

where $GF(f)$ is the frequency-dependent gauge factor, which we evaluate at $f=5$ Hz. In Eq. (1), FFT is the amplitude of the Fast-Fourier transform, G is the conductance, G_0 is the conductance quantum, d is the electrode displacement estimated from the piezo voltage, and d_0 is the length of the molecule estimated from the most probable molecular length in fast-breaking measurements. Essentially, GF involves a Fast-Fourier transform of the conductance signal on a logarithmic scale and of the electrode displacement on a linear scale. The obtained FFT amplitudes at the driving frequency f of 5 Hz are then taken to define GF by taking the ratio of the two. Note that the sign of GF is fixed by the phase of the signal obtained from the FFT spectra, where in-phase gives a positive GF and anti-phase a negative GF. For example, if we use a highly mechano-sensitive molecule with mainly anti-phase behavior, we expect to see $GF < 0$, and a large absolute value $|GF| \neq 0$ indicates a large conductance change. In the case of a non-mechano-sensitive molecule, such as *ps-meta-para* PCP, $|GF|$ is close to 0, while we find $|GF| > 1$ for the mechano-sensitive *ps-para-para* PCP.

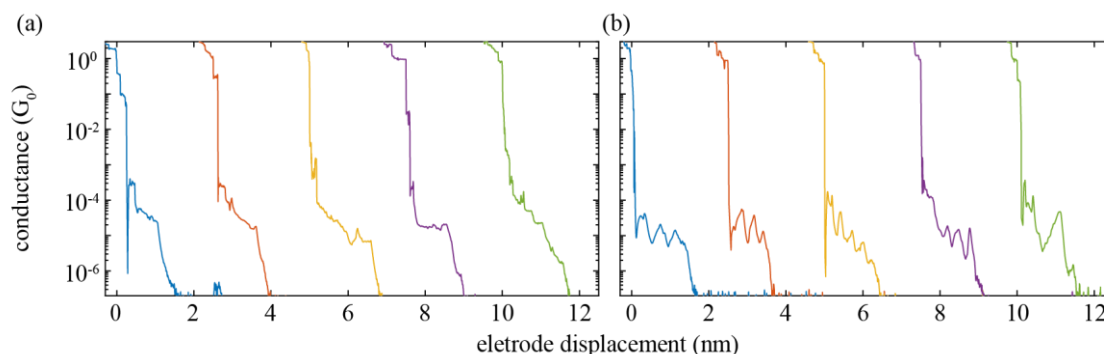
5.4.2.5 *Stick-Slip Motion in Molecular Junctions*

Figure S5: Individual fast-breaking traces for *ps-meta-para* and *ps-para-para* molecules.

In the fast-breaking experiment described in the main text, thousands of breaking traces for *ps-meta-para* and *ps-para-para* molecules were obtained. As suggested by Figure S2, the average conductance value of *ps-meta-para* is slightly larger and exhibits a narrower conductance distribution than those of *ps-para-para*. This is explained by the absence of DQI in the case of *ps-meta-para*. When the individual traces shown in Figure S5 are examined further, it is clear that *ps-para-para* features conductance oscillations during the displacement of electrodes, indicating the presence of DQI. However, oscillations can repeat up to 3 or 4 times instead of the single oscillation expected from crossing a DQI dip. Such a behavior was already observed in the previous experiment with OPE PCP, and we explained it by the stick-slip motion of the molecule in the junction.²²⁴ This stick-slip motion happens, when the molecule is strained sufficiently. As the gold-sulfur connection breaks due to the high strain, the molecule contracts before it establishes a new connection between the sulfur anchor and a nearby electrode gold atom. This process leads to multiple conductance oscillation as observed in the breaking traces. A similar motion can be conceived, if the molecule drags along with it a gold adatom or generally a smaller gold cluster that slides along a macroscopic gold surface. The stick-slip motion is discussed further in the theory section below.

5.4.3 Transport Calculations

5.4.3.1 DFT Calculation Setup

We describe electronic transport through the PCP-based single-molecule junctions as phase-coherent and elastic in terms of the Landauer scattering theory.²²⁵ The conductance at sufficiently low temperatures simplifies to

$$G = G_0 \tau(E_F), \quad (1)$$

i.e. the product of the energy-dependent transmission function $\tau(E)$, evaluated at the Fermi energy E_F , and the conductance quantum $G_0 = 2e^2/h$. The elastic transmission $\tau(E)$ is computed in a parameter-free approach by combining DFT with NEGF techniques. The established theoretical methods have been discussed in detail previously.²²⁶

The calculations to obtain the transmission as a function of energy and electrode displacement for the four PCP derivatives comprise the following steps: First, the molecular structures are optimized in the gas phase. Then terminal hydrogens at each sulfur atom are removed, and the molecules are placed between two tetrahedral gold leads. We distinguish “top-top” and “hollow-hollow” junction geometries, where we use either atomically sharp tips, ending with a single Au tip atom for “top-top”, or blunt tips for hollow-hollow, where the tip atoms are removed on each side. The resulting junction structures are subsequently optimized by relaxing both the molecule and the four (for top-top geometries) or three (for hollow-hollow geometries) gold atoms of each pyramid that are located at the top of each tip. The rest of the gold atoms are fixed in a face-centered cubic lattice configuration. The resulting geometries are displayed in Figure 5a of the main text for the hollow-hollow junction configuration and in Figure S6a for the top-top junction configuration. In the stretching process we separate the gold contacts in steps of 0.1 Å, optimize the geometries as described before, and keep increasing the electrode separation d until the contact ruptures. For compression we proceed in an analogous way until the molecular structure starts to strongly deform. Finally the transmission $\tau(E, d)$ and from Eq. (1) the conductance $G(d)$ are computed for the static geometries within the DFT-NEGF formalism.²²⁶

The DFT calculations are performed with the quantum chemistry code TURBOMOLE²²⁷, employing the def-SV(P) Gaussian basis set²²⁸ for all atoms and the PBE exchange-correlation functional.²²⁹ Total energies are converged to an accuracy of better than 10^{-8} a.u., while geometries are optimized until the change of the maximum norm of the Cartesian gradient is below 10^{-3} a.u. The transport program²³⁰ that we use for computing the elastic transmission is custom-built and interfaced with TURBOMOLE. For evaluating the transmission function, we employ 16×16 transverse k -points to properly describe the semi-infinite gold electrodes.

5.4.3.2 Transmission Maps and Stick-Slip Motion in the Top-Top Configuration

In the main text, we discuss conduction properties of the four PCP molecules immobilized in hollow-hollow junctions. In this part we now focus on a different geometry, namely the behavior of the PCP derivatives in the top-top configuration, see Figure S6a. The conductance and the total energy of DFT are illustrated in Figure S6b for all four PCP derivatives. Considering the example of the *ps-para-para* PCP single-molecule junction, both quantities show pronounced jumps at certain stretching steps during the electrode displacement process. Starting from the initial junction geometry at zero displacement, conductance and total energy grow to a local maximum at 1.5 Å. At this point an anchoring sulfur slips to the next gold atom, see Figure S7a, and the molecule releases the mechanical tension that has been built up due to the mechanical stretching process. An instantaneous decrease of both conductance and energy is observed, restoring the latter to a lower value. After reaching the final tip gold atom, the junction breaks at 5.6 Å, and the molecule snaps back and loses contact to one electrode as the mechanical tension becomes too high, which leads to a sharp drop in the conductance. Molecular contacts based on the other three PCP derivatives show a similar interplay of elastic and plastic stretching stages. The sliding of the anchor group along the surface of the electrode, as presented in Figure S7 and called stick-slip motion, is evident from the experimental data in Figure S5 and has also been observed in our previous work.²²⁴

In the two-dimensional contour maps of transmission in dependence of energy and electrode displacement, see Figure S6c, sudden geometric rearrangements in the junctions (such as the slipping of the anchor group to a neighboring gold atom) result in a discontinuous distance dependence (for *ps-para-para* PCP at 1.5 Å and 4.6 Å, for *ps-meta-para* PCP at 2.3 Å, for *ps-para-meta* PCP at 3.1 Å and 5.0 Å, and for *ps-meta-meta* PCP at 0.8 Å and 2.4 Å).

A closer look at Figure S6c reveals a similar transport behavior of the top-top molecular junctions compared to the hollow-hollow junctions of Figure 5 in the main text. Again, inside the electronic gap between the HOMO and the LUMO the *ps-para-para* PCP junction shows transmission valleys (blue diagonal traces) with transmission values lower than 10^{-6} , which cause DQI conductance dips. In contrast the *ps-meta-para* PCP junction features a rather constant transmission in the range of about 10^{-3} to 10^{-4} . Different from the observations in the main text, remnants of transmission valleys are faintly visible close to the LUMO for the *ps-para-meta* PCP molecular junction in top-top configuration, further consolidating the hypothesis of the central *ps-para* PCP subunit as origin of the DQI phenomenon. Again, rather uniform transmission values are predicted in the molecule's electronic gap for *ps-meta-meta* PCP as structural analogue with a central *ps-meta* PCP subunit.

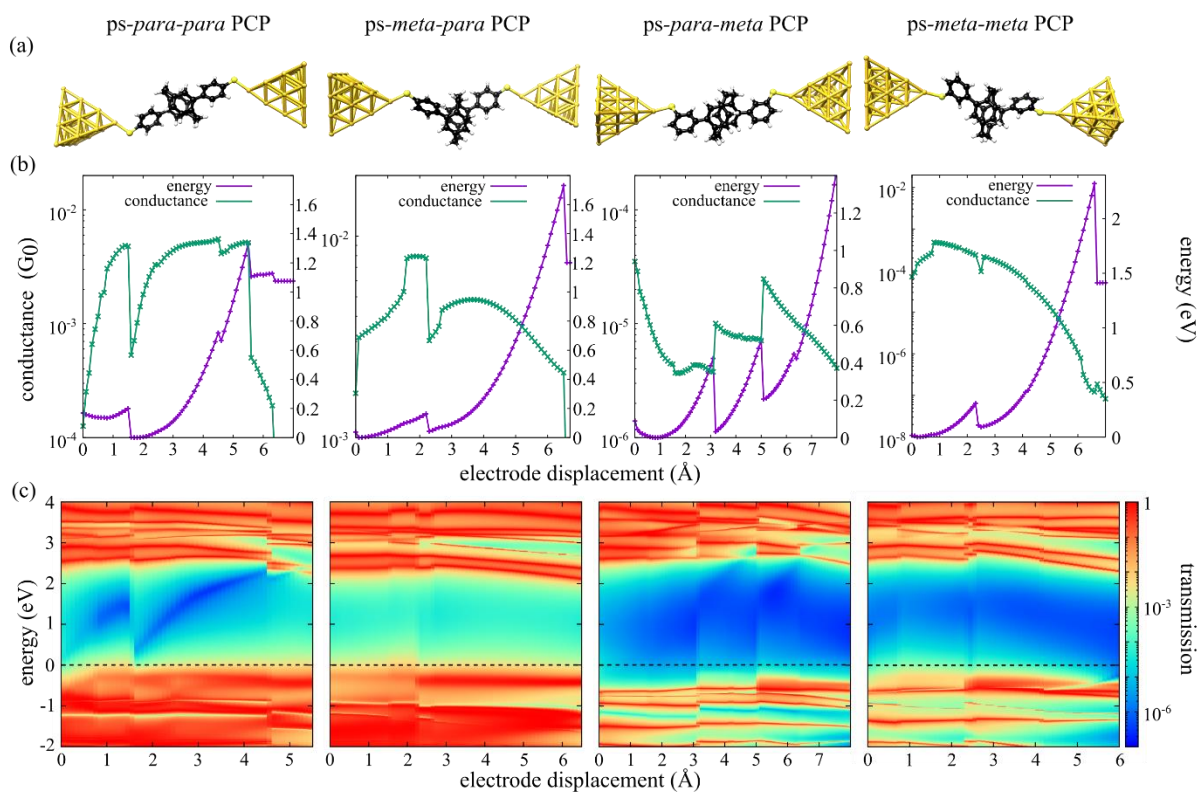


Figure S6: (a) Illustration of the PCP derivatives **1-4**, immobilized in top-top junctions between two gold electrodes. (b) Calculated conductance and total energy of the PCP molecular junctions during the gap opening. (c) Transmission maps of the four types of PCP single-molecule junctions. Horizontal red resonances in the maps arise from molecular frontier orbitals. For the *ps-para-para* PCP molecule, an anti-resonance is observed inside the HOMO-LUMO gap that shifts in energy as the displacement is varied. Analogous behavior can be found for the *ps-para-meta* PCP molecule as well, but the effect is masked by the DQI, resulting from the meta coupling at the terminal benzene rings. Tunable DQI effects are neither found in the simulations of *ps-meta-para* PCP junctions nor *ps-meta-meta* PCP junctions with central *ps-meta* PCP systems. The position of the Fermi energy E_F is indicated as a horizontal dashed line in each plot. The conductance curves of panel b are obtained by tracing the transmission along this line.

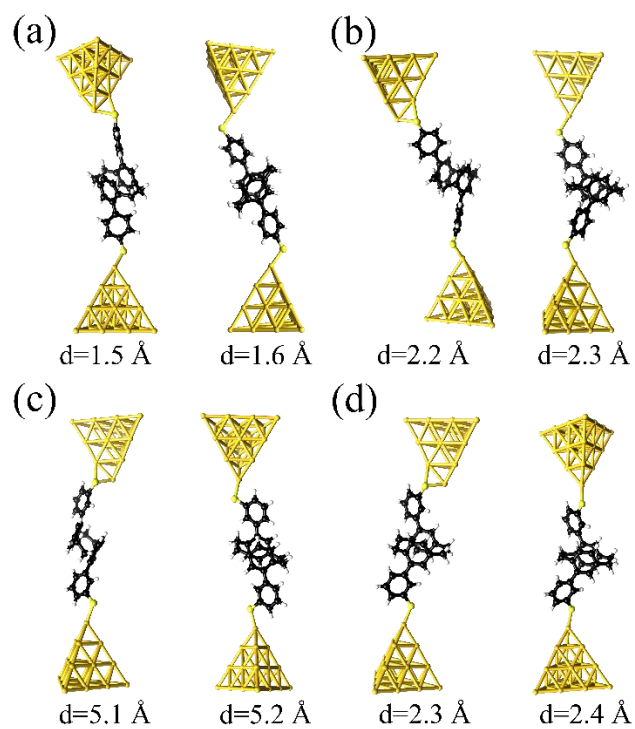


Figure S7: Snapshots illustrating the stick-slip motion of the sulfur anchor group on the gold electrode at different electrode displacements d for the (a) *ps-para-para*, (b) *ps-meta-para*, (c) *ps-para-meta*, and (d) *ps-meta-meta* PCP molecules.

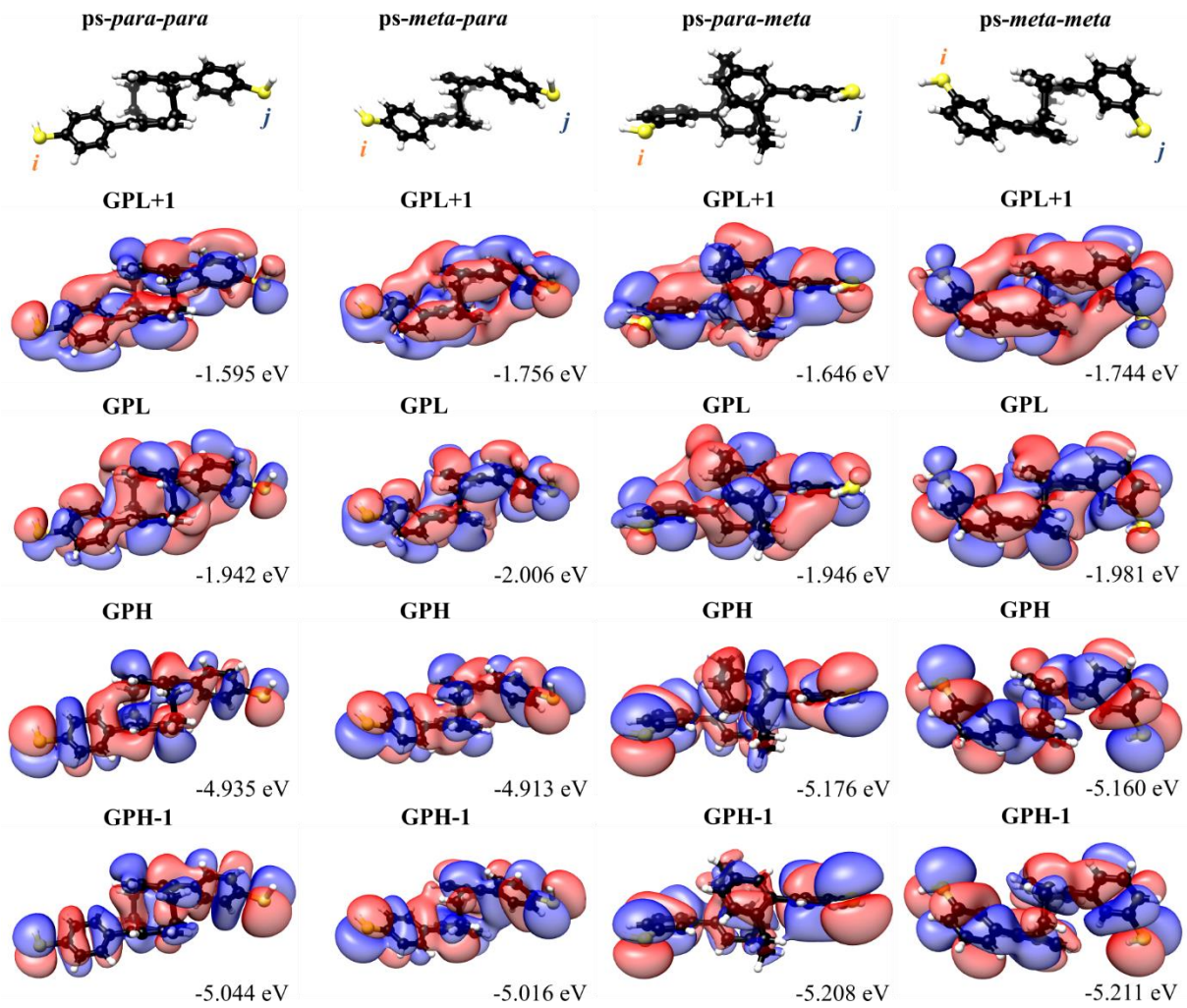
5.4.3.3 *Quantum Interference Effects and Symmetry Rules*

Figure S8: Illustration of frontier molecular orbitals of *ps-para-para*, *ps-meta-para*, *ps-para-meta* and *ps-meta-meta* PCP molecules in the gas phase. Shown are the gas phase HOMO (GPH) and gas phase LUMO (GPL), as in Figure 6 of the manuscript, supplemented by the corresponding lower and higher states GPH-1 and GPL+1. The DFT energies of all orbitals are indicated.

We relate the valleys of low transmission in Figures 5 and S6 to DQI effects, resulting from molecular frontier orbital contributions. The appearance or absence of these valleys can be explained by using orbital symmetry rules for the molecules' gas-phase orbitals, which are documented in the literature.^{98,113,231} For off-resonant transport inside the HOMO-LUMO gap, embedding self-energies of the electrodes can be neglected to first approximation. Therefore, the retarded Green's function $G_{i\alpha,j\beta}^r(E)$ that describes the probability amplitude for the propagation of electrons from orbital α at atom i to orbital β at atom j through the molecule can be approximated by the zeroth-order Green's function

$$G_{i\alpha,j\beta}^{r,(0)}(E) = \sum_k \frac{c_{i\alpha,k} c_{j\beta,k}^*}{E + i\eta - \epsilon_k} \quad (2)$$

with the energy ϵ_k of molecular orbital k , its coefficient $C_{i\alpha,k}$ at atom i and atomic orbital α , and a positive infinitesimal broadening parameter η . We identify the sites i and j with the terminal sulfur atoms of the respective PCPs (see Figure S9). The relation between the transmission and the Green's function

$$\tau(E) \propto \left| G_{i\alpha,j\beta}^{r,(0)}(E) \right|^2 \quad (3)$$

ultimately connects transmission to molecular orbital contributions k . In Eq. (3) a sum should be carried out over all orbitals α and β that couple well to the electrodes, and there should be a weighting factor included that depends on this molecule-electrode coupling. For simplicity and under the assumption that the energy E is located between the HOMO energy ϵ_{HOMO} and the LUMO energy ϵ_{LUMO} , we reduce the Green's function in Eq. (2) to the largest terms and thus only consider the HOMO and LUMO contributions

$$G_{i\alpha,j\beta}^{r,(0)}(E) \approx \frac{C_{i\alpha,\text{HOMO}}C_{j\beta,\text{HOMO}}^*}{E+i\eta-\epsilon_{\text{HOMO}}} + \frac{C_{i\alpha,\text{LUMO}}C_{j\beta,\text{LUMO}}^*}{E+i\eta-\epsilon_{\text{LUMO}}}. \quad (4)$$

For a full description of the transmission behavior further orbital contributions k may need to be taken into account¹¹³, but Eq. (4) still allows for a qualitative explanation of the occurrence or absence of DQI in the case of the studied PCP systems. We will omit the atomic orbital indices α and β in Eqs. (2)-(4) in the following and not specify them further, similar to the presentation in the paper. They will simply be of the form of the HOMO and LUMO wavefunctions at the atoms i and j . It is important though that the orbital characters of HOMO and LUMO wavefunctions are of compatible character in order to interfere as given in Eq. (4). Figure S8 reveals that this is the case here, i.e. all of the relevant HOMOs and LUMOs exhibit the same π -character and spatial orientation at the respective terminal sulfur atoms for each of the four PCP derivatives. The form of the Green's function in Eq. (4) combined with Eq. (3) allows to draw the following conclusions^{229,230}: First, the products of the orbital coefficients $C_{i\text{HOMO}}C_{j\text{HOMO}}^*$ of the HOMO and $C_{i\text{LUMO}}C_{j\text{LUMO}}^*$ of the LUMO need to be of decent size in order to contribute to the transmission. For this reason, the weight of HOMO and LUMO wavefunctions need to be sufficiently large on the anchoring atoms i and j , meaning that these are delocalized orbitals. Second, the parities of the molecule's HOMO and LUMO need to be different ($\text{sign}(C_{i\text{HOMO}}C_{j\text{HOMO}}^*) = -\text{sign}(C_{i\text{LUMO}}C_{j\text{LUMO}}^*)$) in order to achieve high transmission, as in this case the terms in Eq. (4) add up. If the parities of HOMO and LUMO are the same instead, the two terms cancel each other inside the gap, and DQI occurs, resulting in a low transmission. Figure S8 shows relevant frontier molecular orbitals and their energies, from which orbital weights on terminal sulfurs as well as their parity can be inferred. The quantities

are needed to rationalize the transport behavior in Figure 5 of the main text as well as Figure S6 in terms of the orbital symmetry rules.

5.4.3.4 Transmission Eigenchannels

Figure S9 visualizes the wave function of those left-incoming transmission eigenchannels with the highest transmission for each of the four studied PCP isomers at the Fermi energy and at a particular electrode separation d . We see that the amplitude of the eigenchannels decays along the propagation direction inside the molecules, as expected in an off-resonant transport situation.

The spatial distribution of the wave function is quite similar for all four molecules, exhibiting a high weight on the molecular deck that is directly connected through a sulfur anchor to the left electrode and a low weight on the molecular deck that is directly connected to the right electrode. Note the low weight of the wave function on the ethylene braces of the central paracyclophane units. It indicates that they do not contribute to the phase-coherent electronic transmission through the PCP molecules at E_F .

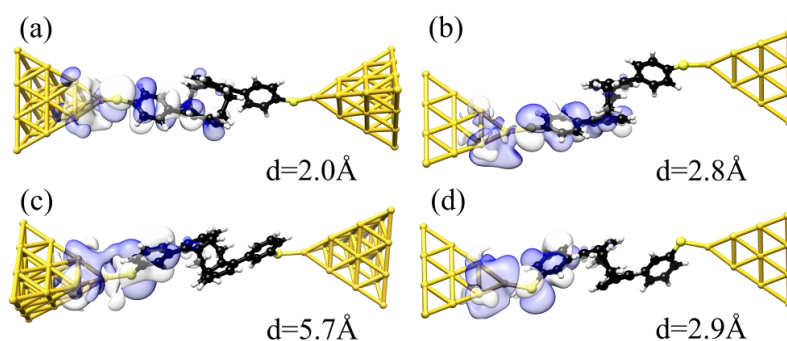
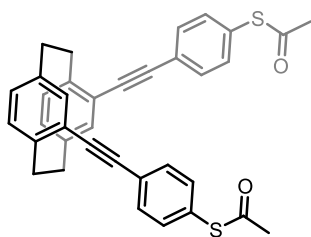


Figure S9: Illustration of the wave function of the most transparent left-incoming transmission eigenchannel, evaluated at the Fermi energy E_F , for electron transport through (a) *ps-para-para*, (b) *ps-meta-para*, (c) *ps-para-meta*, and (d) *ps-meta-meta* PCP molecules connected to gold electrodes. The selected electrode displacement d is indicated separately for each junction.

5.5 Supporting Information: Subchapter 2.3

Previously reported compounds: pseudo-*ortho*-dibromo[2.2]paracyclophane (**42**), pseudo-*ortho*-diethynyl[2.2]paracyclophane (**50**), acetylthioiodobenzene (**51**), (4-(*tert*-butylthio)phenyl)boronic acid (**55**) were prepared following reported procedures.^{89,118,121–125}

Synthesis of pseudo-*ortho*-bis(((4'-acetylthio)phenyl)ethynyl)[2.2]paracyclophane (**47**):



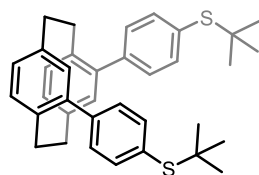
Pseudo-*ortho*-diethynyl[2.2]paracyclophane (**50**) (100 mg, 390 μ mol, 1.0 eq.) was added to a degassed solution of 4-acetylthioiodobenzene (**51**) (434 mg, 1.56 mmol, 4.0 eq.) in THF (10 mL) and DIPA (2.5 mL). The reaction mixture was degassed by bubbling through a stream of argon for 20 min. Then Pd(PPh₃)₄ (45 mg, 39 μ mol, 10 mol%) and CuI (8 mg, 39 μ mol, 10 mol%) were added under Argon. The reaction mixture was placed in preheated oil bath and was stirred at 55 °C for 16 h. Afterwards, the reaction mixture was cooled to RT, filtered over celite and the solvent was removed under reduced pressure. The crude product was purified by column chromatography (cyclohexane/EA 1:1) and GPC to give pseudo-*ortho*-bis(((4'-acetylthio)phenyl)ethynyl)[2.2]paracyclophane (**47**) (115 mg, 207 μ mol, 53%) as a white amorphous solid.

¹H NMR (500 MHz, CDCl₃): δ 7.62 – 7.58 (m, 4H), 7.45 – 7.42 (m, 4H), 7.11 (t, J = 1.1 Hz, 2H), 6.57 (d, J = 1.1 Hz, 4H), 3.65 (ddd, J = 13.0, 10.4, 2.6 Hz, 2H), 3.24 – 3.16 (m, 2H), 3.12 – 3.06 (m, 2H), 2.95 – 2.87 (m, 2H), 2.46 (s, 6H) ppm.

¹³C{¹H} NMR (126 MHz, CDCl₃): δ 193.71, 142.44, 139.80, 134.50, 134.36, 133.68, 133.52, 132.21, 127.92, 125.31, 124.61, 92.45, 91.39, 34.48, 33.91, 30.44 ppm.

HRMS (ESI, +): m/z calcd. for C₃₆H₂₈O₂S₂Ag [M+Ag]⁺ 663.0576; found: 663.0567.

Synthesis of pseudo-*ortho*-bis((4'-*tert*-butylthio)phenyl)[2.2]paracyclophane (**56**):



Pseudo-*ortho*-dibromo [2.2]paracyclophane (**42**) (200 mg, 564 μ mol, 1.0 eq.), 4-(*tert*-butylthio)benzeneboronic acid (**55**) (344 mg, 1.64 mmol, 3.0 eq.) and K₂CO₃ (226 mg, 1.64 mmol, 3.0 eq.) were suspended in toluene (8 mL) and MeOH (8 mL). The reaction mixture was degassed by bubbling through a stream of argon for 20 min. Then, Pd-PEPPSITM-iPr (19 mg, 27.3 μ mol, 5 mol%) was added and the reaction mixture was placed in preheated oil bath and stirred at 70 °C for 1 h. Afterwards, the reaction was cooled to RT and aq. HCl (1 M) was added. The org. layer was separated and the aq. layer was extracted with toluene (3x). The combined organic layers were washed with water, brine and dried over Na₂SO₄, filtered and the solvent

was evaporated under reduced pressure. The crude was purified by column chromatography (cyclohexane/CH₂Cl₂ 4:1) to give pseudo-*ortho*-bis((4'-*tert*-butylthio)phenyl)[2.2]paracyclophane (**56**) (232 mg, 432 μmol, 79%) as a white amorphous solid.

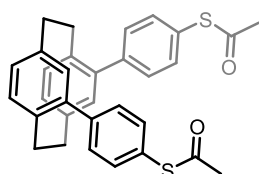
¹H NMR (400 MHz, CD₂Cl₂): δ 7.56 – 7.50 (m, 4H), 7.30 – 7.24 (m, 4H), 6.74 (d, *J* = 7.6 Hz, 2H), 6.68 – 6.63 (m, 4H), 3.57 – 3.48 (m, 2H), 3.18 – 3.09 (m, 2H), 3.04 – 2.95 (m, 2H), 2.82 – 2.73 (m, 2H), 1.33 (s, 18H) ppm.

¹³C{¹H} NMR (101 MHz, CD₂Cl₂): δ 141.96, 140.20, 139.99, 137.82, 137.53, 136.04, 132.98, 131.54, 130.41, 129.48, 46.21, 34.79, 34.50, 31.18 ppm.

HRMS (ESI, +): *m/z* calcd. for C₃₆H₄₀S₂Ag [M+Ag]⁺ 643.1617; found: 643.1610.

Synthesis of pseudo-*ortho*-bis((4'-*tert*-acetylthio)phenyl)[2.2]paracyclophane (**48**):

This reaction was adopted from literature.¹²⁶



Pseudo-*ortho*-bis((4'-*tert*-butylthio)phenyl)[2.2]paracyclophane (**56**)

(30 mg, 55.9 μmol, 1.0 eq.) and acetyl chloride (200 μL, 2.79 mmol, 50 eq) were dissolved in dry toluene (3 mL) and dry MeCN (3 mL) under argon atmosphere. Bismuth(III)trifluoromethanesulfonate (112 mg,

168 μmol, 3.0 eq.) was added and the reaction mixture was stirred at RT for 3 h. Afterwards, water was added. The aq. layer was extracted with CH₂Cl₂ (3x). The combined org. layers were dried over Na₂SO₄, filtered and the solvent was removed under reduced pressure. The crude product was purified by column chromatography (cyclohexane/CH₂ 1:3) and GPC to give pseudo-*ortho*-bis((4'-*tert*-acetylthio)phenyl)[2.2]paracyclophane (**48**) (18 mg, 35.4 μmol, **63%**) as a white amorphous solid.

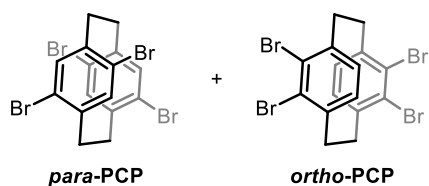
¹H NMR (500 MHz, CD₂Cl₂): δ 7.47 – 7.43 (m, 4H), 7.38 – 7.34 (m, 4H), 6.76 (d, *J* = 7.7 Hz, 2H), 6.69 (dd, *J* = 7.7, 1.9 Hz, 2H), 6.65 (d, *J* = 1.9 Hz, 2H), 3.55 – 3.49 (m, 2H), 3.17 – 3.11 (m, 2H), 3.05 – 2.99 (m, 2H), 2.82 – 2.57 (m, 2H), 2.44 (s, 6H) ppm.

¹³C NMR (126 MHz, CD₂Cl₂): 194.36, 142.65, 140.23, 139.73, 137.62, 136.10, 134.98, 133.23, 130.40, 130.14, 126.93, 34.82, 34.48, 30.47 ppm.

HRMS (ESI, +): *m/z* calcd. for C₃₂H₂₈O₂S₂Na [M+Na]⁺ 531.1423; found: 531.1422
m/z calcd. for (C₃₂H₂₈O₂S₂)₂Na [2M+Na]⁺ 1039.2954; found: 1039.2943.

5.6 Supporting Information: Chapters 3 & 4

Synthesis of 4,7,12,15- (84) and 4,5,12,13-tetrabromo[2.2]paracyclophane (85):



Commercially available [2.2]paracyclophane (20.0 g, 96.0 mmol, 1.0 eq.) and iodine (292 mg, 1.15 mmol, 0.01 eq.) were placed in the flask wrapped with aluminum foil to exclude the daily light. Bromine (60 ml, 1166 mmol, 12 eq.) was slowly added over a dropping funnel and vigorously stirred for 8 d at RT. Afterwards, the excess of bromine was quenched with aq. NaOH (20 %) solution. The precipitate was collected by filtration, washed with hot ethanol (3x) and CH₂Cl₂ to give the pure by-product **85** as a white solid. The CH₂Cl₂ fraction was dried under reduced pressure and showed a mixture of *ortho*-PCP (**85**) and *para*-PCP (**84**) in almost equal amounts. The reaction mixture was recrystallized several times from CH₂Cl₂ to give the pure by-product **85** (18.2 g, 34.7 mmol, 36%) as a white solid. The remained filtrate was concentrated under reduced pressure to give the desired *para*-tetrabromo-PCP **84** (21.2 g, 40.5 mmol, 42%) as a white solid.

4,7,12,15- tetrabromo[2.2]paracyclophane (84):

¹H NMR (400 MHz, CDCl₃): δ 7.20 (s, 4H), 3.29 – 3.18 (m, 4H), 3.03 – 2.93 (m, 4H) ppm.

¹³C{¹H} NMR (101 MHz, CDCl₃): δ 140.47, 134.57, 125.44, 32.84 ppm.

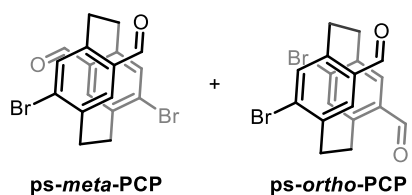
4,5,12,13-tetrabromo[2.2]paracyclophane (85):

¹H NMR (400 MHz, CDCl₃) δ 6.99 (s, 4H), 3.40 – 3.29 (m, 4H), 3.16 – 3.04 (m, 4H) ppm.

¹³C{¹H} NMR (101 MHz, CDCl₃) δ 140.84, 129.42, 128.79, 34.70 ppm.

The analytical data are in agreement with the ones reported in ref.¹⁷⁸

Synthesis of 4,15-dibromo-7,12-diformyl[2.2]paracyclophane (82) and 4,12-dibromo-7,15-diformyl[2.2]paracyclophane (86):



Compound **84** (1.00 g, 1.91 mmol, 1.0 eq.) was dissolved in dry THF (100 mL). The reaction mixture was cooled to -78 °C and *n*-BuLi (2.5 M, 1.6 mL, 4.01 mmol, 2.1 eq.) was added. The solution was stirred for 30 min at -78 °C. Afterward, dry DMF (1.2 mL, 15.6 mmol, 8.1 eq.) was added. The reaction mixture was allowed to warm to RT and stirred for 16 h. Then, the reaction mixture was quenched with dilute

ammonium hydroxide solution and THF was removed under reduced pressure. The resulting solid was extracted with CH₂Cl₂ (3x). The combined org. layers were washed with aq. HCl (1M), water, brine, dried over Na₂SO₄, filtered and the solvent was evaporated under reduced pressure. The crude product was purified by column chromatography (toluene) to give dialdehyde with *ps-meta* (**82**) (197 mg, 466 μmol, 24%) and *ps-ortho* connectivity (**86**) (402 mg, 953 μmol, 50%) as white solids.

4,15-Dibromo-7,12-diformyl[2.2]paracyclophane (82):

¹H NMR (400 MHz, CDCl₃): δ 9.90 (s, 2H), 7.58 (s, 2H), 6.60 (s, 2H), 4.10 – 4.00 (m, 2H), 3.44 – 3.34 (m, 2H), 3.23 – 3.13 (m, 2H), 2.96 – 2.86 (m, 2H) ppm.

¹³C{¹H} NMR (101 MHz, CDCl₃): δ 191.32, 143.77, 139.85, 138.56, 135.48, 134.63, 133.52, 32.89, 32.76 ppm.

HR-MS (ESI, +): *m/z* calcd. for C₁₈H₁₄Br₂O₂Na [M+Na]⁺ 442.9253, found 442.9250.

4,12-Dibromo-7,15-diformyl[2.2]paracyclophane (86):

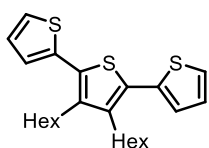
¹H NMR (400 MHz, CDCl₃): δ 9.79 (s, 2H), 7.27 (s, 2H), 6.88 (s, 2H), 3.99 – 3.88 (m, 2H), 3.55 – 3.42 (m, 2H), 3.12 – 2.95 (m, 4H) ppm.

¹³C{¹H} NMR (101 MHz, CDCl₃): δ 191.22, 143.53, 140.20, 137.45, 136.01, 135.55, 133.10, 35.05, 30.59 ppm.

HR-MS (ESI, +): *m/z* calcd. for C₁₈H₁₄Br₂O₂Na [M+Na]⁺ 442.9253, found 442.9247.

The analytical data are in agreement with the ones reported in ref.^{173,174}

Synthesis of 3',4'-dihexyl-2,2':5',2''-terthiophene (90):



2,5-Dibromo-3,4-dihexylthiophene (**88**) (3.0 mL, 9.59 mmol, 1.0 eq.), thiophene-2-boronic acid pinacol ester (**89**) (4.13 g, 19.7 mmol, 2.05 eq.) and K₂CO₃ (7.95 g, 57.5 mmol, 6.0 eq.) were dissolved in toluene (30 mL) and MeOH (30 mL). The reaction mixture was degassed for 20 min with Argon before Pd-

PEPPSI™-IPr (98%, 332 mg, 489 μmol, 5 mol%) was added. The reaction mixture was placed in preheated oil bath and stirred at 70 °C for 30 min. Afterwards, the reaction was allowed to reach room temperature and aq. HCl (1M) was added. The aq. layer was extracted with toluene (3x). The combined organic layer was washed with aq. HCl (1M), water, brine, dried over Na₂SO₄, filtered and the solvent was removed under reduced pressure. The crude product was

purified by column chromatography (pentane) to give dihexylterthiophene **90** (3.92 g, 9.41 mmol, **98%**) as a yellow oil.

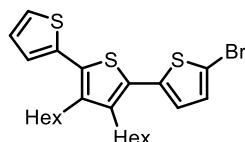
¹H NMR (400 MHz, CDCl₃): δ 7.32 (dd, *J* = 5.2, 1.2 Hz, 2H), 7.16 (dd, *J* = 3.6, 1.2 Hz, 2H), 7.08 (dd, *J* = 5.1, 3.6 Hz, 2H), 2.75 – 2.69 (m, 4H), 1.64 – 1.54 (m, 4H), 1.48 – 1.40 (m, 4H), 1.39 – 1.30 (m, 8H), 0.96 – 0.89 (m, 6H) ppm.

¹³C{¹H} NMR (101 MHz, CDCl₃): δ 140.21, 136.35, 129.95, 127.46, 125.96, 125.40, 31.65, 30.89, 29.73, 28.28, 22.78, 14.23 ppm.

HRMS (ESI, +): *m/z* calcd. for C₂₄H₃₂S₃H [M+H]⁺ 417.1739; found: 417.1731.

The analytical data are in agreement with the ones reported in ref.²³²

Synthesis of 5-bromo-3',4'-dihexyl-2,2':5',2''-terthiophene (**91**):

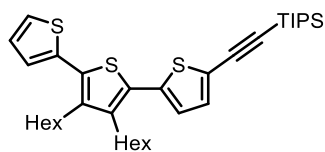


Compound **90** (1.66 g, 3.98 mmol, 1.0 eq.) was dissolved in DMF (30 mL) in the flask wrapped with aluminum foil to exclude the daily light and cooled to -20 °C. *N*-Bromosuccinimide (787 mg, 4.38 mmol, 1.1 eq.) was added in one portion. The reaction mixture was allowed to warm up to RT and stirred for 16 h. Afterwards, water was added and the reaction mixture was extracted with CH₂Cl₂ (3x). The combined org. layers were washed with aq. HCl (1M), water (2x) and brine (2x), dried over Na₂SO₄, filtered and the solvent was removed under reduced pressure. The crude product was purified by column chromatography (pentane) to give monobrominated terthiophene **91** (1.54 g, 3.10 mmol, **78%**) as a yellow oil.

¹H NMR (400 MHz, CDCl₃): δ 7.32 (dd, *J* = 5.1, 1.2 Hz, 1H), 7.14 (dd, *J* = 3.6, 1.2 Hz, 1H), 7.07 (dd, *J* = 5.2, 3.6 Hz, 1H), 7.02 (d, *J* = 3.9 Hz, 1H), 6.88 (d, *J* = 3.9 Hz, 1H), 2.73 – 2.63 (m, 4H), 1.62 – 1.52 (m, 4H), 1.48 – 1.39 (m, 4H), 1.38 – 1.28 (m, 8H), 0.98 – 0.88 (m, 6H) ppm.

¹³C{¹H} NMR (101 MHz, CDCl₃): δ 140.73, 140.23, 137.90, 136.07, 130.53, 130.29, 128.94, 127.49, 126.18, 126.13, 125.61, 111.87, 31.63, 31.62, 30.93, 30.86, 29.71, 29.69, 28.26, 28.24, 22.77, 22.76, 14.22 ppm.

HRMS (ESI, +): *m/z* calcd. for C₂₄H₃₁BrS₃ [M]⁺ 494.0766; found: 494.0757.

Synthesis of ((3',4'-dihexyl-[2,2':5',2''-terthiophen]-5-yl)ethynyl)triisopropylsilane (92):

Brominated terthiophene **91** (816 mg, 1.65 mmol, 1.0 eq.) was dissolved in trimethylamine (16 mL) and degassed for 20 min with Argon. Afterwards, TIPSA (0.5 mL, 2.31 mmol, 1.4 eq.) was added and the reaction mixture was degassed for a further 10 min. Pd(PPh₃)₂Cl₂ (58 mg, 8.25 μmol, 5 mol%) and CuI (8 mg, 4.13 μmol, 2.5 mol%) were added and the reaction mixture was put in preheated oil bath for 16h. Then, the reaction mixture was cooled to RT, plugged over Celite and the solvent was removed under reduced pressure. The crude was purified by column chromatography (pentane) to give the compound **92** (935 mg, 1.57 mmol, **95%**) as a yellow oil.

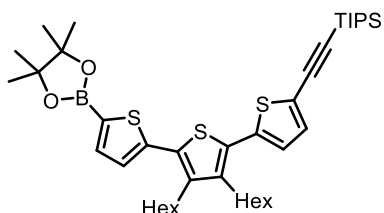
¹H NMR (400 MHz, CDCl₃): δ 7.32 (dd, *J* = 5.2, 1.2 Hz, 1H), 7.18 (d, *J* = 3.8 Hz, 1H), 7.14 (dd, *J* = 3.6, 1.2 Hz, 1H), 7.07 (dd, *J* = 5.1, 3.6 Hz, 1H), 6.98 (d, *J* = 3.8 Hz, 1H), 2.76 – 2.64 (m, 4H), 1.63 – 1.52 (m, 4H), 1.49 – 1.39 (m, 4H), 1.39 – 1.29 (m, 12H), 1.20 – 1.09 (m, 21H), 0.96 – 0.86 (m, 6H) ppm.

¹³C{¹H} NMR (101 MHz, CDCl₃): δ 140.78, 140.38, 137.77, 136.13, 132.93, 130.50, 129.41, 127.51, 126.11, 125.60, 125.35, 123.16, 99.42, 96.83, 31.64, 31.58, 30.86, 30.74, 29.73, 29.68, 28.34, 28.35, 22.78, 22.76, 18.81, 14.23, 14.21, 11.46 ppm.

HRMS (ESI, +): *m/z* calcd. for C₃₅H₅₂S₃Si [M+]⁺ 596.2995; found:596.2984.

UV/Vis: λ_{max} = 358 nm (cyclohexane), 358 nm (toluene), 360 nm (ethyl acetate), 363 nm (chloroform).

Fluorescence: λ_{max} = 461 (438) nm (cyclohexane), 461 (441) nm (toluene), 461 (441) nm (ethyl acetate), 466 (445) nm (chloroform).

Synthesis of ((3',4'-dihexyl-5''-(4,4,5,5-tetramethyl-1,3,2-dioxaborolan-2-yl)-[2,2':5',2''-terthiophen]-5-yl)ethynyl)triisopropylsilane (83b):

Terthiophene **92** (530 mg, 888 μmol, 1.0 eq.) was dissolved in dry THF (90 mL). The reaction mixture was cooled to -78 °C and *n*-BuLi (1.6 M, 0.6 mL, 960 μmol, 1.0 eq.) was added. The solution was stirred for 90 min at -78 °C. Afterwards, 2-isopropoxy-4,4,5,5-tetramethyl-1,3,2-dioxaborolane (0.7 mL, 3.43 mmol, 4.0 eq.) was added. The reaction mixture was allowed to warm to RT and stirred for 16 h. Then, HCl (1M) was added and the reaction mixture was extracted with CH₂Cl₂ (3x). The combined org. layers were washed with aq. HCl (1M), dried over Na₂SO₄, filtered and the

solvent was evaporated under reduced pressure to give a crude product (600 mg) as a mixture of starting material **92** (137 mg, 227 μmol , **26%**) and the desired borester **83b** (432 mg, 639 μmol , **72%**) in ratio 1 to 2.8 (determined in NMR spectrum) as a green oil which was used in the next step without further purification.

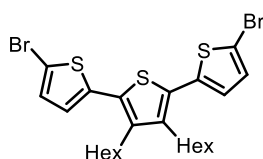
The analytical amount was purified by GPC.

^1H NMR (400 MHz, CDCl_3): δ 7.57 (d, $J = 3.6$ Hz, 1H), 7.20 (d, $J = 3.6$ Hz, 1H), 7.17 (d, $J = 3.8$ Hz, 1H), 6.97 (d, $J = 3.8$ Hz, 1H), 2.77 – 2.65 (m, 4H), 1.62 – 1.50 (m, 4H), 1.48 – 1.39 (m, 4H), 1.36 (s, 12H), 1.35 – 1.28 (m, 8H), 1.18 – 1.08 (m, 21H), 0.94 – 0.87 (m, 6H) ppm.

$^{13}\text{C}\{^1\text{H}\}$ NMR (101 MHz, CDCl_3): δ 143.16, 140.95, 140.79, 137.70, 137.66, 132.94, 130.54, 129.87, 127.26, 125.47, 123.28, 99.39, 96.91, 84.30, 31.60, 31.57, 30.72, 30.63, 29.68, 29.66, 28.33, 28.21, 24.91, 22.75, 18.81, 14.23, 14.20, 11.46 ppm.

MS (MALDI-ToF, RP, DCTB): m/z calcd. for $\text{C}_{41}\text{H}_{63}\text{BO}_2\text{S}_3\text{Si}$ $[\text{M}]^+$ 722.385, found 722.142.

Synthesis of 5,5''-dibromo-3',4'-dihexyl-2,2':5',2''-terthiophene (**100**):



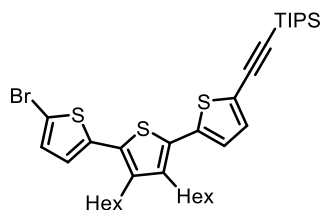
Terthiophene **90** (960 mg, 2.30 mmol, 1.0 eq.) was dissolved in DMF (60 mL) in the flask wrapped with aluminum foil to exclude the daily light and cooled to -20 $^\circ\text{C}$. *N*-Bromosuccinimide (868 mg, 4.83 mmol, 2.1 eq.) was added in one portion. The reaction mixture was allowed to warm up to RT and stirred for 16 h. Afterward, water was added and the reaction mixture was extracted with CH_2Cl_2 (3x). The combined org. layers were washed with aq. HCl (1M), water (2x), dried over Na_2SO_4 , filtered and the solvent was removed under reduced pressure. The crude product was purified by column chromatography (pentane) to give two-fold brominated terthiophene **100** (1.23 g, 2.14 mmol, **93%**) as a yellow oil.

^1H NMR (400 MHz, CDCl_3): δ 7.01 (d, $J = 3.8$ Hz, 2H), 6.86 (d, $J = 3.9$ Hz, 2H), 2.68 – 2.59 (m, 4H), 1.59 – 1.47 (m, 4H), 1.45 – 1.28 (m, 12H), 0.95 – 0.86 (m, 6H) ppm.

$^{13}\text{C}\{^1\text{H}\}$ NMR (101 MHz, CDCl_3): δ 140.80, 137.60, 130.36, 129.50, 126.40, 112.15, 31.61, 30.92, 29.68, 28.23, 22.75, 14.22 ppm.

HRMS (ESI, +): m/z calcd. for $\text{C}_{24}\text{H}_{30}\text{Br}_2\text{S}_3$ $[\text{M}]^+$ 571.9871; found:571.9860.

Synthesis of ((5''-bromo-3',4'-dihexyl-[2,2':5',2''-terthiophen]-5-yl)ethynyl)triisopropylsilane (**101**):



Two-fold brominated terthiophene **100** (700 mg, 1.22 mmol, 1.0 eq.) was dissolved in trimethylamine (30 mL)/toluene (30 mL) and degassed for 20 min with Argon. Afterwards, TIPSA (0.2 mL, 892 μ mol, 0.7 eq.) was added and the reaction mixture was degassed for a further 10 min. Pd(PPh₃)₂Cl₂ (43 mg, 61.0 μ mol, 5 mol%) and CuI (6 mg, 30.5 μ mol, 2.5 mol%) were added and the reaction mixture was put in preheated oil bath for 16 h. Then, the reaction mixture was cooled to RT, plugged over Celite and the solvent was removed under reduced pressure. The crude was purified by column chromatography (pentane) to give the terthiophene **101** (320 mg, 473 μ mol, **55%**) as a yellow oil.

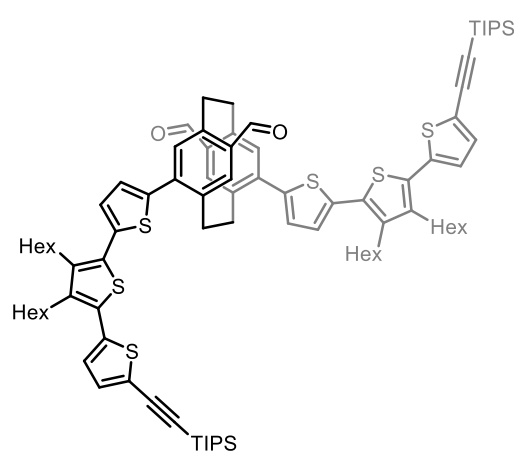
¹H NMR (400 MHz, CD₂Cl₂): δ 7.18 (d, *J* = 3.9 Hz, 1H), 7.05 (d, *J* = 3.9 Hz, 1H), 7.00 (d, *J* = 3.9 Hz, 1H), 6.90 (d, *J* = 3.9 Hz, 1H), 2.73 – 2.62 (m, 4H), 1.59 – 1.48 (m, 4H), 1.47 – 1.38 (m, 4H), 1.36 – 1.28 (m, 8H), 1.17 – 1.10 (m, 21H), 0.93 – 0.87 (m, 6H) ppm.

¹³C NMR {¹H} (101 MHz, CD₂Cl₂): δ 141.5, 141.4, 138.0, 137.8, 133.2, 130.8, 130.1, 129.6, 126.7, 125.9, 123.6, 112.2, 99.5, 97.4, 31.9, 31.9, 31.1, 30.9, 29.9, 29.9, 28.5, 28.4, 23.0, 23.0, 18.8, 14.2, 14.2, 11.7 ppm.

HRMS (ESI, +): *m/z* calcd. for C₃₅H₅₂BrS₃Si [M]⁺ 675.2178; found:675.2186.

m/z calcd. for (C₃₅H₅₂BrS₃Si)₂Ag [2M+Ag]⁺ 1455.3257; found:1455.3264.

Synthesis of Compound **93**:



Dialdehyde **82** (45 mg, 107 μ mol, 1.0 eq.), borester **83b** (309 mg, 428 μ mol, 4.0 eq.) and K₂CO₃ (89 mg, 642 μ mol, 6.0 eq.) were dissolved in toluene (5 mL) and MeOH (1 mL). The reaction mixture was degassed for 20 min with Argon before Pd(PPh₃)₄ (12 mg, 10.7 μ mol, 10 mol%) was added. The reaction mixture was placed in preheated oil bath and stirred at 70 °C for 2 h. Afterward, the reaction was allowed to reach room temperature and aq. HCl (1M) was added. The aq. layer was extracted with toluene (3x). The combined organic layer was washed with aq. HCl (1M), water, brine, dried over Na₂SO₄, filtered and the solvent was removed under reduced pressure. The crude product was purified by column chromatography

(cyclohexane to cyclohexane/CH₂Cl₂ 3:2) to give a compound **93** (150 mg, 103 μmol, **96%**) as a red/orange amorphous solid.

¹H NMR (400 MHz, CDCl₃): δ 10.09 (s, 2H), 7.40 (s, 2H), 7.26 (d, *J* = 3.7 Hz, 2H), 7.21 (d, *J* = 3.8 Hz, 2H), 7.19 (d, *J* = 3.8 Hz, 2H), 7.02 (d, *J* = 3.8 Hz, 2H), 6.65 (s, 2H), 4.21 – 4.08 (m, 2H), 3.89 – 3.74 (m, 2H), 3.10 – 2.95 (m, 2H), 2.83 – 2.64 (m, 10H), 1.68 – 1.55 (m, 8H), 1.52 – 1.44 (m, 8H), 1.39 – 1.32 (m, 16H), 1.18 – 1.10 (m, 42H), 0.95 – 0.88 (m, 12H) ppm.

¹³C{¹H} NMR (101 MHz, CDCl₃): δ 191.04, 143.70, 141.15, 141.10, 140.98, 140.26, 138.54, 137.47, 137.46, 136.43, 135.04, 134.30, 132.97, 130.09, 129.97, 127.77, 126.89, 125.61, 123.50, 99.32, 97.13, 33.74, 33.64,* 31.73, 31.60, 30.82, 30.76, 29.82, 29.67, 28.54, 28.35, 22.81, 22.76, 18.81, 14.27, 14.21, 11.47 ppm.

* was extracted from DEPT-135 experiment

HRMS (ESI, +): *m/z* calcd. for C₈₈H₁₁₆O₂S₆Si₂H [M+H]⁺1453.6911; found:1453.6871;

m/z calcd. for C₈₈H₁₁₆O₂S₆Si₂Na [M+Na]⁺1475.6730; found:1475.6700;

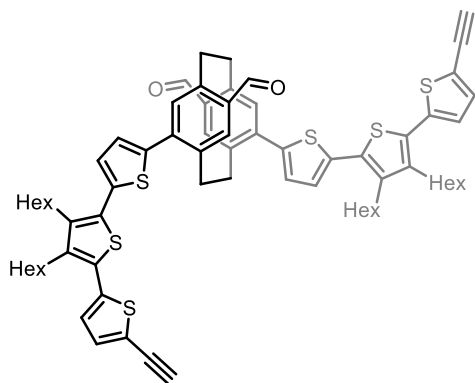
m/z calcd. for C₈₈H₁₁₆O₂S₆Si₂K [M+K]⁺1491.6470; found:1491.6453.

UV/Vis: λ_{max} = 415 nm (cyclohexane), 421 nm (toluene), 413 nm (ethyl acetate), 424 nm (chloroform).

Fluorescence: λ_{max} = 510 (540) nm (cyclohexane), 529 nm (toluene), 540 nm (ethyl acetate), 572 nm (chloroform).

Φ_f (%): 10.1 (cyclohexane), 11.6 (toluene), 8.2 (ethyl acetate), 7.7 (chloroform).

Synthesis of Compound 102:



Compound **93** (205 mg, 141 μmol, 1.0 eq.) was dissolved in THF/water (40/1). The reaction mixture was degassed for 20 min with Argon before TBAF (1.4 mL, 1.41 mmol, 10 eq.) was added. The reaction was stirred at room temperature for 16 h. Afterward, the reaction mixture was diluted with toluene and water. The organic layer was separated and washed with brine (3x), water, dried over Na₂SO₄ filtered and the solvent

was removed under reduced pressure. The crude product was purified by column chromatography (cyclohexane/CH₂Cl₂ 3:2) to give the compound **102** (150 mg, 131 μmol, **93%**) as a red/orange amorphous solid.

¹H NMR (400 MHz, CD₂Cl₂): δ 10.10 (s, 2H), 7.40 (s, 2H), 7.29 (d, *J* = 3.9 Hz, 2H), 7.26 (d, *J* = 3.8 Hz, 2H), 7.25 (d, *J* = 3.9 Hz, 2H), 7.06 (d, *J* = 3.9 Hz, 2H), 6.67 (s, 2H), 4.20 – 4.07 (m, 2H), 3.89 – 3.75 (m, 2H), 3.51 (s, 2H), 3.07 – 2.95 (m, 2H), 2.88 – 2.78 (m, 4H), 2.78 – 2.63 (m, 6H), 1.68 – 1.55 (m, 8H), 1.53 – 1.42 (m, 8H), 1.40 – 1.28 (m, 16H), 0.97 – 0.82 (m, 12H) ppm.

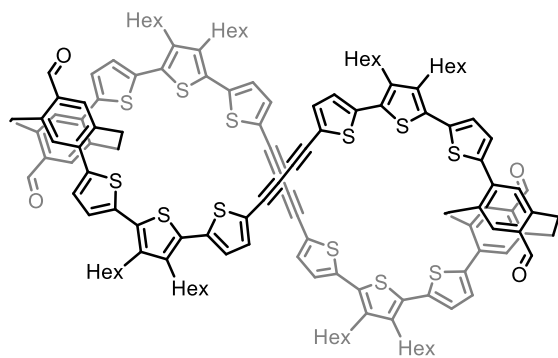
¹³C{¹H} NMR (101 MHz, CD₂Cl₂): δ 191.08, 143.92, 141.80, 141.64, 141.44, 140.36, 138.53, 138.44, 137.94, 136.34, 135.43, 134.47, 134.02, 130.47, 129.83, 128.13, 127.35, 125.92, 121.91, 82.72, 76.99, 33.97, * 33.75, * 32.00, 31.92, 31.04 (2C), 30.02, 29.93, 28.71, 28.62, 23.09, 23.05, 14.30, 14.26 ppm.

* better visible in DEPT-135 experiment

HRMS (ESI, +): *m/z* calcd. for C₇₀H₇₆O₂S₆Na [M+Na]⁺ 1163.4062; found:1163.4059.

Synthesis of Diyne Dimer (103):**Eglinton-Breslow**

CuCl and Cu(Ac)₂ were purified according to the procedure described in the ref.¹⁸⁷



Chemical Formula: C₁₄₀H₁₄₈O₄S₁₂
Exact Mass: 2276.803

CuCl (104 mg, 1.05 mmol, 30 eq.) and Cu(Ac)₂ (267 mg, 1.47 mmol, 42 eq.) were dissolved in dry pyridine (18 mL) and stirred at 80 °C for 20 min. To this reaction mixture, a solution of **102** (40 mg, 35.0 μmol, 1.0 eq.) in dry pyridine (6 mL) was added with a syringe pump over 14 h and stirred for a further 2 h. Afterward, pyridine was removed under reduced pressure, and the residue was redissolved in CH₂Cl₂. The organic

layer was washed with NH₄Cl (2x), HCl (1M), water, dried over Na₂SO₄, filtered, and the solvent was removed under reduced pressure. The crude product was purified by column chromatography (CH₂Cl₂) to give the product (14 mg, 6.13 μmol, **35%**) as a red amorphous solid.

General Procedure I: One-Pot Deprotection and Macrocyclisation

This procedure was modified from ref.¹⁸⁹

Compound **93** was dissolved in pyridine in a round bottom flask equipped with a large magnetic stirrer. Copper(II) fluoride hydrate (6.0 eq.) was added and the reaction mixture was placed in preheated oil bath (40 – 80 °C) and stirred vigorously at open ambient atmosphere for 1-16 h. Afterward, the reaction mixture was allowed to reach room temperature. The organic layer was washed with aq. NH₄Cl (sat., 2x), water, brine, dried over Na₂SO₄, filtered over a plug of silica. The solvent was removed under reduced pressure and the crude product was purified by column chromatography (CH₂Cl₂) and/or GPC to provide the dimer **103** as a red amorphous solid.

General procedure II: Glaser-Hay

Compound **102** was dissolved in CH₂Cl₂. CuCl and TMEDA were added and the reaction mixture was stirred for 1 - 16 h at room temperature. Afterward, the reaction mixture was diluted and washed with aq. NH₄Cl (sat., 2x), water, filtered over a plug of silica. The solvent was removed under reduced pressure and the crude product was purified by column chromatography (CH₂Cl₂) and/or GPC to provide the dimer **103** as a red amorphous solid.

¹H NMR (500 MHz, CD₂Cl₂): δ 10.12 (s, 4H), 7.39 (s, 4H), 7.35 (d, *J* = 3.9 Hz, 4H), 7.31 (d, *J* = 3.8 Hz, 4H), 7.27 (d, *J* = 3.9 Hz, 4H), 7.08 (d, *J* = 3.9 Hz, 4H), 6.72 (s, 4H), 4.18 – 4.08 (m, 4H), 3.93 – 3.84 (m, 4H), 3.05 – 2.97 (m, 4H), 2.84 – 2.71 (m, 16H), 2.71 – 2.64 (m, 4H), 1.66 – 1.56 (m, 16H), 1.50 – 1.42 (m, 16H), 1.39 – 1.32 (m, 32H), 0.94 – 0.89 (m, 24H) ppm.

¹H NMR (600 MHz, CD₂Cl₂): δ 10.11 (s, 4H), 7.38 (s, 4H), 7.35 (d, *J* = 3.7 Hz, 4H), 7.30 (d, *J* = 3.8 Hz, 4H), 7.27 (d, *J* = 3.8 Hz, 4H), 7.07 (d, *J* = 3.8 Hz, 4H), 6.71 (s, 4H), 4.15 – 4.09 (m, 4H), 3.93 – 3.82 (m, 4H), 3.04 – 2.97 (m, 4H), 2.83 – 2.71 (m, 16H), 2.70 – 2.60 (m, 4H), 1.65 – 1.56 (m, 16H), 1.50 – 1.42 (m, 16H), 1.38 – 1.33 (dq_t, *J* = 10.4, 5.7, 2.7 Hz, 32H), 0.94 – 0.90 (m, 24H) ppm.

¹³C NMR (126 MHz, CD₂Cl₂): δ 190.97, 143.93, 142.23, 141.73, 141.57, 140.53, 140.29, 138.99, 138.10, 135.70 (2C),* 135.43, 133.88, 130.95, 129.69, 128.24, 126.71, 125.61, 79.34, 34.20,** 33.89,** 31.99, 31.93, 31.01, 30.93, 29.99, 29.95, 28.62 (2C),** 23.09, 23.06, 14.31, 14.26 ppm. (No clear resonance for the second quarternary carbon atom of acetylene and some of quartier carbons could be observed due to the insufficient amount of prepared dimeric structure).

* overlap is visible in HSQC spectrum

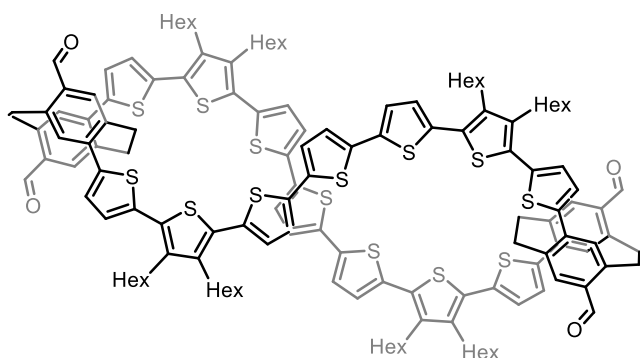
** were detected in DEPT-135 experiment.

MS (MALDI-ToF, RP, DCTB): *m/z* calcd. for C₁₄₀H₁₄₈O₄S₁₂ [M]⁺ 2276.803, found 2276.907.

UV/Vis: λ_{max} = 415 nm (cyclohexane), 426 nm (toluene), 420 nm (ethyl acetate), 427 nm (chloroform).

Fluorescence: λ_{max} = 530 (564) nm (cyclohexane), 541 (577) nm (toluene), 540 (568) nm (ethyl acetate), 581 nm (chloroform).

Φ_f (%): 9.3 (cyclohexane), 10.6 (toluene), 8.9 (ethyl acetate), 10.9 (chloroform).

Synthesis of Thiophene Dimer (125):

Chemical Formula: $C_{140}H_{152}O_4S_{14}$
Exact Mass: 2344.778

Diyne dimer (**103**) (10 mg, 4.39 μ mol, 1.0 eq.) and 1,4,7,10,13-pentaoxacyclopentadecan (77 mg, 351 μ mol, 80 eq.) were dissolved in *p*-xylol (1 mL) and degassed for 20 min. Afterward, sodium sulfide nonahydrate (42 mg, 176 μ mol, 40 eq.) was added. The reaction mixture was put in preheated oil bath and stirred for 90 min at 140 °C. Then, the reaction

was cooled to room temperature, diluted with toluene and washed with aq. HCl (1M), water, brine, dried over Na_2SO_4 , filtered over a plug of silica. The solvent was removed under reduced pressure and the crude product was purified by GPC to give the desired thiophene dimer (**125**) (5 mg, 2.15 μ mol, **49%**) as a red amorphous solid.

1H NMR (600 MHz, C_6D_6): δ 9.91 (s, 4H, H23), 7.38 (s, 4H, H19), 7.27 – 7.22 (m, 8H, H12/13), 7.05 (dd, $J = 3.7, 1.4$ Hz, 4H, H5), 6.94 (d, $J = 3.6$ Hz, 4H, H4), 6.86 (d, $J = 1.1$ Hz, 4H, H1), 6.64 (s, 4H, H16), 3.87 – 3.79 (m, 4H, H21), 3.75 – 3.68 (m, 4H, H22), 2.91 – 2.79 (m, 16H, H24/30), 2.74 – 2.66 (m, 4H, H21), 2.56 – 2.49 (m, 4H, H22), 1.76 – 1.66 (m, 16H, H25/31), 1.51 – 1.45 (m, 16H, H26/32), 1.31 – 1.27 (m, 32H, H27/28/33/34), 0.98 – 0.90 (m, 24H, H29/35 (overlap with the H grease)) ppm.

$^{13}C\{^1H\}$ NMR (151 MHz, C_6D_6):* 190.24 (C23), 143.77 (C17), 141.84 (C14), 141.38 (C8), 140.18 (C15), 139.30 (C11), 137.92 (C20), 137.43 (C3), 136.50 (C2), 136.00 (C6), 135.70 (C19), 135.67 (C18), 135.47 (C9), 133.91 (C16), 131.11 (C7), 130.66 (C10), 128.25 (C12), 126.72 (C5), 126.71 (C13), 124.99 (C1), 124.81 (C4), 34.03 (C22), 33.06 (C21), 32.07 (C27), 31.92 (C33), 31.27 (C25), 31.08 (C31), 30.20 (C26), 29.94 (C32), 28.78 (C24), 28.68 (C30), 23.23 (C28), 23.03 (C34), 14.44 (C29), 14.41 (C35).

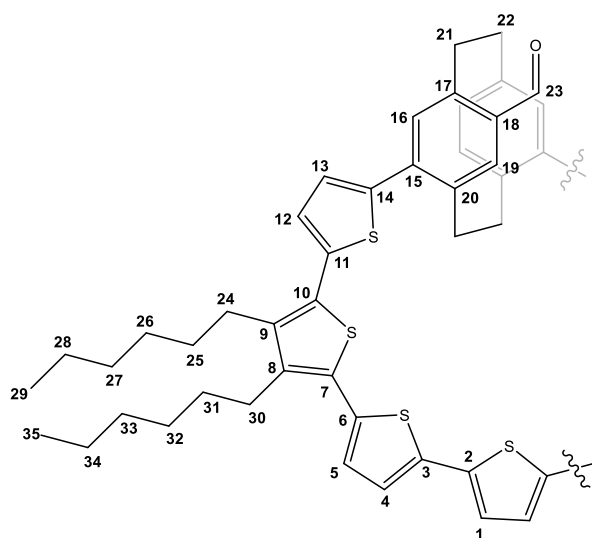
* Was extracted from 2D NMR experiments

MS (MALDI-ToF, RP, DCTB): m/z calcd. for $C_{140}H_{152}O_4S_{14}$ $[M]^+$ 2344.778, found 2344.979.

UV/Vis: λ_{max} = 425 nm (cyclohexane), 433 nm (toluene), 426 nm (ethyl acetate), 435 nm (chloroform).

Fluorescence: λ_{max} = 559 (597) nm (cyclohexane), 573 (610) nm (toluene), 601 nm (ethyl acetate), 626 nm (chloroform).

Φ_f (%): 11.4 (cyclohexane), 11.4 (toluene), 8.5 (ethyl acetate), 9.6 (chloroform).



6 Abbreviations

| | |
|--------|---------------------------------------------------------------------------------------|
| °C | degrees centigrade |
| aq. | aqueous |
| COD | 1,5-cyclooctadien |
| COSY | correlation spectroscopy |
| CPDMS | (3-cyanopropyl)dimethylsilyl |
| CPL | circularly polarized luminescent |
| CPP | cycloparaphenylenes |
| CQI | constructive quantum interference |
| CVD | chemical vapor deposition |
| DCTB | <i>trans</i> -2-[3-(4- <i>tert</i> -Butylphenyl)-2-methyl-propenyldiene]malononitrile |
| DFT | density-functional theory |
| DIPA | diisopropylamine |
| DIPEA | <i>N,N</i> -diisopropylethylamine, or Hünig's base |
| DMF | <i>N,N</i> -dimethylformamide |
| DMSO | dimethyl sulfoxide |
| DOSY | diffusion-ordered spectroscopy |
| dppe | 1,2-bis(diphenylphosphino)ethane |
| DQI | destructive quantum interference |
| EA | ethyl acetate |
| EB | electrical breakdown |
| eq. | equivalent |
| ESI-MS | electrospray ionization mass spectrometry |
| FFT | Fast Fourier transformation |
| GC | gas chromatography |
| GF | gauge factor |
| GPC | gel permeation chromatography |
| GPH | gas-phase HOMO |
| GPL | gas-phase LUMO |
| h | hour(s) |
| Hex | hexyl = C ₆ H ₁₃ |
| HMBC | heteronuclear multiple-quantum correlation |
| HOMO | highest occupied molecular orbital |
| HOP | 2-hydroxyprop-2-yl |
| HSQC | heteronuclear single quantum correlation |
| Hz | hertz [s ⁻¹] |

| | |
|----------------------------------|------------------------------------------------------------|
| J (NMR) | coupling constant [Hz] |
| LDA | lithium diisopropylamide |
| LUMO | lowest unoccupied molecular orbital |
| M | molarity [mol/L] |
| <i>m</i> | meta |
| MALDI-TOF | matrix-assisted laser desorption ionization-time of flight |
| MCBJ | mechanically controlled break junction |
| MeOH | methanol |
| min | minutes |
| MS | mass spectrometry |
| NBS | N-Bromosuccinimide |
| NEGF | nonequilibrium Green's function |
| NEt₃ | triethylamine |
| NMR | nuclear magnetic resonance |
| NOESY | nuclear overhauser effect spectroscopy |
| <i>o</i> | ortho |
| OPE | oligo(phenylene ethynylene) |
| <i>p</i> | para |
| PCP | [2.2]paracyclophane |
| PG | protecting group |
| ppm | parts per million |
| ps | pseudo |
| QI | quantum interference |
| QUIET | Quantum Interference Enhanced Thermoelectricity |
| RT | room temperature |
| sat. | saturated |
| STM | scanning tunneling microscope |
| TADF | thermally activated delayed fluorescence |
| TBAF | tetra- <i>n</i> -butylammonium fluoride |
| TCE | tetrachloroethane |
| TLC | thin layer chromatography |
| THF | tetrahydrofuran |
| TMEDA | tetramethylethylenediamine |
| UV-Vis | ultraviolet-visible spectroscopy |
| δ (NMR) | chemical shift [ppm] |

7 References

- (1) Aviram, A.; Ratner, M. A. Molecular Rectifiers. *Chem. Phys. Lett.* **1974**, *29* (2), 277–283. [https://doi.org/10.1016/0009-2614\(74\)85031-1](https://doi.org/10.1016/0009-2614(74)85031-1).
- (2) Xiang, D.; Wang, X.; Jia, C.; Lee, T.; Guo, X. Molecular-Scale Electronics: From Concept to Function. *Chem. Rev.* **2016**, *116* (7), 4318–4440. <https://doi.org/10.1021/acs.chemrev.5b00680>.
- (3) Mathew, P. T.; Fang, F. Advances in Molecular Electronics: A Brief Review. *Engineering* **2018**, *4* (6), 760–771. <https://doi.org/10.1016/j.eng.2018.11.001>.
- (4) Tang, C.; Ayinla, R. T.; Wang, K. Beyond Electrical Conductance: Progress and Prospects in Single-Molecule Junctions. *J. Mater. Chem. C* **2022**, *10* (37), 13717–13733. <https://doi.org/10.1039/D2TC01155G>.
- (5) Binnig, G.; Rohrer, H. Scanning Tunneling Microscopy. *IBM J. Res. Dev.* **2000**, *44* (1/2), 279.
- (6) Xiang, D.; Jeong, H.; Lee, T.; Mayer, D. Mechanically Controllable Break Junctions for Molecular Electronics. *Adv. Mater.* **2013**, *25* (35), 4845–4867.
- (7) Liang, W.; Shores, M. P.; Bockrath, M.; Long, J. R.; Park, H. Kondo Resonance in a Single-Molecule Transistor. *Nature* **2002**, *417* (6890), 725–729. <https://doi.org/10.1038/nature00790>.
- (8) Prins, F.; Barreiro, A.; Ruitenbergh, J. W.; Seldenthuis, J. S.; Aliaga-Alcalde, N.; Vandersypen, L. M. K.; van der Zant, H. S. J. Room-Temperature Gating of Molecular Junctions Using Few-Layer Graphene Nanogap Electrodes. *Nano Lett.* **2011**, *11* (11), 4607–4611. <https://doi.org/10.1021/nl202065x>.
- (9) Mol, J. A.; Lau, C. S.; Lewis, W. J. M.; Sadeghi, H.; Roche, C.; Crossen, A.; Warner, J. H.; Lambert, C. J.; Anderson, H. L.; Briggs, G. A. D. Graphene-Porphyrin Single-Molecule Transistors. *Nanoscale* **2015**, *7* (31), 13181–13185. <https://doi.org/10.1039/C5NR03294F>.
- (10) Lau, C. S.; Mol, J. A.; Warner, J. H.; Briggs, G. A. D. Nanoscale Control of Graphene Electrodes. *Phys. Chem. Chem. Phys.* **2014**, *16* (38), 20398–20401. <https://doi.org/10.1039/C4CP03257H>.
- (11) Vazquez, H.; Skouta, R.; Schneebeli, S.; Kamenetska, M.; Breslow, R.; Venkataraman, L.; Hybertsen, M. S. Probing the Conductance Superposition Law in Single-Molecule Circuits with Parallel Paths. *Nat. Nanotechnol.* **2012**, *7* (10), 663–667. <https://doi.org/10.1038/nnano.2012.147>.
- (12) Guédon, C. M.; Valkenier, H.; Markussen, T.; Thygesen, K. S.; Hummelen, J. C.; van der Molen, S. J. Observation of Quantum Interference in Molecular Charge Transport. *Nat. Nanotechnol.* **2012**, *7* (5), 305–309. <https://doi.org/10.1038/nnano.2012.37>.
- (13) Vezzoli, A. Mechanoresistive Single-Molecule Junctions. *Nanoscale* **2022**, *14* (8), 2874–2884. <https://doi.org/10.1039/D1NR06891A>.
- (14) Jia, C.; Migliore, A.; Xin, N.; Huang, S.; Wang, J.; Yang, Q.; Wang, S.; Chen, H.; Wang, D.; Feng, B.; Liu, Z.; Zhang, G.; Qu, D.-H.; Tian, H.; Ratner, M. A.; Xu, H. Q.; Nitzan, A.; Guo, X. Covalently Bonded Single-Molecule Junctions with Stable and Reversible Photoswitched Conductivity. *Science* **2016**, *352* (6292), 1443–1445. <https://doi.org/10.1126/science.aaf6298>.
- (15) Kim, Y.; Jeong, W.; Kim, K.; Lee, W.; Reddy, P. Electrostatic Control of Thermoelectricity in Molecular Junctions. *Nat. Nanotechnol.* **2014**, *9* (11), 881–885. <https://doi.org/10.1038/nnano.2014.209>.
- (16) Cao, Y.; Dong, S.; Liu, S.; He, L.; Gan, L.; Yu, X.; Steigerwald, M. L.; Wu, X.; Liu, Z.; Guo, X. Building High-Throughput Molecular Junctions Using Indented Graphene Point Contacts. *Angew. Chem.* **2012**, *124* (49), 12394–12398. <https://doi.org/10.1002/ange.201205607>.
- (17) Braun, O.; Overbeck, J.; El Abbassi, M.; Käser, S.; Furrer, R.; Olziersky, A.; Flasby, A.; Borin Barin, G.; Sun, Q.; Darawish, R.; Müllen, K.; Ruffieux, P.; Fasel, R.; Shorubalko, I.; Perrin, M. L.; Calame, M. Optimized Graphene Electrodes for Contacting Graphene Nanoribbons. *Carbon* **2021**, *184*, 331–339. <https://doi.org/10.1016/j.carbon.2021.08.001>.
- (18) Sadeghi, H.; Sangtarash, S.; Lambert, C. Robust Molecular Anchoring to Graphene Electrodes. *Nano Lett.* **2017**, *17* (8), 4611–4618. <https://doi.org/10.1021/acs.nanolett.7b01001>.

- (19) Xu, Q.; Scuri, G.; Mathewson, C.; Kim, P.; Nuckolls, C.; Bouilly, D. Single Electron Transistor with Single Aromatic Ring Molecule Covalently Connected to Graphene Nanogaps. *Nano Lett.* **2017**, *17* (9), 5335–5341. <https://doi.org/10.1021/acs.nanolett.7b01745>.
- (20) Lee, C.-H.; Lee, G.-H.; van der Zande, A. M.; Chen, W.; Li, Y.; Han, M.; Cui, X.; Arefe, G.; Nuckolls, C.; Heinz, T. F.; Guo, J.; Hone, J.; Kim, P. Atomically Thin p–n Junctions with van Der Waals Heterointerfaces. *Nat. Nanotechnol.* **2014**, *9* (9), 676–681. <https://doi.org/10.1038/nnano.2014.150>.
- (21) Nef, C.; Pósa, L.; Makk, P.; Fu, W.; Halbritter, A.; Schönenberger, C.; Calame, M. High-Yield Fabrication of Nm-Size Gaps in Monolayer CVD Graphene. *Nanoscale* **2014**, *6* (13), 7249–7254. <https://doi.org/10.1039/C4NR01838A>.
- (22) Abbassi, M. E.; Pósa, L.; Makk, P.; Nef, C.; Thodkar, K.; Halbritter, A.; Calame, M. From Electroburning to Sublimation: Substrate and Environmental Effects in the Electrical Breakdown Process of Monolayer Graphene. *Nanoscale* **2017**, *9* (44), 17312–17317. <https://doi.org/10.1039/C7NR05348G>.
- (23) Thodkar, K.; El Abbassi, M.; Lüönd, F.; Overney, F.; Schönenberger, C.; Jeanneret, B.; Calame, M. Comparative Study of Single and Multi Domain CVD Graphene Using Large-Area Raman Mapping and Electrical Transport Characterization. *Phys. Status Solidi RRL – Rapid Res. Lett.* **2016**, *10* (11), 807–811. <https://doi.org/10.1002/pssr.201600211>.
- (24) Schmuck, O.; Beretta, D.; Furrer, R.; Oswald, J.; Calame, M. A Method to Fabricate Nanoscale Gaps in Graphene Nano-Constrictions by Electrical Breakdown. *AIP Adv.* **2022**, *12* (5), 055312. <https://doi.org/10.1063/5.0087564>.
- (25) Zhou, Y.; Maguire, P.; Jadwiszczak, J.; Muruganathan, M.; Mizuta, H.; Zhang, H. Precise Milling of Nano-Gap Chains in Graphene with a Focused Helium Ion Beam. *Nanotechnology* **2016**, *27* (32), 325302. <https://doi.org/10.1088/0957-4484/27/32/325302>.
- (26) Song, B.; Schneider, G. F.; Xu, Q.; Pandraud, G.; Dekker, C.; Zandbergen, H. Atomic-Scale Electron-Beam Sculpting of Near-Defect-Free Graphene Nanostructures. *Nano Lett.* **2011**, *11* (6), 2247–2250. <https://doi.org/10.1021/nl200369r>.
- (27) Xie, L.; Liao, M.; Wang, S.; Yu, H.; Du, L.; Tang, J.; Zhao, J.; Zhang, J.; Chen, P.; Lu, X.; Wang, G.; Xie, G.; Yang, R.; Shi, D.; Zhang, G. Graphene-Contacted Ultrashort Channel Monolayer MoS₂ Transistors. *Adv. Mater.* **2017**, *29* (37), 1702522. <https://doi.org/10.1002/adma.201702522>.
- (28) Zhang, K.; Fu, Q.; Pan, N.; Yu, X.; Liu, J.; Luo, Y.; Wang, X.; Yang, J.; Hou, J. Direct Writing of Electronic Devices on Graphene Oxide by Catalytic Scanning Probe Lithography. *Nat. Commun.* **2012**, *3* (1), 1194. <https://doi.org/10.1038/ncomms2200>.
- (29) Limburg, B.; Thomas, J. O.; Holloway, G.; Sadeghi, H.; Sangtarash, S.; Hou, I. C.-Y.; Cremers, J.; Narita, A.; Müllen, K.; Lambert, C. J.; Briggs, G. A. D.; Mol, J. A.; Anderson, H. L. Anchor Groups for Graphene-Porphyrin Single-Molecule Transistors. *Adv. Funct. Mater.* **2018**, *28* (45), 1803629. <https://doi.org/10.1002/adfm.201803629>.
- (30) Elmahdy, M. M.; Dou, X.; Mondeshki, M.; Floudas, G.; Butt, H.-J.; Spiess, H. W.; Müllen, K. Self-Assembly, Molecular Dynamics, and Kinetics of Structure Formation in Dipole-Functionalized Discotic Liquid Crystals. *J. Am. Chem. Soc.* **2008**, *130* (15), 5311–5319. <https://doi.org/10.1021/ja7113618>.
- (31) El Abbassi, M.; Sangtarash, S.; Liu, X.; Perrin, M. L.; Braun, O.; Lambert, C.; van der Zant, H. S. J.; Yitzchaik, S.; Decurtins, S.; Liu, S.-X.; Sadeghi, H.; Calame, M. Robust Graphene-Based Molecular Devices. *Nat. Nanotechnol.* **2019**, *14* (10), 957–961. <https://doi.org/10.1038/s41565-019-0533-8>.
- (32) Sadeghi, H.; Mol, J. A.; Lau, C. S.; Briggs, G. A. D.; Warner, J.; Lambert, C. J. Conductance Enlargement in Picoscale Electroburnt Graphene Nanojunctions. *Proc. Natl. Acad. Sci.* **2015**, *112* (9), 2658–2663. <https://doi.org/10.1073/pnas.1418632112>.
- (33) Sonogashira, K.; Tohda, Y.; Hagihara, N. A Convenient Synthesis of Acetylenes: Catalytic Substitutions of Acetylenic Hydrogen with Bromoalkenes, Iodoarenes, and Bromopyridines. *Tetrahedron Lett.* **1975**, *50* (16), 4467–4470. [https://doi.org/10.1016/S0040-4039\(00\)91094-3](https://doi.org/10.1016/S0040-4039(00)91094-3).
- (34) Bunz, U. H. F.; Rubin, Y.; Tobe, Y. Polyethynylated Cyclic P-Systems: Scaffoldings for Novel Two and Three-Dimensional Carbon Networks. **13**.

- (35) Le Pleux, L.; Kapatsina, E.; Hildesheim, J.; Häußinger, D.; Mayor, M. A Molecular Turnstile as an E-Field-Triggered Single-Molecule Switch: Concept and Synthesis. *Eur. J. Org. Chem.* **2017**, 2017 (22), 3165–3178. <https://doi.org/10.1002/ejoc.201700318>.
- (36) Grunder, S.; Muñoz Torres, D.; Marquardt, C.; Błaszczuk, A.; Krupke, R.; Mayor, M. Synthesis and Optical Properties of Molecular Rods Comprising a Central Core-Substituted Naphthalenediimide Chromophore for Carbon Nanotube Junctions. *Eur. J. Org. Chem.* **2011**, 2011 (3), 478–496. <https://doi.org/10.1002/ejoc.201001415>.
- (37) Jenny, N. M.; Mayor, M.; Eaton, T. R. Phenyl–Acetylene Bond Assembly: A Powerful Tool for the Construction of Nanoscale Architectures. *Eur. J. Org. Chem.* **2011**, 2011 (26), 4965–4983. <https://doi.org/10.1002/ejoc.201100176>.
- (38) Ko, S.-B.; Cho, A.-N.; Kim, M.-J.; Lee, C.-R.; Park, N.-G. Alkyloxy substituted organic dyes for high voltage dye-sensitized solar cell: Effect of alkyloxy chain length on open-circuit voltage. *Dyes and Pigments.* **2012**, 94 (1), 88–98. <https://doi.org/10.1016/j.dyepig.2011.10.014>.
- (39) Höger, S.; Bonrad, K. [(3-Cyanopropyl)Dimethylsilyl]Acetylene, a Polar Analogue of (Trimethylsilyl)Acetylene: Synthesis and Applications in the Preparation of Monoprotected Bisacetylenes. *J. Org. Chem.* **2000**, 65 (7), 2243–2245. <https://doi.org/10.1021/jo991746m>.
- (40) Wang, C.; Batsanov, A. S.; Bryce, M. R. Convergent Synthesis of 10 Nm Aryleneethynylene Molecular Wires by an Iterative Regioselective Deprotection/Sonogashira Coupling Protocol. *J. Org. Chem.* **2006**, 71 (1), 108–116. <https://doi.org/10.1021/jo051711o>.
- (41) Havens, S. J.; Hergenrother, P. M. Synthesis of Arylacetylenes by the Sodium Hydride Catalyzed Cleavage of 4-Aryl-2-Methyl-3-Butyn-2-Ols. *J. Org. Chem.* **1985**, 50 (10), 1763–1765. <https://doi.org/10.1021/jo00210a042>.
- (42) Zhang, J.; Cui, Y.; Wang, M.; Liu, J. Synthesis of Double-Conjugated-Segment Molecules and Their Application as Ultra-Broad Two-Photon-Absorption Optical Limiters. *Chem. Commun.* **2002**, No. 21, 2526–2527. <https://doi.org/10.1039/B208190C>.
- (43) Wuts, P. G.; Greene, T. W. *Greene's protective groups in organic synthesis*. John Wiley & Sons., **2006**.
- (44) Speier, J. L.; Webster, J. A.; Barnes, G. H. The Addition of Silicon Hydrides to Olefinic Double Bonds. Part II. The Use of Group VIII Metal Catalysts. *J. Am. Chem. Soc.* **1957**, 79 (4), 974–979. <https://doi.org/10.1021/ja01561a054>.
- (45) Lewis, L. N.; Stein, J.; Gao, Y.; Colborn, R. E.; Hutchins, G. Platinum Catalysts Used in the Silicones Industry: Their Synthesis and Activity in Hydrosilylation. *Platin. Met. Rev.* **1997**, 41 (2), 66–75.
- (46) Nakajima, Y.; Shimada, S. Hydrosilylation Reaction of Olefins: Recent Advances and Perspectives. *RSC Adv.* **2015**, 5 (26), 20603–20616. <https://doi.org/10.1039/C4RA17281G>.
- (47) Gigler, P.; Drees, M.; Riener, K.; Bechlars, B.; Herrmann, W. A.; Kühn, F. E. Mechanistic Insights into the Hydrosilylation of Allyl Compounds – Evidence for Different Coexisting Reaction Pathways. *J. Catal.* **2012**, 295, 1–14. <https://doi.org/10.1016/j.jcat.2012.06.006>.
- (48) Riener, K.; Meister, T. K.; Gigler, P.; Herrmann, W. A.; Kühn, F. E. Mechanistic Insights into the Iridium-Catalyzed Hydrosilylation of Allyl Compounds. *J. Catal.* **2015**, 331, 203–209. <https://doi.org/10.1016/j.jcat.2015.09.003>.
- (49) Troegel, D.; Stohrer, J. Recent Advances and Actual Challenges in Late Transition Metal Catalyzed Hydrosilylation of Olefins from an Industrial Point of View. *Coord. Chem. Rev.* **2011**, 255 (13), 1440–1459. <https://doi.org/10.1016/j.ccr.2010.12.025>.
- (50) Brown, C. J.; Farthing, A. C. Preparation and Structure of Di- p -Xylylene. *Nature* **1949**, 164 (4178), 915–916. <https://doi.org/10.1038/164915b0>.
- (51) Cram, D. J.; Steinberg, H. Macro Rings. I. Preparation and Spectra of the Paracyclophanes. *J. Am. Chem. Soc.* **1951**, 73 (12), 5691–5704. <https://doi.org/10.1021/ja01156a059>.
- (52) Winberg, H. E.; Fawcett, F. S.; Mochel, W. E.; Theobald, C. W. Dimethylenedihydroheteroaromatic Compounds and Heterocyclophanes by 1,6-Hofmann Elimination Reactions. *J. Am. Chem. Soc.* **1960**, 82 (6), 1428–1435. <https://doi.org/10.1021/ja01491a037>.

- (53) Chow, H.-F.; Low, K.-H.; Wong, K. Y. An Improved Method for the Regiospecific Synthesis of Polysubstituted [2.2]Paracyclophanes. *Synlett* **2005**, 2005 (14), 2130–2134. <https://doi.org/10.1055/s-2005-872270>.
- (54) Otsubo, T.; Horita, H.; Misumi, S. Studies on the Syntheses of Multilayered [2. 2] Paracyclophanes. *Synth. Commun.* **1976**, 6 (8), 591–596. <https://doi.org/10.1080/00397917608063553>.
- (55) Pan, D.; Wang, Y.; Xiao, G. A New Protocol for the Synthesis of 4,7,12,15-Tetrachloro[2.2]Paracyclophane. *Beilstein J. Org. Chem.* **2016**, 12 (1), 2443–2449. <https://doi.org/10.3762/bjoc.12.237>.
- (56) Paradies, J. [2.2]Paracyclophane Derivatives: Synthesis and Application in Catalysis. *Synthesis* **2011**, 2011 (23), 3749–3766. <https://doi.org/10.1055/s-0031-1289296>.
- (57) David, O. R. P. Syntheses and Applications of Disubstituted [2.2]Paracyclophanes. *Tetrahedron* **2012**, 68 (44), 8977–8993. <https://doi.org/10.1016/j.tet.2012.08.009>.
- (58) Hassan, Z.; Spuling, E.; Knoll, D. M.; Bräse, S. Regioselective Functionalization of [2.2]Paracyclophanes: Recent Synthetic Progress and Perspectives. *Angew. Chem. Int. Ed.* **2020**, 59 (6), 2156–2170. <https://doi.org/10.1002/anie.201904863>.
- (59) Weiland, K. J.; Gallego, A.; Mayor, M. Beyond Simple Substitution Patterns – Symmetrically Tetrasubstituted [2.2]Paracyclophanes as 3D Functional Materials. *Eur. J. Org. Chem.* **2019**, 2019 (20), 3073–3085. <https://doi.org/10.1002/ejoc.201900061>.
- (60) Hopf, H. [2.2]Paracyclophanes in Polymer Chemistry and Materials Science. *Angew. Chem. Int. Ed.* **2008**, 47 (51), 9808–9812. <https://doi.org/10.1002/anie.200800969>.
- (61) Dahmen, S.; Bräse, S. The Asymmetric Dialkylzinc Addition to Imines Catalyzed by [2.2]Paracyclophane-Based N,O-Ligands. *J. Am. Chem. Soc.* **2002**, 124 (21), 5940–5941. <https://doi.org/10.1021/ja025831e>.
- (62) Bolm, C.; Focken, T.; Raabe, G. Synthesis of Iridium Complexes with Novel Planar Chiral Chelating Imidazolylidene Ligands. *Tetrahedron Asymmetry* **2003**, 14 (12), 1733–1746. [https://doi.org/10.1016/S0957-4166\(03\)00353-7](https://doi.org/10.1016/S0957-4166(03)00353-7).
- (63) Pye, P. J.; Rossen, K.; Reamer, R. A.; Tsou, N. N.; Volante, R. P.; Reider, P. J. A New Planar Chiral Bisphosphine Ligand for Asymmetric Catalysis: Highly Enantioselective Hydrogenations under Mild Conditions. *J. Am. Chem. Soc.* **1997**, 119 (26), 6207–6208. <https://doi.org/10.1021/ja970654g>.
- (64) Gon, M.; Morisaki, Y.; Sawada, R.; Chujo, Y. Synthesis of Optically Active, X-Shaped, Conjugated Compounds and Dendrimers Based on Planar Chiral [2.2]Paracyclophane, Leading to Highly Emissive Circularly Polarized Luminescence. *Chem. Eur. J.* **2016**, 22, 2291–2298. <https://doi.org/10.1002/chem.201504270>.
- (65) Weiland, K. J.; Brandl, T.; Atz, K.; Prescimone, A.; Häussinger, D.; Šolomek, T.; Mayor, M. Mechanical Stabilization of Helical Chirality in a Macrocyclic Oligothiophene. *J. Am. Chem. Soc.* **2019**, 141 (5), 2104–2110. <https://doi.org/10.1021/jacs.8b11797>.
- (66) Weiland, K. J.; Münch, N.; Gschwind, W.; Häussinger, D.; Mayor, M. A Chiral Macrocyclic Oligothiophene with Broken Conjugation – Rapid Racemization through Internal Rotation. *Helv. Chim. Acta* **2019**, 102 (1), e1800205. <https://doi.org/10.1002/hlca.201800205>.
- (67) He, J.; Yu, M.; Pang, M.; Fan, Y.; Lian, Z.; Wang, Y.; Wang, W.; Liu, Y.; Jiang, H. Nanosized Carbon Macrocycles Based on a Planar Chiral Pseudo Meta-[2.2]Paracyclophane. *Chem. – Eur. J.* **2022**, 28 (13), e202103832. <https://doi.org/10.1002/chem.202103832>.
- (68) Wu, Y.; Zhuang, G.; Cui, S.; Zhou, Y.; Wang, J.; Huang, Q.; Du, P. Through-Space π -Delocalization in a Conjugated Macrocyclic Consisting of [2.2]Paracyclophane. *Chem. Commun.* **2019**, 55 (97), 14617–14620. <https://doi.org/10.1039/C9CC06492C>.
- (69) Sidler, E.; Zwick, P.; Kress, C.; Reznikova, K.; Fuhr, O.; Fenske, D.; Mayor, M. Intense Molar Circular Dichroism in Fully Conjugated All-Carbon Macrocyclic 1,3-Butadiyne Linked Pseudo-Meta [2.2]Paracyclophanes. *Chem. Eur. J.* **2022**, 28, e2022017. <https://doi.org/10.1002/chem.202201764>.
- (70) Hasegawa, M.; Kobayakawa, K.; Matsuzawa, H.; Nishinaga, T.; Hirose, T.; Sako, K.; Mazaki, Y. Macrocyclic Oligothiophene with Stereogenic [2.2]Paracyclophane Scaffolds: Chiroptical Properties from π -Transannular Interactions. *Chem. – Eur. J.* **2017**, 23 (14), 3267–3271. <https://doi.org/10.1002/chem.201605842>.

- (71) Marrocchi, A.; Tomasi, I.; Vaccaro, L. Organic Small Molecules for Photonics and Electronics from the [2.2]Paracyclophane Scaffold. *Isr. J. Chem.* **2012**, *52* (1–2), 41–52. <https://doi.org/10.1002/ijch.201100091>.
- (72) Stefani, D.; Weiland, K. J.; Skripnik, M.; Hsu, C.; Perrin, M. L.; Mayor, M.; Pauly, F.; van der Zant, H. S. J. Large Conductance Variations in a Mechanosensitive Single-Molecule Junction. *Nano Lett.* **2018**, *18* (9), 5981–5988. <https://doi.org/10.1021/acs.nanolett.8b02810>.
- (73) Wielopolski, M.; Molina-Ontoria, A.; Schubert, C.; Margraf, J. T.; Krokos, E.; Kirschner, J.; Gouloumis, A.; Clark, T.; Guldi, D. M.; Martín, N. Blending Through-Space and Through-Bond π - π -Coupling in [2.2]-Paracyclophane-Oligophenylenevinylene Molecular Wires. *J. Am. Chem. Soc.* **2013**, *135* (28), 10372–10381. <https://doi.org/10.1021/ja401239r>.
- (74) Morisaki, Y.; Chujo, Y. Through-Space Conjugated Polymers Based on Cyclophanes. *Angew. Chem. Int. Ed.* **2006**, *45* (39), 6430–6437. <https://doi.org/10.1002/anie.200600752>.
- (75) Sharma, N.; Spuling, E.; Mattern, C. M.; Li, W.; Fuhr, O.; Tsuchiya, Y.; Adachi, C.; Bräse, S.; Samuel, I. D. W.; Zysman-Colman, E. Turn on of Sky-Blue Thermally Activated Delayed Fluorescence and Circularly Polarized Luminescence (CPL) via Increased Torsion by a Bulky Carbazolophane Donor. *Chem. Sci.* **2019**, *10* (27), 6689–6696. <https://doi.org/10.1039/C9SC01821B>.
- (76) Teng, J.-M.; Zhang, D.-W.; Chen, C.-F. Recent Progress in Circularly Polarized Luminescence of [2.2]Paracyclophane Derivatives. *ChemPhotoChem* **2022**, *6* (3), e202100228. <https://doi.org/10.1002/cptc.202100228>.
- (77) Spuling, E.; Sharma, N.; Samuel, I. D. W.; Zysman-Colman, E.; Bräse, S. (Deep) Blue through-Space Conjugated TADF Emitters Based on [2.2]Paracyclophanes. *Chem. Commun.* **2018**, *54* (67), 9278–9281. <https://doi.org/10.1039/C8CC04594A>.
- (78) Hassan, Z.; Spuling, E.; Knoll, D. M.; Lahann, J.; Bräse, S. Planar Chiral [2.2]Paracyclophanes: From Synthetic Curiosity to Applications in Asymmetric Synthesis and Materials. *Chem. Soc. Rev.* **2018**, *47* (18), 6947–6963. <https://doi.org/10.1039/C7CS00803A>.
- (79) Reich, H. J.; Cram, D. J. Transannular Directive Influences in Electrophilic Substitution of 2.2-Paracyclophane. *J. Am. Chem. Soc.* **1968**, *90* (5), 1365–1367. <https://doi.org/10.1021/ja01007a055>.
- (80) Cram, D. J.; Bauer, R. H.; Allinger, N. L.; Reeves, R. A.; Wechter, W. J.; Heilbronner, E. Macro Rings. XXI. Mono- and Polysubstituted [2.2]Paracyclophanes. *J. Am. Chem. Soc.* **1959**, *81* (22), 5977–5983. <https://doi.org/10.1021/ja01531a032>.
- (81) Hopf, H.; Mlynek, C. Cyclophanes. 32. Bridging of the [2.2]Paracyclophane Nucleus by a Phenanthrene Unit. *J. Org. Chem.* **1990**, *55* (4), 1361–1363. <https://doi.org/10.1021/jo00291a052>.
- (82) Staab, H. A.; Haffner, H. Orientierungseffekte auf Charge-Transfer-Wechselwirkungen, VIII. Diastereomere 4,7-Dimethoxy-12,15-dinitro[2.2]paracyclophane. *Chem. Ber.* **1977**, *110* (10), 3358–3365. <https://doi.org/10.1002/cber.19771101015>.
- (83) Vorontsova, N. V.; Rozenberg, V. I.; Sergeeva, E. V.; Vorontsov, E. V.; Starikova, Z. A.; Lyssenko, K. A.; Hopf, H. Symmetrically Tetrasubstituted [2.2]Paracyclophanes: Their Systematization and Regioselective Synthesis of Several Types of Bis-Bifunctional Derivatives by Double Electrophilic Substitution. *Chem. – Eur. J.* **2008**, *14* (15), 4600–4617. <https://doi.org/10.1002/chem.200701683>.
- (84) Dodziuk, H.; Szymański, S.; Jaźwiński, J.; Ostrowski, M.; Demissie, T. B.; Ruud, K.; Kuś, P.; Hopf, H.; Lin, S.-T. Structure and NMR Spectra of Some [2.2]Paracyclophanes. The Dilemma of [2.2]Paracyclophane Symmetry. *J. Phys. Chem. A* **2011**, *115* (38), 10638–10649. <https://doi.org/10.1021/jp205693a>.
- (85) Cahn, R. S.; Ingold, C.; Prelog, V. Specification of Molecular Chirality. *Angew. Chem. Int. Ed. Engl.* **1966**, *5* (4), 385–415. <https://doi.org/10.1002/anie.196603851>.
- (86) Felder, S.; Wu, S.; Brom, J.; Micouin, L.; Benedetti, E. Enantiopure Planar Chiral [2.2]Paracyclophanes: Synthesis and Applications in Asymmetric Organocatalysis. *Chirality* **2021**, *33* (9), 506–527. <https://doi.org/10.1002/chir.23335>.
- (87) Reich, H. J.; Cram, D. J. Macro Rings. XXXV. Transannular Directive Influences in Electrophilic Substitution of Monosubstituted [2.2]Paracyclophanes. *J. Am. Chem. Soc.* **1969**, *91* (13), 3505–3516. <https://doi.org/10.1021/ja01041a015>.

- (88) Reich, H. J.; Cram, D. J. Macro Rings. XXXVII. Multiple Electrophilic Substitution Reactions of [2.2]Paracyclophanes and Interconversions of Polysubstituted Derivatives. *J. Am. Chem. Soc.* **1969**, *91* (13), 3527–3533. <https://doi.org/10.1021/ja01041a017>.
- (89) Braddock, D. C.; MacGilp, I. D.; Perry, B. G. Improved Synthesis of (\pm)-4,12-Dihydroxy[2.2]Paracyclophane and Its Enantiomeric Resolution by Enzymatic Methods: Planar Chiral (*R*)- and (*S*)-Phanol. *J. Org. Chem.* **2002**, *67* (24), 8679–8681. <https://doi.org/10.1021/jo020451x>.
- (90) Bondarenko, L.; Dix, I.; Hinrichs, H.; Hopf, H. Cyclophanes. Part LII: Ethynyl[2.2]Paracyclophanes - New Building Blocks for Molecular Scaffolding. *Synthesis* **2004**, *2004* (16), 2751–2759. <https://doi.org/10.1055/s-2004-834872>.
- (91) Reich, H. J.; Cram, D. J. Macro Rings. XXXVI. Ring Expansion, Racemization, and Isomer Interconversions in the [2.2]Paracyclophane System through a Diradical Intermediate. *J. Am. Chem. Soc.* **1969**, *91* (13), 3517–3526. <https://doi.org/10.1021/ja01041a016>.
- (92) Tsuji, Y.; Hoffmann, R.; Movassagh, R.; Datta, S. Quantum Interference in Polyenes. *J. Chem. Phys.* **2014**, *141* (22), 224311. <https://doi.org/10.1063/1.4903043>.
- (93) Tsuji, Y.; Estrada, E.; Movassagh, R.; Hoffmann, R. Quantum Interference, Graphs, Walks, and Polynomials. *Chem. Rev.* **2018**, *118* (10), 4887–4911. <https://doi.org/10.1021/acs.chemrev.7b00733>.
- (94) Lambert, C. J. Basic Concepts of Quantum Interference and Electron Transport in Single-Molecule Electronics. *Chem. Soc. Rev.* **2015**, *44* (4), 875–888. <https://doi.org/10.1039/C4CS00203B>.
- (95) Taylor, G. I. Interference Fringes with Feeble Light. In *Proceedings of the Cambridge Philosophical Society*; 1909; Vol. 15, pp 114–115.
- (96) Su, T. A.; Neupane, M.; Steigerwald, M. L.; Venkataraman, L.; Nuckolls, C. Chemical Principles of Single-Molecule Electronics. *Nat. Rev. Mater.* **2016**, *1* (3), 16002. <https://doi.org/10.1038/natrevmats.2016.2>.
- (97) Gunasekaran, S.; Greenwald, J. E.; Venkataraman, L. Visualizing Quantum Interference in Molecular Junctions. *Nano Lett.* **2020**, *20* (4), 2843–2848. <https://doi.org/10.1021/acs.nanolett.0c00605>.
- (98) Yoshizawa, K.; Tada, T.; Staykov, A. Orbital Views of the Electron Transport in Molecular Devices. *J. Am. Chem. Soc.* **2008**, *130* (29), 9406–9413. <https://doi.org/10.1021/ja800638t>.
- (99) Yoshizawa, K. An Orbital Rule for Electron Transport in Molecules. *Acc. Chem. Res.* **2012**, *45* (9), 1612–1621. <https://doi.org/10.1021/ar300075f>.
- (100) Koga, J.; Tsuji, Y.; Yoshizawa, K. Orbital Control of Single-Molecule Conductance Perturbed by π -Accepting Anchor Groups: Cyanide and Isocyanide. *J. Phys. Chem. C* **2012**, *116* (38), 20607–20616. <https://doi.org/10.1021/jp3068156>.
- (101) Tsuji, Y.; Yoshizawa, K. Frontier Orbital Perspective for Quantum Interference in Alternant and Nonalternant Hydrocarbons. *J. Phys. Chem. C* **2017**, *121* (17), 9621–9626. <https://doi.org/10.1021/acs.jpcc.7b02274>.
- (102) Liu, X.; Sangtarash, S.; Reber, D.; Zhang, D.; Sadeghi, H.; Shi, J.; Xiao, Z.-Y.; Hong, W.; Lambert, C. J.; Liu, S.-X. Gating of Quantum Interference in Molecular Junctions by Heteroatom Substitution. *Angew. Chem. Int. Ed.* **2017**, *56* (1), 173–176. <https://doi.org/10.1002/anie.201609051>.
- (103) Jiang, F.; Trupp, D. I.; Algethami, N.; Zheng, H.; He, W.; Alqorashi, A.; Zhu, C.; Tang, C.; Li, R.; Liu, J.; Sadeghi, H.; Shi, J.; Davidson, R.; Korb, M.; Sobolev, A. N.; Naher, M.; Sangtarash, S.; Low, P. J.; Hong, W.; Lambert, C. J. Turning the Tap: Conformational Control of Quantum Interference to Modulate Single-Molecule Conductance. *Angew. Chem. Int. Ed.* **2019**, *58* (52), 18987–18993. <https://doi.org/10.1002/anie.201909461>.
- (104) Arroyo, C. R.; Tarkuc, S.; Frisenda, R.; Seldenthuis, J. S.; Woerde, C. H. M.; Eelkema, R.; Grozema, F. C.; van der Zant, H. S. J. Signatures of Quantum Interference Effects on Charge Transport Through a Single Benzene Ring. *Angew. Chem. Int. Ed.* **2013**, *52* (11), 3152–3155. <https://doi.org/10.1002/anie.201207667>.
- (105) Manrique, D. Z.; Huang, C.; Baghernejad, M.; Zhao, X.; Al-Owaedi, O. A.; Sadeghi, H.; Kaliginedi, V.; Hong, W.; Gulcur, M.; Wandlowski, T.; Bryce, M. R.; Lambert, C. J. A Quantum Circuit Rule for Interference Effects in Single-Molecule Electrical Junctions. *Nat. Commun.* **2015**, *6* (1), 6389. <https://doi.org/10.1038/ncomms7389>.

- (106) Mayor, M.; Weber, H. B.; Reichert, J.; Elbing, M.; Hänisch, C. von; Beckmann, D.; Fischer, M. Electric Current through a Molecular Rod—Relevance of the Position of the Anchor Groups. *Angew. Chem. Int. Ed.* **2003**, *42* (47), 5834–5838. <https://doi.org/10.1002/anie.200352179>.
- (107) Sautet, P.; Joachim, C. Electronic Interference Produced by a Benzene Embedded in a Polyacetylene Chain. *Chem. Phys. Lett.* **1988**, *153* (6), 511–516. [https://doi.org/10.1016/0009-2614\(88\)85252-7](https://doi.org/10.1016/0009-2614(88)85252-7).
- (108) Brandbyge, M.; Mozos, J.-L.; Ordejón, P.; Taylor, J.; Stokbro, K. Density-Functional Method for Nonequilibrium Electron Transport. *Phys. Rev. B* **2002**, *65* (16), 165401. <https://doi.org/10.1103/PhysRevB.65.165401>.
- (109) Stokbro, K. First-Principles Modeling of Electron Transport. *J. Phys. Condens. Matter* **2008**, *20* (6), 064216. <https://doi.org/10.1088/0953-8984/20/6/064216>.
- (110) Perdew, J. P.; Burke, K.; Ernzerhof, M. Generalized Gradient Approximation Made Simple. *Phys. Rev. Lett.* **1996**, *77* (18), 3865–3868. <https://doi.org/10.1103/PhysRevLett.77.3865>.
- (111) Bürkle, M.; Viljas, J. K.; Vonlanthen, D.; Mishchenko, A.; Schön, G.; Mayor, M.; Wandlowski, T.; Pauly, F. Conduction Mechanisms in Biphenyl Dithiol Single-Molecule Junctions. *Phys. Rev. B* **2012**, *85* (7), 075417. <https://doi.org/10.1103/PhysRevB.85.075417>.
- (112) Tada, T.; Yoshizawa, K. Molecular Design of Electron Transport with Orbital Rule: Toward Conductance-Decay Free Molecular Junctions. *Phys. Chem. Chem. Phys.* **2015**, *17* (48), 32099–32110. <https://doi.org/10.1039/C5CP05423K>.
- (113) Tsuji, Y.; Yoshizawa, K. Frontier Orbital Perspective for Quantum Interference in Alternant and Nonalternant Hydrocarbons. *J. Phys. Chem. C* **2017**, *121* (17), 9621–9626. <https://doi.org/10.1021/acs.jpcc.7b02274>.
- (114) Li, X.; Staykov, A.; Yoshizawa, K. Orbital Views on Electron-Transport Properties of Cyclophanes: Insight into Intermolecular Transport. *Bull. Chem. Soc. Jpn.* **2012**, *85* (2), 181–188. <https://doi.org/10.1246/bcsj.20110256>.
- (115) Hsu, C.; Schosser, W. M.; Zwick, P.; Dulić, D.; Mayor, M.; Pauly, F.; van der Zant, H. S. J. Mechanical Compression in Cofacial Porphyrin Cyclophane Pincers. *Chem. Sci.* **2022**, *13* (27), 8017–8024. <https://doi.org/10.1039/D2SC00937D>.
- (116) Schosser, W. M.; Hsu, C.; Zwick, P.; Beltako, K.; Dulić, D.; Mayor, M.; Zant, H. S. J. van der; Pauly, F. Mechanical Conductance Tunability of a Porphyrin–Cyclophane Single-Molecule Junction. *Nanoscale* **2022**, *14* (3), 984–992. <https://doi.org/10.1039/D1NR06484C>.
- (117) Reznikova, K.; Hsu, C.; Schosser, W. M.; Gallego, A.; Beltako, K.; Pauly, F.; van der Zant, H. S. J.; Mayor, M. Substitution Pattern Controlled Quantum Interference in [2.2]Paracyclophane-Based Single-Molecule Junctions. *J. Am. Chem. Soc.* **2021**, *143* (34), 13944–13951. <https://doi.org/10.1021/jacs.1c06966>.
- (118) Meyer-Eppler, G.; Vogelsang, E.; Benkhäuser, C.; Schneider, A.; Schnakenburg, G.; Lützen, A. Synthesis, Chiral Resolution, and Absolute Configuration of Dissymmetric 4,12-Difunctionalized [2.2]Paracyclophanes. *Eur. J. Org. Chem.* **2013**, *2013* (21), 4523–4532. <https://doi.org/10.1002/ejoc.201300412>.
- (119) Müller, S.; Liepold, B.; Roth, G. J.; Bestmann, H. J. An Improved One-Pot Procedure for the Synthesis of Alkynes from Aldehydes. *Synlett* **1996**, *1996* (06), 521–522. <https://doi.org/10.1055/s-1996-5474>.
- (120) Ohira, S. Methanolysis of Dimethyl (1-Diazo-2-Oxopropyl) Phosphonate: Generation of Dimethyl (Diazomethyl) Phosphonate and Reaction with Carbonyl Compounds. *Synth. Commun.* **1989**, *19* (3–4), 561–564. <https://doi.org/10.1080/00397918908050700>.
- (121) O'Driscoll, L. J.; Wang, X.; Jay, M.; Batsanov, A. S.; Sadeghi, H.; Lambert, C. J.; Robinson, B. J.; Bryce, M. R. Carbazole-Based Tetrapodal Anchor Groups for Gold Surfaces: Synthesis and Conductance Properties. *Angew. Chem.* **2020**, *132* (2), 892–899. <https://doi.org/10.1002/ange.201911652>.
- (122) Li, R.; Zhang, C.-C.; Wang, D.; Hu, Y.-F.; Li, Y.-L.; Xie, W. Reaction Pathway Change on Plasmonic Au Nanoparticles Studied by Surface-Enhanced Raman Spectroscopy. *Chin. Chem. Lett.* **2021**, *32* (9), 2846–2850. <https://doi.org/10.1016/j.ccl.2021.02.014>.

- (123) Søndergaard, R.; Krebs, F. C. The Challenge of Synthesizing Oligomers for Molecular Wires. *Polymers* **2011**, *3* (1), 545–557. <https://doi.org/10.3390/polym3010545>.
- (124) Kahrs, C.; Wickleder, M. S.; Christoffers, J. Biphenyl Sulfonic and Disulfonic Acids with Perfluorinated Alkyl Residues. *Eur. J. Org. Chem.* **2018**, *2018* (41), 5754–5762. <https://doi.org/10.1002/ejoc.201800882>.
- (125) Zeng, X.; Wang, C.; Batsanov, A. S.; Bryce, M. R.; Gigon, J.; Urasinska-Wojcik, B.; Ashwell, G. J. Synthesis and Properties of Functionalized Oligo(Arylene) Molecular Wires with Thiolated Termini: Competing Thiol-Au and Nitro-Au Assembly. *J. Org. Chem.* **2010**, *75* (1), 130–136. <https://doi.org/10.1021/jo902205p>.
- (126) Jevric, M.; Petersen, A. U.; Mansø, M.; Madsen, A. Ø.; Nielsen, M. B. Bismuth(III)-Promoted Acetylation of Thio-ethers into Thioacetates. *Eur. J. Org. Chem.* **2015**, No. 21, 4675–4688. <https://doi.org/10.1002/ejoc.201500420>.
- (127) Hopf, H.; Greiving, H.; Beck, C.; Dix, I.; Jones, P. G.; Desvergne, J.-P.; Bouas-Laurent, H. One-Pot Preparation of [n]Ladderanes by [2 π + 2 π] Photocycloaddition. *Eur. J. Org. Chem.* **2005**, *2005* (3), 567–581. <https://doi.org/10.1002/ejoc.200400596>.
- (128) Weiland, K. J. Molecular Loops – Mating Cyclophanes and Macrocycles. Thesis, University_of_Basel, 2018. <https://doi.org/10.5451/unibas-007140708>.
- (129) Miki, K.; Ohe, K. π -Conjugated Macrocycles Bearing Angle-Strained Alkynes. *Chem. – Eur. J.* **2020**, *26* (12), 2529–2575. <https://doi.org/10.1002/chem.201904114>.
- (130) Gholami, M.; Tykwinski, R. R. Oligomeric and Polymeric Systems with a Cross-Conjugated π -Framework. *Chem. Rev.* **2006**, *106* (12), 4997–5027. <https://doi.org/10.1021/cr0505573>.
- (131) Maraval, V.; Chauvin, R. From Macrocyclic Oligo-Acetylenes to Aromatic Ring Carbo-Mers. *Chem. Rev.* **2006**, *106* (12), 5317–5343. <https://doi.org/10.1021/cr050964e>.
- (132) Spitler, E. L.; Johnson, C. A.; Haley, M. M. Renaissance of Annulene Chemistry. *Chem. Rev.* **2006**, *106* (12), 5344–5386. <https://doi.org/10.1021/cr050541c>.
- (133) Hisaki, I.; Sonoda, M.; Tobe, Y. Strained Dehydrobenzoannulenes. *Eur. J. Org. Chem.* **2006**, *2006* (4), 833–847. <https://doi.org/10.1002/ejoc.200500705>.
- (134) Iyoda, M.; Yamakawa, J.; Rahman, M. J. Conjugated Macrocycles: Concepts and Applications. *Angew. Chem. Int. Ed.* **2011**, *50* (45), 10522–10553. <https://doi.org/10.1002/anie.201006198>.
- (135) Zhang, W.; Moore, J. S. Shape-Persistent Macrocycles: Structures and Synthetic Approaches from Arylene and Ethynylene Building Blocks. *Angew. Chem. Int. Ed.* **2006**, *45* (27), 4416–4439. <https://doi.org/10.1002/anie.200503988>.
- (136) Mayor, M.; Lehn, J.-M. Reducible Nanosize Macrocycles. *J. Am. Chem. Soc.* **1999**, *121* (48), 11231–11232. <https://doi.org/10.1021/ja992617q>.
- (137) Zhang, J.; Pesak, D. J.; Ludwick, J. L.; Moore, J. S. Geometrically-Controlled and Site-Specifically-Functionalized Phenylacetylene Macrocycles. *J. Am. Chem. Soc.* **1994**, *116* (10), 4227–4239. <https://doi.org/10.1021/ja00089a012>.
- (138) Toyota, S.; Suzuki, S.; Goichi, M. Chemistry of Anthracene–Acetylene Oligomers: Synthesis and Enantiomeric Resolution of a Chiral 1,8-Anthrylene–Ethynylene Cyclic Tetramer. *Chem. – Eur. J.* **2006**, *12* (9), 2482–2487. <https://doi.org/10.1002/chem.200501111>.
- (139) Höger, S.; Enkelmann, V. Synthese Und Struktur Eines Formtreuen Makrocyclischen Amphiphils. *Angew. Chem.* **1995**, *107* (23–24), 2917–2919. <https://doi.org/10.1002/ange.19951072331>.
- (140) Baxter, P. N. W. Cyclic Donor–Acceptor Circuits: Synthesis and Fluorescence Ion Sensory Properties of a Mixed-Heterocyclic Dehydroannulene-Type Cyclophane. *J. Org. Chem.* **2004**, *69* (6), 1813–1821. <https://doi.org/10.1021/jo0302410>.
- (141) Höger, S. Highly Efficient Methods for the Preparation of Shape-Persistent Macrocyclics. *J. Polym. Sci. Part Polym. Chem.* **1999**, *37* (15), 2685–2698. [https://doi.org/10.1002/\(SICI\)1099-0518\(19990801\)37:15<2685::AID-POLA1>3.0.CO;2-S](https://doi.org/10.1002/(SICI)1099-0518(19990801)37:15<2685::AID-POLA1>3.0.CO;2-S).

- (142) Kondratuk, D. V.; Perdigo, L. M. A.; O'Sullivan, M. C.; Svatek, S.; Smith, G.; O'Shea, J. N.; Beton, P. H.; Anderson, H. L. Two Vernier-Templated Routes to a 24-Porphyrin Nanoring. *Angew. Chem.* **2012**, *124* (27), 6800–6803. <https://doi.org/10.1002/ange.201202870>.
- (143) Cremers, J.; Haver, R.; Rickhaus, M.; Gong, J. Q.; Favereau, L.; Peeks, M. D.; Claridge, T. D. W.; Herz, L. M.; Anderson, H. L. Template-Directed Synthesis of a Conjugated Zinc Porphyrin Nanoball. *J. Am. Chem. Soc.* **2018**, *140* (16), 5352–5355. <https://doi.org/10.1021/jacs.8b02552>.
- (144) Krebs, A.; Wilke, J. Angle Strained Cycloalkynes. In *Wittig Chemistry*; Topics in Current Chemistry; Springer: Berlin, Heidelberg, 1983; pp 189–233. <https://doi.org/10.1007/BFb0018059>.
- (145) Agard, N. J.; Prescher, J. A.; Bertozzi, C. R. A Strain-Promoted [3 + 2] Azide–Alkyne Cycloaddition for Covalent Modification of Biomolecules in Living Systems. *J. Am. Chem. Soc.* **2004**, *126* (46), 15046–15047. <https://doi.org/10.1021/ja044996f>.
- (146) Agard, N. J.; Baskin, J. M.; Prescher, J. A.; Lo, A.; Bertozzi, C. R. A Comparative Study of Bioorthogonal Reactions with Azides. *ACS Chem. Biol.* **2006**, *1* (10), 644–648. <https://doi.org/10.1021/cb6003228>.
- (147) MacKenzie, D. A.; Sherratt, A. R.; Chigrinova, M.; Cheung, L. L.; Pezacki, J. P. Strain-Promoted Cycloadditions Involving Nitrones and Alkynes—Rapid Tunable Reactions for Bioorthogonal Labeling. *Curr. Opin. Chem. Biol.* **2014**, *21*, 81–88. <https://doi.org/10.1016/j.cbpa.2014.05.023>.
- (148) Siemsen, P.; Livingston, R. C.; Diederich, F. Acetylenkupplungen: eine leistungsfähige Methode für den Aufbau von Molekülen. *Angew. Chem.* **2000**, *112* (15), 2740–2767. [https://doi.org/10.1002/1521-3757\(20000804\)112:15<2740::AID-ANGE2740>3.0.CO;2-F](https://doi.org/10.1002/1521-3757(20000804)112:15<2740::AID-ANGE2740>3.0.CO;2-F).
- (149) Alonso, F.; Yus, M. Heterogeneous Catalytic Homocoupling of Terminal Alkynes. *ACS Catal.* **2012**, *2* (7), 1441–1451. <https://doi.org/10.1021/cs300195r>.
- (150) Fuhrmann, G.; Debaerdemaeker, T.; Baeuerle, P. C—C Bond Formation Through Oxidatively Induced Elimination of Platinum Complexes — A Novel Approach Towards Conjugated Macrocycles. *ChemInform* **2003**, *34* (31). <https://doi.org/10.1002/chin.200331189>.
- (151) Glaser, C. Beiträge Zur Kenntniss Des Acetylnylbenzols. *Berichte Dtsch. Chem. Ges.* **1869**, *2* (1), 422–424. <https://doi.org/10.1002/cber.186900201183>.
- (152) Eglinton, G.; Galbraith, A. R. *Chem. Ind.(London)*; 1956.
- (153) Hay, A. S. Oxidative Coupling of Acetylenes. II1. *J. Org. Chem.* **1962**, *27* (9), 3320–3321.
- (154) Li, J. J. Cadiot–Chodkiewicz Coupling. In *Name Reactions*; Springer, 2021; pp 67–69.
- (155) Sindhu, K. S.; Thankachan, A. P.; Sajitha, P. S.; Anilkumar, G. Recent Developments and Applications of the Cadiot–Chodkiewicz Reaction. *Org. Biomol. Chem.* **2015**, *13* (25), 6891–6905. <https://doi.org/10.1039/C5OB00697J>.
- (156) Fomina, L.; Vazquez, B.; Tkatchouk, E.; Fomine, S. The Glaser Reaction Mechanism. A DFT Study. *Tetrahedron* **2002**, *58* (33), 6741–6747. [https://doi.org/10.1016/S0040-4020\(02\)00669-5](https://doi.org/10.1016/S0040-4020(02)00669-5).
- (157) Vilhelmsen, M. H.; Jensen, J.; Tortzen, C. G.; Nielsen, M. B. The Glaser–Hay Reaction: Optimization and Scope Based on ¹³C NMR Kinetics Experiments. *Eur. J. Org. Chem.* **2013**, *2013* (4), 701–711. <https://doi.org/10.1002/ejoc.201201159>.
- (158) Qi, X.; Bai, R.; Zhu, L.; Jin, R.; Lei, A.; Lan, Y. Mechanism of Synergistic Cu(II)/Cu(I)-Mediated Alkyne Coupling: Dinuclear 1,2-Reductive Elimination after Minimum Energy Crossing Point. *J. Org. Chem.* **2016**, *81* (4), 1654–1660. <https://doi.org/10.1021/acs.joc.5b02797>.
- (159) Travis, C. R.; Mazur, L. E.; Peairs, E. M.; Gaunt, G. H.; Young, D. D. Mechanistic Investigation and Further Optimization of the Aqueous Glaser–Hay Bioconjugation. *Org. Biomol. Chem.* **2019**, *17* (13), 3396–3402. <https://doi.org/10.1039/C9OB00327D>.
- (160) Zhang, G.; Yi, H.; Zhang, G.; Deng, Y.; Bai, R.; Zhang, H.; Miller, J. T.; Kropf, A. J.; Bunel, E. E.; Lei, A. Direct Observation of Reduction of Cu(II) to Cu(I) by Terminal Alkynes. *J. Am. Chem. Soc.* **2014**, *136* (3), 924–926. <https://doi.org/10.1021/ja410756b>.

- (161) Sindhu, K. S.; Anilkumar, G. Recent Advances and Applications of Glaser Coupling Employing Greener Protocols. *RSC Adv* **2014**, *4* (53), 27867–27887. <https://doi.org/10.1039/C4RA02416H>.
- (162) Marsden, J. A.; Miller, J. J.; Haley, M. M. Let the Best Ring Win: Selective Macrocyclic Formation through Pd-Catalyzed or Cu-Mediated Alkyne Homocoupling. *Angew. Chem. Int. Ed.* **2004**, *43* (13), 1694–1697. <https://doi.org/10.1002/anie.200353043>.
- (163) Yamago, S.; Watanabe, Y.; Iwamoto, T. Synthesis of [8]Cycloparaphenylene from a Square-Shaped Tetranuclear Platinum Complex. *Angew. Chem. Int. Ed.* **2010**, *49* (4), 757–759. <https://doi.org/10.1002/anie.200905659>.
- (164) Majewski, M. A.; Stępień, M. Bowls, Hoops, and Saddles: Synthetic Approaches to Curved Aromatic Molecules. *Angew. Chem. Int. Ed.* **2019**, *58* (1), 86–116. <https://doi.org/10.1002/anie.201807004>.
- (165) Yahav, A.; Goldberg, I.; Vigalok, A. Iodine Oxidative Addition to Isomeric Platinum(II) Phosphine Complexes. *Organometallics* **2005**, *24* (23), 5654–5659. <https://doi.org/10.1021/om050507o>.
- (166) Yahav-Levi, A.; Goldberg, I.; Vigalok, A. Aryl-Halide versus Aryl–Aryl Reductive Elimination in Pt(IV)–Phosphine Complexes. *J. Am. Chem. Soc.* **2006**, *128* (27), 8710–8711. <https://doi.org/10.1021/ja062166r>.
- (167) Vigalok, A. Metal-Mediated Formation of Carbon–Halogen Bonds. *Chem. – Eur. J.* **2008**, *14* (17), 5102–5108. <https://doi.org/10.1002/chem.200701738>.
- (168) Krömer, J.; Rios-Carreras, I.; Fuhrmann, G.; Musch, C.; Wunderlin, M.; Debaerdemaeker, T.; Mena-Osteritz, E.; Bäuerle, P. Synthesis of the First Fully α -Conjugated Macrocyclic Oligothiophenes: Cyclo[n]Thiophenes with Tunable Cavities in the Nanometer Regime. *Angew. Chem. Int. Ed.* **2000**, *39* (19), 3481–3486. [https://doi.org/10.1002/1521-3773\(20001002\)39:19<3481::AID-ANIE3481>3.0.CO;2-O](https://doi.org/10.1002/1521-3773(20001002)39:19<3481::AID-ANIE3481>3.0.CO;2-O).
- (169) Fuhrmann, G. L. Synthesis and Characterization of Fully P-Conjugated Oligothiophene-Based Macrocycles. Dissertation, Universität Ulm, 2006. <https://doi.org/10.18725/OPARU-454>.
- (170) Iyoda, M.; Shimizu, H. Multifunctional π -Expanded Oligothiophene Macrocycles. *Chem. Soc. Rev.* **2015**, *44* (18), 6411–6424. <https://doi.org/10.1039/C5CS00388A>.
- (171) Mishra, A.; Ma, C.-Q.; Bäuerle, P. Functional Oligothiophenes: Molecular Design for Multidimensional Nanoarchitectures and Their Applications. *Chem. Rev.* **2009**, *109* (3), 1141–1276. <https://doi.org/10.1021/cr8004229>.
- (172) Corey, E. J.; Fuchs, P. L. A Synthetic Method for Formyl→ethynyl Conversion (RCHO→RC≡CH or RC≡CR'). *Tetrahedron Lett.* **1972**, *13* (36), 3769–3772. [https://doi.org/10.1016/S0040-4039\(01\)94157-7](https://doi.org/10.1016/S0040-4039(01)94157-7).
- (173) Bartholomew, G. P.; Bazan, G. C. Synthesis, Characterization, and Spectroscopy of 4,7,12,15-[2.2]Paracyclophane Containing Donor and Acceptor Groups: Impact of Substitution Patterns on Through-Space Charge Transfer. *J. Am. Chem. Soc.* **2002**, *124* (18), 5183–5196. <https://doi.org/10.1021/ja0121383>.
- (174) Biliz, F.; Cakici, M. Regioselective Synthesis of 4,7,12,15-Tetrasubstituted [2.2]Paracyclophanes: A Modular Route Involving Optical Resolution. *Eur. J. Org. Chem.* **2021**, *2021* (34), 4828–4834. <https://doi.org/10.1002/ejoc.202100762>.
- (175) Nishii, Y.; Ikeda, M.; Hayashi, Y.; Kawauchi, S.; Miura, M. Triptycenylium Sulfide: A Practical and Active Catalyst for Electrophilic Aromatic Halogenation Using N-Halosuccinimides. *J. Am. Chem. Soc.* **2020**, *142* (3), 1621–1629. <https://doi.org/10.1021/jacs.9b12672>.
- (176) König, B.; Knieriem, B.; Meijere, A. D. Double-Layered 1,4-Distyrylbenzene Chromophores—Synthesis, UV and Fluorescence Spectra. *Chem. Ber.* **1993**, *126* (7), 1643–1650. <https://doi.org/10.1002/cber.19931260723>.
- (177) Reich, H. J.; Cram, D. J. Macro Rings. XXXVII. Multiple Electrophilic Substitution Reactions of [2.2]Paracyclophanes and Interconversions of Polysubstituted Derivatives. 7.
- (178) Vaghi, L.; Cirilli, R.; Pierini, M.; Rizzo, S.; Terraneo, G.; Benincori, T. PHANE-TetraPHOS, the First D2 Symmetric Chiral Tetraphosphane. Synthesis, Metal Complexation, and Application in Homogeneous Stereoselective Hydrogenation. *Eur. J. Org. Chem.* **2021**, *2021* (17), 2367–2374. <https://doi.org/10.1002/ejoc.202100109>.

- (179) Dienes, Y.; Durben, S.; Kárpáti, T.; Neumann, T.; Englert, U.; Nyulászi, L.; Baumgartner, T. Selective Tuning of the Band Gap of π -Conjugated Dithieno[3,2-b:2',3'-d]Phospholes toward Different Emission Colors. *Chem. – Eur. J.* **2007**, *13* (26), 7487–7500. <https://doi.org/10.1002/chem.200700399>.
- (180) Haid, S.; Marszalek, M.; Mishra, A.; Wielopolski, M.; Teuscher, J.; Moser, J.-E.; Humphry-Baker, R.; Zakeeruddin, S. M.; Grätzel, M.; Bäuerle, P. Significant Improvement of Dye-Sensitized Solar Cell Performance by Small Structural Modification in π -Conjugated Donor–Acceptor Dyes. *Adv. Funct. Mater.* **2012**, *22* (6), 1291–1302. <https://doi.org/10.1002/adfm.201102519>.
- (181) Casoni, G.; Myers, E. L.; Aggarwal, V. K. Synthesis of 3-Aryl-1-Aminopropane Derivatives: Lithiation–Boryl-ation–Ring-Opening of Azetidinium Ions. *Synthesis* **2016**, *48* (19), 3241–3253. <https://doi.org/10.1055/s-0035-1562447>.
- (182) Hitosugi, S.; Tanimoto, D.; Nakanishi, W.; Isobe, H. A Facile Chromatographic Method for Purification of Pinacol Boronic Esters. *Chem. Lett.* **2012**, *41* (9), 972–973. <https://doi.org/10.1246/cl.2012.972>.
- (183) Zotti, G.; Zecchin, S.; Vercelli, B.; Pasini, M.; Destri, S.; Bertini, F.; Berlin, A. Electrochemical, Magnetic, and Electrical Properties of α,ω -Capped Sexithiophene Films. 2. Conduction in Sexithiophenes with α,ω -Aryl-Extended Conjugation. *Chem. Mater.* **2006**, *18* (13), 3151–3161. <https://doi.org/10.1021/cm060671h>.
- (184) Porzio, W.; Destri, S.; Pasini, M.; Giovanella, U.; Ragazzi, M.; Scavia, G.; Kotowski, D.; Zotti, G.; Vercelli, B. Synthesis and Characterisation of Fluorenone–Thiophene-Based Donor–Acceptor Oligomers: Role of Moiety Sequence upon Packing and Electronic Properties. *New J. Chem.* **2010**, *34* (9), 1961–1973. <https://doi.org/10.1039/C0NJ00045K>.
- (185) Scott, L. T.; Cooney, M. J.; Otte, C.; Puls, C.; Haumann, T.; Boese, R.; Smith, A. B.; Carroll, P. J.; de Meijere, A. Enhancement of Through-Space and Through-Bond. π -Orbital Interactions. Syntheses and Properties of Permethylated and Perspirocyclopropanated Cyclotetradeca-1,3,6,9,12-Pentayne. *J. Am. Chem. Soc.* **1994**, *116* (22), 10275–10283. <https://doi.org/10.1021/ja00101a051>.
- (186) de Meijere, A.; Kozhushkov, S.; Haumann, T.; Boese, R.; Puls, C.; Cooney, M. J.; Scott, L. T. Completely Spirocyclopropanated Macrocyclic Oligodiacylenes: The Family of “Exploding” [n]Rotanes. *Chem. – Eur. J.* **1995**, *1* (2), 124–131. <https://doi.org/10.1002/chem.19950010206>.
- (187) Bannwart, L. M.; Jundt, L.; Müntener, T.; Neuburger, M.; Häussinger, D.; Mayor, M. A Phenyl-Ethynyl-Macrocyclic Model Compound for “Geländer” Oligomers Comprising Reactive Conjugated Banisters. *Eur. J. Org. Chem.* **2018**, *2018* (26), 3391–3402. <https://doi.org/10.1002/ejoc.201800586>.
- (188) Bannwart, L. M.; Müntener, T.; Rickhaus, M.; Jundt, L.; Häussinger, D.; Mayor, M. Bicyclic Phenyl–Ethynyl Architectures: Synthesis of a 1,4-Bis(Phenylbuta-1,3-Diyn-1-Yl) Benzene Banister. *Chem. – Eur. J.* **2021**, *27* (20), 6295–6307. <https://doi.org/10.1002/chem.202005207>.
- (189) D’Addio, A.; Malinčik, J.; Fuhr, O.; Fenske, D.; Häussinger, D.; Mayor, M. Geländer Molecules with Orthogonal Joints: Synthesis of Macrocyclic Dimers. *Chem. – Eur. J.* **2022**, *28*, e2022016. <https://doi.org/10.1002/chem.202201678>.
- (190) Dix, I.; Bondarenko, L.; Jones, P. G.; Oeser, T.; Hopf, H. Building Complex Carbon Skeletons with Ethynyl[2.2]Paracyclophanes. *Beilstein J. Org. Chem.* **2014**, *10*, 2013–2020. <https://doi.org/10.3762/bjoc.10.209>.
- (191) Liu, Q.; Burton, D. J. A Facile Synthesis of Diynes. *Tetrahedron Lett.* **1997**, *38* (25), 4371–4374. [https://doi.org/10.1016/S0040-4039\(97\)00969-6](https://doi.org/10.1016/S0040-4039(97)00969-6).
- (192) Yamamoto, T.; Wakabayashi, S.; Osakada, K. Mechanism of C–C Coupling Reactions of Aromatic Halides, Promoted by Ni(COD)₂ in the Presence of 2,2'-Bipyridine and PPh₃, to Give Biaryls. *J. Organomet. Chem.* **1992**, *428* (1), 223–237. [https://doi.org/10.1016/0022-328X\(92\)83232-7](https://doi.org/10.1016/0022-328X(92)83232-7).
- (193) Grave, C.; Schlüter, A. D. Shape-Persistent, Nano-Sized Macrocycles. *Eur. J. Org. Chem.* **2002**, *2002* (18), 3075–3098. [https://doi.org/10.1002/1099-0690\(200209\)2002:18<3075::AID-EJOC3075>3.0.CO;2-3](https://doi.org/10.1002/1099-0690(200209)2002:18<3075::AID-EJOC3075>3.0.CO;2-3).
- (194) Kawase, T.; Kurata, H. Ball-, Bowl-, and Belt-Shaped Conjugated Systems and Their Complexing Abilities: Exploration of the Concave–Convex π – π Interaction. *Chem. Rev.* **2006**, *106* (12), 5250–5273. <https://doi.org/10.1021/cr0509657>.

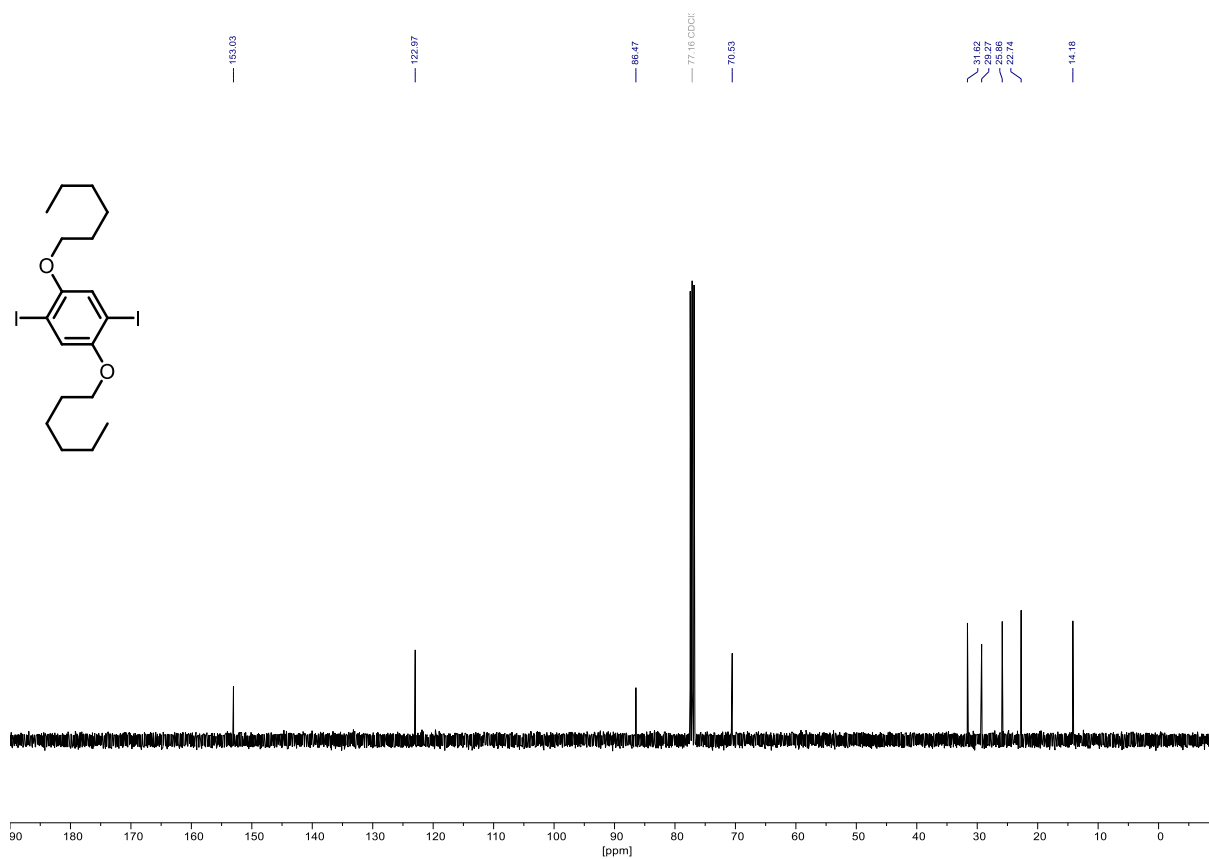
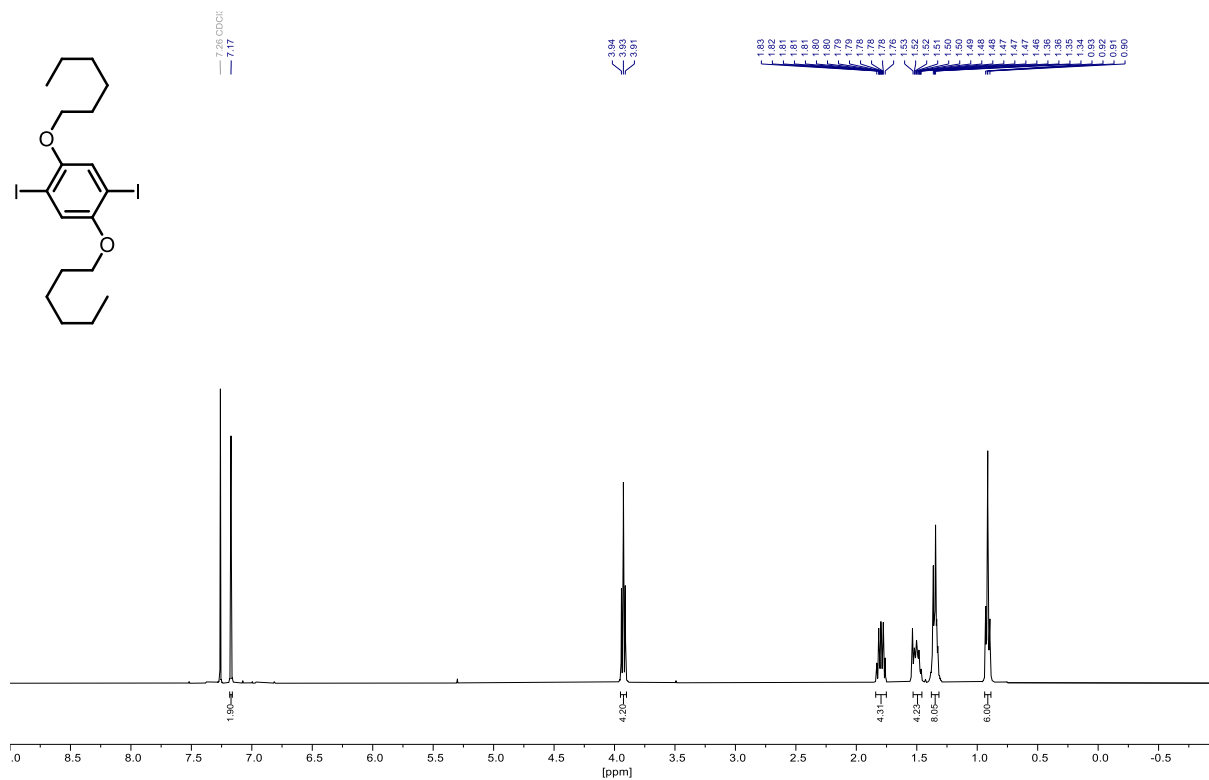
- (195) Jasti, R.; Bhattacharjee, J.; Neaton, J. B.; Bertozzi, C. R. Synthesis, Characterization, and Theory of [9]-, [12]-, and [18]Cycloparaphenylene: Carbon Nano hoop Structures. *J. Am. Chem. Soc.* **2008**, *130* (52), 17646–17647. <https://doi.org/10.1021/ja807126u>.
- (196) Wassy, D.; Pfeifer, M.; Esser, B. Synthesis and Properties of Conjugated Nano hoops Incorporating Dibenzo[a,e]Pentalenes: [2]DBP[12]CPPs. *J. Org. Chem.* **2020**, *85* (1), 34–43. <https://doi.org/10.1021/acs.joc.9b01195>.
- (197) Zhang, F.; Bäuerle, P. A Controlled Approach to Well-Defined Oligothiophenes via Oxidatively Induced Reductive Elimination of Stable Pt(II) Oligothiophenyl Complexes. *J. Am. Chem. Soc.* **2007**, *129* (11), 3090–3091. <https://doi.org/10.1021/ja070083k>.
- (198) Zhang, Z.; Cha, W.-Y.; Williams, N. J.; Rush, E. L.; Ishida, M.; Lynch, V. M.; Kim, D.; Sessler, J. L. Cyclo[6]Pyridine[6]Pyrrole: A Dynamic, Twisted Macrocyclic with No Meso Bridges. *J. Am. Chem. Soc.* **2014**, *136* (21), 7591–7594. <https://doi.org/10.1021/ja503451m>.
- (199) Ito, H.; Mitamura, Y.; Segawa, Y.; Itami, K. Thiophene-Based, Radial π -Conjugation: Synthesis, Structure, and Photophysical Properties of Cyclo-1,4-Phenylene-2',5'-Thienylenes. *Angew. Chem.* **2015**, *127* (1), 161–165. <https://doi.org/10.1002/ange.201409389>.
- (200) Morisaki, Y.; Inoshita, K.; Chujo, Y. Planar-Chiral Through-Space Conjugated Oligomers: Synthesis and Characterization of Chiroptical Properties. *Chem. – Eur. J.* **2014**, *20* (27), 8386–8390. <https://doi.org/10.1002/chem.201402930>.
- (201) Morisaki, Y.; Hifumi, R.; Lin, L.; Inoshita, K.; Chujo, Y. Through-Space Conjugated Polymers Consisting of Planar Chiral Pseudo-Ortho-Linked [2.2]Paracyclophane. *Polym. Chem.* **2012**, *3* (10), 2727–2730. <https://doi.org/10.1039/C2PY20530K>.
- (202) Gon, M.; Morisaki, Y.; Chujo, Y. Optically Active Cyclic Compounds Based on Planar Chiral [2.2]Paracyclophane: Extension of the Conjugated Systems and Chiroptical Properties. *J. Mater. Chem. C* **2014**, *3* (3), 521–529. <https://doi.org/10.1039/C4TC02339K>.
- (203) Gon, M.; Kozuka, H.; Morisaki, Y.; Chujo, Y. Optically Active Cyclic Compounds Based on Planar Chiral [2.2]Paracyclophane with Naphthalene Units. *Asian J. Org. Chem.* **2016**, *5* (3), 353–359. <https://doi.org/10.1002/ajoc.201500468>.
- (204) Gon, M.; Morisaki, Y.; Chujo, Y. Highly Emissive Optically Active Conjugated Dimers Consisting of a Planar Chiral [2.2]Paracyclophane Showing Circularly Polarized Luminescence. *Eur. J. Org. Chem.* **2015**, *2015* (35), 7756–7762. <https://doi.org/10.1002/ejoc.201501181>.
- (205) Riehl, J. P.; Richardson, F. S. Circularly Polarized Luminescence Spectroscopy. *Chem. Rev.* **1986**, *86* (1), 1–16. <https://doi.org/10.1021/cr00071a001>.
- (206) Chen, Y. Circularly Polarized Luminescence Based on Small Organic Fluorophores. *Mater. Today Chem.* **2022**, *23*, 100651. <https://doi.org/10.1016/j.mtchem.2021.100651>.
- (207) Morisaki, Y.; Sawada, R.; Gon, M.; Chujo, Y. New Types of Planar Chiral [2.2]Paracyclophanes and Construction of One-Handed Double Helices. *Chem. – Asian J.* **2016**, *11* (18), 2524–2527. <https://doi.org/10.1002/asia.201601028>.
- (208) Tsuchiya, M.; Maeda, H.; Inoue, R.; Morisaki, Y. Construction of Helical Structures with Planar Chiral [2.2]Paracyclophane: Fusing Helical and Planar Chiralities. *Chem. Commun.* **2021**, *57* (73), 9256–9259. <https://doi.org/10.1039/D1CC03320D>.
- (209) Hasegawa, M.; Ishida, Y.; Sasaki, H.; Ishioka, S.; Usui, K.; Hara, N.; Kitahara, M.; Imai, Y.; Mazaki, Y. Helical Oligophenylene Linked with [2.2]Paracyclophane: Stereogenic π -Conjugated Dye for Highly Emissive Chiroptical Properties. *Chem. – Eur. J.* **2021**, *27* (65), 16225–16231. <https://doi.org/10.1002/chem.202103158>.
- (210) Tanaka, K.; Inoue, R.; Morisaki, Y. Optically Active Cyclic Oligomers Based on Planar Chiral [2.2]Paracyclophane. *Chem. – Asian J.* **2022**, *17* (2), e202101267. <https://doi.org/10.1002/asia.202101267>.
- (211) Zhang, G.; Yi, H.; Chen, H.; Bian, C.; Liu, C.; Lei, A. Trisulfur Radical Anion as the Key Intermediate for the Synthesis of Thiophene via the Interaction between Elemental Sulfur and NaO *t* Bu. *Org. Lett.* **2014**, *16* (23), 6156–6159. <https://doi.org/10.1021/ol503015b>.

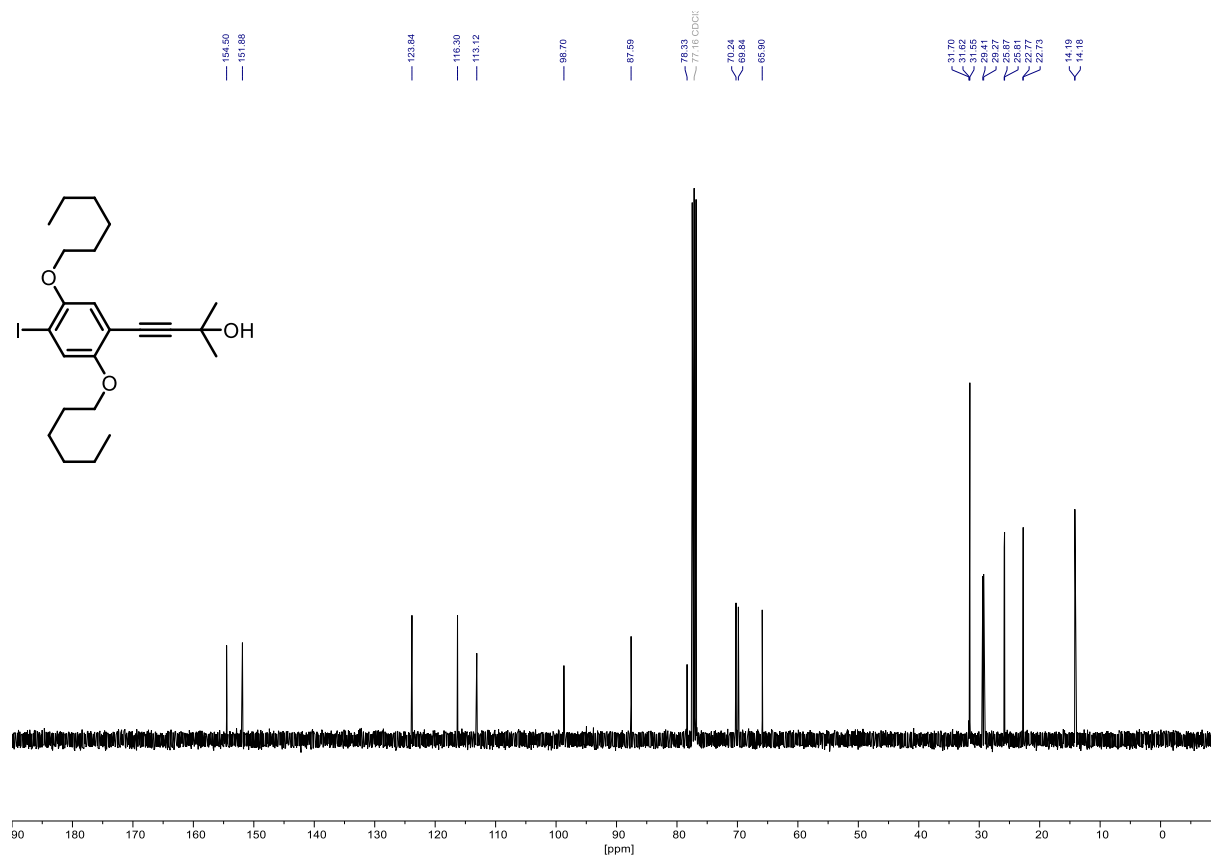
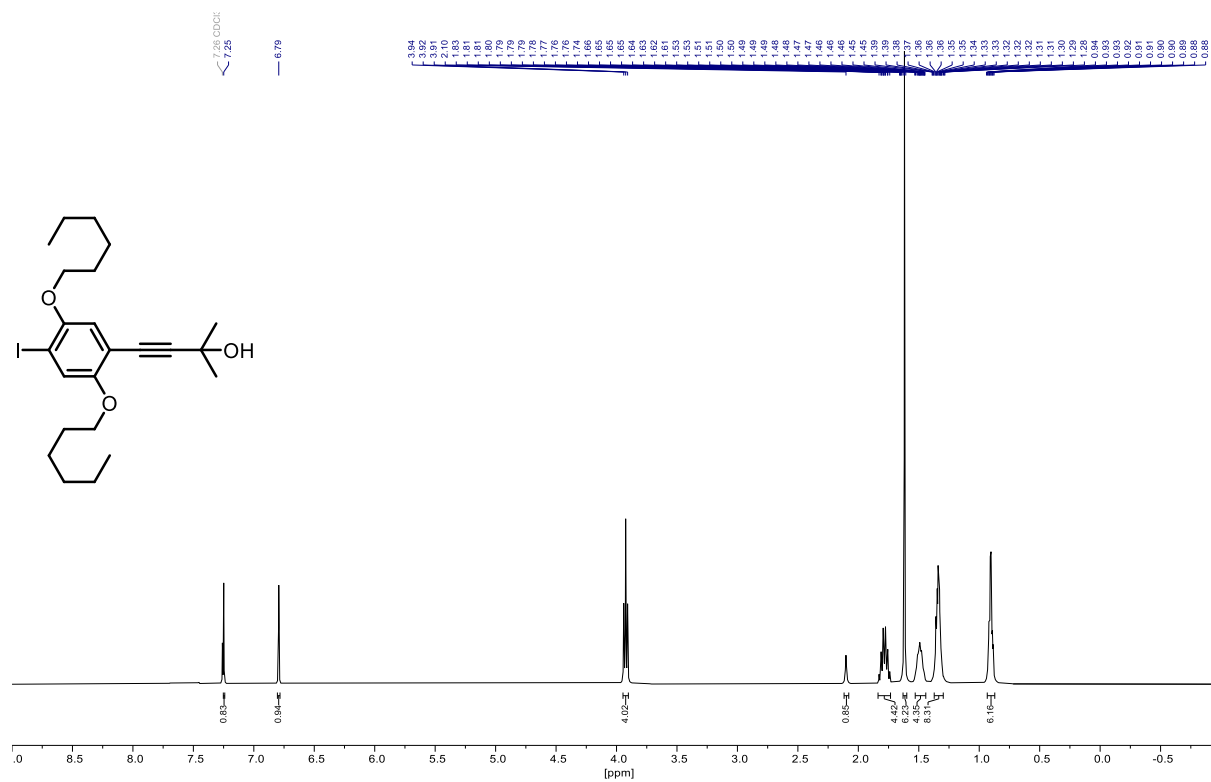
- (212) Feng, L.; Hu, T.; Zhang, S.; Xiong, H.-Y.; Zhang, G. Copper-Mediated Deacylative Coupling of Ynones via C–C Bond Activation under Mild Conditions. *Org. Lett.* **2019**, *21* (23), 9487–9492. <https://doi.org/10.1021/acs.orglett.9b03684>.
- (213) Krömer, J.; Bäuerle, P. Homologous Series of Regioregular Alkylsubstituted Oligothiophenes up to an 11-Mer. *Tetrahedron* **2001**, *57* (17), 3785–3794. [https://doi.org/10.1016/S0040-4020\(01\)00254-X](https://doi.org/10.1016/S0040-4020(01)00254-X).
- (214) Jiang, H.; Zeng, W.; Li, Y.; Wu, W.; Huang, L.; Fu, W. Copper(I)-Catalyzed Synthesis of 2,5-Disubstituted Furans and Thiophenes from Haloalkynes or 1,3-Diynes. *J. Org. Chem.* **2012**, *77* (11), 5179–5183. <https://doi.org/10.1021/jo300692d>.
- (215) Rao, M. L. N.; Islam, S. S.; Dasgupta, P. Rapid Access to Unsymmetrical 1,3-Diynes and 2,5-Disubstituted Thiophenes under Ligand and Pd/Ni-Free Cu-Catalysis. *RSC Adv.* **2015**, *5* (95), 78090–78098. <https://doi.org/10.1039/C5RA15705F>.
- (216) Nakayama, J.; Konishi, T.; Murabayashi, S.; Hoshino, M. Preparation of A-Quater-, a-Sexi-, and a-Octithiophenes. *HETEROCYCLES* **1987**, *26* (7), 1793. <https://doi.org/10.3987/R-1987-07-1793>.
- (217) Zhang, F.; Götz, G.; Winkler, H. D. F.; Schalley, C. A.; Bäuerle, P. Giant Cyclo[n]Thiophenes with Extended π Conjugation. *Angew. Chem. Int. Ed.* **2009**, *48* (36), 6632–6635. <https://doi.org/10.1002/anie.200900101>.
- (218) Reichardt, C. Solvatochromic Dyes as Solvent Polarity Indicators. *Chem. Rev.* **1994**, *94* (8), 2319–2358. <https://doi.org/10.1021/cr00032a005>.
- (219) Duncan, K. D.; Fang, R.; Yuan, J.; Chu, R. K.; Dey, S. K.; Burnum-Johnson, K. E.; Lanekoff, I. Quantitative Mass Spectrometry Imaging of Prostaglandins as Silver Ion Adducts with Nanospray Desorption Electrospray Ionization. *Anal. Chem.* **2018**, *90* (12), 7246–7252. <https://doi.org/10.1021/acs.analchem.8b00350>.
- (220) Munakata, M.; Wu, L. P.; Sugimoto, K.; Kuroda-Sowa, T.; Maekawa, M.; Suenaga, Y.; Maeno, N.; Fujita, M. Silver(I) Complex Assemblies with Nonplanar Aromatic Compounds. *Inorg. Chem.* **1999**, *38* (25), 5674–5680. <https://doi.org/10.1021/ic990391m>.
- (221) Ko, S.-B.; Cho, A.-N.; Kim, M.-J.; Lee, C.-R.; Park, N.-G. Alkyloxy Substituted Organic Dyes for High Voltage Dye-Sensitized Solar Cell: Effect of Alkyloxy Chain Length on Open-Circuit Voltage. *Dyes Pigments* **2012**, *94* (1), 88–98. <https://doi.org/10.1016/j.dyepig.2011.10.014>.
- (222) Swager, T. M.; Gil, C. J.; Wrighton, M. S. Fluorescence Studies of Poly(p-Phenyleneethynylene)s: The Effect of Anthracene Substitution. *J. Phys. Chem.* **1995**, *99* (14), 4886–4893. <https://doi.org/10.1021/j100014a003>.
- (223) Jevric, M.; Petersen, A. U.; Mansø, M.; Madsen, A. Ø.; Nielsen, M. B. Bismuth(III)-Promoted Acetylation of Thio-ethers into Thioacetates: Bismuth(III)-Promoted Acetylation of Thioethers into Thioacetates. *Eur. J. Org. Chem.* **2015**, *2015* (21), 4675–4688. <https://doi.org/10.1002/ejoc.201500420>.
- (224) Stefani, D.; Weiland, K. J.; Skripnik, M.; Hsu, C.; Perrin, M. L.; Mayor, M.; Pauly, F.; van der Zant, H. S. J. Large Conductance Variations in a Mechanosensitive Single-Molecule Junction. *Nano Lett.* **2018**, *18* (9), 5981–5988. <https://doi.org/10.1021/acs.nanolett.8b02810>.
- (225) Cuevas, J. C.; Scheer, E. *Molecular Electronics: An Introduction to Theory and Experiment*, 2nd ed.; World Scientific series in nanoscience and nanotechnology, v. 15.; World Scientific: Singapore, **2017**.
- (226) Pauly, F.; Viljas, J. K.; Huniar, U.; Häfner, M.; Wohlthat, S.; Bürkle, M.; Cuevas, J. C.; Schön, G. Cluster-Based Density-Functional Approach to Quantum Transport through Molecular and Atomic Contacts. *New J. Phys.* **2008**, *10* (12), 125019. <https://doi.org/10.1088/1367-2630/10/12/125019>.
- (227) Ahlrichs, R.; Bär, M.; Häser, M.; Horn, H.; Kölmel, C. Electronic Structure Calculations on Workstation Computers: The Program System Turbomole. *Chem. Phys. Lett.* **1989**, *162* (3), 165–169. [https://doi.org/10.1016/0009-2614\(89\)85118-8](https://doi.org/10.1016/0009-2614(89)85118-8).
- (228) Schäfer, A.; Horn, H.; Ahlrichs, R. Fully Optimized Contracted Gaussian Basis Sets for Atoms Li to Kr. *J. Chem. Phys.* **1992**, *97* (4), 2571–2577. <https://doi.org/10.1063/1.463096>.
- (229) Perdew, J. P.; Burke, K.; Ernzerhof, M. Generalized Gradient Approximation Made Simple. *Phys. Rev. Lett.* **1996**, *77* (18), 3865–3868. <https://doi.org/10.1103/PhysRevLett.77.3865>.

- (230) Bürkle, M.; Viljas, J. K.; Vonlanthen, D.; Mishchenko, A.; Schön, G.; Mayor, M.; Wandlowski, T.; Pauly, F. Conduction Mechanisms in Biphenyl Dithiol Single-Molecule Junctions. *Phys. Rev. B* **2012**, *85* (7), 075417. <https://doi.org/10.1103/PhysRevB.85.075417>.
- (231) Nozaki, D.; Lucke, A.; Schmidt, W. G. Molecular Orbital Rule for Quantum Interference in Weakly Coupled Dimers: Low-Energy Giant Conductivity Switching Induced by Orbital Level Crossing. *J Phys Chem Lett* **2017**, No. 8 (4), 727–732. <https://doi.org/10.1021/acs.jpcclett.6b02989>.
- (232) Vidal, P.-L.; Divisia-Blohorn, B.; Bidan, G.; Hazemann, J.-L.; Kern, J.-M.; Sauvage, J.-P. π -Conjugated Ligand Polymers Entwined around Copper Centres. *Chem. – Eur. J.* **2000**, *6* (9), 1663–1673. [https://doi.org/10.1002/\(SICI\)1521-3765\(20000502\)6:9<1663::AID-CHEM1663>3.0.CO;2-Q](https://doi.org/10.1002/(SICI)1521-3765(20000502)6:9<1663::AID-CHEM1663>3.0.CO;2-Q).

8 Appendix

^1H and $^{13}\text{C}\{^1\text{H}\}$ NMR (400/101 MHz, CDCl_3) spectra of 1,4-bis(hexyloxy)-2,5-diiodobenzene (16):

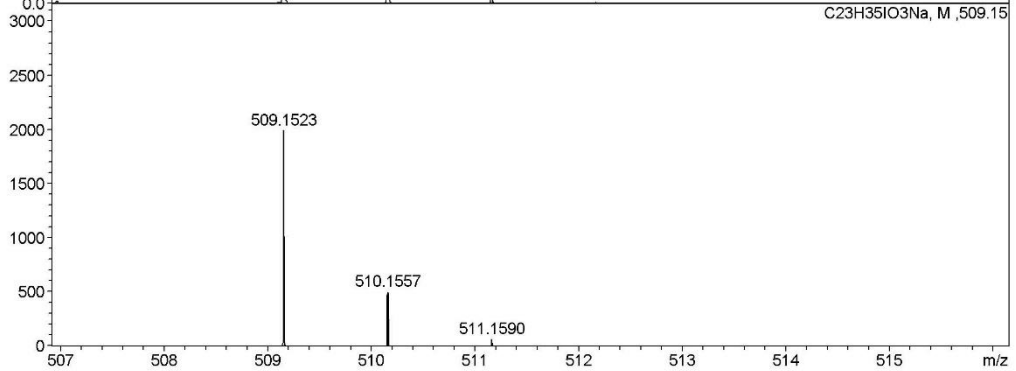
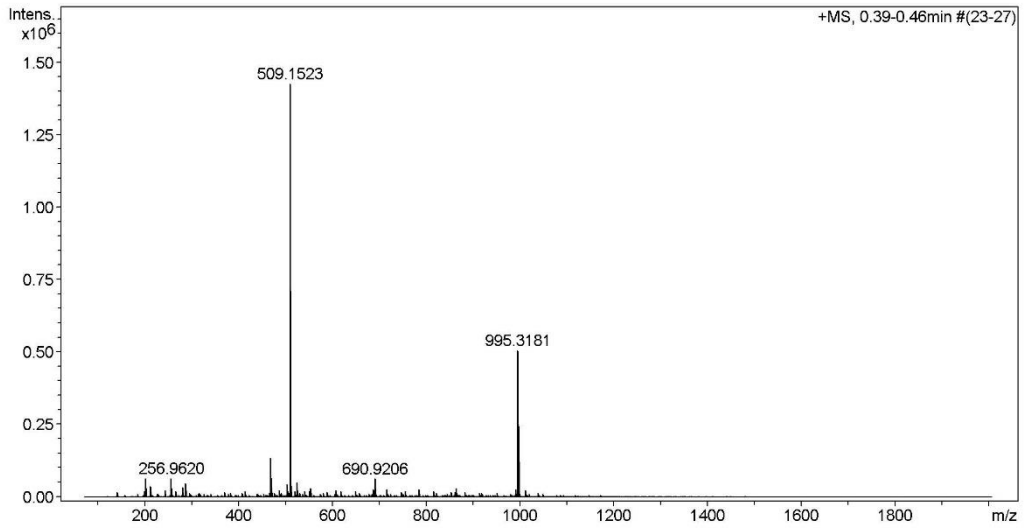


^1H , $^{13}\text{C}\{^1\text{H}\}$ (400/101 MHz, CDCl_3) NMR and HR-ESI-MS Spectra of 4-(2,5-bis(hexyloxy)-4-iodophenyl)-2-methylbut-3-yn-2-ol (10):

High Resolution Mass Spectrometry Report

Sample Name **KR-242**
Comment

Instrument **maXis 4G**
Method **ms_nocolumn_mid_pos.m**



 High Resolution Mass Spectrometry Report

Measured m/z vs. theoretical m/z

| Meas. m/z | # | Formula | Score | m/z | err [mDa] | err [ppm] | mSigma | rdb | e ⁻ Conf | z |
|-----------|---|------------------------------------------------------------------|--------|-----------|-----------|-----------|--------|------|---------------------|----|
| 504.1959 | 1 | C ₂₃ H ₃₉ I N O ₃ | 100.00 | 504.1969 | 1.0 | 1.9 | 4.7 | 4.5 | even | 1+ |
| 509.1523 | 1 | C ₂₃ H ₃₅ I Na O ₃ | 100.00 | 509.1523 | -0.0 | -0.1 | 21.1 | 5.5 | even | |
| 990.3614 | 1 | C ₄₆ H ₇₄ I ₂ N O ₆ | 100.00 | 990.3600 | -1.4 | -1.4 | 18.8 | 9.5 | even | |
| 995.3181 | 1 | C ₄₆ H ₇₀ I ₂ Na O ₆ | 100.00 | 995.3154 | -2.7 | -2.7 | 13.0 | 10.5 | even | |
| 1011.2908 | 1 | C ₄₆ H ₇₀ I ₂ K O ₆ | 100.00 | 1011.2893 | -1.4 | -1.4 | 26.3 | 10.5 | even | |

Mass list

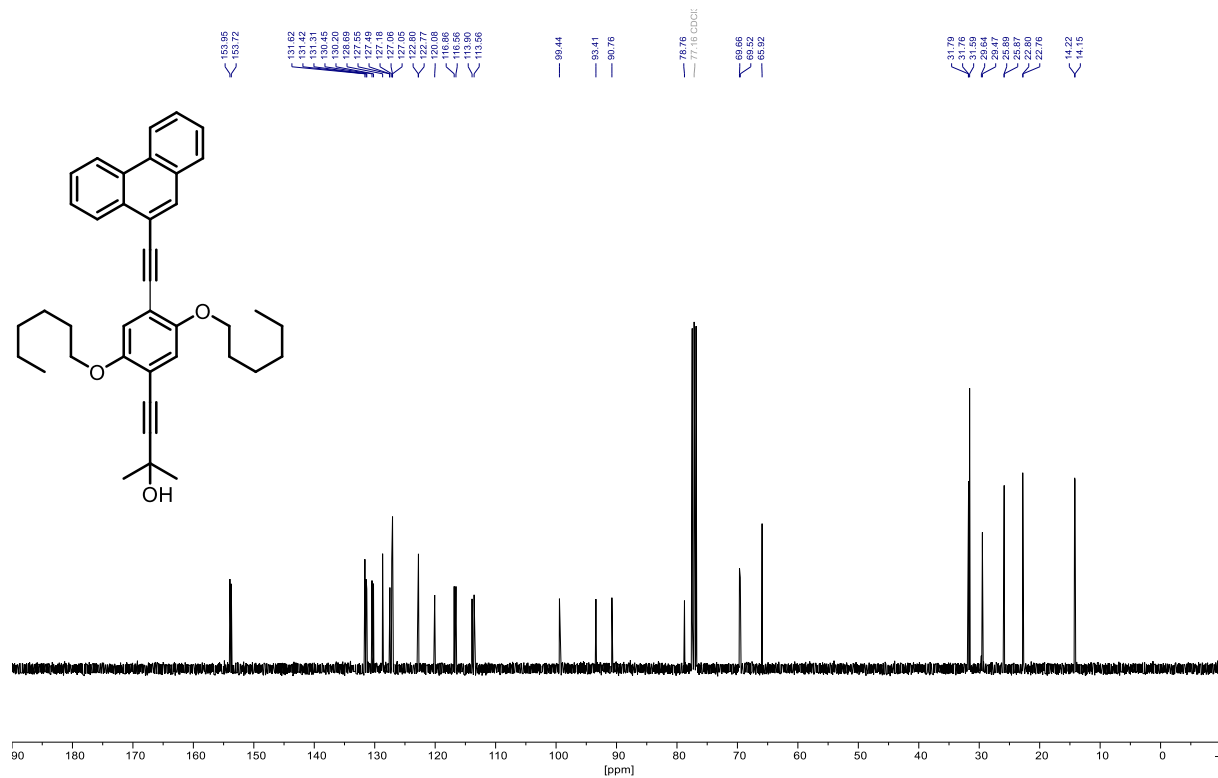
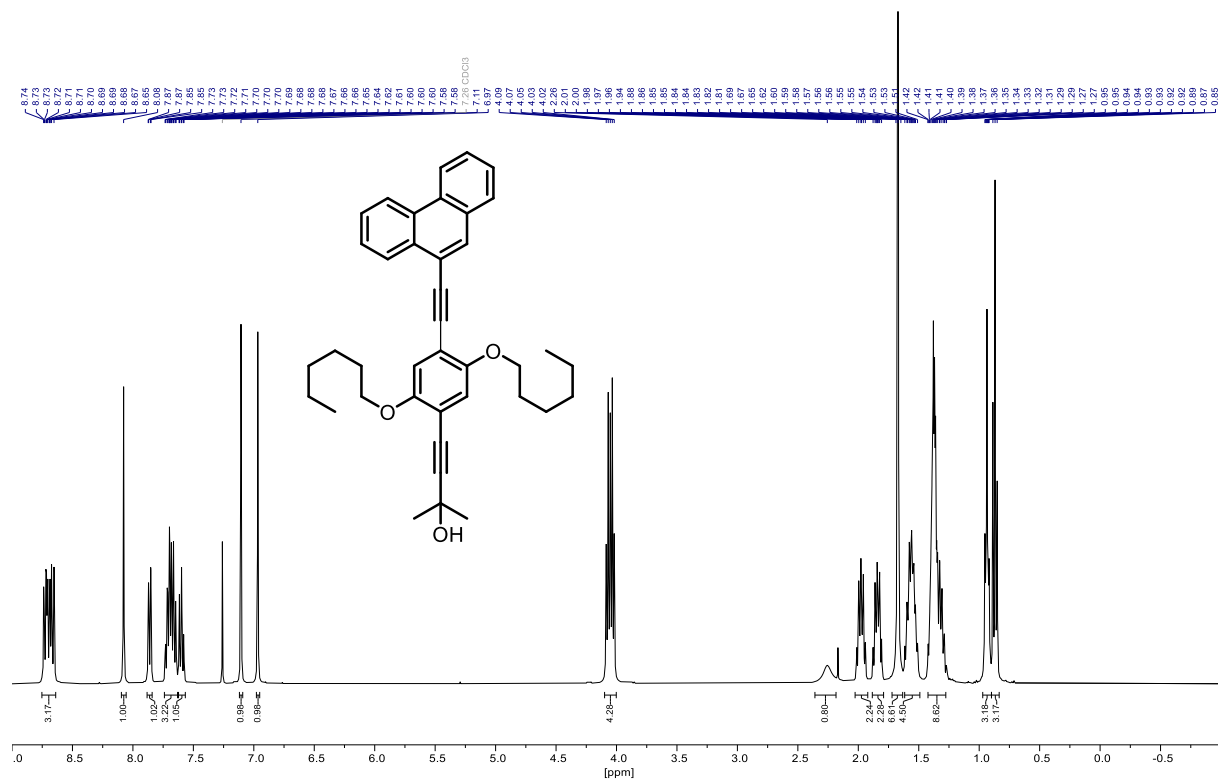
| # | m/z | I % | I |
|----|----------|-------|---------|
| 1 | 141.0019 | 1.2 | 16611 |
| 2 | 185.1146 | 0.6 | 9148 |
| 3 | 198.9565 | 0.7 | 10373 |
| 4 | 198.9927 | 1.3 | 18648 |
| 5 | 201.1096 | 4.4 | 62538 |
| 6 | 212.9720 | 2.6 | 37759 |
| 7 | 226.9514 | 0.8 | 10728 |
| 8 | 229.0034 | 0.6 | 9031 |
| 9 | 242.9827 | 1.6 | 22198 |
| 10 | 256.9620 | 4.6 | 65398 |
| 11 | 257.0630 | 0.6 | 9205 |
| 12 | 266.9814 | 1.4 | 20258 |
| 13 | 280.9404 | 2.2 | 31140 |
| 14 | 280.9609 | 2.3 | 32827 |
| 15 | 286.9724 | 3.3 | 46541 |
| 16 | 294.9195 | 1.0 | 14041 |
| 17 | 296.9906 | 0.8 | 10732 |
| 18 | 315.1925 | 0.6 | 8992 |
| 19 | 316.9826 | 0.9 | 13184 |
| 20 | 319.2602 | 0.7 | 10160 |
| 21 | 327.0009 | 0.7 | 10451 |
| 22 | 340.9801 | 0.7 | 9379 |
| 23 | 370.9906 | 1.1 | 16233 |
| 24 | 378.9568 | 0.6 | 8768 |
| 25 | 379.2992 | 0.7 | 9479 |
| 26 | 383.2545 | 0.9 | 12145 |
| 27 | 408.9674 | 0.9 | 12621 |
| 28 | 413.2652 | 0.7 | 9385 |
| 29 | 414.9804 | 1.4 | 19779 |
| 30 | 438.9780 | 0.6 | 8846 |
| 31 | 441.2962 | 0.7 | 9634 |
| 32 | 467.1009 | 0.8 | 11906 |
| 33 | 469.1591 | 9.5 | 135912 |
| 34 | 470.1620 | 2.3 | 33295 |
| 35 | 476.9544 | 1.0 | 13981 |
| 36 | 487.1690 | 1.6 | 22418 |
| 37 | 490.9338 | 1.0 | 14102 |
| 38 | 504.1959 | 3.0 | 43428 |
| 39 | 505.1989 | 0.8 | 11335 |
| 40 | 506.9652 | 1.0 | 14463 |
| 41 | 509.1523 | 100.0 | 1426841 |
| 42 | 510.1552 | 21.7 | 309902 |
| 43 | 511.1577 | 2.9 | 40785 |
| 44 | 520.9442 | 1.3 | 19053 |
| 45 | 525.1251 | 3.6 | 51427 |
| 46 | 526.1281 | 1.0 | 13962 |
| 47 | 531.1328 | 0.9 | 13122 |
| 48 | 536.1638 | 0.7 | 10340 |
| 49 | 541.1193 | 1.3 | 18639 |
| 50 | 542.1203 | 0.7 | 10079 |
| 51 | 550.9546 | 1.3 | 18920 |
| 52 | 553.4577 | 2.0 | 29005 |
| 53 | 554.4611 | 0.8 | 11971 |
| 54 | 574.9521 | 0.8 | 11663 |
| 55 | 580.9650 | 0.8 | 11998 |
| 56 | 588.9318 | 1.1 | 15874 |
| 57 | 604.9623 | 0.7 | 9964 |
| 58 | 607.1490 | 1.7 | 24882 |

 High Resolution Mass Spectrometry Report

| # | m/z | I % | I |
|-----|-----------|------|--------|
| 59 | 618.9421 | 1.5 | 21042 |
| 60 | 648.9527 | 1.4 | 19970 |
| 61 | 656.9194 | 1.0 | 14930 |
| 62 | 678.9634 | 0.7 | 9997 |
| 63 | 685.4340 | 0.7 | 9971 |
| 64 | 686.9298 | 1.9 | 27589 |
| 65 | 688.9259 | 1.6 | 23386 |
| 66 | 689.9256 | 0.8 | 11923 |
| 67 | 690.9206 | 4.4 | 63062 |
| 68 | 691.9216 | 1.4 | 19536 |
| 69 | 692.9212 | 0.7 | 10619 |
| 70 | 716.9409 | 1.9 | 27532 |
| 71 | 724.9069 | 0.7 | 9511 |
| 72 | 746.9511 | 1.2 | 17102 |
| 73 | 754.9174 | 1.4 | 20069 |
| 74 | 784.9285 | 1.8 | 25393 |
| 75 | 814.9384 | 1.5 | 21117 |
| 76 | 822.9050 | 0.8 | 11830 |
| 77 | 844.9492 | 0.8 | 11121 |
| 78 | 852.9163 | 1.2 | 17003 |
| 79 | 860.9479 | 1.1 | 15243 |
| 80 | 861.9469 | 0.8 | 11067 |
| 81 | 862.9432 | 2.0 | 29098 |
| 82 | 863.9429 | 1.2 | 17725 |
| 83 | 864.9421 | 0.6 | 9210 |
| 84 | 882.9272 | 1.2 | 16534 |
| 85 | 912.9380 | 0.9 | 12213 |
| 86 | 916.9501 | 0.8 | 12111 |
| 87 | 920.9048 | 0.7 | 10256 |
| 88 | 950.9158 | 0.9 | 12473 |
| 89 | 980.9259 | 0.8 | 10845 |
| 90 | 990.3614 | 2.0 | 28334 |
| 91 | 991.3648 | 1.0 | 14551 |
| 92 | 995.3181 | 35.5 | 507055 |
| 93 | 996.3210 | 17.2 | 245362 |
| 94 | 997.3238 | 4.4 | 62430 |
| 95 | 998.3260 | 0.9 | 12148 |
| 96 | 1011.2908 | 1.6 | 23158 |
| 97 | 1012.2941 | 0.9 | 12753 |
| 98 | 1018.9043 | 0.6 | 8629 |
| 99 | 1039.6234 | 0.9 | 13451 |
| 100 | 1048.9139 | 0.7 | 9852 |

Acquisition Parameter

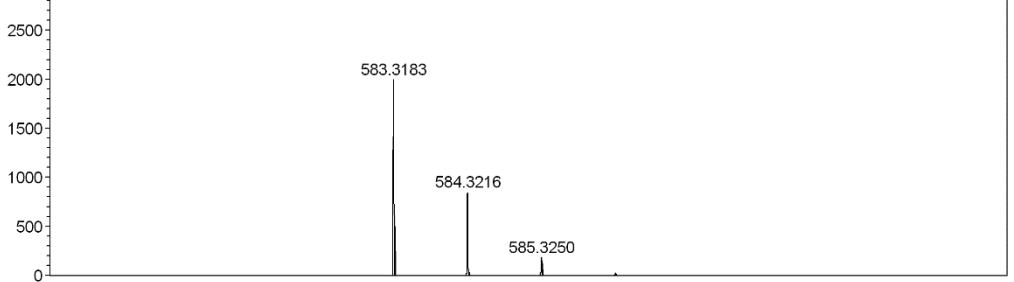
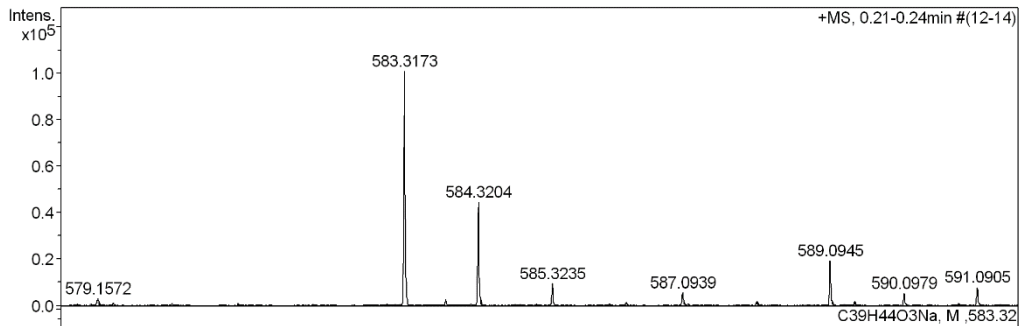
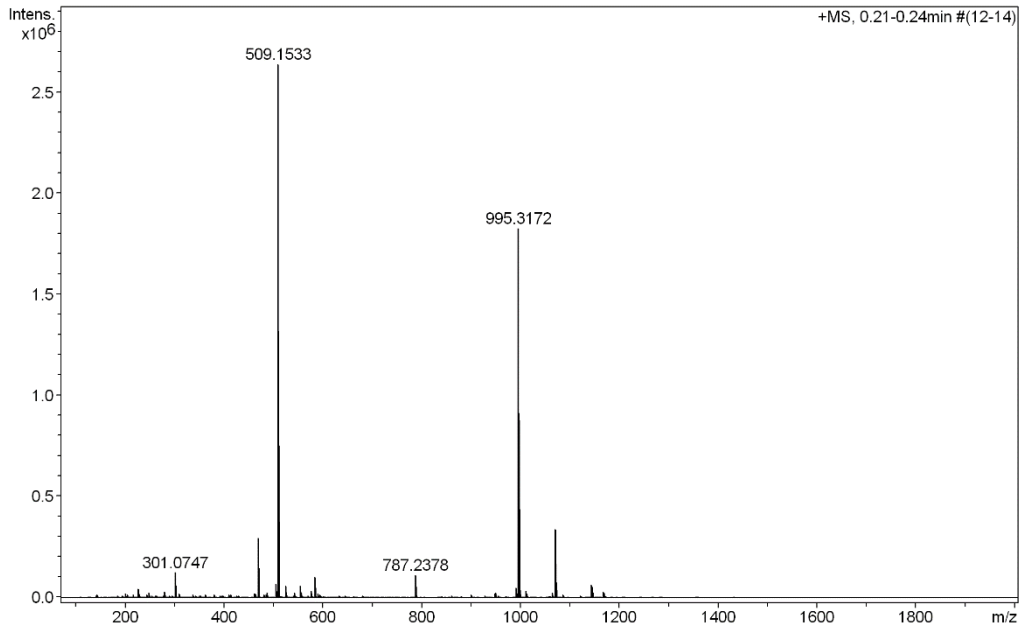
| | | | | | | |
|-------------------|------------------------------|----------------|---------------------------------------|----------------|--------------|-----------|
| General | Fore Vacuum | 3.36e+000 mBar | High Vacuum | 9.18e-008 mBar | Source Type | ESI |
| | Scan Begin | 75 m/z | Scan End | 2000 m/z | Ion Polarity | Positive |
| Source | Set Nebulizer | 2.0 Bar | Set Capillary | 4500 V | Set Dry Gas | 8.0 l/min |
| | Set Dry Heater | 200 °C | Set End Plate Offset | -500 V | | |
| Quadrupole | Set Ion Energy (MS only) | 4.0 eV | | | 100.0 Vpp | |
| Coll. Cell | Collision Energy | 8.0 eV | Set Collision Cell RF | 600.0 Vpp | | |
| Ion Cooler | Set Ion Cooler Transfer Time | 75.0 µs | Set Ion Cooler Pre Pulse Storage Time | 10.0 µs | | |

^1H , $^{13}\text{C}\{^1\text{H}\}$ (400/101 MHz, CDCl_3) NMR and HR-ESI-MS Spectra of Compound 20:

High Resolution Mass Spectrometry Report

Sample Name **KR289**
Comment

Instrument maXis 4G
Method ms_nocolumn_mid_pos.m



 High Resolution Mass Spectrometry Report

Measured m/z vs. theoretical m/z

| Meas. m/z | # | Formula | Score | m/z | err [mDa] | err [ppm] | mSigma | rdb | e ⁻ Conf | z |
|-----------|---|------------------|--------|-----------|-----------|-----------|--------|------|---------------------|----|
| 583.3173 | 1 | C 39 H 44 Na O 3 | 100.00 | 583.3183 | 1.0 | 1.7 | 10.9 | 17.5 | even | 1+ |
| 1143.6477 | 1 | C 78 H 88 Na O 6 | 100.00 | 1143.6473 | -0.4 | -0.3 | 13.1 | 34.5 | even | |

Mass list

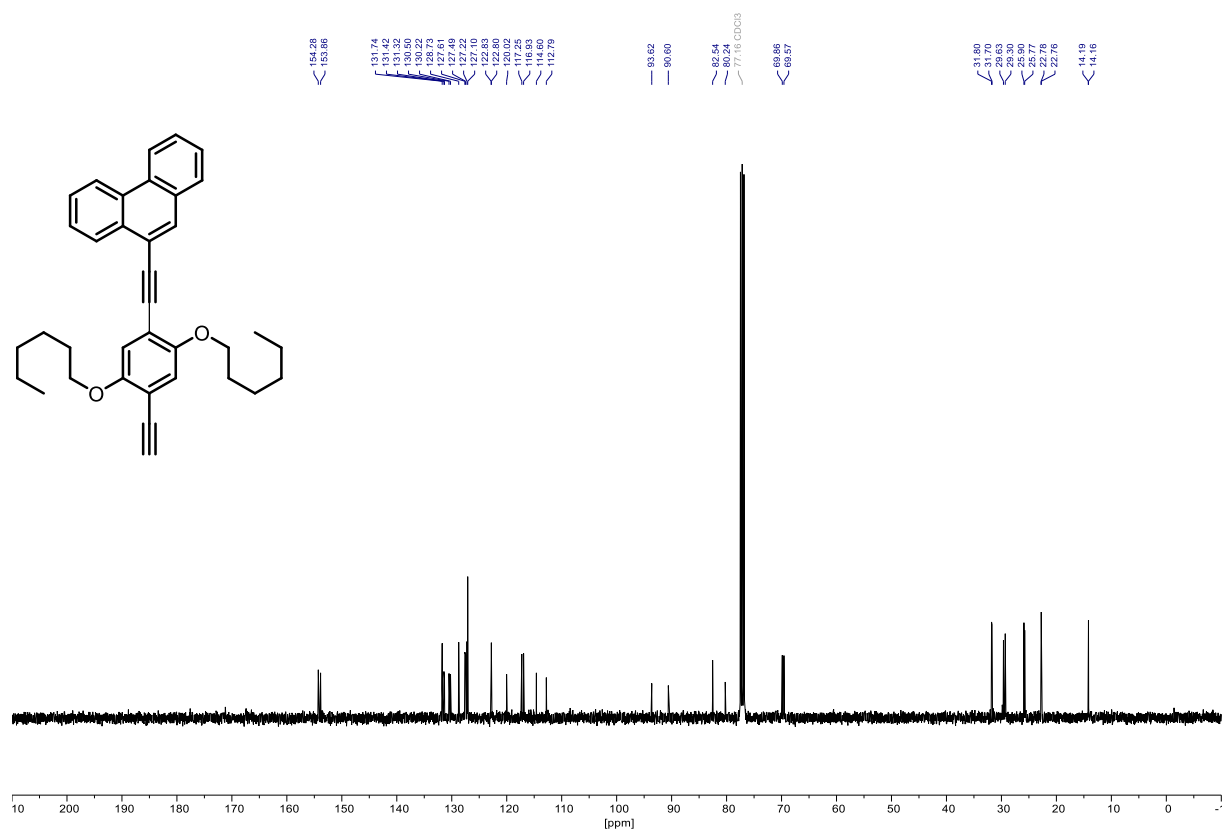
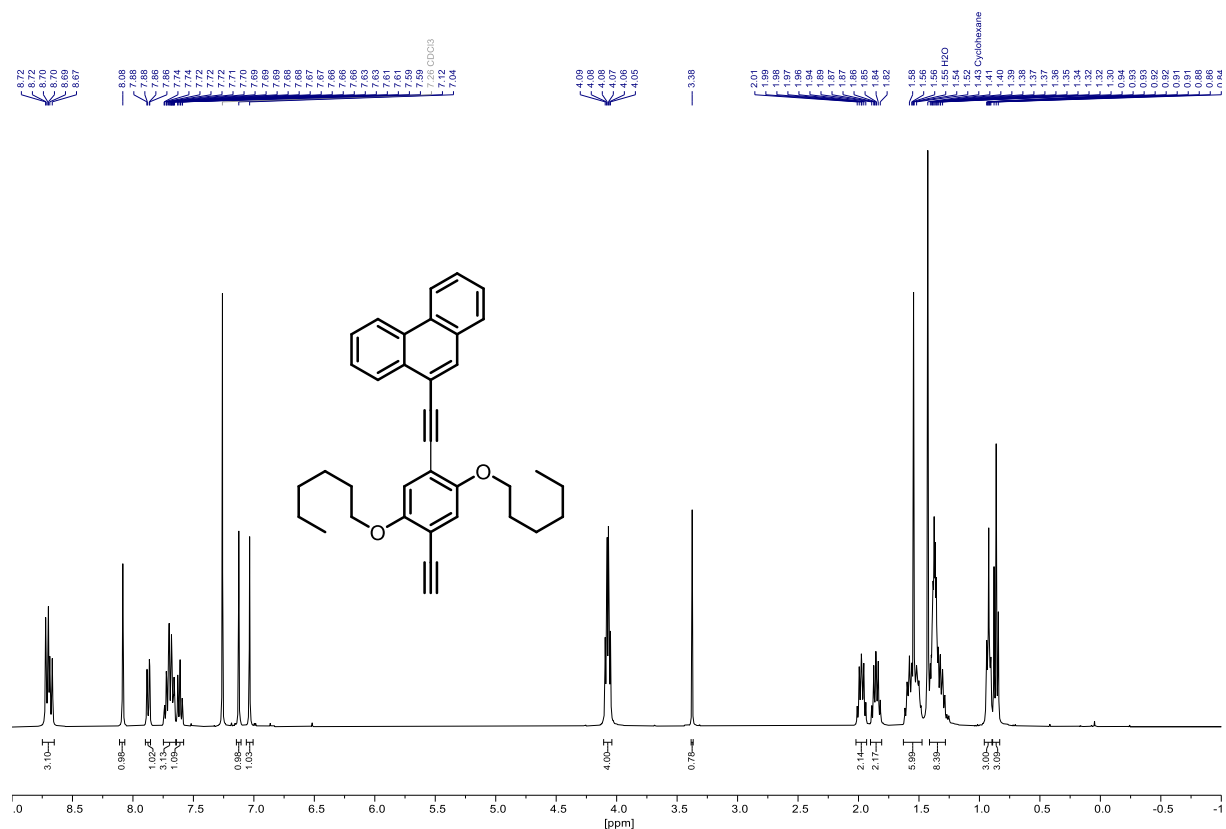
| # | m/z | I % | I |
|----|----------|-------|---------|
| 1 | 141.0023 | 0.4 | 10006 |
| 2 | 143.9591 | 0.5 | 12196 |
| 3 | 201.1095 | 0.7 | 19633 |
| 4 | 205.0596 | 0.4 | 11326 |
| 5 | 217.1043 | 0.5 | 14505 |
| 6 | 226.9512 | 1.6 | 41021 |
| 7 | 229.0500 | 0.7 | 17331 |
| 8 | 243.9412 | 0.5 | 14259 |
| 9 | 249.1092 | 0.9 | 24702 |
| 10 | 253.1405 | 0.3 | 8696 |
| 11 | 261.1305 | 0.3 | 7368 |
| 12 | 263.0554 | 0.4 | 9932 |
| 13 | 279.0927 | 1.0 | 27350 |
| 14 | 294.9194 | 0.4 | 9992 |
| 15 | 301.0747 | 4.6 | 122377 |
| 16 | 301.1402 | 0.8 | 21135 |
| 17 | 302.0778 | 0.9 | 22710 |
| 18 | 309.1299 | 0.8 | 20516 |
| 19 | 337.0743 | 0.5 | 12837 |
| 20 | 353.1563 | 0.4 | 10861 |
| 21 | 353.2655 | 0.3 | 7644 |
| 22 | 362.9258 | 0.4 | 11741 |
| 23 | 381.2963 | 0.4 | 11823 |
| 24 | 393.2968 | 0.3 | 8562 |
| 25 | 399.0806 | 0.3 | 9145 |
| 26 | 411.0929 | 0.5 | 12847 |
| 27 | 413.2652 | 0.4 | 11789 |
| 28 | 430.9133 | 0.4 | 10492 |
| 29 | 461.1650 | 0.8 | 19819 |
| 30 | 463.1631 | 0.7 | 18857 |
| 31 | 469.1594 | 11.1 | 293803 |
| 32 | 470.1623 | 2.7 | 69969 |
| 33 | 471.1652 | 0.4 | 10768 |
| 34 | 481.2644 | 0.5 | 13093 |
| 35 | 485.1112 | 0.4 | 11300 |
| 36 | 487.1690 | 0.8 | 22083 |
| 37 | 504.1959 | 2.6 | 67412 |
| 38 | 505.1990 | 0.6 | 16543 |
| 39 | 509.1167 | 0.6 | 15398 |
| 40 | 509.1533 | 100.0 | 2639470 |
| 41 | 509.7169 | 0.4 | 9478 |
| 42 | 510.1557 | 28.6 | 755332 |
| 43 | 511.1579 | 3.4 | 90623 |
| 44 | 512.1603 | 0.4 | 9800 |
| 45 | 525.1254 | 2.1 | 55981 |
| 46 | 526.1286 | 0.5 | 14290 |
| 47 | 541.1199 | 0.4 | 9424 |
| 48 | 543.3244 | 0.8 | 22053 |
| 49 | 544.3281 | 0.4 | 10007 |
| 50 | 553.4579 | 0.3 | 9082 |
| 51 | 555.1444 | 2.1 | 56069 |
| 52 | 556.1466 | 0.8 | 20846 |
| 53 | 557.1445 | 0.4 | 10836 |
| 54 | 559.1303 | 0.4 | 9400 |
| 55 | 571.1215 | 0.3 | 9135 |
| 56 | 577.1385 | 1.2 | 32129 |
| 57 | 578.1418 | 0.4 | 9319 |
| 58 | 583.3173 | 3.8 | 101077 |
| 59 | 584.3204 | 1.7 | 44782 |
| 60 | 585.3235 | 0.4 | 9611 |
| 61 | 589.0945 | 0.7 | 19524 |

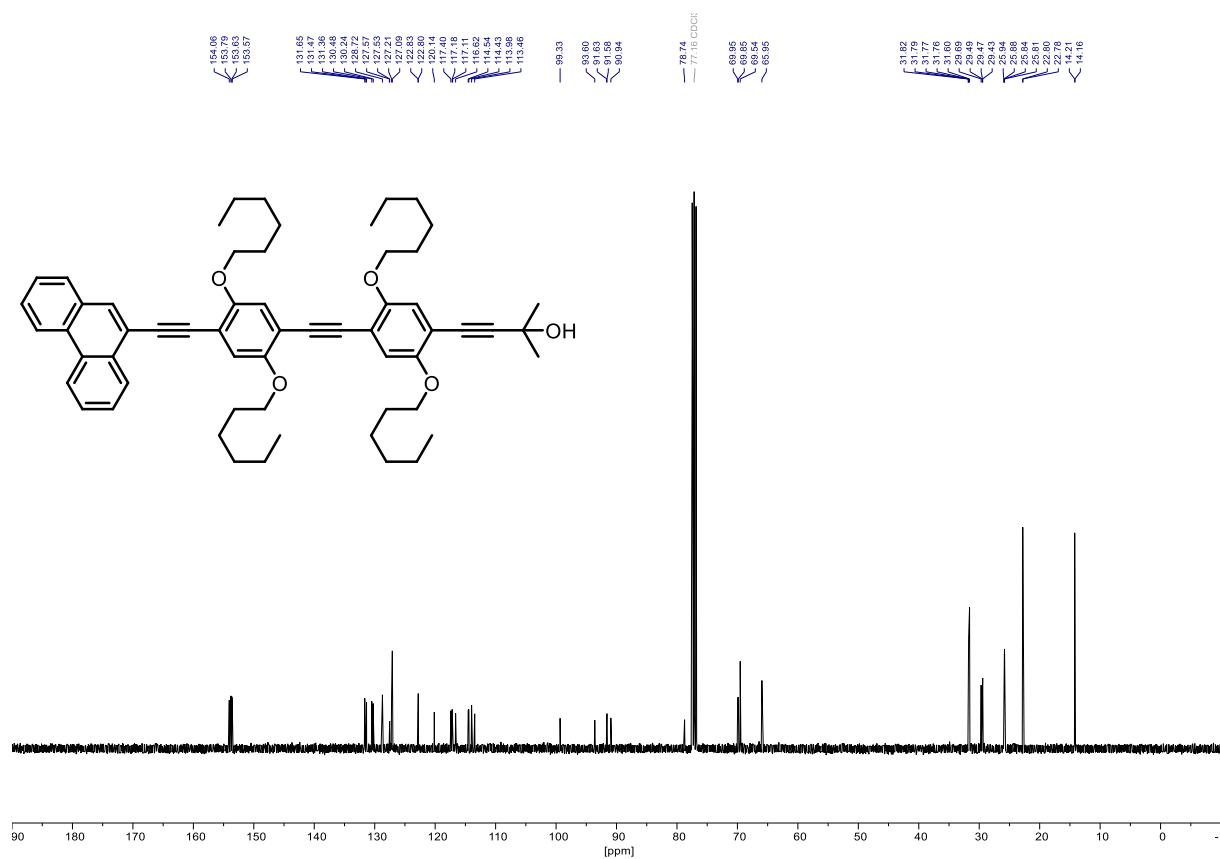
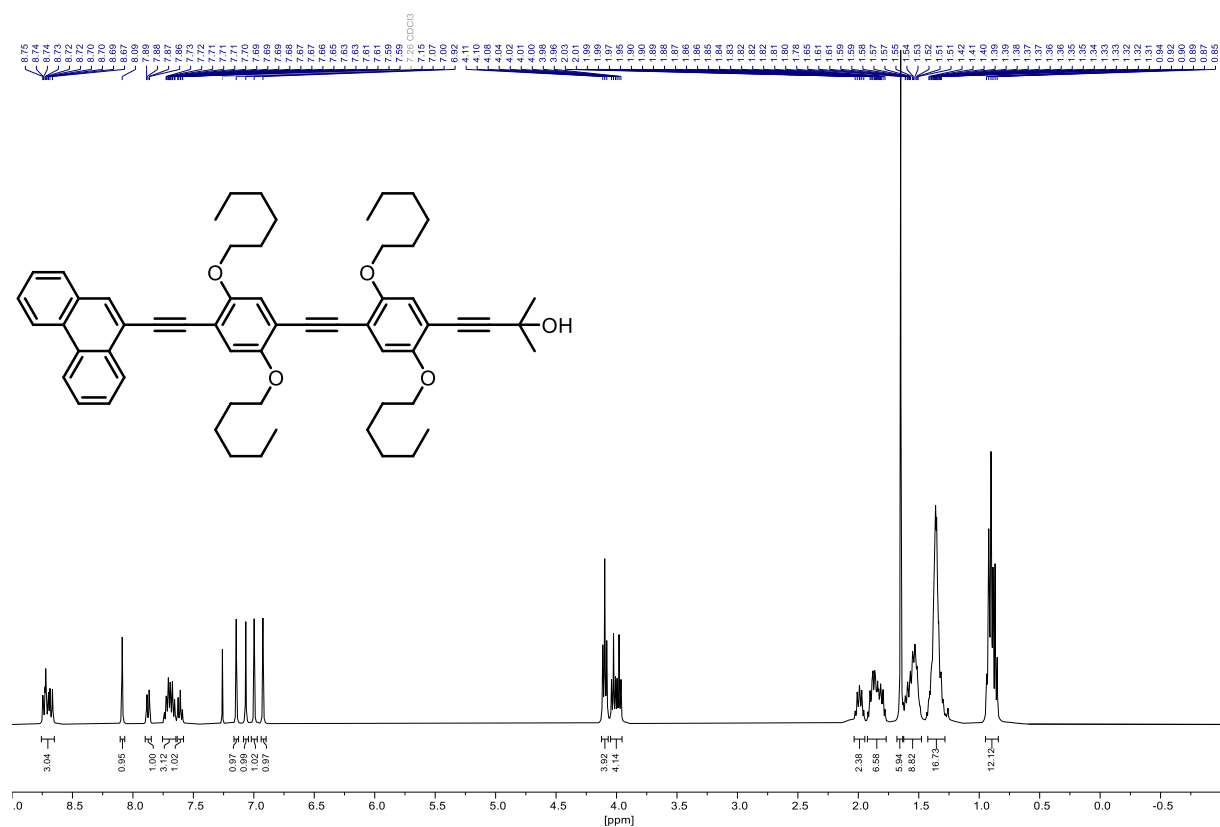
 High Resolution Mass Spectrometry Report

| # | m/z | I % | I |
|-----|-----------|------|---------|
| 62 | 591.0905 | 0.3 | 8242 |
| 63 | 594.1290 | 0.5 | 12248 |
| 64 | 681.3722 | 0.4 | 9820 |
| 65 | 787.2378 | 4.2 | 111477 |
| 66 | 787.3009 | 0.4 | 10464 |
| 67 | 788.2409 | 1.9 | 50589 |
| 68 | 789.2439 | 0.4 | 11207 |
| 69 | 861.4031 | 0.3 | 7669 |
| 70 | 899.4287 | 0.5 | 12223 |
| 71 | 947.3283 | 0.8 | 20365 |
| 72 | 948.3320 | 0.4 | 10543 |
| 73 | 949.3273 | 0.8 | 21745 |
| 74 | 950.3301 | 0.4 | 10030 |
| 75 | 990.3596 | 1.7 | 45965 |
| 76 | 991.3629 | 0.9 | 24604 |
| 77 | 995.3172 | 69.3 | 1828200 |
| 78 | 996.3200 | 33.4 | 880908 |
| 79 | 997.3224 | 7.4 | 196200 |
| 80 | 998.3247 | 1.4 | 36469 |
| 81 | 1011.2890 | 1.2 | 31350 |
| 82 | 1012.2923 | 0.6 | 16331 |
| 83 | 1063.3026 | 0.9 | 22750 |
| 84 | 1064.3060 | 0.4 | 11219 |
| 85 | 1064.5256 | 0.6 | 15082 |
| 86 | 1065.5285 | 0.4 | 10901 |
| 87 | 1069.4822 | 12.8 | 338561 |
| 88 | 1070.4854 | 8.6 | 227679 |
| 89 | 1071.4881 | 2.9 | 76900 |
| 90 | 1072.4904 | 0.8 | 20615 |
| 91 | 1085.4555 | 0.5 | 13676 |
| 92 | 1086.4577 | 0.3 | 8932 |
| 93 | 1121.2124 | 0.3 | 8364 |
| 94 | 1143.6477 | 2.3 | 61083 |
| 95 | 1144.6508 | 2.0 | 52372 |
| 96 | 1145.6539 | 0.9 | 23626 |
| 97 | 1167.5366 | 1.0 | 26599 |
| 98 | 1168.5398 | 0.8 | 21066 |
| 99 | 1169.5423 | 0.4 | 9403 |
| 100 | 1171.5984 | 0.3 | 8094 |

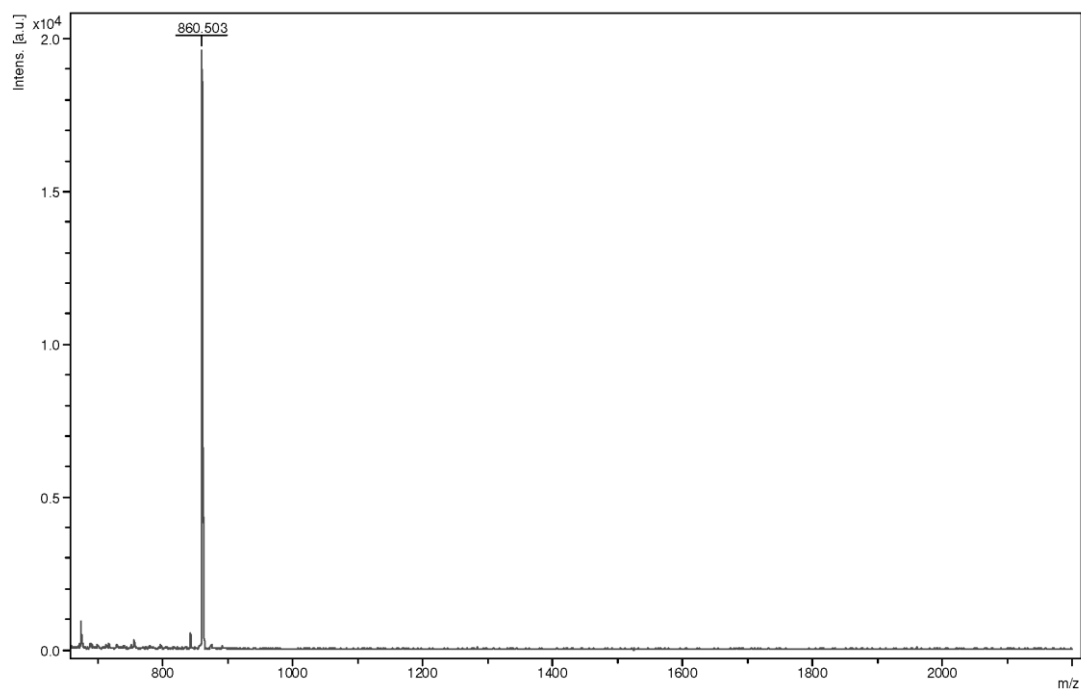
Acquisition Parameter

| | | | | | | |
|-------------------|------------------------------|----------------|---------------------------------------|----------------|--------------|-----------|
| General | Fore Vacuum | 3.27e+000 mBar | High Vacuum | 9.05e-008 mBar | Source Type | ESI |
| | Scan Begin | 75 m/z | Scan End | 2000 m/z | Ion Polarity | Positive |
| Source | Set Nebulizer | 2.0 Bar | Set Capillary | 4500 V | Set Dry Gas | 8.0 l/min |
| | Set Dry Heater | 200 °C | Set End Plate Offset | -500 V | | |
| Quadrupole | Set Ion Energy (MS only) | 4.0 eV | | | | |
| Coll. Cell | Collision Energy | 8.0 eV | Set Collision Cell RF | 600.0 Vpp | | 100.0 Vpp |
| Ion Cooler | Set Ion Cooler Transfer Time | 75.0 µs | Set Ion Cooler Pre Pulse Storage Time | | | 10.0 µs |

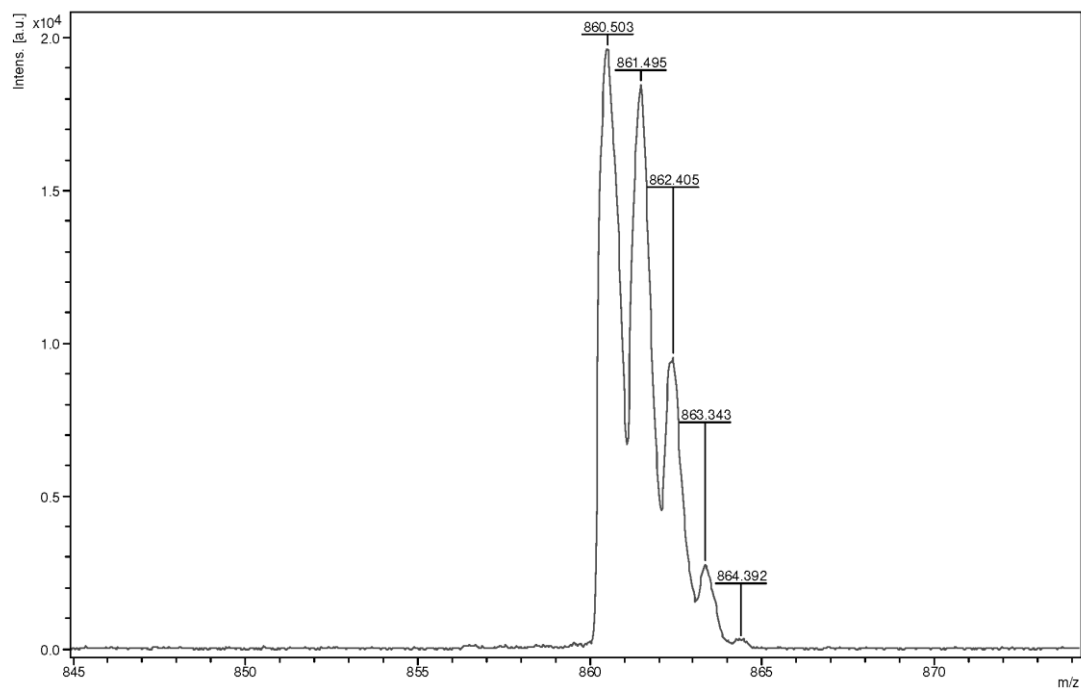
^1H and $^{13}\text{C}\{^1\text{H}\}$ (400/101 MHz, CDCl_3) NMR spectra of Compound 21:

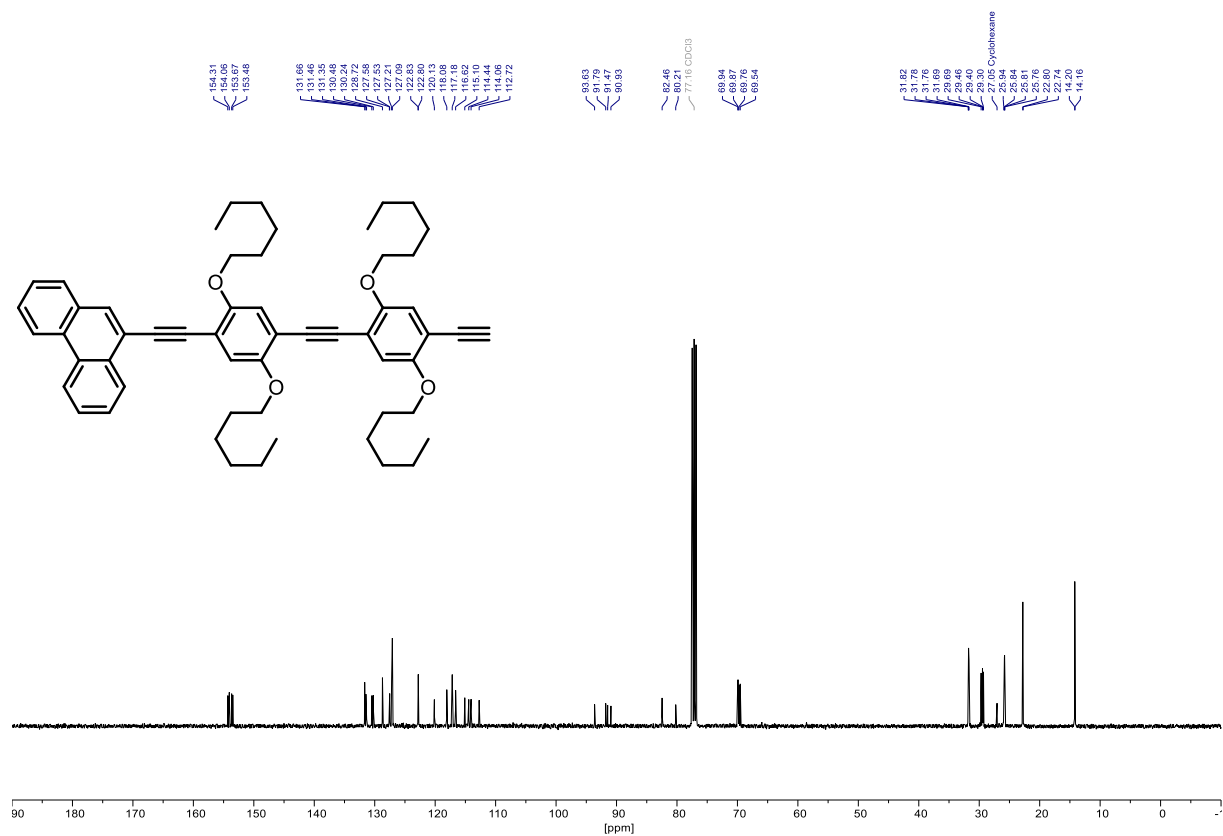
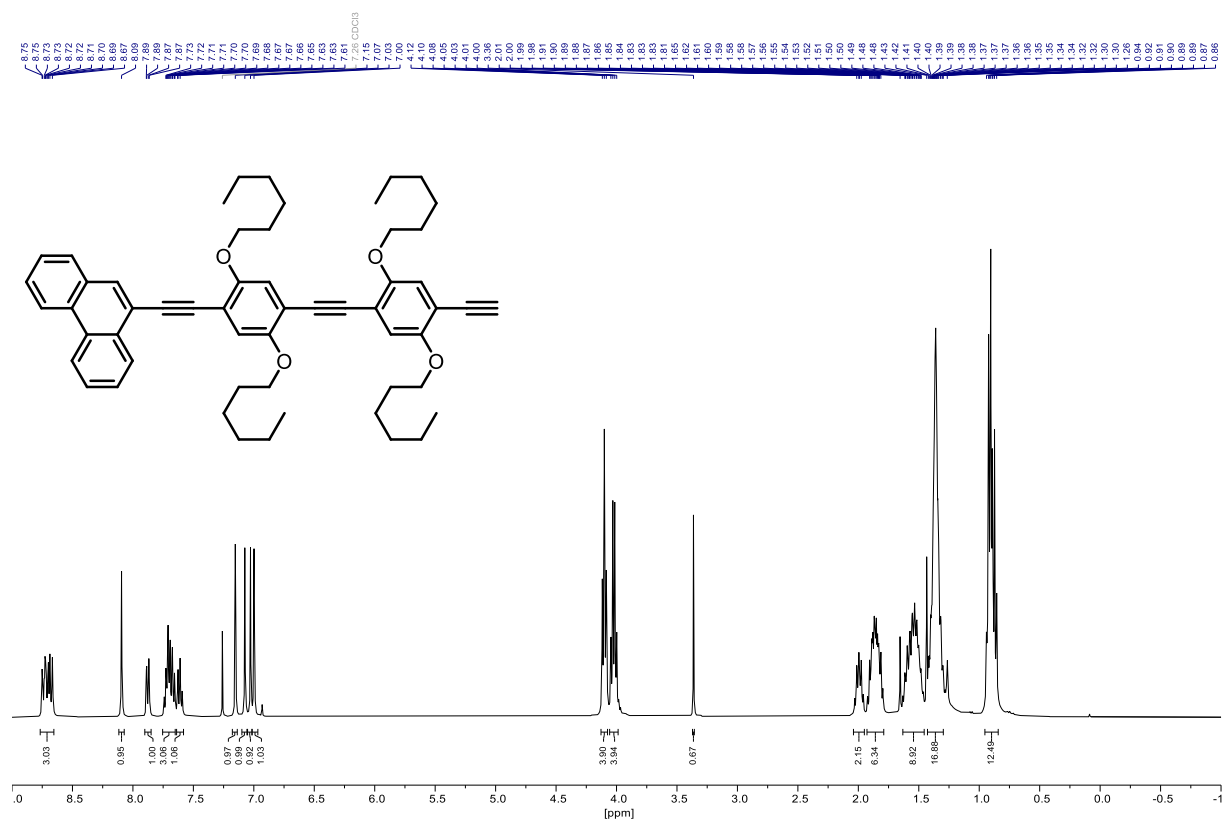
^1H , $^{13}\text{C}\{^1\text{H}\}$ (400/101 MHz, CDCl_3) NMR and MALDI-ToF-MS Spectra of Compound 22:

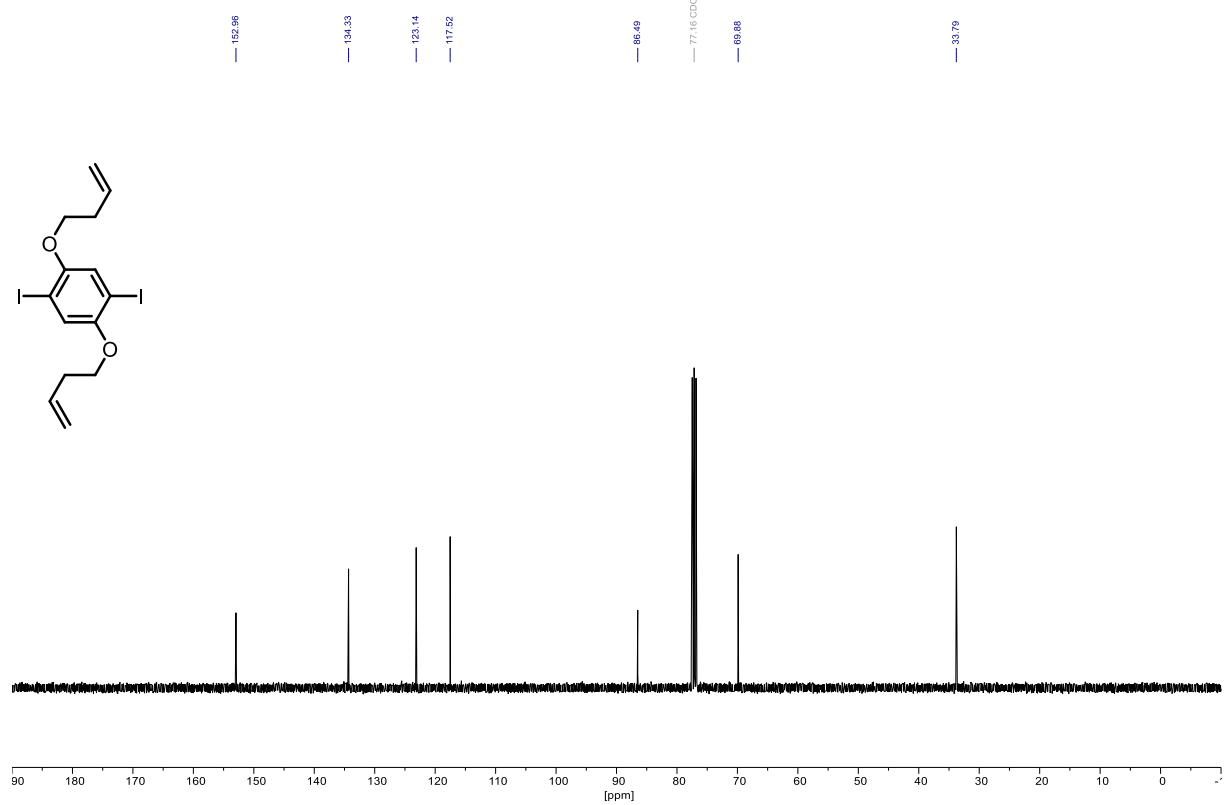
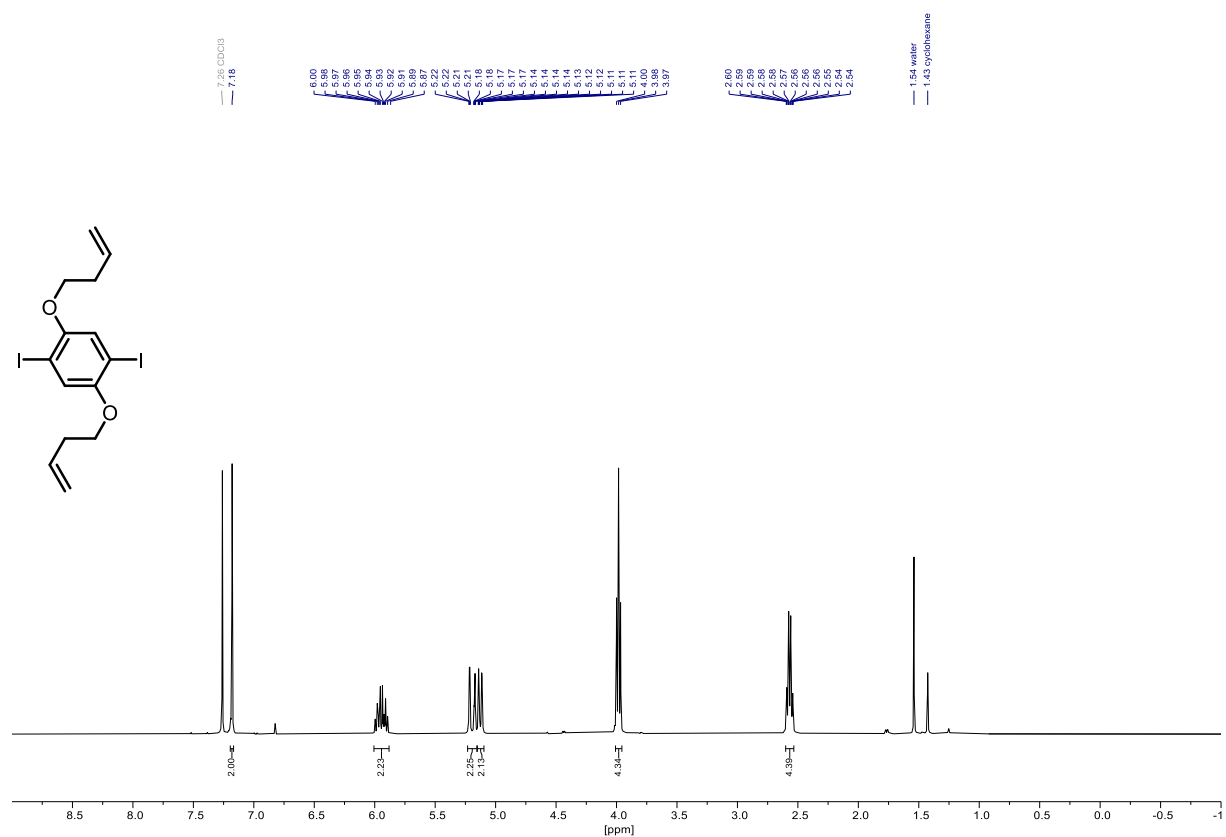
MALDI-ToF-MS (RP, DCTB) Spectrum of Compound 22:



Zoom in of MALDI-ToF-MS (RP, DCTB) Spectrum of Compound 22:



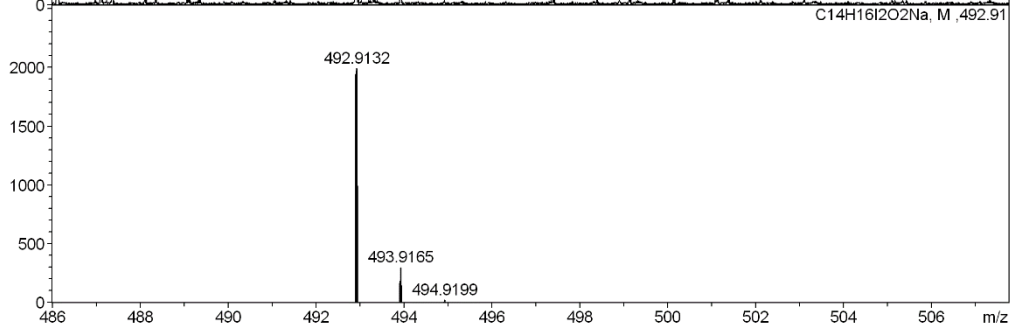
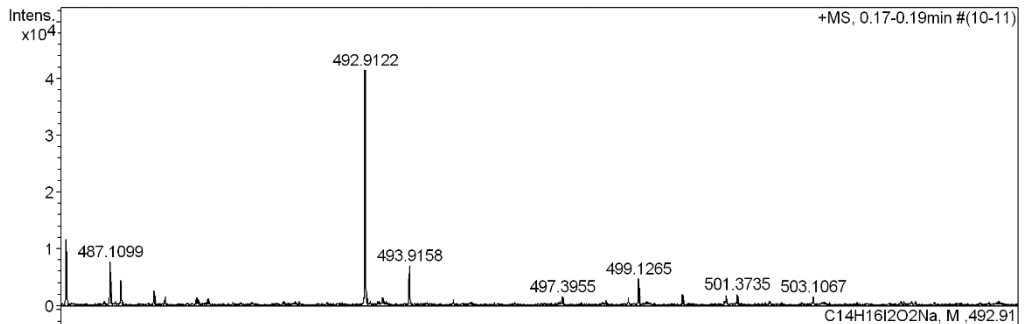
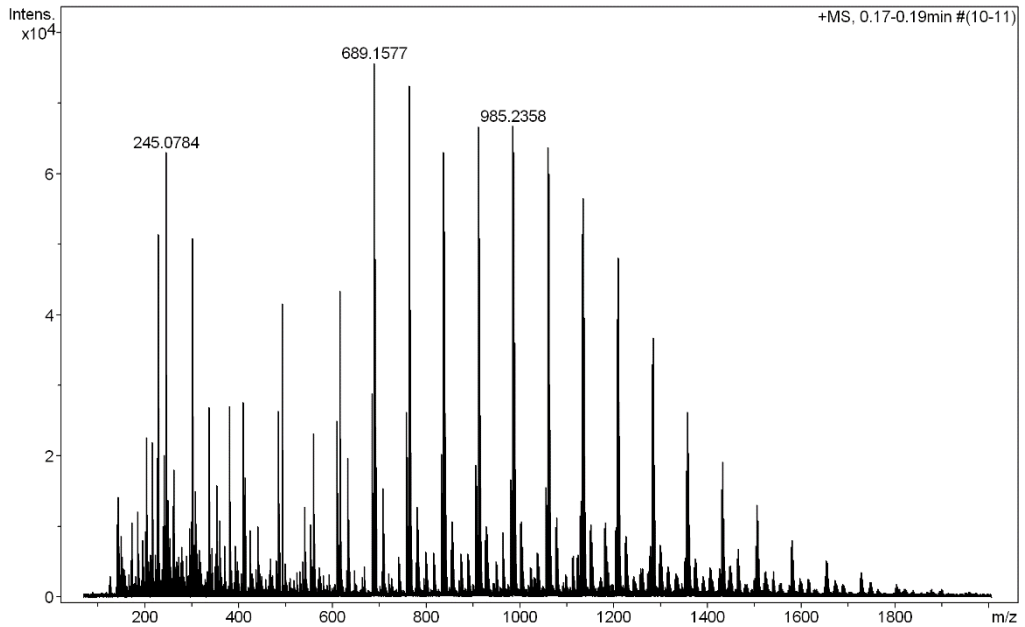
^1H , $^{13}\text{C}\{^1\text{H}\}$ (400/101 MHz, CDCl_3) NMR Spectra of Compound 23:

^1H , $^{13}\text{C}\{^1\text{H}\}$ (400/101 MHz, CDCl_3) NMR and HR-ESI-MS Spectra of 1,4-bis(but-3-en-1-yloxy)-2,5-diiodobenzene (11):

High Resolution Mass Spectrometry Report

Sample Name **KR287**
Comment

Instrument maXis 4G
Method ms_nocolumn_mid_pos.m



High Resolution Mass Spectrometry Report

Measured m/z vs. theoretical m/z

| Meas. m/z | # | Formula | Score | m/z | err [mDa] | err [ppm] | mSigma | rdb | e ⁻ Conf | z |
|-----------|---|----------------------|--------|----------|-----------|-----------|--------|------|---------------------|----|
| 492.9122 | 1 | C 14 H 16 I 2 Na O 2 | 100.00 | 492.9132 | 1.0 | 2.0 | 14.6 | 5.5 | even | 1+ |
| 962.8382 | 1 | C 28 H 32 I 4 Na O 4 | 100.00 | 962.8372 | -1.0 | -1.1 | 31.9 | 10.5 | even | |

Mass list

| # | m/z | I % | I |
|----|----------|-------|-------|
| 1 | 143.9584 | 18.9 | 14286 |
| 2 | 205.0601 | 29.9 | 22643 |
| 3 | 217.0831 | 23.7 | 17908 |
| 4 | 217.1047 | 29.0 | 21964 |
| 5 | 226.9515 | 26.1 | 19737 |
| 6 | 229.0505 | 67.9 | 51390 |
| 7 | 241.0681 | 26.6 | 20117 |
| 8 | 245.0784 | 83.3 | 63057 |
| 9 | 249.1095 | 18.2 | 13764 |
| 10 | 263.0559 | 23.9 | 18082 |
| 11 | 301.0749 | 31.1 | 23532 |
| 12 | 301.1407 | 67.2 | 50867 |
| 13 | 309.1305 | 19.9 | 15092 |
| 14 | 337.0746 | 35.6 | 26986 |
| 15 | 337.2344 | 32.3 | 24455 |
| 16 | 353.2656 | 21.0 | 15895 |
| 17 | 381.2971 | 35.9 | 27147 |
| 18 | 411.0930 | 36.5 | 27669 |
| 19 | 413.2656 | 22.5 | 17060 |
| 20 | 485.1115 | 34.9 | 26407 |
| 21 | 492.9122 | 54.9 | 41601 |
| 22 | 559.1303 | 30.7 | 23257 |
| 23 | 610.1829 | 33.1 | 25044 |
| 24 | 611.1837 | 19.5 | 14734 |
| 25 | 615.1385 | 57.4 | 43455 |
| 26 | 616.1388 | 33.7 | 25493 |
| 27 | 617.1358 | 25.9 | 19641 |
| 28 | 633.1485 | 26.0 | 19722 |
| 29 | 684.2020 | 38.1 | 28837 |
| 30 | 685.2024 | 24.1 | 18218 |
| 31 | 686.2003 | 18.0 | 13628 |
| 32 | 689.1577 | 100.0 | 75709 |
| 33 | 690.1580 | 63.5 | 48041 |
| 34 | 691.1560 | 52.6 | 39808 |
| 35 | 692.1550 | 24.5 | 18530 |
| 36 | 707.1683 | 20.5 | 15491 |
| 37 | 758.2209 | 34.7 | 26282 |
| 38 | 759.2215 | 26.3 | 19906 |
| 39 | 760.2196 | 19.4 | 14683 |
| 40 | 763.1766 | 95.7 | 72459 |
| 41 | 764.1775 | 66.0 | 49968 |
| 42 | 765.1751 | 54.0 | 40856 |
| 43 | 766.1747 | 28.2 | 21341 |
| 44 | 832.2401 | 26.8 | 20306 |
| 45 | 833.2407 | 23.1 | 17458 |
| 46 | 834.2395 | 19.5 | 14755 |
| 47 | 837.1961 | 83.3 | 63045 |
| 48 | 838.1969 | 68.5 | 51853 |
| 49 | 839.1943 | 58.1 | 43973 |
| 50 | 840.1938 | 30.2 | 22863 |
| 51 | 841.1911 | 17.6 | 13350 |
| 52 | 906.2599 | 24.9 | 18832 |
| 53 | 907.2605 | 21.1 | 15943 |
| 54 | 908.2585 | 20.2 | 15321 |
| 55 | 911.2155 | 88.0 | 66617 |
| 56 | 912.2169 | 79.3 | 60061 |
| 57 | 913.2143 | 67.1 | 50834 |
| 58 | 914.2138 | 36.0 | 27289 |
| 59 | 915.2120 | 20.7 | 15668 |
| 60 | 980.2799 | 22.1 | 16720 |
| 61 | 981.2798 | 21.0 | 15911 |

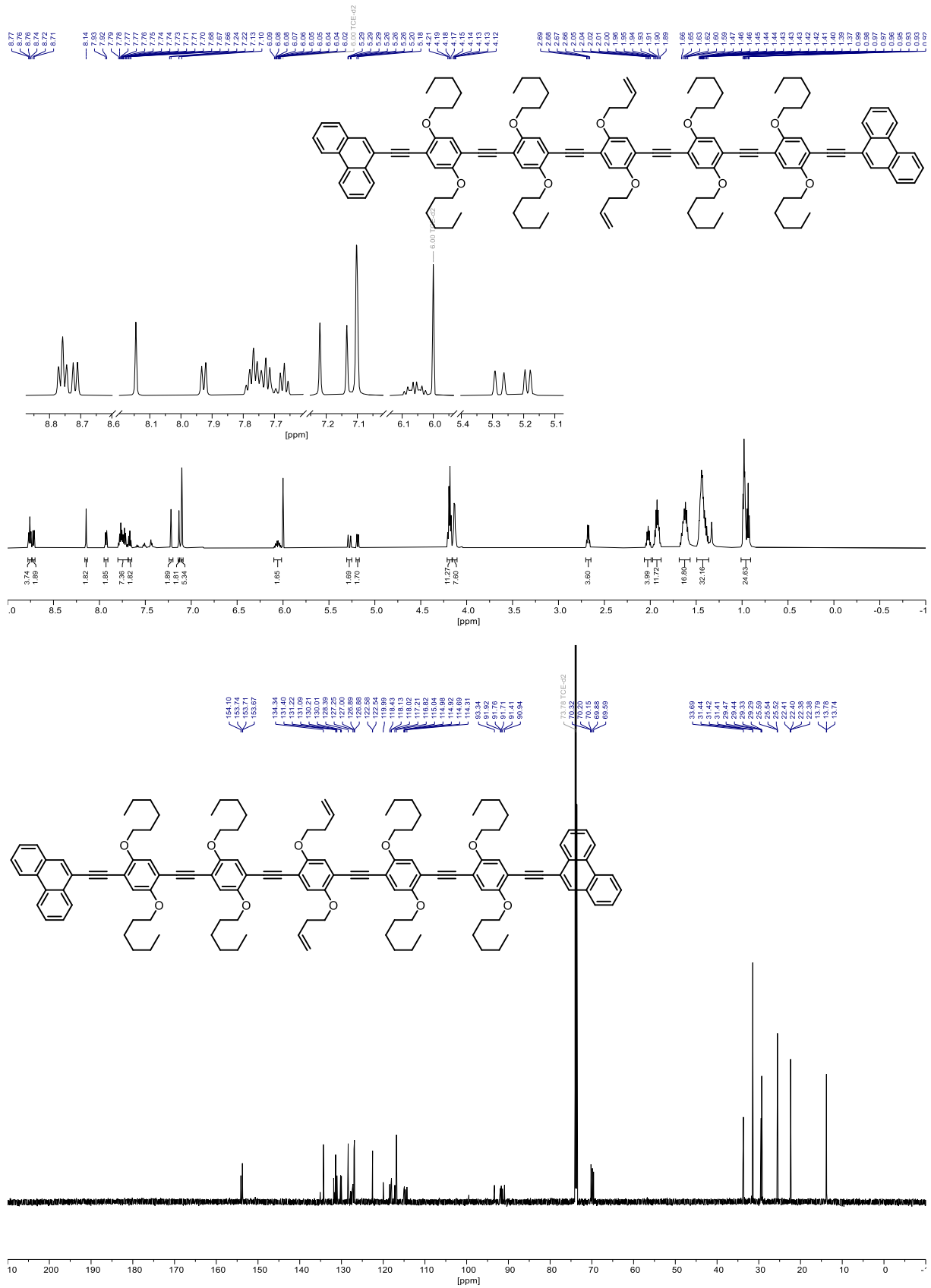
 High Resolution Mass Spectrometry Report

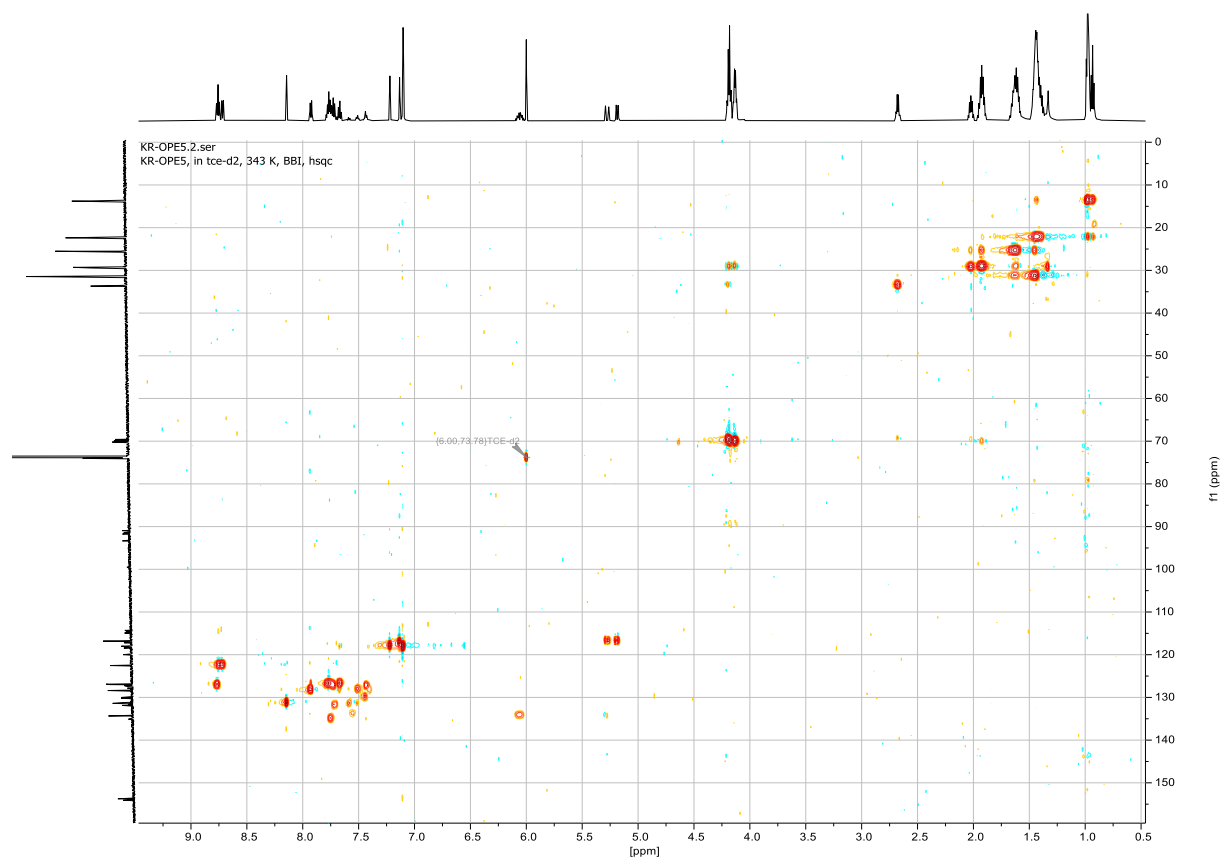
| # | m/z | I % | I |
|-----|-----------|------|-------|
| 62 | 982.2789 | 20.1 | 15232 |
| 63 | 985.2358 | 88.2 | 66771 |
| 64 | 986.2361 | 83.4 | 63116 |
| 65 | 987.2345 | 78.2 | 59178 |
| 66 | 988.2336 | 47.6 | 36024 |
| 67 | 989.2324 | 28.3 | 21420 |
| 68 | 1054.2988 | 18.8 | 14225 |
| 69 | 1055.3008 | 20.0 | 15136 |
| 70 | 1056.2980 | 20.5 | 15556 |
| 71 | 1059.2554 | 81.1 | 61420 |
| 72 | 1060.2564 | 84.3 | 63820 |
| 73 | 1061.2547 | 79.2 | 59981 |
| 74 | 1062.2539 | 52.3 | 39623 |
| 75 | 1063.2524 | 31.3 | 23726 |
| 76 | 1130.3193 | 18.0 | 13610 |
| 77 | 1133.2756 | 68.0 | 51505 |
| 78 | 1134.2761 | 73.8 | 55850 |
| 79 | 1135.2751 | 74.7 | 56591 |
| 80 | 1136.2746 | 52.4 | 39696 |
| 81 | 1137.2729 | 31.8 | 24088 |
| 82 | 1207.2963 | 52.1 | 39472 |
| 83 | 1208.2969 | 58.4 | 44233 |
| 84 | 1209.2955 | 63.6 | 48153 |
| 85 | 1210.2955 | 45.1 | 34116 |
| 86 | 1211.2936 | 30.2 | 22886 |
| 87 | 1281.3174 | 35.9 | 27195 |
| 88 | 1282.3178 | 43.7 | 33096 |
| 89 | 1283.3163 | 48.6 | 36790 |
| 90 | 1284.3158 | 34.4 | 26076 |
| 91 | 1285.3144 | 24.9 | 18825 |
| 92 | 1355.3373 | 23.7 | 17942 |
| 93 | 1356.3390 | 30.6 | 23139 |
| 94 | 1357.3376 | 34.7 | 26242 |
| 95 | 1358.3368 | 27.1 | 20493 |
| 96 | 1359.3358 | 18.5 | 13975 |
| 97 | 1430.3600 | 20.2 | 15330 |
| 98 | 1431.3590 | 25.5 | 19276 |
| 99 | 1432.3586 | 19.9 | 15104 |
| 100 | 1505.3816 | 17.3 | 13077 |

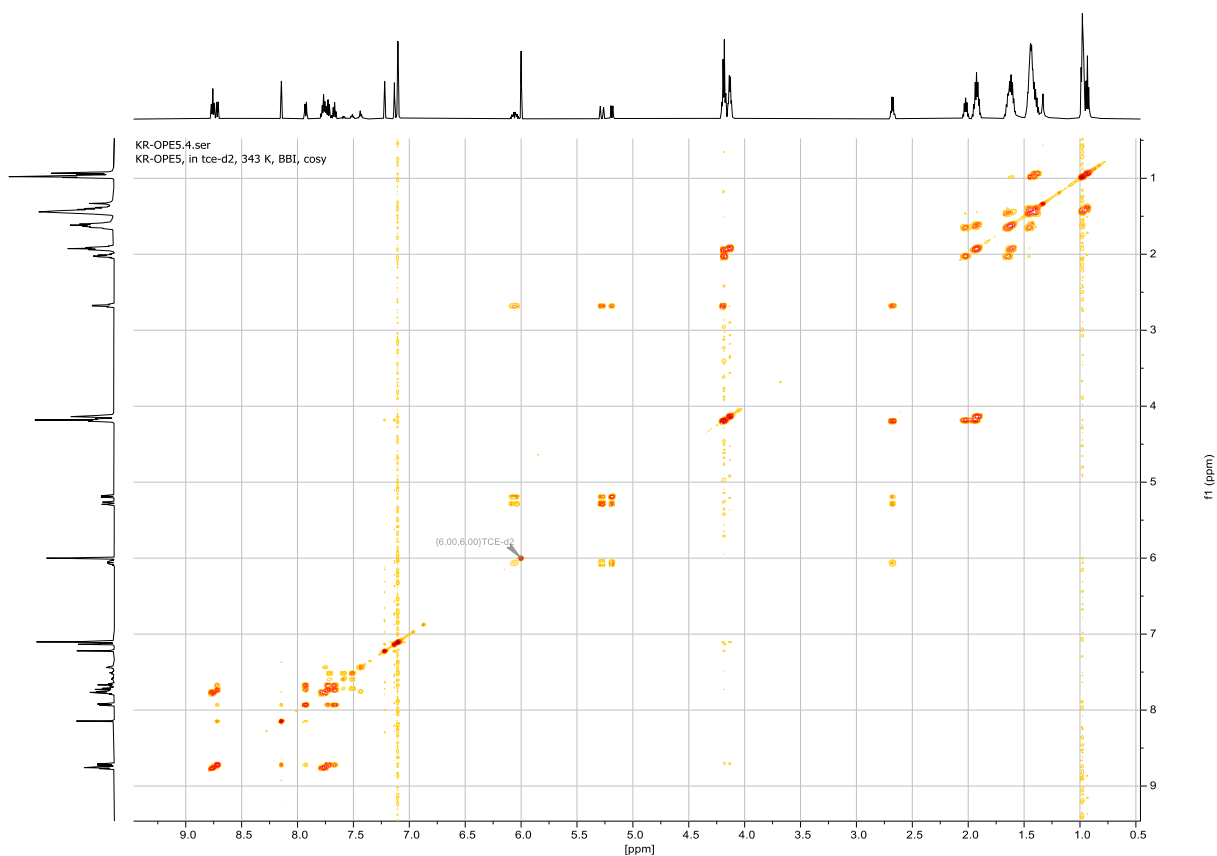
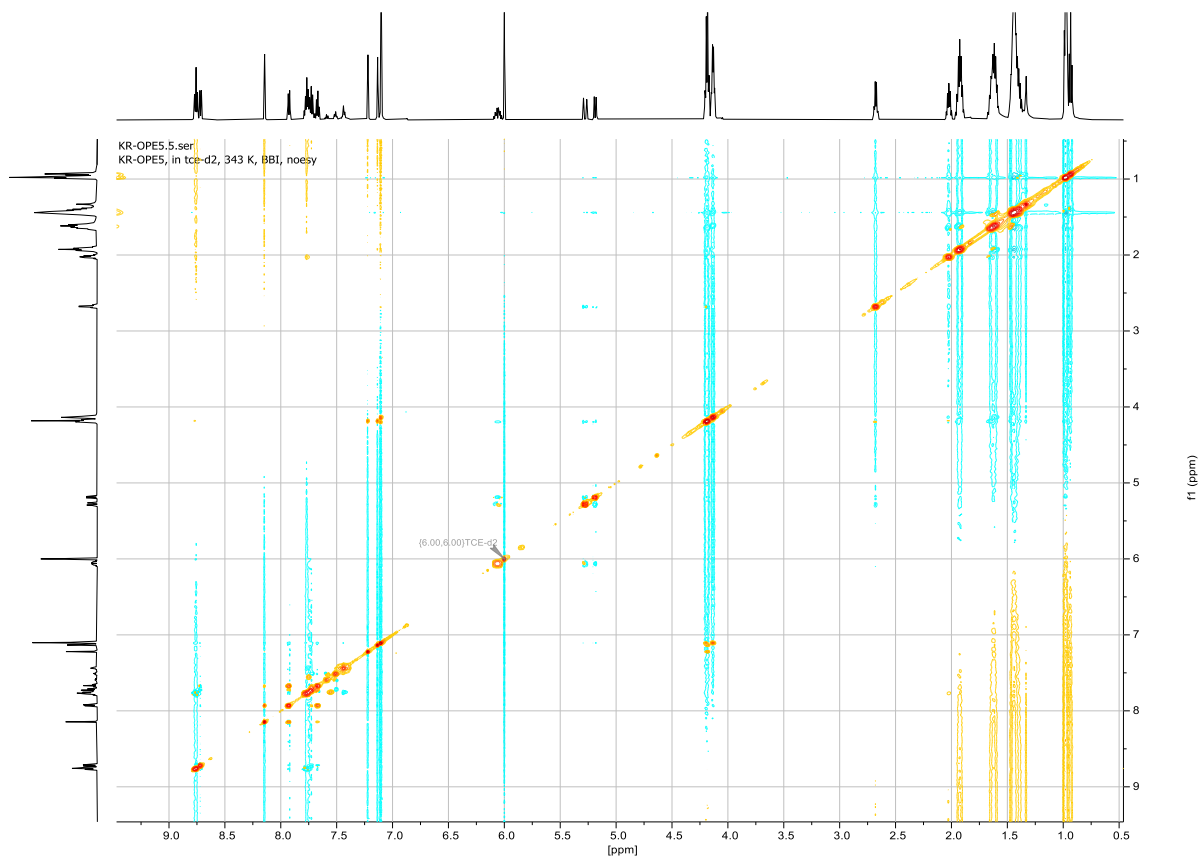
Acquisition Parameter

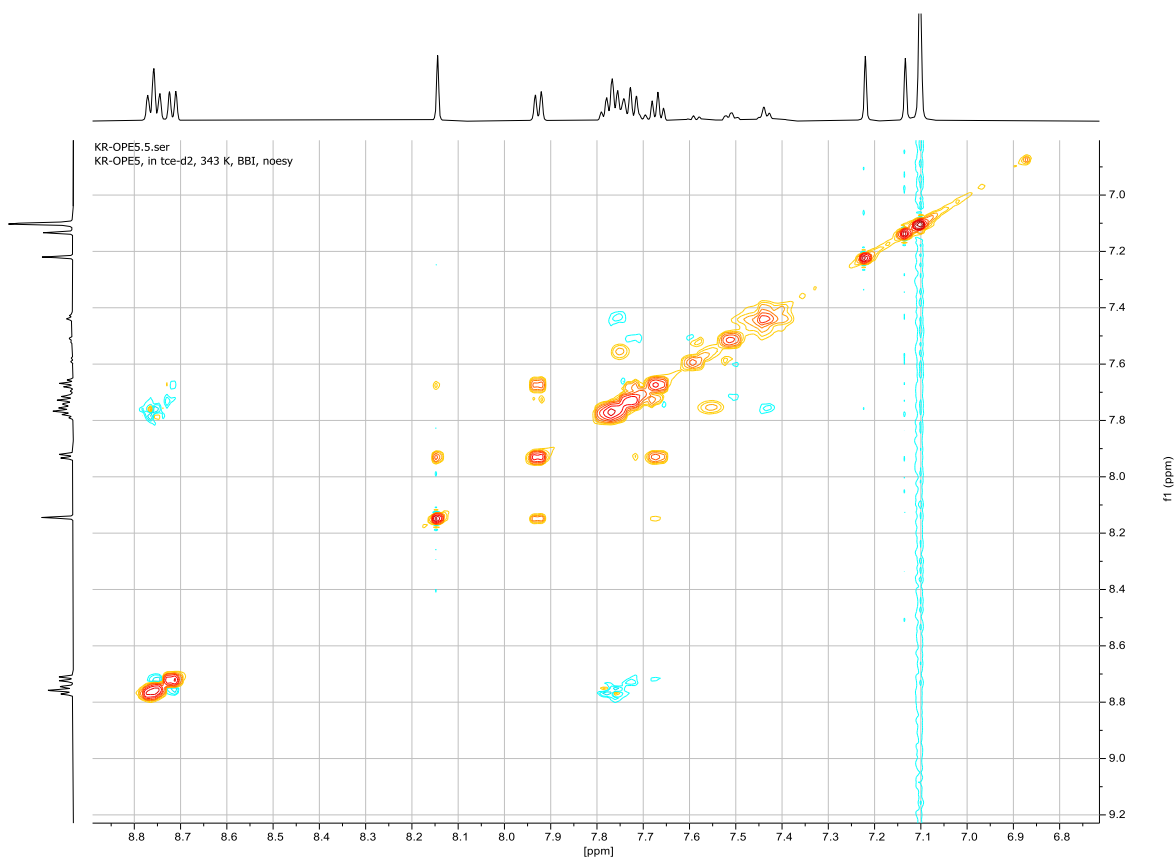
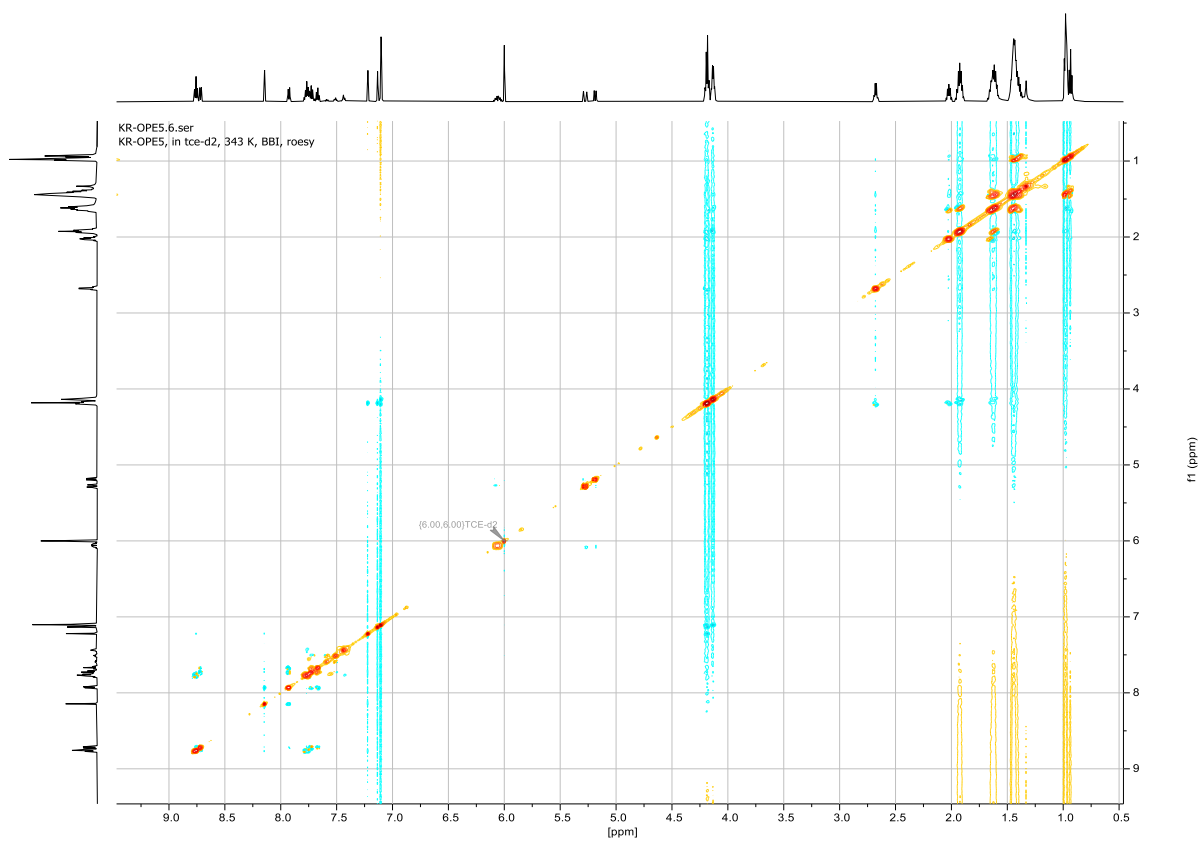
| | | | | | | |
|-------------------|------------------------------|----------------|---------------------------------------|----------------|--------------|-----------|
| General | Fore Vacuum | 3.28e+000 mBar | High Vacuum | 9.09e-008 mBar | Source Type | ESI |
| | Scan Begin | 75 m/z | Scan End | 2000 m/z | Ion Polarity | Positive |
| Source | Set Nebulizer | 2.0 Bar | Set Capillary | 4500 V | Set Dry Gas | 8.0 l/min |
| | Set Dry Heater | 200 °C | Set End Plate Offset | -500 V | | |
| Quadrupole | Set Ion Energy (MS only) | 4.0 eV | | | | |
| Coll. Cell | Collision Energy | 8.0 eV | Set Collision Cell RF | 600.0 Vpp | | 100.0 Vpp |
| Ion Cooler | Set Ion Cooler Transfer Time | 75.0 µs | Set Ion Cooler Pre Pulse Storage Time | | | 10.0 µs |

^1H , $^{13}\text{C}\{^1\text{H}\}$, 2D (600 MHz, TCE-d₂, 343 K) NMR and MALDI-MS Spectra of OPE5 Precursor (8):

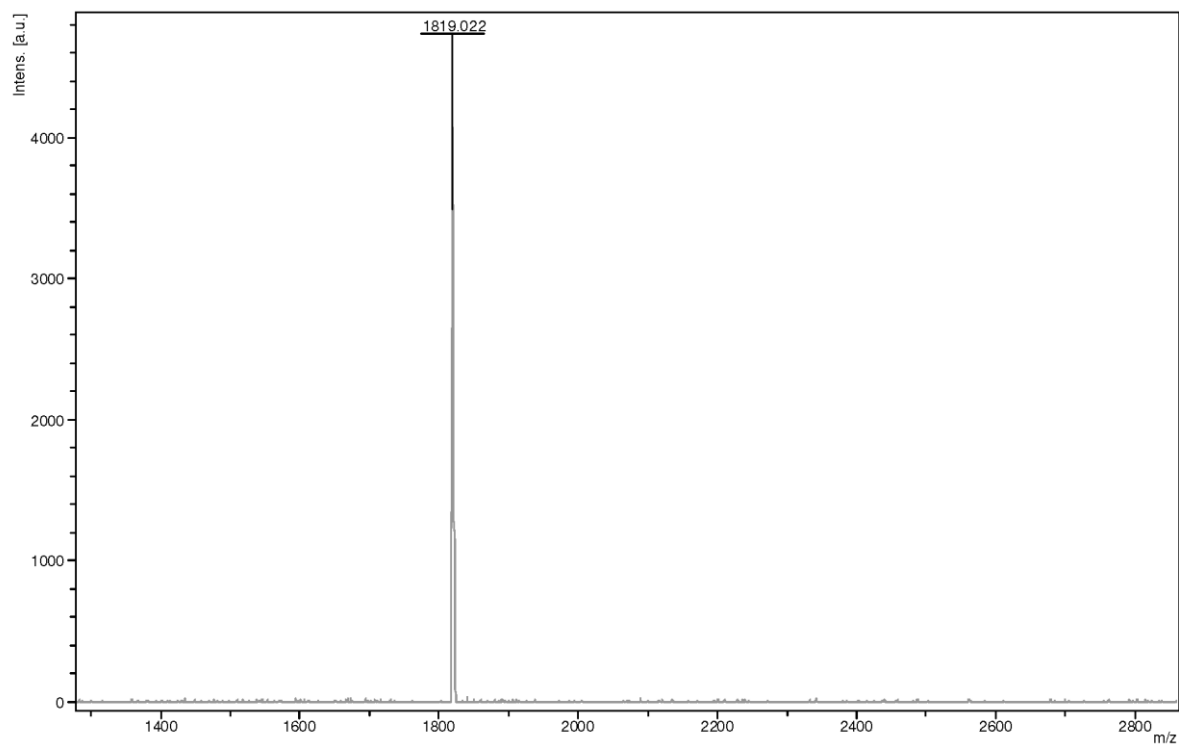


HSQC Spectrum of OPE5 Precursor (8):HMBC Spectrum of OPE5 Precursor (8):

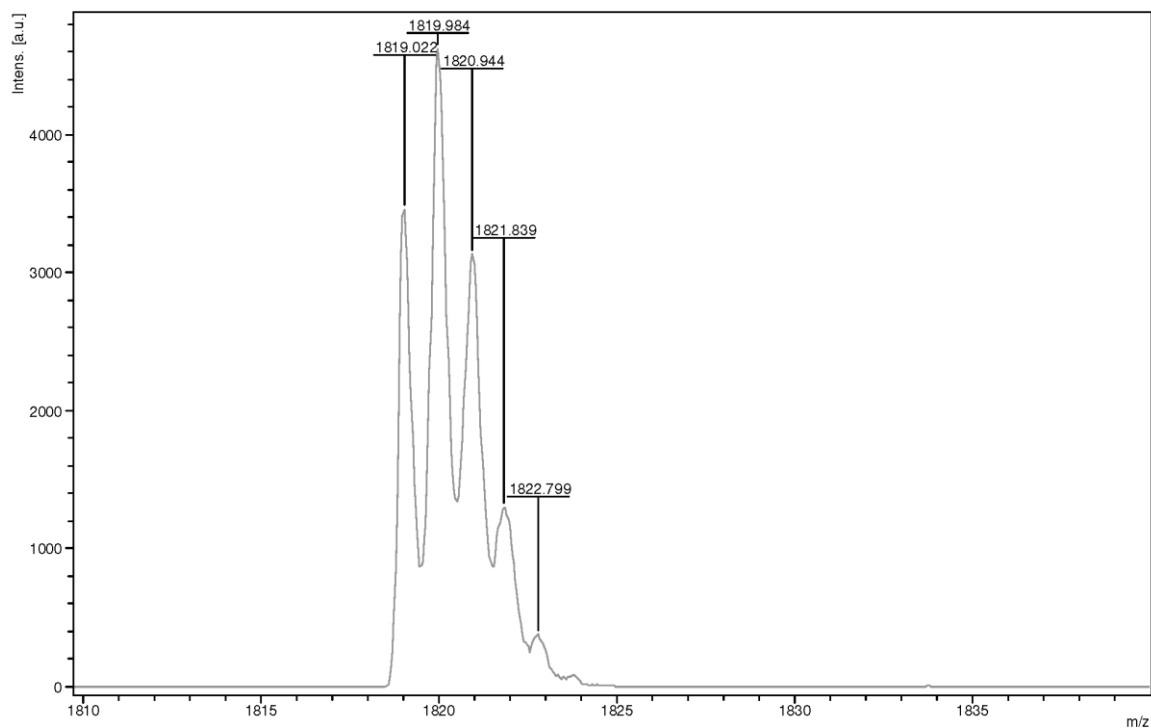
COSY Spectrum of OPE5 Precursor (8):NOESY Spectrum of OPE5 Precursor (8):

Aromatic region of the NOESY Spectrum of OPE5 Precursor (8):ROESY Spectrum of OPE5 Precursor (8):

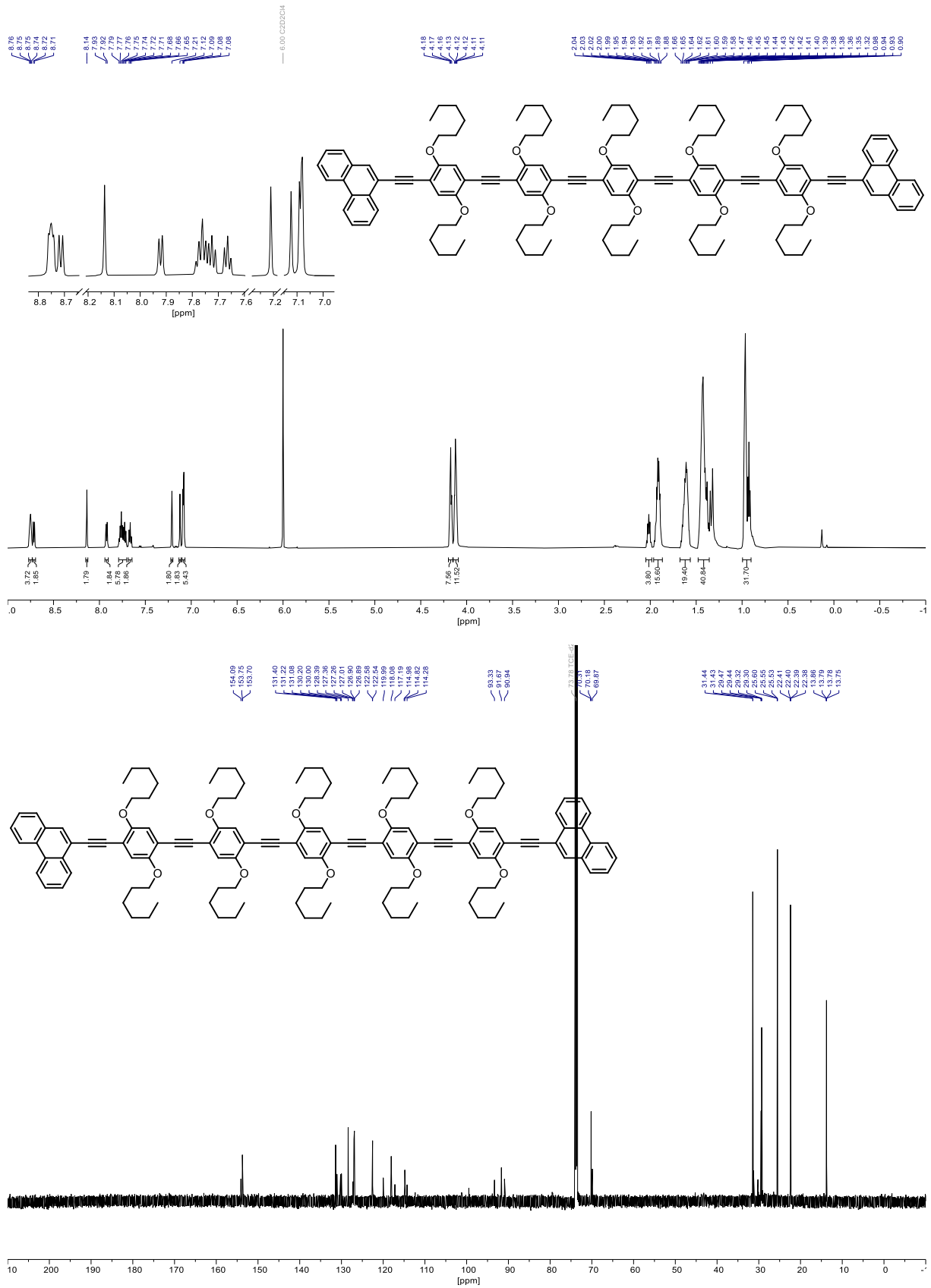
MALDI-ToF-MS (RP, DCTB) Spectrum of OPE5 Precursor (8):

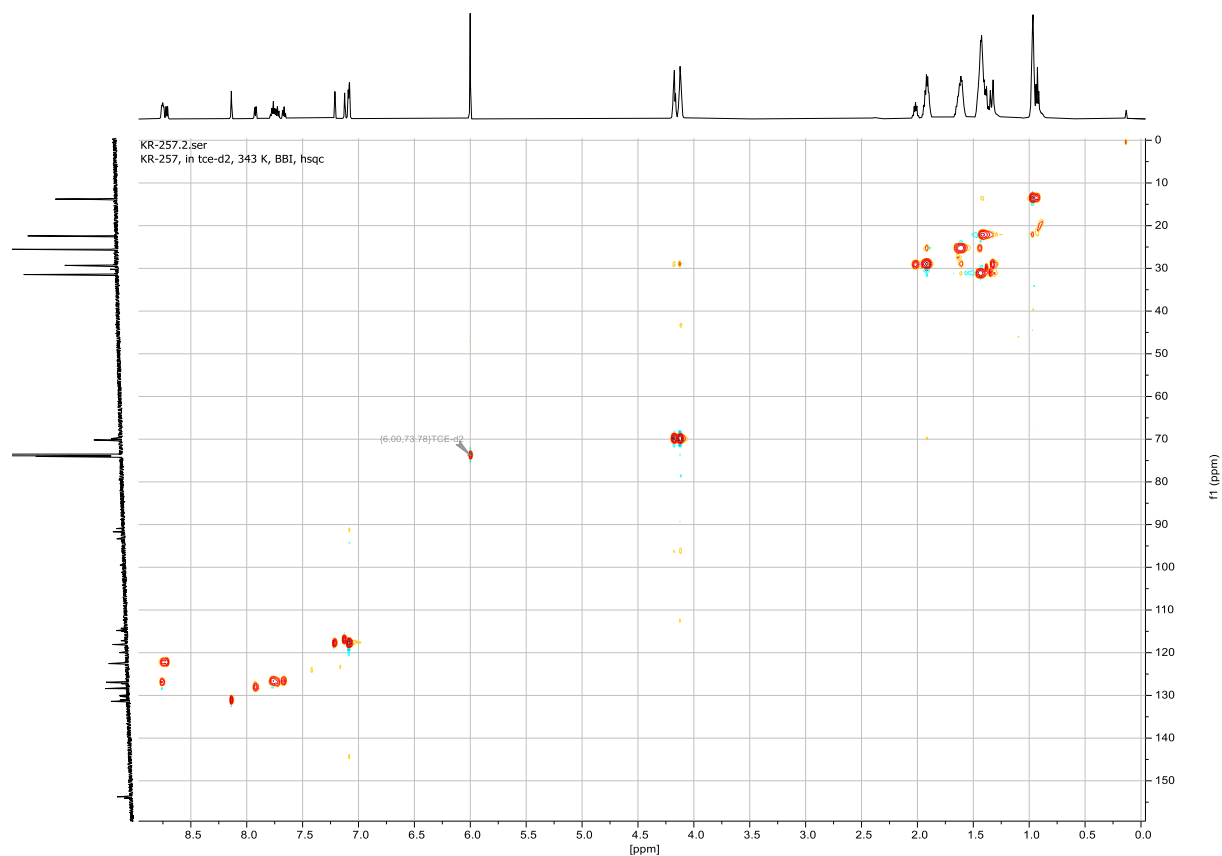
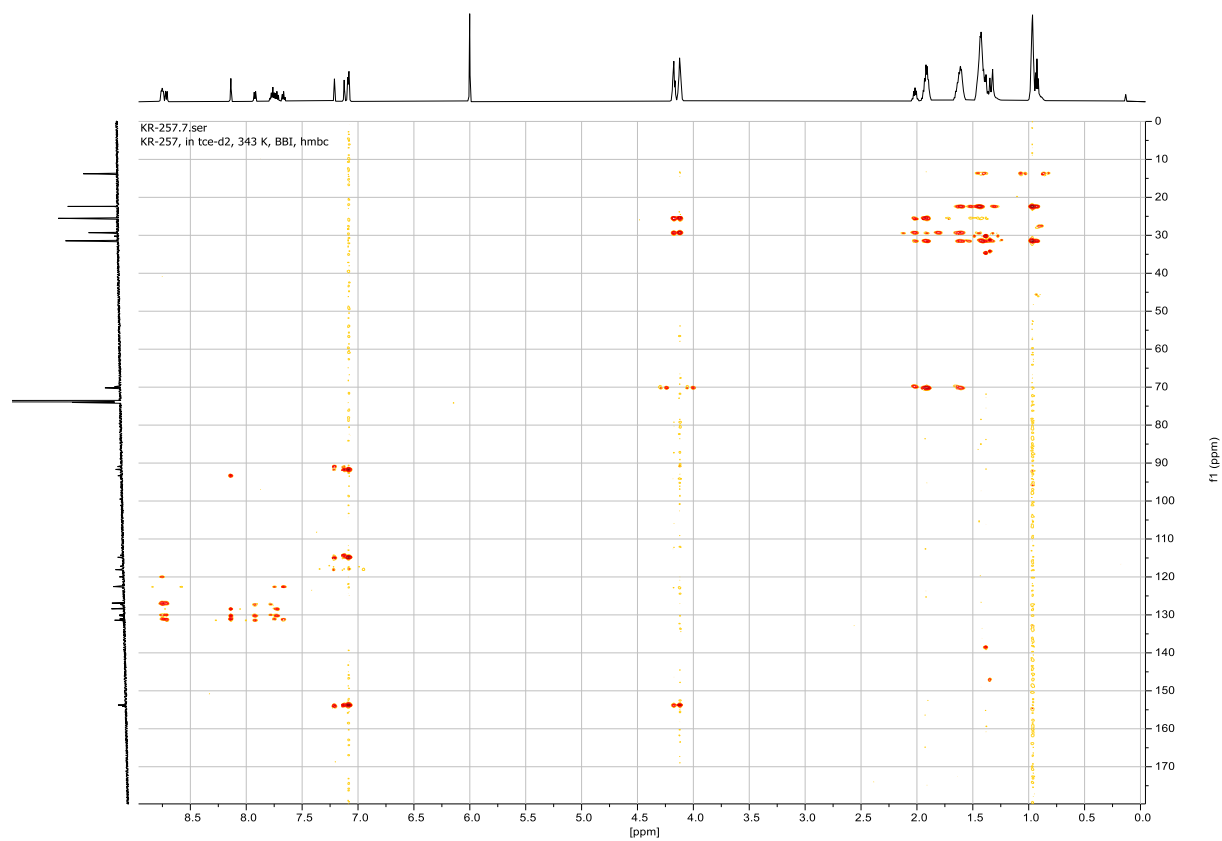


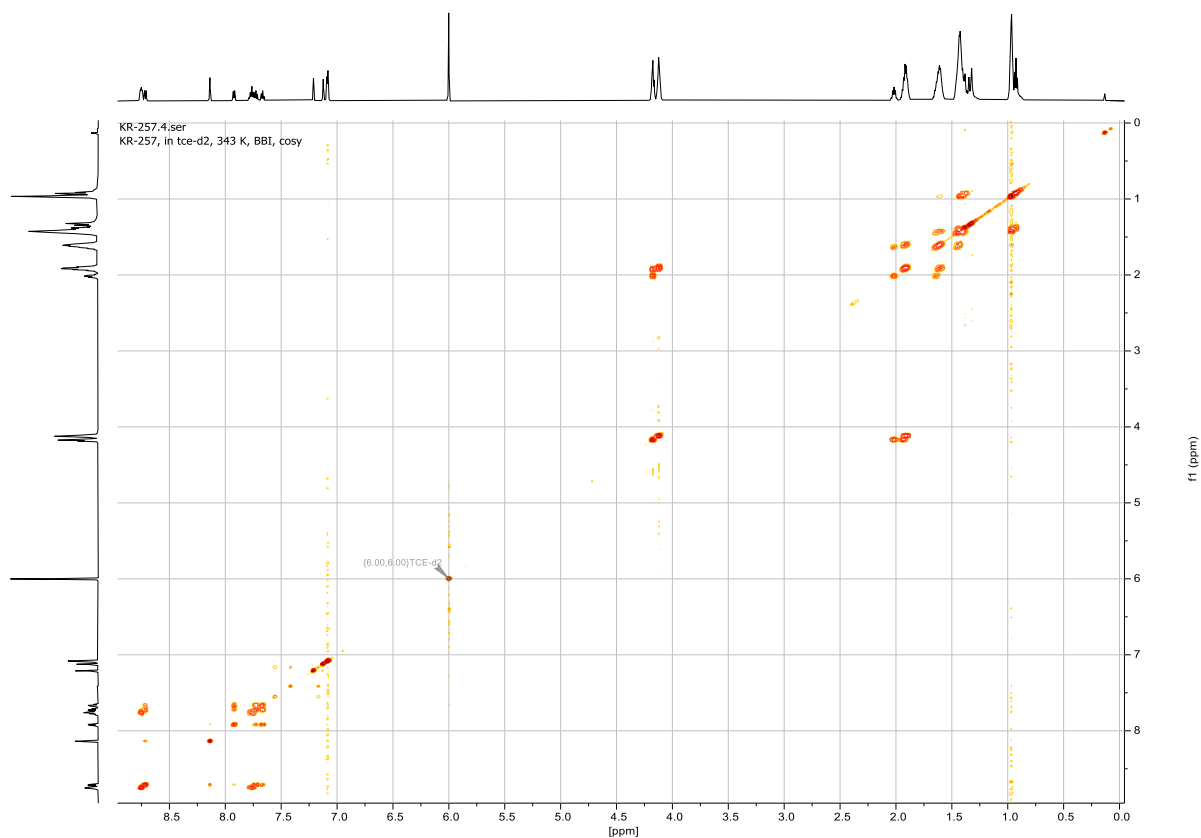
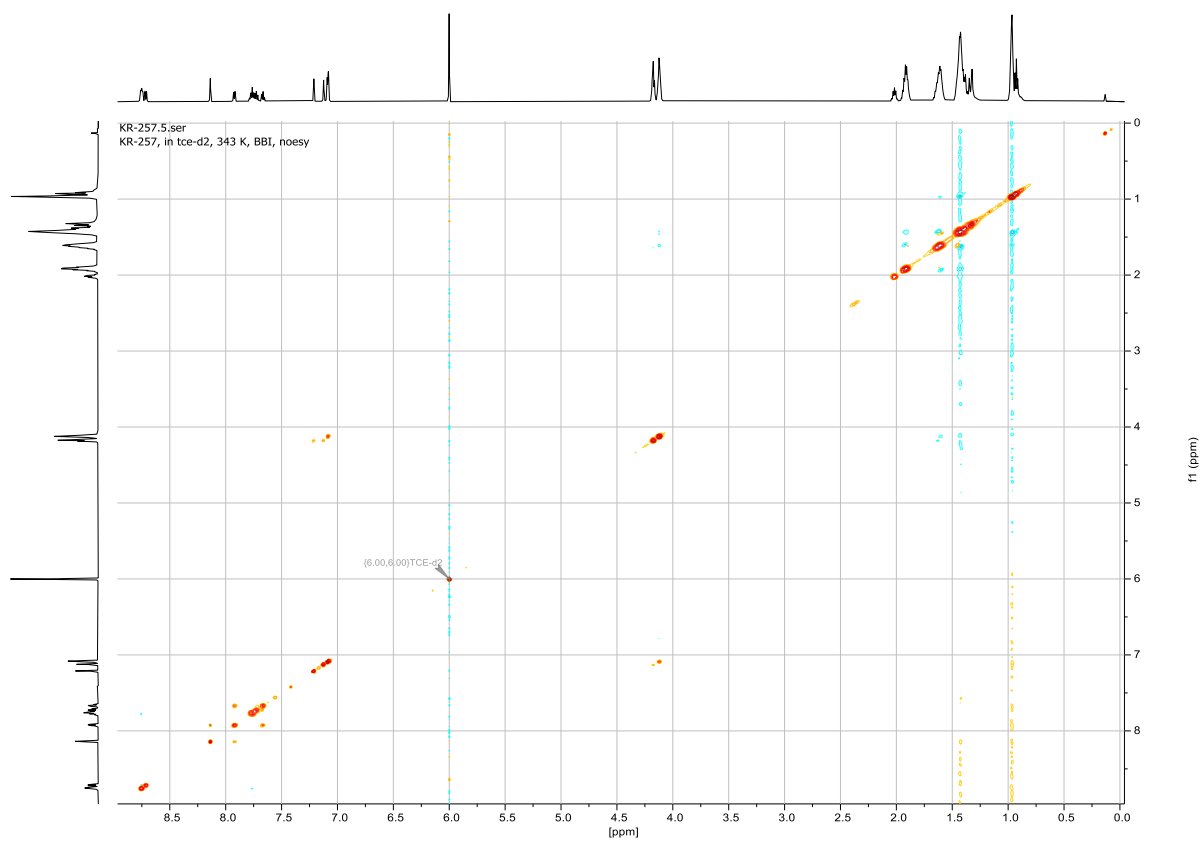
Zoom in of MALDI-ToF-MS (RP, DCTB) Spectrum of OPE5 Precursor (8):

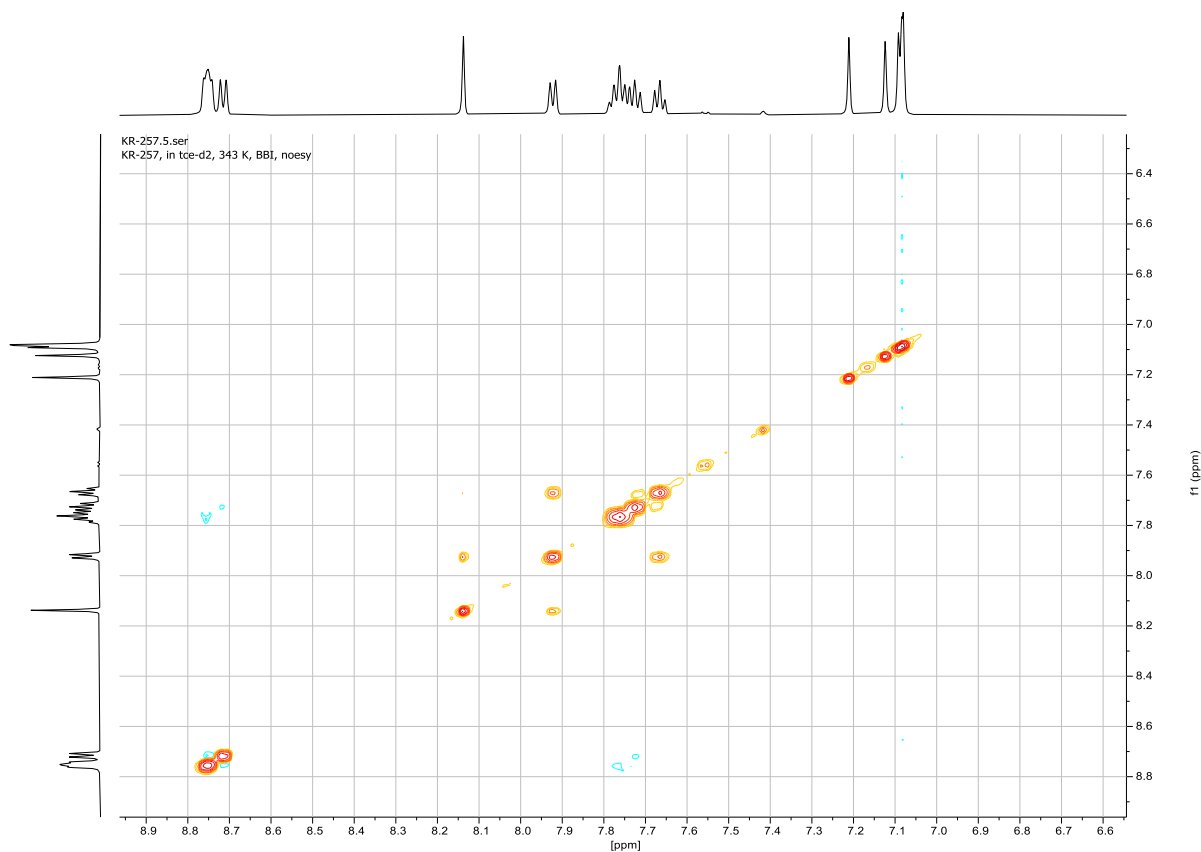
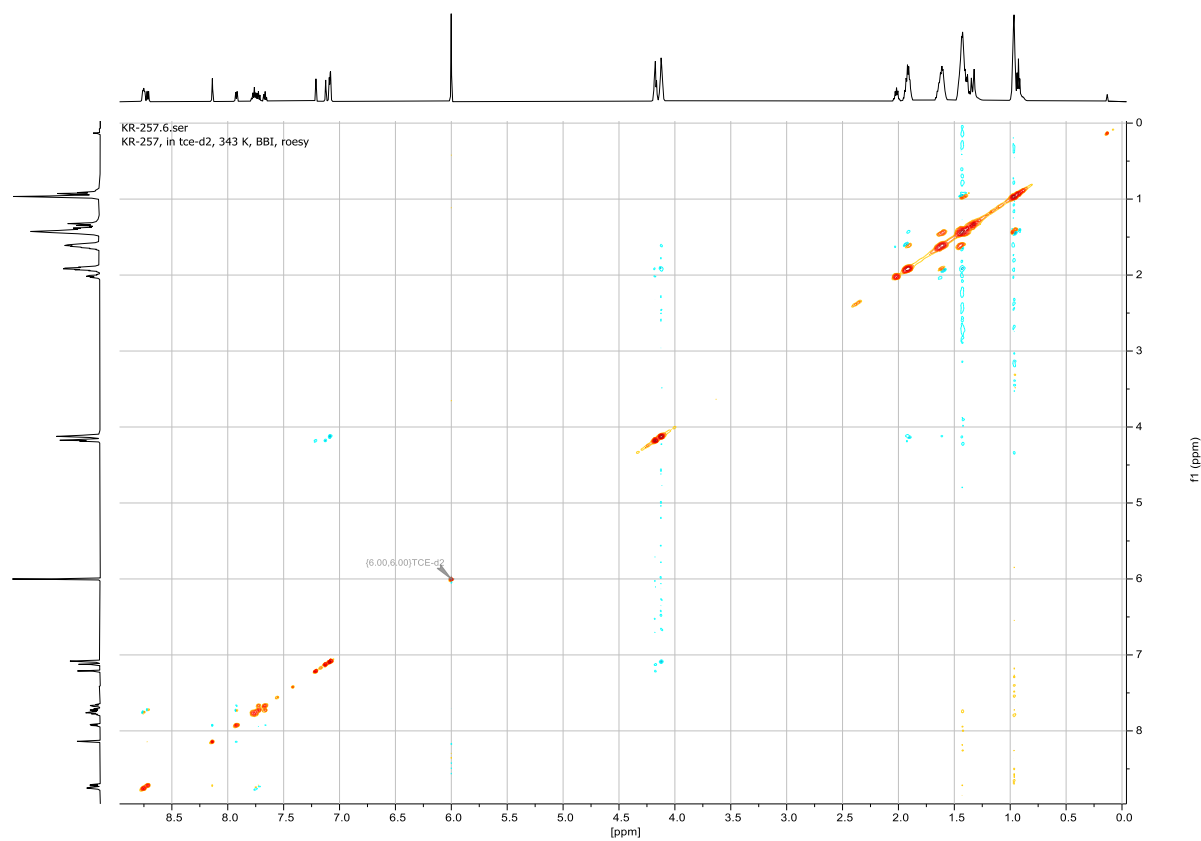


^1H , $^{13}\text{C}\{^1\text{H}\}$, 2D (600 MHz, TCE-d₂, 343 K) NMR and MALDI-MS Spectra of OPE5 Reference (27):

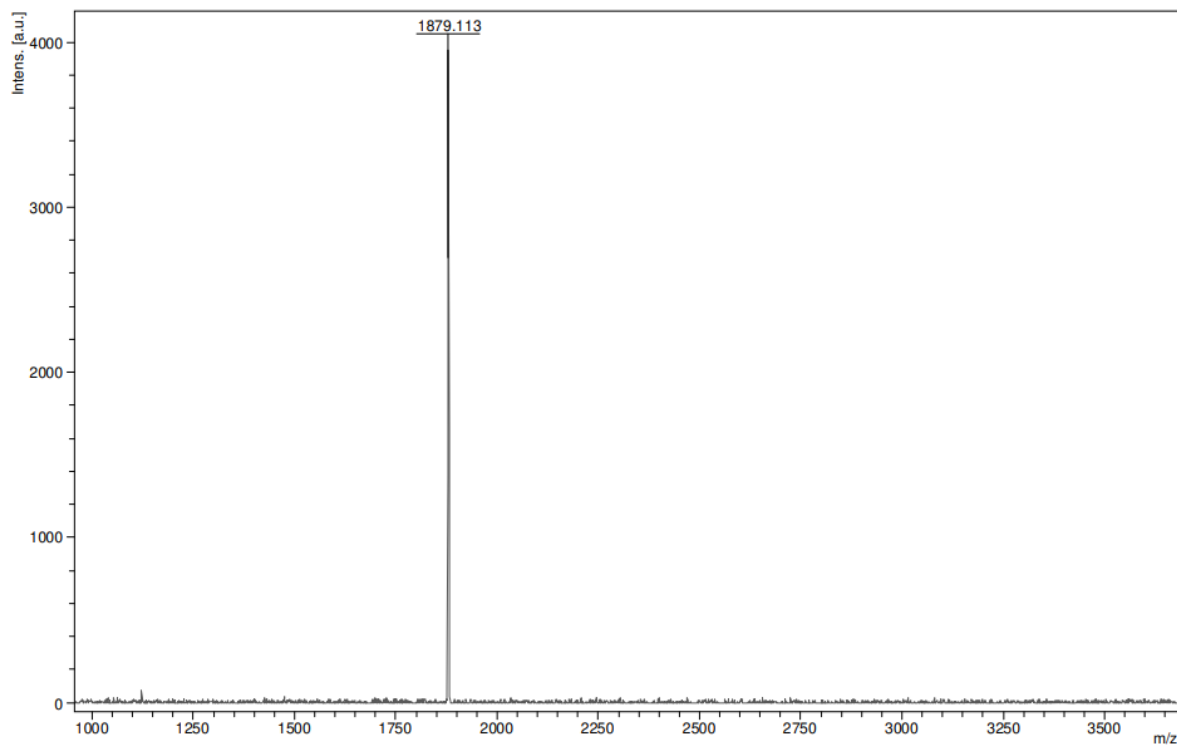


HSQC Spectrum of OPE5 Reference (27):**HMBC Spectrum of OPE5 Reference (27):**

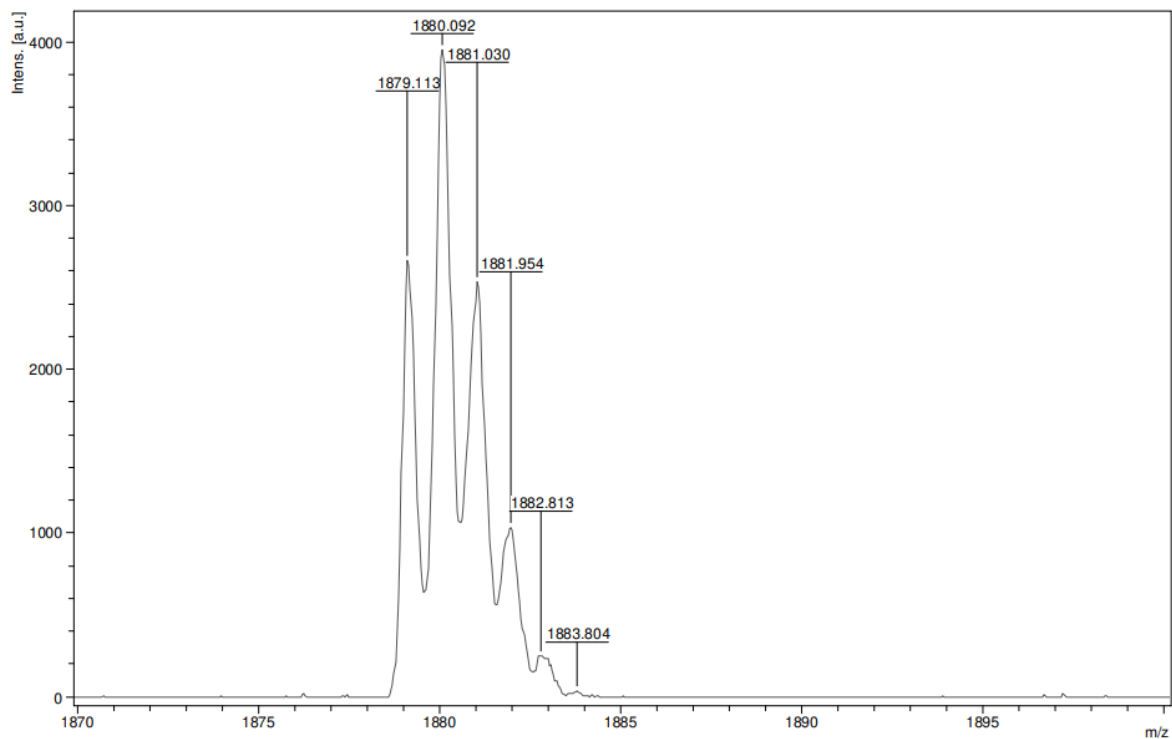
COSY Spectrum of OPE5 Reference (27):**NOESY Spectrum of OPE5 Reference (27):**

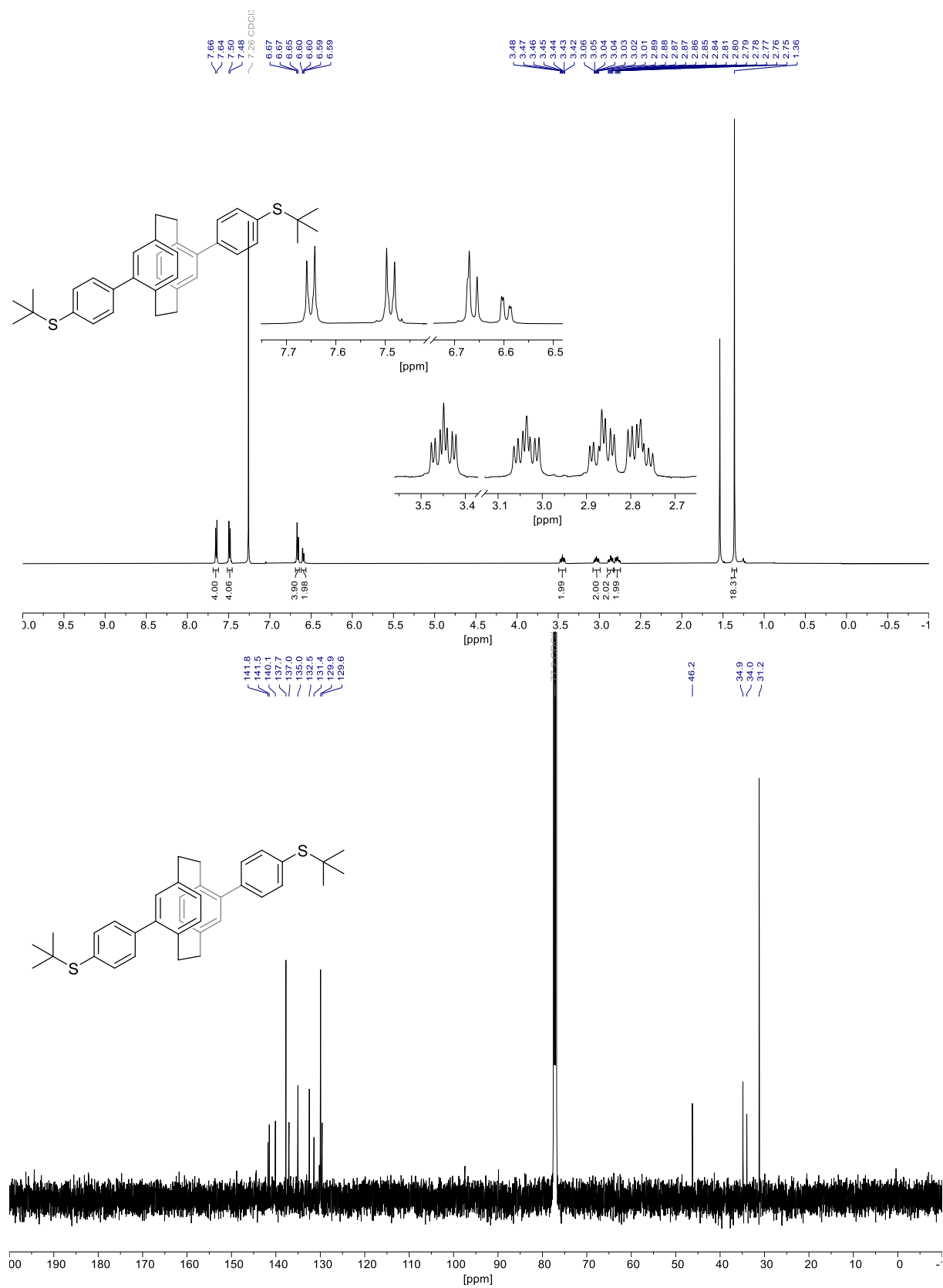
Aromatic region of the NOESY Spectrum of OPE5 Reference (27):**ROESY Spectrum of OPE5 Reference (27):**

MALDI-ToF-MS (RP, DCTB) Spectrum of OPE5 Reference (27):



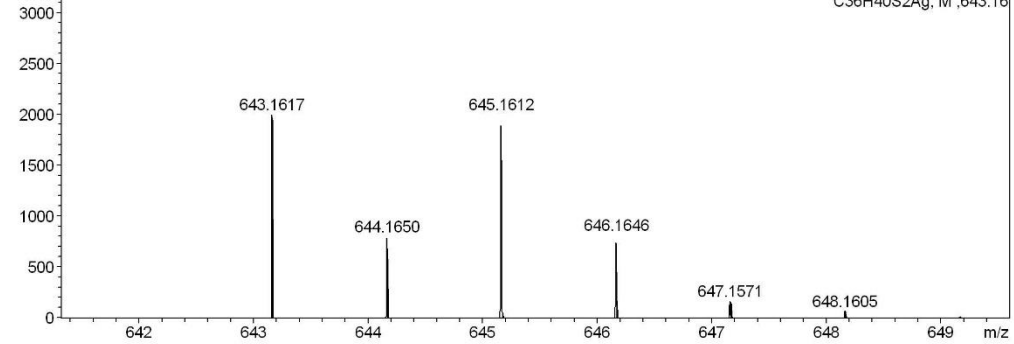
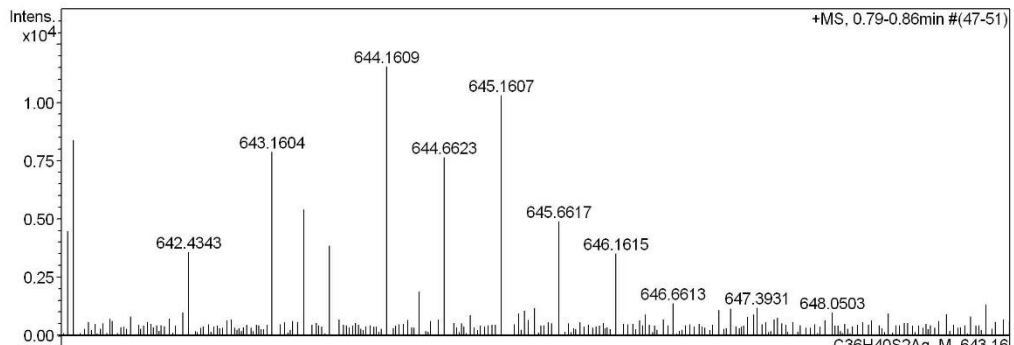
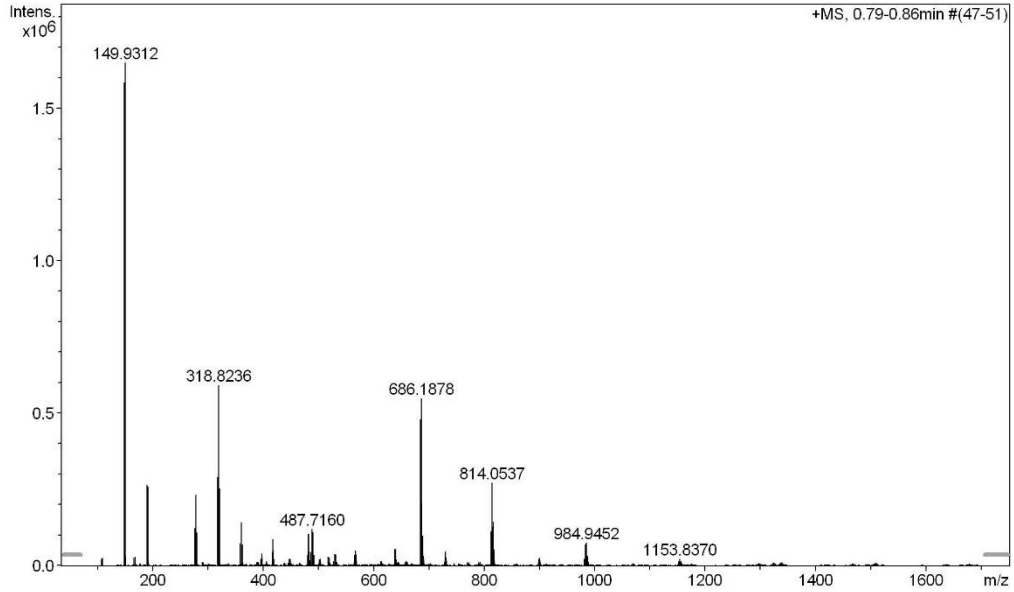
Zoom in of MALDI-ToF-MS (RP, DCTB) Spectrum of OPE5 Reference (27):



^1H , $^{13}\text{C}\{^1\text{H}\}$ (500/126 MHz, CDCl_3) NMR and HR-ESI-MS Spectra of *ps-para-para* StBu PCP:

High Resolution Mass Spectrometry Report

Sample Name **KR-262** Instrument **maXis 4G**
Comment **in MeOH+ AgNO3 (1mM)** Method **22 Direct_pos_mid.m**



 High Resolution Mass Spectrometry Report

Measured m/z vs. theoretical m/z

| Meas. m/z | # | Formula | Score | m/z | err [mDa] | err [ppm] | mSigma | rdb | e ⁻ Conf | z |
|-----------|---|------------------|--------|----------|-----------|-----------|--------|------|---------------------|----|
| 643.1604 | 1 | C 36 H 40 Ag S 2 | 100.00 | 643.1617 | 1.3 | 2.0 | 258.3 | 16.5 | even | 1+ |

Mass list

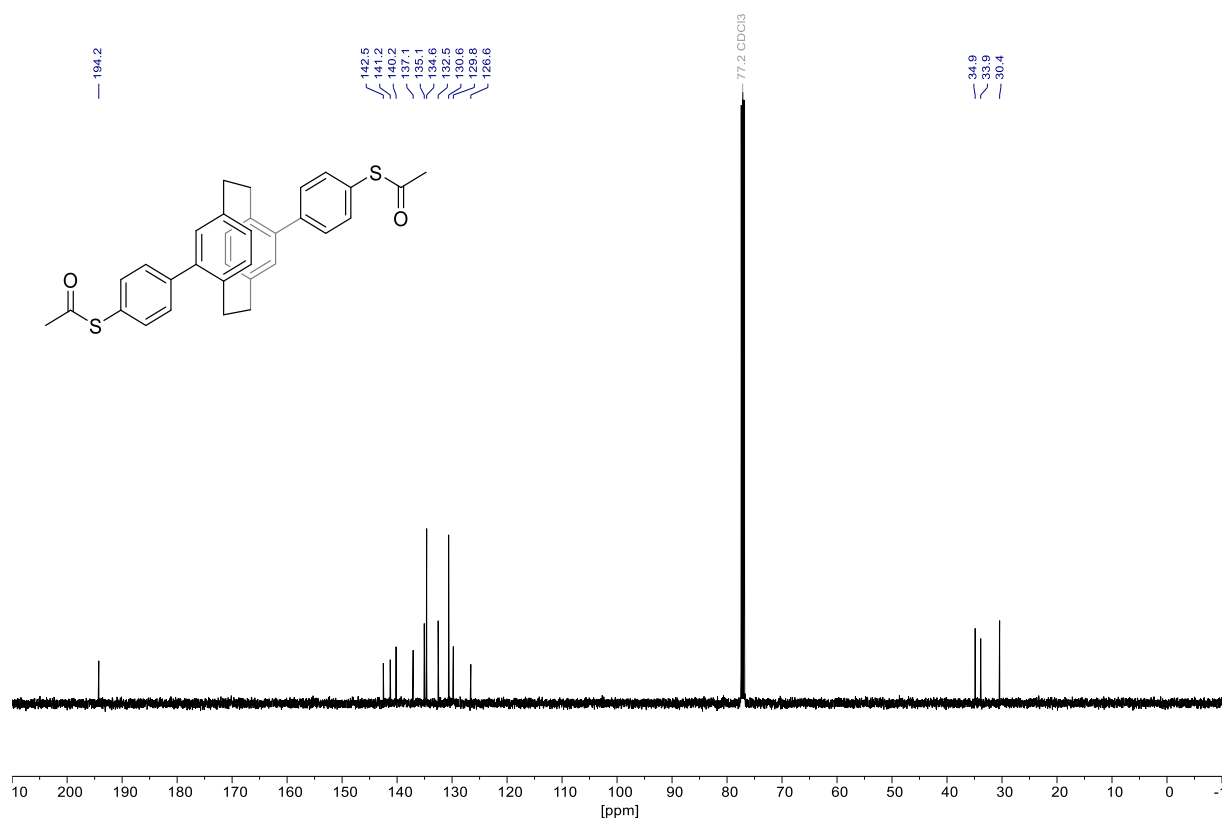
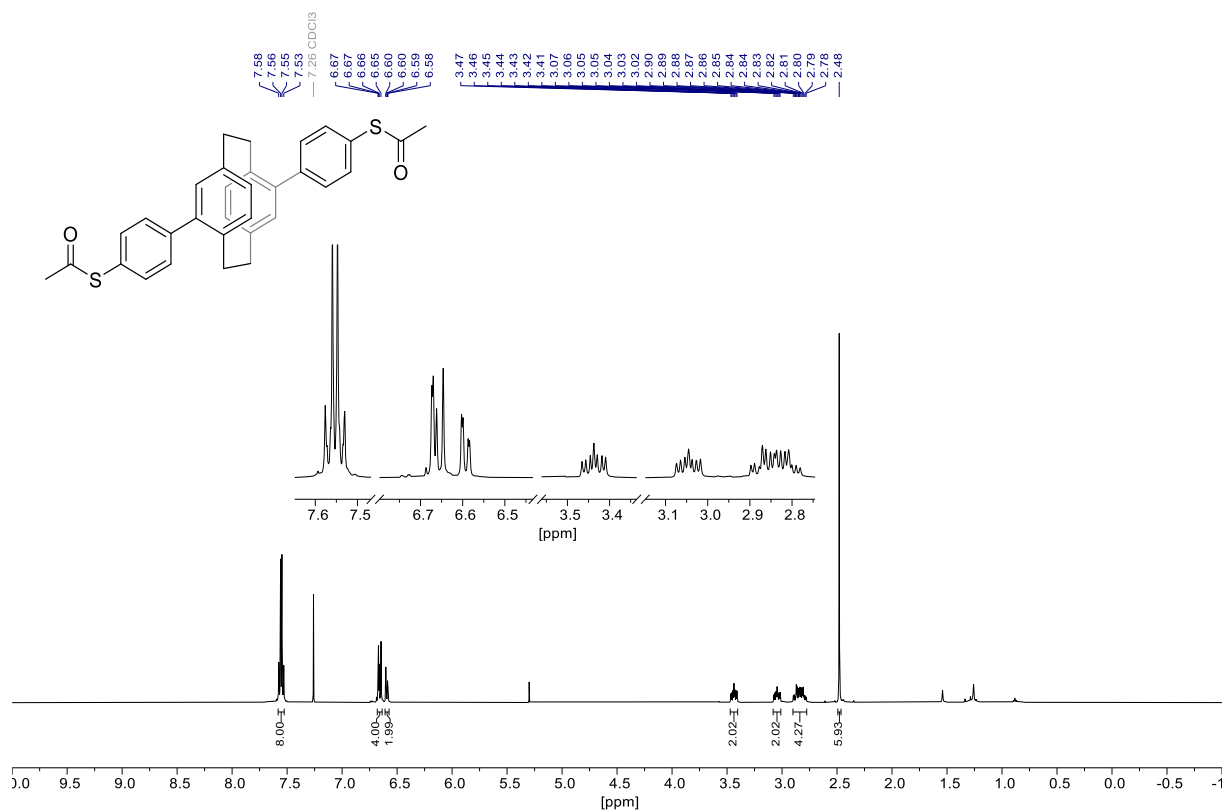
| # | m/z | I % | I |
|----|----------|-------|---------|
| 1 | 106.9052 | 1.2 | 20279 |
| 2 | 108.9048 | 1.4 | 23458 |
| 3 | 147.9315 | 96.0 | 1581629 |
| 4 | 148.9343 | 1.6 | 26334 |
| 5 | 149.9312 | 100.0 | 1647778 |
| 6 | 150.9339 | 1.7 | 28649 |
| 7 | 165.9418 | 1.6 | 25731 |
| 8 | 167.9415 | 1.7 | 27880 |
| 9 | 188.9575 | 16.0 | 263703 |
| 10 | 189.9602 | 0.8 | 13354 |
| 11 | 190.9572 | 15.6 | 257458 |
| 12 | 275.7969 | 7.4 | 121156 |
| 13 | 277.7967 | 14.0 | 230062 |
| 14 | 279.7962 | 6.5 | 107139 |
| 15 | 316.8237 | 17.6 | 290533 |
| 16 | 318.8236 | 35.9 | 591526 |
| 17 | 320.8230 | 15.2 | 250711 |
| 18 | 357.8499 | 4.4 | 72285 |
| 19 | 359.8499 | 8.6 | 141120 |
| 20 | 361.8494 | 4.1 | 66776 |
| 21 | 395.5457 | 1.3 | 20663 |
| 22 | 396.5457 | 2.4 | 39104 |
| 23 | 397.0472 | 1.1 | 18085 |
| 24 | 397.5456 | 1.5 | 24121 |
| 25 | 405.5510 | 0.8 | 13571 |
| 26 | 416.0588 | 2.5 | 41310 |
| 27 | 416.5606 | 1.2 | 19402 |
| 28 | 417.0589 | 5.1 | 84232 |
| 29 | 417.5602 | 2.4 | 38866 |
| 30 | 418.0588 | 3.0 | 50053 |
| 31 | 418.5600 | 1.3 | 21243 |
| 32 | 446.6891 | 1.3 | 21215 |
| 33 | 448.6888 | 1.2 | 20346 |
| 34 | 479.9921 | 2.1 | 33840 |
| 35 | 480.4938 | 0.9 | 14740 |
| 36 | 480.9922 | 6.2 | 102317 |
| 37 | 481.4935 | 2.7 | 44129 |
| 38 | 481.9921 | 6.2 | 101927 |
| 39 | 482.4933 | 2.7 | 44896 |
| 40 | 482.9919 | 2.6 | 42563 |
| 41 | 483.4932 | 1.0 | 16473 |
| 42 | 485.7161 | 2.6 | 43245 |
| 43 | 487.7160 | 7.2 | 117873 |
| 44 | 489.7158 | 6.6 | 108685 |
| 45 | 491.7152 | 2.0 | 33477 |
| 46 | 501.5051 | 1.2 | 19699 |
| 47 | 502.5052 | 1.2 | 20438 |
| 48 | 517.2947 | 1.6 | 26448 |
| 49 | 519.2945 | 1.6 | 25673 |
| 50 | 526.7423 | 0.8 | 13289 |
| 51 | 528.7423 | 2.2 | 37020 |
| 52 | 530.7422 | 2.1 | 34571 |
| 53 | 565.4383 | 2.0 | 33729 |
| 54 | 565.9395 | 0.9 | 14453 |
| 55 | 566.4384 | 3.0 | 48686 |
| 56 | 566.9396 | 1.3 | 22132 |
| 57 | 567.4383 | 2.2 | 35497 |
| 58 | 567.9397 | 0.9 | 14124 |
| 59 | 612.4247 | 0.8 | 13127 |
| 60 | 637.3733 | 3.2 | 53324 |
| 61 | 638.3763 | 1.3 | 20631 |
| 62 | 639.3734 | 3.2 | 52899 |

 High Resolution Mass Spectrometry Report

| # | m/z | I % | I |
|-----|-----------|------|--------|
| 63 | 640.3765 | 1.2 | 19479 |
| 64 | 658.6079 | 0.8 | 13811 |
| 65 | 684.1878 | 29.0 | 478559 |
| 66 | 685.1907 | 11.7 | 192316 |
| 67 | 686.1878 | 33.2 | 547250 |
| 68 | 687.1903 | 12.4 | 205018 |
| 69 | 688.1882 | 5.8 | 95824 |
| 70 | 689.1889 | 1.8 | 29673 |
| 71 | 690.1874 | 1.2 | 19446 |
| 72 | 728.6070 | 2.2 | 35542 |
| 73 | 729.1084 | 1.8 | 29596 |
| 74 | 729.6072 | 2.7 | 45273 |
| 75 | 730.1081 | 1.9 | 31479 |
| 76 | 730.6076 | 1.5 | 25081 |
| 77 | 731.1080 | 0.9 | 14453 |
| 78 | 812.0534 | 6.7 | 110291 |
| 79 | 813.0553 | 4.1 | 67761 |
| 80 | 813.5548 | 1.4 | 22506 |
| 81 | 814.0537 | 16.4 | 270196 |
| 82 | 814.5546 | 2.0 | 33543 |
| 83 | 815.0555 | 7.5 | 124269 |
| 84 | 815.5542 | 1.5 | 25068 |
| 85 | 816.0535 | 8.6 | 141865 |
| 86 | 817.0554 | 3.1 | 50592 |
| 87 | 818.0534 | 1.0 | 16277 |
| 88 | 898.4994 | 1.3 | 20785 |
| 89 | 899.0009 | 1.0 | 16009 |
| 90 | 899.4999 | 1.4 | 23565 |
| 91 | 900.0006 | 1.0 | 16252 |
| 92 | 900.5002 | 0.9 | 15574 |
| 93 | 980.9450 | 1.3 | 21169 |
| 94 | 982.9453 | 4.2 | 68581 |
| 95 | 983.9475 | 2.2 | 35753 |
| 96 | 984.9452 | 4.5 | 73890 |
| 97 | 985.9476 | 1.8 | 30258 |
| 98 | 986.9451 | 1.6 | 27076 |
| 99 | 1153.8370 | 1.2 | 20362 |
| 100 | 1155.8374 | 0.9 | 14825 |

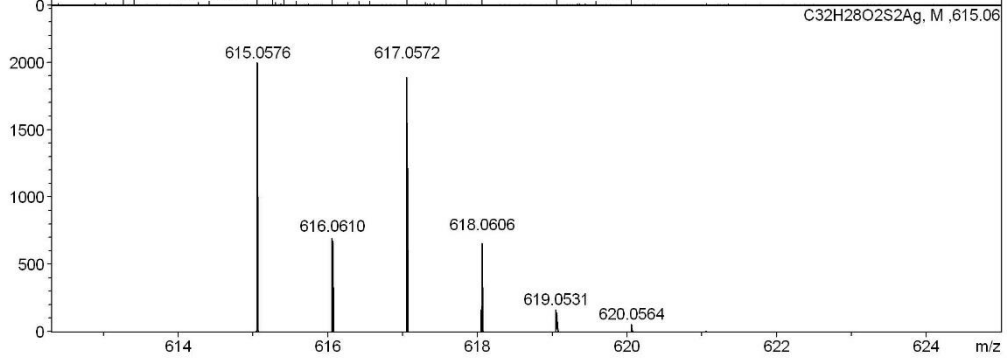
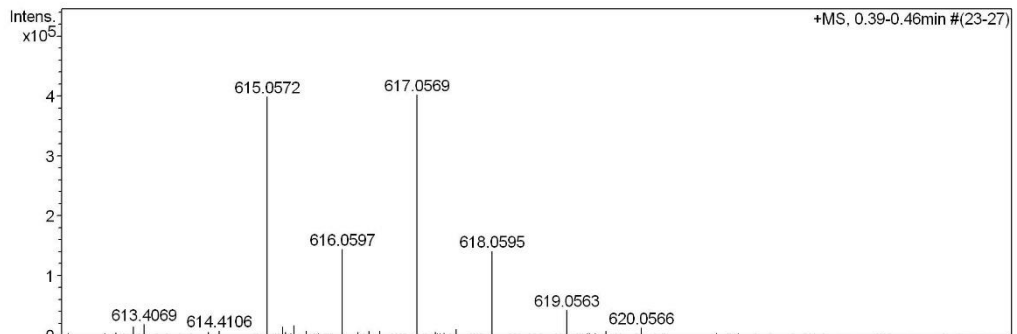
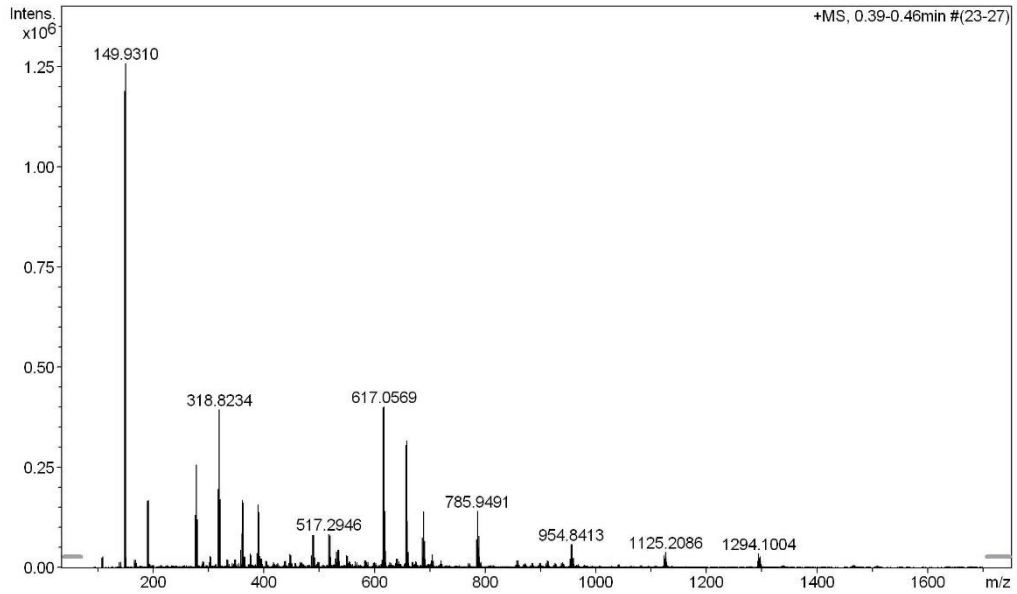
Acquisition Parameter

| | | | | | | |
|-------------------|------------------------------|----------------|---------------------------------------|----------------|--------------|-----------|
| General | Fore Vacuum | 2.48e+000 mBar | High Vacuum | 1.14e-007 mBar | Source Type | ESI |
| | Scan Begin | 75 m/z | Scan End | 1700 m/z | Ion Polarity | Positive |
| Source | Set Nebulizer | 0.4 Bar | Set Capillary | 3600 V | Set Dry Gas | 4.0 l/min |
| | Set Dry Heater | 180 °C | Set End Plate Offset | -500 V | | |
| Quadrupole | Set Ion Energy (MS only) | 4.0 eV | | | | |
| Coll. Cell | Collision Energy | 8.0 eV | Set Collision Cell RF | 350.0 Vpp | | 100.0 Vpp |
| Ion Cooler | Set Ion Cooler Transfer Time | 75.0 µs | Set Ion Cooler Pre Pulse Storage Time | | | 10.0 µs |

^1H , $^{13}\text{C}\{^1\text{H}\}$ (500/126 MHz, CDCl_3) NMR and HR-ESI-MS Spectra of *ps-para-para* PCP:

High Resolution Mass Spectrometry Report

| | | | |
|-------------|----------------------------------|------------|---------------------|
| Sample Name | KR-263 | Instrument | maXis 4G |
| Comment | in MeOH+ AgNO ₃ (1mM) | Method | 22 Direct_pos_mid.m |



High Resolution Mass Spectrometry Report

Measured m/z vs. theoretical m/z

| Meas. m/z | # | Formula | Score | m/z | err [mDa] | err [ppm] | mSigma | rdb | e ⁻ Conf | z |
|-----------|---|----------------------|--------|----------|-----------|-----------|--------|------|---------------------|----|
| 615.0572 | 1 | C 32 H 28 Ag O 2 S 2 | 100.00 | 615.0576 | 0.4 | 0.7 | 32.6 | 18.5 | even | 1+ |

Mass list

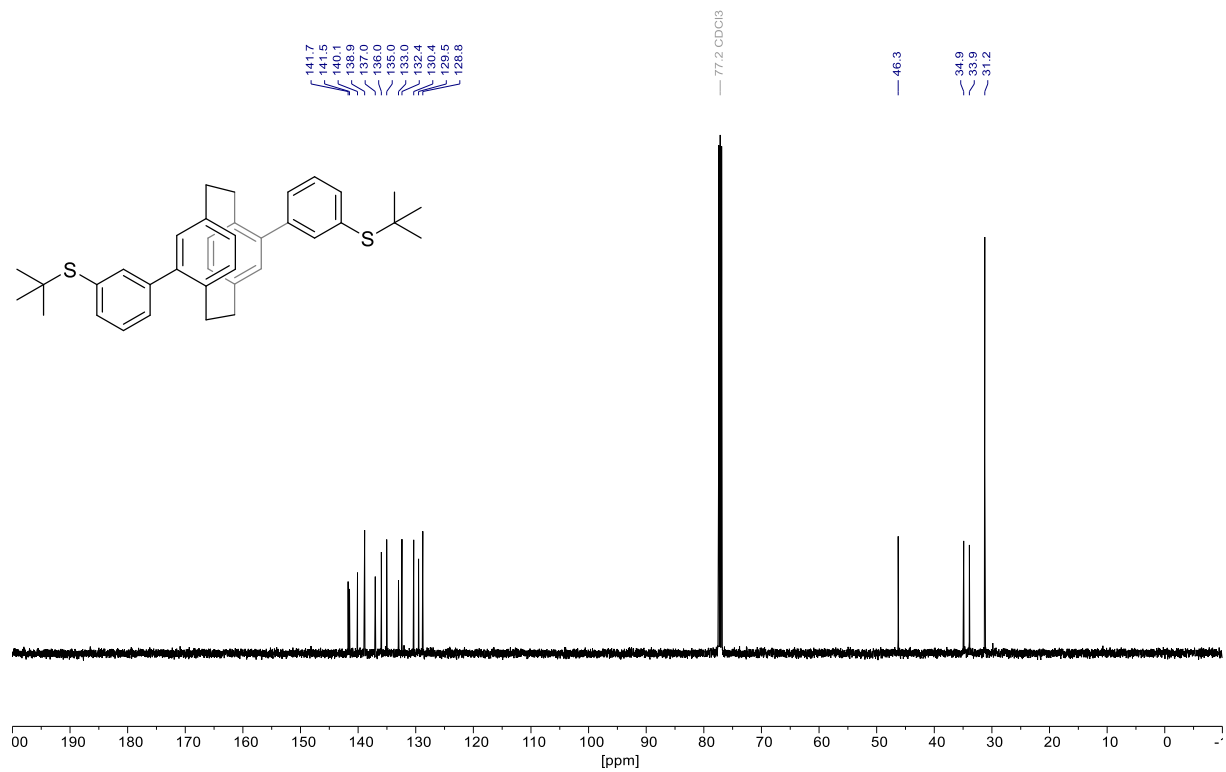
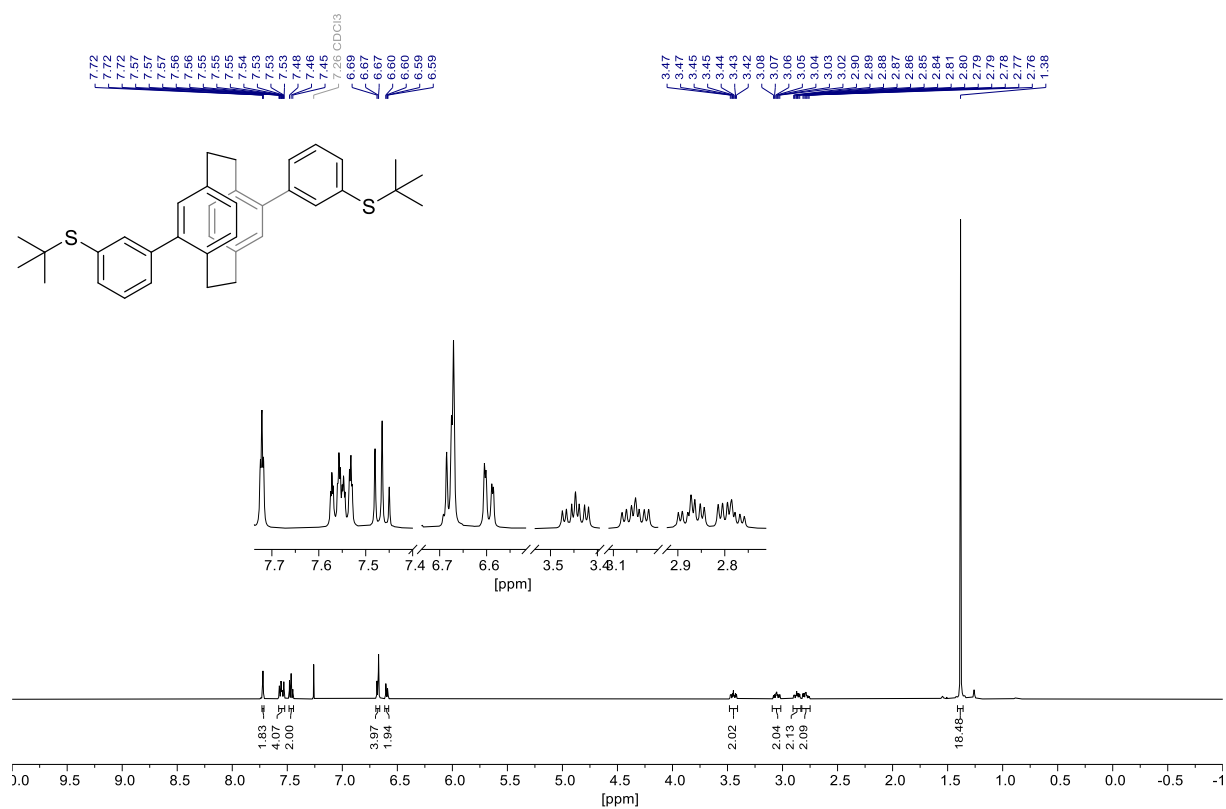
| # | m/z | I % | I |
|----|----------|-------|---------|
| 1 | 106.9050 | 1.9 | 23660 |
| 2 | 108.9047 | 2.2 | 27107 |
| 3 | 147.9313 | 94.4 | 1187570 |
| 4 | 148.9341 | 1.6 | 20441 |
| 5 | 149.9310 | 100.0 | 1257418 |
| 6 | 150.9336 | 1.9 | 24031 |
| 7 | 165.9417 | 1.5 | 18271 |
| 8 | 167.9414 | 1.4 | 18231 |
| 9 | 188.9573 | 13.2 | 165848 |
| 10 | 190.9570 | 13.2 | 166362 |
| 11 | 275.7968 | 10.4 | 130154 |
| 12 | 277.7966 | 20.3 | 255627 |
| 13 | 279.7961 | 9.5 | 119021 |
| 14 | 301.9602 | 2.2 | 27662 |
| 15 | 303.9597 | 2.1 | 26151 |
| 16 | 316.8234 | 15.5 | 194421 |
| 17 | 318.8234 | 31.3 | 393288 |
| 18 | 320.8227 | 13.4 | 169063 |
| 19 | 333.0967 | 1.5 | 19119 |
| 20 | 335.0968 | 1.5 | 18864 |
| 21 | 347.1123 | 1.6 | 19538 |
| 22 | 349.1124 | 1.5 | 19008 |
| 23 | 357.8497 | 3.4 | 43273 |
| 24 | 359.8495 | 6.7 | 83930 |
| 25 | 361.1284 | 13.4 | 168196 |
| 26 | 361.8491 | 3.2 | 40623 |
| 27 | 362.1314 | 2.4 | 30025 |
| 28 | 363.1283 | 12.8 | 160916 |
| 29 | 364.1313 | 2.1 | 26811 |
| 30 | 365.1430 | 2.1 | 26027 |
| 31 | 375.1436 | 2.7 | 33855 |
| 32 | 377.1435 | 2.4 | 30415 |
| 33 | 387.1435 | 2.8 | 34911 |
| 34 | 389.1592 | 12.4 | 156450 |
| 35 | 390.1626 | 2.3 | 29459 |
| 36 | 391.1595 | 10.9 | 137667 |
| 37 | 392.1627 | 2.3 | 28500 |
| 38 | 394.1494 | 1.8 | 22241 |
| 39 | 396.1492 | 1.7 | 21480 |
| 40 | 446.6889 | 2.6 | 32334 |
| 41 | 448.6886 | 2.4 | 30221 |
| 42 | 485.7158 | 2.4 | 29742 |
| 43 | 487.7157 | 6.4 | 80979 |
| 44 | 489.7153 | 6.4 | 79962 |
| 45 | 491.7148 | 1.9 | 24464 |
| 46 | 517.2946 | 6.6 | 82573 |
| 47 | 518.2978 | 2.2 | 27284 |
| 48 | 519.2945 | 6.3 | 79621 |
| 49 | 520.2973 | 2.1 | 26123 |
| 50 | 528.7421 | 1.7 | 21944 |
| 51 | 530.7417 | 1.7 | 21017 |
| 52 | 531.2588 | 3.1 | 39050 |
| 53 | 533.2590 | 3.1 | 39554 |
| 54 | 533.2885 | 3.5 | 44438 |
| 55 | 534.2902 | 1.3 | 16864 |
| 56 | 535.2891 | 3.4 | 42412 |
| 57 | 549.2845 | 2.5 | 31056 |
| 58 | 551.2844 | 2.2 | 27751 |
| 59 | 581.2738 | 1.4 | 17629 |
| 60 | 583.2738 | 1.3 | 16908 |
| 61 | 613.4069 | 1.4 | 18135 |
| 62 | 615.0572 | 31.7 | 397975 |

 High Resolution Mass Spectrometry Report

| # | m/z | I % | I |
|-----|-----------|------|--------|
| 63 | 616.0597 | 11.4 | 143376 |
| 64 | 617.0569 | 31.9 | 400812 |
| 65 | 618.0595 | 11.2 | 140297 |
| 66 | 619.0563 | 3.3 | 41228 |
| 67 | 639.4242 | 1.7 | 21173 |
| 68 | 641.4300 | 1.6 | 20709 |
| 69 | 656.0835 | 24.3 | 304927 |
| 70 | 657.0861 | 8.8 | 110302 |
| 71 | 658.0834 | 25.1 | 315449 |
| 72 | 659.0858 | 9.1 | 114072 |
| 73 | 660.0834 | 3.0 | 38024 |
| 74 | 686.1875 | 5.9 | 74801 |
| 75 | 687.1904 | 2.1 | 26466 |
| 76 | 688.1876 | 11.1 | 139410 |
| 77 | 689.1900 | 3.7 | 46245 |
| 78 | 690.1875 | 5.2 | 65533 |
| 79 | 691.1900 | 1.7 | 21000 |
| 80 | 704.1818 | 2.5 | 31264 |
| 81 | 783.9490 | 5.5 | 69485 |
| 82 | 784.9517 | 2.1 | 26566 |
| 83 | 785.9491 | 11.1 | 139938 |
| 84 | 786.9515 | 4.0 | 49781 |
| 85 | 787.9487 | 6.2 | 78496 |
| 86 | 788.9512 | 2.2 | 27129 |
| 87 | 857.0797 | 1.4 | 17593 |
| 88 | 952.8408 | 1.6 | 20109 |
| 89 | 954.8413 | 4.6 | 57478 |
| 90 | 955.8442 | 1.7 | 21908 |
| 91 | 956.8412 | 4.6 | 57220 |
| 92 | 957.8440 | 1.7 | 21398 |
| 93 | 958.8405 | 1.8 | 22896 |
| 94 | 1123.2074 | 2.3 | 29368 |
| 95 | 1124.2112 | 1.7 | 21832 |
| 96 | 1125.2086 | 3.0 | 38040 |
| 97 | 1126.2109 | 2.0 | 25531 |
| 98 | 1294.1004 | 2.8 | 34667 |
| 99 | 1295.1035 | 1.9 | 23566 |
| 100 | 1296.1016 | 2.1 | 26333 |

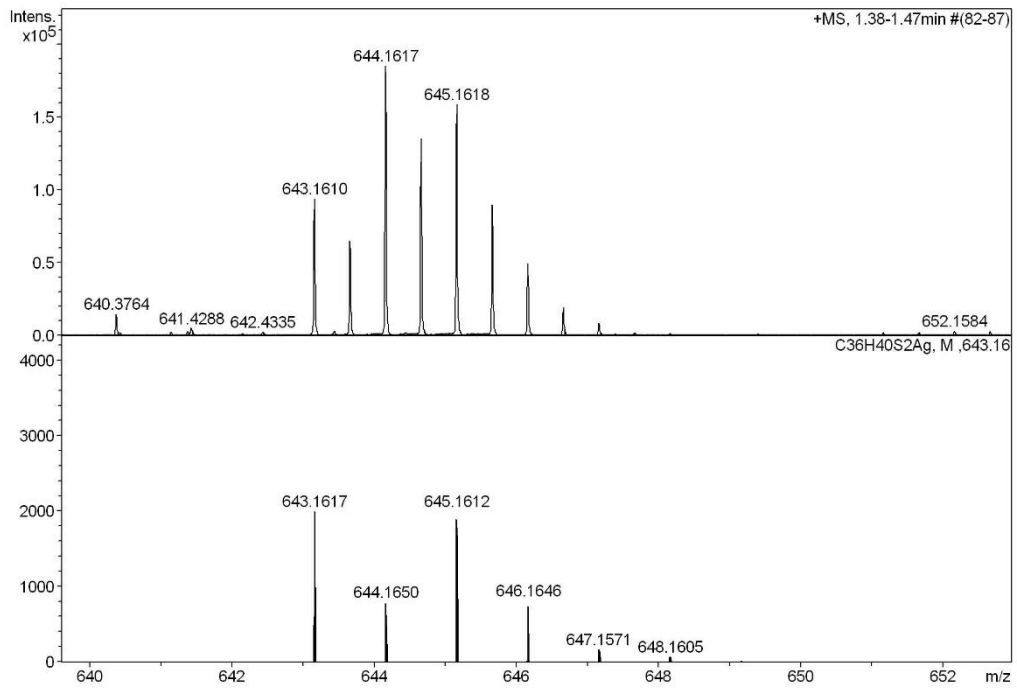
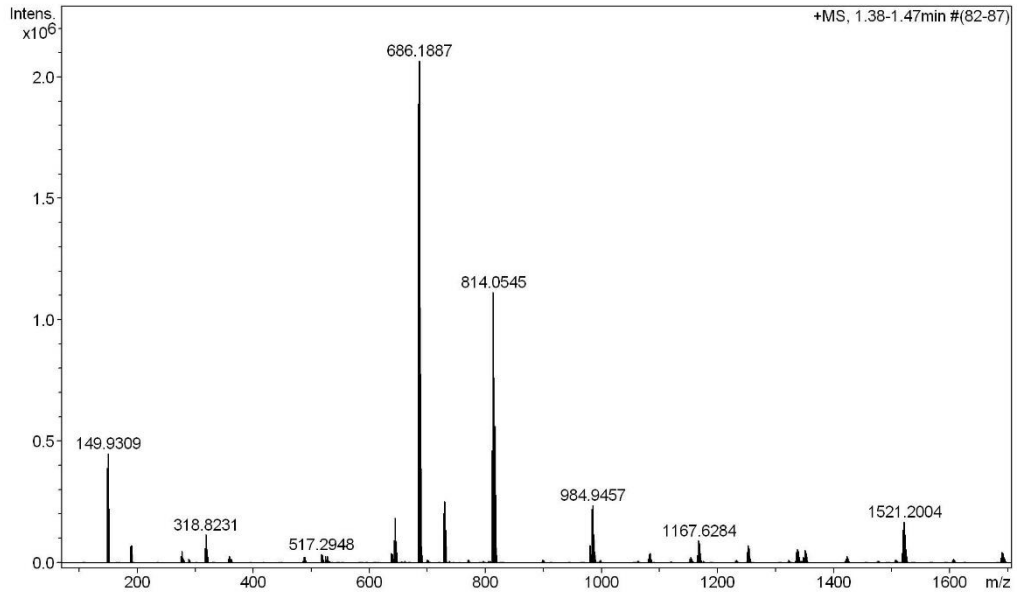
Acquisition Parameter

| | | | | | | |
|-------------------|------------------------------|----------------|---------------------------------------|----------------|--------------|-----------|
| General | Fore Vacuum | 2.48e+000 mBar | High Vacuum | 1.14e-007 mBar | Source Type | ESI |
| | Scan Begin | 75 m/z | Scan End | 1700 m/z | Ion Polarity | Positive |
| Source | Set Nebulizer | 0.4 Bar | Set Capillary | 3600 V | Set Dry Gas | 4.0 l/min |
| | Set Dry Heater | 180 °C | Set End Plate Offset | -500 V | | |
| Quadrupole | Set Ion Energy (MS only) | 4.0 eV | | | | |
| Coll. Cell | Collision Energy | 8.0 eV | Set Collision Cell RF | 350.0 Vpp | | 100.0 Vpp |
| Ion Cooler | Set Ion Cooler Transfer Time | 75.0 µs | Set Ion Cooler Pre Pulse Storage Time | | | 10.0 µs |

^1H , $^{13}\text{C}\{^1\text{H}\}$ (500/126 MHz, CDCl_3) NMR and HR-ESI-MS Spectra of *ps*-*para*-*meta* StBu PCP:

High Resolution Mass Spectrometry Report

Sample Name **KR-168** Instrument **maXis 4G**
Comment **in MeOH+ AgNO3 (1mM)** Method **22 Direct_pos_mid.m**



High Resolution Mass Spectrometry Report

Measured m/z vs. theoretical m/z

| Meas. m/z | # | Formula | Score | m/z | err [mDa] | err [ppm] | mSigma | rdB | e ⁻ Conf | z |
|-----------|---|------------------|--------|----------|-----------|-----------|--------|------|---------------------|----|
| 643.1610 | 1 | C 36 H 40 Ag S 2 | 100.00 | 643.1617 | 0.7 | 1.1 | 293.0 | 16.5 | even | 1+ |

Mass list

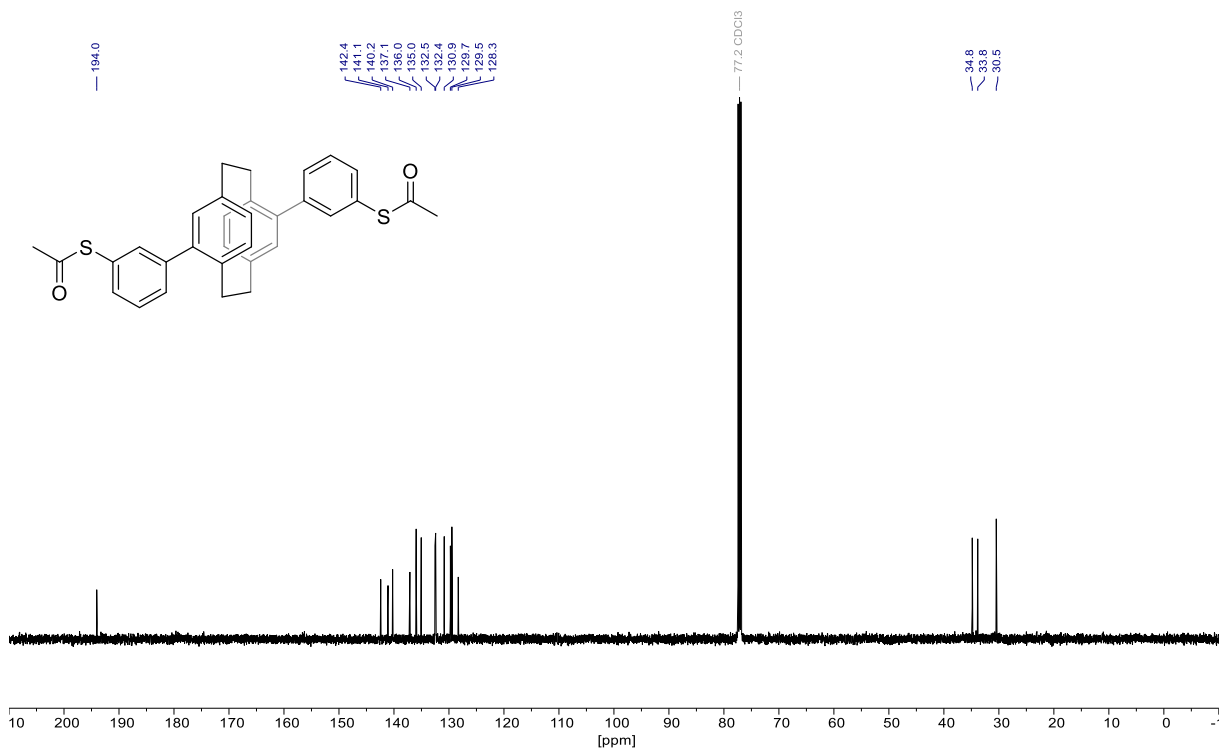
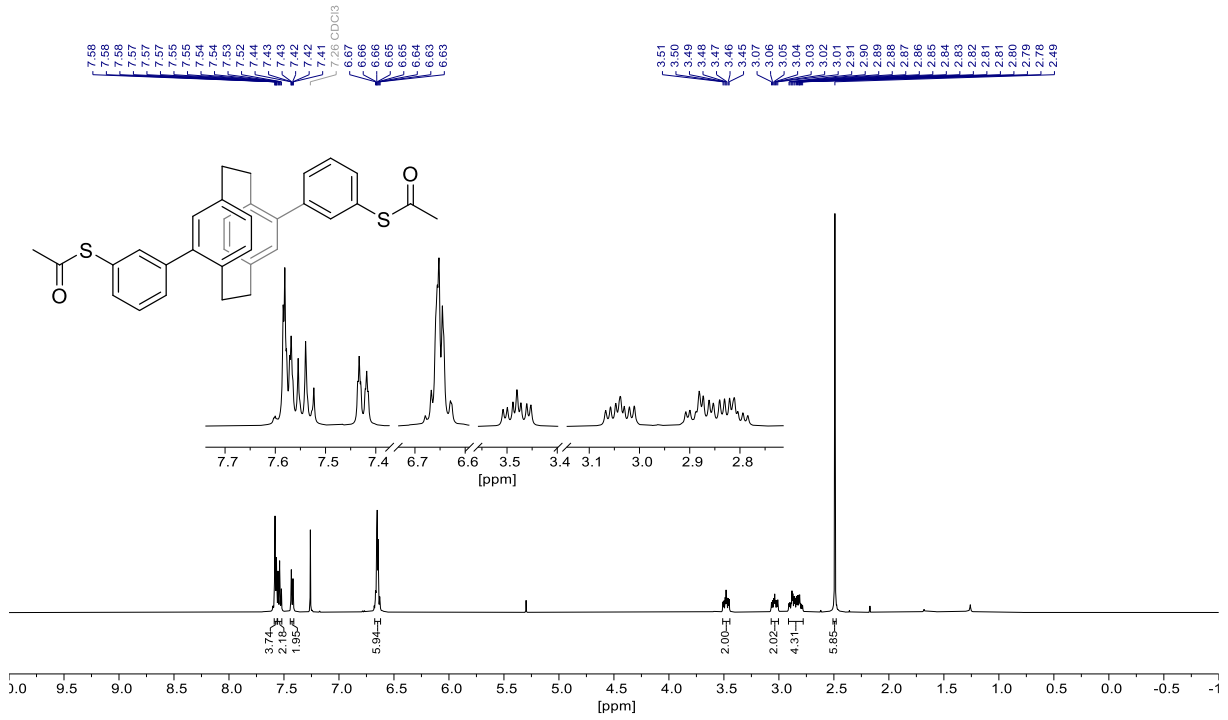
| # | m/z | I % | I |
|----|-----------|-------|---------|
| 1 | 147.9312 | 18.8 | 389268 |
| 2 | 149.9309 | 21.8 | 451621 |
| 3 | 188.9573 | 3.4 | 70271 |
| 4 | 190.9569 | 3.5 | 71482 |
| 5 | 275.7966 | 1.3 | 26828 |
| 6 | 277.7963 | 2.4 | 49709 |
| 7 | 316.8233 | 2.9 | 59523 |
| 8 | 318.8231 | 5.7 | 116904 |
| 9 | 320.8227 | 2.5 | 51865 |
| 10 | 359.8496 | 1.5 | 30367 |
| 11 | 517.2948 | 1.7 | 35064 |
| 12 | 519.2946 | 1.6 | 33150 |
| 13 | 525.2118 | 1.4 | 28896 |
| 14 | 527.2118 | 1.4 | 28663 |
| 15 | 637.3733 | 1.9 | 39343 |
| 16 | 639.3734 | 1.8 | 37374 |
| 17 | 643.1610 | 4.6 | 94388 |
| 18 | 643.6626 | 3.2 | 65222 |
| 19 | 644.1617 | 9.0 | 185578 |
| 20 | 644.6627 | 6.6 | 135848 |
| 21 | 645.1618 | 7.7 | 159043 |
| 22 | 645.6625 | 4.4 | 90336 |
| 23 | 646.1620 | 2.4 | 49784 |
| 24 | 684.1887 | 91.4 | 1890306 |
| 25 | 685.1914 | 34.9 | 722384 |
| 26 | 686.1887 | 100.0 | 2068073 |
| 27 | 687.1910 | 37.8 | 781310 |
| 28 | 688.1890 | 11.2 | 232171 |
| 29 | 689.1885 | 3.3 | 68240 |
| 30 | 727.6072 | 3.0 | 61701 |
| 31 | 728.1089 | 2.4 | 50471 |
| 32 | 728.6080 | 9.9 | 204185 |
| 33 | 729.1092 | 7.4 | 152583 |
| 34 | 729.6083 | 12.2 | 252757 |
| 35 | 730.1091 | 8.4 | 174099 |
| 36 | 730.6083 | 6.7 | 137821 |
| 37 | 731.1089 | 3.7 | 77529 |
| 38 | 731.6082 | 1.9 | 38610 |
| 39 | 812.0542 | 22.5 | 464648 |
| 40 | 813.0566 | 10.1 | 208728 |
| 41 | 814.0545 | 54.0 | 1116478 |
| 42 | 814.5542 | 1.7 | 34172 |
| 43 | 815.0568 | 20.1 | 415004 |
| 44 | 815.5545 | 1.3 | 27161 |
| 45 | 816.0541 | 27.3 | 565402 |
| 46 | 817.0560 | 9.3 | 192527 |
| 47 | 818.0539 | 3.1 | 64765 |
| 48 | 980.9454 | 3.5 | 73172 |
| 49 | 981.9480 | 1.6 | 32870 |
| 50 | 982.9458 | 10.7 | 220944 |
| 51 | 983.9483 | 4.3 | 88879 |
| 52 | 984.9457 | 11.6 | 239374 |
| 53 | 985.9479 | 4.3 | 89671 |
| 54 | 986.9453 | 4.6 | 95619 |
| 55 | 987.9474 | 1.6 | 33557 |
| 56 | 1082.1818 | 1.8 | 37301 |
| 57 | 1082.6822 | 1.7 | 35271 |
| 58 | 1083.1822 | 1.9 | 39448 |
| 59 | 1083.6824 | 1.6 | 32867 |
| 60 | 1165.6273 | 1.4 | 28661 |
| 61 | 1166.1287 | 1.5 | 31878 |
| 62 | 1166.6280 | 3.3 | 68509 |

 High Resolution Mass Spectrometry Report

| # | m/z | I % | I |
|-----|-----------|-----|--------|
| 63 | 1167.1289 | 3.4 | 71073 |
| 64 | 1167.6284 | 4.5 | 92192 |
| 65 | 1168.1291 | 4.0 | 81940 |
| 66 | 1168.6287 | 3.7 | 75907 |
| 67 | 1169.1287 | 2.7 | 55121 |
| 68 | 1169.6286 | 1.9 | 38691 |
| 69 | 1251.0740 | 2.1 | 43450 |
| 70 | 1251.5746 | 2.1 | 44035 |
| 71 | 1252.0743 | 3.5 | 72679 |
| 72 | 1252.5750 | 3.3 | 67484 |
| 73 | 1253.0750 | 3.5 | 73035 |
| 74 | 1253.5752 | 2.9 | 60775 |
| 75 | 1254.0745 | 2.4 | 49800 |
| 76 | 1254.5745 | 1.7 | 34763 |
| 77 | 1336.5209 | 2.2 | 44598 |
| 78 | 1337.0211 | 2.1 | 43377 |
| 79 | 1337.5204 | 2.8 | 57168 |
| 80 | 1338.0212 | 2.3 | 48449 |
| 81 | 1338.5205 | 2.3 | 47646 |
| 82 | 1339.0212 | 1.7 | 36012 |
| 83 | 1339.5213 | 1.4 | 28790 |
| 84 | 1350.3075 | 2.6 | 53334 |
| 85 | 1351.3095 | 2.0 | 42288 |
| 86 | 1352.3077 | 2.1 | 42464 |
| 87 | 1353.3093 | 1.3 | 27181 |
| 88 | 1421.9673 | 1.3 | 26904 |
| 89 | 1517.1988 | 2.0 | 41485 |
| 90 | 1518.2023 | 1.7 | 35710 |
| 91 | 1519.1994 | 6.6 | 136915 |
| 92 | 1520.2019 | 5.3 | 108861 |
| 93 | 1521.2004 | 8.2 | 169619 |
| 94 | 1522.2019 | 5.7 | 118640 |
| 95 | 1523.2006 | 4.8 | 99479 |
| 96 | 1524.2012 | 2.7 | 56865 |
| 97 | 1525.2011 | 1.3 | 27609 |
| 98 | 1690.0927 | 2.2 | 46019 |
| 99 | 1691.0952 | 1.9 | 38978 |
| 100 | 1692.0936 | 2.0 | 41471 |

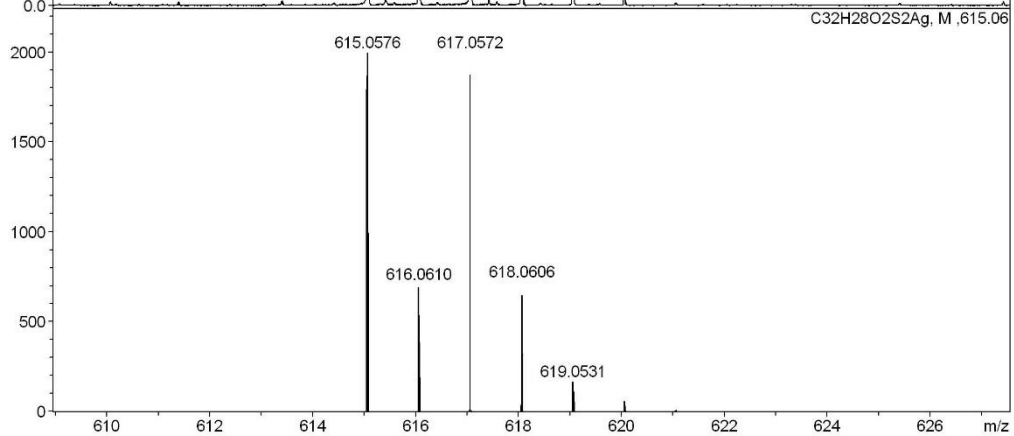
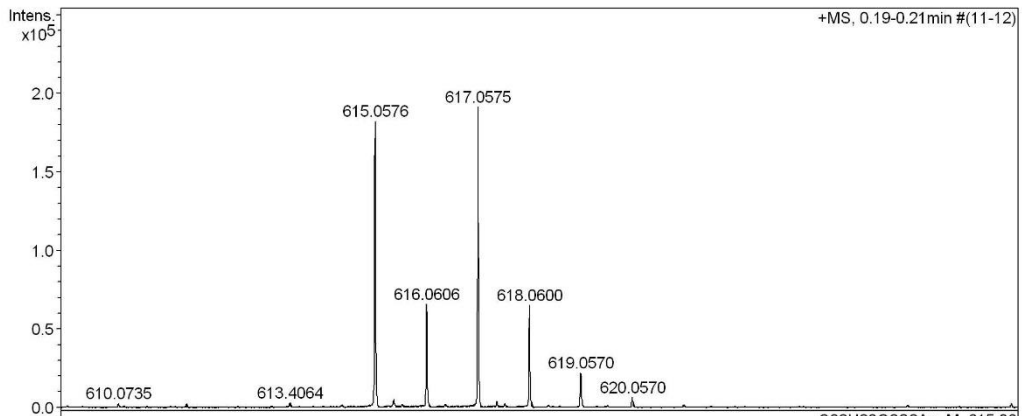
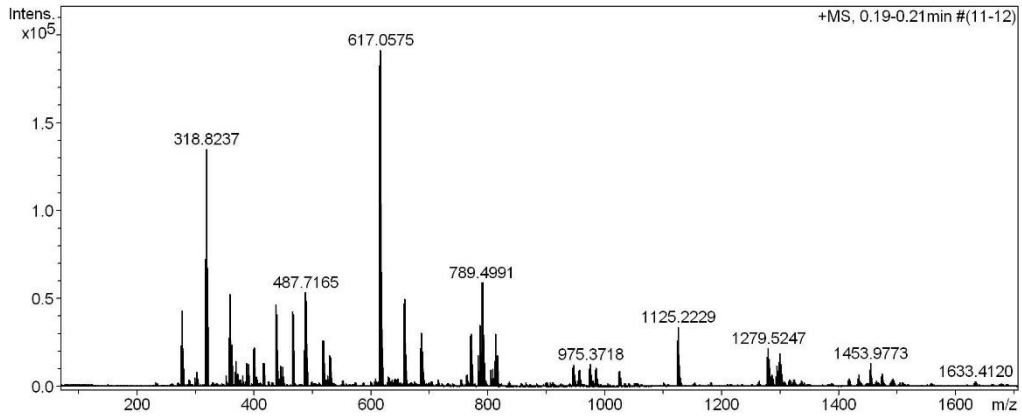
Acquisition Parameter

| | | | | | | |
|-------------------|------------------------------|----------------|---------------------------------------|----------------|--------------|-----------|
| General | Fore Vacuum | 2.48e+000 mBar | High Vacuum | 1.14e-007 mBar | Source Type | ESI |
| | Scan Begin | 75 m/z | Scan End | 1700 m/z | Ion Polarity | Positive |
| Source | Set Nebulizer | 0.4 Bar | Set Capillary | 3600 V | Set Dry Gas | 4.0 l/min |
| | Set Dry Heater | 180 °C | Set End Plate Offset | -500 V | | |
| Quadrupole | Set Ion Energy (MS only) | 4.0 eV | | | | |
| Coll. Cell | Collision Energy | 8.0 eV | Set Collision Cell RF | 350.0 Vpp | | 100.0 Vpp |
| Ion Cooler | Set Ion Cooler Transfer Time | 75.0 µs | Set Ion Cooler Pre Pulse Storage Time | | | 10.0 µs |

^1H , $^{13}\text{C}\{^1\text{H}\}$ (500/126 MHz, CDCl_3) NMR and HR-ESI-MS Spectra of *ps*-*para*-*meta* PCP:

High Resolution Mass Spectrometry Report

| | | | |
|-------------|-----------------------------------------------|------------|------------------------|
| Sample Name | Ksenia Reznikova / KR 178 | Instrument | maXis 4G |
| Comment | 10 ug / mL in DCM, analyzed in MeOH+AgNO3 5mM | Method | 23 Direct_pos_higher.m |



High Resolution Mass Spectrometry Report

Measured m/z vs. theoretical m/z

| Meas. m/z | # | Formula | Score | m/z | err [mDa] | err [ppm] | mSigma | rdb | e ⁻ Conf | z |
|-----------|---|----------------------|--------|----------|-----------|-----------|--------|------|---------------------|----|
| 615.0576 | 1 | C 32 H 28 Ag O 2 S 2 | 100.00 | 615.0576 | 0.0 | 0.1 | 16.1 | 18.5 | even | 1+ |

Mass list

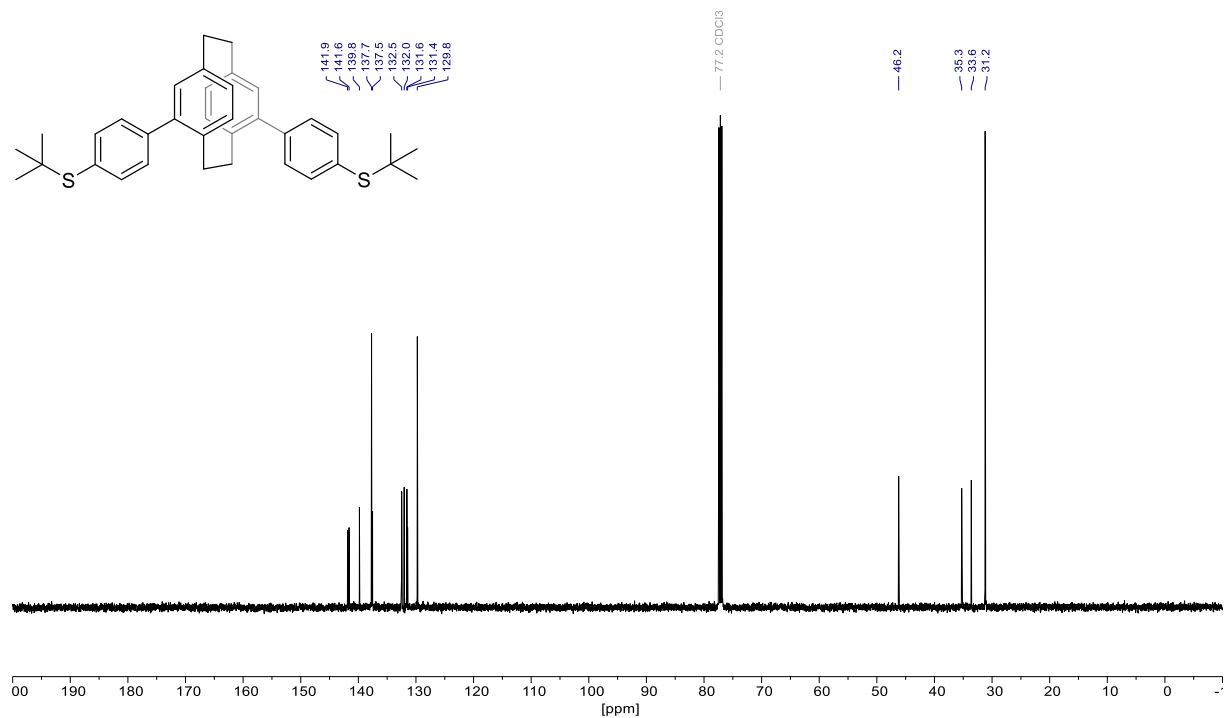
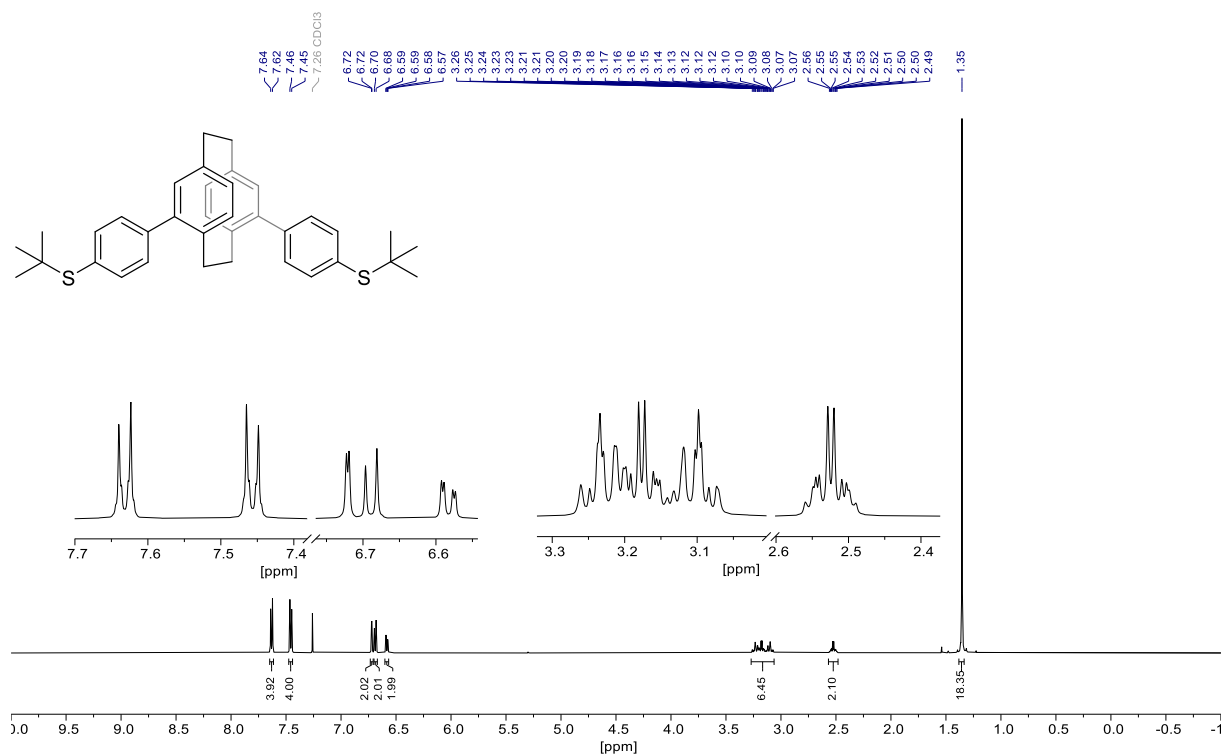
| # | m/z | I % | I |
|----|----------|-------|--------|
| 1 | 275.7970 | 12.3 | 23666 |
| 2 | 277.7967 | 22.7 | 43541 |
| 3 | 279.7964 | 10.9 | 20989 |
| 4 | 301.8333 | 4.7 | 8952 |
| 5 | 316.8238 | 38.0 | 72843 |
| 6 | 318.8237 | 70.5 | 135252 |
| 7 | 320.8232 | 35.5 | 67977 |
| 8 | 357.8505 | 14.6 | 28038 |
| 9 | 359.8501 | 27.5 | 52648 |
| 10 | 361.8498 | 12.7 | 24275 |
| 11 | 367.8210 | 4.5 | 8543 |
| 12 | 369.8206 | 7.7 | 14737 |
| 13 | 388.1757 | 7.2 | 13887 |
| 14 | 390.1755 | 6.9 | 13274 |
| 15 | 399.1079 | 11.2 | 21421 |
| 16 | 401.1078 | 11.6 | 22306 |
| 17 | 415.1025 | 7.1 | 13581 |
| 18 | 417.1030 | 7.1 | 13648 |
| 19 | 437.1813 | 24.4 | 46812 |
| 20 | 438.1845 | 5.5 | 10560 |
| 21 | 439.1810 | 21.5 | 41285 |
| 22 | 440.1843 | 4.8 | 9149 |
| 23 | 446.6898 | 6.4 | 12260 |
| 24 | 448.6894 | 6.1 | 11629 |
| 25 | 465.2125 | 22.4 | 42981 |
| 26 | 466.2157 | 5.2 | 9877 |
| 27 | 467.2123 | 21.6 | 41457 |
| 28 | 468.2157 | 5.2 | 9938 |
| 29 | 485.7166 | 10.9 | 20803 |
| 30 | 487.7165 | 28.1 | 53844 |
| 31 | 489.7163 | 25.6 | 49023 |
| 32 | 491.7158 | 8.8 | 16811 |
| 33 | 517.2954 | 13.7 | 26180 |
| 34 | 518.2987 | 5.0 | 9673 |
| 35 | 519.2950 | 13.8 | 26420 |
| 36 | 528.7429 | 9.3 | 17923 |
| 37 | 530.7430 | 8.9 | 17110 |
| 38 | 615.0576 | 95.3 | 182661 |
| 39 | 616.0606 | 34.5 | 66068 |
| 40 | 617.0575 | 100.0 | 191719 |
| 41 | 618.0600 | 34.1 | 65355 |
| 42 | 619.0570 | 11.8 | 22541 |
| 43 | 656.0838 | 24.7 | 47436 |
| 44 | 657.0868 | 10.1 | 19450 |
| 45 | 658.0836 | 26.2 | 50185 |
| 46 | 659.0866 | 9.8 | 18720 |
| 47 | 684.1877 | 11.5 | 21983 |
| 48 | 685.1907 | 4.7 | 8991 |
| 49 | 686.1880 | 16.1 | 30859 |
| 50 | 687.1912 | 6.5 | 12434 |
| 51 | 688.1886 | 10.5 | 20116 |
| 52 | 690.1886 | 4.5 | 8541 |
| 53 | 769.3519 | 15.1 | 28960 |
| 54 | 770.3546 | 7.4 | 14242 |
| 55 | 771.3518 | 15.7 | 30076 |
| 56 | 772.3543 | 6.8 | 12965 |
| 57 | 783.9514 | 9.3 | 17846 |
| 58 | 785.9511 | 18.3 | 35043 |
| 59 | 786.9539 | 7.0 | 13439 |
| 60 | 787.9507 | 10.5 | 20142 |
| 61 | 789.4991 | 31.0 | 59366 |
| 62 | 790.5021 | 14.3 | 27368 |

 High Resolution Mass Spectrometry Report

| # | m/z | I % | I |
|-----|-----------|------|-------|
| 63 | 791.4993 | 31.0 | 59338 |
| 64 | 792.5019 | 14.3 | 27416 |
| 65 | 793.5031 | 4.8 | 9112 |
| 66 | 805.4939 | 5.1 | 9735 |
| 67 | 807.4933 | 5.3 | 10187 |
| 68 | 812.0556 | 7.7 | 14702 |
| 69 | 814.0559 | 15.8 | 30282 |
| 70 | 815.0584 | 6.4 | 12320 |
| 71 | 816.0558 | 9.3 | 17892 |
| 72 | 945.3382 | 5.8 | 11083 |
| 73 | 947.3400 | 6.7 | 12824 |
| 74 | 954.8482 | 4.9 | 9299 |
| 75 | 956.8479 | 5.0 | 9552 |
| 76 | 973.3714 | 5.4 | 10322 |
| 77 | 975.3718 | 6.7 | 12895 |
| 78 | 982.9529 | 5.1 | 9782 |
| 79 | 984.9532 | 5.7 | 10870 |
| 80 | 1023.5182 | 4.5 | 8544 |
| 81 | 1025.5196 | 4.8 | 9255 |
| 82 | 1123.2227 | 13.6 | 26119 |
| 83 | 1124.2248 | 10.5 | 20112 |
| 84 | 1125.2229 | 17.8 | 34134 |
| 85 | 1126.2255 | 11.7 | 22372 |
| 86 | 1127.2249 | 6.5 | 12370 |
| 87 | 1277.5239 | 8.8 | 16794 |
| 88 | 1278.5268 | 7.7 | 14792 |
| 89 | 1279.5247 | 11.6 | 22234 |
| 90 | 1280.5284 | 8.3 | 15920 |
| 91 | 1294.1245 | 6.2 | 11821 |
| 92 | 1296.1262 | 4.9 | 9423 |
| 93 | 1297.6717 | 7.4 | 14116 |
| 94 | 1298.6742 | 5.9 | 11274 |
| 95 | 1299.6735 | 10.1 | 19295 |
| 96 | 1300.6760 | 6.8 | 13109 |
| 97 | 1451.9765 | 5.2 | 9917 |
| 98 | 1452.9797 | 4.7 | 8968 |
| 99 | 1453.9773 | 7.0 | 13482 |
| 100 | 1454.9801 | 5.5 | 10472 |

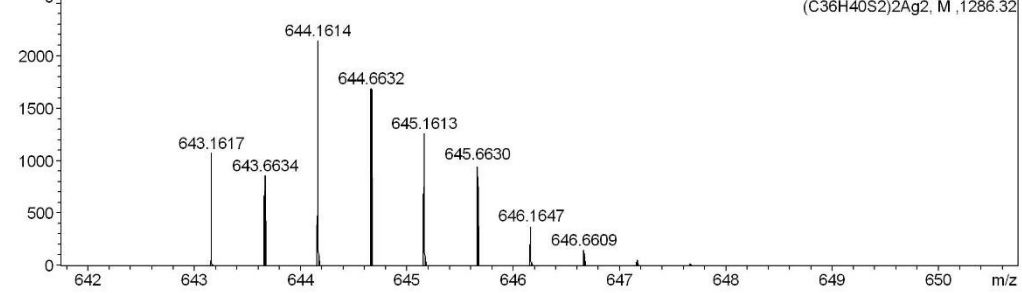
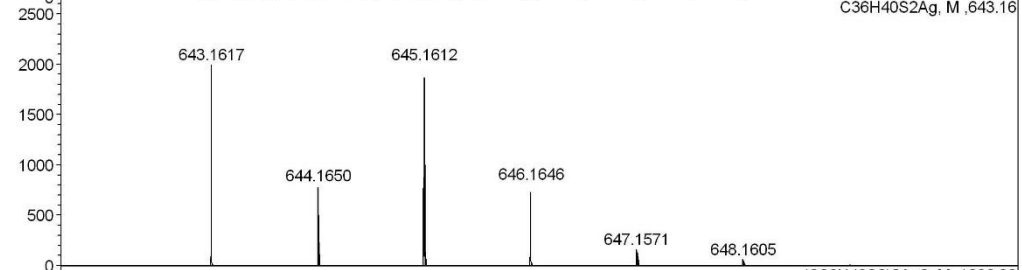
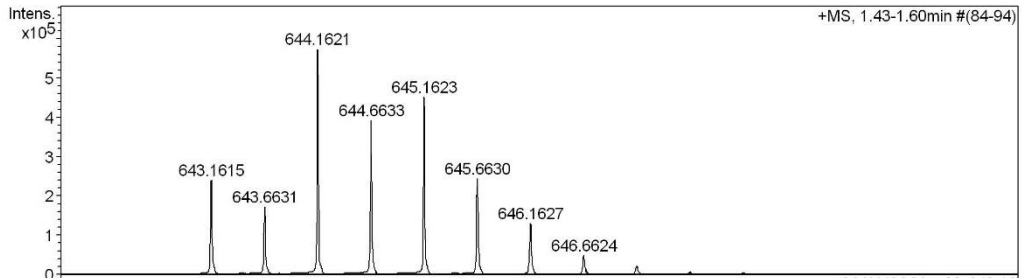
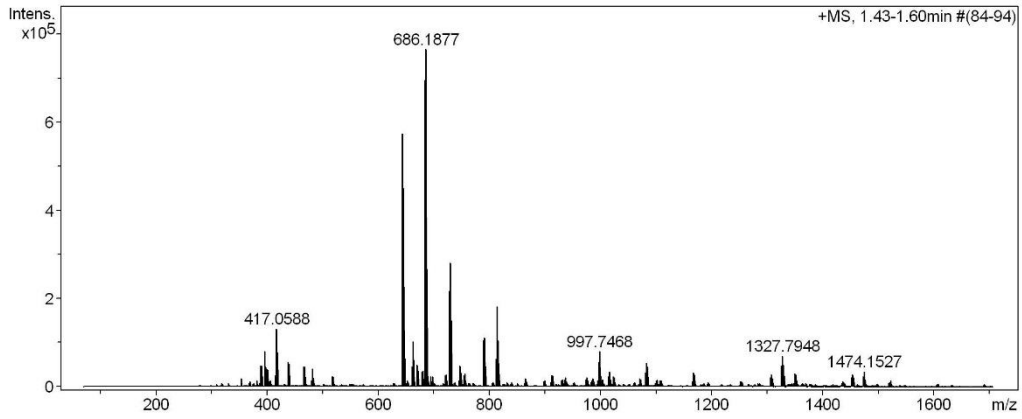
Acquisition Parameter

| | | | | | | |
|-------------------|------------------------------|----------------|---------------------------------------|----------------|--------------|-----------|
| General | Fore Vacuum | 2.59e+000 mBar | High Vacuum | 9.65e-008 mBar | Source Type | ESI |
| | Scan Begin | 75 m/z | Scan End | 1700 m/z | Ion Polarity | Positive |
| Source | Set Nebulizer | 0.4 Bar | Set Capillary | 3600 V | Set Dry Gas | 4.0 l/min |
| | Set Dry Heater | 180 °C | Set End Plate Offset | -500 V | | |
| Quadrupole | Set Ion Energy (MS only) | 4.0 eV | | | | |
| Coll. Cell | Collision Energy | 8.0 eV | Set Collision Cell RF | 500.0 Vpp | | |
| Ion Cooler | Set Ion Cooler Transfer Time | 100.0 µs | Set Ion Cooler Pre Pulse Storage Time | 18.0 µs | | |

^1H , $^{13}\text{C}\{^1\text{H}\}$ (500/126 MHz, CDCl_3) NMR and HR-ESI-MS Spectra of ps-*meta*-*para* StBu PCP:

High Resolution Mass Spectrometry Report

| | | | |
|-------------|-----------------------------------------------|------------|------------------------|
| Sample Name | Ksenia Reznikova / KR 166 | Instrument | maXis 4G |
| Comment | 10 ug / mL in DCM, analyzed in MeOH+AgNO3 5mM | Method | 23 Direct_pos_higher.m |



High Resolution Mass Spectrometry Report

Measured m/z vs. theoretical m/z

| Meas. m/z | # | Formula | Score | m/z | err [mDa] | err [ppm] | mSigma | rdB | e ⁻ Conf | z |
|-----------|---|------------------|--------|----------|-----------|-----------|--------|------|---------------------|----|
| 643.1615 | 1 | C 36 H 40 Ag S 2 | 100.00 | 643.1617 | 0.2 | 0.3 | 320.0 | 16.5 | even | 1+ |

Mass list

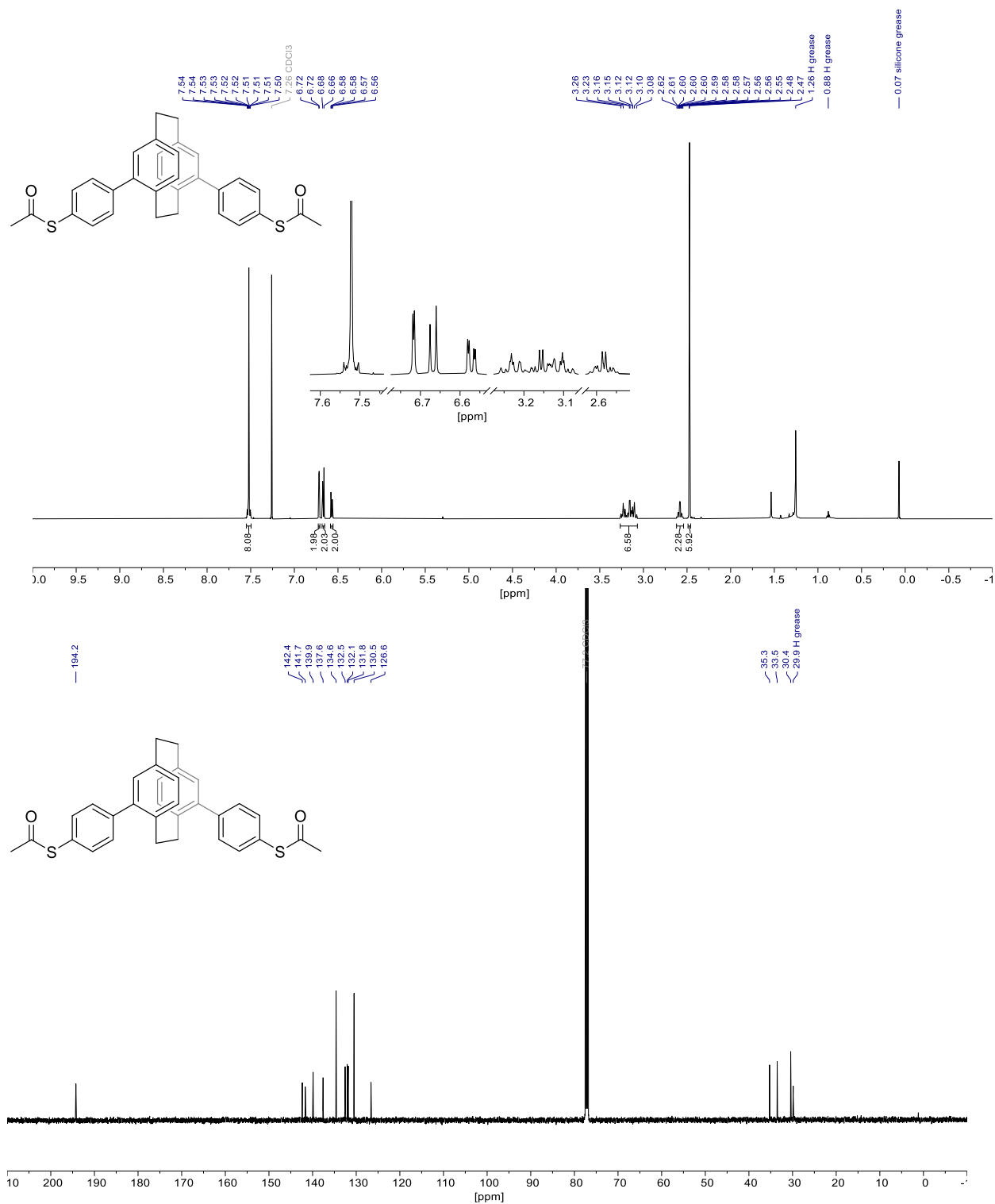
| # | m/z | I % | I |
|----|----------|-------|--------|
| 1 | 388.1743 | 6.2 | 47551 |
| 2 | 390.1744 | 6.1 | 46954 |
| 3 | 395.5449 | 5.3 | 40379 |
| 4 | 396.5450 | 10.6 | 81329 |
| 5 | 397.0463 | 4.7 | 35899 |
| 6 | 397.5448 | 6.1 | 46752 |
| 7 | 399.1068 | 5.3 | 40724 |
| 8 | 401.1067 | 5.1 | 38760 |
| 9 | 416.0588 | 8.8 | 67005 |
| 10 | 416.5603 | 4.1 | 31707 |
| 11 | 417.0588 | 17.3 | 132215 |
| 12 | 417.5602 | 7.9 | 60584 |
| 13 | 418.0588 | 10.2 | 77837 |
| 14 | 418.5599 | 4.4 | 33699 |
| 15 | 437.1806 | 7.5 | 57425 |
| 16 | 439.1804 | 6.9 | 52638 |
| 17 | 465.2119 | 6.1 | 46456 |
| 18 | 467.2120 | 5.9 | 44976 |
| 19 | 480.9924 | 5.0 | 38205 |
| 20 | 481.9923 | 5.3 | 40557 |
| 21 | 643.1615 | 31.5 | 241523 |
| 22 | 643.6631 | 22.5 | 172602 |
| 23 | 644.1621 | 75.0 | 574700 |
| 24 | 644.6633 | 51.3 | 393098 |
| 25 | 645.1623 | 59.1 | 452473 |
| 26 | 645.6630 | 32.0 | 245069 |
| 27 | 646.1627 | 17.0 | 130443 |
| 28 | 646.6624 | 6.4 | 49310 |
| 29 | 661.1481 | 6.1 | 46837 |
| 30 | 661.6493 | 4.9 | 37844 |
| 31 | 662.1483 | 13.3 | 102037 |
| 32 | 662.6494 | 9.8 | 74769 |
| 33 | 663.1486 | 10.0 | 76413 |
| 34 | 663.6493 | 6.4 | 48658 |
| 35 | 670.1454 | 6.5 | 49687 |
| 36 | 670.6465 | 4.9 | 37150 |
| 37 | 671.1456 | 4.9 | 37375 |
| 38 | 679.1340 | 4.6 | 35133 |
| 39 | 681.1340 | 5.0 | 38066 |
| 40 | 684.1878 | 90.9 | 696002 |
| 41 | 685.1908 | 33.8 | 258945 |
| 42 | 686.1877 | 100.0 | 765771 |
| 43 | 687.1902 | 35.0 | 268172 |
| 44 | 688.1883 | 11.5 | 87696 |
| 45 | 722.1605 | 3.7 | 28313 |
| 46 | 727.6081 | 8.5 | 65380 |
| 47 | 728.1098 | 7.4 | 56802 |
| 48 | 728.6086 | 28.5 | 218196 |
| 49 | 729.1100 | 21.4 | 164250 |
| 50 | 729.6090 | 36.8 | 281790 |
| 51 | 730.1099 | 24.8 | 189765 |
| 52 | 730.6091 | 19.8 | 151516 |
| 53 | 731.1095 | 11.1 | 85163 |
| 54 | 731.6091 | 5.6 | 42881 |
| 55 | 746.5950 | 5.2 | 40065 |
| 56 | 747.0964 | 4.2 | 32029 |
| 57 | 747.5954 | 6.2 | 47777 |
| 58 | 748.0962 | 4.4 | 33584 |
| 59 | 748.5955 | 3.6 | 27335 |
| 60 | 755.1013 | 3.8 | 29471 |
| 61 | 755.5968 | 3.9 | 30188 |
| 62 | 789.4979 | 13.8 | 105944 |

 High Resolution Mass Spectrometry Report

| # | m/z | I % | I |
|-----|-----------|------|--------|
| 63 | 790.5011 | 6.3 | 48168 |
| 64 | 791.4984 | 14.6 | 111681 |
| 65 | 792.5008 | 6.2 | 47337 |
| 66 | 812.0555 | 8.3 | 63347 |
| 67 | 813.0570 | 8.6 | 65615 |
| 68 | 813.5575 | 4.6 | 35135 |
| 69 | 814.0561 | 24.0 | 183512 |
| 70 | 814.5574 | 7.1 | 54609 |
| 71 | 815.0575 | 13.9 | 106166 |
| 72 | 815.5572 | 5.6 | 42509 |
| 73 | 816.0559 | 11.5 | 87919 |
| 74 | 817.0572 | 4.0 | 30375 |
| 75 | 996.7461 | 6.9 | 52893 |
| 76 | 997.2474 | 7.4 | 56659 |
| 77 | 997.7468 | 10.6 | 81004 |
| 78 | 998.2476 | 9.2 | 70069 |
| 79 | 998.7474 | 7.9 | 60636 |
| 80 | 999.2476 | 5.6 | 42799 |
| 81 | 1015.7345 | 4.6 | 35450 |
| 82 | 1016.2350 | 4.1 | 31313 |
| 83 | 1081.1986 | 3.6 | 27249 |
| 84 | 1081.7001 | 4.1 | 31706 |
| 85 | 1082.1988 | 6.8 | 52334 |
| 86 | 1082.7001 | 6.7 | 51416 |
| 87 | 1083.1995 | 7.3 | 55656 |
| 88 | 1083.7001 | 6.1 | 46619 |
| 89 | 1084.1997 | 4.5 | 34534 |
| 90 | 1167.6527 | 4.2 | 32220 |
| 91 | 1168.1536 | 3.7 | 27996 |
| 92 | 1307.6452 | 3.7 | 28642 |
| 93 | 1325.7937 | 6.3 | 48324 |
| 94 | 1326.7968 | 5.6 | 43181 |
| 95 | 1327.7948 | 9.3 | 70911 |
| 96 | 1328.7971 | 6.6 | 50597 |
| 97 | 1350.3554 | 3.8 | 29426 |
| 98 | 1351.3569 | 3.8 | 28985 |
| 99 | 1454.0035 | 3.7 | 28562 |
| 100 | 1474.1527 | 4.6 | 35176 |

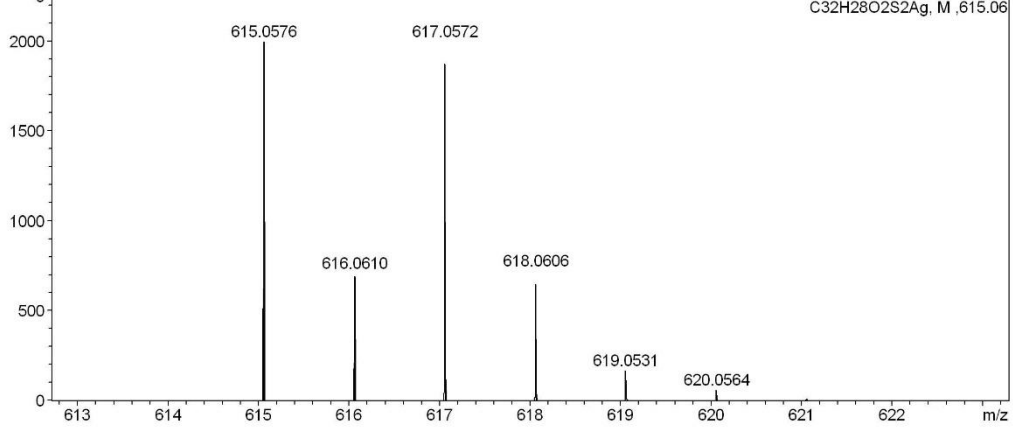
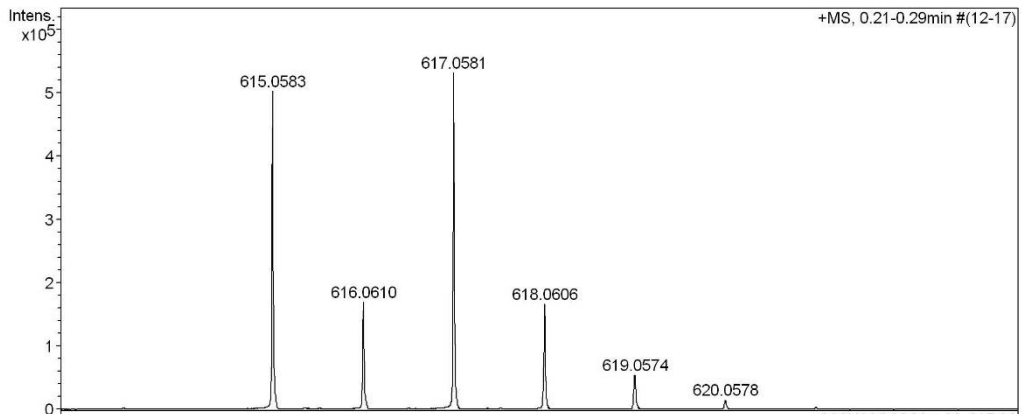
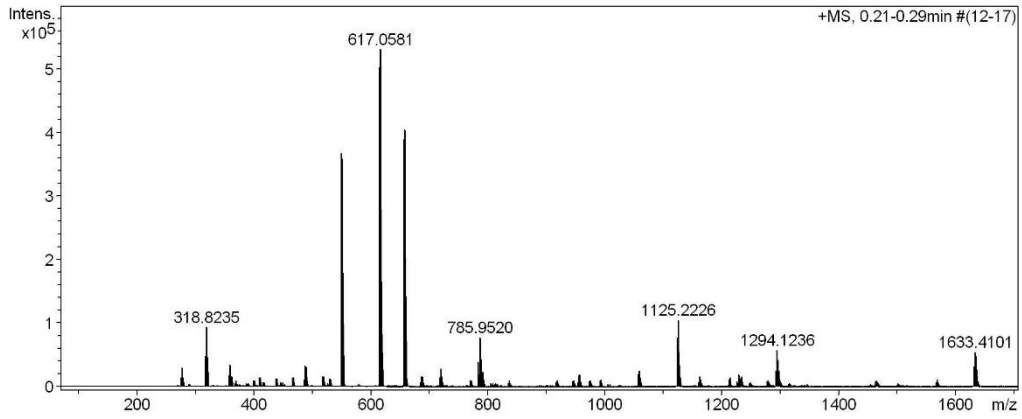
Acquisition Parameter

| | | | | | | |
|-------------------|------------------------------|----------------|---------------------------------------|----------------|--------------|-----------|
| General | Fore Vacuum | 2.59e+000 mBar | High Vacuum | 9.68e-008 mBar | Source Type | ESI |
| | Scan Begin | 75 m/z | Scan End | 1700 m/z | Ion Polarity | Positive |
| Source | Set Nebulizer | 0.4 Bar | Set Capillary | 3600 V | Set Dry Gas | 4.0 l/min |
| | Set Dry Heater | 180 °C | Set End Plate Offset | -500 V | | |
| Quadrupole | Set Ion Energy (MS only) | 4.0 eV | | | | |
| Coll. Cell | Collision Energy | 8.0 eV | Set Collision Cell RF | 500.0 Vpp | | |
| Ion Cooler | Set Ion Cooler Transfer Time | 100.0 µs | Set Ion Cooler Pre Pulse Storage Time | 18.0 µs | | |

^1H , $^{13}\text{C}\{^1\text{H}\}$ (500/126 MHz, CDCl_3) NMR and HR-ESI-MS Spectra of ps-meta-para PCP:

High Resolution Mass Spectrometry Report

| | | | |
|-------------|-----------------------------------------------|------------|------------------------|
| Sample Name | Ksenia Reznikova / KR 212 | Instrument | maXis 4G |
| Comment | 10 ug / mL in DCM, analyzed in MeOH+AgNO3 5mM | Method | 23 Direct_pos_higher.m |



High Resolution Mass Spectrometry Report

Measured m/z vs. theoretical m/z

| Meas. m/z | # | Formula | Score | m/z | err [mDa] | err [ppm] | mSigma | rdb | e ⁻ Conf | z |
|-----------|---|----------------------|--------|----------|-----------|-----------|--------|------|---------------------|----|
| 615.0583 | 1 | C 32 H 28 Ag O 2 S 2 | 100.00 | 615.0576 | -0.7 | -1.1 | 21.8 | 18.5 | even | 1+ |

Mass list

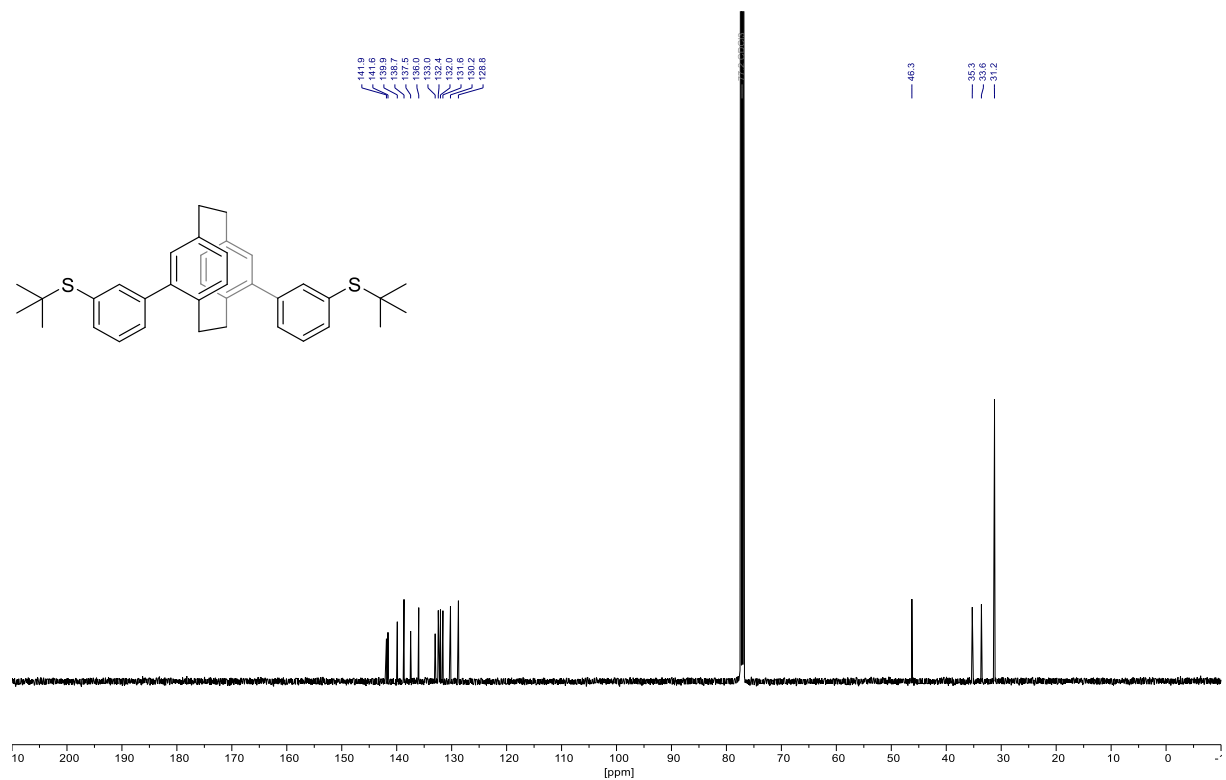
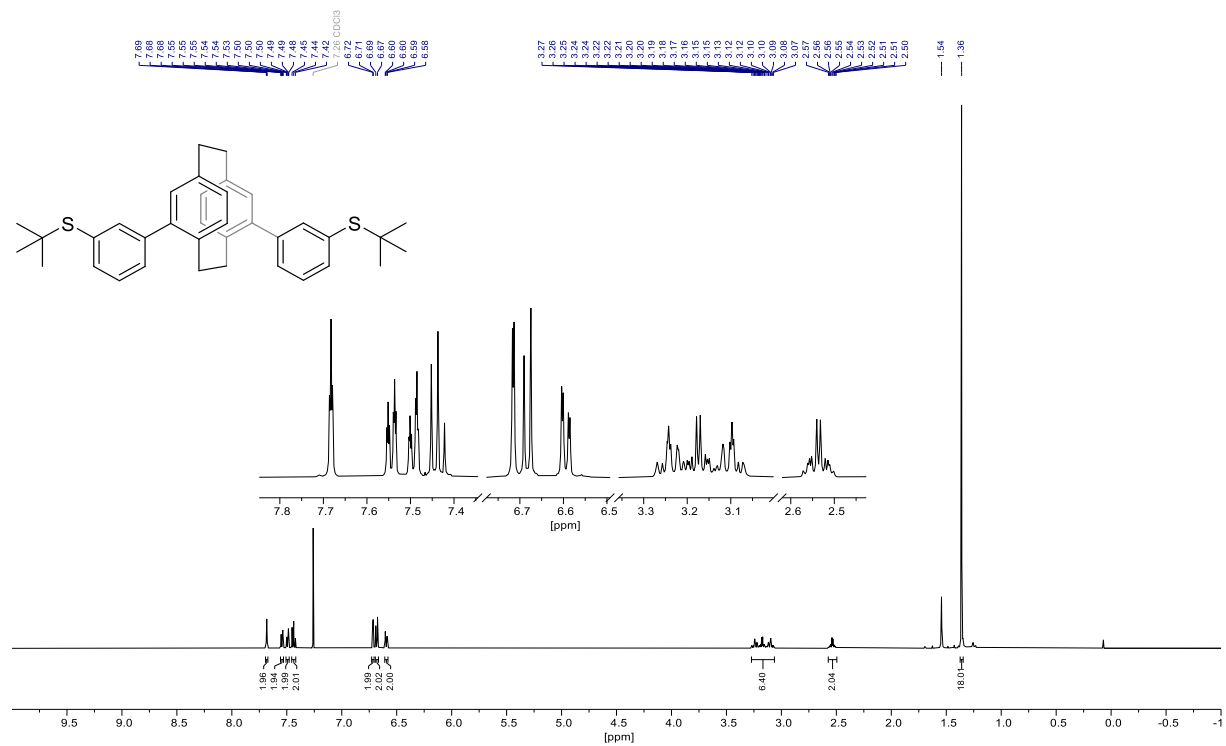
| # | m/z | I % | I |
|----|----------|-------|--------|
| 1 | 275.7969 | 2.9 | 15572 |
| 2 | 277.7966 | 5.6 | 29917 |
| 3 | 279.7962 | 2.7 | 14576 |
| 4 | 316.8237 | 9.2 | 48685 |
| 5 | 318.8235 | 17.7 | 94297 |
| 6 | 320.8231 | 8.7 | 46407 |
| 7 | 357.8504 | 3.5 | 18653 |
| 8 | 359.8501 | 6.6 | 35050 |
| 9 | 361.8498 | 3.2 | 17014 |
| 10 | 369.8208 | 2.0 | 10659 |
| 11 | 399.1080 | 2.1 | 10943 |
| 12 | 401.1078 | 2.1 | 11011 |
| 13 | 408.9479 | 2.9 | 15206 |
| 14 | 410.9469 | 2.8 | 14946 |
| 15 | 437.1811 | 2.6 | 13830 |
| 16 | 439.1810 | 2.4 | 12853 |
| 17 | 465.2123 | 2.9 | 15522 |
| 18 | 467.2123 | 2.8 | 14650 |
| 19 | 485.7170 | 2.4 | 12578 |
| 20 | 487.7167 | 6.4 | 33854 |
| 21 | 489.7162 | 6.0 | 31872 |
| 22 | 491.7158 | 2.0 | 10727 |
| 23 | 517.2955 | 3.2 | 17090 |
| 24 | 519.2953 | 3.0 | 15974 |
| 25 | 528.7431 | 2.4 | 12655 |
| 26 | 530.7431 | 2.3 | 11977 |
| 27 | 549.1231 | 69.1 | 367566 |
| 28 | 550.1258 | 19.0 | 100959 |
| 29 | 551.1229 | 67.6 | 359303 |
| 30 | 552.1254 | 18.7 | 99249 |
| 31 | 553.1240 | 4.7 | 25228 |
| 32 | 615.0583 | 94.5 | 502324 |
| 33 | 616.0610 | 31.9 | 169795 |
| 34 | 617.0581 | 100.0 | 531631 |
| 35 | 618.0606 | 31.4 | 166745 |
| 36 | 619.0574 | 10.3 | 54831 |
| 37 | 620.0578 | 3.0 | 15970 |
| 38 | 656.0848 | 73.4 | 390175 |
| 39 | 657.0875 | 25.5 | 135747 |
| 40 | 658.0846 | 76.0 | 404282 |
| 41 | 659.0871 | 26.9 | 143168 |
| 42 | 660.0843 | 9.3 | 49519 |
| 43 | 661.0846 | 2.6 | 13816 |
| 44 | 686.1882 | 3.0 | 16134 |
| 45 | 688.1886 | 3.0 | 15711 |
| 46 | 718.0153 | 2.9 | 15285 |
| 47 | 720.0153 | 5.4 | 28801 |
| 48 | 722.0154 | 3.1 | 16334 |
| 49 | 769.3515 | 2.0 | 10369 |
| 50 | 783.9518 | 7.4 | 39281 |
| 51 | 784.9548 | 2.8 | 15080 |
| 52 | 785.9520 | 14.7 | 78353 |
| 53 | 786.9543 | 5.5 | 29277 |
| 54 | 787.9513 | 8.3 | 44202 |
| 55 | 788.9538 | 3.0 | 15797 |
| 56 | 789.4987 | 4.1 | 21936 |
| 57 | 790.5015 | 2.1 | 10989 |
| 58 | 791.4990 | 4.6 | 24343 |
| 59 | 792.5020 | 2.1 | 10963 |
| 60 | 836.9494 | 1.9 | 10349 |
| 61 | 954.8485 | 3.5 | 18500 |
| 62 | 956.8483 | 3.6 | 19338 |

 High Resolution Mass Spectrometry Report

| # | m/z | I % | I |
|-----|-----------|------|--------|
| 63 | 993.3463 | 2.1 | 11403 |
| 64 | 1057.2832 | 3.7 | 19418 |
| 65 | 1058.2867 | 2.5 | 13131 |
| 66 | 1059.2844 | 4.8 | 25461 |
| 67 | 1060.2867 | 2.8 | 14742 |
| 68 | 1123.2219 | 14.6 | 77491 |
| 69 | 1124.2250 | 10.9 | 57889 |
| 70 | 1125.2226 | 19.8 | 105219 |
| 71 | 1126.2249 | 12.5 | 66588 |
| 72 | 1127.2239 | 6.6 | 34831 |
| 73 | 1128.2242 | 3.0 | 15696 |
| 74 | 1162.2461 | 3.2 | 17017 |
| 75 | 1164.2462 | 2.2 | 11530 |
| 76 | 1211.5842 | 2.1 | 11396 |
| 77 | 1213.5855 | 2.7 | 14210 |
| 78 | 1228.1846 | 3.7 | 19687 |
| 79 | 1229.1874 | 2.2 | 11647 |
| 80 | 1230.1847 | 2.6 | 13826 |
| 81 | 1231.7312 | 2.6 | 13719 |
| 82 | 1232.7343 | 2.0 | 10898 |
| 83 | 1233.7322 | 3.2 | 17227 |
| 84 | 1234.7355 | 2.2 | 11817 |
| 85 | 1279.5236 | 2.0 | 10381 |
| 86 | 1292.1233 | 4.8 | 25440 |
| 87 | 1293.1259 | 3.6 | 19259 |
| 88 | 1294.1236 | 10.9 | 57960 |
| 89 | 1295.1266 | 7.6 | 40302 |
| 90 | 1296.1241 | 8.1 | 43236 |
| 91 | 1297.1257 | 5.0 | 26326 |
| 92 | 1298.1258 | 2.5 | 13353 |
| 93 | 1567.4685 | 2.2 | 11848 |
| 94 | 1568.4704 | 2.0 | 10397 |
| 95 | 1631.4078 | 6.0 | 32062 |
| 96 | 1632.4114 | 6.6 | 34919 |
| 97 | 1633.4101 | 10.4 | 55447 |
| 98 | 1634.4121 | 9.1 | 48363 |
| 99 | 1635.4116 | 6.0 | 31975 |
| 100 | 1636.4123 | 3.4 | 18131 |

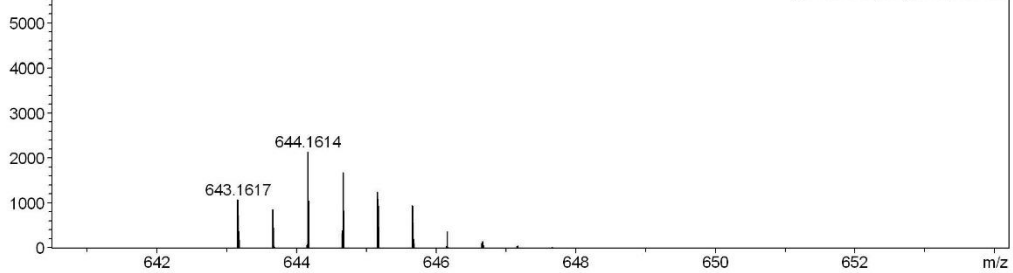
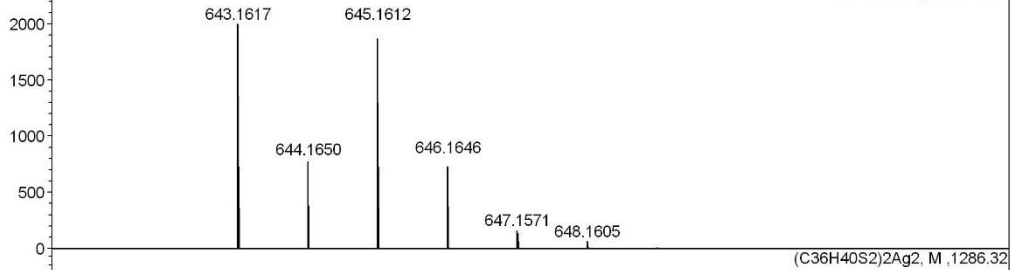
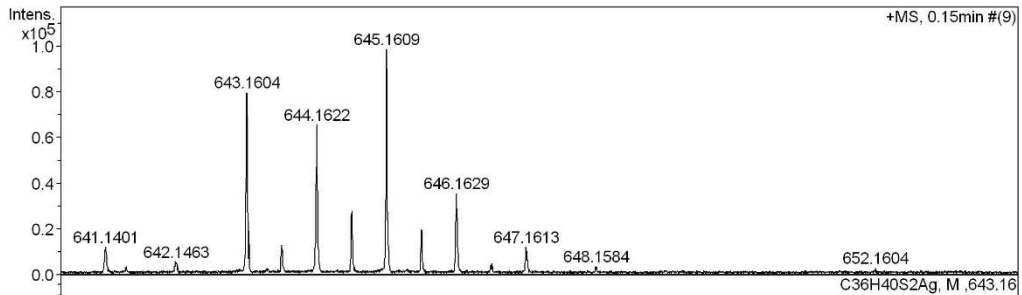
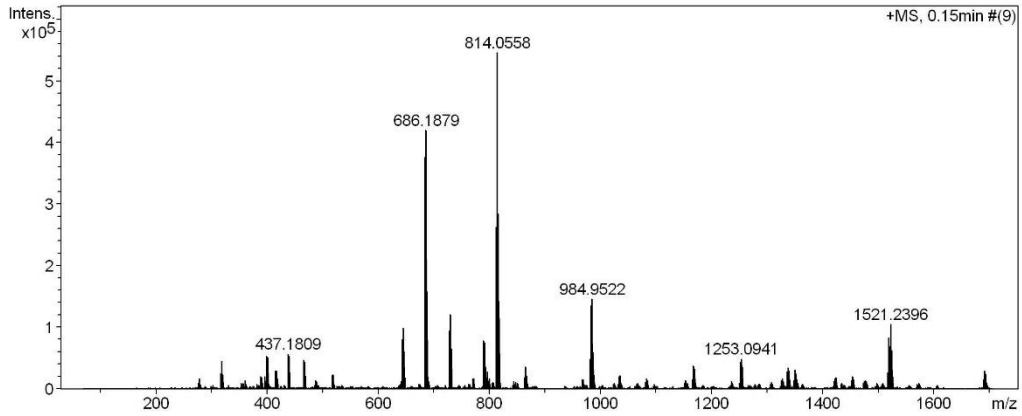
Acquisition Parameter

| | | | | | | |
|-------------------|------------------------------|----------------|---------------------------------------|----------------|--------------|-----------|
| General | Fore Vacuum | 2.59e+000 mBar | High Vacuum | 9.65e-008 mBar | Source Type | ESI |
| | Scan Begin | 75 m/z | Scan End | 1700 m/z | Ion Polarity | Positive |
| Source | Set Nebulizer | 0.4 Bar | Set Capillary | 3600 V | Set Dry Gas | 4.0 l/min |
| | Set Dry Heater | 180 °C | Set End Plate Offset | -500 V | | |
| Quadrupole | Set Ion Energy (MS only) | 4.0 eV | | | | |
| Coll. Cell | Collision Energy | 8.0 eV | Set Collision Cell RF | 500.0 Vpp | | |
| Ion Cooler | Set Ion Cooler Transfer Time | 100.0 µs | Set Ion Cooler Pre Pulse Storage Time | 18.0 µs | | |

^1H , $^{13}\text{C}\{^1\text{H}\}$ (500/126 MHz, CDCl_3) NMR and HR-ESI-MS Spectra of ps-meta-meta StBu PCP:

High Resolution Mass Spectrometry Report

| | | | |
|-------------|-----------------------------------------------|------------|------------------------|
| Sample Name | Ksenia Reznikova / KR 167 | Instrument | maXis 4G |
| Comment | 10 ug / mL in DCM, analyzed in MeOH+AgNO3 5mM | Method | 23 Direct_pos_higher.m |



High Resolution Mass Spectrometry Report

Measured m/z vs. theoretical m/z

| Meas. m/z | # | Formula | Score | m/z | err [mDa] | err [ppm] | mSigma | rdB | e ⁻ Conf | z |
|-----------|---|------------------|--------|----------|-----------|-----------|--------|------|---------------------|----|
| 643.1604 | 1 | C 36 H 40 Ag S 2 | 100.00 | 643.1617 | 1.3 | 2.0 | 117.6 | 16.5 | even | 1+ |

Mass list

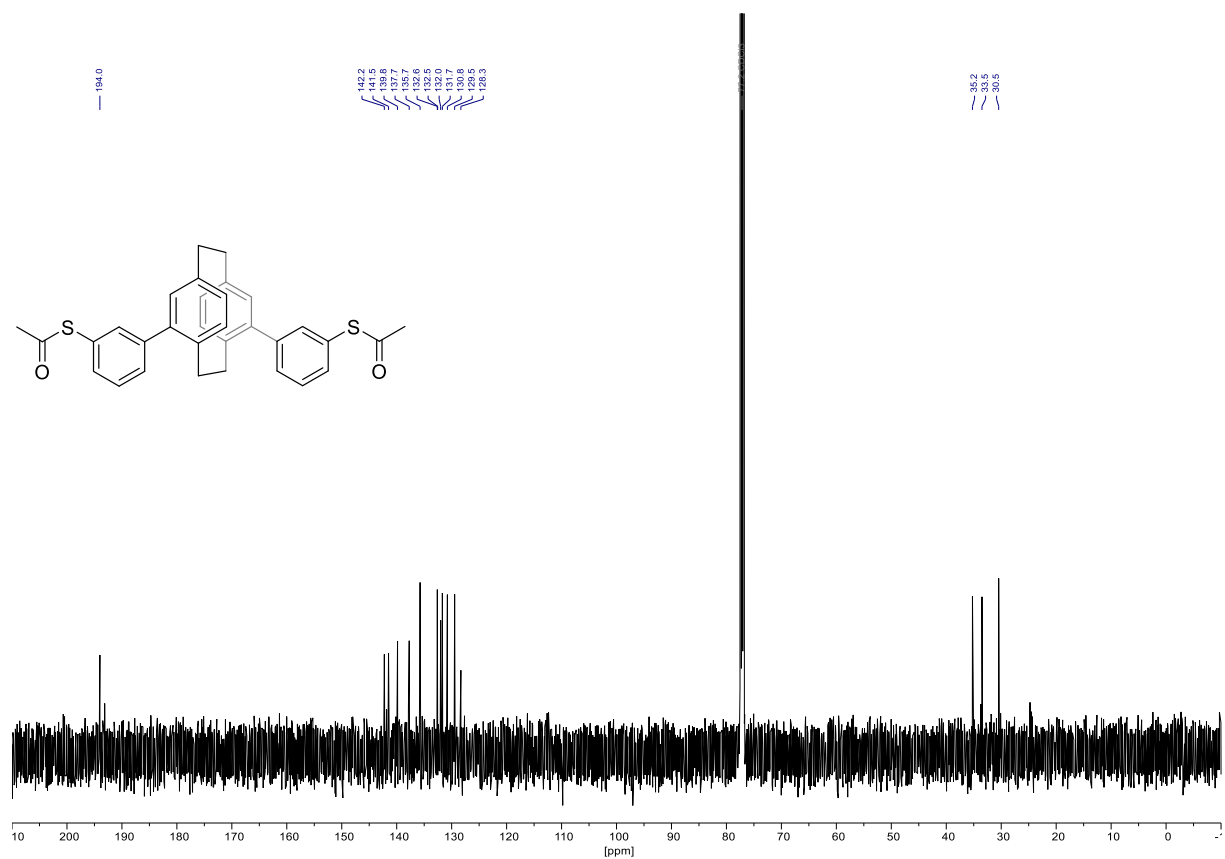
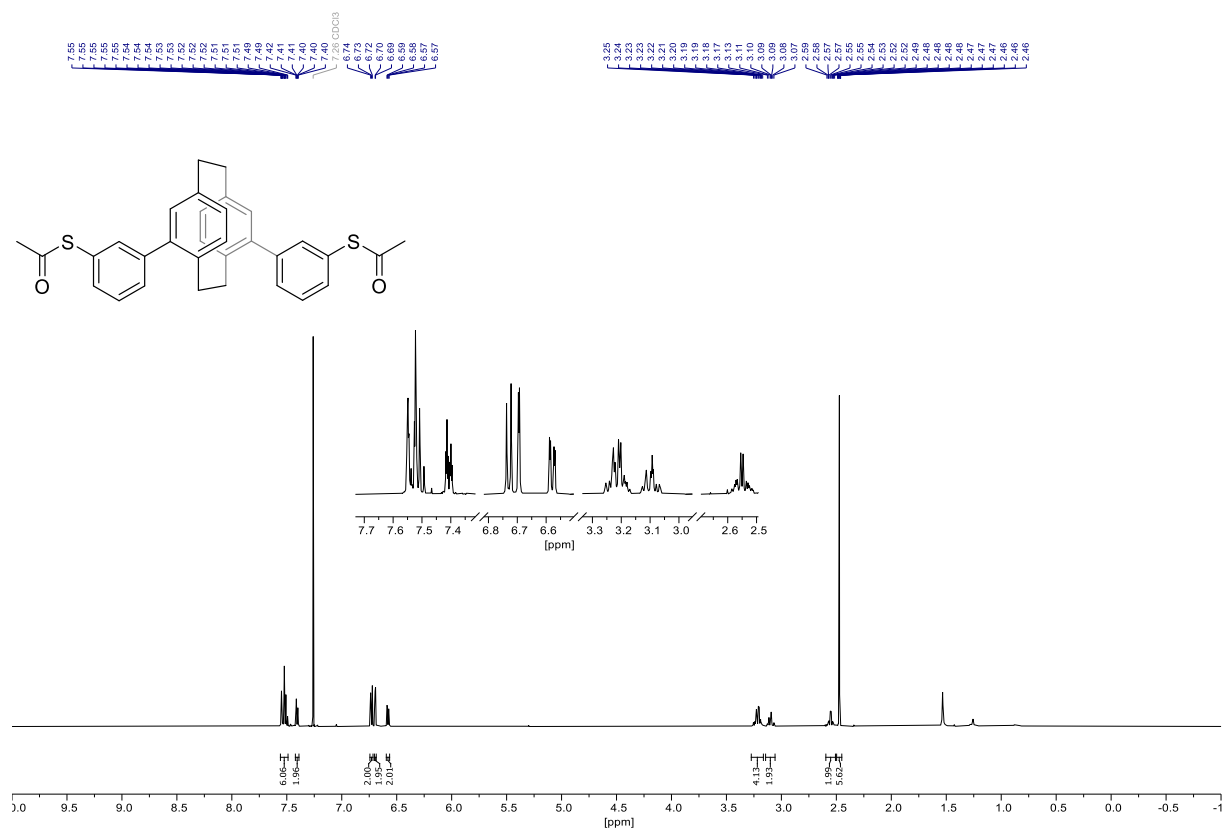
| # | m/z | I % | I |
|----|-----------|-------|--------|
| 1 | 316.8236 | 4.6 | 24986 |
| 2 | 318.8234 | 8.3 | 45604 |
| 3 | 320.8227 | 4.3 | 23530 |
| 4 | 388.1756 | 3.9 | 21376 |
| 5 | 390.1753 | 3.6 | 19860 |
| 6 | 396.5457 | 3.8 | 20814 |
| 7 | 399.1078 | 10.0 | 54398 |
| 8 | 401.1076 | 9.5 | 52178 |
| 9 | 415.1027 | 5.6 | 30846 |
| 10 | 417.0596 | 5.6 | 30334 |
| 11 | 417.1026 | 5.7 | 30925 |
| 12 | 437.1809 | 10.5 | 57229 |
| 13 | 439.1807 | 9.8 | 53698 |
| 14 | 465.2122 | 8.7 | 47604 |
| 15 | 467.2122 | 8.3 | 45137 |
| 16 | 517.2951 | 4.2 | 23177 |
| 17 | 519.2951 | 4.3 | 23572 |
| 18 | 643.1604 | 14.6 | 79965 |
| 19 | 644.1622 | 12.0 | 65718 |
| 20 | 644.6622 | 5.1 | 27922 |
| 21 | 645.1609 | 18.1 | 98801 |
| 22 | 645.6625 | 3.6 | 19877 |
| 23 | 646.1629 | 6.6 | 35912 |
| 24 | 684.1881 | 69.0 | 377318 |
| 25 | 685.1908 | 28.2 | 154362 |
| 26 | 686.1879 | 76.9 | 420044 |
| 27 | 687.1903 | 29.2 | 159770 |
| 28 | 688.1884 | 12.3 | 67288 |
| 29 | 689.1889 | 3.9 | 21402 |
| 30 | 727.6082 | 5.9 | 32090 |
| 31 | 728.1098 | 4.6 | 25168 |
| 32 | 728.6089 | 17.2 | 94229 |
| 33 | 729.1099 | 14.0 | 76597 |
| 34 | 729.6088 | 22.1 | 120896 |
| 35 | 730.1105 | 15.1 | 82433 |
| 36 | 730.6092 | 12.3 | 67078 |
| 37 | 731.1092 | 7.7 | 41925 |
| 38 | 731.6094 | 3.8 | 20790 |
| 39 | 789.4978 | 14.4 | 78770 |
| 40 | 790.5009 | 6.9 | 37825 |
| 41 | 791.4983 | 13.9 | 76074 |
| 42 | 792.5008 | 6.6 | 35842 |
| 43 | 797.0640 | 5.3 | 28820 |
| 44 | 812.0559 | 48.1 | 262717 |
| 45 | 813.0585 | 18.7 | 102440 |
| 46 | 814.0558 | 100.0 | 546516 |
| 47 | 815.0584 | 37.2 | 203105 |
| 48 | 816.0556 | 52.3 | 285774 |
| 49 | 817.0577 | 21.2 | 116037 |
| 50 | 818.0548 | 6.9 | 37945 |
| 51 | 863.0527 | 3.5 | 19289 |
| 52 | 865.0531 | 6.7 | 36889 |
| 53 | 867.0524 | 4.1 | 22672 |
| 54 | 980.9515 | 9.1 | 49798 |
| 55 | 981.9555 | 3.9 | 21308 |
| 56 | 982.9522 | 24.7 | 135017 |
| 57 | 983.9550 | 10.5 | 57282 |
| 58 | 984.9522 | 26.8 | 146340 |
| 59 | 985.9546 | 10.5 | 57646 |
| 60 | 986.9519 | 11.0 | 59988 |
| 61 | 987.9549 | 4.5 | 24765 |
| 62 | 1033.9503 | 4.0 | 21597 |

 High Resolution Mass Spectrometry Report

| # | m/z | I % | I |
|-----|-----------|------|--------|
| 63 | 1035.9504 | 4.0 | 21808 |
| 64 | 1166.6426 | 5.4 | 29345 |
| 65 | 1167.1446 | 5.8 | 31622 |
| 66 | 1167.6432 | 7.0 | 38369 |
| 67 | 1168.1436 | 6.1 | 33314 |
| 68 | 1168.6431 | 6.2 | 33678 |
| 69 | 1169.1443 | 4.6 | 25312 |
| 70 | 1251.0944 | 5.4 | 29249 |
| 71 | 1251.5949 | 5.4 | 29270 |
| 72 | 1252.0945 | 8.1 | 44178 |
| 73 | 1252.5948 | 7.4 | 40386 |
| 74 | 1253.0941 | 9.1 | 49640 |
| 75 | 1253.5948 | 7.0 | 38241 |
| 76 | 1254.0950 | 6.6 | 35916 |
| 77 | 1254.5948 | 4.2 | 23118 |
| 78 | 1336.5457 | 5.3 | 29085 |
| 79 | 1337.0462 | 5.1 | 27864 |
| 80 | 1337.5466 | 6.4 | 35244 |
| 81 | 1338.0460 | 6.0 | 33061 |
| 82 | 1338.5467 | 5.5 | 29998 |
| 83 | 1339.0456 | 4.4 | 24125 |
| 84 | 1339.5456 | 3.6 | 19556 |
| 85 | 1350.3331 | 5.9 | 32257 |
| 86 | 1351.3357 | 4.7 | 25724 |
| 87 | 1352.3338 | 4.3 | 23570 |
| 88 | 1453.9729 | 3.8 | 20621 |
| 89 | 1517.2378 | 4.8 | 26472 |
| 90 | 1518.2414 | 4.2 | 22788 |
| 91 | 1519.2386 | 15.3 | 83590 |
| 92 | 1520.2410 | 12.7 | 69337 |
| 93 | 1521.2396 | 19.3 | 105338 |
| 94 | 1522.2412 | 13.7 | 74884 |
| 95 | 1523.2403 | 11.5 | 62782 |
| 96 | 1524.2408 | 6.5 | 35322 |
| 97 | 1525.2425 | 3.7 | 20461 |
| 98 | 1690.1485 | 5.6 | 30777 |
| 99 | 1691.1477 | 4.4 | 24241 |
| 100 | 1692.1488 | 4.7 | 25510 |

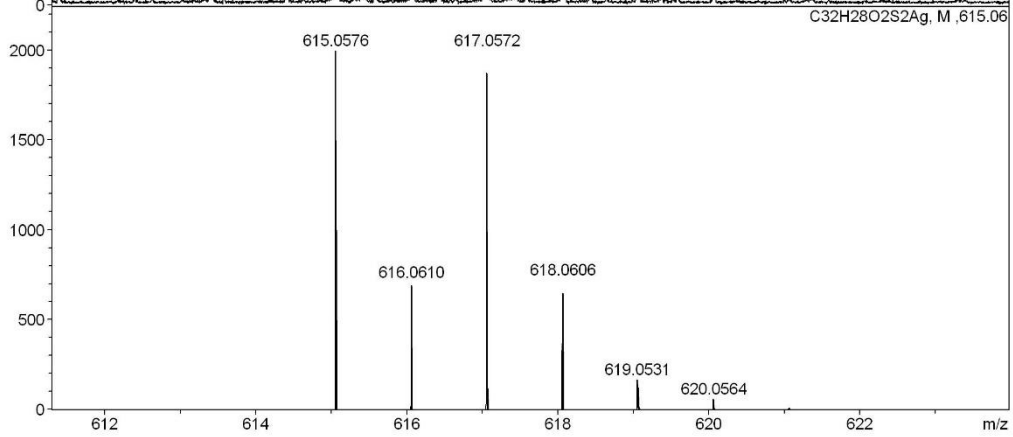
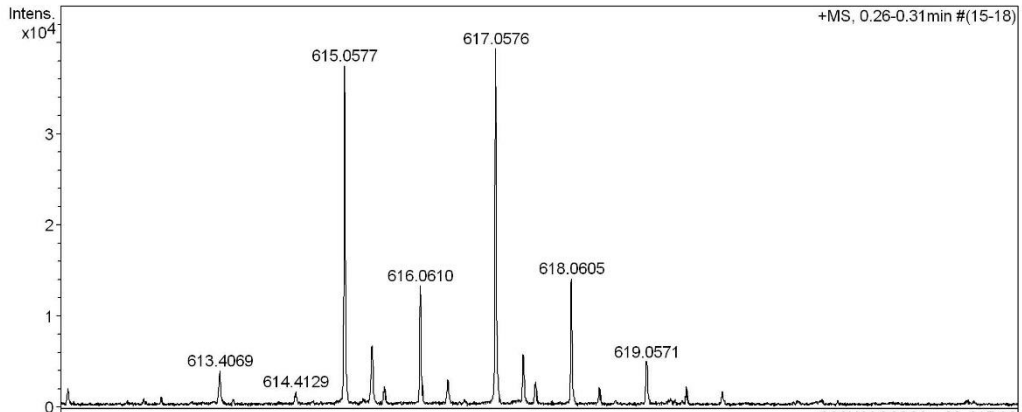
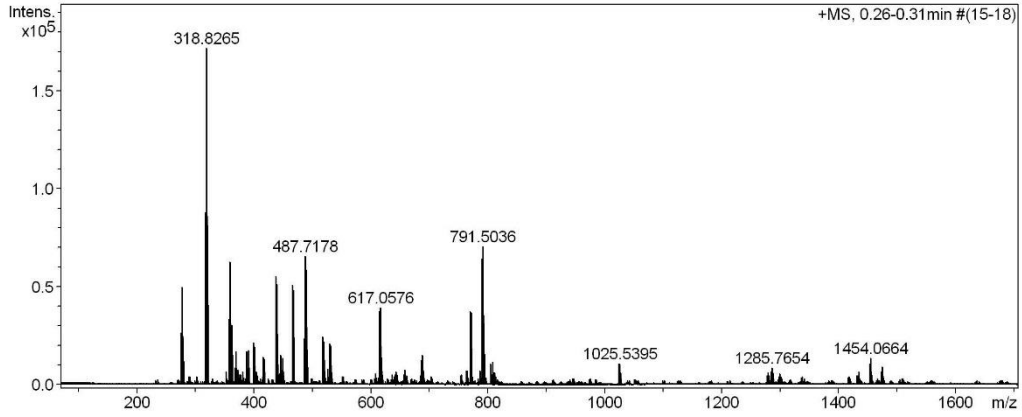
Acquisition Parameter

| | | | | | | |
|-------------------|------------------------------|----------------|---------------------------------------|----------------|--------------|-----------|
| General | Fore Vacuum | 2.59e+000 mBar | High Vacuum | 9.68e-008 mBar | Source Type | ESI |
| | Scan Begin | 75 m/z | Scan End | 1700 m/z | Ion Polarity | Positive |
| Source | Set Nebulizer | 0.4 Bar | Set Capillary | 3600 V | Set Dry Gas | 4.0 l/min |
| | Set Dry Heater | 180 °C | Set End Plate Offset | -500 V | | |
| Quadrupole | Set Ion Energy (MS only) | 4.0 eV | | | | |
| Coll. Cell | Collision Energy | 8.0 eV | Set Collision Cell RF | 500.0 Vpp | | |
| Ion Cooler | Set Ion Cooler Transfer Time | 100.0 µs | Set Ion Cooler Pre Pulse Storage Time | 18.0 µs | | |

^1H , $^{13}\text{C}\{^1\text{H}\}$ (500/126 MHz, CDCl_3) NMR and HR-ESI-MS Spectra of *ps-meta-meta* PCP:

High Resolution Mass Spectrometry Report

| | | | |
|-------------|-----------------------------------------------|------------|------------------------|
| Sample Name | Ksenia Reznikova / KR176 | Instrument | maXis 4G |
| Comment | 10 ug / mL in DCM, analyzed in MeOH+AgNO3 5mM | Method | 23 Direct_pos_higher.m |



High Resolution Mass Spectrometry Report

Measured m/z vs. theoretical m/z

| Meas. m/z | # | Formula | Score | m/z | err [mDa] | err [ppm] | mSigma | rdb | e ⁻ Conf | z |
|-----------|---|----------------------|--------|----------|-----------|-----------|--------|------|---------------------|----|
| 615.0577 | 1 | C 32 H 28 Ag O 2 S 2 | 100.00 | 615.0576 | -0.1 | -0.2 | 15.3 | 18.5 | even | 1+ |

Mass list

| # | m/z | I % | I |
|----|----------|-------|--------|
| 1 | 275.7992 | 15.4 | 26512 |
| 2 | 277.7990 | 29.0 | 49862 |
| 3 | 279.7987 | 14.2 | 24413 |
| 4 | 316.8265 | 51.4 | 88348 |
| 5 | 318.8265 | 100.0 | 171959 |
| 6 | 320.8259 | 47.4 | 81549 |
| 7 | 353.2684 | 4.0 | 6807 |
| 8 | 357.8531 | 19.5 | 33557 |
| 9 | 359.8529 | 36.7 | 63055 |
| 10 | 361.1314 | 4.0 | 6819 |
| 11 | 361.8525 | 17.7 | 30482 |
| 12 | 363.1313 | 4.1 | 7072 |
| 13 | 367.8236 | 5.2 | 9028 |
| 14 | 369.8232 | 10.0 | 17274 |
| 15 | 371.8229 | 4.6 | 7919 |
| 16 | 377.1469 | 3.1 | 5314 |
| 17 | 381.2997 | 3.8 | 6591 |
| 18 | 388.1784 | 10.0 | 17203 |
| 19 | 389.1628 | 5.0 | 8665 |
| 20 | 390.1780 | 10.3 | 17783 |
| 21 | 391.1625 | 4.4 | 7627 |
| 22 | 399.1103 | 12.6 | 21689 |
| 23 | 401.1100 | 11.4 | 19679 |
| 24 | 403.8031 | 4.1 | 7036 |
| 25 | 415.1050 | 8.2 | 14093 |
| 26 | 417.1048 | 7.7 | 13228 |
| 27 | 437.1833 | 32.3 | 55554 |
| 28 | 438.1865 | 6.9 | 11904 |
| 29 | 439.1830 | 29.9 | 51439 |
| 30 | 440.1862 | 6.2 | 10660 |
| 31 | 444.6914 | 3.4 | 5930 |
| 32 | 446.6916 | 8.8 | 15122 |
| 33 | 448.6913 | 8.0 | 13787 |
| 34 | 465.2141 | 29.6 | 50825 |
| 35 | 466.2172 | 7.2 | 12390 |
| 36 | 467.2138 | 28.1 | 48272 |
| 37 | 468.2171 | 6.5 | 11138 |
| 38 | 485.7180 | 13.8 | 23713 |
| 39 | 487.7178 | 38.3 | 65811 |
| 40 | 489.7174 | 34.3 | 58969 |
| 41 | 491.7172 | 10.7 | 18361 |
| 42 | 517.2963 | 14.3 | 24560 |
| 43 | 518.2999 | 4.7 | 8097 |
| 44 | 519.2963 | 13.0 | 22326 |
| 45 | 520.2990 | 4.3 | 7458 |
| 46 | 526.7442 | 4.7 | 8166 |
| 47 | 528.7439 | 12.4 | 21365 |
| 48 | 530.7434 | 11.7 | 20151 |
| 49 | 532.7430 | 4.1 | 6979 |
| 50 | 608.0739 | 3.4 | 5845 |
| 51 | 615.0577 | 21.8 | 37519 |
| 52 | 615.4221 | 4.0 | 6802 |
| 53 | 616.0610 | 7.8 | 13376 |
| 54 | 617.0576 | 22.9 | 39358 |
| 55 | 617.4258 | 3.4 | 5845 |
| 56 | 618.0605 | 8.2 | 14162 |
| 57 | 643.4553 | 4.0 | 6958 |
| 58 | 656.6103 | 3.1 | 5342 |
| 59 | 658.6102 | 4.5 | 7730 |
| 60 | 686.1893 | 7.3 | 12564 |
| 61 | 688.1898 | 8.8 | 15196 |
| 62 | 689.1927 | 3.2 | 5437 |

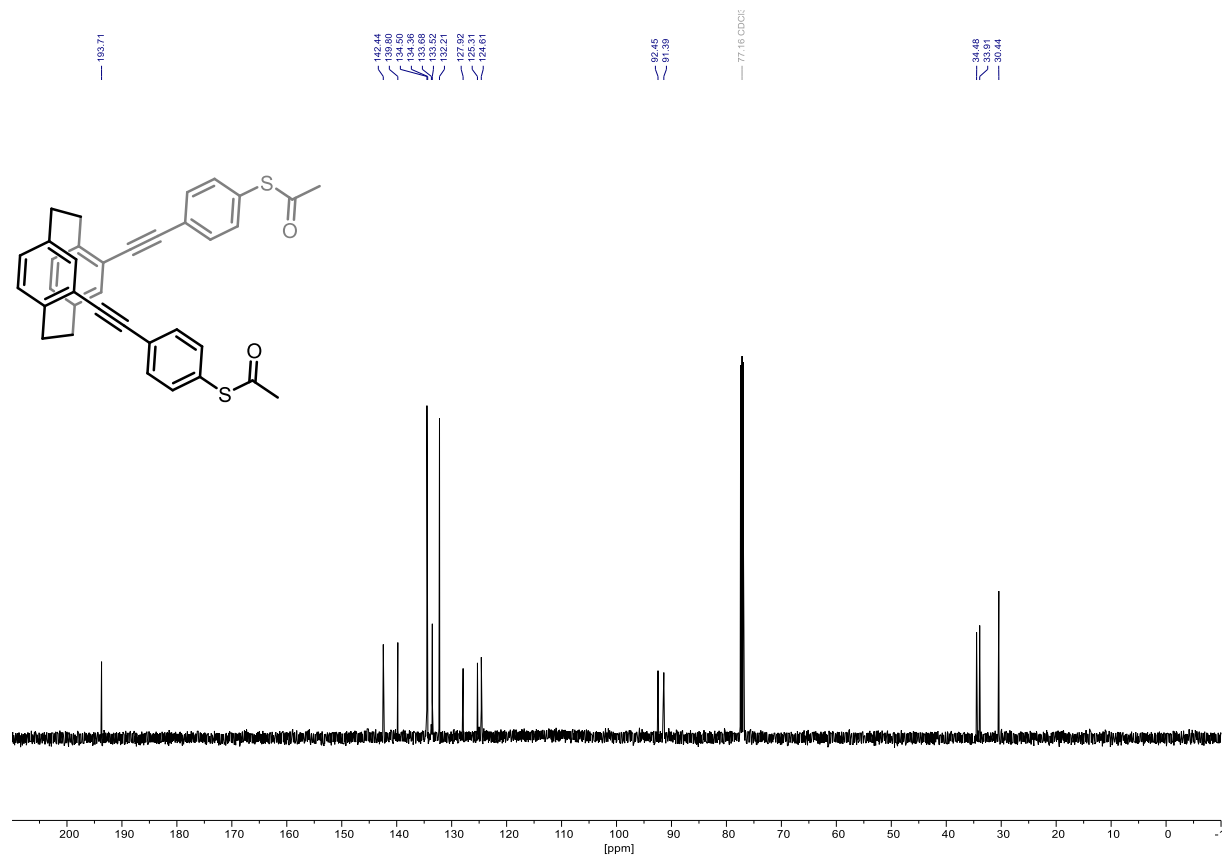
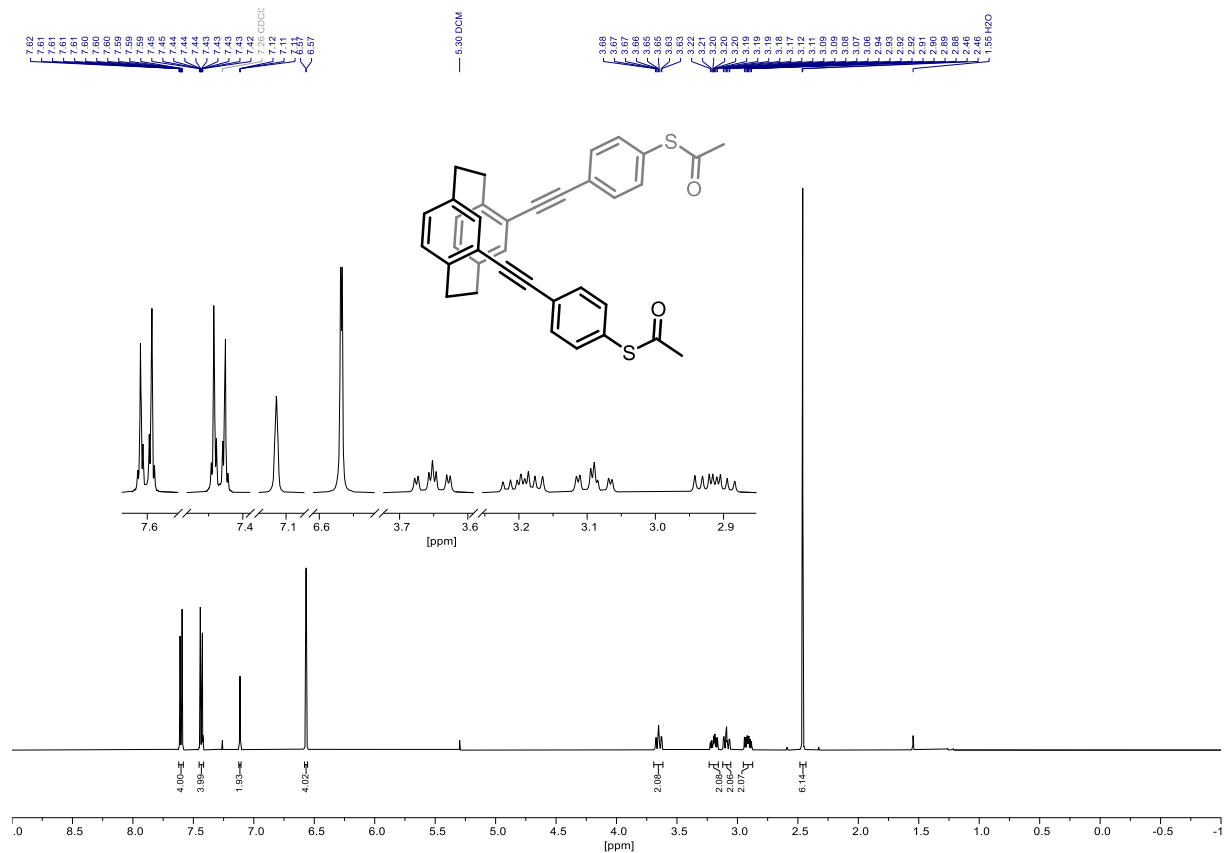
 High Resolution Mass Spectrometry Report

| # | m/z | I % | I |
|-----|-----------|------|-------|
| 63 | 690.1901 | 4.2 | 7267 |
| 64 | 763.3371 | 4.3 | 7432 |
| 65 | 765.3372 | 4.3 | 7334 |
| 66 | 769.3550 | 21.8 | 37412 |
| 67 | 770.3582 | 10.3 | 17688 |
| 68 | 771.3556 | 21.4 | 36859 |
| 69 | 772.3586 | 9.9 | 16981 |
| 70 | 785.9552 | 4.2 | 7207 |
| 71 | 789.5033 | 37.4 | 64311 |
| 72 | 790.5061 | 18.7 | 32143 |
| 73 | 791.5036 | 41.1 | 70609 |
| 74 | 792.5060 | 18.5 | 31751 |
| 75 | 793.5064 | 5.4 | 9248 |
| 76 | 805.4991 | 6.3 | 10839 |
| 77 | 806.5019 | 3.1 | 5345 |
| 78 | 807.4992 | 6.7 | 11603 |
| 79 | 810.3834 | 3.6 | 6199 |
| 80 | 812.3844 | 3.8 | 6576 |
| 81 | 1023.5381 | 6.1 | 10574 |
| 82 | 1024.5412 | 3.8 | 6541 |
| 83 | 1025.5395 | 6.3 | 10860 |
| 84 | 1026.5436 | 3.8 | 6528 |
| 85 | 1279.5806 | 3.8 | 6578 |
| 86 | 1283.7650 | 4.1 | 7072 |
| 87 | 1284.7677 | 3.3 | 5674 |
| 88 | 1285.7654 | 5.0 | 8604 |
| 89 | 1286.7686 | 3.6 | 6123 |
| 90 | 1299.7346 | 3.5 | 6063 |
| 91 | 1433.9135 | 3.9 | 6698 |
| 92 | 1452.0633 | 6.2 | 10611 |
| 93 | 1453.0679 | 5.5 | 9397 |
| 94 | 1454.0664 | 8.0 | 13748 |
| 95 | 1455.0693 | 6.0 | 10399 |
| 96 | 1456.0706 | 3.2 | 5578 |
| 97 | 1472.2177 | 3.9 | 6669 |
| 98 | 1473.2212 | 3.7 | 6396 |
| 99 | 1474.2197 | 5.5 | 9448 |
| 100 | 1475.2217 | 4.2 | 7274 |

Acquisition Parameter

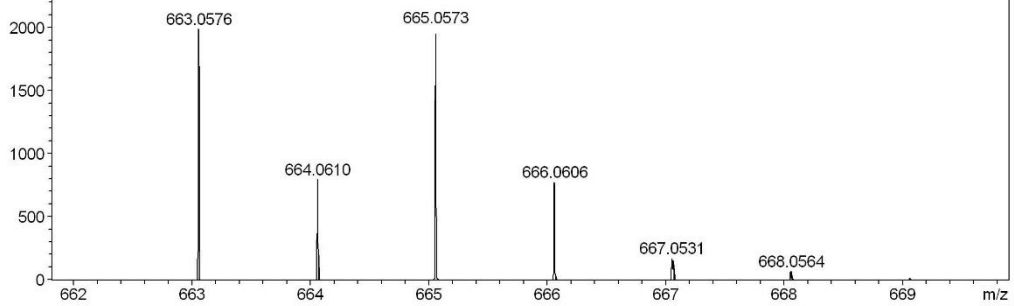
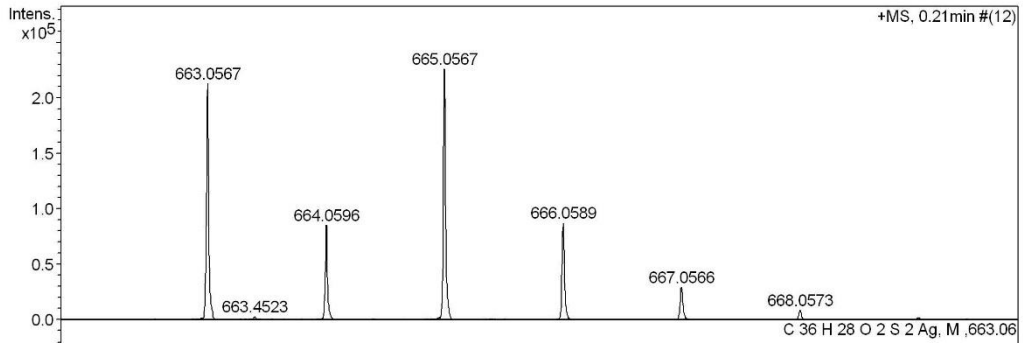
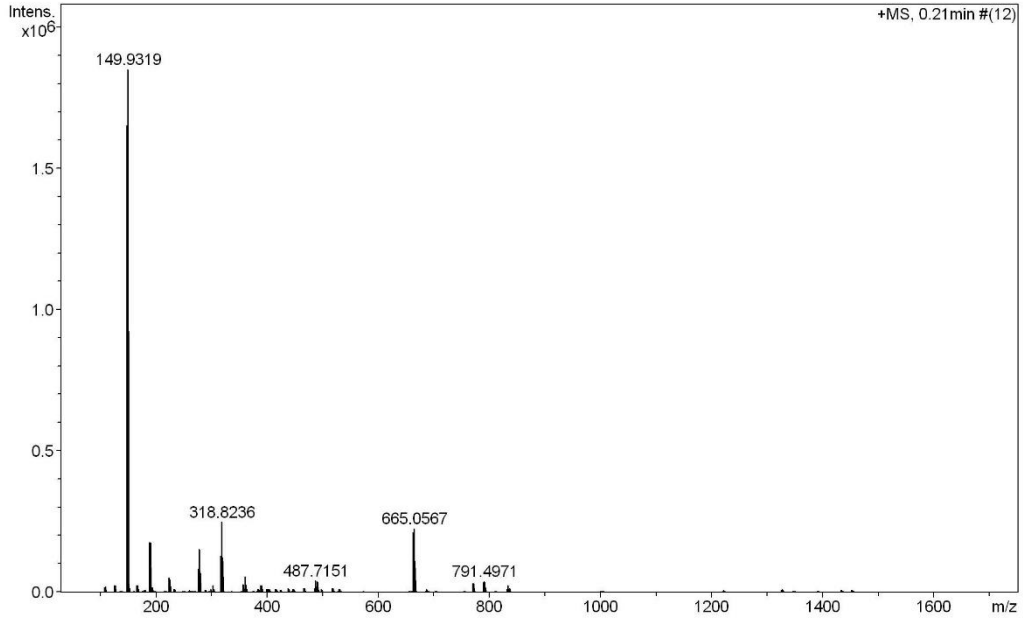
| | | | | | | |
|-------------------|------------------------------|----------------|---------------------------------------|----------------|--------------|-----------|
| General | Fore Vacuum | 2.54e+000 mBar | High Vacuum | 9.65e-008 mBar | Source Type | ESI |
| | Scan Begin | 75 m/z | Scan End | 1700 m/z | Ion Polarity | Positive |
| Source | Set Nebulizer | 0.4 Bar | Set Capillary | 3600 V | Set Dry Gas | 4.0 l/min |
| | Set Dry Heater | 180 °C | Set End Plate Offset | -500 V | | |
| Quadrupole | Set Ion Energy (MS only) | 4.0 eV | | | | |
| Coll. Cell | Collision Energy | 8.0 eV | Set Collision Cell RF | 500.0 Vpp | | |
| Ion Cooler | Set Ion Cooler Transfer Time | 100.0 µs | Set Ion Cooler Pre Pulse Storage Time | 18.0 µs | | |

^1H , $^{13}\text{C}\{\text{H}\}$ (500/126 MHz, CDCl_3) NMR and HR-ESI-MS Spectra of *ps-ortho-bis*((4'-acetylthio)phenyl)ethynyl)[2.2]paracyclophane (47):



High Resolution Mass Spectrometry Report

| | | | |
|-------------|-------------------------------------------|------------|---------------------|
| Sample Name | KR305 | Instrument | maXis 4G |
| Comment | dissolved in MeOH + AgNO ₃ 1mM | Method | 22 Direct_pos_mid.m |



 High Resolution Mass Spectrometry Report

Measured m/z vs. theoretical m/z

| Meas. m/z | # | Formula | Score | m/z | err [mDa] | err [ppm] | mSigma | rdb | e ⁻ Conf | z |
|-----------|---|----------------------|--------|----------|-----------|-----------|--------|------|---------------------|----|
| 663.0567 | 1 | C 36 H 28 Ag O 2 S 2 | 100.00 | 663.0576 | 0.9 | 1.4 | 16.6 | 22.5 | even | 1+ |

Mass list

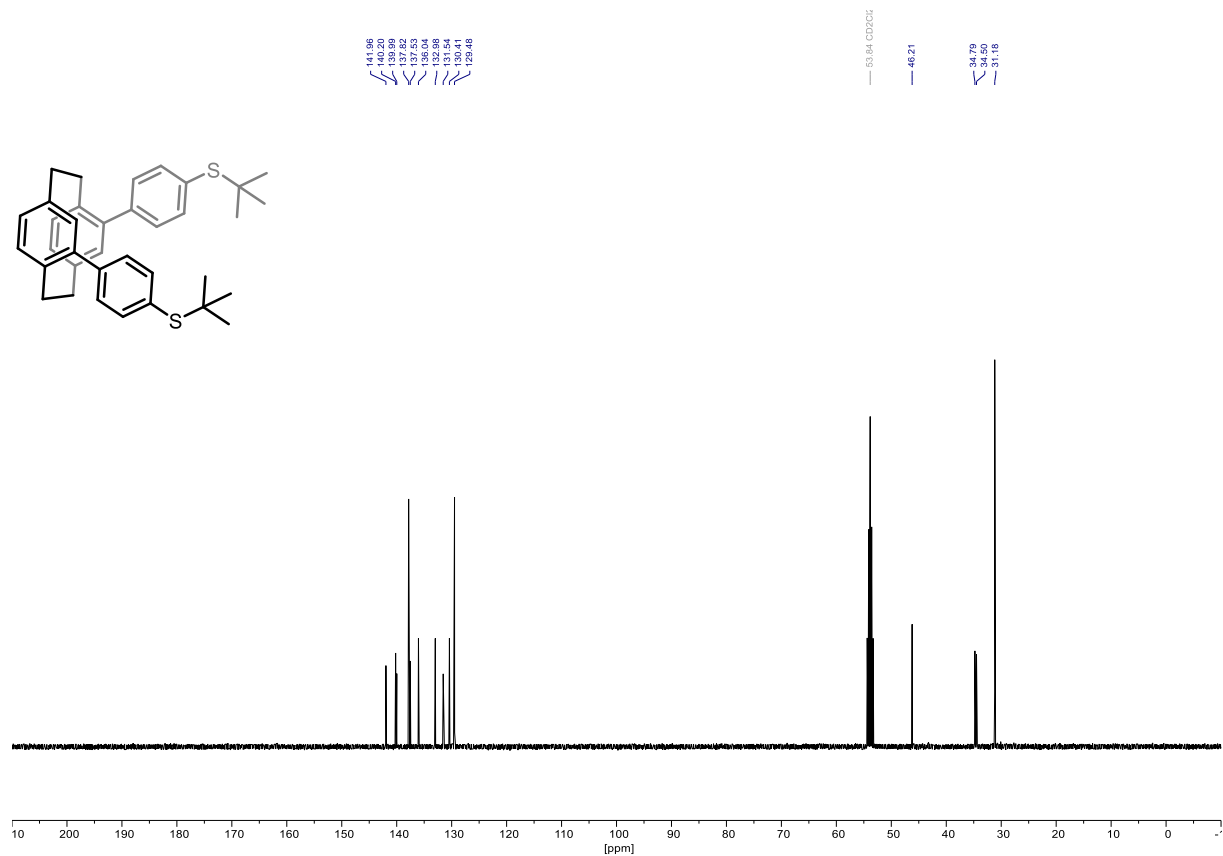
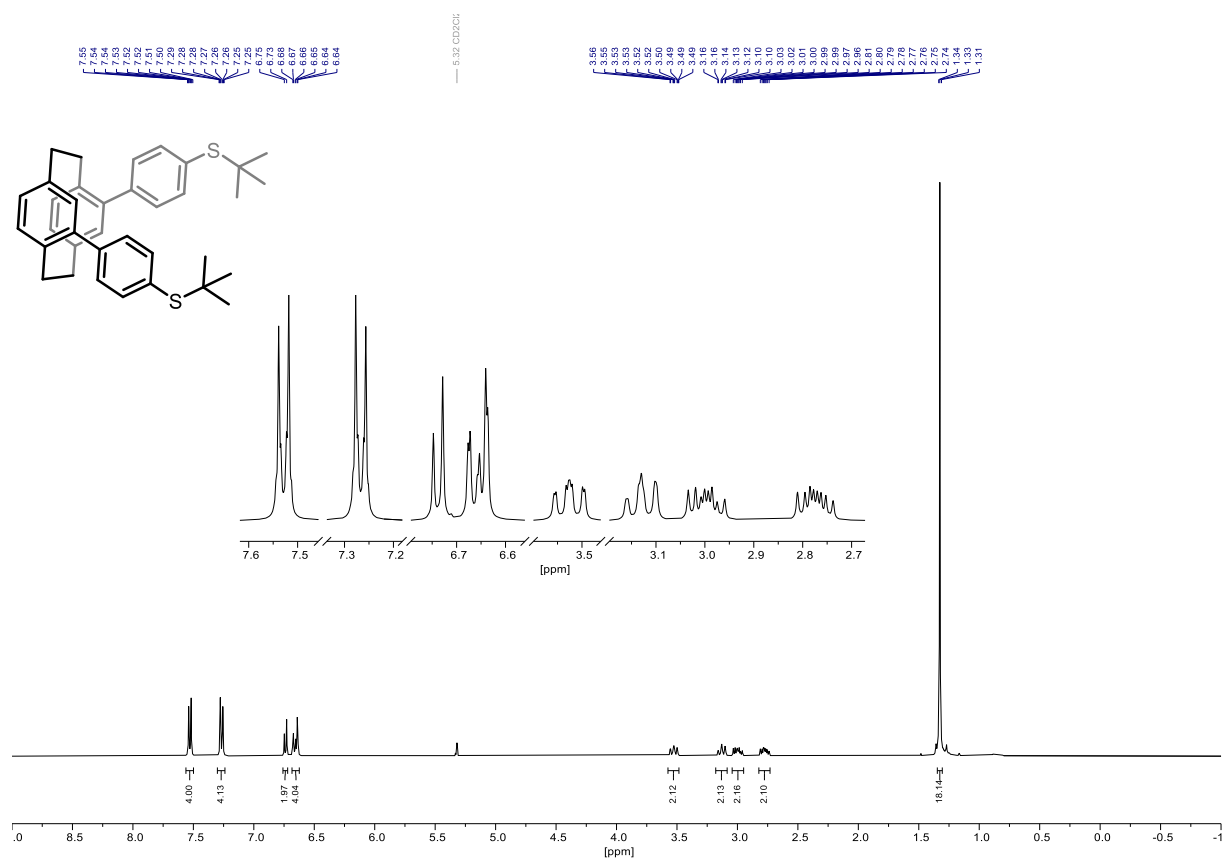
| # | m/z | I % | I |
|----|----------|-------|---------|
| 1 | 106.9047 | 0.9 | 17040 |
| 2 | 108.9043 | 1.1 | 20241 |
| 3 | 124.9157 | 1.3 | 23670 |
| 4 | 126.9154 | 1.4 | 26360 |
| 5 | 147.9322 | 89.2 | 1652485 |
| 6 | 148.9349 | 1.7 | 31592 |
| 7 | 149.9319 | 100.0 | 1851735 |
| 8 | 150.9344 | 1.7 | 31214 |
| 9 | 165.9426 | 1.4 | 25959 |
| 10 | 167.9423 | 1.4 | 25401 |
| 11 | 178.9626 | 0.4 | 8274 |
| 12 | 180.9621 | 0.4 | 7902 |
| 13 | 188.9584 | 9.5 | 176613 |
| 14 | 189.9611 | 0.5 | 8665 |
| 15 | 190.9580 | 9.6 | 177266 |
| 16 | 191.8825 | 1.0 | 18922 |
| 17 | 191.9609 | 0.4 | 8237 |
| 18 | 193.8822 | 0.9 | 17288 |
| 19 | 222.9886 | 2.8 | 51322 |
| 20 | 224.9881 | 2.5 | 46815 |
| 21 | 232.9090 | 0.7 | 12126 |
| 22 | 234.9087 | 0.6 | 11808 |
| 23 | 260.8067 | 0.4 | 7673 |
| 24 | 275.7973 | 4.6 | 84300 |
| 25 | 277.7970 | 8.3 | 153644 |
| 26 | 279.7967 | 3.8 | 70663 |
| 27 | 288.9747 | 0.4 | 7660 |
| 28 | 290.9746 | 0.4 | 7556 |
| 29 | 299.8333 | 0.7 | 12874 |
| 30 | 301.8331 | 1.3 | 24724 |
| 31 | 303.8330 | 0.7 | 12060 |
| 32 | 316.8237 | 7.0 | 128770 |
| 33 | 318.8236 | 13.5 | 249444 |
| 34 | 319.8254 | 0.4 | 6696 |
| 35 | 320.8230 | 5.9 | 110074 |
| 36 | 357.8500 | 1.6 | 28910 |
| 37 | 359.8495 | 3.0 | 55777 |
| 38 | 361.1281 | 0.6 | 10701 |
| 39 | 361.8489 | 1.4 | 25308 |
| 40 | 362.7738 | 0.4 | 7627 |
| 41 | 363.1273 | 0.6 | 10970 |
| 42 | 383.0762 | 0.5 | 9785 |
| 43 | 385.0752 | 0.5 | 9589 |
| 44 | 388.1746 | 1.4 | 25444 |
| 45 | 389.1593 | 0.7 | 13387 |
| 46 | 390.1744 | 1.3 | 23652 |
| 47 | 391.1592 | 0.6 | 11906 |
| 48 | 399.1069 | 0.6 | 10690 |
| 49 | 401.1067 | 0.6 | 11566 |
| 50 | 403.1737 | 0.5 | 10147 |
| 51 | 403.8000 | 0.4 | 8096 |
| 52 | 405.1742 | 0.5 | 9533 |
| 53 | 415.1019 | 0.7 | 12433 |
| 54 | 417.1018 | 0.7 | 12344 |
| 55 | 424.1023 | 0.3 | 6163 |
| 56 | 437.1800 | 0.7 | 13028 |
| 57 | 439.1796 | 0.7 | 12434 |
| 58 | 446.6886 | 0.6 | 10344 |
| 59 | 448.6879 | 0.6 | 10346 |
| 60 | 465.2106 | 0.8 | 14082 |
| 61 | 467.2109 | 0.8 | 13993 |
| 62 | 485.7152 | 0.8 | 14898 |

 High Resolution Mass Spectrometry Report

| # | m/z | I % | I |
|-----|-----------|------|--------|
| 63 | 487.7151 | 2.3 | 41928 |
| 64 | 489.7148 | 2.1 | 39512 |
| 65 | 491.7146 | 0.7 | 12449 |
| 66 | 497.1791 | 0.5 | 9777 |
| 67 | 499.1793 | 0.4 | 7501 |
| 68 | 517.2938 | 0.8 | 14153 |
| 69 | 519.2940 | 0.8 | 13982 |
| 70 | 528.7416 | 0.7 | 12166 |
| 71 | 530.7413 | 0.6 | 11440 |
| 72 | 531.2577 | 0.3 | 6217 |
| 73 | 663.0567 | 11.5 | 213111 |
| 74 | 664.0596 | 4.6 | 85398 |
| 75 | 665.0567 | 12.2 | 226266 |
| 76 | 666.0589 | 4.7 | 87764 |
| 77 | 667.0566 | 1.6 | 29606 |
| 78 | 668.0573 | 0.5 | 8825 |
| 79 | 688.1871 | 0.6 | 10866 |
| 80 | 769.3499 | 1.6 | 30437 |
| 81 | 770.3532 | 0.8 | 14798 |
| 82 | 771.3505 | 1.7 | 30912 |
| 83 | 772.3524 | 0.7 | 13633 |
| 84 | 789.4970 | 2.0 | 36887 |
| 85 | 790.5004 | 0.9 | 17496 |
| 86 | 791.4971 | 2.1 | 38939 |
| 87 | 792.4999 | 1.0 | 18180 |
| 88 | 831.9506 | 0.6 | 10658 |
| 89 | 833.9504 | 1.3 | 23422 |
| 90 | 834.9529 | 0.5 | 9375 |
| 91 | 835.9507 | 0.7 | 13252 |
| 92 | 1221.2219 | 0.4 | 6926 |
| 93 | 1325.5187 | 0.5 | 8959 |
| 94 | 1326.5205 | 0.4 | 7102 |
| 95 | 1327.5186 | 0.7 | 12173 |
| 96 | 1328.5207 | 0.5 | 8589 |
| 97 | 1431.8147 | 0.3 | 6316 |
| 98 | 1433.8178 | 0.5 | 8650 |
| 99 | 1434.8210 | 0.3 | 6276 |
| 100 | 1453.9650 | 0.4 | 7326 |

Acquisition Parameter

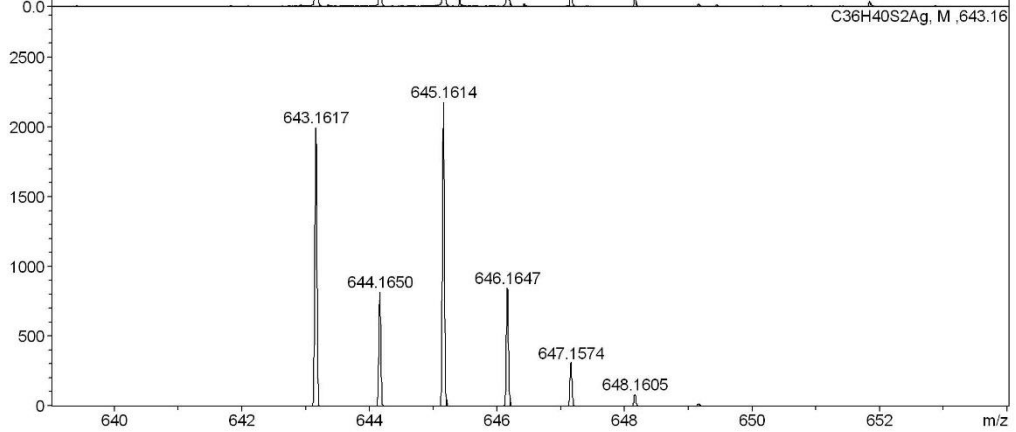
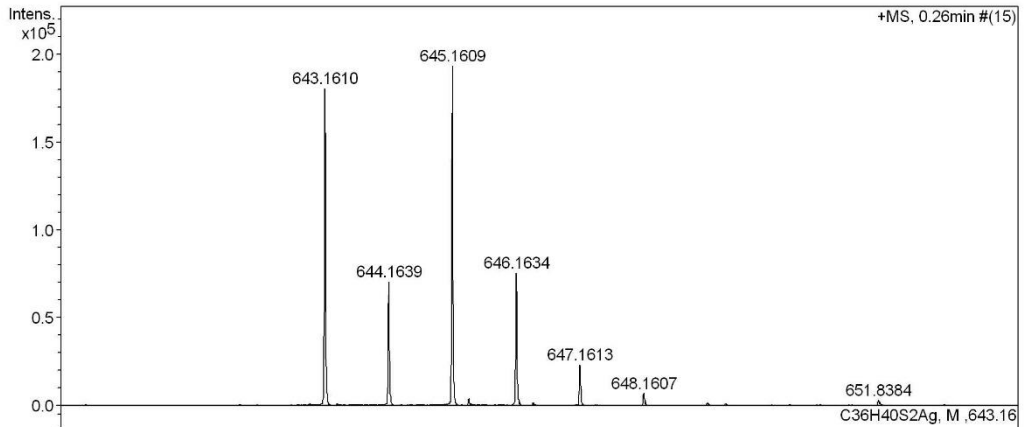
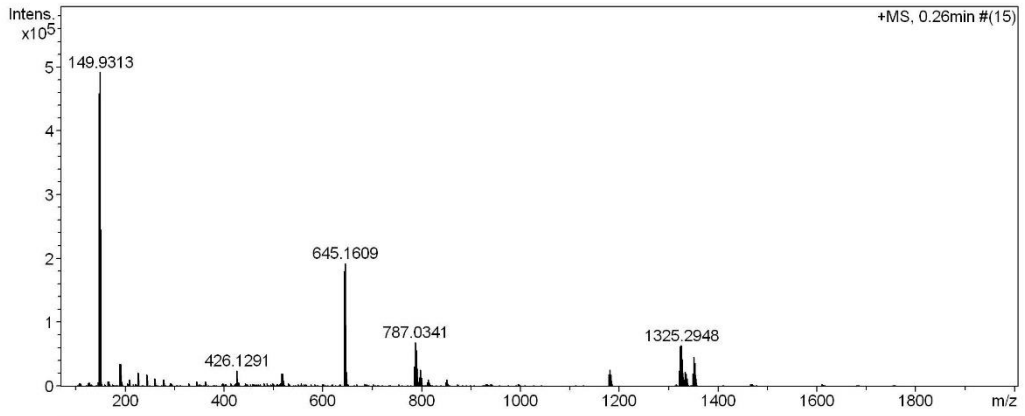
| | | | | | | |
|-------------------|------------------------------|----------------|---------------------------------------|----------------|--------------|-----------|
| General | Fore Vacuum | 3.46e+000 mBar | High Vacuum | 9.21e-008 mBar | Source Type | ESI |
| | Scan Begin | 75 m/z | Scan End | 1700 m/z | Ion Polarity | Positive |
| Source | Set Nebulizer | 0.4 Bar | Set Capillary | 3600 V | Set Dry Gas | 4.0 l/min |
| | Set Dry Heater | 180 °C | Set End Plate Offset | -500 V | | |
| Quadrupole | Set Ion Energy (MS only) | 4.0 eV | | | | |
| Coll. Cell | Collision Energy | 8.0 eV | Set Collision Cell RF | 350.0 Vpp | 100.0 Vpp | |
| Ion Cooler | Set Ion Cooler Transfer Time | 75.0 µs | Set Ion Cooler Pre Pulse Storage Time | 10.0 µs | | |

^1H , $^{13}\text{C}\{^1\text{H}\}$ (500/126 MHz, CDCl_3) NMR and HR-ESI-MS Spectra of *ps-ortho-bis*((4'-*tert*-butylthio)phenyl)[2.2]paracyclophane (56**):**

High Resolution Mass Spectrometry Report

Sample Name KR311+Ag
Comment

Instrument maXis 4G
Method ms_nocolumn_mid_pos.m



 High Resolution Mass Spectrometry Report

Measured m/z vs. theoretical m/z

| Meas. m/z | # | Formula | Score | m/z | err [mDa] | err [ppm] | mSigma | rdb | e ⁻ Conf | z |
|-----------|---|------------------|--------|----------|-----------|-----------|--------|------|---------------------|----|
| 643.1610 | 1 | C 36 H 40 Ag S 2 | 100.00 | 643.1617 | 0.7 | 1.1 | 15.5 | 16.5 | even | 1+ |

Mass list

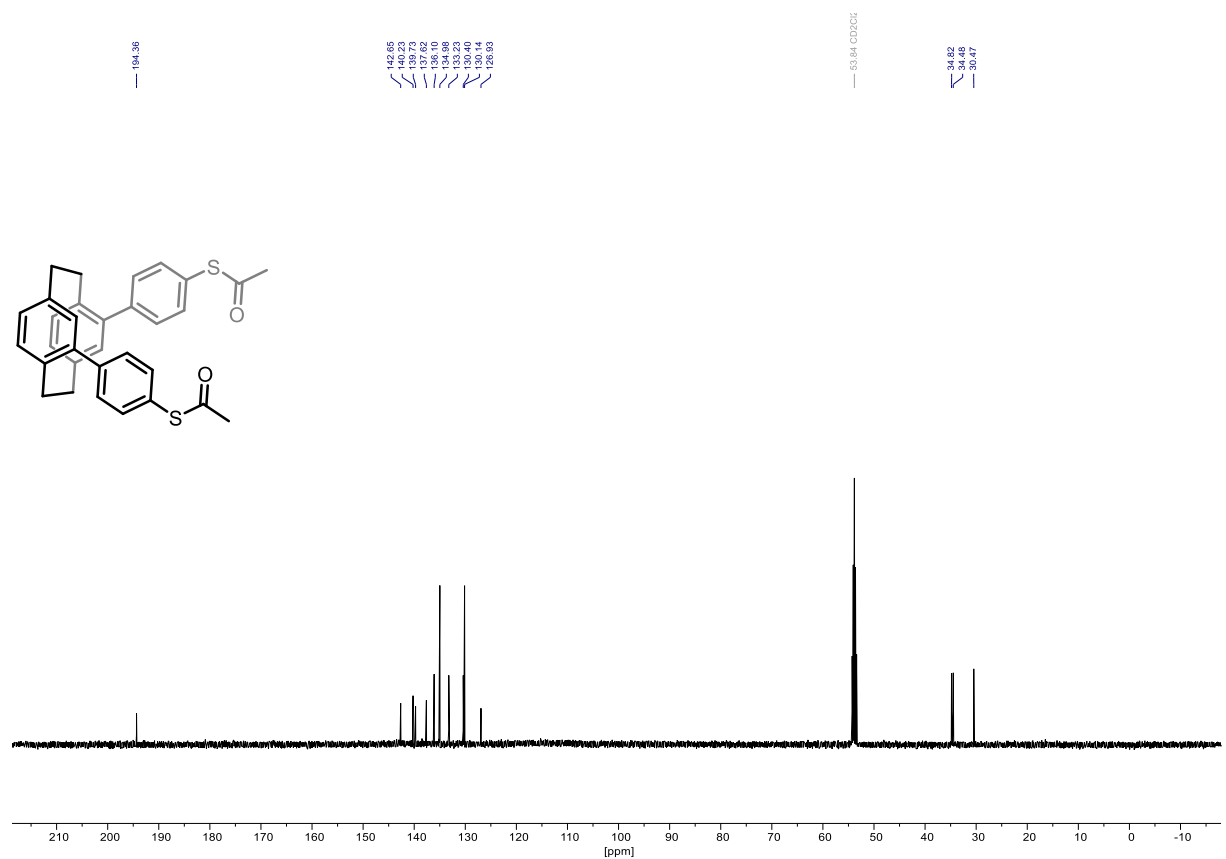
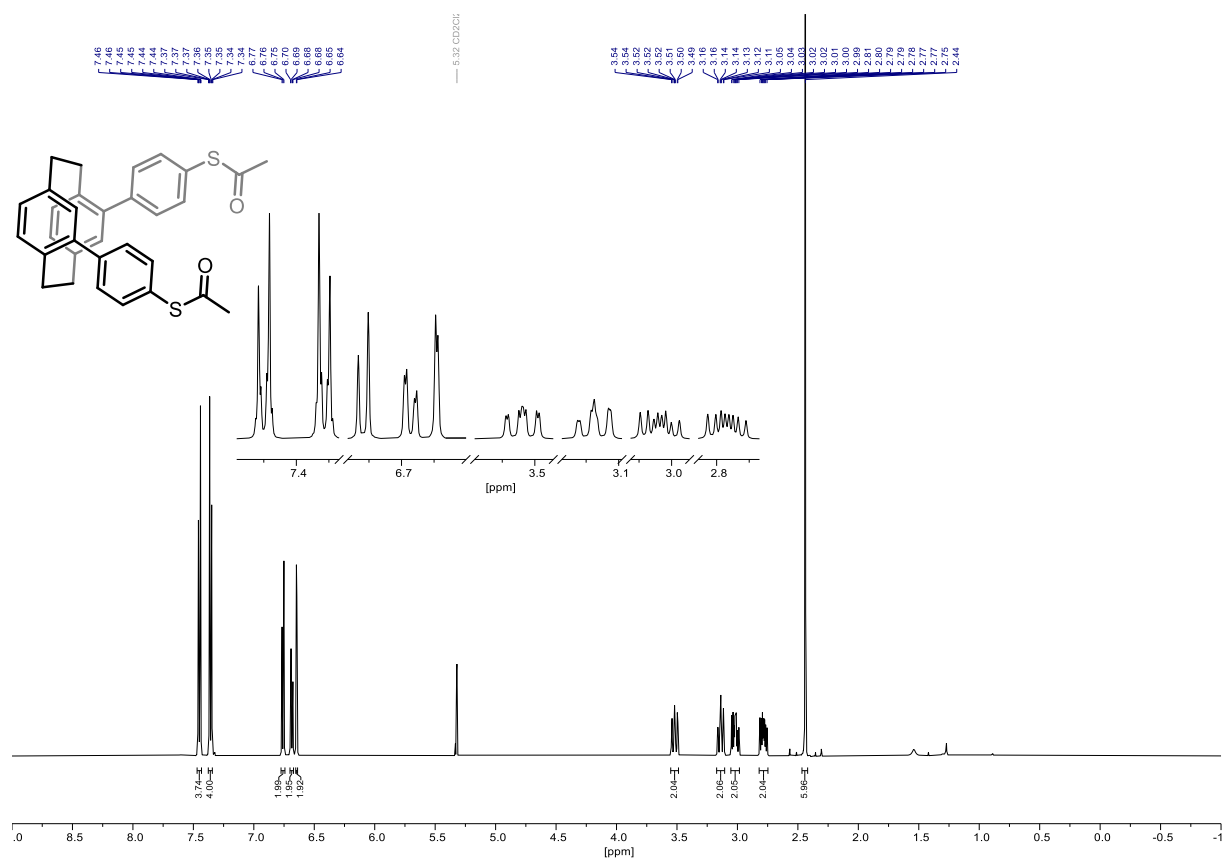
| # | m/z | I % | I |
|----|----------|-------|--------|
| 1 | 106.9046 | 1.1 | 5313 |
| 2 | 108.9043 | 1.1 | 5453 |
| 3 | 124.9156 | 1.1 | 5350 |
| 4 | 126.9152 | 1.3 | 6320 |
| 5 | 144.9823 | 1.3 | 6576 |
| 6 | 147.9316 | 93.1 | 458322 |
| 7 | 148.9344 | 1.7 | 8378 |
| 8 | 149.9313 | 100.0 | 492539 |
| 9 | 150.9341 | 1.7 | 8352 |
| 10 | 165.9421 | 1.6 | 7662 |
| 11 | 167.9417 | 1.5 | 7592 |
| 12 | 188.9577 | 7.2 | 35298 |
| 13 | 190.9574 | 7.3 | 35753 |
| 14 | 192.9444 | 1.7 | 8140 |
| 15 | 203.9307 | 1.1 | 5301 |
| 16 | 205.0603 | 1.1 | 5574 |
| 17 | 209.0216 | 2.4 | 11848 |
| 18 | 226.9514 | 4.3 | 21308 |
| 19 | 243.9415 | 3.7 | 18070 |
| 20 | 260.9317 | 2.6 | 12762 |
| 21 | 277.0090 | 0.9 | 4364 |
| 22 | 277.9212 | 2.1 | 10435 |
| 23 | 328.9183 | 0.9 | 4551 |
| 24 | 345.9087 | 1.7 | 8264 |
| 25 | 362.8992 | 1.7 | 8304 |
| 26 | 362.9258 | 1.3 | 6173 |
| 27 | 399.3071 | 0.9 | 4530 |
| 28 | 413.8964 | 1.0 | 5066 |
| 29 | 423.6270 | 1.0 | 4788 |
| 30 | 426.1291 | 5.0 | 24853 |
| 31 | 426.6304 | 2.0 | 9880 |
| 32 | 430.8864 | 1.3 | 6369 |
| 33 | 430.9126 | 1.2 | 5858 |
| 34 | 443.3334 | 1.1 | 5652 |
| 35 | 481.8834 | 1.1 | 5228 |
| 36 | 487.3594 | 1.1 | 5438 |
| 37 | 498.8735 | 1.2 | 5689 |
| 38 | 515.8641 | 1.0 | 4709 |
| 39 | 517.2945 | 4.1 | 19952 |
| 40 | 518.2974 | 1.3 | 6478 |
| 41 | 519.2948 | 4.2 | 20462 |
| 42 | 520.2979 | 1.3 | 6636 |
| 43 | 531.3858 | 0.9 | 4591 |
| 44 | 643.1610 | 36.7 | 180857 |
| 45 | 644.1639 | 14.4 | 70834 |
| 46 | 645.1609 | 39.3 | 193580 |
| 47 | 646.1634 | 15.4 | 75918 |
| 48 | 647.1613 | 4.8 | 23481 |
| 49 | 648.1607 | 1.5 | 7218 |
| 50 | 785.0343 | 6.2 | 30530 |
| 51 | 786.0376 | 2.7 | 13350 |
| 52 | 787.0341 | 14.1 | 69597 |
| 53 | 788.0368 | 5.7 | 28075 |
| 54 | 789.0335 | 11.7 | 57529 |
| 55 | 790.0359 | 4.2 | 20690 |
| 56 | 791.0323 | 3.2 | 15941 |
| 57 | 792.0339 | 1.2 | 5751 |
| 58 | 795.0625 | 2.8 | 13717 |
| 59 | 796.0656 | 1.0 | 5074 |
| 60 | 797.0632 | 5.4 | 26463 |
| 61 | 798.0662 | 2.2 | 10706 |
| 62 | 799.0629 | 3.0 | 14643 |

 High Resolution Mass Spectrometry Report

| # | m/z | I % | I |
|-----|-----------|------|-------|
| 63 | 800.0647 | 1.2 | 5742 |
| 64 | 812.0533 | 1.4 | 6756 |
| 65 | 814.0540 | 2.3 | 11324 |
| 66 | 815.0565 | 1.0 | 4834 |
| 67 | 816.0530 | 1.4 | 6766 |
| 68 | 849.2701 | 1.3 | 6218 |
| 69 | 851.2592 | 2.0 | 9631 |
| 70 | 852.2684 | 1.1 | 5360 |
| 71 | 1179.4191 | 3.8 | 18733 |
| 72 | 1180.4225 | 3.3 | 16352 |
| 73 | 1181.4196 | 5.3 | 26102 |
| 74 | 1182.4214 | 3.8 | 18769 |
| 75 | 1183.4227 | 2.0 | 10050 |
| 76 | 1184.4210 | 1.0 | 4784 |
| 77 | 1321.2945 | 5.1 | 25121 |
| 78 | 1322.2971 | 4.0 | 19645 |
| 79 | 1323.2946 | 12.8 | 63282 |
| 80 | 1324.2971 | 10.1 | 49739 |
| 81 | 1325.2948 | 13.0 | 64188 |
| 82 | 1326.2960 | 8.6 | 42578 |
| 83 | 1327.2950 | 5.6 | 27767 |
| 84 | 1328.2945 | 3.1 | 15219 |
| 85 | 1329.2943 | 1.4 | 6735 |
| 86 | 1331.3230 | 2.3 | 11463 |
| 87 | 1332.3249 | 2.0 | 9960 |
| 88 | 1333.3234 | 4.7 | 23338 |
| 89 | 1334.3255 | 3.7 | 18333 |
| 90 | 1335.3236 | 4.0 | 19612 |
| 91 | 1336.3259 | 2.5 | 12544 |
| 92 | 1337.3261 | 1.4 | 6804 |
| 93 | 1348.3142 | 4.2 | 20904 |
| 94 | 1349.3164 | 3.6 | 17785 |
| 95 | 1350.3136 | 9.3 | 46020 |
| 96 | 1351.3169 | 7.3 | 35769 |
| 97 | 1352.3147 | 7.5 | 36874 |
| 98 | 1353.3158 | 5.4 | 26385 |
| 99 | 1354.3149 | 2.5 | 12436 |
| 100 | 1355.3146 | 1.1 | 5430 |

Acquisition Parameter

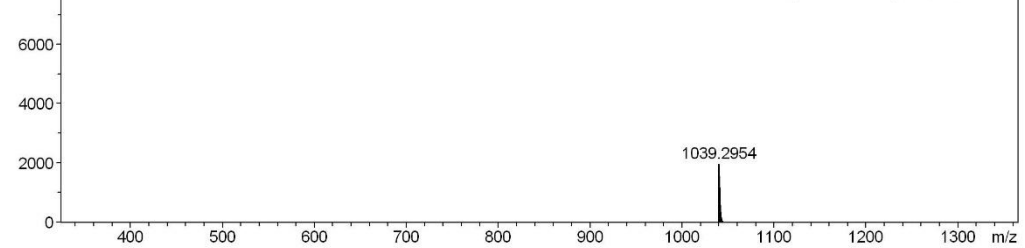
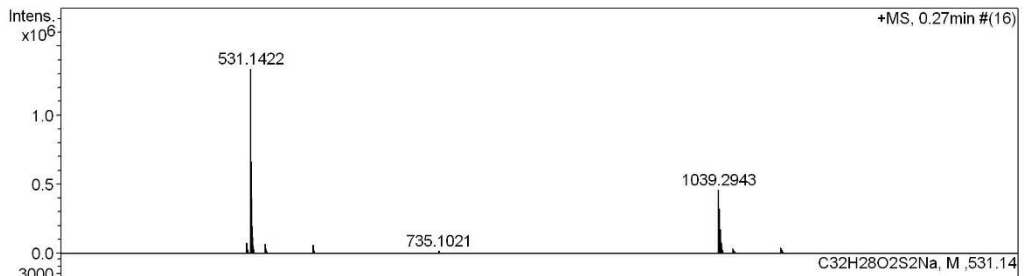
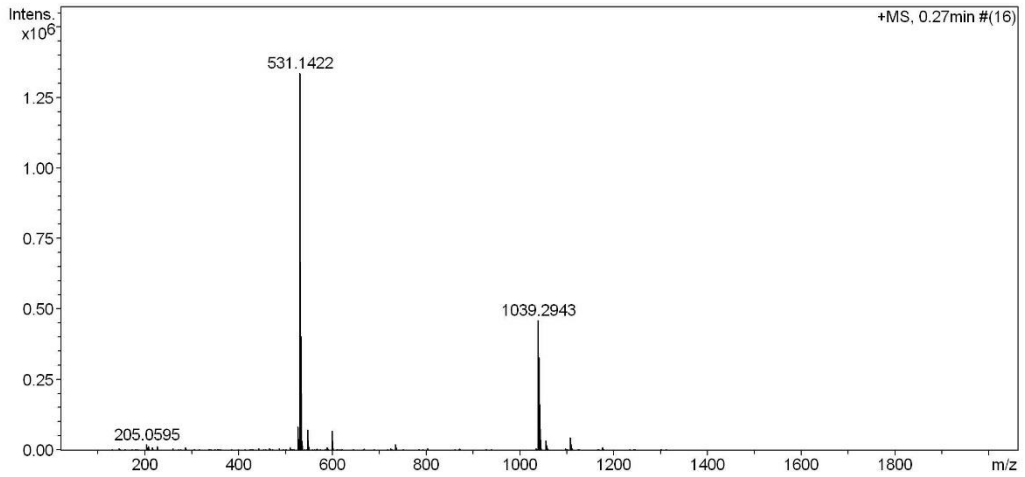
| | | | | | | |
|-------------------|------------------------------|----------------|---------------------------------------|----------------|--------------|-----------|
| General | Fore Vacuum | 3.36e+000 mBar | High Vacuum | 9.61e-008 mBar | Source Type | ESI |
| | Scan Begin | 75 m/z | Scan End | 2000 m/z | Ion Polarity | Positive |
| Source | Set Nebulizer | 2.0 Bar | Set Capillary | 4500 V | Set Dry Gas | 8.0 l/min |
| | Set Dry Heater | 200 °C | Set End Plate Offset | -500 V | | |
| Quadrupole | Set Ion Energy (MS only) | 4.0 eV | | | | |
| Coll. Cell | Collision Energy | 8.0 eV | Set Collision Cell RF | 600.0 Vpp | 100.0 Vpp | |
| Ion Cooler | Set Ion Cooler Transfer Time | 75.0 µs | Set Ion Cooler Pre Pulse Storage Time | 10.0 µs | | |

^1H , $^{13}\text{C}\{\text{H}\}$ (500/126 MHz, CDCl_3) NMR and HR-ESI-MS Spectra of *ps*-*ortho*-bis((4'-*tert*-acetylthio)phenyl)[2.2]paracyclophane (48):

High Resolution Mass Spectrometry Report

Sample Name **KR315**
Comment

Instrument **maXis 4G**
Method **ms_nocolumn_mid_pos.m**



High Resolution Mass Spectrometry Report

Measured m/z vs. theoretical m/z

| Meas. m/z | # | Formula | Score | m/z | err [mDa] | err [ppm] | mSigma | rdb | e ⁻ Conf | z |
|-----------|---|----------------------|--------|-----------|-----------|-----------|--------|------|---------------------|----|
| 531.1422 | 1 | C 32 H 28 Na O 2 S 2 | 100.00 | 531.1423 | 0.1 | 0.2 | 39.5 | 18.5 | even | 1+ |
| 1039.2943 | 1 | C 64 H 56 Na O 4 S 4 | 100.00 | 1039.2954 | 1.0 | 1.0 | 31.4 | 36.5 | even | |

Mass list

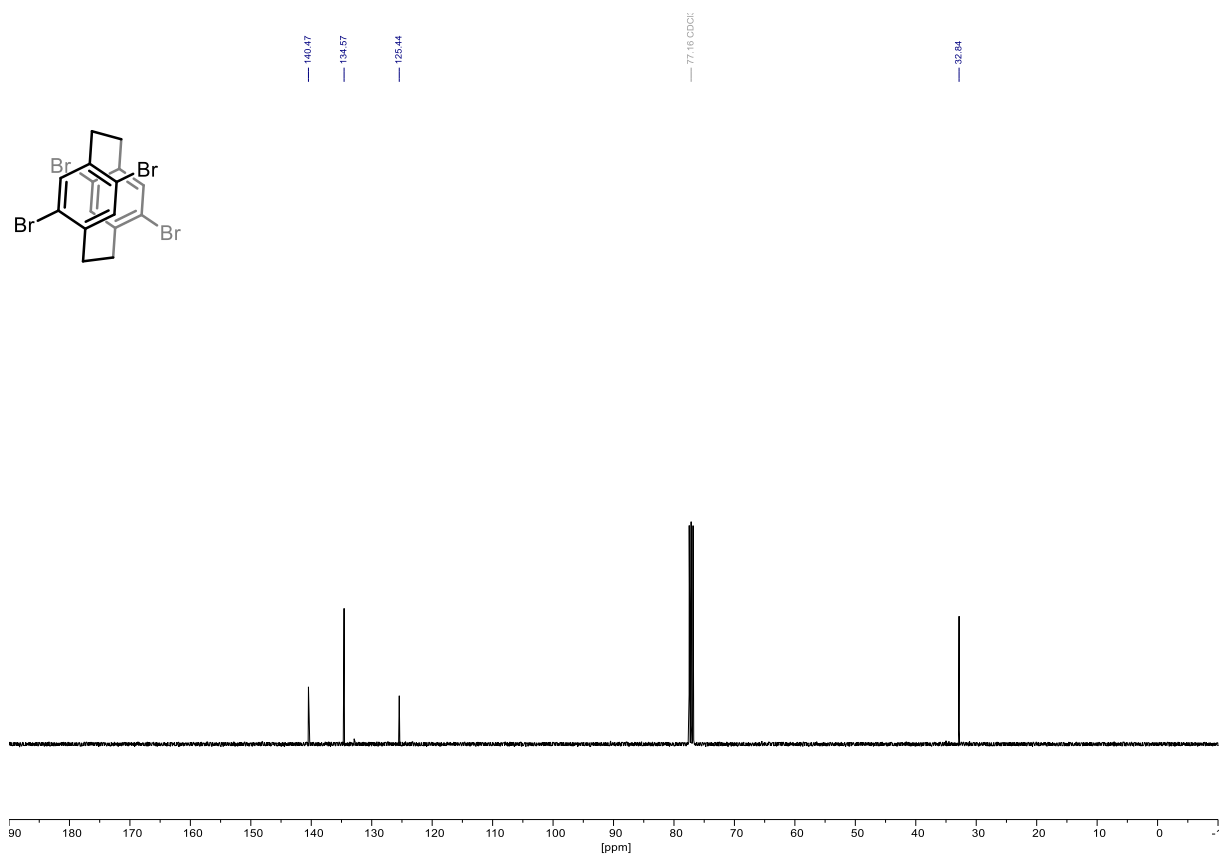
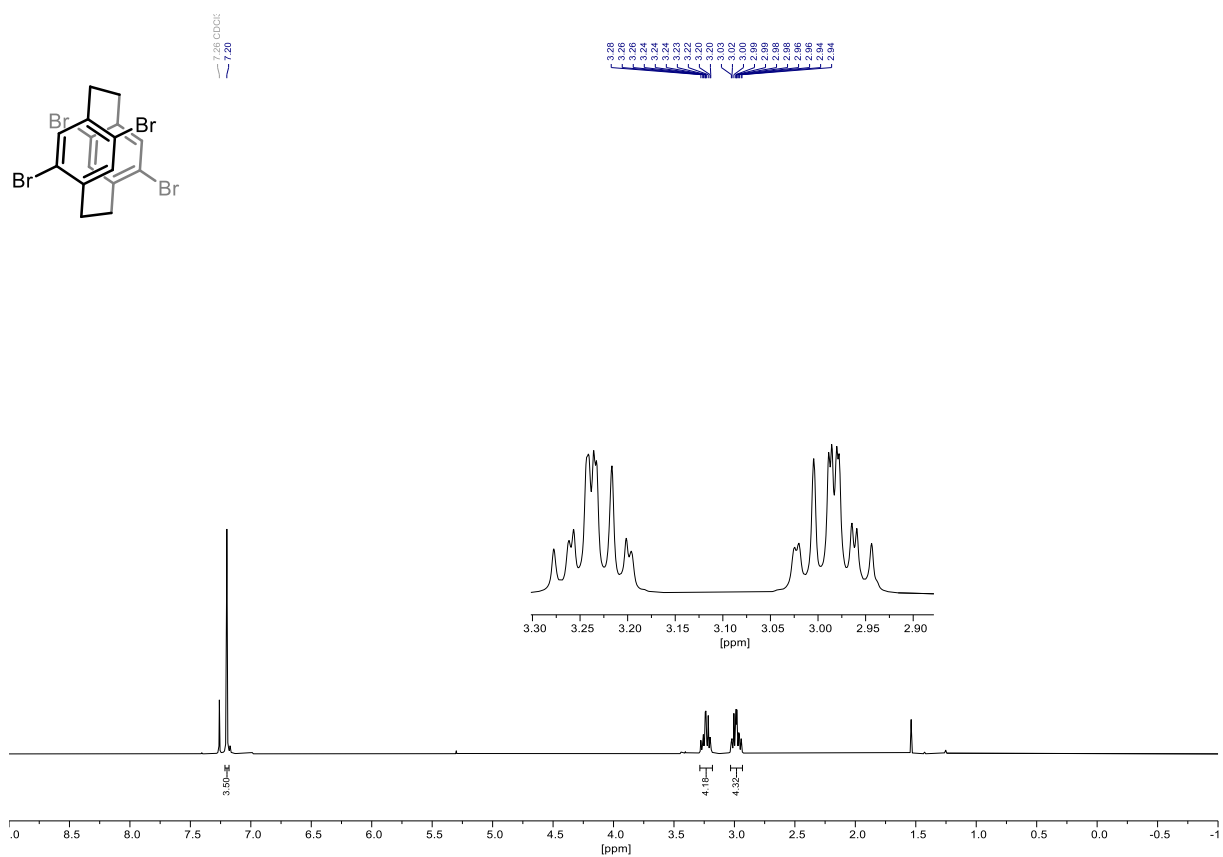
| # | m/z | I % | I |
|----|----------|-------|---------|
| 1 | 144.9820 | 0.5 | 6344 |
| 2 | 146.9799 | 0.3 | 3861 |
| 3 | 185.1146 | 0.3 | 3842 |
| 4 | 203.9304 | 0.7 | 8994 |
| 5 | 205.0595 | 1.5 | 20136 |
| 6 | 205.9273 | 0.4 | 5758 |
| 7 | 209.0213 | 1.0 | 13004 |
| 8 | 217.1045 | 0.7 | 9525 |
| 9 | 226.9511 | 1.1 | 14791 |
| 10 | 261.1303 | 0.5 | 6595 |
| 11 | 277.0085 | 0.3 | 4460 |
| 12 | 288.2888 | 0.8 | 10080 |
| 13 | 316.3202 | 0.3 | 3937 |
| 14 | 341.2650 | 0.3 | 4579 |
| 15 | 350.2658 | 0.4 | 5632 |
| 16 | 355.2811 | 0.3 | 3796 |
| 17 | 362.9256 | 0.4 | 5092 |
| 18 | 385.2914 | 0.3 | 4530 |
| 19 | 399.3070 | 0.4 | 5676 |
| 20 | 429.3179 | 0.4 | 4928 |
| 21 | 430.9126 | 0.4 | 4692 |
| 22 | 443.3329 | 0.5 | 7248 |
| 23 | 453.7844 | 0.4 | 4808 |
| 24 | 457.3483 | 0.3 | 4269 |
| 25 | 467.1482 | 0.5 | 6098 |
| 26 | 469.3123 | 0.3 | 4513 |
| 27 | 473.3433 | 0.3 | 4368 |
| 28 | 487.3592 | 0.5 | 6994 |
| 29 | 494.8106 | 0.4 | 5880 |
| 30 | 509.1585 | 0.9 | 11532 |
| 31 | 510.1623 | 0.3 | 4338 |
| 32 | 513.3383 | 0.4 | 5546 |
| 33 | 517.3700 | 0.3 | 4152 |
| 34 | 526.1858 | 6.2 | 82588 |
| 35 | 527.1885 | 2.2 | 29481 |
| 36 | 528.1860 | 0.8 | 10374 |
| 37 | 531.1422 | 100.0 | 1338616 |
| 38 | 531.3866 | 0.5 | 7142 |
| 39 | 532.1450 | 30.4 | 407289 |
| 40 | 533.1419 | 9.2 | 123709 |
| 41 | 534.1416 | 2.8 | 36919 |
| 42 | 535.1416 | 0.6 | 8109 |
| 43 | 547.1151 | 5.4 | 72565 |
| 44 | 548.1180 | 2.0 | 26700 |
| 45 | 549.1145 | 1.1 | 14266 |
| 46 | 550.1158 | 0.3 | 4670 |
| 47 | 557.3644 | 0.4 | 5424 |
| 48 | 575.4114 | 0.3 | 4097 |
| 49 | 589.0993 | 0.9 | 11524 |
| 50 | 590.1026 | 0.3 | 4304 |
| 51 | 591.0971 | 0.4 | 5472 |
| 52 | 599.1282 | 5.1 | 68644 |
| 53 | 600.1312 | 1.8 | 24747 |
| 54 | 601.1282 | 0.7 | 9089 |
| 55 | 601.3899 | 0.4 | 5450 |
| 56 | 611.1872 | 0.4 | 5959 |
| 57 | 616.1188 | 0.4 | 5948 |
| 58 | 645.4172 | 0.3 | 4550 |
| 59 | 667.1151 | 0.3 | 4138 |
| 60 | 717.1725 | 0.4 | 4809 |
| 61 | 725.0734 | 0.7 | 8797 |

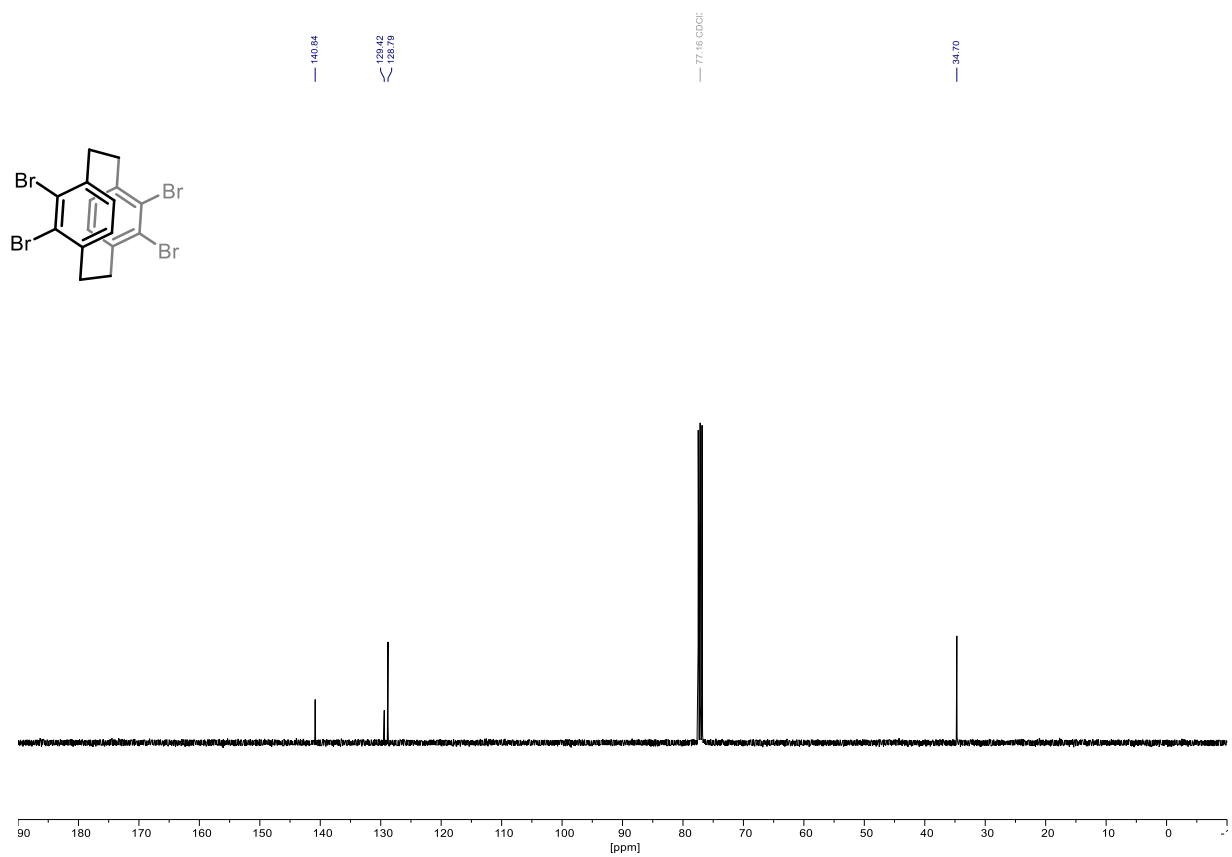
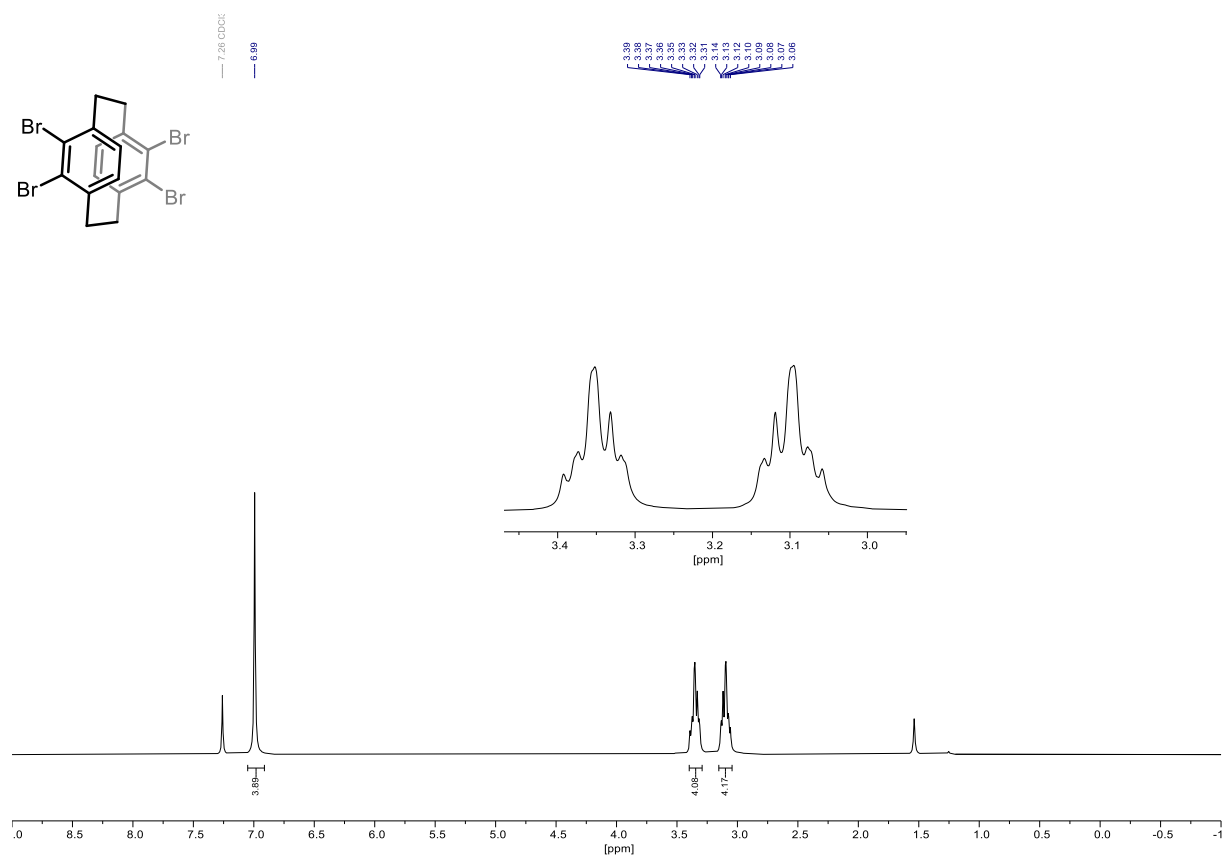
 High Resolution Mass Spectrometry Report

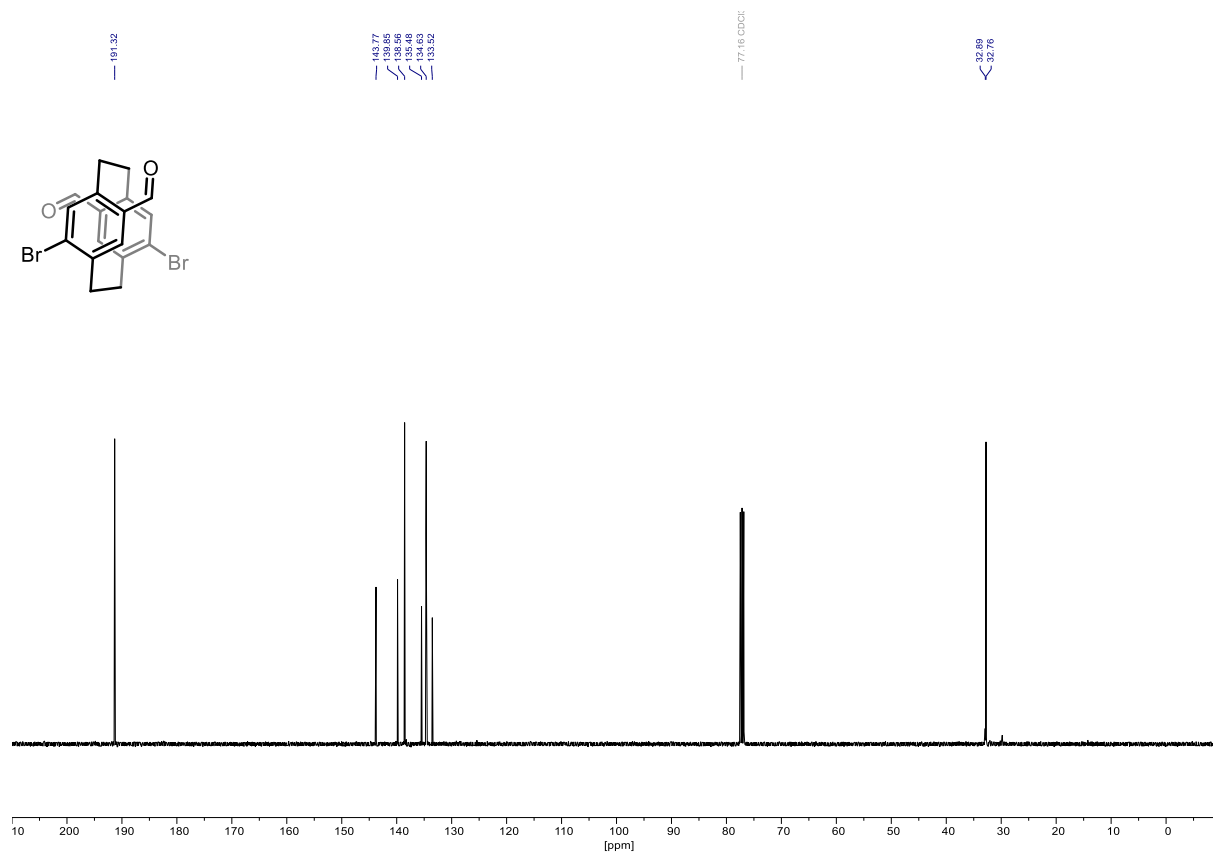
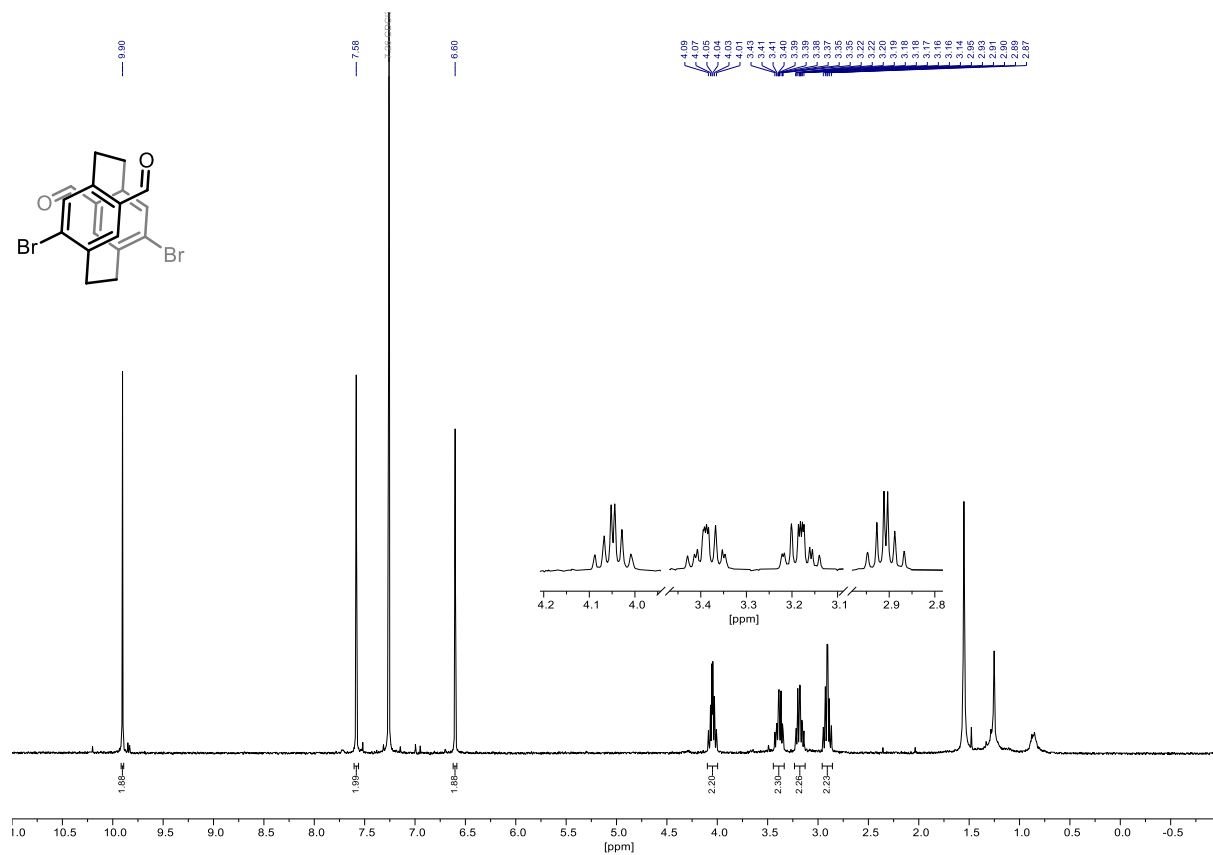
| # | m/z | I % | I |
|-----|-----------|------|--------|
| 62 | 727.0706 | 0.3 | 4368 |
| 63 | 735.1021 | 1.6 | 21099 |
| 64 | 736.1066 | 0.6 | 8306 |
| 65 | 793.0612 | 0.3 | 3956 |
| 66 | 803.0903 | 0.6 | 8410 |
| 67 | 804.0942 | 0.3 | 3834 |
| 68 | 861.0485 | 0.3 | 3782 |
| 69 | 871.0772 | 0.4 | 5200 |
| 70 | 1034.3366 | 0.6 | 7422 |
| 71 | 1035.3399 | 0.4 | 5382 |
| 72 | 1039.2943 | 34.5 | 461849 |
| 73 | 1040.2974 | 24.6 | 328665 |
| 74 | 1041.2962 | 13.4 | 178880 |
| 75 | 1042.2958 | 5.7 | 76090 |
| 76 | 1043.2948 | 2.1 | 27464 |
| 77 | 1044.2951 | 0.7 | 8973 |
| 78 | 1055.2668 | 2.6 | 35225 |
| 79 | 1056.2696 | 1.9 | 25534 |
| 80 | 1057.2682 | 1.2 | 16256 |
| 81 | 1058.2690 | 0.6 | 8612 |
| 82 | 1097.2505 | 0.6 | 7525 |
| 83 | 1098.2537 | 0.4 | 5688 |
| 84 | 1099.2518 | 0.4 | 4827 |
| 85 | 1107.2809 | 3.4 | 45662 |
| 86 | 1108.2839 | 2.4 | 31977 |
| 87 | 1109.2835 | 1.4 | 18887 |
| 88 | 1110.2823 | 0.6 | 8460 |
| 89 | 1124.2693 | 0.4 | 5362 |
| 90 | 1125.2713 | 0.3 | 3962 |
| 91 | 1165.2390 | 0.4 | 5374 |
| 92 | 1166.2410 | 0.3 | 4434 |
| 93 | 1167.2383 | 0.3 | 4098 |
| 94 | 1175.2685 | 0.7 | 9564 |
| 95 | 1176.2711 | 0.5 | 7300 |
| 96 | 1177.2692 | 0.3 | 4258 |
| 97 | 1233.2274 | 0.3 | 4178 |
| 98 | 1243.2559 | 0.3 | 4214 |
| 99 | 1244.2606 | 0.3 | 3905 |
| 100 | 1311.2435 | 0.3 | 3857 |

Acquisition Parameter

| | | | | | | |
|-------------------|------------------------------|----------------|---------------------------------------|----------------|--------------|-----------|
| General | Fore Vacuum | 3.46e+000 mBar | High Vacuum | 9.92e-008 mBar | Source Type | ESI |
| | Scan Begin | 75 m/z | Scan End | 2000 m/z | Ion Polarity | Positive |
| Source | Set Nebulizer | 2.0 Bar | Set Capillary | 4500 V | Set Dry Gas | 8.0 l/min |
| | Set Dry Heater | 200 °C | Set End Plate Offset | -500 V | | |
| Quadrupole | Set Ion Energy (MS only) | 4.0 eV | | | | |
| Coll. Cell | Collision Energy | 8.0 eV | Set Collision Cell RF | 600.0 Vpp | | 100.0 Vpp |
| Ion Cooler | Set Ion Cooler Transfer Time | 75.0 µs | Set Ion Cooler Pre Pulse Storage Time | | | 10.0 µs |

^1H , $^{13}\text{C}\{^1\text{H}\}$ (400/101 MHz, CDCl_3) NMR Spectra of 4,7,12,15-tetrabromo[2.2]paracyclophane (84):

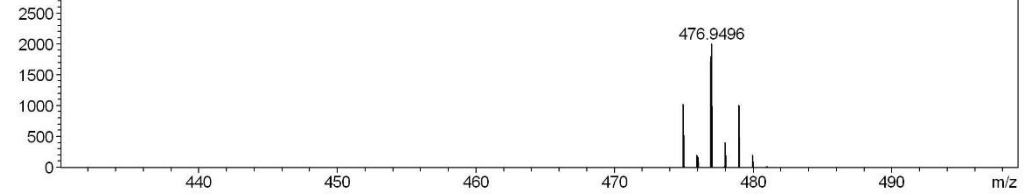
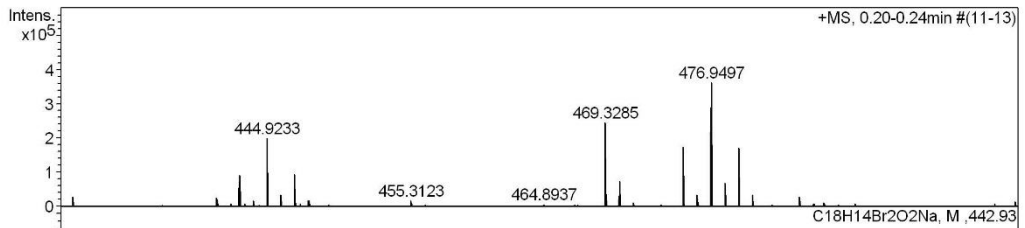
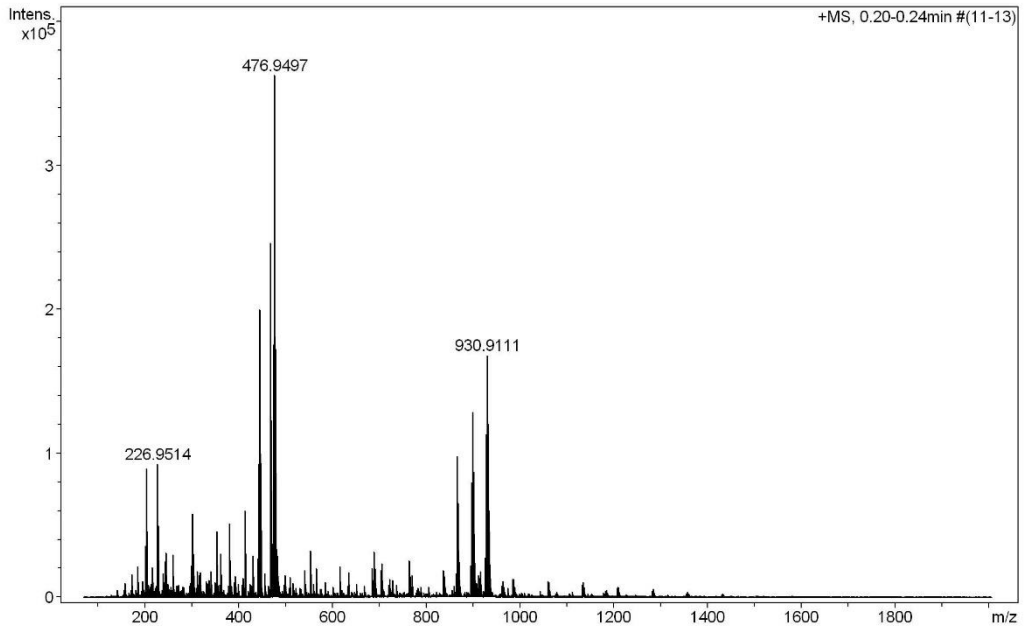
^1H , $^{13}\text{C}\{^1\text{H}\}$ (400/101 MHz, CDCl_3) NMR Spectra of 4,5,12,13-tetrabromo[2.2]paracyclophane (85):

^1H , $^{13}\text{C}\{^1\text{H}\}$ (400/101 MHz, CDCl_3) NMR and HR-ESI-MS Spectra of 4,15-dibromo-7,12-diformyl[2.2]paracyclophane (82):

High Resolution Mass Spectrometry Report

Sample Name KR333_1
Comment

Instrument maXis 4G
Method ms_nocolumn_mid_pos.m



High Resolution Mass Spectrometry Report

Measured m/z vs. theoretical m/z

| Meas. m/z | # | Formula | Score | m/z | err [mDa] | err [ppm] | mSigma | rdb | e ⁻ Conf | z |
|-----------|---|-----------------------|--------|----------|-----------|-----------|--------|------|---------------------|----|
| 442.9250 | 1 | C 18 H 14 Br 2 Na O 2 | 100.00 | 442.9253 | 0.3 | 0.7 | 22.2 | 10.5 | even | 1+ |
| 474.9514 | 1 | C 19 H 18 Br 2 Na O 3 | 100.00 | 474.9515 | 0.1 | 0.2 | 15.5 | 9.5 | even | |
| 862.8607 | 1 | C 36 H 28 Br 4 Na O 4 | 100.00 | 862.8613 | 0.6 | 0.7 | 13.3 | 20.5 | even | |
| 894.8878 | 1 | C 37 H 32 Br 4 Na O 5 | 100.00 | 894.8875 | -0.3 | -0.3 | 14.5 | 19.5 | even | |
| 926.9137 | 1 | C 38 H 36 Br 4 Na O 6 | 100.00 | 926.9138 | 0.1 | 0.1 | 8.2 | 18.5 | even | |

Mass list

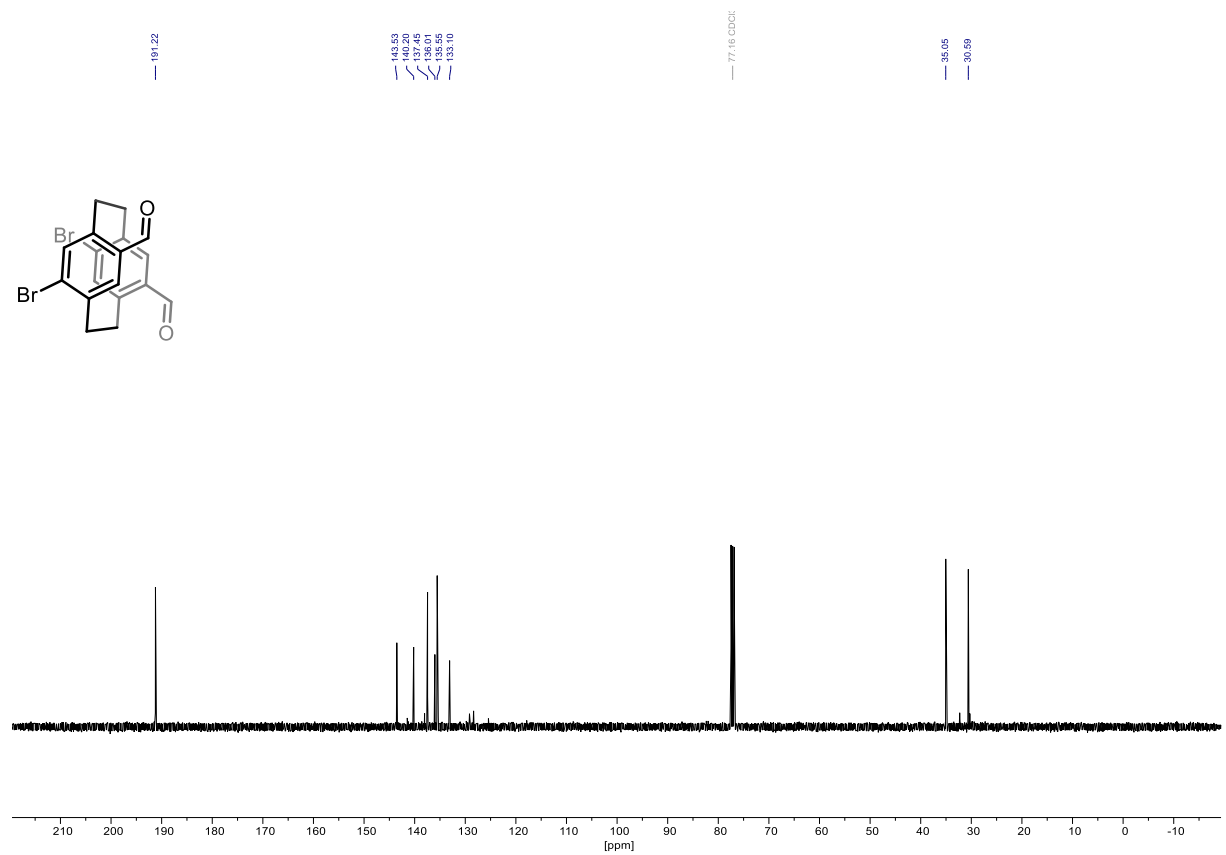
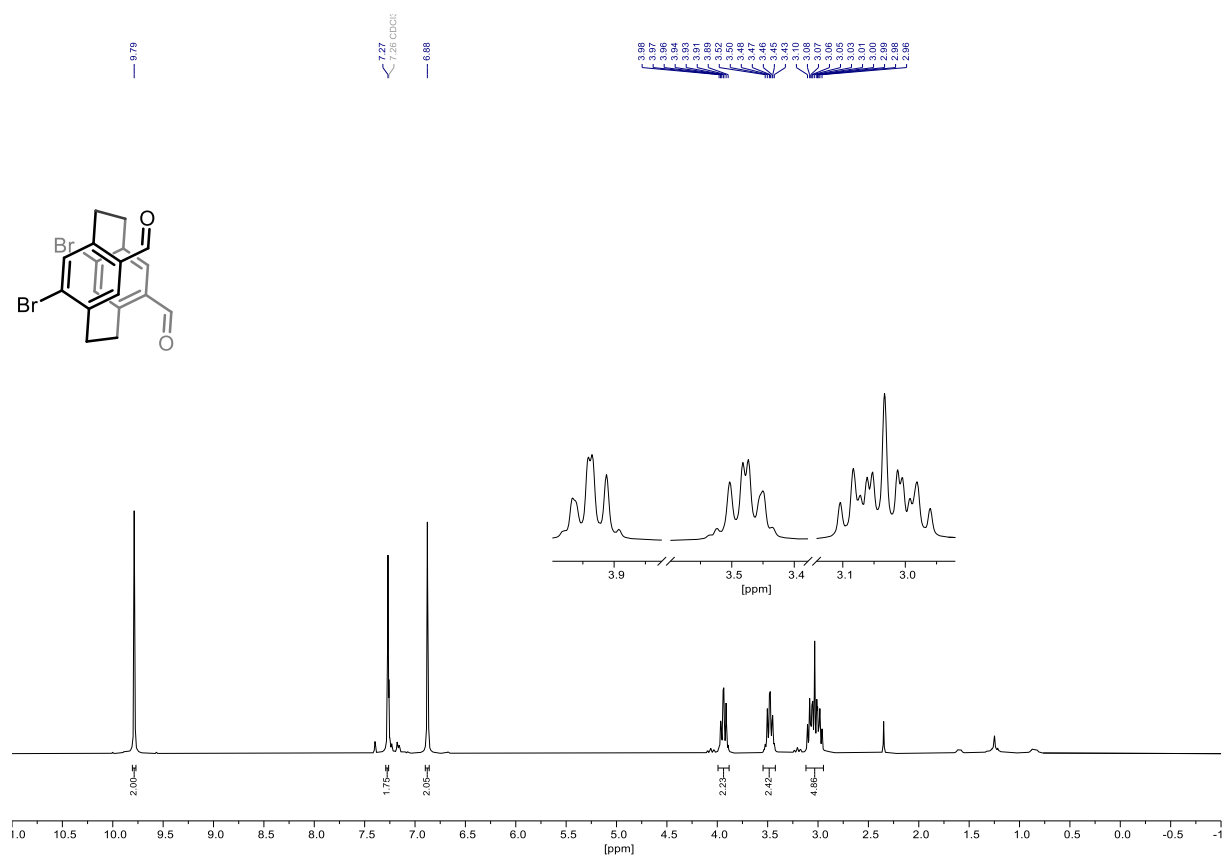
| # | m/z | I % | I |
|----|----------|-------|--------|
| 1 | 173.0783 | 4.4 | 16022 |
| 2 | 185.1145 | 5.9 | 21492 |
| 3 | 201.1096 | 9.8 | 35577 |
| 4 | 205.0599 | 24.6 | 89302 |
| 5 | 217.0467 | 4.1 | 14740 |
| 6 | 217.1043 | 5.8 | 21217 |
| 7 | 226.9514 | 25.6 | 92824 |
| 8 | 229.0503 | 13.8 | 49888 |
| 9 | 239.0886 | 4.6 | 16780 |
| 10 | 243.9414 | 6.8 | 24778 |
| 11 | 245.0781 | 8.6 | 31338 |
| 12 | 261.1305 | 8.2 | 29566 |
| 13 | 299.1613 | 6.2 | 22405 |
| 14 | 301.1406 | 16.1 | 58562 |
| 15 | 304.2607 | 8.3 | 30218 |
| 16 | 313.2345 | 5.0 | 18216 |
| 17 | 317.1716 | 3.6 | 13087 |
| 18 | 317.2444 | 4.2 | 15248 |
| 19 | 319.2601 | 4.8 | 17333 |
| 20 | 341.2656 | 5.0 | 18282 |
| 21 | 353.2657 | 12.7 | 45942 |
| 22 | 362.9260 | 8.4 | 30494 |
| 23 | 381.2969 | 14.1 | 51283 |
| 24 | 393.2967 | 4.1 | 14832 |
| 25 | 411.0930 | 3.7 | 13578 |
| 26 | 413.2260 | 7.5 | 27093 |
| 27 | 413.2655 | 16.6 | 60275 |
| 28 | 414.2690 | 4.3 | 15764 |
| 29 | 430.9134 | 8.1 | 29417 |
| 30 | 441.2966 | 7.5 | 27371 |
| 31 | 442.9250 | 25.6 | 92904 |
| 32 | 443.9279 | 5.1 | 18491 |
| 33 | 444.9233 | 55.1 | 200028 |
| 34 | 445.9262 | 9.7 | 35049 |
| 35 | 446.9211 | 25.9 | 93784 |
| 36 | 447.9043 | 3.8 | 13893 |
| 37 | 447.9232 | 5.3 | 19143 |
| 38 | 455.3123 | 4.6 | 16796 |
| 39 | 469.3285 | 67.9 | 246423 |
| 40 | 470.3316 | 20.6 | 74869 |
| 41 | 471.3343 | 3.7 | 13425 |
| 42 | 474.9514 | 48.4 | 175562 |
| 43 | 475.9543 | 10.0 | 36092 |
| 44 | 476.9497 | 100.0 | 362702 |
| 45 | 477.9524 | 18.9 | 68587 |
| 46 | 478.9475 | 47.6 | 172694 |
| 47 | 479.9503 | 9.3 | 33812 |
| 48 | 483.3434 | 8.1 | 29397 |
| 49 | 498.9009 | 4.3 | 15420 |
| 50 | 508.9749 | 3.9 | 14223 |
| 51 | 541.1200 | 5.1 | 18609 |
| 52 | 553.4581 | 8.9 | 32191 |
| 53 | 554.4612 | 3.6 | 13076 |
| 54 | 566.8881 | 5.5 | 20030 |
| 55 | 615.1386 | 6.0 | 21593 |
| 56 | 634.8755 | 4.9 | 17756 |
| 57 | 685.4342 | 5.6 | 20415 |
| 58 | 689.1576 | 8.7 | 31641 |

 High Resolution Mass Spectrometry Report

| # | m/z | I% | I |
|-----|----------|------|--------|
| 59 | 690.1583 | 5.6 | 20396 |
| 60 | 691.1562 | 4.8 | 17243 |
| 61 | 702.8633 | 5.2 | 19019 |
| 62 | 705.5816 | 6.5 | 23727 |
| 63 | 763.1767 | 7.1 | 25679 |
| 64 | 764.1784 | 5.1 | 18612 |
| 65 | 765.1752 | 4.1 | 14866 |
| 66 | 770.8508 | 4.3 | 15674 |
| 67 | 837.1951 | 5.3 | 19095 |
| 68 | 838.1962 | 4.1 | 14896 |
| 69 | 838.8379 | 3.8 | 13927 |
| 70 | 839.1938 | 3.8 | 13683 |
| 71 | 862.8607 | 4.7 | 17003 |
| 72 | 864.8597 | 17.5 | 63457 |
| 73 | 865.8626 | 7.2 | 26070 |
| 74 | 866.8582 | 27.1 | 98115 |
| 75 | 867.8605 | 10.6 | 38621 |
| 76 | 868.8561 | 18.1 | 65615 |
| 77 | 869.8584 | 6.8 | 24734 |
| 78 | 870.8554 | 5.3 | 19215 |
| 79 | 894.8878 | 6.1 | 22205 |
| 80 | 896.8861 | 22.2 | 80344 |
| 81 | 897.8886 | 9.3 | 33695 |
| 82 | 898.8845 | 35.6 | 129151 |
| 83 | 899.8871 | 13.4 | 48483 |
| 84 | 900.8827 | 24.2 | 87717 |
| 85 | 901.8848 | 9.0 | 32680 |
| 86 | 902.8813 | 6.8 | 24535 |
| 87 | 911.2143 | 4.2 | 15284 |
| 88 | 912.2153 | 3.7 | 13524 |
| 89 | 913.2127 | 3.7 | 13312 |
| 90 | 915.6678 | 5.0 | 18305 |
| 91 | 926.9137 | 7.7 | 28026 |
| 92 | 928.9125 | 31.2 | 113163 |
| 93 | 929.9156 | 12.5 | 45237 |
| 94 | 930.9111 | 46.4 | 168391 |
| 95 | 931.9136 | 18.7 | 67689 |
| 96 | 932.9094 | 33.2 | 120591 |
| 97 | 933.9116 | 12.7 | 45937 |
| 98 | 934.9084 | 9.1 | 33167 |
| 99 | 935.9104 | 3.6 | 13220 |
| 100 | 985.2338 | 3.5 | 12752 |

Acquisition Parameter

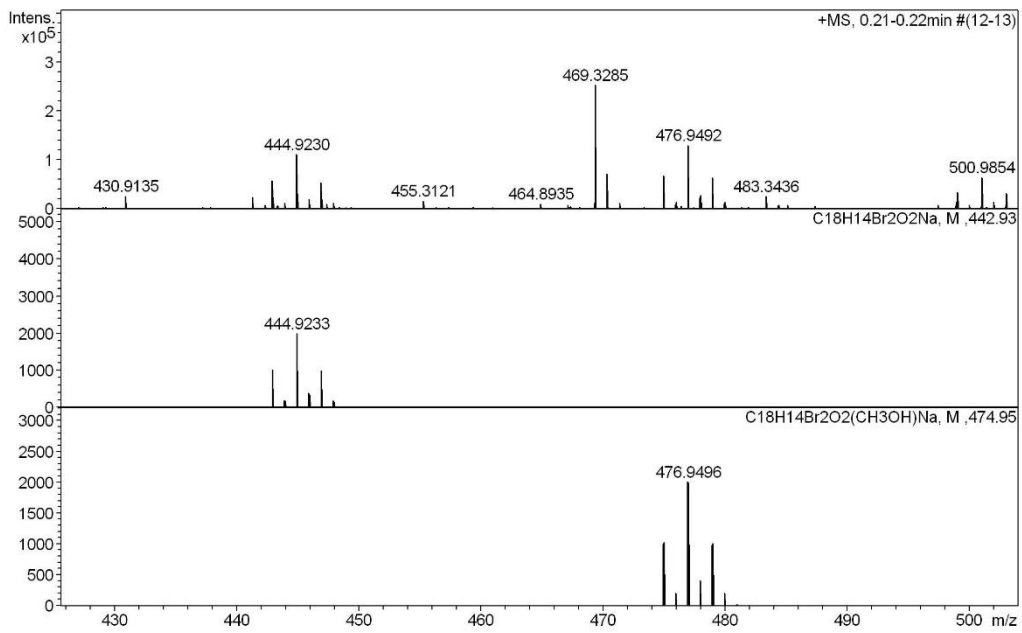
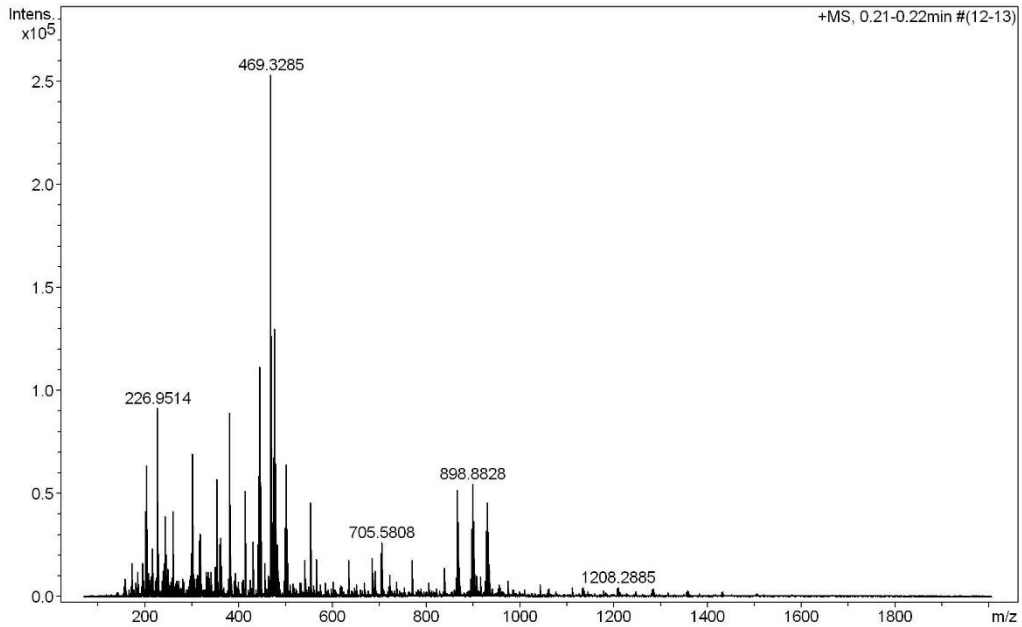
| | | | | | | |
|-------------------|------------------------------|----------------|---------------------------------------|----------------|--------------|-----------|
| General | Fore Vacuum | 3.46e+000 mBar | High Vacuum | 9.61e-008 mBar | Source Type | ESI |
| | Scan Begin | 75 m/z | Scan End | 2000 m/z | Ion Polarity | Positive |
| Source | Set Nebulizer | 2.0 Bar | Set Capillary | 4500 V | Set Dry Gas | 8.0 l/min |
| | Set Dry Heater | 200 °C | Set End Plate Offset | -500 V | | |
| Quadrupole | Set Ion Energy (MS only) | 4.0 eV | | | 100.0 Vpp | |
| Coll. Cell | Collision Energy | 8.0 eV | Set Collision Cell RF | 600.0 Vpp | | |
| Ion Cooler | Set Ion Cooler Transfer Time | 75.0 µs | Set Ion Cooler Pre Pulse Storage Time | 10.0 µs | | |

^1H , $^{13}\text{C}\{\text{H}\}$ (400/101 MHz, CDCl_3) NMR and HR-ESI-MS Spectra of 4,12-dibromo-7,15-diformyl[2.2]paracyclophane (86):

High Resolution Mass Spectrometry Report

Sample Name KR333_2
Comment

Instrument maXis 4G
Method ms_nocolumn_mid_pos.m



High Resolution Mass Spectrometry Report

Measured m/z vs. theoretical m/z

| Meas. m/z | # | Formula | Score | m/z | err [mDa] | err [ppm] | mSigma | rdb | e ⁻ Conf | z |
|-----------|---|-----------------------|--------|----------|-----------|-----------|--------|------|---------------------|----|
| 442.9247 | 1 | C 18 H 14 Br 2 Na O 2 | 100.00 | 442.9253 | 0.6 | 1.3 | 12.9 | 10.5 | even | 1+ |
| 474.9508 | 1 | C 19 H 18 Br 2 Na O 3 | 100.00 | 474.9515 | 0.7 | 1.5 | 10.7 | 9.5 | even | |
| 862.8596 | 1 | C 36 H 28 Br 4 Na O 4 | 100.00 | 862.8613 | 1.7 | 2.0 | 15.9 | 20.5 | even | |
| 926.9119 | 1 | C 38 H 36 Br 4 Na O 6 | 100.00 | 926.9138 | 1.8 | 2.0 | 21.1 | 18.5 | even | |

Mass list

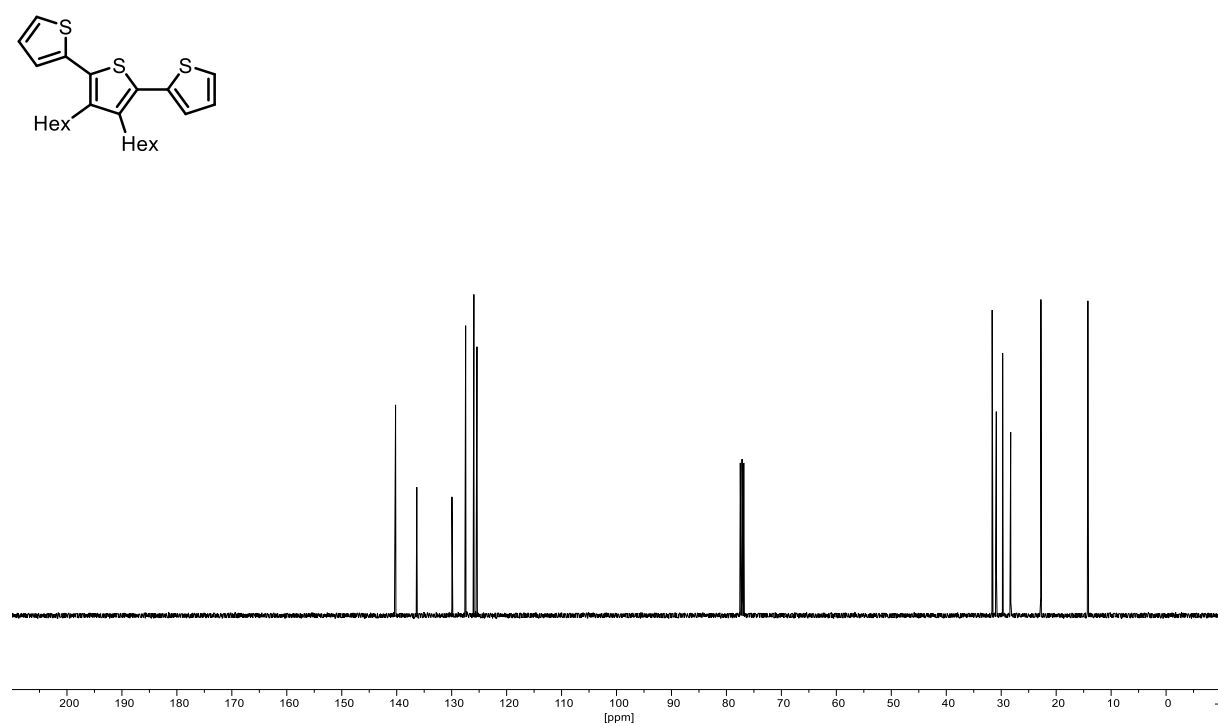
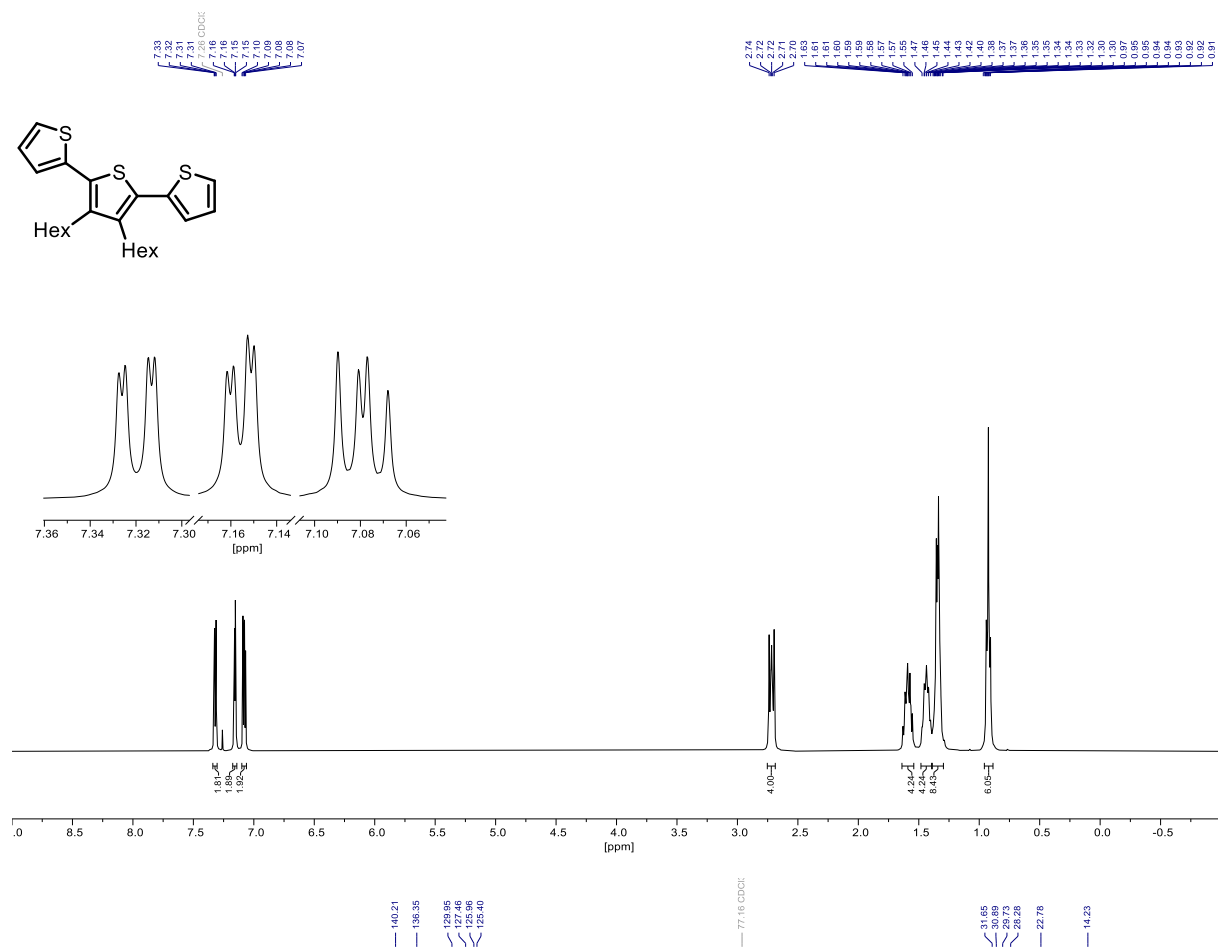
| # | m/z | I % | I |
|----|----------|-------|--------|
| 1 | 173.0783 | 6.5 | 16559 |
| 2 | 185.1146 | 4.9 | 12347 |
| 3 | 195.0989 | 6.5 | 16382 |
| 4 | 201.1095 | 16.3 | 41409 |
| 5 | 205.0599 | 25.2 | 63909 |
| 6 | 209.1144 | 4.6 | 11719 |
| 7 | 217.0468 | 7.8 | 19693 |
| 8 | 217.1043 | 9.4 | 23796 |
| 9 | 226.9514 | 36.2 | 91707 |
| 10 | 229.0501 | 8.3 | 21062 |
| 11 | 239.0887 | 5.0 | 12708 |
| 12 | 241.0679 | 6.5 | 16520 |
| 13 | 241.1405 | 4.7 | 11833 |
| 14 | 243.9414 | 15.5 | 39186 |
| 15 | 245.0780 | 8.2 | 20753 |
| 16 | 249.1818 | 5.5 | 13884 |
| 17 | 261.1305 | 16.4 | 41622 |
| 18 | 299.1613 | 8.3 | 21139 |
| 19 | 301.1406 | 27.5 | 69616 |
| 20 | 302.1438 | 4.9 | 12327 |
| 21 | 304.2603 | 4.4 | 11238 |
| 22 | 313.2343 | 4.3 | 11006 |
| 23 | 315.2288 | 4.1 | 10426 |
| 24 | 317.1718 | 6.4 | 16197 |
| 25 | 317.2445 | 10.9 | 27619 |
| 26 | 319.2602 | 12.2 | 30789 |
| 27 | 331.1871 | 4.9 | 12295 |
| 28 | 335.2548 | 4.8 | 12183 |
| 29 | 341.2658 | 4.9 | 12410 |
| 30 | 348.9894 | 5.7 | 14444 |
| 31 | 350.9865 | 5.8 | 14719 |
| 32 | 353.2657 | 22.6 | 57281 |
| 33 | 354.2688 | 4.9 | 12343 |
| 34 | 360.3229 | 10.1 | 25597 |
| 35 | 362.3384 | 11.4 | 28824 |
| 36 | 362.9262 | 10.4 | 26418 |
| 37 | 381.2970 | 35.2 | 89218 |
| 38 | 382.3003 | 7.8 | 19878 |
| 39 | 393.2968 | 4.6 | 11769 |
| 40 | 413.2654 | 20.3 | 51326 |
| 41 | 414.2690 | 5.4 | 13559 |
| 42 | 430.9135 | 10.7 | 27150 |
| 43 | 441.2965 | 10.0 | 25372 |
| 44 | 442.9247 | 23.2 | 58725 |
| 45 | 443.9274 | 4.6 | 11590 |
| 46 | 444.9230 | 44.1 | 111815 |
| 47 | 445.9258 | 7.8 | 19732 |
| 48 | 446.9209 | 21.2 | 53717 |
| 49 | 447.9041 | 4.8 | 12075 |
| 50 | 447.9222 | 4.5 | 11524 |
| 51 | 455.3121 | 6.5 | 16471 |
| 52 | 464.8935 | 4.2 | 10545 |
| 53 | 469.3285 | 100.0 | 253400 |
| 54 | 470.3314 | 28.6 | 72393 |
| 55 | 471.3340 | 5.2 | 13060 |
| 56 | 474.9508 | 26.6 | 67525 |
| 57 | 475.9540 | 5.7 | 14554 |
| 58 | 476.9492 | 51.4 | 130359 |
| 59 | 477.9521 | 11.5 | 29233 |

 High Resolution Mass Spectrometry Report

| # | m/z | I% | I |
|-----|----------|------|-------|
| 60 | 478.9471 | 25.5 | 64595 |
| 61 | 479.9500 | 5.5 | 13940 |
| 62 | 483.3436 | 10.1 | 25635 |
| 63 | 498.9007 | 5.6 | 14073 |
| 64 | 498.9868 | 13.2 | 33505 |
| 65 | 500.9854 | 25.5 | 64495 |
| 66 | 501.9883 | 5.9 | 15054 |
| 67 | 502.9835 | 13.0 | 33053 |
| 68 | 541.1195 | 7.1 | 17873 |
| 69 | 553.4581 | 18.1 | 45772 |
| 70 | 554.4613 | 7.2 | 18213 |
| 71 | 566.8881 | 7.2 | 18223 |
| 72 | 634.8754 | 7.2 | 18145 |
| 73 | 685.4338 | 7.4 | 18829 |
| 74 | 690.9204 | 5.1 | 12920 |
| 75 | 702.8630 | 8.5 | 21457 |
| 76 | 705.5808 | 10.5 | 26658 |
| 77 | 706.5841 | 4.9 | 12427 |
| 78 | 721.5755 | 4.3 | 10785 |
| 79 | 770.8504 | 7.0 | 17811 |
| 80 | 838.8374 | 5.6 | 14231 |
| 81 | 864.8583 | 13.2 | 33411 |
| 82 | 865.8609 | 5.4 | 13619 |
| 83 | 866.8565 | 20.6 | 52183 |
| 84 | 867.8591 | 7.8 | 19657 |
| 85 | 868.8541 | 14.4 | 36555 |
| 86 | 869.8573 | 5.8 | 14802 |
| 87 | 870.8531 | 4.5 | 11403 |
| 88 | 896.8843 | 13.1 | 33204 |
| 89 | 897.8874 | 5.5 | 13910 |
| 90 | 898.8828 | 21.7 | 55074 |
| 91 | 899.8855 | 8.2 | 20685 |
| 92 | 900.8814 | 14.6 | 36924 |
| 93 | 901.8836 | 5.6 | 14287 |
| 94 | 902.8801 | 4.4 | 11187 |
| 95 | 928.9108 | 12.6 | 32014 |
| 96 | 929.9139 | 5.1 | 12851 |
| 97 | 930.9090 | 18.0 | 45655 |
| 98 | 931.9116 | 7.7 | 19467 |
| 99 | 932.9071 | 12.4 | 31445 |
| 100 | 933.9101 | 5.4 | 13775 |

Acquisition Parameter

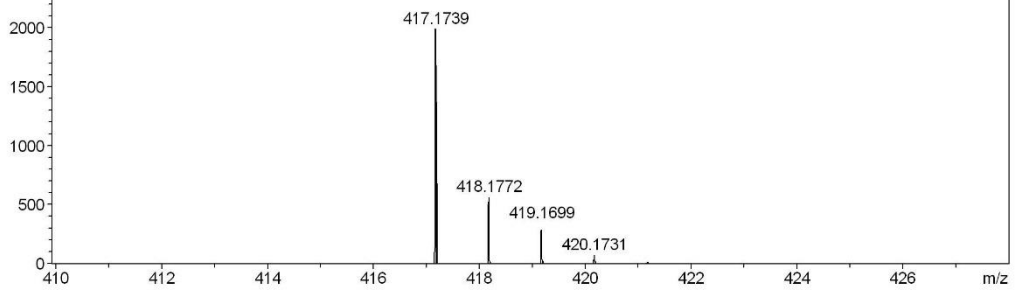
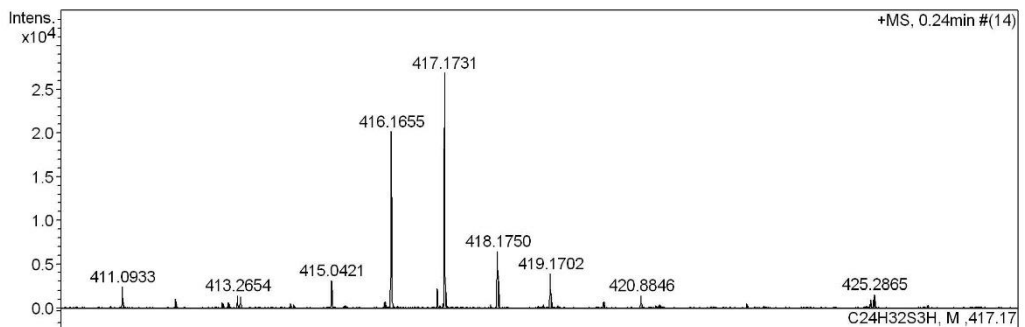
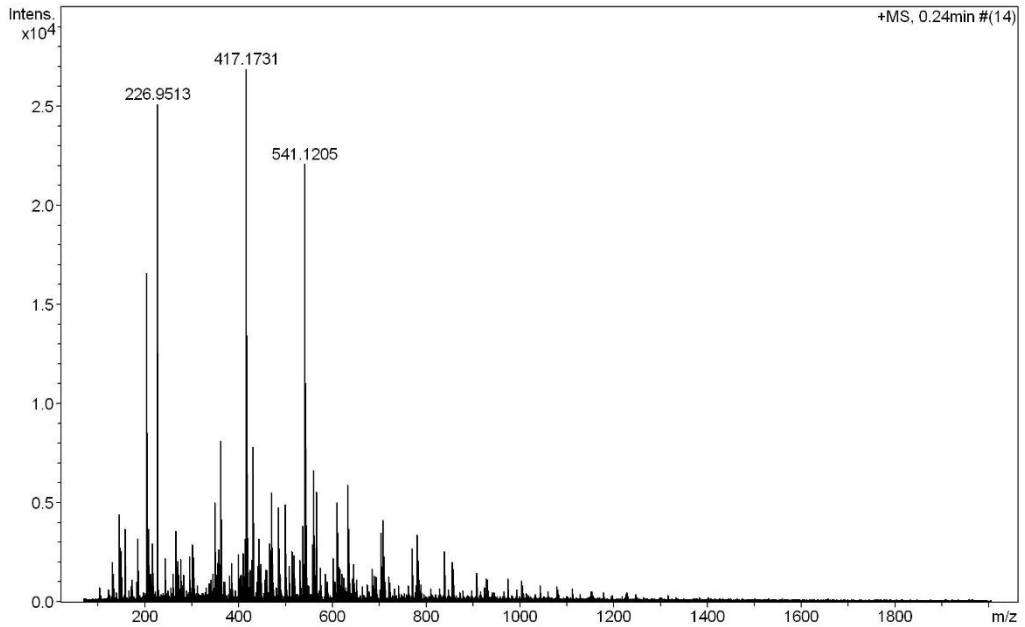
| | | | | | | |
|-------------------|------------------------------|----------------|---------------------------------------|----------------|--------------|-----------|
| General | Fore Vacuum | 3.46e+000 mBar | High Vacuum | 9.61e-008 mBar | Source Type | ESI |
| | Scan Begin | 75 m/z | Scan End | 2000 m/z | Ion Polarity | Positive |
| Source | Set Nebulizer | 2.0 Bar | Set Capillary | 4500 V | Set Dry Gas | 8.0 l/min |
| | Set Dry Heater | 200 °C | Set End Plate Offset | -500 V | | |
| Quadrupole | Set Ion Energy (MS only) | 4.0 eV | | | | |
| Coll. Cell | Collision Energy | 8.0 eV | Set Collision Cell RF | 600.0 Vpp | | 100.0 Vpp |
| Ion Cooler | Set Ion Cooler Transfer Time | 75.0 µs | Set Ion Cooler Pre Pulse Storage Time | | | 10.0 µs |

^1H , $^{13}\text{C}\{^1\text{H}\}$ (400/101 MHz, CDCl_3) NMR and HR-ESI-MS Spectra of 3',4'-dihexyl-2,2':5',2''-terthiophene (90):

High Resolution Mass Spectrometry Report

Sample Name **KR307**
Comment

Instrument maXis 4G
Method ms_nocolumn_mid_pos.m



High Resolution Mass Spectrometry Report

Measured m/z vs. theoretical m/z

| Meas. m/z | # | Formula | Score | m/z | err [mDa] | err [ppm] | mSigma | rdb | e ⁻ Conf | z |
|-----------|---|---------------|--------|----------|-----------|-----------|--------|-----|---------------------|----|
| 417.1731 | 1 | C 24 H 33 S 3 | 100.00 | 417.1739 | 0.8 | 1.8 | 29.3 | 8.5 | even | 1+ |

Mass list

| # | m/z | I % | I |
|----|----------|-------|-------|
| 1 | 131.9616 | 7.6 | 2033 |
| 2 | 144.9818 | 16.5 | 4432 |
| 3 | 146.9802 | 8.5 | 2292 |
| 4 | 147.9309 | 10.3 | 2780 |
| 5 | 149.9307 | 9.6 | 2592 |
| 6 | 158.9639 | 13.8 | 3700 |
| 7 | 185.1143 | 12.0 | 3229 |
| 8 | 205.0599 | 61.8 | 16624 |
| 9 | 206.0623 | 5.8 | 1561 |
| 10 | 209.0214 | 13.8 | 3706 |
| 11 | 216.9224 | 10.4 | 2808 |
| 12 | 217.1043 | 11.1 | 2976 |
| 13 | 226.9513 | 93.4 | 25133 |
| 14 | 243.9413 | 8.3 | 2235 |
| 15 | 265.9620 | 13.4 | 3592 |
| 16 | 270.9773 | 7.8 | 2104 |
| 17 | 277.0087 | 8.0 | 2164 |
| 18 | 294.9385 | 8.7 | 2336 |
| 19 | 301.1402 | 10.9 | 2935 |
| 20 | 302.9827 | 8.5 | 2288 |
| 21 | 350.2661 | 18.7 | 5025 |
| 22 | 355.2814 | 7.3 | 1974 |
| 23 | 358.9798 | 9.9 | 2651 |
| 24 | 360.9771 | 7.1 | 1916 |
| 25 | 362.9263 | 30.2 | 8130 |
| 26 | 385.2916 | 7.3 | 1974 |
| 27 | 399.3074 | 9.1 | 2441 |
| 28 | 411.0933 | 9.1 | 2450 |
| 29 | 413.2654 | 5.7 | 1524 |
| 30 | 415.0421 | 11.9 | 3200 |
| 31 | 416.1655 | 75.2 | 20224 |
| 32 | 417.0402 | 8.3 | 2242 |
| 33 | 417.1731 | 100.0 | 26906 |
| 34 | 418.1750 | 24.2 | 6509 |
| 35 | 419.1702 | 14.8 | 3980 |
| 36 | 420.8846 | 5.7 | 1525 |
| 37 | 425.2865 | 6.0 | 1616 |
| 38 | 429.3176 | 7.9 | 2130 |
| 39 | 430.9139 | 29.2 | 7860 |
| 40 | 441.2969 | 6.8 | 1836 |
| 41 | 443.3343 | 12.0 | 3222 |
| 42 | 447.9040 | 7.2 | 1949 |
| 43 | 457.3498 | 6.0 | 1624 |
| 44 | 459.0174 | 5.9 | 1596 |
| 45 | 461.0173 | 6.1 | 1633 |
| 46 | 467.1017 | 11.1 | 2987 |
| 47 | 469.3138 | 9.7 | 2615 |
| 48 | 471.1450 | 20.5 | 5517 |
| 49 | 472.1493 | 7.3 | 1951 |
| 50 | 473.3443 | 6.6 | 1789 |
| 51 | 485.1119 | 17.8 | 4786 |
| 52 | 486.1123 | 8.9 | 2397 |
| 53 | 487.1101 | 6.3 | 1692 |
| 54 | 487.3598 | 10.2 | 2743 |
| 55 | 498.9010 | 18.4 | 4948 |
| 56 | 506.9449 | 6.8 | 1824 |
| 57 | 513.3390 | 9.6 | 2587 |
| 58 | 515.8913 | 5.6 | 1503 |
| 59 | 517.2957 | 8.8 | 2369 |
| 60 | 517.3712 | 6.0 | 1609 |
| 61 | 519.2950 | 8.8 | 2365 |
| 62 | 531.3863 | 7.9 | 2136 |

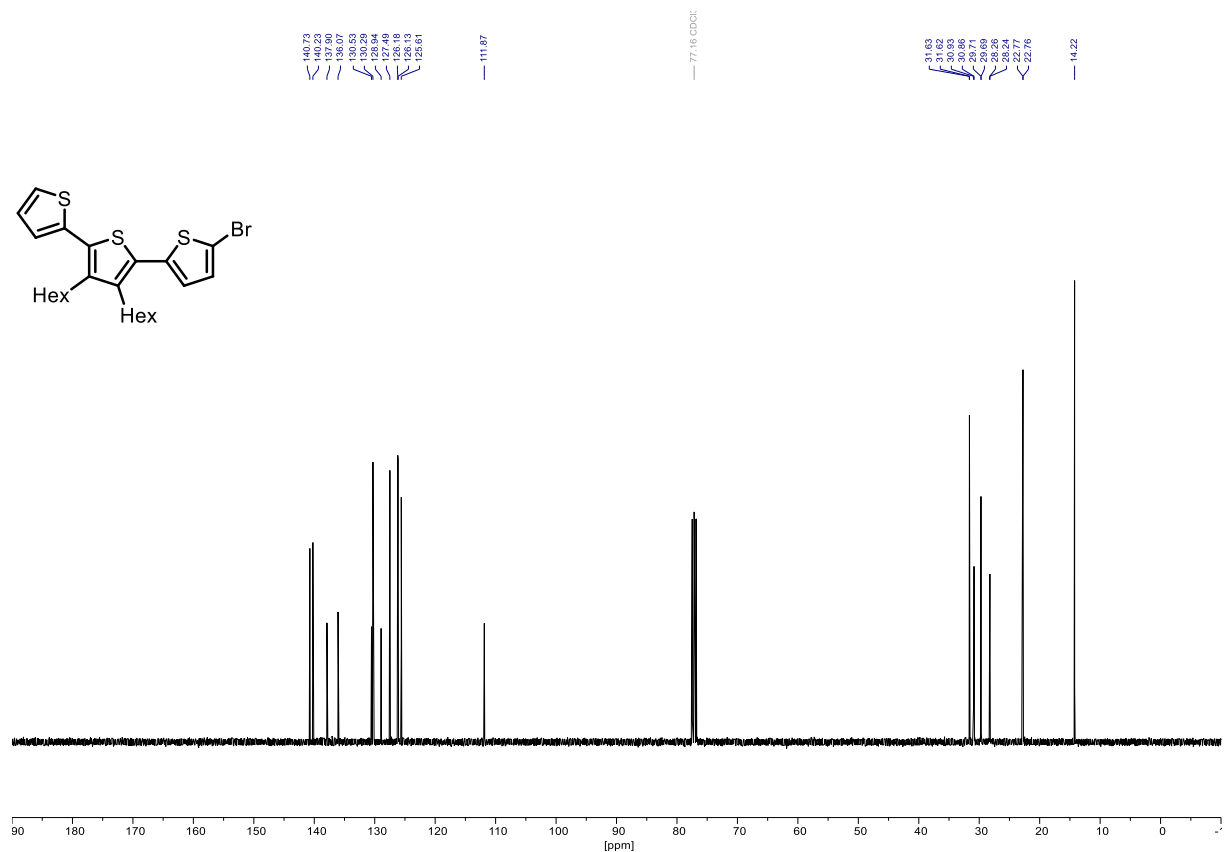
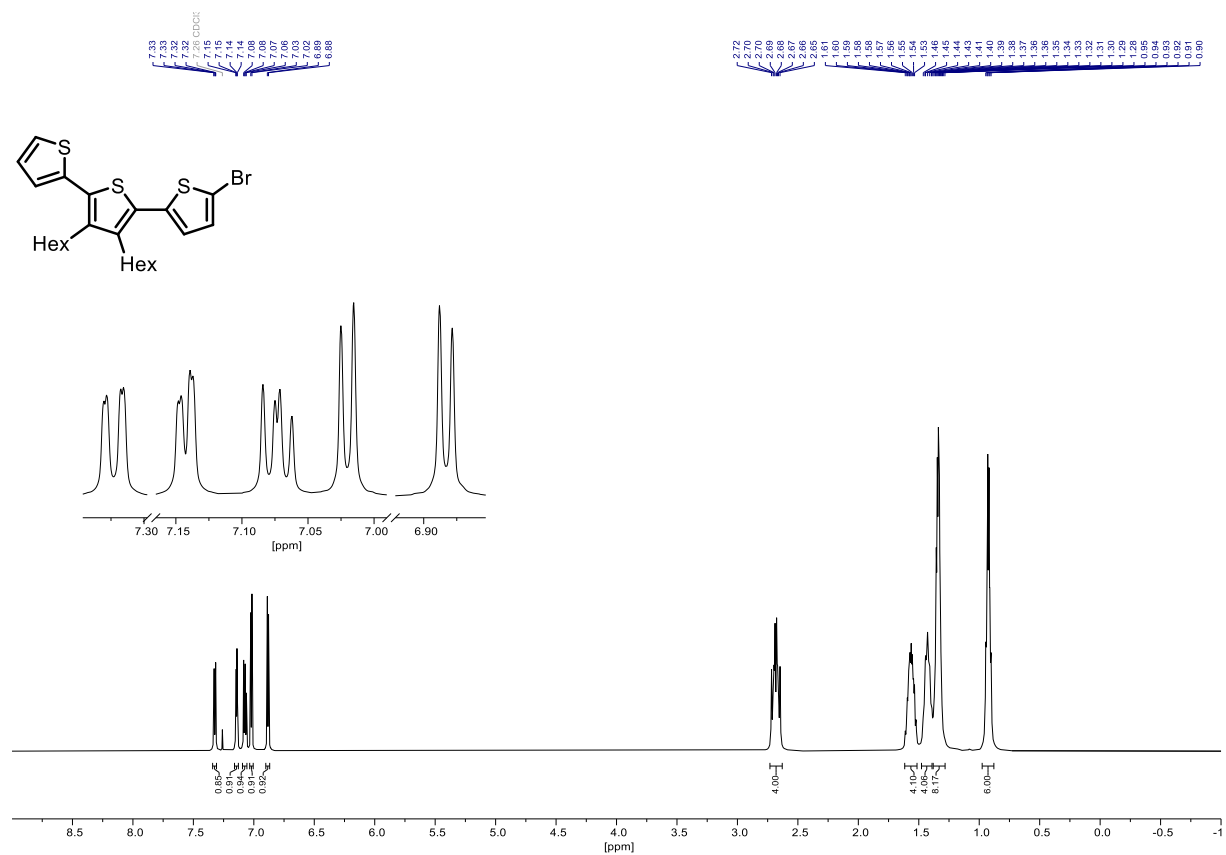
High Resolution Mass Spectrometry Report

| # | m/z | I% | I |
|-----|----------|------|-------|
| 63 | 536.1654 | 14.3 | 3838 |
| 64 | 537.1654 | 7.7 | 2081 |
| 65 | 538.1631 | 5.6 | 1498 |
| 66 | 541.1205 | 82.2 | 22104 |
| 67 | 542.1210 | 40.2 | 10817 |
| 68 | 543.1186 | 28.9 | 7779 |
| 69 | 544.1193 | 11.8 | 3172 |
| 70 | 557.0944 | 6.1 | 1630 |
| 71 | 557.3653 | 10.8 | 2900 |
| 72 | 559.1312 | 24.7 | 6640 |
| 73 | 560.1322 | 11.2 | 3009 |
| 74 | 561.1288 | 10.3 | 2760 |
| 75 | 566.8887 | 20.8 | 5585 |
| 76 | 575.4138 | 5.9 | 1585 |
| 77 | 601.3917 | 8.3 | 2224 |
| 78 | 610.1837 | 18.7 | 5029 |
| 79 | 611.1847 | 13.1 | 3529 |
| 80 | 612.1819 | 7.6 | 2040 |
| 81 | 615.1400 | 6.2 | 1669 |
| 82 | 633.1504 | 22.1 | 5942 |
| 83 | 634.1508 | 13.0 | 3500 |
| 84 | 634.8762 | 13.8 | 3709 |
| 85 | 635.1475 | 9.9 | 2672 |
| 86 | 645.4182 | 7.2 | 1941 |
| 87 | 685.4335 | 6.2 | 1680 |
| 88 | 702.8637 | 13.0 | 3490 |
| 89 | 707.1693 | 15.3 | 4124 |
| 90 | 708.1692 | 11.9 | 3205 |
| 91 | 709.1670 | 8.6 | 2308 |
| 92 | 770.8517 | 10.1 | 2709 |
| 93 | 781.1880 | 12.7 | 3425 |
| 94 | 782.1899 | 7.9 | 2126 |
| 95 | 783.1872 | 6.5 | 1740 |
| 96 | 838.8388 | 9.6 | 2578 |
| 97 | 855.2064 | 7.6 | 2038 |
| 98 | 856.2064 | 5.7 | 1537 |
| 99 | 857.2064 | 6.3 | 1692 |
| 100 | 906.8271 | 5.6 | 1499 |

Acquisition Parameter

| | | | | | | |
|-------------------|------------------------------|----------------|---------------------------------------|----------------|--------------|-----------|
| General | Fore Vacuum | 3.46e+000 mBar | High Vacuum | 9.88e-008 mBar | Source Type | ESI |
| | Scan Begin | 75 m/z | Scan End | 2000 m/z | Ion Polarity | Positive |
| Source | Set Nebulizer | 2.0 Bar | Set Capillary | 4500 V | Set Dry Gas | 8.0 l/min |
| | Set Dry Heater | 200 °C | Set End Plate Offset | -500 V | | |
| Quadrupole | Set Ion Energy (MS only) | 4.0 eV | | | | |
| Coll. Cell | Collision Energy | 8.0 eV | Set Collision Cell RF | 600.0 Vpp | 100.0 Vpp | |
| Ion Cooler | Set Ion Cooler Transfer Time | 75.0 µs | Set Ion Cooler Pre Pulse Storage Time | 10.0 µs | | |

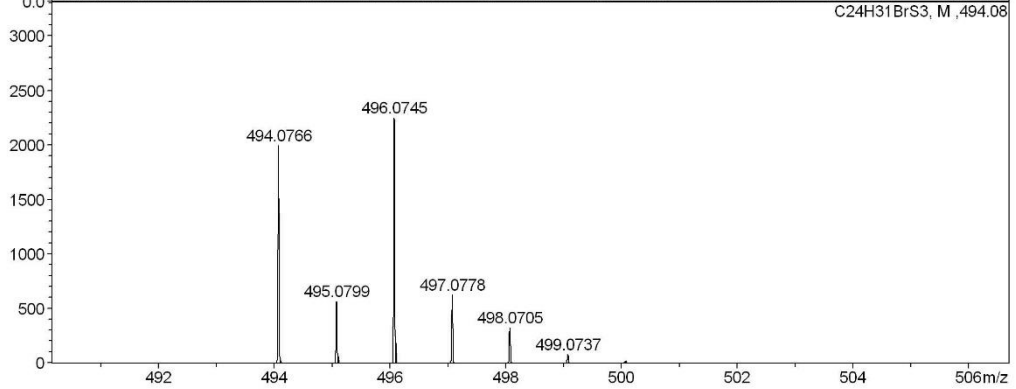
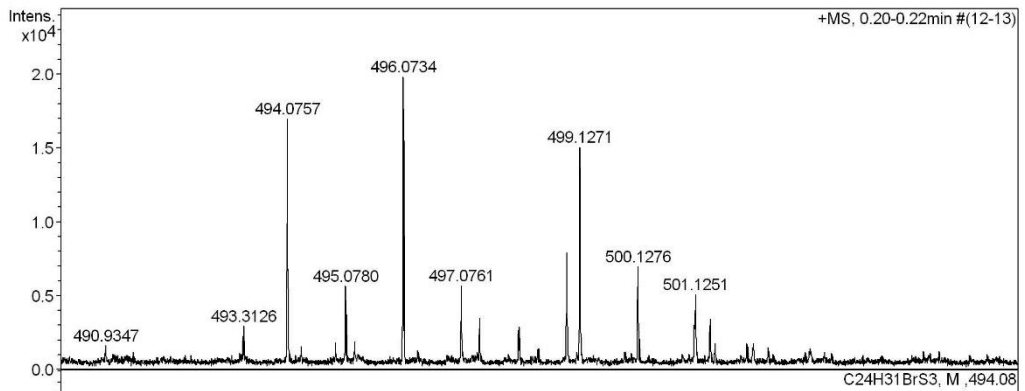
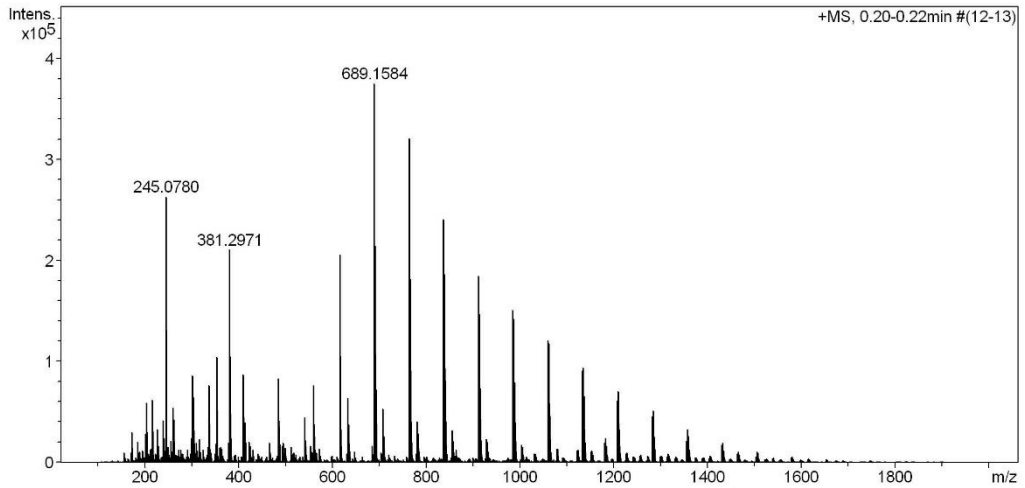
^1H , $^{13}\text{C}\{^1\text{H}\}$ (400/101 MHz, CDCl_3) NMR and HR-ESI-MS Spectra of 5-bromo-3',4'-dihexyl-2,2':5',2''-terthiophene (91):



High Resolution Mass Spectrometry Report

Sample Name **KR341_1Br**
Comment

Instrument **maXis 4G**
Method **ms_nocolumn_mid_pos.m**



 High Resolution Mass Spectrometry Report

Measured m/z vs. theoretical m/z

| Meas. m/z | # | Formula | Score | m/z | err [mDa] | err [ppm] | mSigma | rdb | e ⁻ Conf | z |
|-----------|---|------------------|--------|----------|-----------|-----------|--------|-----|---------------------|----|
| 494.0757 | 1 | C 24 H 31 Br S 3 | 100.00 | 494.0766 | 0.9 | 1.8 | 20.6 | 9.0 | odd | 1+ |

Mass list

| # | m/z | I % | I |
|----|----------|-------|--------|
| 1 | 173.0780 | 8.0 | 30015 |
| 2 | 201.1091 | 7.5 | 28017 |
| 3 | 205.0596 | 15.7 | 58959 |
| 4 | 217.0827 | 16.4 | 61671 |
| 5 | 217.1039 | 11.8 | 44278 |
| 6 | 226.9510 | 8.9 | 33381 |
| 7 | 239.0883 | 11.1 | 41637 |
| 8 | 241.0676 | 6.4 | 24122 |
| 9 | 245.0780 | 70.1 | 263232 |
| 10 | 246.0812 | 8.9 | 33354 |
| 11 | 261.1301 | 14.6 | 54803 |
| 12 | 263.0553 | 11.3 | 42476 |
| 13 | 299.1609 | 6.6 | 24869 |
| 14 | 301.1403 | 22.9 | 86066 |
| 15 | 304.2604 | 17.3 | 64822 |
| 16 | 317.1713 | 6.3 | 23599 |
| 17 | 337.0741 | 20.5 | 76872 |
| 18 | 353.2656 | 27.8 | 104534 |
| 19 | 354.2688 | 6.1 | 22992 |
| 20 | 381.2971 | 56.1 | 210848 |
| 21 | 382.3001 | 12.9 | 48336 |
| 22 | 411.0932 | 23.2 | 87309 |
| 23 | 412.0936 | 8.3 | 31230 |
| 24 | 413.2654 | 10.5 | 39603 |
| 25 | 485.1120 | 22.3 | 83711 |
| 26 | 486.1125 | 9.5 | 35648 |
| 27 | 487.1099 | 6.5 | 24470 |
| 28 | 541.1198 | 12.0 | 45180 |
| 29 | 559.1307 | 20.4 | 76813 |
| 30 | 560.1313 | 9.9 | 37195 |
| 31 | 561.1290 | 7.1 | 26644 |
| 32 | 615.1393 | 55.0 | 206578 |
| 33 | 616.1399 | 29.3 | 109928 |
| 34 | 617.1374 | 22.2 | 83319 |
| 35 | 618.1368 | 8.9 | 33248 |
| 36 | 633.1497 | 17.0 | 63739 |
| 37 | 634.1504 | 10.0 | 37522 |
| 38 | 635.1476 | 7.4 | 27836 |
| 39 | 689.1584 | 100.0 | 375627 |
| 40 | 690.1590 | 57.2 | 214980 |
| 41 | 690.9208 | 6.7 | 25343 |
| 42 | 691.1567 | 45.5 | 170800 |
| 43 | 692.1562 | 19.4 | 72759 |
| 44 | 693.1540 | 9.1 | 34066 |
| 45 | 707.1686 | 14.2 | 53213 |
| 46 | 708.1693 | 8.5 | 31850 |
| 47 | 709.1666 | 7.0 | 26267 |
| 48 | 763.1773 | 85.5 | 321096 |
| 49 | 764.1778 | 60.0 | 225454 |
| 50 | 765.1757 | 48.4 | 181708 |
| 51 | 766.1752 | 21.9 | 82176 |
| 52 | 767.1733 | 10.8 | 40392 |
| 53 | 781.1872 | 10.9 | 40967 |
| 54 | 782.1878 | 7.8 | 29175 |
| 55 | 783.1861 | 6.3 | 23666 |
| 56 | 837.1958 | 64.1 | 240931 |
| 57 | 838.1966 | 49.8 | 187204 |
| 58 | 839.1944 | 42.1 | 158314 |
| 59 | 840.1935 | 21.7 | 81620 |
| 60 | 841.1915 | 11.3 | 42507 |
| 61 | 855.2061 | 8.6 | 32404 |
| 62 | 856.2067 | 6.1 | 22873 |

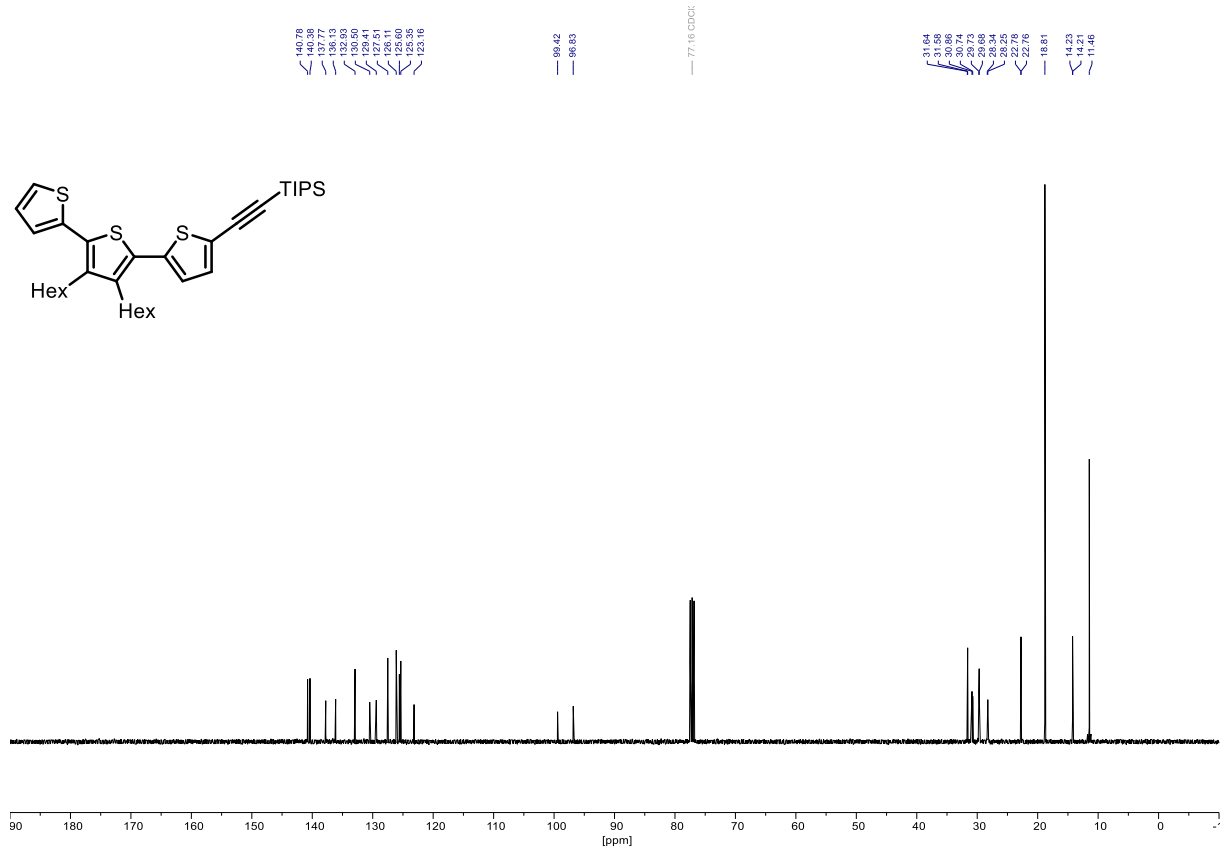
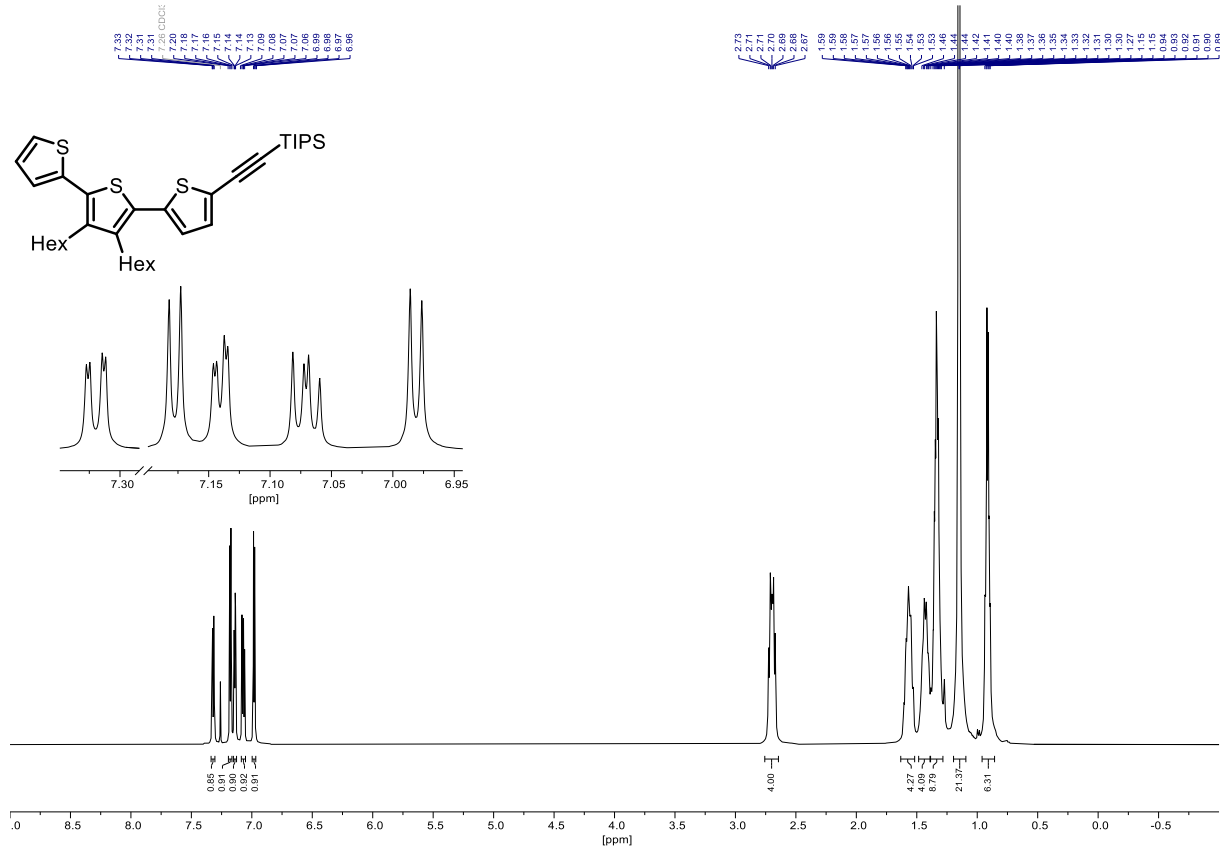
 High Resolution Mass Spectrometry Report

| # | m/z | I % | I |
|-----|-----------|------|--------|
| 63 | 911.2147 | 49.3 | 185293 |
| 64 | 912.2152 | 43.9 | 165037 |
| 65 | 913.2133 | 39.3 | 147521 |
| 66 | 914.2125 | 21.7 | 81450 |
| 67 | 915.2105 | 11.7 | 43811 |
| 68 | 929.2256 | 6.1 | 22983 |
| 69 | 985.2332 | 40.1 | 150709 |
| 70 | 986.2339 | 37.9 | 142359 |
| 71 | 987.2320 | 34.5 | 129511 |
| 72 | 988.2315 | 21.1 | 79422 |
| 73 | 989.2295 | 11.9 | 44650 |
| 74 | 990.2287 | 5.7 | 21522 |
| 75 | 1059.2519 | 32.3 | 121146 |
| 76 | 1060.2526 | 31.8 | 119532 |
| 77 | 1061.2508 | 31.5 | 118473 |
| 78 | 1062.2501 | 20.4 | 76746 |
| 79 | 1063.2480 | 12.3 | 46342 |
| 80 | 1064.2470 | 5.9 | 22167 |
| 81 | 1133.2706 | 24.3 | 91220 |
| 82 | 1134.2717 | 24.9 | 93440 |
| 83 | 1135.2698 | 24.9 | 93632 |
| 84 | 1136.2694 | 17.5 | 65560 |
| 85 | 1137.2680 | 10.5 | 39559 |
| 86 | 1182.1650 | 5.8 | 21793 |
| 87 | 1183.1633 | 6.5 | 24549 |
| 88 | 1207.2893 | 16.3 | 61336 |
| 89 | 1208.2899 | 18.8 | 70788 |
| 90 | 1209.2888 | 18.8 | 70726 |
| 91 | 1210.2881 | 14.2 | 53178 |
| 92 | 1211.2862 | 8.9 | 33337 |
| 93 | 1281.3080 | 10.1 | 38000 |
| 94 | 1282.3087 | 12.2 | 45908 |
| 95 | 1283.3074 | 13.6 | 51134 |
| 96 | 1284.3069 | 9.9 | 37339 |
| 97 | 1285.3053 | 6.7 | 25178 |
| 98 | 1356.3270 | 7.8 | 29156 |
| 99 | 1357.3261 | 8.9 | 33482 |
| 100 | 1358.3251 | 6.9 | 25901 |

Acquisition Parameter

| | | | | | | |
|-------------------|------------------------------|----------------|---------------------------------------|----------------|--------------|-----------|
| General | Fore Vacuum | 3.46e+000 mBar | High Vacuum | 9.88e-008 mBar | Source Type | ESI |
| | Scan Begin | 75 m/z | Scan End | 2000 m/z | Ion Polarity | Positive |
| Source | Set Nebulizer | 2.0 Bar | Set Capillary | 4500 V | Set Dry Gas | 8.0 l/min |
| | Set Dry Heater | 200 °C | Set End Plate Offset | -500 V | | |
| Quadrupole | Set Ion Energy (MS only) | 4.0 eV | | | | |
| Coll. Cell | Collision Energy | 8.0 eV | Set Collision Cell RF | 600.0 Vpp | 100.0 Vpp | |
| Ion Cooler | Set Ion Cooler Transfer Time | 75.0 µs | Set Ion Cooler Pre Pulse Storage Time | 10.0 µs | | |

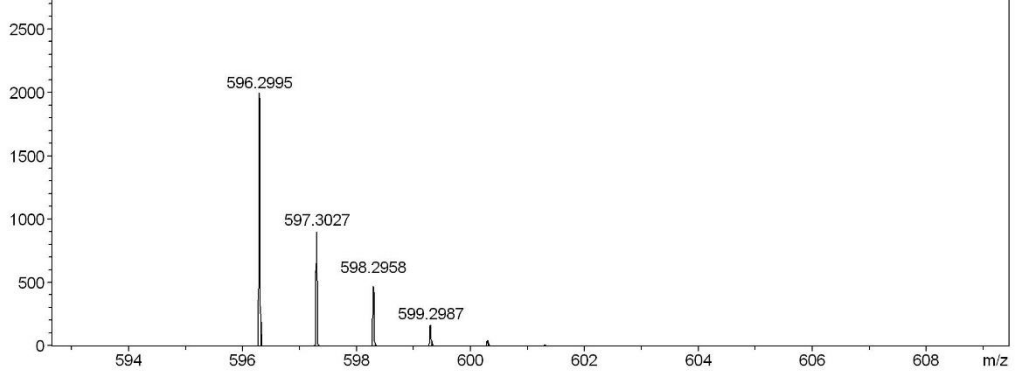
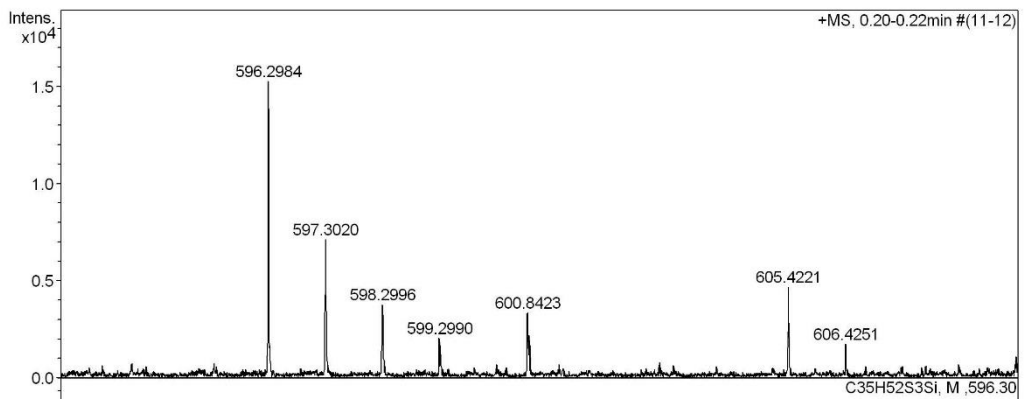
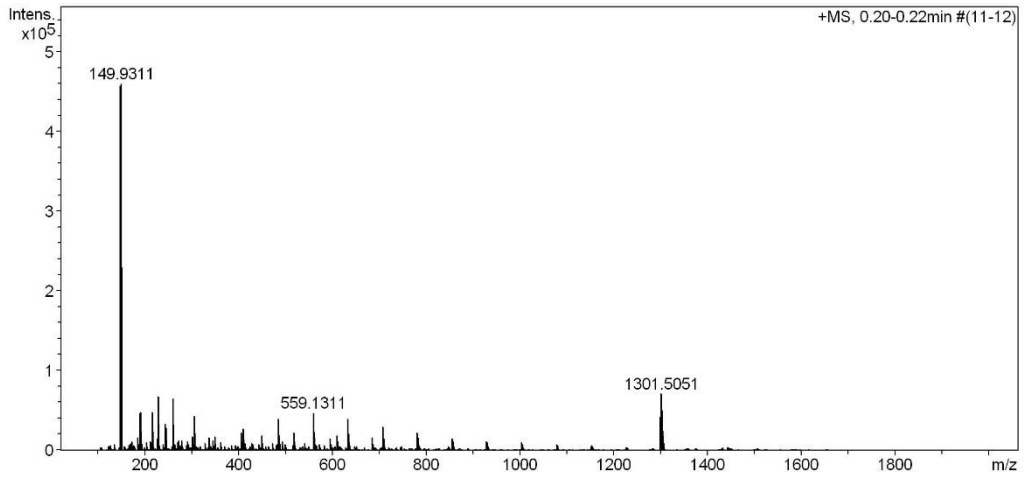
^1H , $^{13}\text{C}\{^1\text{H}\}$ (400/101 MHz, CDCl_3) NMR and HR-ESI-MS Spectra of ((3',4'-dihexyl-[2,2':5',2''-terthiophen]-5-yl)ethynyl)tri-isopropylsilane (92):



High Resolution Mass Spectrometry Report

Sample Name **KR323**
Comment

Instrument **maXis 4G**
Method **ms_nocolumn_mid_pos.m**



 High Resolution Mass Spectrometry Report

Measured m/z vs. theoretical m/z

| Meas. m/z | # | Formula | Score | m/z | err [mDa] | err [ppm] | mSigma | rdb | e ⁻ Conf | z |
|-----------|---|------------------|--------|----------|-----------|-----------|--------|------|---------------------|----|
| 596.2984 | 1 | C 35 H 52 S 3 Si | 100.00 | 596.2995 | 1.1 | 1.9 | 26.9 | 11.0 | odd | 1+ |

Mass list

| # | m/z | I % | I |
|----|----------|-------|--------|
| 1 | 136.1122 | 1.7 | 7870 |
| 2 | 147.9314 | 99.4 | 457899 |
| 3 | 148.9342 | 1.9 | 8626 |
| 4 | 149.9311 | 100.0 | 460668 |
| 5 | 150.9340 | 2.0 | 9134 |
| 6 | 167.9416 | 1.6 | 7287 |
| 7 | 171.0993 | 1.8 | 8396 |
| 8 | 173.0786 | 2.5 | 11583 |
| 9 | 185.1147 | 3.6 | 16690 |
| 10 | 188.9578 | 10.3 | 47499 |
| 11 | 190.9574 | 10.4 | 48050 |
| 12 | 192.9445 | 2.1 | 9460 |
| 13 | 205.0604 | 2.1 | 9864 |
| 14 | 213.1097 | 1.9 | 8953 |
| 15 | 213.1460 | 2.5 | 11738 |
| 16 | 215.1252 | 1.8 | 8350 |
| 17 | 217.1046 | 10.4 | 47695 |
| 18 | 226.9513 | 3.2 | 14591 |
| 19 | 227.1252 | 1.7 | 7990 |
| 20 | 229.1410 | 14.7 | 67774 |
| 21 | 230.1445 | 1.5 | 7033 |
| 22 | 239.0890 | 1.8 | 8220 |
| 23 | 243.9416 | 7.2 | 33198 |
| 24 | 245.0782 | 6.3 | 28988 |
| 25 | 260.9319 | 3.7 | 16840 |
| 26 | 261.1308 | 14.1 | 65099 |
| 27 | 262.1339 | 1.6 | 7240 |
| 28 | 263.0557 | 1.6 | 7252 |
| 29 | 265.1043 | 1.7 | 7730 |
| 30 | 271.1877 | 2.1 | 9512 |
| 31 | 273.1673 | 2.7 | 12289 |
| 32 | 277.9220 | 2.7 | 12332 |
| 33 | 291.8044 | 2.4 | 10912 |
| 34 | 293.8032 | 1.7 | 7976 |
| 35 | 301.1407 | 3.8 | 17683 |
| 36 | 305.1569 | 9.5 | 43630 |
| 37 | 328.9194 | 1.8 | 8508 |
| 38 | 337.0746 | 3.6 | 16510 |
| 39 | 345.9092 | 2.8 | 13005 |
| 40 | 349.1829 | 3.7 | 16875 |
| 41 | 361.2348 | 1.7 | 8050 |
| 42 | 362.8994 | 2.2 | 10099 |
| 43 | 405.2606 | 4.7 | 21845 |
| 44 | 411.0935 | 6.0 | 27451 |
| 45 | 412.0944 | 2.0 | 9272 |
| 46 | 413.8970 | 1.8 | 8347 |
| 47 | 429.3183 | 2.0 | 9335 |
| 48 | 430.8868 | 1.8 | 8240 |
| 49 | 443.3338 | 1.6 | 7156 |
| 50 | 449.2866 | 4.2 | 19254 |
| 51 | 473.3442 | 2.0 | 9186 |
| 52 | 481.8844 | 1.7 | 7941 |
| 53 | 485.1123 | 8.5 | 39184 |
| 54 | 486.1130 | 3.7 | 16842 |
| 55 | 487.1103 | 2.4 | 11115 |
| 56 | 493.3127 | 2.6 | 11911 |
| 57 | 498.8741 | 1.7 | 7884 |
| 58 | 517.2951 | 4.8 | 21960 |
| 59 | 518.2985 | 1.7 | 7614 |
| 60 | 519.2951 | 4.7 | 21553 |
| 61 | 541.1199 | 2.0 | 9338 |
| 62 | 559.1311 | 10.2 | 47213 |

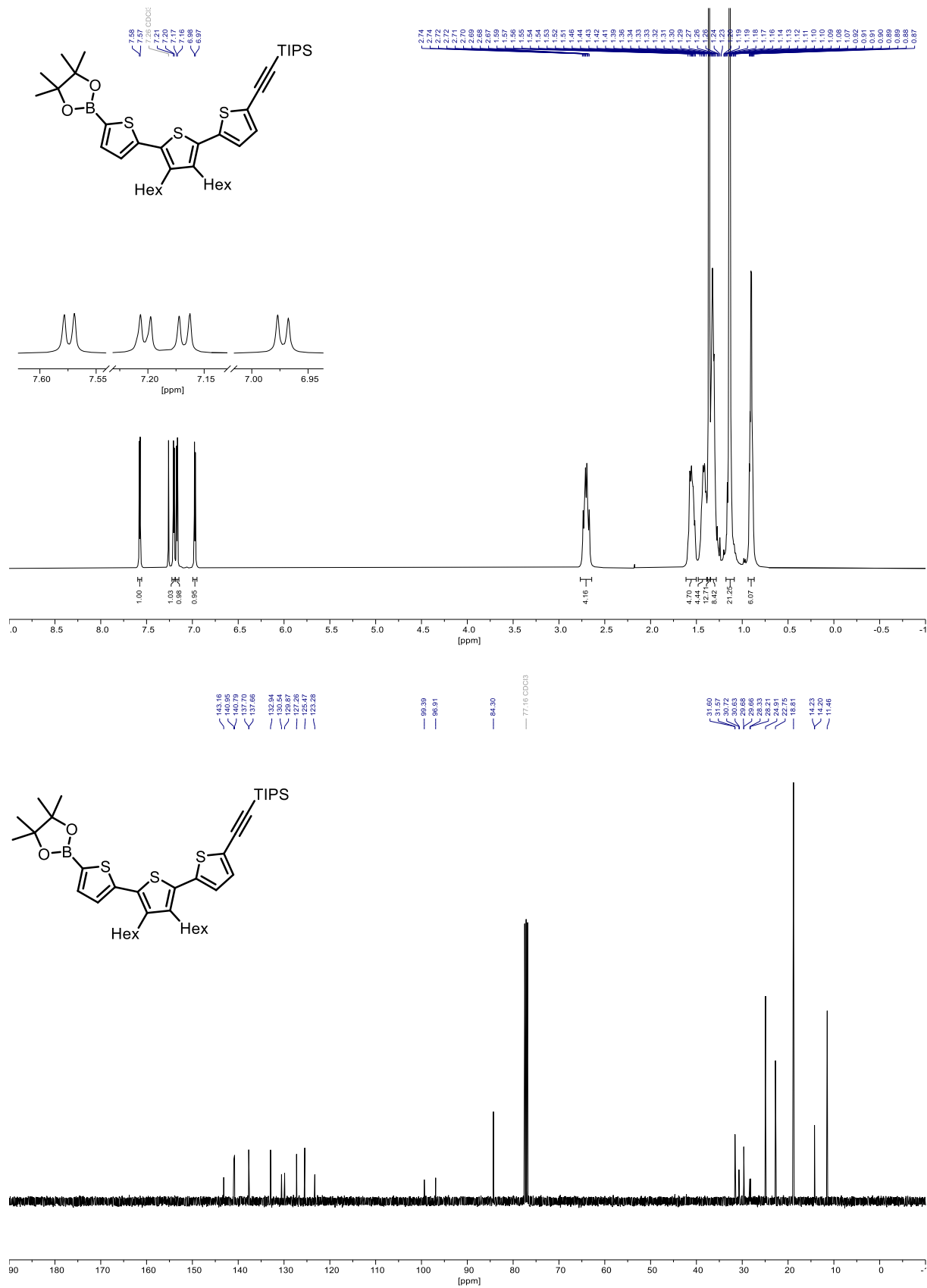
 High Resolution Mass Spectrometry Report

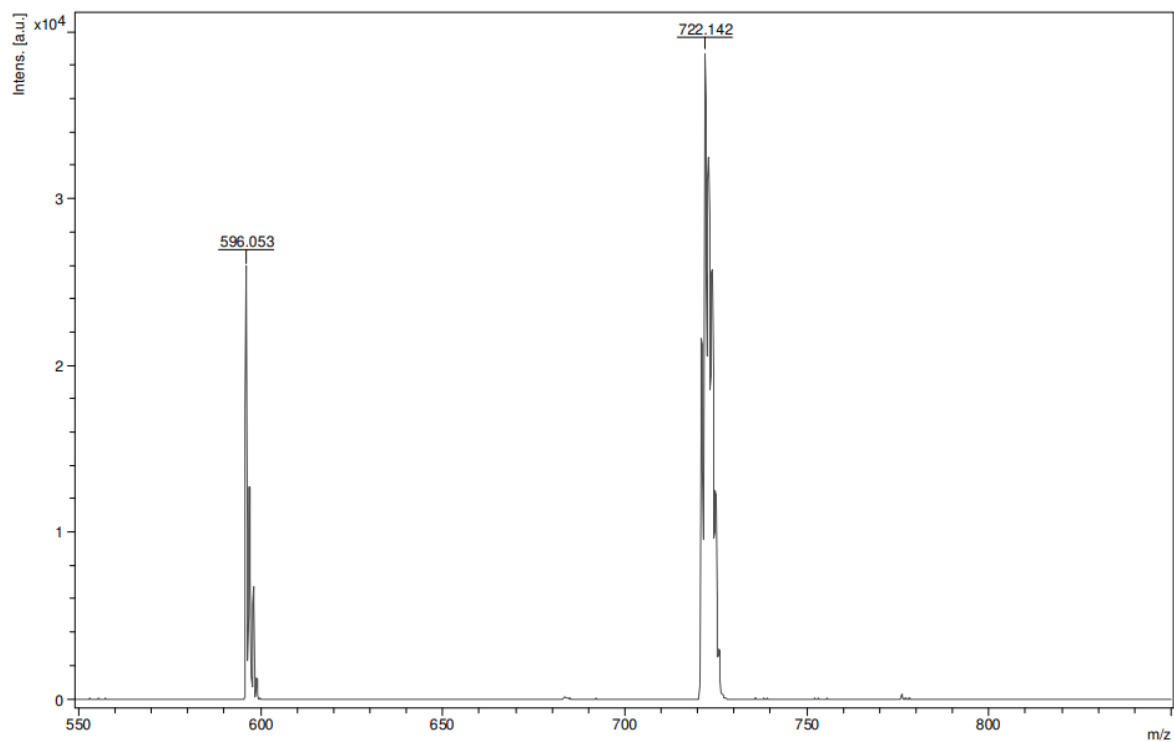
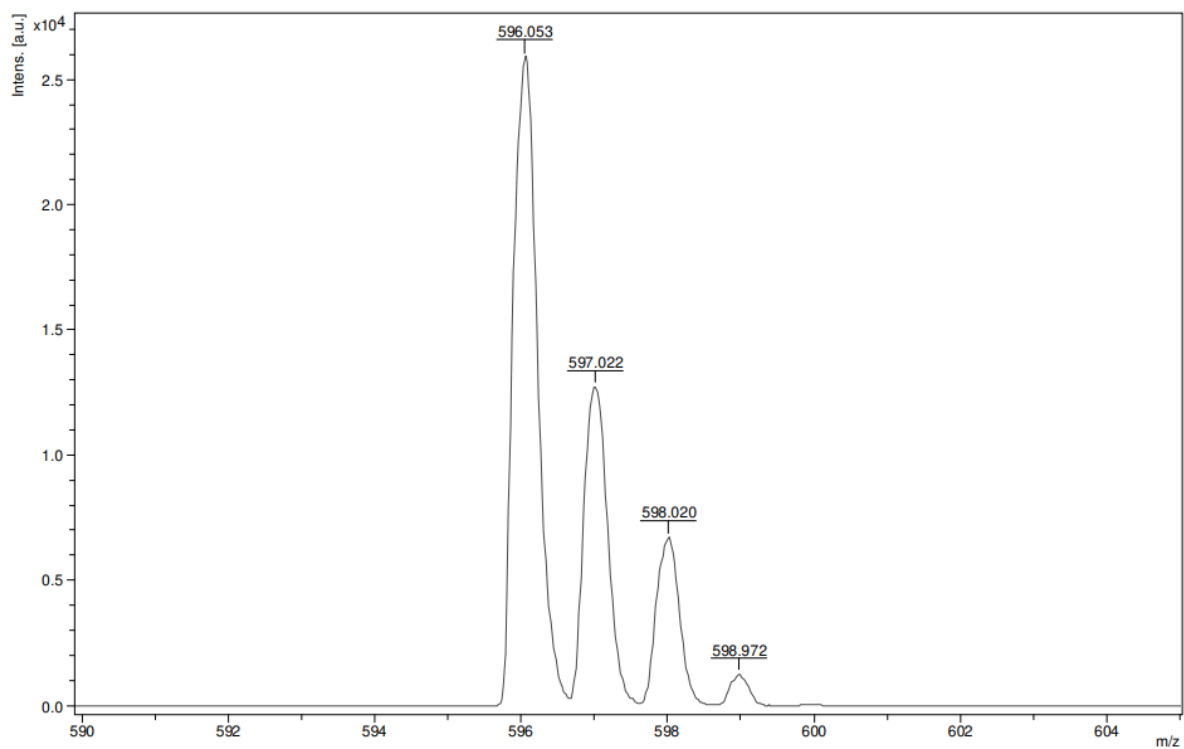
| # | m/z | I % | I |
|-----|-----------|------|-------|
| 63 | 560.1316 | 5.0 | 23050 |
| 64 | 561.1290 | 3.6 | 16377 |
| 65 | 573.1463 | 1.7 | 7747 |
| 66 | 596.2984 | 3.3 | 15280 |
| 67 | 597.3020 | 1.5 | 7129 |
| 68 | 610.1835 | 3.9 | 18182 |
| 69 | 611.1843 | 2.4 | 11197 |
| 70 | 612.1815 | 1.9 | 8787 |
| 71 | 633.1499 | 8.5 | 38956 |
| 72 | 634.1503 | 4.7 | 21515 |
| 73 | 635.1478 | 3.8 | 17499 |
| 74 | 636.1481 | 1.5 | 6996 |
| 75 | 685.4344 | 3.6 | 16552 |
| 76 | 686.4387 | 1.7 | 7721 |
| 77 | 707.1684 | 6.6 | 30204 |
| 78 | 708.1691 | 4.4 | 20356 |
| 79 | 709.1671 | 3.4 | 15489 |
| 80 | 781.1875 | 4.8 | 22171 |
| 81 | 782.1880 | 3.4 | 15893 |
| 82 | 783.1857 | 2.7 | 12492 |
| 83 | 855.2064 | 3.3 | 15386 |
| 84 | 856.2067 | 2.7 | 12395 |
| 85 | 857.2047 | 2.4 | 11247 |
| 86 | 929.2249 | 2.6 | 11942 |
| 87 | 930.2256 | 2.2 | 10071 |
| 88 | 931.2242 | 2.0 | 9156 |
| 89 | 1003.2446 | 2.1 | 9646 |
| 90 | 1004.2437 | 1.9 | 8736 |
| 91 | 1005.2420 | 1.8 | 8257 |
| 92 | 1077.2616 | 1.6 | 7307 |
| 93 | 1078.2631 | 1.5 | 7017 |
| 94 | 1299.5046 | 9.0 | 41558 |
| 95 | 1300.5076 | 8.3 | 38010 |
| 96 | 1301.5051 | 15.5 | 71271 |
| 97 | 1302.5066 | 11.0 | 50738 |
| 98 | 1303.5053 | 7.5 | 34471 |
| 99 | 1304.5058 | 4.1 | 19014 |
| 100 | 1305.5031 | 2.1 | 9729 |

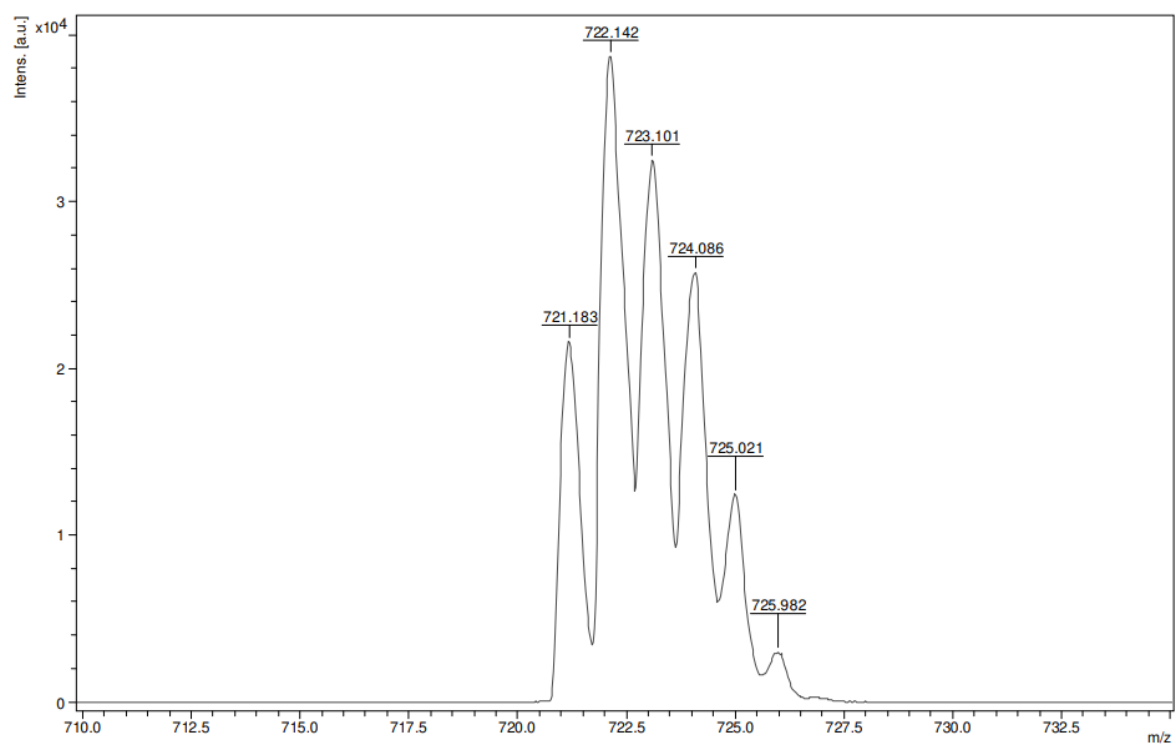
Acquisition Parameter

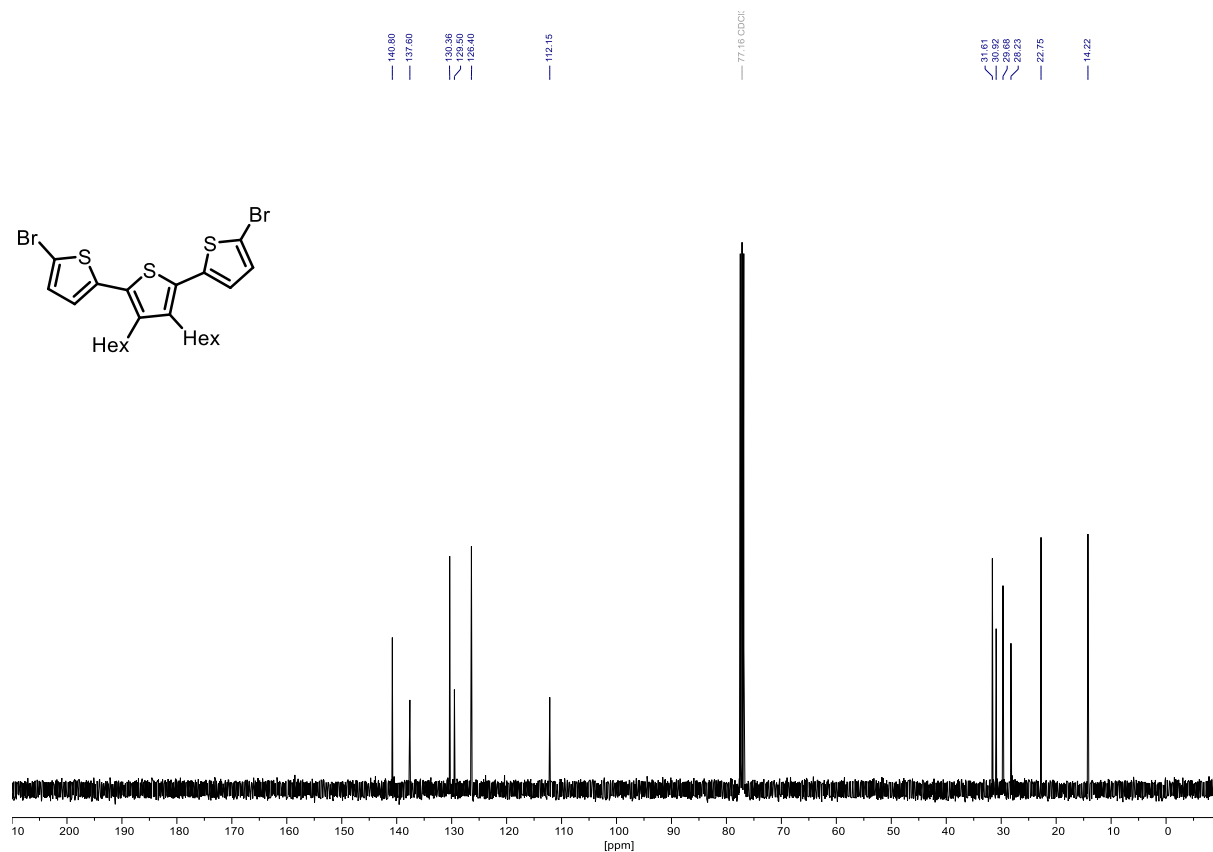
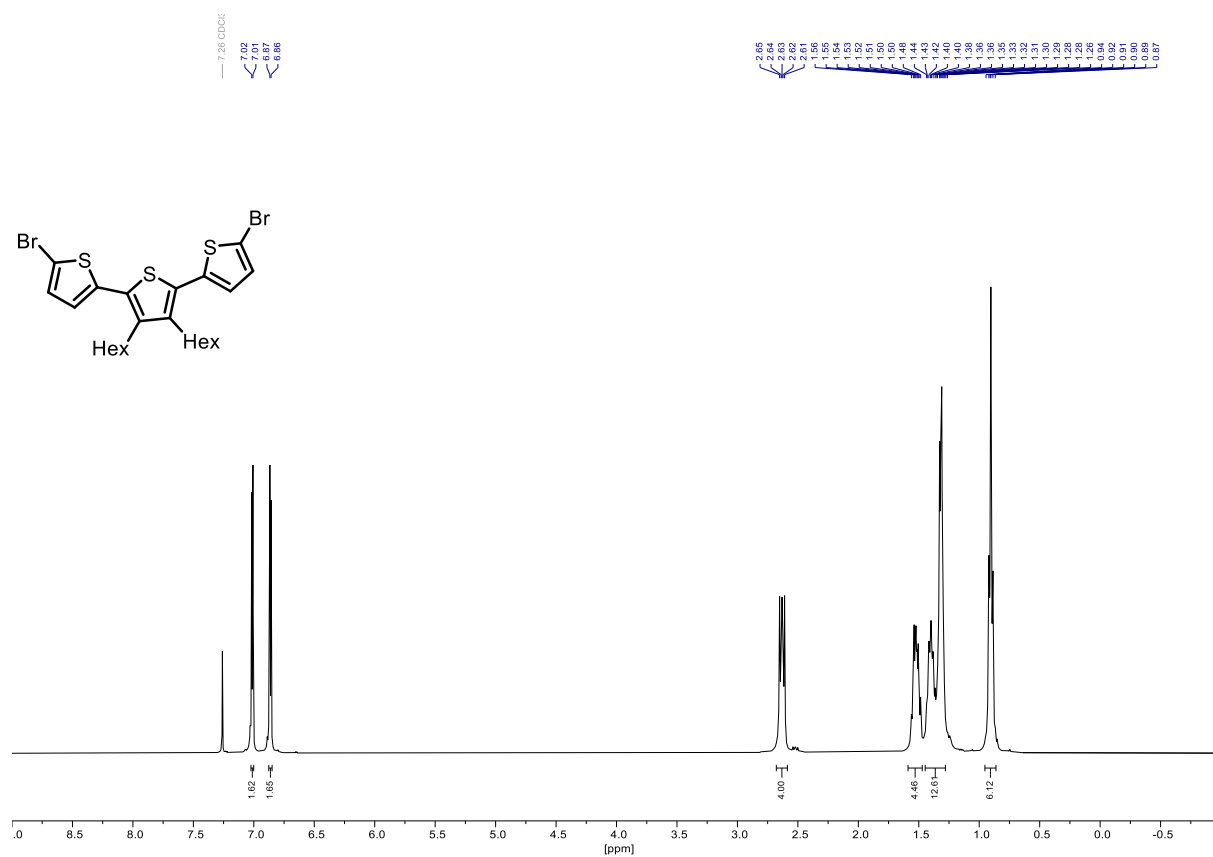
| | | | | | | |
|-------------------|------------------------------|----------------|---------------------------------------|----------------|--------------|-----------|
| General | Fore Vacuum | 3.36e+000 mBar | High Vacuum | 9.92e-008 mBar | Source Type | ESI |
| | Scan Begin | 75 m/z | Scan End | 2000 m/z | Ion Polarity | Positive |
| Source | Set Nebulizer | 2.0 Bar | Set Capillary | 4500 V | Set Dry Gas | 8.0 l/min |
| | Set Dry Heater | 200 °C | Set End Plate Offset | -500 V | | |
| Quadrupole | Set Ion Energy (MS only) | 4.0 eV | | | | |
| Coll. Cell | Collision Energy | 8.0 eV | Set Collision Cell RF | 600.0 Vpp | | 100.0 Vpp |
| Ion Cooler | Set Ion Cooler Transfer Time | 75.0 µs | Set Ion Cooler Pre Pulse Storage Time | | | 10.0 µs |

^1H , $^{13}\text{C}\{\text{H}\}$ (400/101 MHz, CDCl_3) NMR and HR-ESI-MS Spectra of ((3',4'-dihexyl-5'-(4,4,5,5-tetramethyl-1,3,2-dioxaborolan-2-yl)-[2,2':5',2''-terthiophen]-5-yl)ethynyl)triisopropylsilane (83b):



MALDI-ToF-MSZoom in of MALDI-ToF-MS (deborylated, see compound 92)

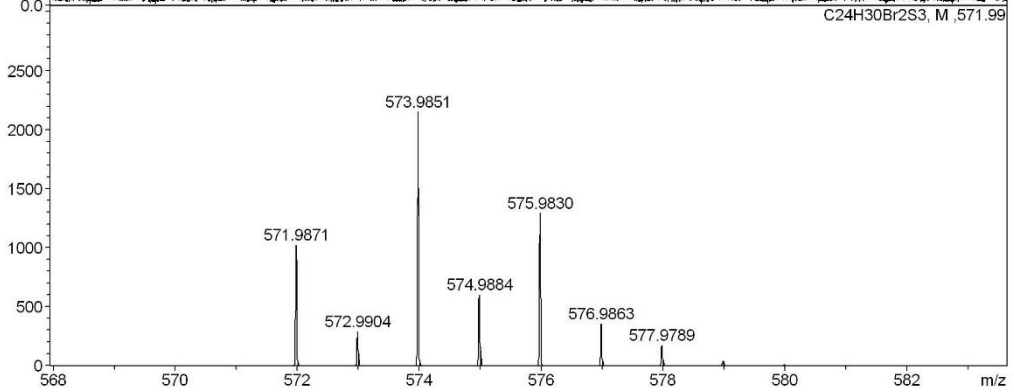
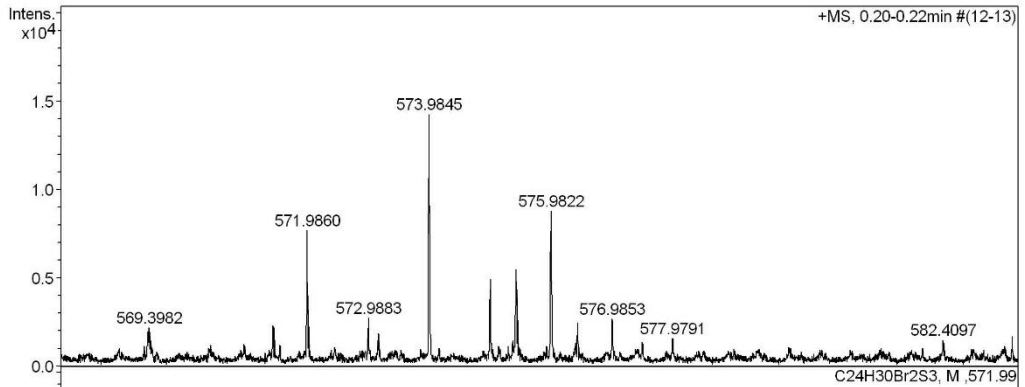
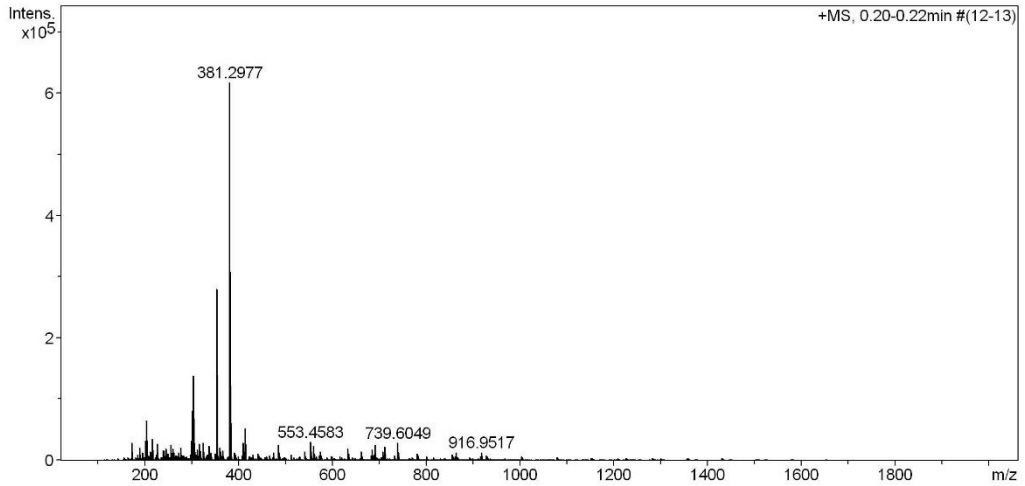
Zoom in of MALDI-ToF-MS of Compound 83b

^1H , $^{13}\text{C}\{\text{H}\}$ (400/101 MHz, CDCl_3) NMR and HR-ESI-MS Spectra of 5,5'-dibromo-3',4'-dihexyl-2,2':5',2''-terthiophene (100):

High Resolution Mass Spectrometry Report

Sample Name **KR341_2Br**
Comment

Instrument **maXis 4G**
Method **ms_nocolumn_mid_pos.m**



High Resolution Mass Spectrometry Report

Measured m/z vs. theoretical m/z

| Meas. m/z | # | Formula | Score | m/z | err [mDa] | err [ppm] | mSigma | rdb | e ⁻ Conf | z |
|-----------|---|--------------------|--------|----------|-----------|-----------|--------|-----|---------------------|----|
| 571.9860 | 1 | C 24 H 30 Br 2 S 3 | 100.00 | 571.9871 | 1.1 | 1.9 | 42.7 | 9.0 | odd | 1+ |

Mass list

| # | m/z | I % | I |
|----|----------|-------|--------|
| 1 | 173.0784 | 4.6 | 28687 |
| 2 | 185.1147 | 1.7 | 10594 |
| 3 | 189.0732 | 3.4 | 20797 |
| 4 | 195.0988 | 2.2 | 13447 |
| 5 | 201.1095 | 5.3 | 32763 |
| 6 | 205.0600 | 10.6 | 65709 |
| 7 | 209.1144 | 1.4 | 8470 |
| 8 | 212.9719 | 2.3 | 14520 |
| 9 | 215.1252 | 2.1 | 13024 |
| 10 | 217.0468 | 3.0 | 18511 |
| 11 | 217.1045 | 5.7 | 35109 |
| 12 | 225.1093 | 1.6 | 9611 |
| 13 | 226.9514 | 4.6 | 28213 |
| 14 | 239.0888 | 2.6 | 16109 |
| 15 | 241.0679 | 2.6 | 16007 |
| 16 | 241.1406 | 1.4 | 8833 |
| 17 | 245.0782 | 3.1 | 19215 |
| 18 | 249.1822 | 1.8 | 11132 |
| 19 | 256.9619 | 4.1 | 25516 |
| 20 | 261.1305 | 3.1 | 19397 |
| 21 | 263.0559 | 2.1 | 13197 |
| 22 | 273.1670 | 2.1 | 13215 |
| 23 | 276.2293 | 3.5 | 21455 |
| 24 | 281.1720 | 1.4 | 8920 |
| 25 | 283.1514 | 1.5 | 9036 |
| 26 | 297.2397 | 1.5 | 9562 |
| 27 | 299.1614 | 5.1 | 31744 |
| 28 | 301.1407 | 13.1 | 81180 |
| 29 | 302.1439 | 2.4 | 14557 |
| 30 | 302.2451 | 3.6 | 21976 |
| 31 | 304.2608 | 22.5 | 139025 |
| 32 | 305.2639 | 4.6 | 28652 |
| 33 | 309.2029 | 1.5 | 9546 |
| 34 | 311.2553 | 1.7 | 10370 |
| 35 | 313.2343 | 2.8 | 17350 |
| 36 | 317.1718 | 4.5 | 27966 |
| 37 | 317.2446 | 2.6 | 15802 |
| 38 | 319.2602 | 2.7 | 16944 |
| 39 | 325.2343 | 4.7 | 28869 |
| 40 | 333.1682 | 1.7 | 10247 |
| 41 | 333.2394 | 1.5 | 9279 |
| 42 | 335.2550 | 1.5 | 9522 |
| 43 | 337.0747 | 3.9 | 23879 |
| 44 | 341.2655 | 2.1 | 12953 |
| 45 | 348.9896 | 1.9 | 11720 |
| 46 | 350.9868 | 2.0 | 12055 |
| 47 | 353.2662 | 45.3 | 280065 |
| 48 | 354.2692 | 9.1 | 56473 |
| 49 | 355.2754 | 1.4 | 8578 |
| 50 | 360.3230 | 3.3 | 20496 |
| 51 | 362.2408 | 2.3 | 14182 |
| 52 | 362.3388 | 1.8 | 11219 |
| 53 | 362.9261 | 1.6 | 9633 |
| 54 | 367.2814 | 2.6 | 16150 |
| 55 | 381.2977 | 100.0 | 618154 |
| 56 | 382.3007 | 19.9 | 123318 |
| 57 | 383.3032 | 2.9 | 18006 |
| 58 | 391.2087 | 2.0 | 12589 |
| 59 | 393.2970 | 1.6 | 9748 |
| 60 | 409.3281 | 1.9 | 11826 |
| 61 | 411.0934 | 4.6 | 28544 |
| 62 | 412.0939 | 1.7 | 10488 |

 High Resolution Mass Spectrometry Report

| # | m/z | I% | I |
|-----|----------|-----|-------|
| 63 | 413.2657 | 8.4 | 52148 |
| 64 | 414.2688 | 2.1 | 12945 |
| 65 | 430.9136 | 1.5 | 9517 |
| 66 | 441.2964 | 2.0 | 12312 |
| 67 | 443.3335 | 1.4 | 8401 |
| 68 | 475.3246 | 2.2 | 13305 |
| 69 | 485.1118 | 4.2 | 25846 |
| 70 | 486.1127 | 2.1 | 12870 |
| 71 | 511.2717 | 1.5 | 9262 |
| 72 | 541.1204 | 2.4 | 15095 |
| 73 | 553.4583 | 4.9 | 30530 |
| 74 | 554.4617 | 1.9 | 11646 |
| 75 | 555.2983 | 1.4 | 8418 |
| 76 | 559.1306 | 4.0 | 24606 |
| 77 | 560.1311 | 1.8 | 11110 |
| 78 | 561.1289 | 1.5 | 9249 |
| 79 | 573.9845 | 2.3 | 14290 |
| 80 | 575.9822 | 1.4 | 8808 |
| 81 | 633.1498 | 3.1 | 19132 |
| 82 | 634.1504 | 1.8 | 11091 |
| 83 | 634.5368 | 1.6 | 9607 |
| 84 | 635.1480 | 1.4 | 8579 |
| 85 | 662.5688 | 2.5 | 15237 |
| 86 | 683.5421 | 1.4 | 8666 |
| 87 | 685.4348 | 2.9 | 18054 |
| 88 | 688.9250 | 1.6 | 9706 |
| 89 | 690.9211 | 4.2 | 26024 |
| 90 | 707.1686 | 2.4 | 14550 |
| 91 | 708.1693 | 1.6 | 9909 |
| 92 | 711.5737 | 3.8 | 23260 |
| 93 | 712.5774 | 1.8 | 11049 |
| 94 | 739.6049 | 4.6 | 28389 |
| 95 | 740.6083 | 2.0 | 12432 |
| 96 | 781.1871 | 1.8 | 11410 |
| 97 | 782.1886 | 1.4 | 8519 |
| 98 | 855.2060 | 1.5 | 9516 |
| 99 | 862.9436 | 2.1 | 13154 |
| 100 | 916.9517 | 2.2 | 13765 |

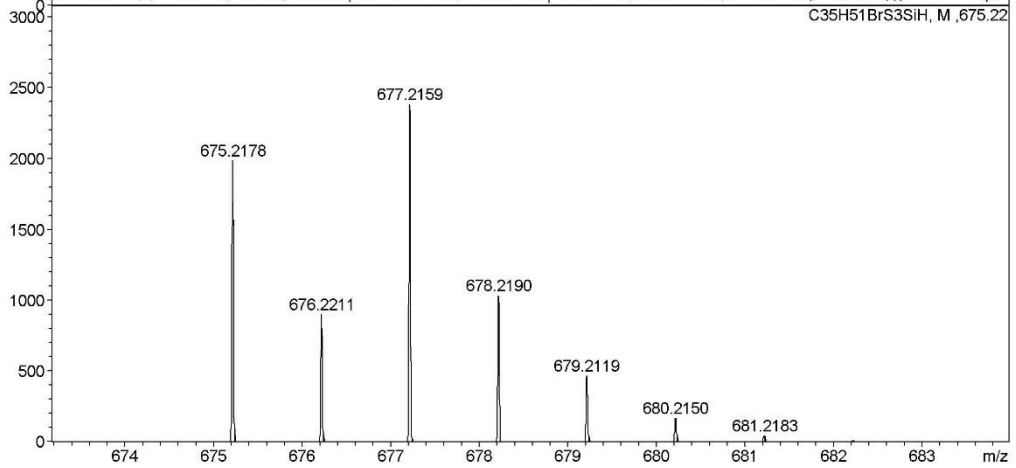
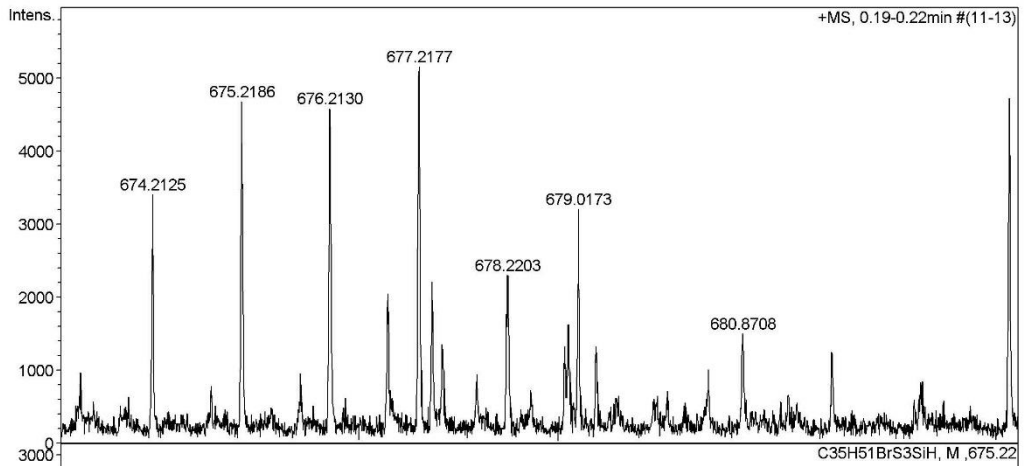
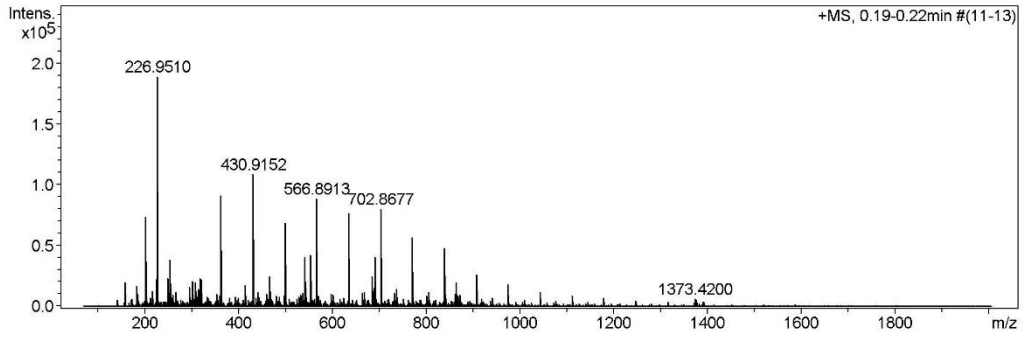
Acquisition Parameter

| | | | | | | |
|-------------------|------------------------------|----------------|---------------------------------------|----------------|--------------|-----------|
| General | Fore Vacuum | 3.45e+000 mBar | High Vacuum | 9.88e-008 mBar | Source Type | ESI |
| | Scan Begin | 75 m/z | Scan End | 2000 m/z | Ion Polarity | Positive |
| Source | Set Nebulizer | 2.0 Bar | Set Capillary | 4500 V | Set Dry Gas | 8.0 l/min |
| | Set Dry Heater | 200 °C | Set End Plate Offset | -500 V | | |
| Quadrupole | Set Ion Energy (MS only) | 4.0 eV | | | | |
| Coll. Cell | Collision Energy | 8.0 eV | Set Collision Cell RF | 600.0 Vpp | 100.0 Vpp | |
| Ion Cooler | Set Ion Cooler Transfer Time | 75.0 µs | Set Ion Cooler Pre Pulse Storage Time | 10.0 µs | | |

High Resolution Mass Spectrometry Report

Sample Name **KR346**
Comment

Instrument maXis 4G
Method ms_nocolumn_mid_pos.m



High Resolution Mass Spectrometry Report

Measured m/z vs. theoretical m/z

| Meas. m/z | # | Formula | Score | m/z | err [mDa] | err [ppm] | mSigma | rdb | e ⁻ Conf | z |
|-----------|---|---------------------|--------|----------|-----------|-----------|--------|------|---------------------|----|
| 675.2186 | 1 | C 35 H 52 Br S 3 Si | 100.00 | 675.2178 | -0.7 | -1.1 | 202.6 | 10.5 | even | 1+ |

Mass list

| # | m/z | I % | I |
|----|----------|-------|--------|
| 1 | 158.9632 | 10.3 | 19574 |
| 2 | 183.0982 | 8.8 | 16643 |
| 3 | 185.1141 | 5.6 | 10686 |
| 4 | 201.1089 | 38.9 | 73642 |
| 5 | 205.0591 | 4.2 | 7913 |
| 6 | 212.9712 | 3.7 | 7003 |
| 7 | 217.1037 | 6.9 | 13089 |
| 8 | 225.1090 | 11.7 | 22119 |
| 9 | 226.9510 | 100.0 | 189425 |
| 10 | 227.9542 | 3.7 | 7089 |
| 11 | 249.1090 | 12.2 | 23187 |
| 12 | 254.1509 | 20.3 | 38437 |
| 13 | 255.1549 | 4.2 | 7987 |
| 14 | 256.9614 | 7.8 | 14699 |
| 15 | 257.0626 | 4.0 | 7654 |
| 16 | 261.1304 | 5.1 | 9603 |
| 17 | 267.1563 | 6.2 | 11772 |
| 18 | 294.9388 | 8.5 | 16107 |
| 19 | 301.1410 | 11.0 | 20865 |
| 20 | 309.1305 | 10.4 | 19767 |
| 21 | 309.2034 | 5.3 | 10001 |
| 22 | 310.2351 | 4.0 | 7642 |
| 23 | 311.2552 | 4.1 | 7855 |
| 24 | 315.1927 | 7.4 | 13937 |
| 25 | 315.2291 | 3.7 | 6948 |
| 26 | 317.2448 | 7.2 | 13679 |
| 27 | 318.0463 | 12.0 | 22799 |
| 28 | 319.2605 | 10.6 | 20102 |
| 29 | 320.0442 | 11.8 | 22309 |
| 30 | 333.1682 | 4.0 | 7558 |
| 31 | 335.2557 | 3.6 | 6744 |
| 32 | 353.1571 | 5.3 | 10013 |
| 33 | 360.3240 | 4.6 | 8725 |
| 34 | 362.9268 | 48.4 | 91602 |
| 35 | 381.2978 | 3.6 | 6893 |
| 36 | 393.2979 | 4.0 | 7546 |
| 37 | 399.3087 | 3.7 | 6993 |
| 38 | 413.2668 | 9.2 | 17395 |
| 39 | 430.9152 | 57.4 | 108741 |
| 40 | 431.9181 | 4.1 | 7719 |
| 41 | 437.3240 | 3.6 | 6729 |
| 42 | 441.2984 | 6.4 | 12063 |
| 43 | 443.3349 | 4.2 | 7897 |
| 44 | 460.9257 | 5.6 | 10515 |
| 45 | 467.1028 | 13.0 | 24626 |
| 46 | 468.1040 | 6.1 | 11564 |
| 47 | 469.1016 | 3.6 | 6755 |
| 48 | 481.3512 | 4.5 | 8462 |
| 49 | 487.3625 | 4.3 | 8079 |
| 50 | 497.3972 | 4.7 | 8834 |
| 51 | 498.9032 | 36.4 | 68993 |
| 52 | 506.9464 | 3.5 | 6710 |
| 53 | 528.9133 | 4.3 | 8169 |
| 54 | 531.3880 | 3.5 | 6722 |
| 55 | 532.8972 | 5.0 | 9401 |
| 56 | 536.1671 | 5.8 | 10894 |
| 57 | 541.1229 | 21.6 | 40842 |
| 58 | 542.1232 | 10.3 | 19458 |
| 59 | 543.1215 | 7.8 | 14772 |
| 60 | 553.4610 | 22.3 | 42243 |
| 61 | 554.4643 | 8.8 | 16649 |
| 62 | 566.8913 | 46.8 | 88639 |

 High Resolution Mass Spectrometry Report

| # | m/z | I % | I |
|-----|-----------|------|-------|
| 63 | 567.8949 | 4.4 | 8302 |
| 64 | 569.4346 | 4.6 | 8805 |
| 65 | 596.9017 | 5.6 | 10545 |
| 66 | 600.8856 | 4.8 | 9184 |
| 67 | 624.8505 | 3.6 | 6897 |
| 68 | 634.8796 | 40.6 | 76969 |
| 69 | 635.8823 | 4.6 | 8692 |
| 70 | 664.8895 | 5.7 | 10837 |
| 71 | 668.8734 | 6.2 | 11798 |
| 72 | 685.4387 | 13.1 | 24898 |
| 73 | 686.4415 | 6.5 | 12335 |
| 74 | 688.9296 | 7.8 | 14793 |
| 75 | 689.9298 | 4.3 | 8209 |
| 76 | 690.9251 | 21.6 | 40938 |
| 77 | 691.9260 | 6.9 | 13004 |
| 78 | 702.8677 | 42.5 | 80443 |
| 79 | 703.8705 | 4.9 | 9247 |
| 80 | 732.8779 | 6.0 | 11335 |
| 81 | 736.8619 | 7.5 | 14252 |
| 82 | 770.8561 | 30.1 | 56997 |
| 83 | 771.8586 | 4.1 | 7692 |
| 84 | 800.8661 | 4.7 | 8859 |
| 85 | 804.8497 | 6.4 | 12107 |
| 86 | 838.8439 | 25.3 | 47832 |
| 87 | 839.8467 | 3.8 | 7228 |
| 88 | 839.9380 | 5.3 | 10066 |
| 89 | 860.9529 | 5.3 | 10123 |
| 90 | 861.9537 | 4.1 | 7807 |
| 91 | 862.9488 | 10.6 | 20147 |
| 92 | 863.9499 | 4.8 | 9037 |
| 93 | 868.8539 | 4.5 | 8449 |
| 94 | 871.9646 | 4.7 | 8880 |
| 95 | 872.8390 | 4.9 | 9351 |
| 96 | 906.8324 | 14.0 | 26538 |
| 97 | 940.8265 | 3.9 | 7396 |
| 98 | 974.8206 | 9.5 | 18061 |
| 99 | 1042.8085 | 6.5 | 12292 |
| 100 | 1110.7971 | 4.7 | 8884 |

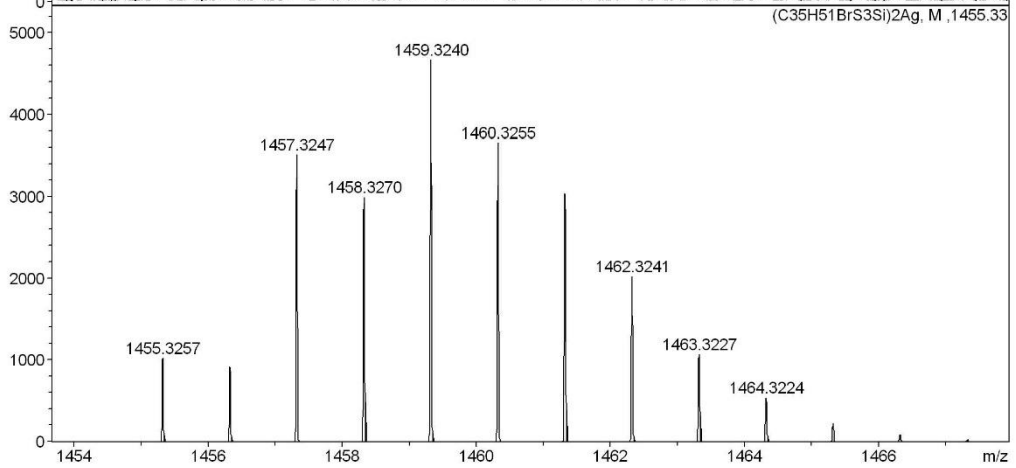
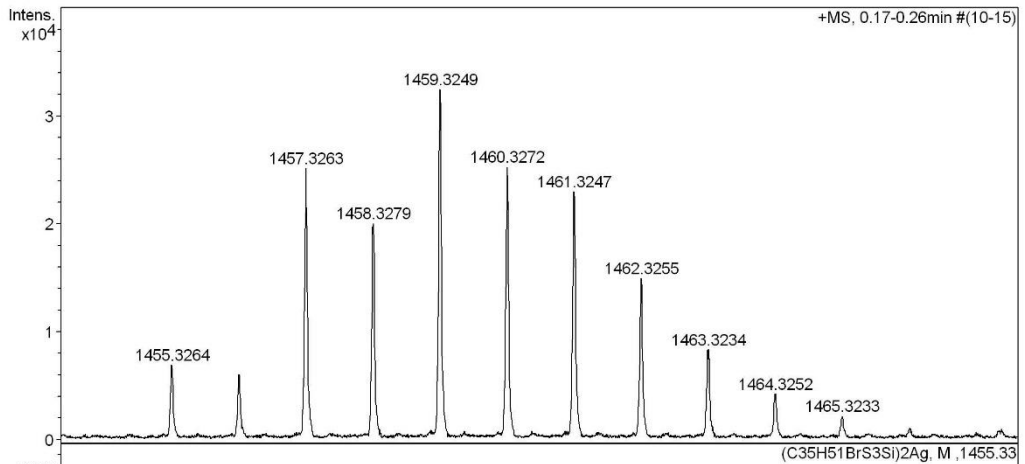
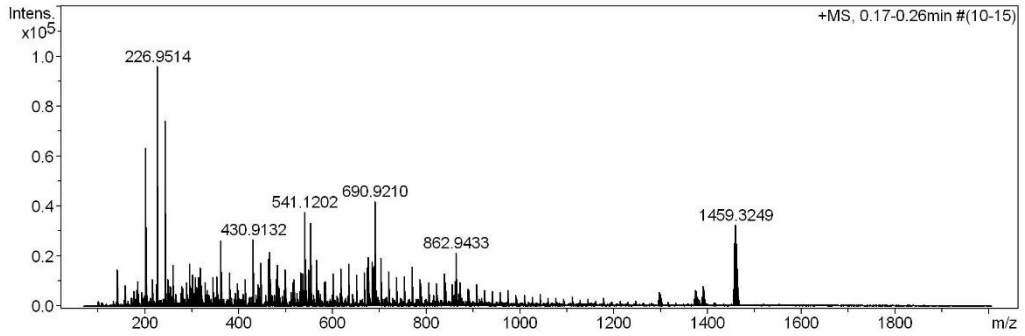
Acquisition Parameter

| | | | | | | |
|-------------------|------------------------------|----------------|---------------------------------------|----------------|--------------|-----------|
| General | Fore Vacuum | 3.36e+000 mBar | High Vacuum | 1.02e-007 mBar | Source Type | ESI |
| | Scan Begin | 75 m/z | Scan End | 2000 m/z | Ion Polarity | Positive |
| Source | Set Nebulizer | 2.0 Bar | Set Capillary | 4500 V | Set Dry Gas | 8.0 l/min |
| | Set Dry Heater | 200 °C | Set End Plate Offset | -500 V | | |
| Quadrupole | Set Ion Energy (MS only) | 4.0 eV | | | | |
| Coll. Cell | Collision Energy | 8.0 eV | Set Collision Cell RF | 600.0 Vpp | | 100.0 Vpp |
| Ion Cooler | Set Ion Cooler Transfer Time | 75.0 µs | Set Ion Cooler Pre Pulse Storage Time | | | 10.0 µs |

High Resolution Mass Spectrometry Report

Sample Name **KR346 +Ag**
 Comment

Instrument maXis 4G
 Method ms_nocolumn_mid_pos.m



High Resolution Mass Spectrometry Report

Measured m/z vs. theoretical m/z

| Meas. m/z | # | Formula | Score | m/z | err [mDa] | err [ppm] | mSigma | rdb | e ⁻ Conf | z |
|-----------|---|-----------------------------|--------|-----------|-----------|-----------|--------|------|---------------------|----|
| 1455.3264 | 1 | C 70 H 102 Ag Br 2 S 6 Si 2 | 100.00 | 1455.3257 | -0.8 | -0.5 | 25.4 | 20.5 | even | 1+ |

Mass list

| # | m/z | I % | I |
|----|----------|-------|-------|
| 1 | 141.0024 | 15.5 | 14905 |
| 2 | 158.9641 | 9.0 | 8607 |
| 3 | 185.1146 | 10.3 | 9874 |
| 4 | 201.1096 | 66.0 | 63386 |
| 5 | 205.0597 | 9.0 | 8609 |
| 6 | 217.1043 | 11.5 | 11007 |
| 7 | 225.1094 | 9.4 | 9046 |
| 8 | 226.9514 | 100.0 | 96090 |
| 9 | 243.9414 | 77.3 | 74257 |
| 10 | 249.1093 | 11.1 | 10700 |
| 11 | 260.9315 | 17.5 | 16852 |
| 12 | 261.1304 | 8.6 | 8220 |
| 13 | 277.9217 | 8.4 | 8116 |
| 14 | 288.9215 | 10.2 | 9845 |
| 15 | 294.9195 | 17.9 | 17204 |
| 16 | 301.1405 | 13.3 | 12778 |
| 17 | 309.1300 | 11.9 | 11449 |
| 18 | 315.1924 | 12.1 | 11632 |
| 19 | 317.2443 | 12.2 | 11748 |
| 20 | 318.0456 | 8.9 | 8516 |
| 21 | 319.2601 | 16.2 | 15556 |
| 22 | 320.0437 | 8.7 | 8388 |
| 23 | 328.9184 | 10.2 | 9781 |
| 24 | 345.9090 | 12.0 | 11540 |
| 25 | 353.2654 | 12.3 | 11853 |
| 26 | 362.9260 | 27.5 | 26413 |
| 27 | 379.9162 | 9.8 | 9461 |
| 28 | 381.2967 | 14.0 | 13472 |
| 29 | 396.9059 | 9.8 | 9394 |
| 30 | 413.2654 | 11.4 | 10914 |
| 31 | 413.8962 | 10.4 | 9980 |
| 32 | 430.9132 | 27.7 | 26630 |
| 33 | 441.2969 | 9.4 | 9053 |
| 34 | 447.9034 | 18.1 | 17428 |
| 35 | 464.8937 | 19.8 | 19028 |
| 36 | 467.1014 | 22.8 | 21908 |
| 37 | 468.1020 | 9.8 | 9422 |
| 38 | 481.8840 | 17.5 | 16808 |
| 39 | 498.8750 | 13.1 | 12574 |
| 40 | 498.8999 | 15.3 | 14680 |
| 41 | 515.8897 | 9.9 | 9485 |
| 42 | 517.2949 | 11.2 | 10734 |
| 43 | 519.2948 | 10.3 | 9943 |
| 44 | 532.8803 | 13.9 | 13399 |
| 45 | 536.1644 | 13.7 | 13127 |
| 46 | 541.1202 | 39.4 | 37857 |
| 47 | 542.1206 | 19.1 | 18386 |
| 48 | 543.1185 | 13.5 | 12945 |
| 49 | 549.8714 | 15.4 | 14757 |
| 50 | 553.4582 | 34.7 | 33390 |
| 51 | 554.4613 | 13.2 | 12648 |
| 52 | 566.8632 | 14.4 | 13880 |
| 53 | 566.8873 | 19.6 | 18804 |
| 54 | 583.8545 | 10.1 | 9744 |
| 55 | 583.8759 | 10.5 | 10090 |
| 56 | 600.8676 | 13.9 | 13324 |
| 57 | 617.8582 | 15.7 | 15111 |
| 58 | 634.8511 | 15.8 | 15152 |
| 59 | 634.8737 | 17.9 | 17205 |
| 60 | 651.8413 | 13.3 | 12826 |
| 61 | 668.8549 | 14.1 | 13592 |
| 62 | 674.2089 | 16.2 | 15600 |

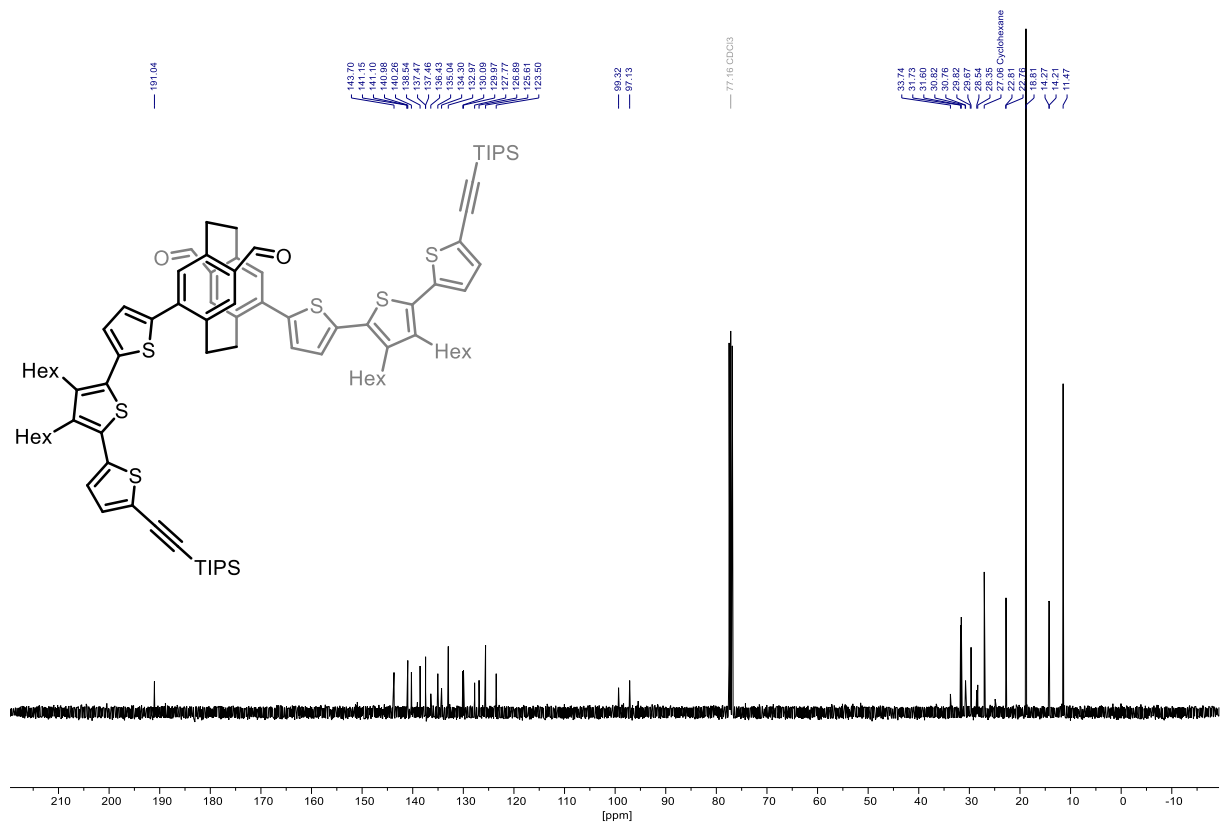
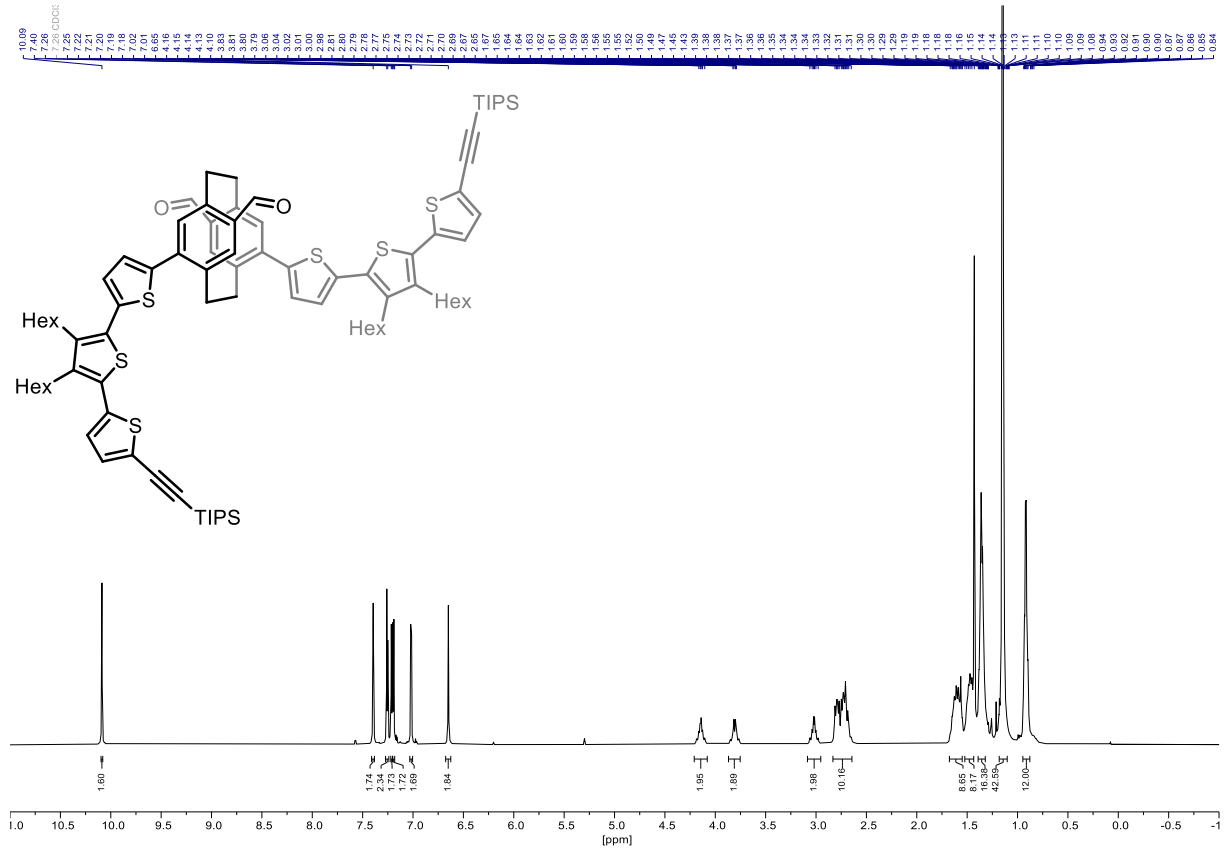
 High Resolution Mass Spectrometry Report

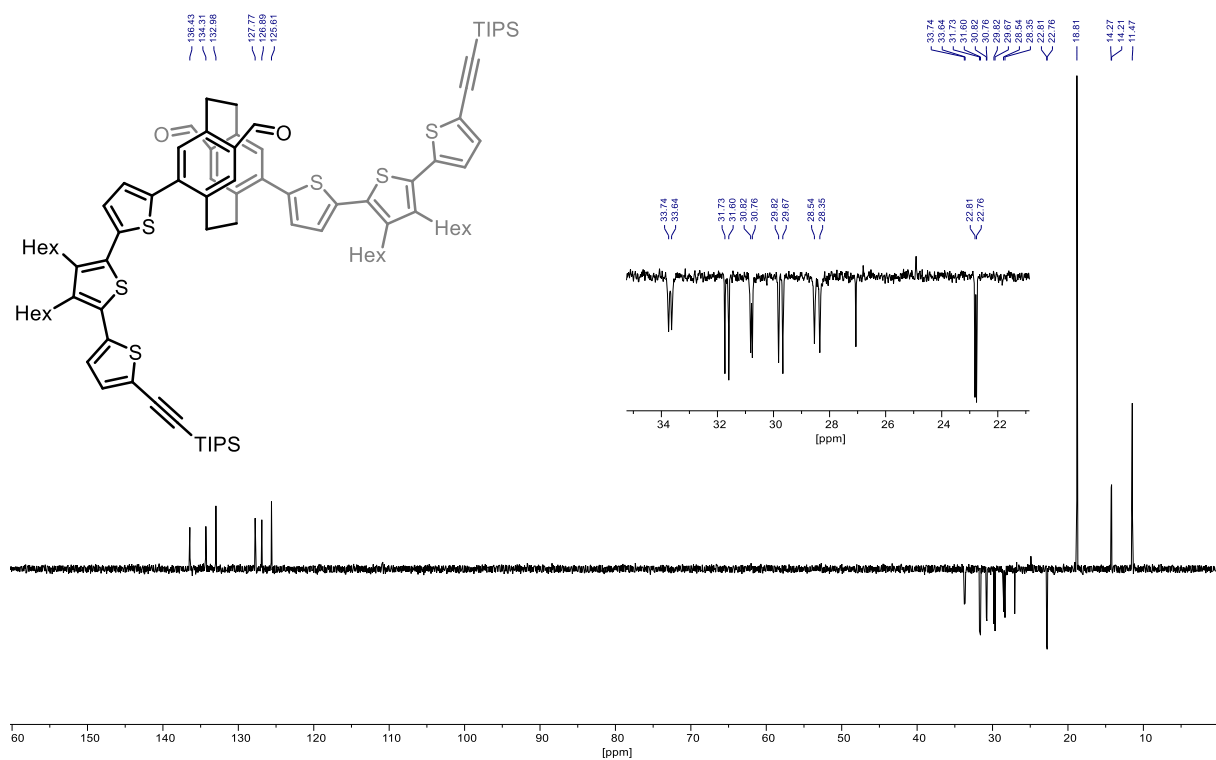
| # | m/z | I % | I |
|-----|-----------|------|-------|
| 63 | 675.2135 | 11.0 | 10609 |
| 64 | 676.2080 | 20.7 | 19934 |
| 65 | 677.2119 | 13.5 | 12982 |
| 66 | 685.4346 | 18.7 | 17951 |
| 67 | 685.8451 | 14.3 | 13705 |
| 68 | 686.4375 | 8.4 | 8088 |
| 69 | 688.9251 | 17.0 | 16317 |
| 70 | 689.9256 | 8.9 | 8547 |
| 71 | 690.9210 | 43.9 | 42151 |
| 72 | 691.9226 | 13.7 | 13183 |
| 73 | 702.8408 | 15.5 | 14864 |
| 74 | 702.8616 | 20.2 | 19364 |
| 75 | 719.8293 | 14.3 | 13747 |
| 76 | 736.8431 | 12.0 | 11484 |
| 77 | 753.8319 | 12.5 | 11989 |
| 78 | 770.8483 | 16.5 | 15811 |
| 79 | 787.8163 | 11.4 | 10980 |
| 80 | 804.8116 | 10.0 | 9564 |
| 81 | 804.8272 | 9.1 | 8708 |
| 82 | 821.8176 | 9.6 | 9262 |
| 83 | 838.8345 | 13.7 | 13209 |
| 84 | 839.9324 | 9.9 | 9548 |
| 85 | 855.8040 | 9.4 | 9011 |
| 86 | 860.9477 | 10.5 | 10122 |
| 87 | 862.9433 | 22.4 | 21502 |
| 88 | 863.9441 | 9.2 | 8826 |
| 89 | 871.9598 | 10.1 | 9671 |
| 90 | 872.7980 | 8.8 | 8485 |
| 91 | 906.8212 | 9.0 | 8628 |
| 92 | 1389.3834 | 8.5 | 8211 |
| 93 | 1391.3833 | 8.6 | 8223 |
| 94 | 1457.3263 | 26.2 | 25197 |
| 95 | 1458.3279 | 20.9 | 20097 |
| 96 | 1459.3249 | 33.8 | 32464 |
| 97 | 1460.3272 | 26.3 | 25318 |
| 98 | 1461.3247 | 24.0 | 23015 |
| 99 | 1462.3255 | 15.6 | 15014 |
| 100 | 1463.3234 | 8.7 | 8392 |

Acquisition Parameter

| | | | | | | |
|-------------------|------------------------------|----------------|---------------------------------------|----------------|--------------|-----------|
| General | Fore Vacuum | 3.39e+000 mBar | High Vacuum | 1.01e-007 mBar | Source Type | ESI |
| | Scan Begin | 75 m/z | Scan End | 2000 m/z | Ion Polarity | Positive |
| Source | Set Nebulizer | 2.0 Bar | Set Capillary | 4500 V | Set Dry Gas | 8.0 l/min |
| | Set Dry Heater | 200 °C | Set End Plate Offset | -500 V | | |
| Quadrupole | Set Ion Energy (MS only) | 4.0 eV | | | | |
| Coll. Cell | Collision Energy | 8.0 eV | Set Collision Cell RF | 600.0 Vpp | | 100.0 Vpp |
| Ion Cooler | Set Ion Cooler Transfer Time | 75.0 µs | Set Ion Cooler Pre Pulse Storage Time | | | 10.0 µs |

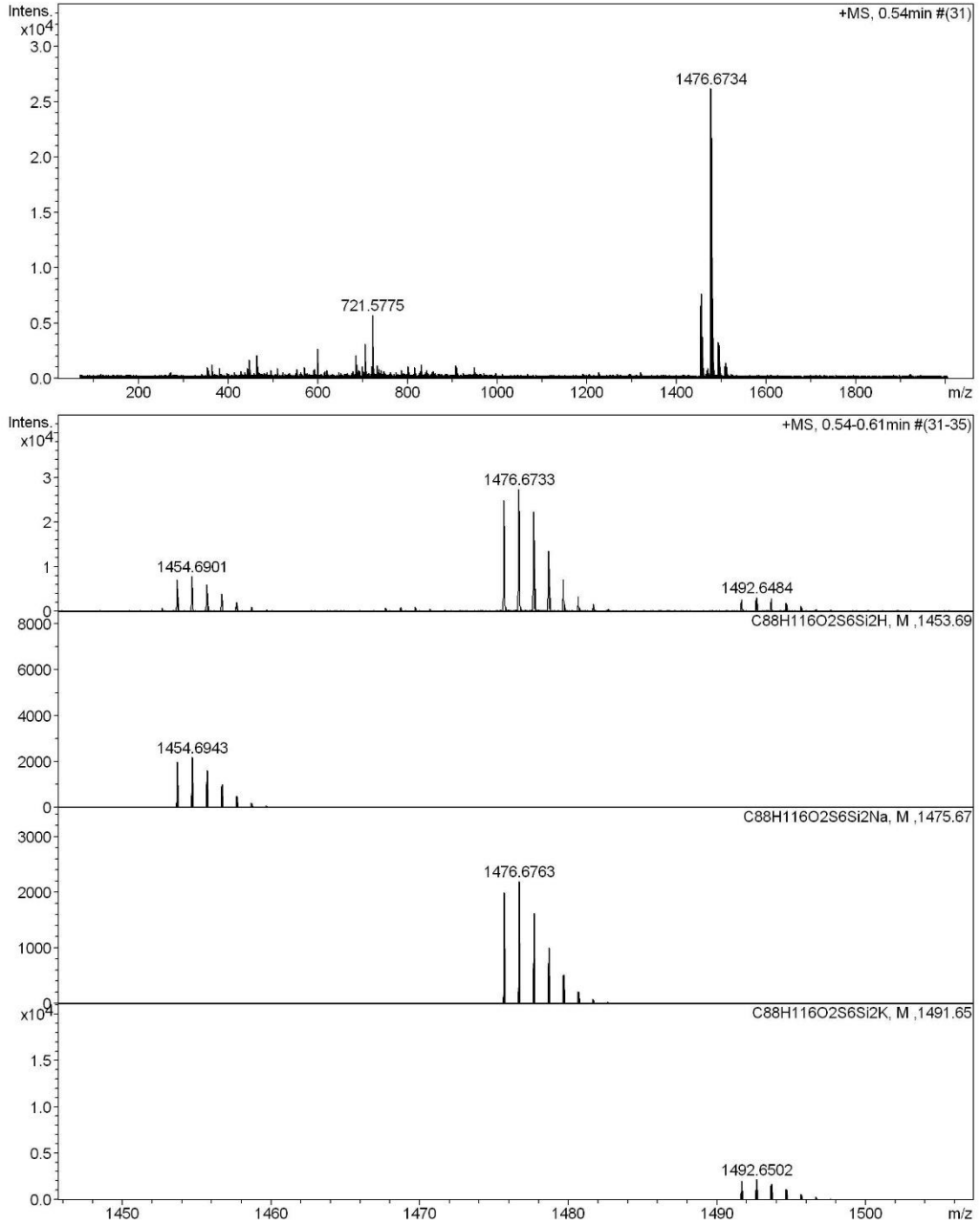
^1H , $^{13}\text{C}\{^1\text{H}\}$ (400/101 MHz, CDCl_3) NMR, DEPT-135 and HR-ESI-MS Spectra of Compound 93:





High Resolution Mass Spectrometry Report

Sample Name **KR_361** Instrument **maXis 4G**
Comment **direct infusion** Method **24 Direct_pos_high.m**



High Resolution Mass Spectrometry Report

Measured m/z vs. theoretical m/z

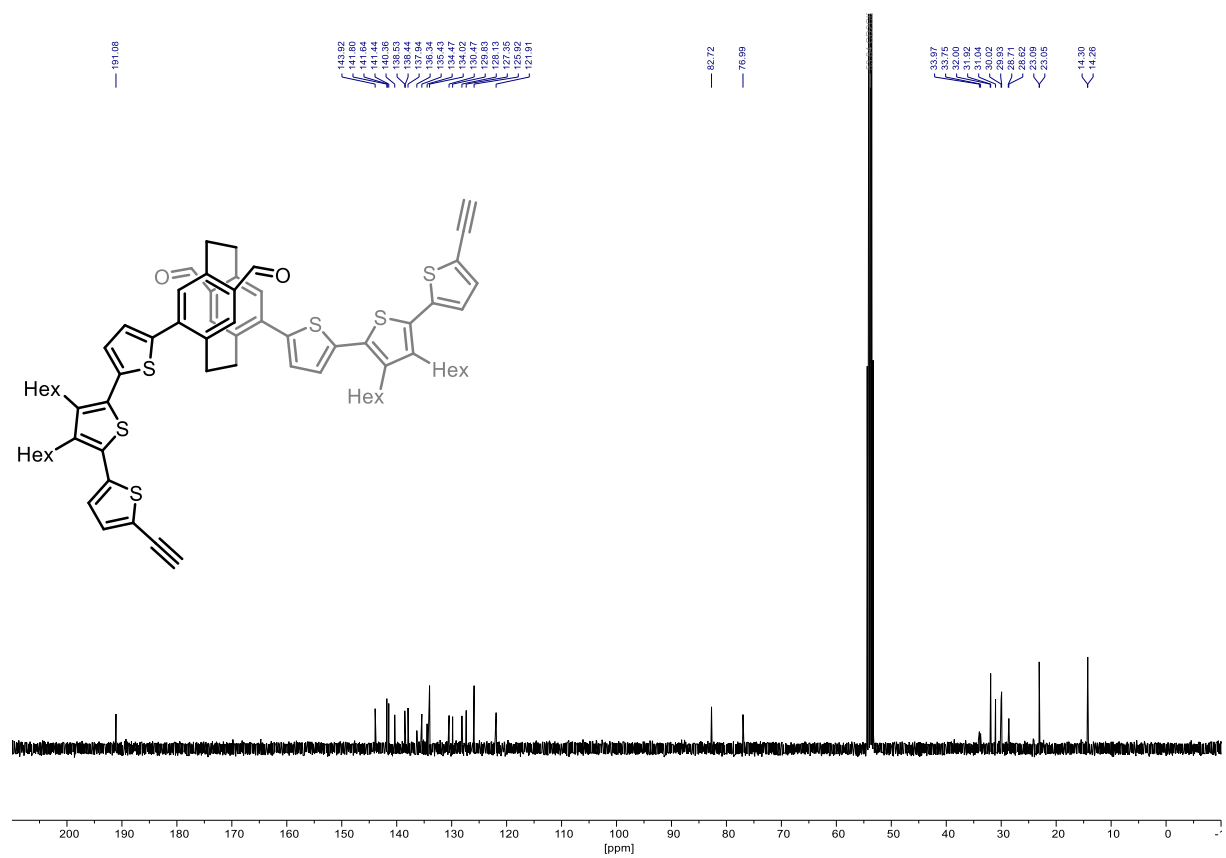
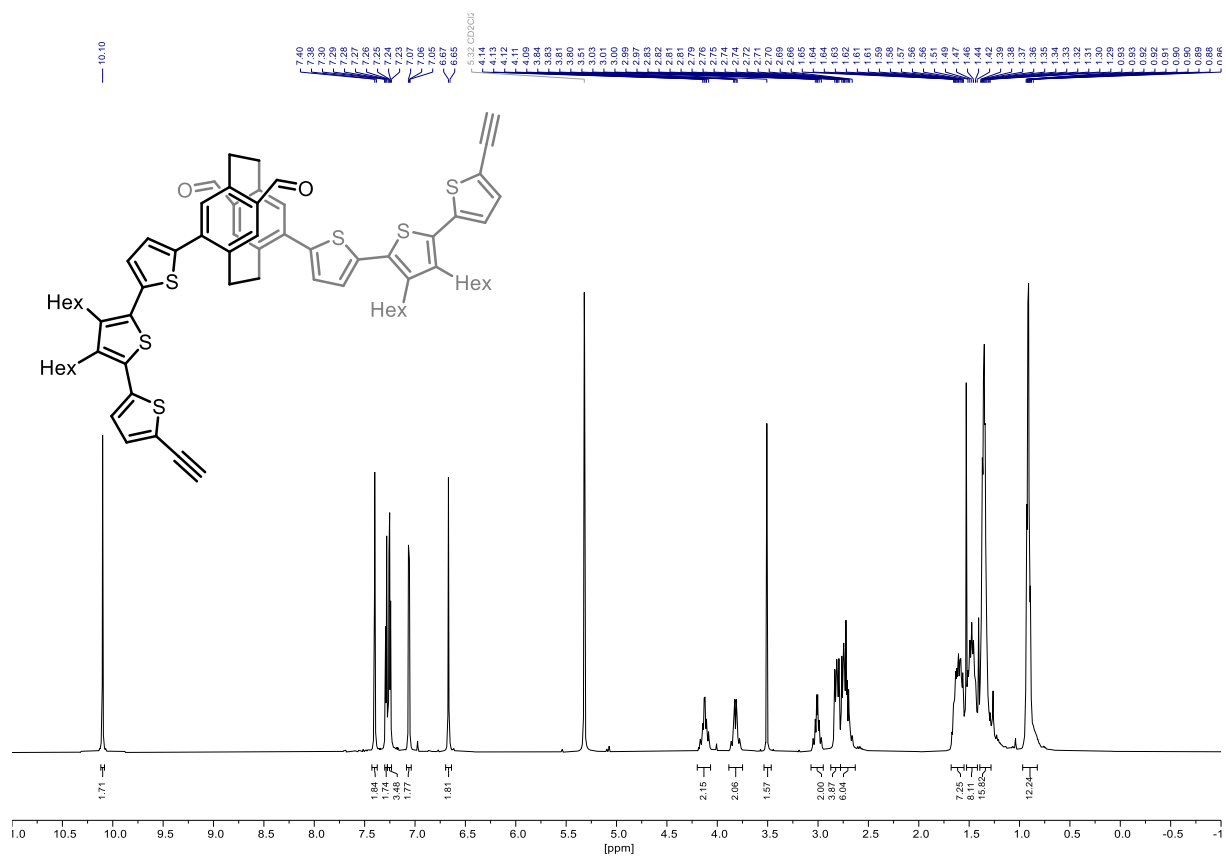
| Meas. m/z | # | Formula | Score | m/z | err [mDa] | err [ppm] | mSigma | rdB | e ⁻ Conf | z |
|-----------|---|----------------------------------------------------------------------------------|--------|-----------|-----------|-----------|--------|------|---------------------|----|
| 1453.6871 | 1 | C ₈₈ H ₁₁₇ O ₂ S ₆ Si ₂ | 100.00 | 1453.6911 | 4.0 | 2.7 | 65.4 | 32.5 | even | 1+ |
| 1475.6700 | 1 | C ₈₈ H ₁₁₆ NaO ₂ S ₆ Si ₂ | 100.00 | 1475.6730 | 3.0 | 2.1 | 22.2 | 32.5 | even | |
| 1491.6453 | 1 | C ₈₈ H ₁₁₆ KO ₂ S ₆ Si ₂ | 100.00 | 1491.6470 | 1.7 | 1.1 | 66.6 | 32.5 | even | |

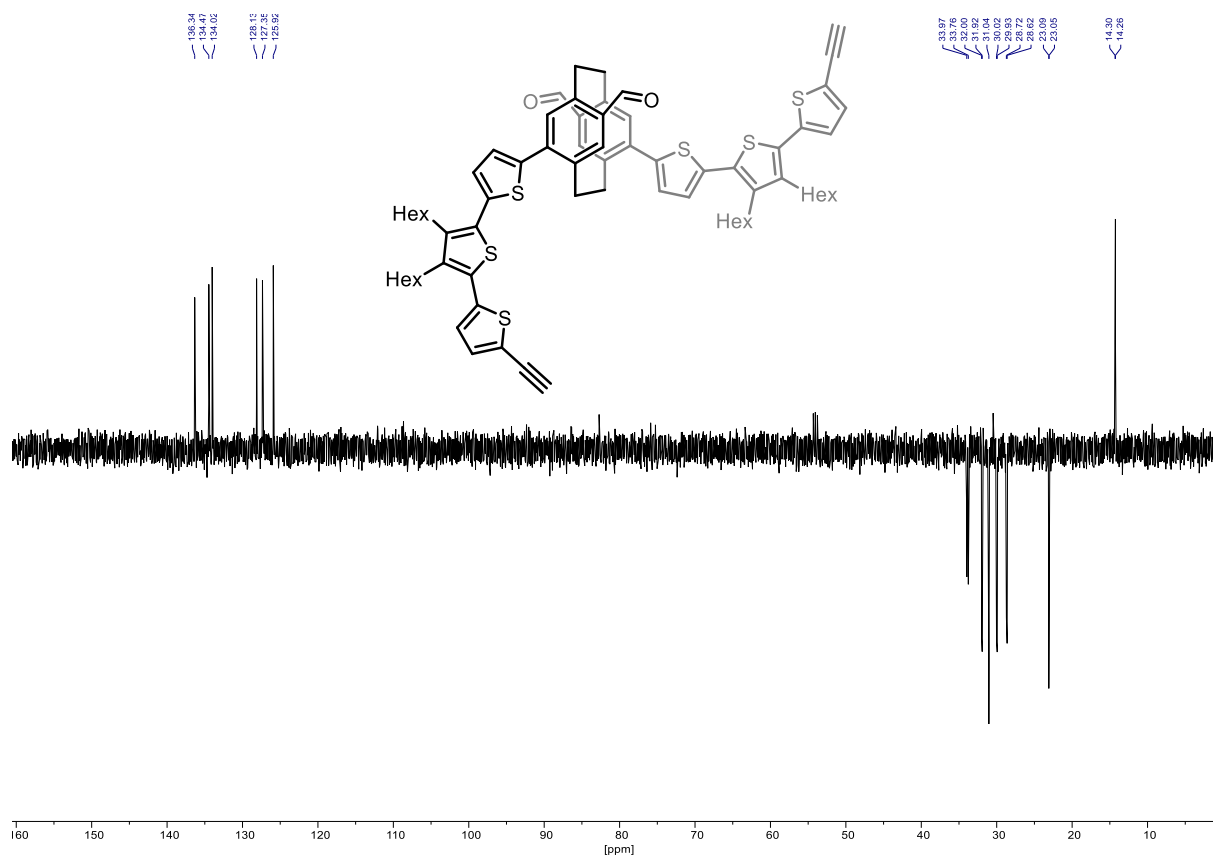
Mass list

| # | m/z | I % | I |
|----|-----------|-------|-------|
| 1 | 365.1062 | 4.8 | 1313 |
| 2 | 447.3435 | 5.5 | 1499 |
| 3 | 464.9891 | 8.0 | 2190 |
| 4 | 599.1169 | 10.2 | 2812 |
| 5 | 685.4359 | 7.8 | 2134 |
| 6 | 686.4387 | 5.0 | 1376 |
| 7 | 699.5957 | 4.3 | 1185 |
| 8 | 705.5828 | 11.9 | 3271 |
| 9 | 706.5856 | 6.2 | 1690 |
| 10 | 721.5774 | 21.4 | 5870 |
| 11 | 722.5808 | 9.7 | 2662 |
| 12 | 829.7241 | 4.1 | 1127 |
| 13 | 1453.6871 | 26.2 | 7177 |
| 14 | 1454.6901 | 29.0 | 7948 |
| 15 | 1455.6896 | 22.0 | 6035 |
| 16 | 1456.6904 | 13.0 | 3564 |
| 17 | 1457.6896 | 8.0 | 2196 |
| 18 | 1475.6700 | 90.7 | 24876 |
| 19 | 1476.6733 | 100.0 | 27441 |
| 20 | 1477.6725 | 81.7 | 22407 |
| 21 | 1478.6726 | 49.4 | 13566 |
| 22 | 1479.6719 | 26.3 | 7222 |
| 23 | 1480.6727 | 12.1 | 3321 |
| 24 | 1481.6712 | 6.0 | 1651 |
| 25 | 1491.6453 | 10.0 | 2736 |
| 26 | 1492.6484 | 11.9 | 3264 |
| 27 | 1493.6465 | 10.9 | 2993 |
| 28 | 1494.6472 | 7.0 | 1934 |
| 29 | 1495.6461 | 4.4 | 1210 |
| 30 | 1508.6952 | 4.8 | 1305 |
| 31 | 1509.6895 | 4.3 | 1192 |

Acquisition Parameter

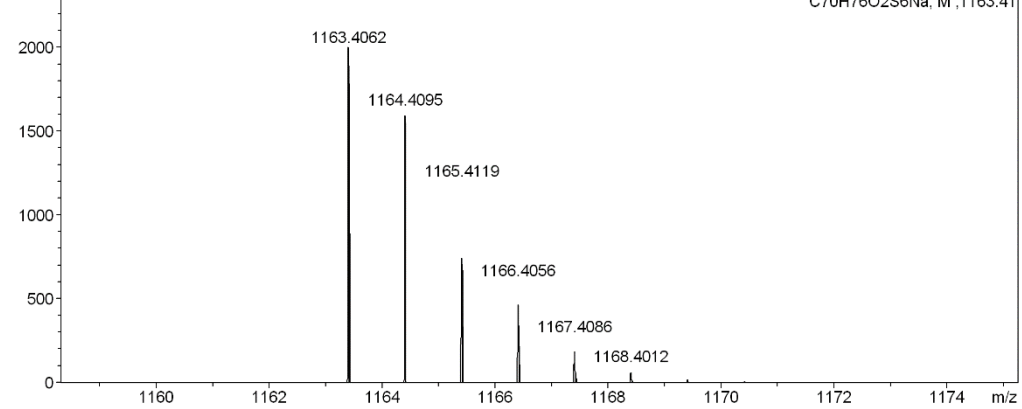
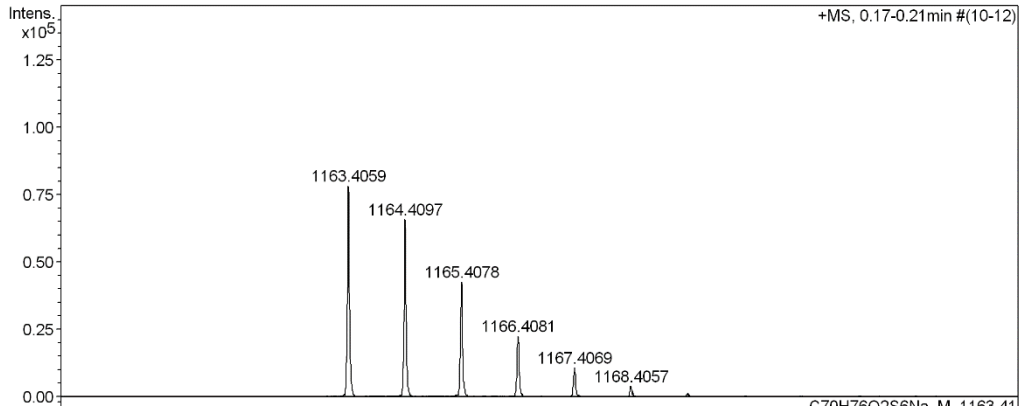
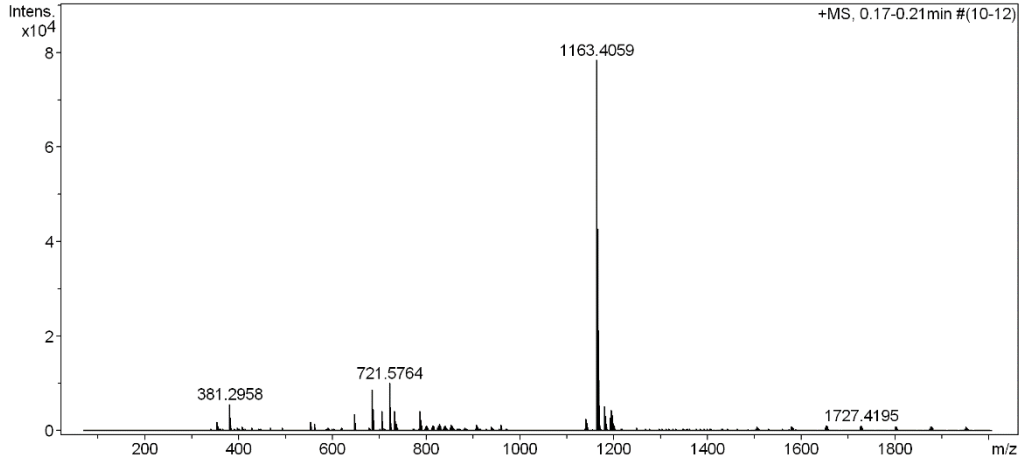
| | | | | | | |
|-------------------|------------------------------|----------------|---------------------------------------|----------------|--------------|-----------|
| General | Fore Vacuum | 3.46e+000 mBar | High Vacuum | 8.83e-008 mBar | Source Type | ESI |
| | Scan Begin | 75 m/z | Scan End | 2000 m/z | Ion Polarity | Positive |
| Source | Set Nebulizer | 0.4 Bar | Set Capillary | 3600 V | Set Dry Gas | 4.0 l/min |
| | Set Dry Heater | 180 °C | Set End Plate Offset | -500 V | | |
| Quadrupole | Set Ion Energy (MS only) | 4.0 eV | | | 300.0 Vpp | |
| Coll. Cell | Collision Energy | 10.0 eV | Set Collision Cell RF | 1000.0 Vpp | | |
| Ion Cooler | Set Ion Cooler Transfer Time | 160.0 µs | Set Ion Cooler Pre Pulse Storage Time | | 18.0 µs | |

^1H , $^{13}\text{C}\{^1\text{H}\}$ (400/101 MHz, CD_2Cl_2) NMR and HR-ESI-MS Spectra of Compound 102:



High Resolution Mass Spectrometry Report

| | | | |
|-------------|------------------|------------|----------------------|
| Sample Name | KR-374 | Instrument | maXis 4G |
| Comment | analyzed in MeOH | Method | 24 Direct_pos_high.m |



High Resolution Mass Spectrometry Report

Measured m/z vs. theoretical m/z

| Meas. m/z | # | Formula | Score | m/z | err [mDa] | err [ppm] | mSigma | rdb | e ⁻ Conf | z |
|-----------|---|----------------------|--------|-----------|-----------|-----------|--------|------|---------------------|----|
| 1140.4141 | 1 | C 70 H 76 O 2 S 6 | 100.00 | 1140.4164 | 2.3 | 2.0 | 73.3 | 33.0 | odd | 1+ |
| 1163.4059 | 1 | C 70 H 76 Na O 2 S 6 | 100.00 | 1163.4062 | 0.3 | 0.3 | 24.8 | 32.5 | even | |
| 1179.3803 | 1 | C 70 H 76 K O 2 S 6 | 100.00 | 1179.3801 | -0.2 | -0.2 | 86.5 | 32.5 | even | |

Mass list

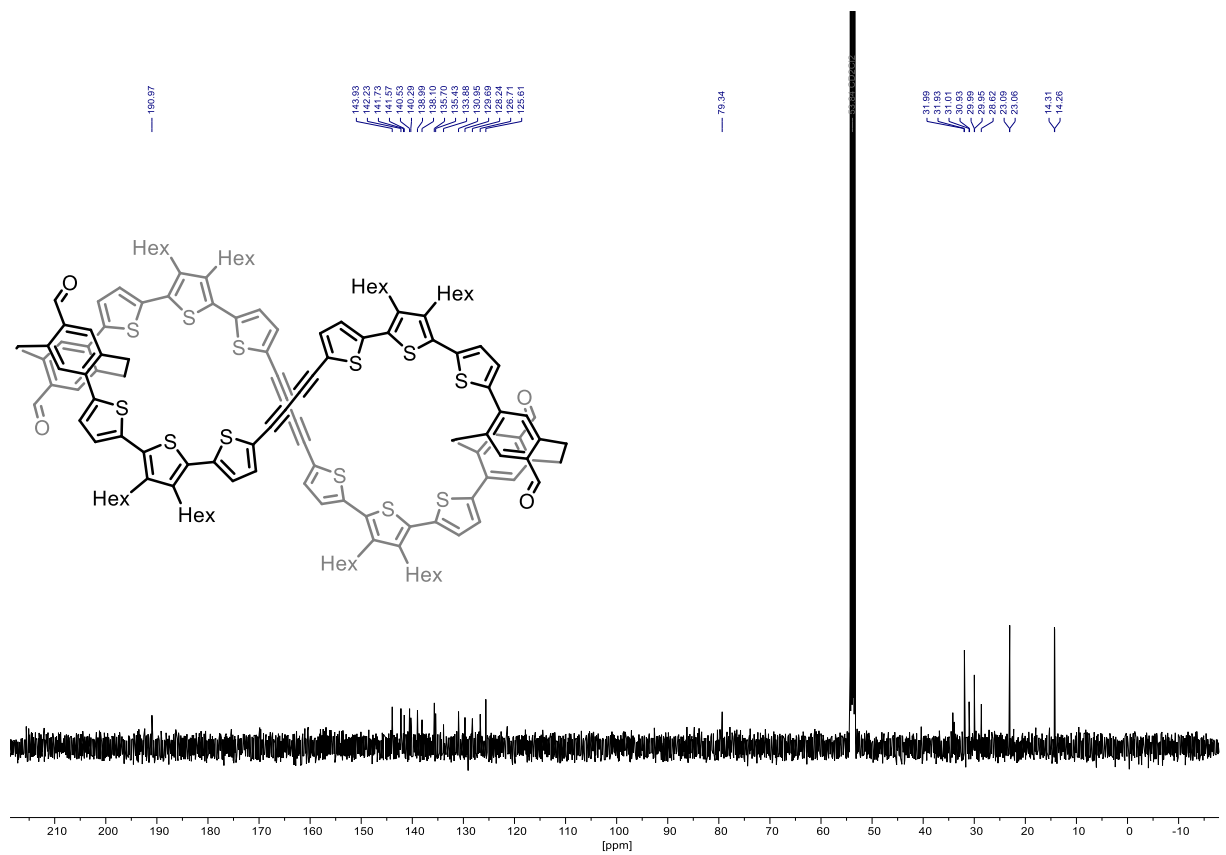
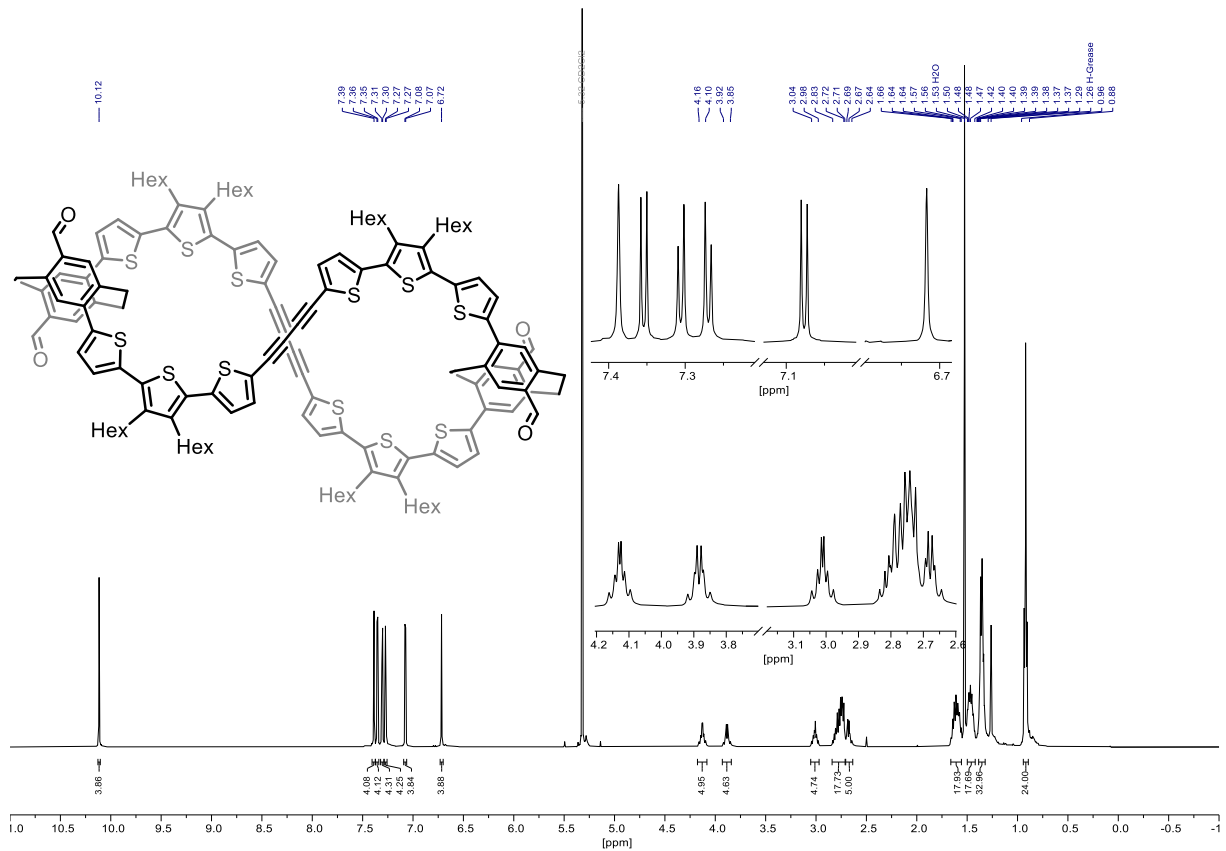
| # | m/z | I % | I |
|----|-----------|-------|-------|
| 1 | 353.2663 | 2.4 | 1855 |
| 2 | 355.0700 | 1.4 | 1101 |
| 3 | 381.2958 | 7.3 | 5751 |
| 4 | 382.2986 | 1.6 | 1255 |
| 5 | 553.4571 | 2.5 | 1930 |
| 6 | 561.2198 | 1.7 | 1355 |
| 7 | 647.2109 | 4.7 | 3687 |
| 8 | 648.2136 | 2.0 | 1566 |
| 9 | 685.4345 | 11.2 | 8779 |
| 10 | 686.4381 | 5.9 | 4606 |
| 11 | 687.4413 | 1.7 | 1322 |
| 12 | 705.5816 | 5.4 | 4204 |
| 13 | 706.5842 | 2.2 | 1737 |
| 14 | 721.5764 | 12.9 | 10099 |
| 15 | 722.5805 | 6.7 | 5244 |
| 16 | 723.5801 | 2.2 | 1762 |
| 17 | 732.1891 | 5.5 | 4288 |
| 18 | 733.1913 | 2.3 | 1833 |
| 19 | 737.5700 | 1.9 | 1504 |
| 20 | 787.3190 | 5.4 | 4230 |
| 21 | 788.3219 | 3.1 | 2462 |
| 22 | 801.6927 | 1.4 | 1104 |
| 23 | 825.6945 | 1.5 | 1205 |
| 24 | 827.7078 | 1.9 | 1462 |
| 25 | 841.7250 | 1.4 | 1101 |
| 26 | 853.7255 | 1.6 | 1275 |
| 27 | 907.7729 | 1.5 | 1215 |
| 28 | 959.3227 | 1.6 | 1268 |
| 29 | 1140.4141 | 3.3 | 2599 |
| 30 | 1141.4193 | 2.7 | 2129 |
| 31 | 1142.4191 | 2.1 | 1680 |
| 32 | 1143.4193 | 1.4 | 1108 |
| 33 | 1163.4059 | 100.0 | 78451 |
| 34 | 1164.4097 | 83.9 | 65822 |
| 35 | 1165.4078 | 54.5 | 42762 |
| 36 | 1166.4081 | 28.9 | 22638 |
| 37 | 1167.4069 | 13.9 | 10872 |
| 38 | 1168.4057 | 5.1 | 4014 |
| 39 | 1169.4044 | 1.8 | 1381 |
| 40 | 1179.3803 | 6.6 | 5191 |
| 41 | 1180.3828 | 4.7 | 3721 |
| 42 | 1181.3816 | 4.1 | 3210 |
| 43 | 1182.3819 | 2.2 | 1729 |
| 44 | 1193.4171 | 3.4 | 2694 |
| 45 | 1194.4189 | 2.4 | 1918 |
| 46 | 1195.4282 | 5.7 | 4437 |
| 47 | 1196.4327 | 4.3 | 3387 |
| 48 | 1197.4313 | 3.1 | 2448 |
| 49 | 1198.4321 | 1.9 | 1472 |
| 50 | 1199.7720 | 1.5 | 1194 |
| 51 | 1653.4015 | 1.4 | 1137 |
| 52 | 1654.4035 | 1.5 | 1140 |
| 53 | 1727.4195 | 1.5 | 1161 |

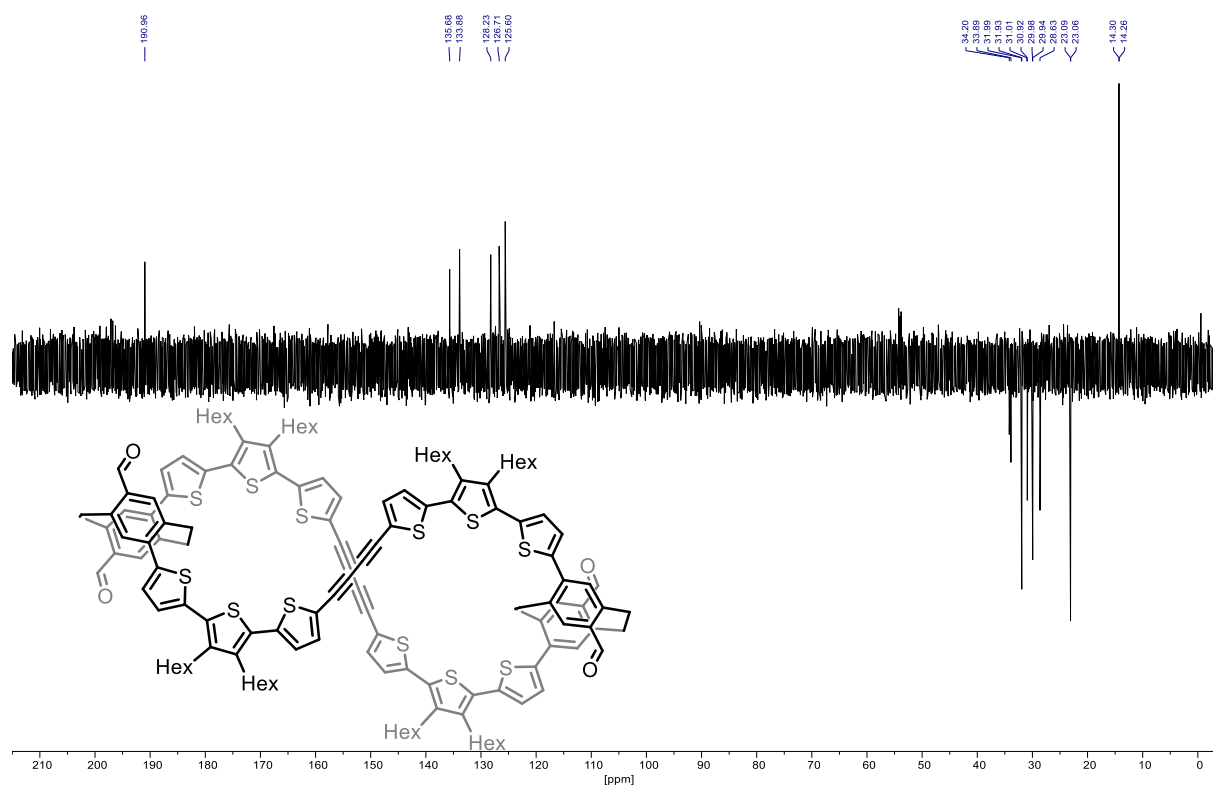
Acquisition Parameter

| | | | | | | |
|----------------|-------------|----------------|-------------|----------------|--------------|----------|
| General | Fore Vacuum | 3.36e+000 mBar | High Vacuum | 9.38e-008 mBar | Source Type | ESI |
| | Scan Begin | 75 m/z | Scan End | 2000 m/z | Ion Polarity | Positive |

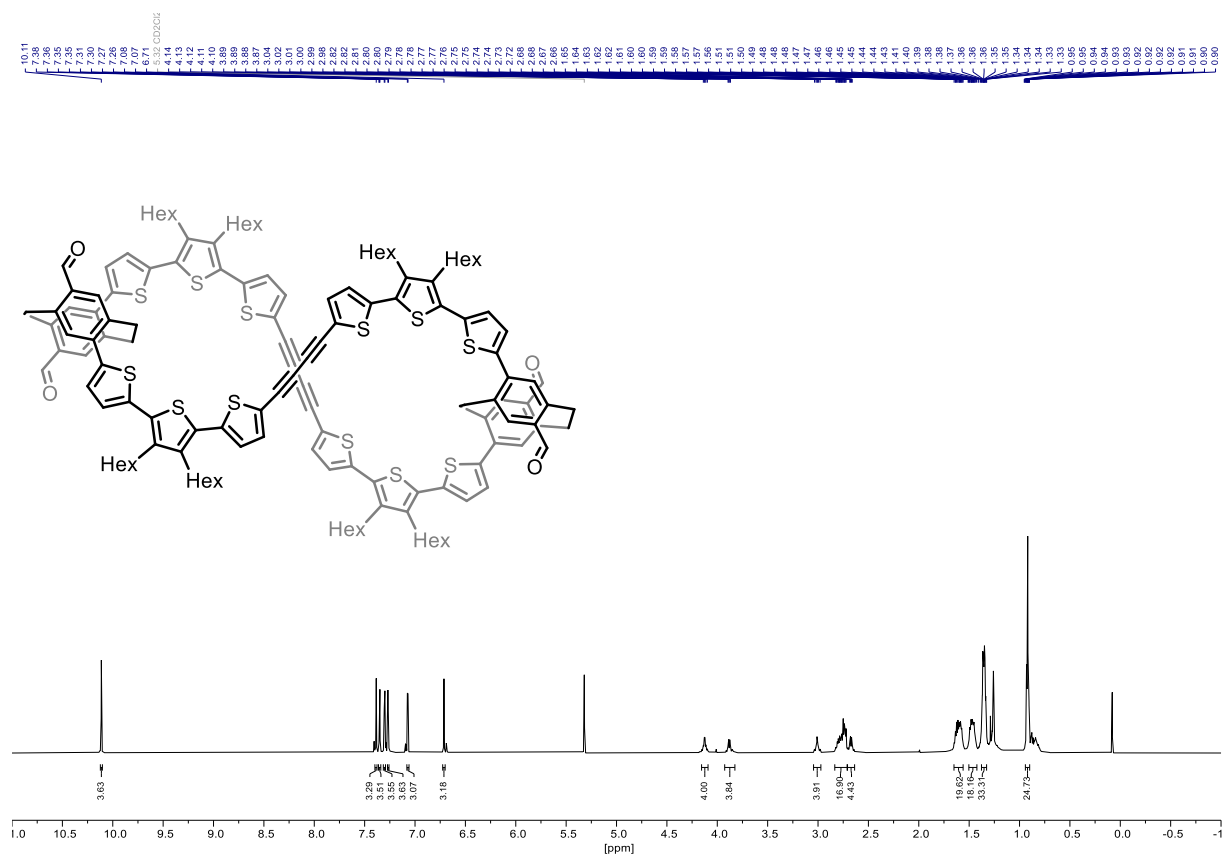
High Resolution Mass Spectrometry Report

| | | | | | | |
|-------------------|------------------------------|----------|---------------------------------------|------------|-------------|-----------|
| Source | Set Nebulizer | 0.4 Bar | Set Capillary | 3600 V | Set Dry Gas | 4.0 l/min |
| | Set Dry Heater | 180 °C | Set End Plate Offset | -500 V | | |
| Quadrupole | Set Ion Energy (MS only) | 4.0 eV | | | | |
| Coll. Cell | Collision Energy | 100.0 eV | Set Collision Cell RF | 2000.0 Vpp | 300.0 Vpp | |
| Ion Cooler | Set Ion Cooler Transfer Time | 160.0 µs | Set Ion Cooler Pre Pulse Storage Time | 22.0 µs | | |

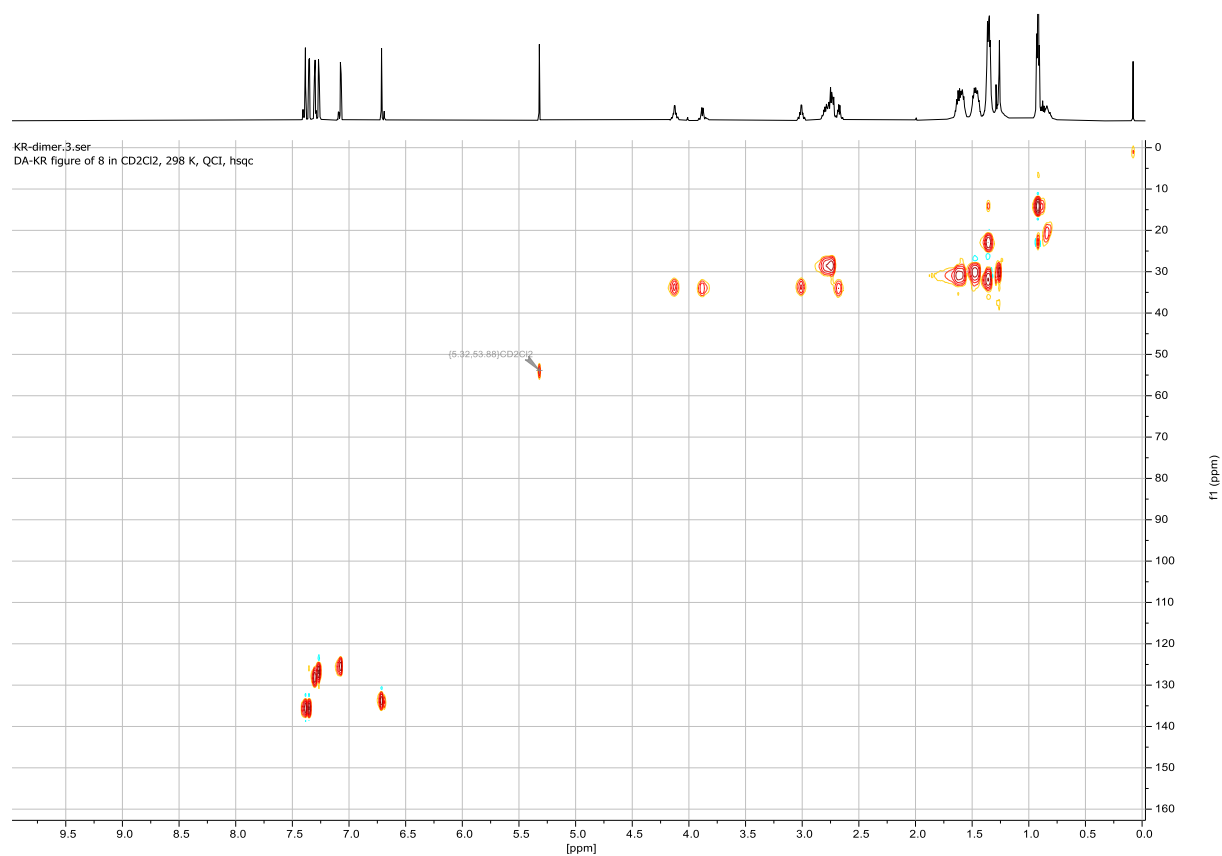
^1H , $^{13}\text{C}\{^1\text{H}\}$, DEPT, 2D (500/126 and 600/151 MHz, CD_2Cl_2) NMR and MALDI-ToF-MS Spectra of Diyne Dimer (103):



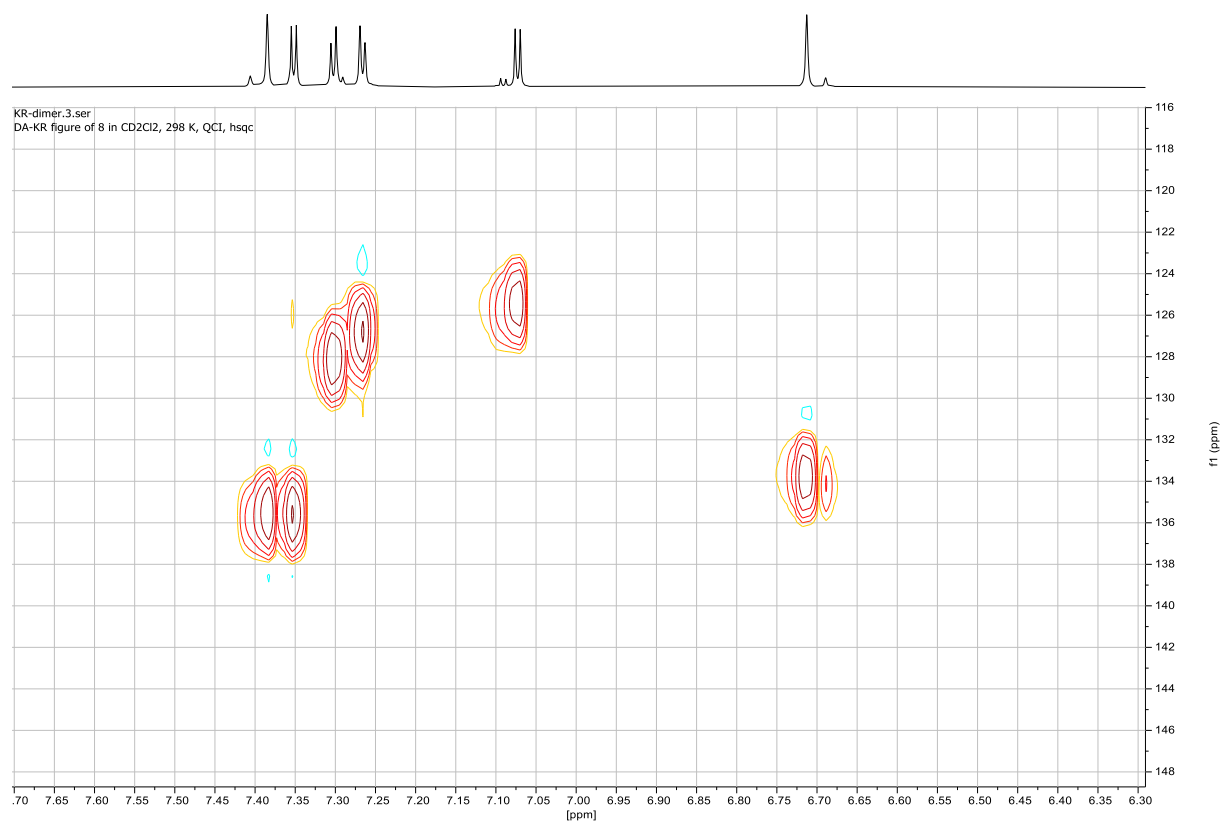
¹H NMR (600 MHz, CD₂Cl₂):

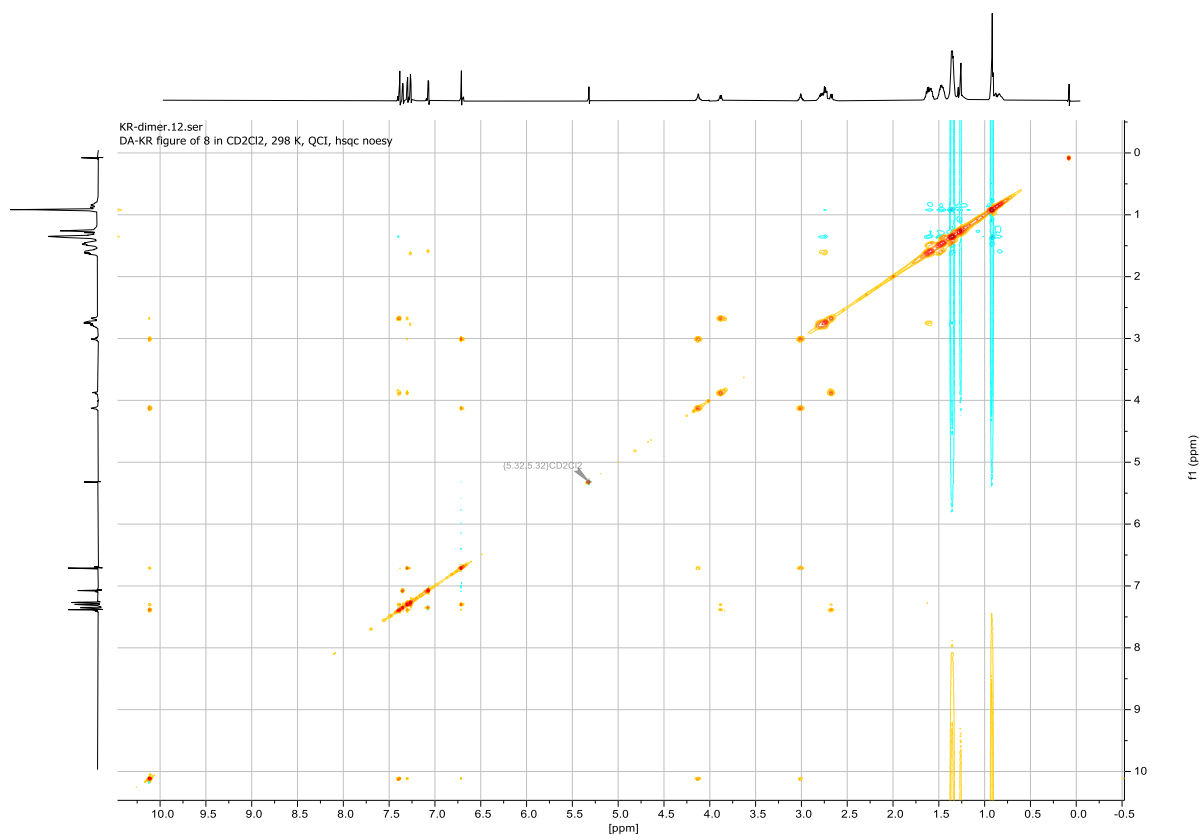
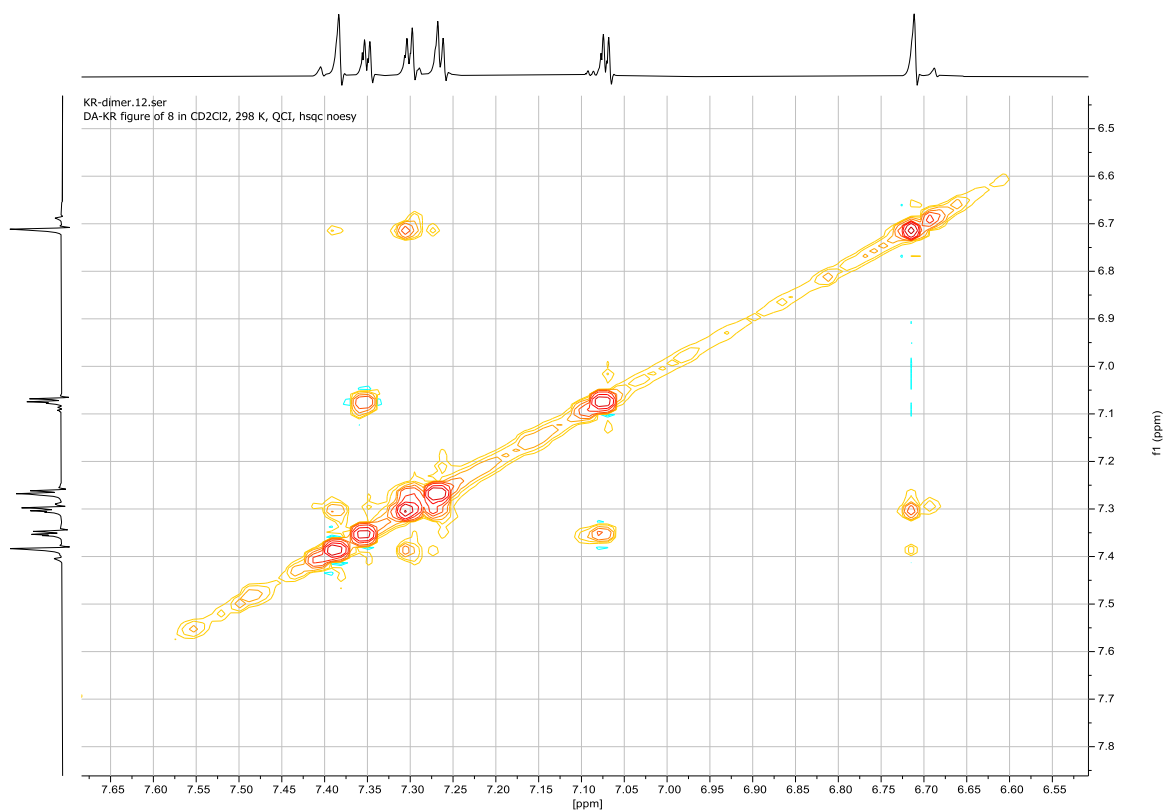


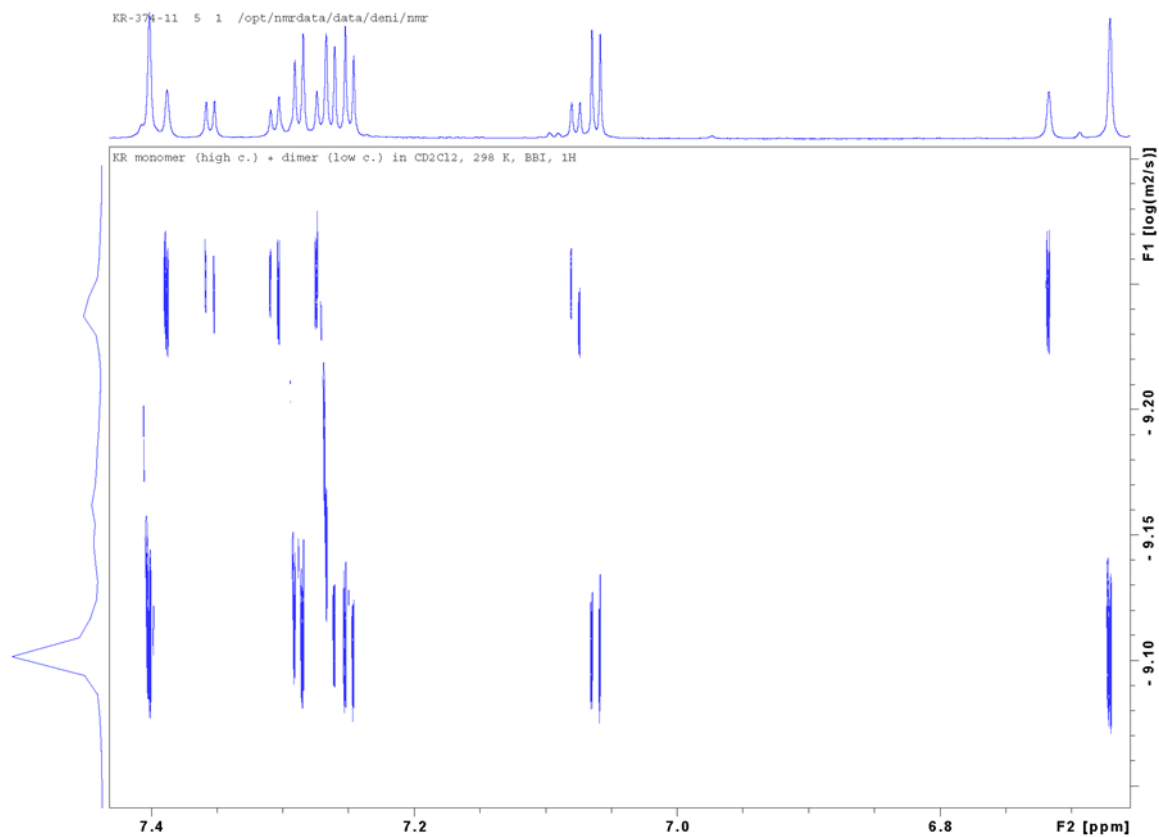
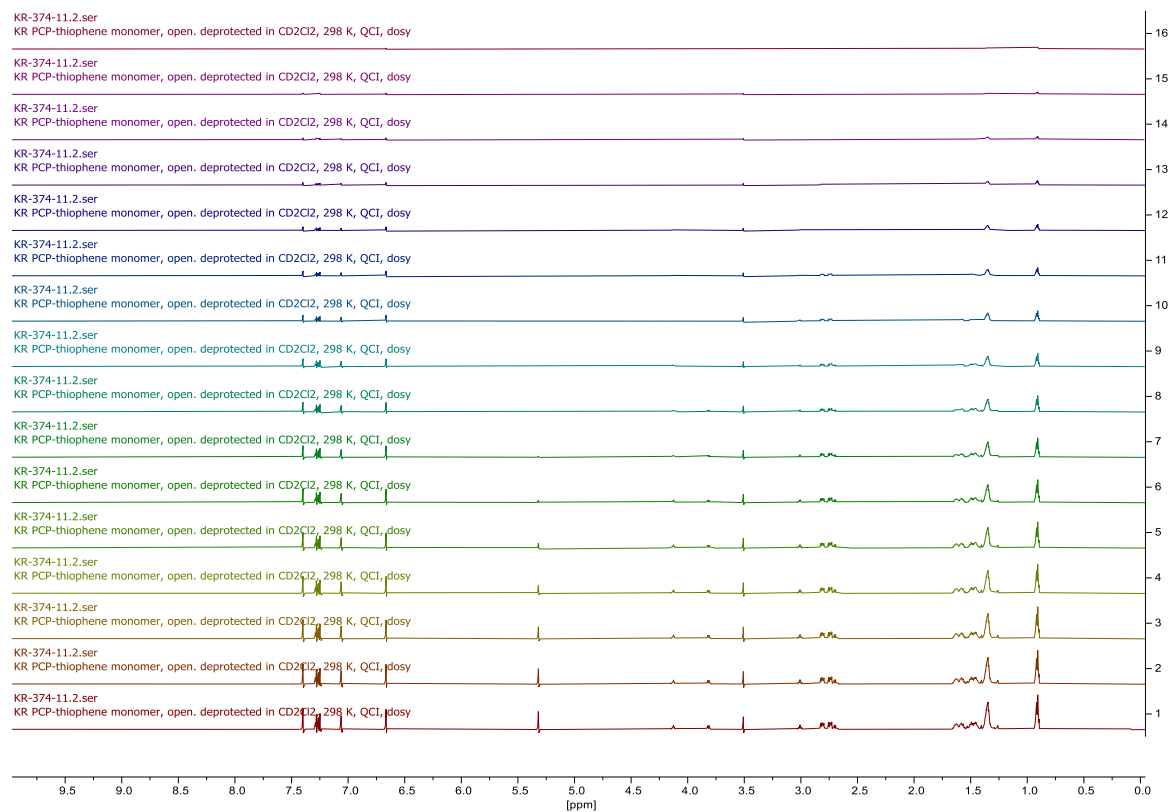
HSQC Spectrum of Dyine Dimer (103):



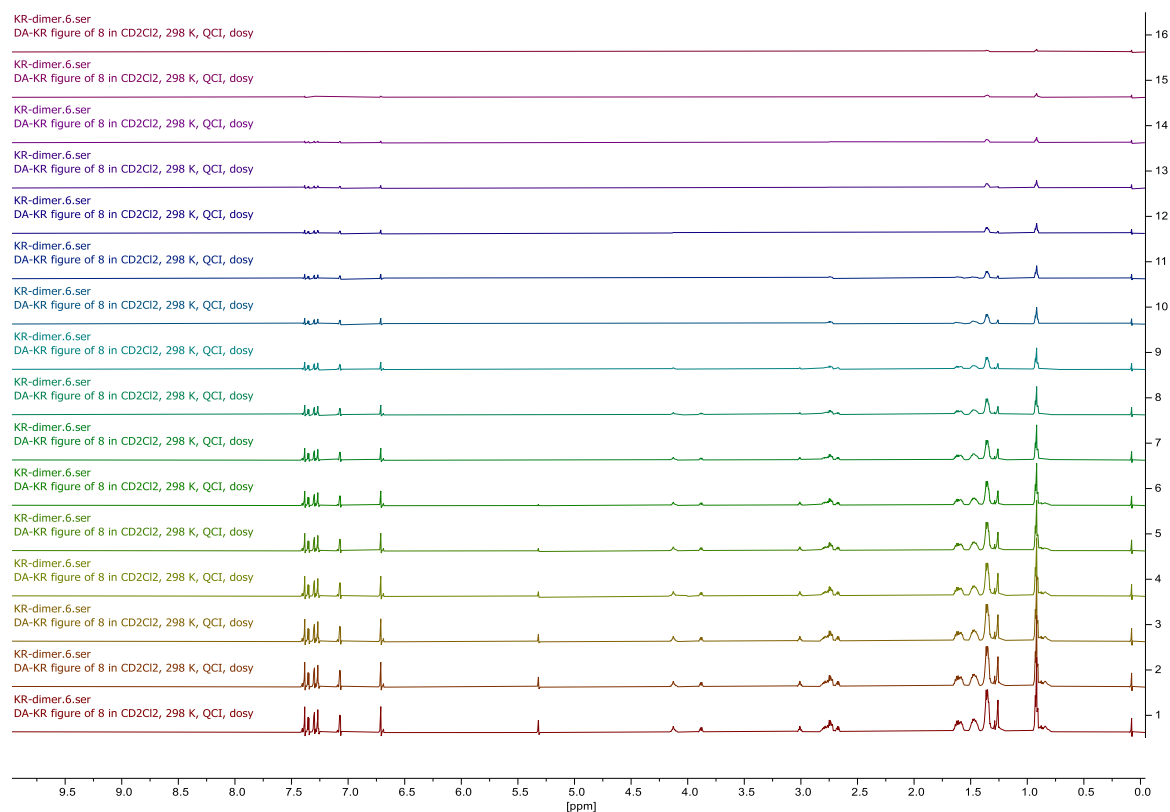
Aromatic region of the HSQC Spectrum of Dyine Dimer (103):



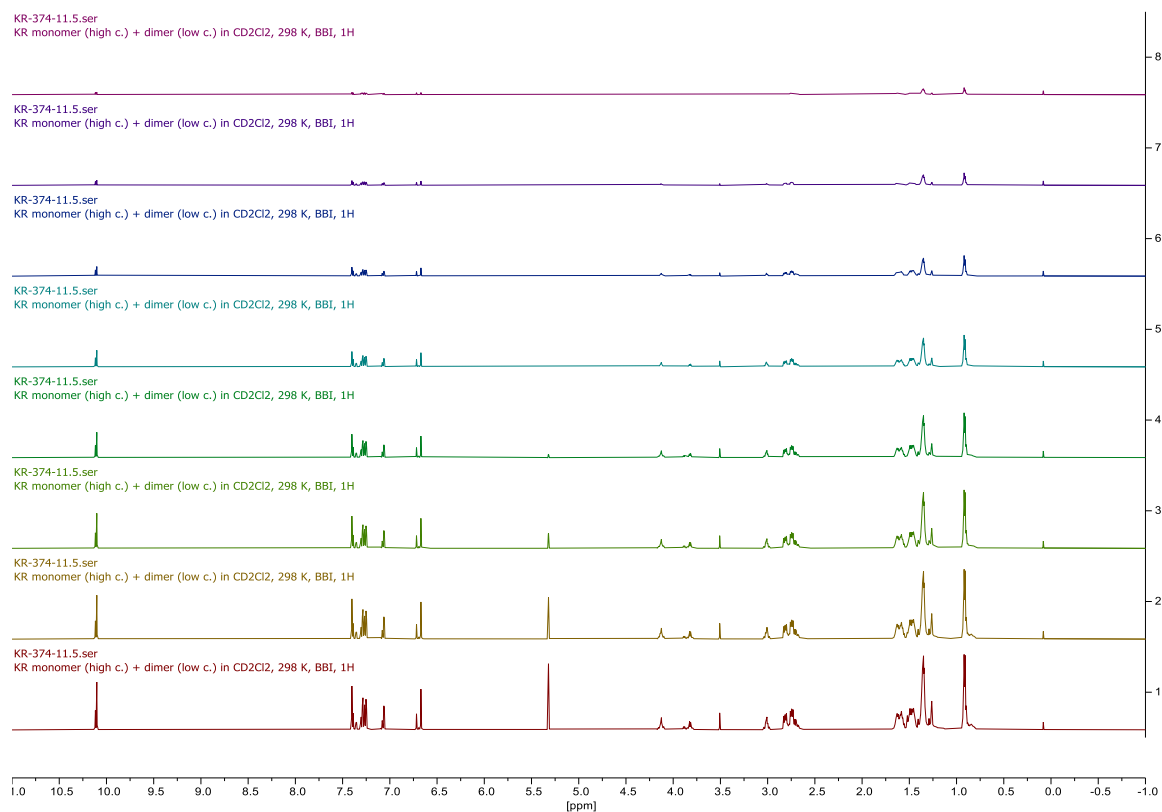
NOESY Spectrum of Dyine Dimer (103):**Aromatic region of the NOESY Spectrum of Dyine Dimer (103):**

DOSY Spectrum:Compound 102

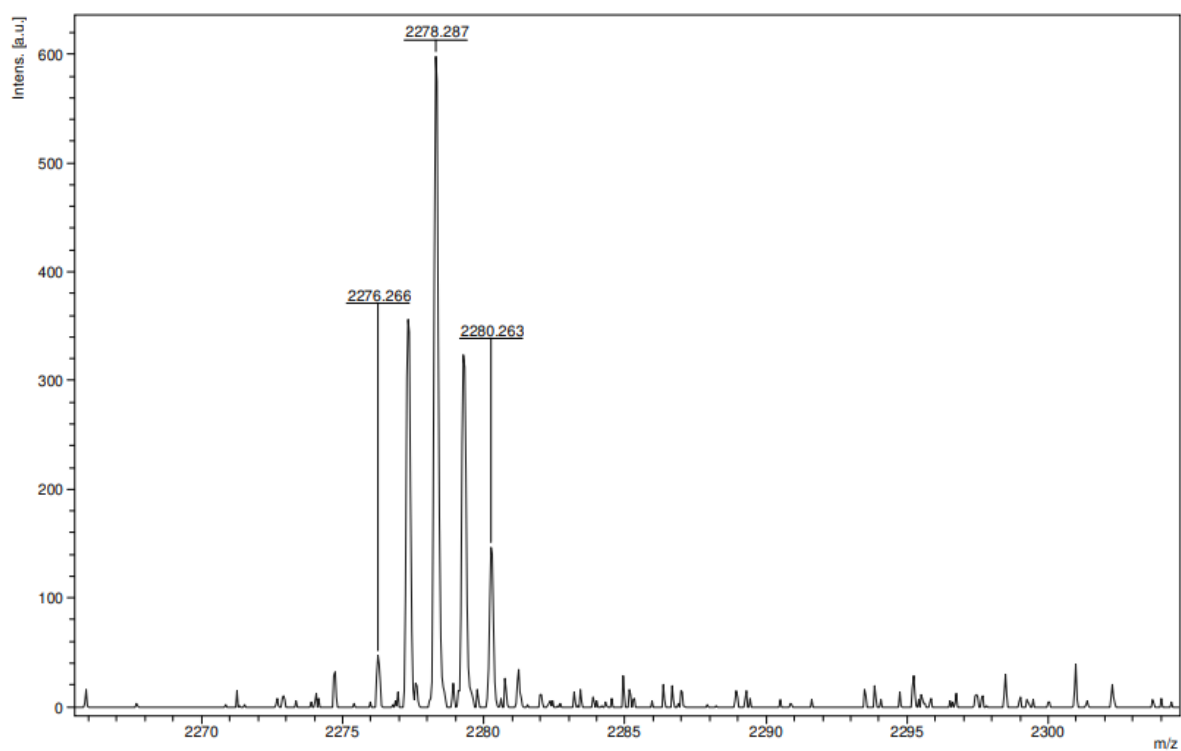
Dyine Dimer (103)

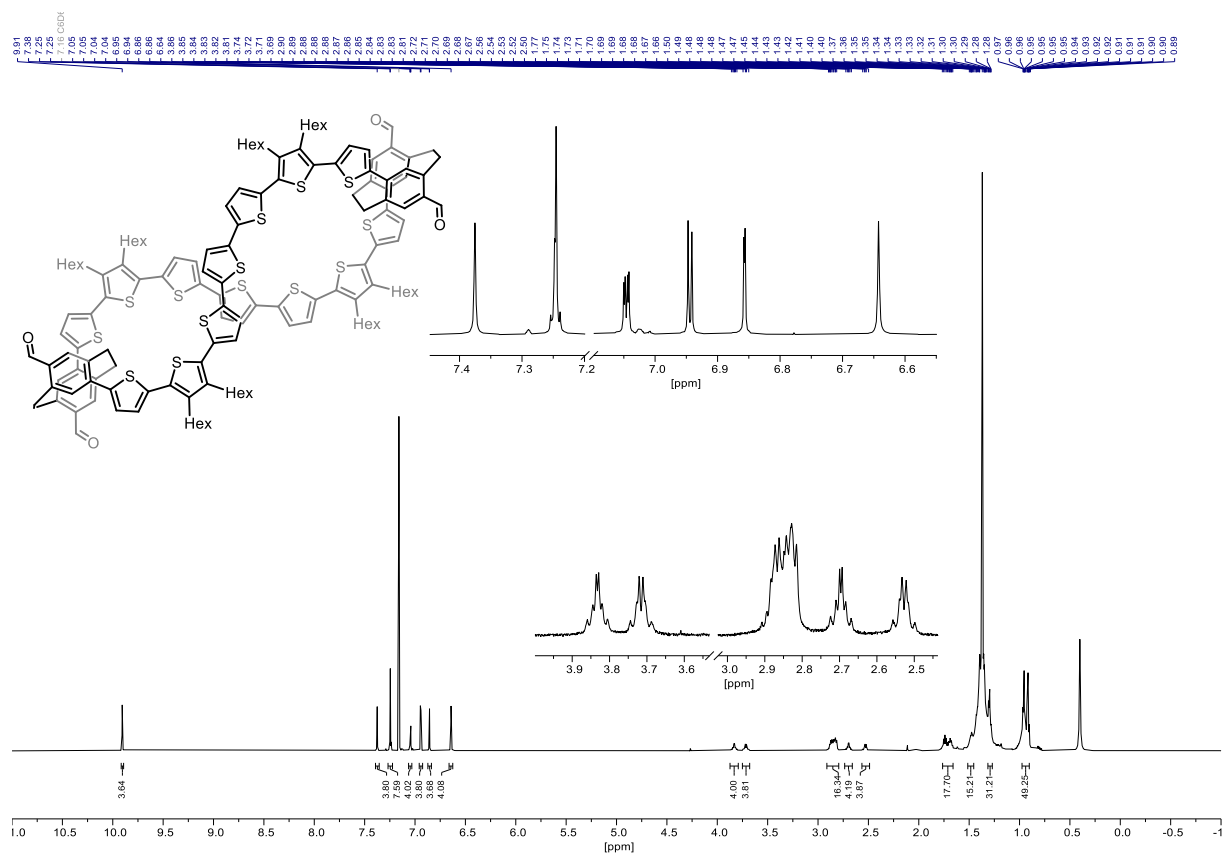
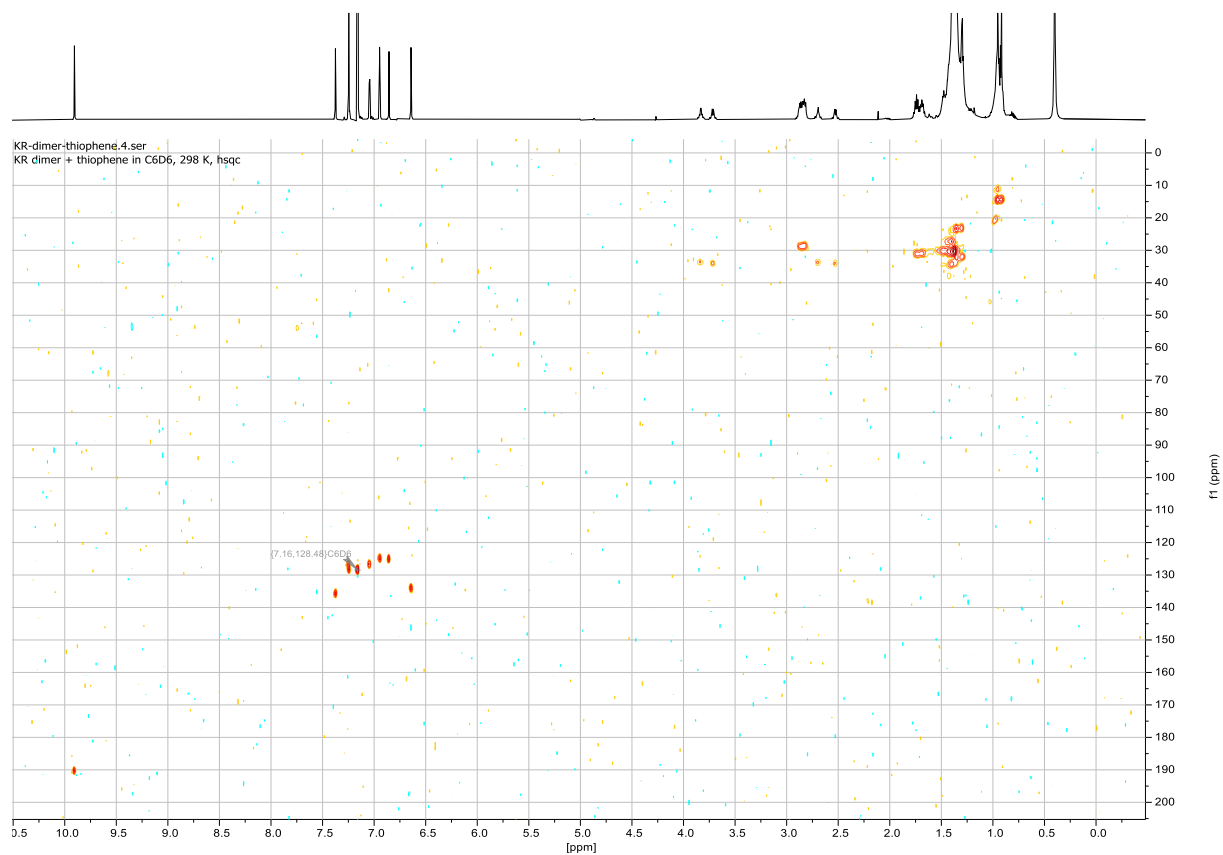


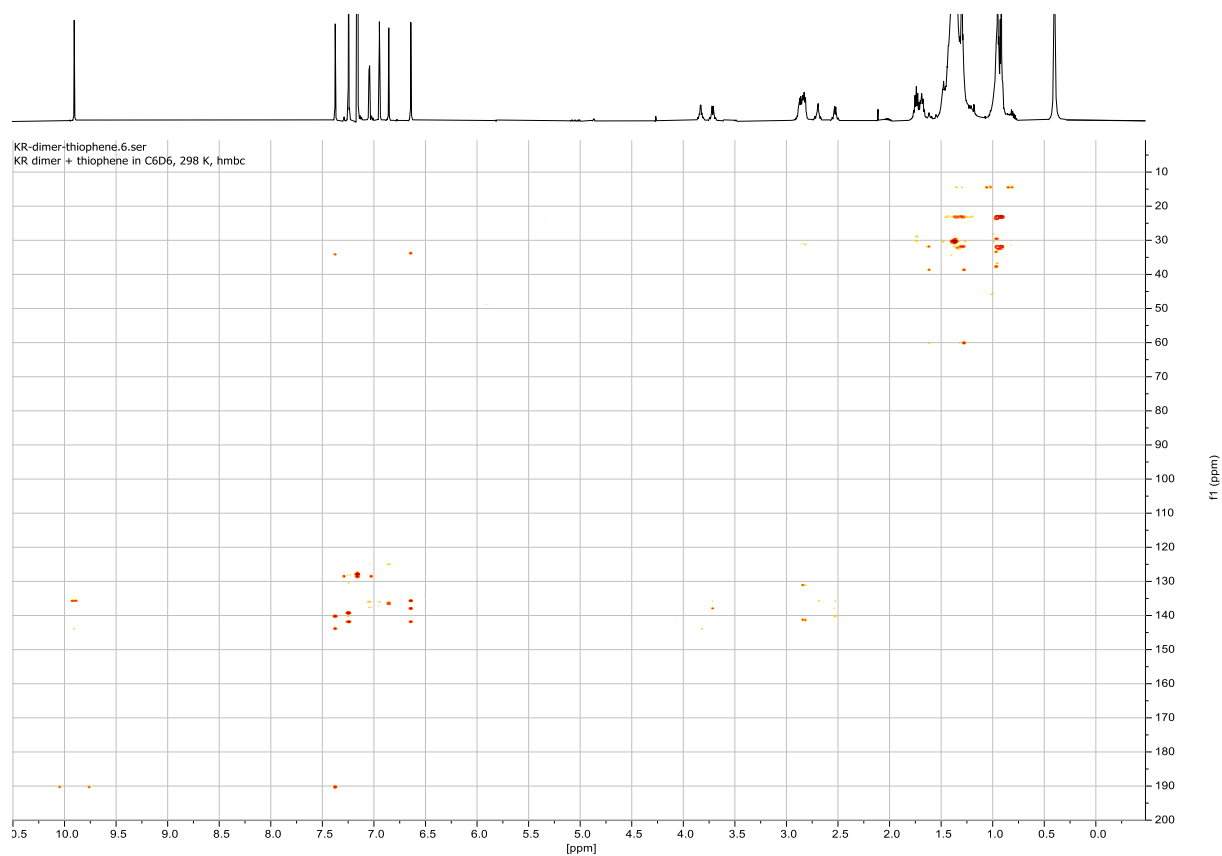
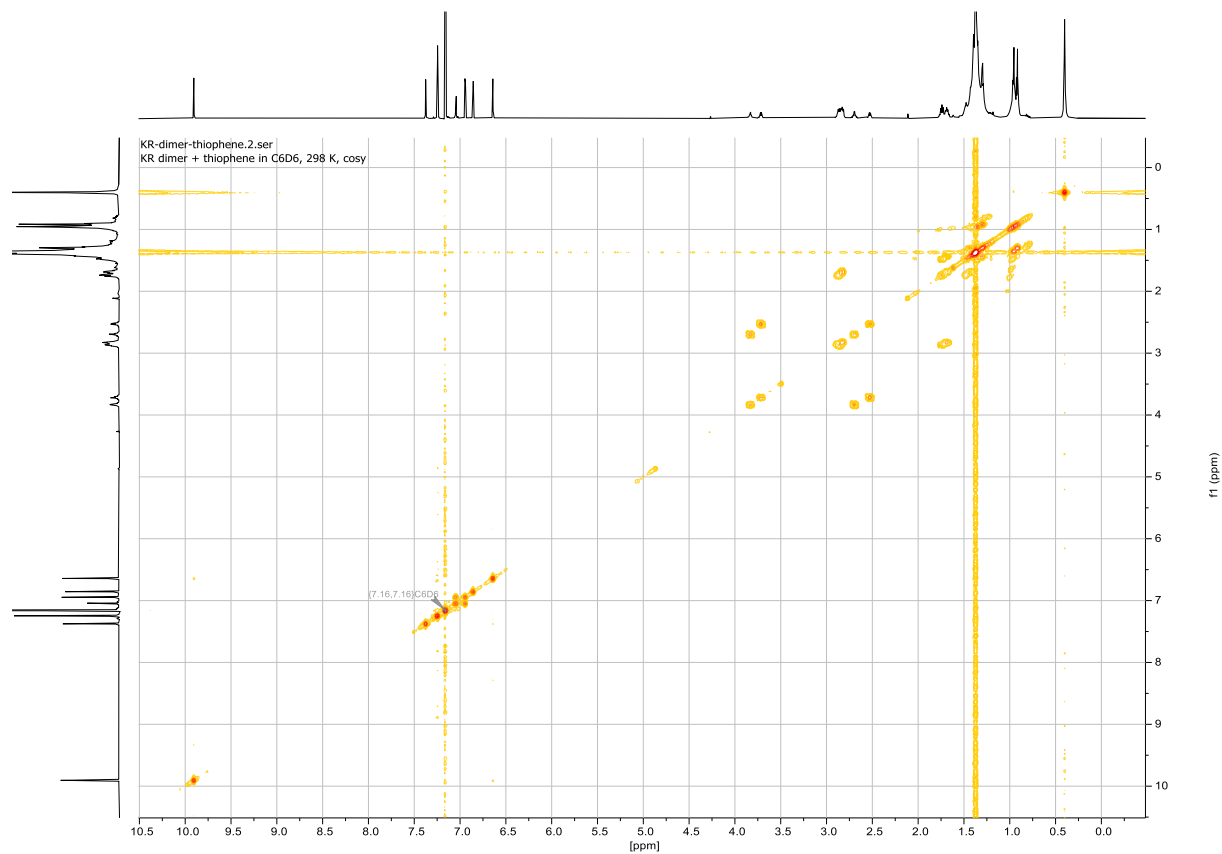
Compound 102 and Dyine Dimer (103)

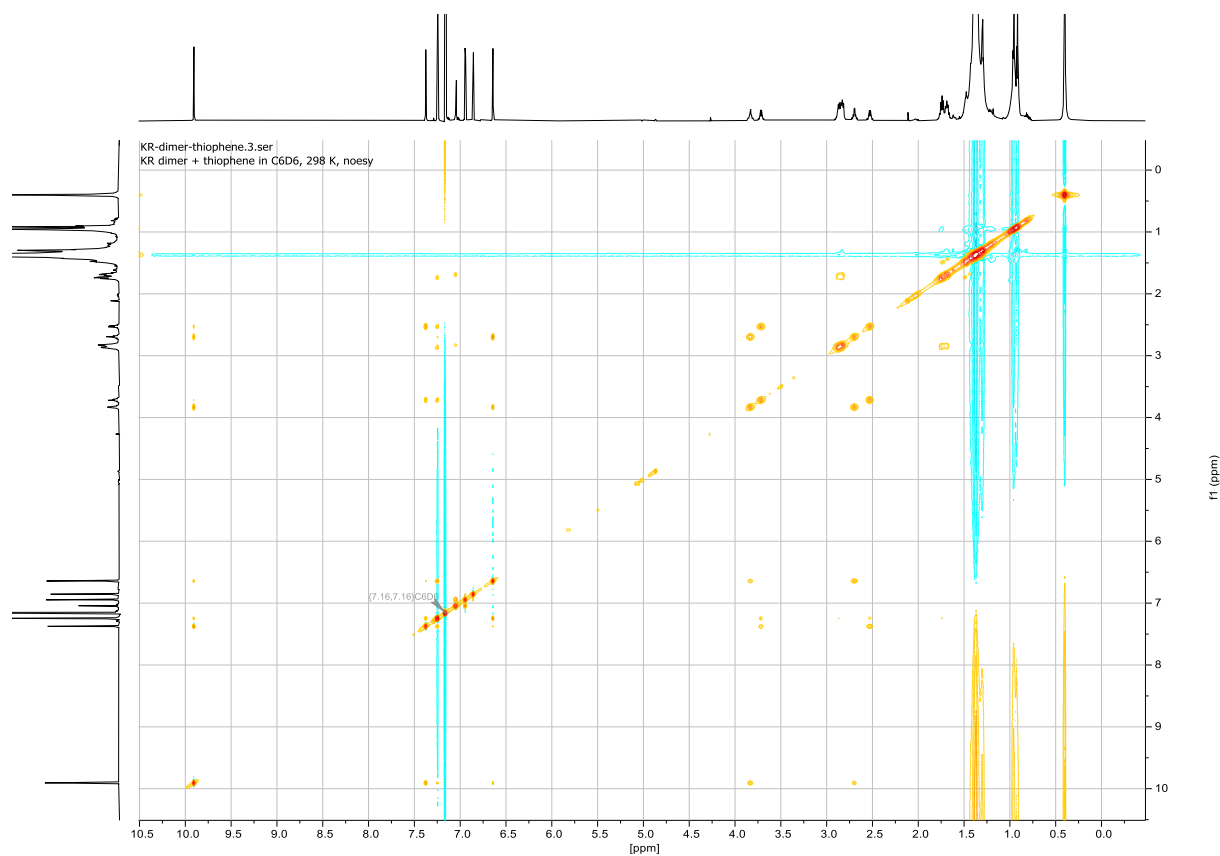
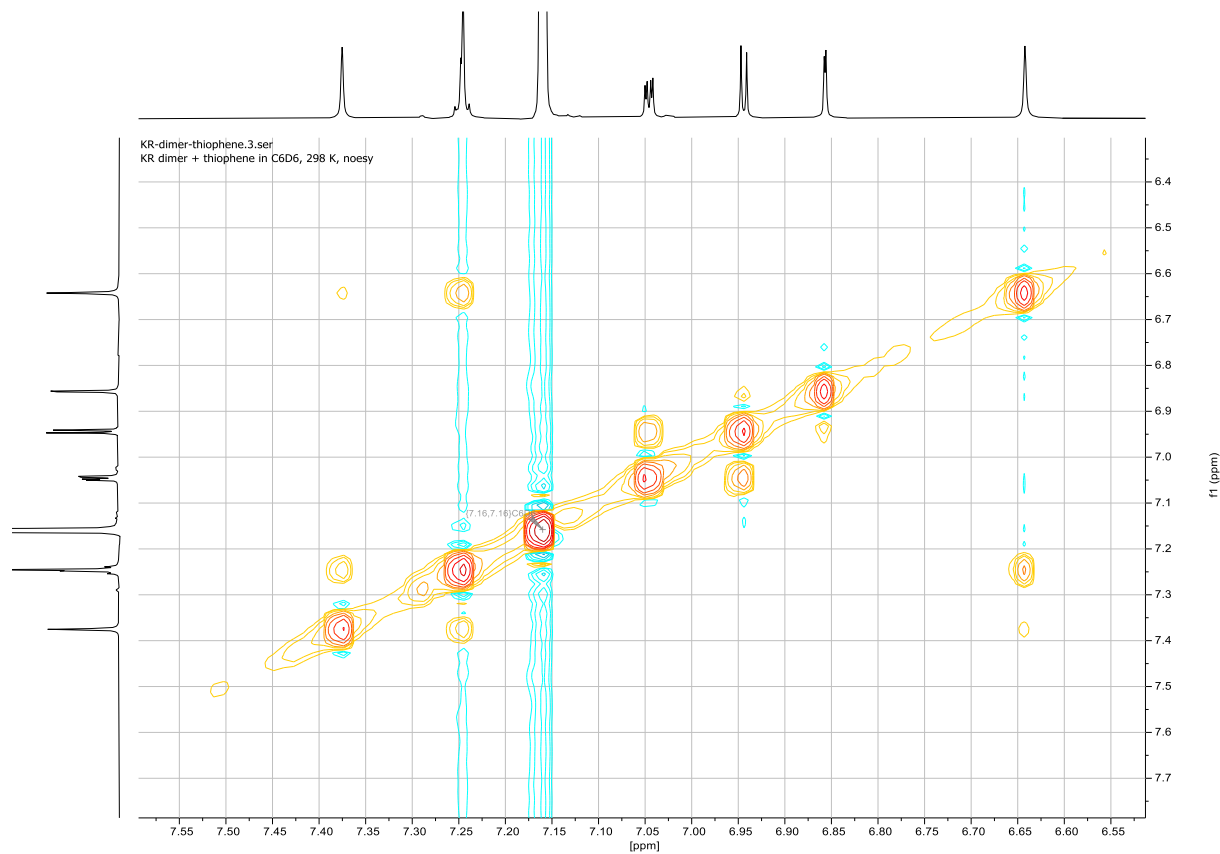


Zoom in of MALDI-ToF-MS of Dyne Dimer (103)

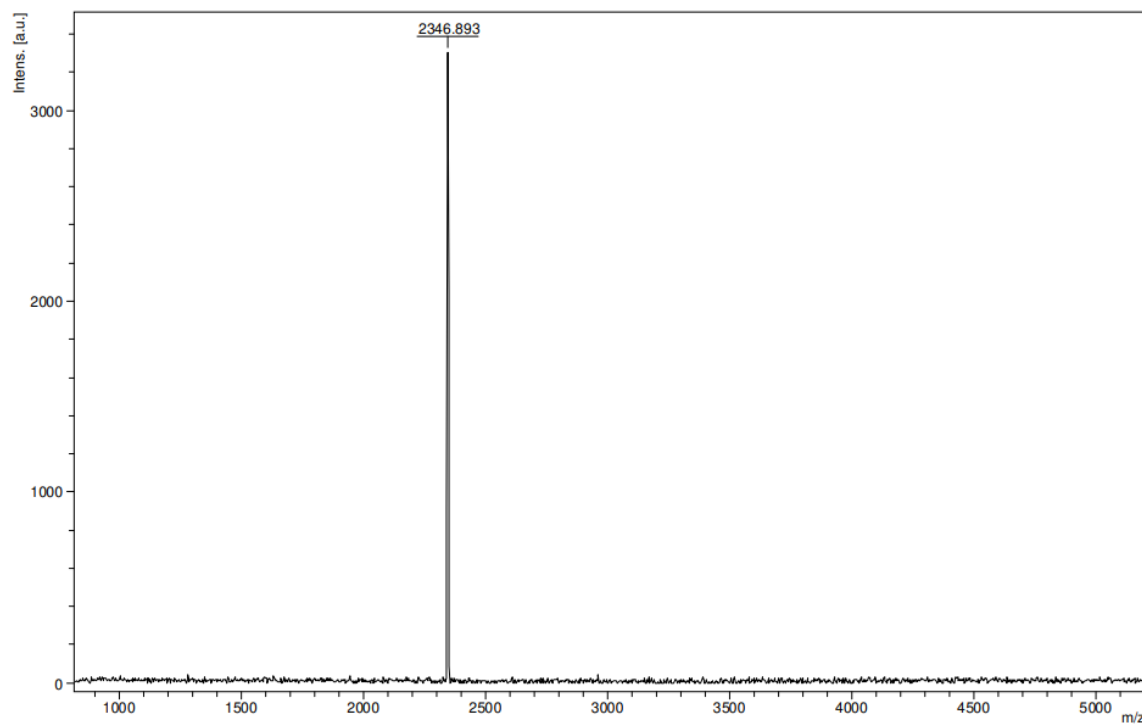


^1H , 2D (600/151 MHz, benzene) NMR and MALDI-ToF-MS Spectra of Thiophene Dimer (125):**HSQC Spectrum of Thiophene Dimer (125):**

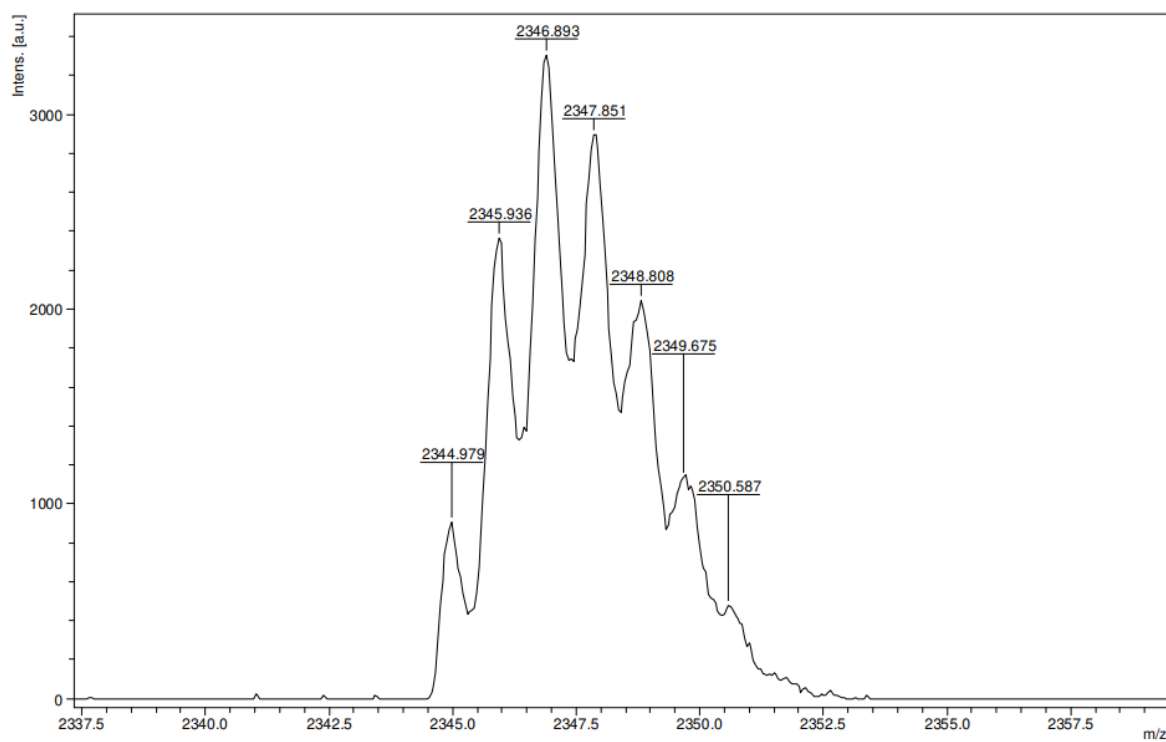
HMBC Spectrum of Thiophene Dimer (125):**COSY Spectrum of Thiophene Dimer (125):**

NOESY Spectrum of Thiophene Dimer (125):**Aromatic region of the NOESY Spectrum of Thiophene Dimer (125):**

MALDI-ToF-MS of Thiophene Dimer (125)



Zoom in of MALDI-ToF-MS of Thiophene Dimer (125)



Curriculum Vitae:

PERSONAL INFORMATION

Name: Ksenia Reznikova
Date & Place of Birth: 18.12.1993, St. Petersburg, Russia
Citizenship: russian

EDUCATION

06/2018 – 02/2023 **Ph. D. studies in organic chemistry**, University of Basel, Basel
“Tailor-Made Structures for Molecular Junctions: From Linear Wires to Molecular Loops.”
Thesis Advisor: Prof. Dr. Marcel Mayor

02/2017 – 04/2018 **Master of Science in Chemistry**, University of Basel, Basel
10/2017 – 04/2018 **Master Thesis: “Tailor-Made Molecular Rods for Graphene Junctions.”**
Advisor: Prof. Dr. Marcel Mayor

06/2017 – 07/2018 **Internship: “Development of Novel Amide Catalysts for Transfer Functionalization of C(sp³)-H Bonds.”**
Advisor: Prof. Dr. Konrad Tiefenbacher

09/2016 – 10/2016 **Internship: “Synthetic Strategies Toward the Synthesis of a Concave Ligand for the Encapsulation and Stabilization of Nanoparticles.”**
Advisor: Prof. Dr. Marcel Mayor

08/2013 – 01/2017 **Bachelor of Science in Chemistry**, University of Basel, Basel
2006 – 2013 **High School Degree (Abitur)**, Kant – Gymnasium, Weil am Rhein, Germany

TEACHING EXPERIENCE

2018 – 2021 **Teaching Assistant**, University of Basel, Basel

HONOR AND AWARDS

03/2021 – 11/2021 **ZOOM@Novartis 2021**, Mentoring Program of the University of Basel in cooperation with Novartis

2018 **Emilie-Louise-Frey Prize 2018**, for outstanding master thesis

EXTRACURRICULAR

2019 – 2021 **Board Member of the “PhD Chemistry Community (PCC)”**, University of Basel

SELECTED CONFERENCES

16/02/2022 **8th QUeT Meeting**, via ZOOM, Talk
“Synthetic Approaches for Molecular Thermoelectronics”

07/07/2021 **7th QUeT Meeting**, via ZOOM, Talk
“Synthetic Approaches for Molecular Thermoelectronics”

08/02/2021 **6th QUeT Meeting**, via ZOOM, Talk
“Synthetic Approaches for Molecular Thermoelectronics”

04/12/2020 **Christmas Symposium Basel 2020**, University of Basel, Switzerland,
Poster

| | |
|-----------------|----------------------------------------------------------------------------------------------------------------------------------------------------------------------------------------|
| 25/09/2020 | <i>"Tailor-Made Molecular Rods for Graphene Junctions"</i> 5th QuIET Meeting , Durham, England, Poster |
| 25/08/2020 | <i>"Synthetic Approaches for Molecular Thermoelectronics"</i> SCS Fall Meeting , Online Conference, Poster |
| 27 – 31/01/2020 | <i>"Tailor-Made Molecular Rods for Graphene Junctions"</i> International Conference on Molecular-Scale Charge and Thermal Transport , Engelberg, Switzerland, Posters |
| 09 – 10/07/2019 | <i>"Tailor-Made Molecular Rods for Graphene Junctions"</i> <i>"Compact[2.2]Paracyclophane-Based Systems"</i> 4th QuIET Meeting , Durham, England, Poster |
| 07 – 08/02/2019 | <i>"Synthetic Approaches for Molecular Thermoelectronics"</i> 3rd QuIET Meeting , Dubendorf, Switzerland, Poster |
| 04/10/2018 | <i>"Synthetic Approaches for Molecular Thermoelectronics"</i> Clariant Chemistry Day , University of Basel, Switzerland, Poster |
| | <i>"Tailor-Made Molecular Rods for Graphene Junctions"</i> |

LANGUAGE SKILLS

| | |
|---------|-----------------|
| Russian | native language |
| German | fluent |
| English | fluent |

PUBLICATION LIST

- **"Intense Molar Circular Dichroism in Fully Conjugated All-Carbon Macrocyclic 1,3-Butadiyne Linked pseudo-meta [2.2]Paracyclophanes."**
Eric Sidler, Patrick Zwick, Charlotte Kress, [Ksenia Reznikova](#), Olaf Fuhr, Dieter Fenske, Marcel Mayor, *Chem. Eur. J.* **2022**, *28*, e2022017.
- **"Substitution Pattern Controlled Quantum Interference in [2.2]Paracyclophane-Based Single-Molecule Junctions."**
[Ksenia Reznikova](#), Chunwei Hsu, Werner M. Schosser, Almudena Gallego, Katawoura Beltako, Fabian Pauly, Herre S. J. van der Zant, and Marcel Mayor, *J. Am. Chem. Soc.* **2021**, *143* (34), 13944–13951.
- **"Christmas Symposium Basel 2020"**
Daniel Joss, Alain Baiyoumy, Vittoria Chimisso, Claire E. Meyer, Dzmitry A. Miarzlou, Gosia M. Murawska, Nadja Niggli, Björn Pfund, [Ksenia Reznikova](#), and Pascal Rieder, *Chimia*, **2021**, *75*, 112.
- **"Christmas Symposium Basel 2019"**
Daniel Joss, Jaicy Vallapurackal, Alain Baiyoumy, Vittoria Chimisso, Fadri Christoffel, Patrick Herr, Claire Meyer, Dzmitry Miarzlou, Gosia Murawska, Nadja Niggli, [Ksenia Reznikova](#), Ivan Urosev, and Puck van Gerwen, *Chimia*, **2020**, *74*, 63.